

H24/3617

ad:
clie:

MONASH UNIVERSITY
THESIS ACCEPTED IN SATISFACTION OF THE
REQUIREMENTS FOR THE DEGREE OF
DOCTOR OF PHILOSOPHY

ON..... 17 February 2004

Sec. Research Graduate School Committee

Under the Copyright Act 1968, this thesis must be used only under the normal conditions of scholarly fair dealing for the purposes of research, criticism or review. In particular no results or conclusions should be extracted from it, nor should it be copied or closely paraphrased in whole or in part without the written consent of the author. Proper written acknowledgement should be made for any assistance obtained from this thesis.

STRESS-STRAIN BEHAVIOUR OF CONFINED HIGH
STRENGTH CONCRETE UNDER MONOTONICALLY
INCREASING AND CYCLIC LOADINGS

BY

W. P. LOKUGE
B.Sc(ENG) HONORS II, M.ENG

A THESIS SUBMITTED IN FULFILLMENT OF THE
REQUIREMENTS FOR THE DEGREE OF
DOCTOR OF PHILOSOPHY

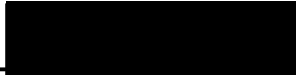
DEPARTMENT OF CIVIL ENGINEERING

MONASH
UNIVERSITY

OCTOBER 22, 2003

DECLARATION

I, W. P. Lokuge, hereby declare that this thesis contains no material which has been accepted for the award of any other degree or diploma in any university. Further to the best of my knowledge and belief, this thesis contains no material previously published or written by another person except where due reference is made in the text of the thesis.


W. P. Lokuge

22-10-2003
date

Contents

List of Tables	ix
List of Figures	x
Abstract	xvii
Acknowledgements	xix
List of publications from this study	xx
Acronyms and Symbols	xxii
1 Introduction	1
1.1 Background	2
1.1.1 Definition of high strength concrete	2
1.1.2 Applications	3
1.2 Research significance and project objectives	4
1.2.1 Objectives of the thesis	5
1.3 Structure of the thesis	6
1.3.1 Monotonically increasing loads	6
1.3.2 Cyclic loads	7
1.4 Contributions to knowledge	8
1.4.1 Important observations	9
2 MONOTONICALLY INCREASING LOADS:	
Lateral reinforcement requirement in high strength concrete columns	
using existing model	10

2.1	Introduction	10
2.2	Ductility	11
2.2.1	Ductility improvement	12
2.2.2	Measure of ductility	12
2.3	Axial load versus curvature relationship	13
2.3.1	Stress-strain model for concrete proposed by Mander et al. (1988b)	14
2.3.2	Stress-strain model for steel	15
2.3.3	Load-curvature analysis	15
2.4	Example	17
2.4.1	Results	18
2.5	Conclusions	20

3 MONOTONICALLY INCREASING LOADS:

	Development of a constitutive model for confined concrete	21
3.1	Introduction	21
3.2	Existing stress-strain models	22
3.2.1	Sargin et al. (1971) type models	23
3.2.2	Kent and Park (1971) type models	25
3.2.3	Popovics (1973) type models	27
3.2.4	Models capable of predicting lateral strain	31
3.2.5	Axial strain at peak axial stress (ϵ_{cc})	33
3.2.6	Peak axial stress for confined concrete (f_{cc})	35
3.2.7	Experimental investigations on high strength concrete	36
3.3	Damage models for concrete	37
3.4	Effect of strain rate on stress-strain behaviour	37
3.5	Gaps in knowledge	37
3.6	Model formulation	38
3.6.1	Experimental results	38
3.6.2	Basis of model formulation	39
3.6.3	Developing a relationship between axial strain and lateral strain	40
3.6.4	Lateral strain at peak axial stress (ϵ'_{cc})	43

3.6.5	Relationship between axial stress, axial strain and lateral strain	45
3.7	Model application in columns with passive confinement	49
3.7.1	Experimental program	50
3.7.2	Results	54
3.7.3	Discussion	54
3.8	Conclusions	58
4	MONOTONICALLY INCREASING LOADS:	
	Development of load-deformation characteristics of columns	61
4.1	Introduction	61
4.2	Previous work on eccentrically loaded columns	62
4.2.1	Analytical model used by Saatcioglu et al. (1995)	64
4.3	Experimental program	65
4.3.1	Short column tests	66
4.3.2	Slender column tests	69
4.4	Stress-strain model for concrete	70
4.4.1	Cover concrete	70
4.4.2	Effective lateral confining pressure	72
4.4.3	Effect of strain gradient	76
4.5	Stress-strain model for steel	76
4.6	Load-deformation analysis	77
4.6.1	Ductility measurement	79
4.6.2	Analysis of slender columns	79
4.7	Analytical findings	82
4.7.1	Comparison with experimental results of Attard and Foster (1995) .	82
4.7.2	Comparison with experimental results of Saatcioglu et al. (1995) . .	91
4.7.3	Comparison with experimental results of Lloyd and Rangan (1995)	94
4.8	Conclusions	99
5	MONOTONICALLY INCREASING LOADS:	
	Application of the constitutive model to estimate the strength of high	

strength concrete column-slab joints	101
5.1 Introduction	101
5.2 Background	102
5.2.1 Reported work on the behaviour of column-slab joints	103
5.3 Experimental program	105
5.4 Application of the constitutive model for the confined column-slab interface	107
5.5 Analytical procedure	107
5.5.1 Unloaded slab	107
5.5.2 Loaded slab	108
5.6 Comparison of the model predictions with reported experimental results . .	109
5.7 Conclusions	115
6 CYCLIC LOADS:	
Previous works on constitutive models of concrete and steel	117
6.1 Introduction	117
6.2 Previous work on models for cyclic loading of concrete	120
6.2.1 Experimental work	120
6.3 Envelope curve	121
6.4 Plastic strain	122
6.4.1 Plastic strain based on unloading strain only	122
6.4.2 Plastic strain based on unloading stress and strain	123
6.4.3 Plastic strain based on unloading strain and number of cycles . . .	124
6.4.4 Summary of plastic strain works	125
6.5 Unloading curve	125
6.5.1 Unloading curve as a parabolic function	126
6.5.2 Unloading curve as a bilinear function	127
6.5.3 Unloading curve as a trilinear function	128
6.5.4 Unloading curve as a power function	132
6.5.5 Unloading curve as a modified form of ascending branch of mono- tonic loading curve	132
6.5.6 Summary of models for unloading curve	134
6.6 Damage due to each cycle	134

6.7	Reloading curve	135
6.7.1	Reloading curve as a straight line	136
6.7.2	Reloading curve as a parabolic function	137
6.7.3	Reloading curve as a combination of straight line and a parabolic function	137
6.7.4	Reloading curve as a power function	139
6.7.5	Common points	139
6.7.6	Summary of the models for reloading curve	140
6.8	Partial unloading and reloading	140
6.8.1	Location of reloading point for partial unloading	141
6.9	Unloading/reloading cycles in the elastic region	142
6.10	Validation of the models	142
6.11	Previous work on models for cyclic loading of reinforcing steel	143
6.12	Conclusions	145
7	CYCLIC LOADS:	
	Experimental program	147
7.1	Introduction	147
7.2	Test variables	148
7.2.1	Compressive strength	148
7.2.2	Confining pressure	148
7.2.3	Loading regime	149
7.3	Concrete mixes and specimen preparation	149
7.3.1	Details of concrete mixes	149
7.3.2	Specimen preparation	151
7.3.3	Uniaxial compressive strengths	153
7.4	The test equipment	155
7.4.1	Triaxial cell	155
7.4.2	Application of confining pressure	155
7.4.3	Measurement of axial and lateral strains	157
7.5	Experimental setup	158
7.6	Test procedure	158

7.7	Trial tests	161
7.7.1	Problems encountered	166
7.8	Conclusions	168
8	CYCLIC LOADS:	
	Experimental results and analysis	170
8.1	Introduction	170
8.2	Calibrations	170
8.2.1	Calibration of LVDTs	170
8.2.2	Calibration of clip gauge	171
8.3	Experimental results	172
8.3.1	Grade 40 test series	174
8.3.2	Grade 60 test series	179
8.3.3	Grade 80 test series	184
8.3.4	Grade 100 test series	189
8.4	Discussion	194
8.4.1	Envelope curve	194
8.4.2	Hysteresis loops	194
8.4.3	Stress loss during hysteresis loops (damage)	194
8.4.4	Poisson's ratio	199
8.5	Conclusions	204
9	CYCLIC LOADS:	
	Development of a constitutive model for confined concrete	205
9.1	Introduction	205
9.2	Comparison of the experimental results with the existing models	206
9.2.1	Grade 40 concrete	207
9.2.2	Grade 60 concrete	207
9.2.3	Grade 80 concrete	208
9.2.4	Grade 100 concrete	208
9.3	Preliminary modelling process	208
9.3.1	Different attempted approaches	208
9.3.2	Shear failure approach	217

9.4	Description of the proposed model	218
9.4.1	Ascending branch of monotonic loading curve (AB)	221
9.4.2	Determination of plastic strain (ϵ_{pl})	224
9.4.3	Unloading curve (BC, GH)	225
9.4.4	Reloading curve (DE, HJ)	230
9.4.5	Parabolic transition curve (EF, JK)	235
9.4.6	Modified monotonic loading curve for the descending branch (FG or KL)	236
9.5	Poisson's ratio	236
9.6	Results	237
9.6.1	Comparison of the proposed model with the experimental results . .	237
9.6.2	Comparison of the proposed model with experimental results re- ported in the literature	251
9.7	Conclusions	253
 10 CYCLIC LOADS:		
	Prediction of load-deformation characteristics of columns	255
10.1	Introduction	255
10.2	Examples for poor design of columns	256
10.3	Previous work on the behaviour of columns under cyclic flexure and con- stant axial load	257
10.3.1	Experimental programs	258
10.3.2	Effect of concrete compressive strength	258
10.3.3	Effect of transverse reinforcement	259
10.3.4	Effect of axial load	260
10.3.5	Ductility	261
10.3.6	Length of plastic hinge	262
10.3.7	Spalling of cover	263
10.3.8	Code provisions	263
10.3.9	Behaviour of HSC columns under cyclic loading	264
10.4	Computational procedure	265
10.4.1	Basic assumptions	265

10.4.2 Methodology	265
10.5 Computer program	268
10.5.1 General description	268
10.5.2 Program outline	268
10.6 Comparison with experimental results	285
10.6.1 Experimental program	285
10.6.2 Load versus displacement relationship	286
10.6.3 Predicted and experimental behaviour	289
10.6.4 Discussion	290
10.7 Conclusions	297
11 Conclusions and recommendations	299
11.1 Conclusions	299
11.1.1 Monotonically increasing loads	299
11.1.2 Cyclic loads	300
11.1.3 Important features of both models	301
11.2 Recommendations	302
A Comparison of experimental results with the existing models for mono-	
tonically increasing loads	304

List of Tables

1.1	Development of concrete strength in Chicago (Laogan and Elnashai 1999).	3
3.1	Stress-strain models for confined concrete based on Sargin et al. (1971).	24
3.2	Stress-strain models for confined concrete based on Kent and Park (1971).	26
3.3	Stress-strain models for confined concrete based on Popovics (1973).	29
3.4	Material parameters in Equations (3.50) and (3.61).	43
3.5	Mix proportions for carbon fibre wrapped specimens.	50
3.6	Uniaxial strengths (specimens to be wrapped by carbon fibre).	51
4.1	Details of column specimens (Foster and Attard 1995).	67
4.2	Details of column specimens (Saatcioglu et al. 1995).	68
4.3	Details of column specimens (Lloyd and Rangan 1995).	70
4.4	Peak loads of eccentrically loaded reinforced concrete columns reported by Attard and Foster (1995).	89
4.5	Ductility of eccentrically loaded reinforced concrete columns reported by Attard and Foster (1995).	90
4.6	Peak loads of eccentrically loaded reinforced concrete columns reported by Lloyd and Rangan (1995).	94
5.1	A summary of previous research.	104
5.2	Provisions of design codes.	105
5.3	Details of the specimens.	106
6.1	Terminology used in the stress-strain curve for cyclic loading of concrete.	119
7.1	Gradings of fine and coarse aggregate.	151
7.2	Mix proportions.	151
7.3	Uniaxial strengths at 28 days and at time of testing.	155
7.4	Planning of testing for Grade 40 (44 MPa) concrete.	162
7.5	Planning of testing for Grade 60 (58 MPa) concrete.	163
7.6	Planning of testing for Grade 80 (83 MPa) concrete.	164
7.7	Planning of testing for Grade 100 (106 MPa) concrete.	165
10.1	Details of test specimens.	287
10.2	Plastic hinge length for selected specimens.	290

List of Figures

2.1	Load versus curvature relationship with ultimate and yielding points. . . .	13
2.2	Cross section analysis.	16
2.3	Section details.	18
2.4	Load-curvature curve for 40 MPa and 100 MPa with same stirrup spacing (300 mm).	19
2.5	Load-curvature curve for 40 MPa and 100 MPa with same ductility 5.8. . .	19
3.1	Typical stress-strain relationship for Sargin et al. (1971) type models. . . .	23
3.2	Typical stress-strain relationship for Kent and Park (1971) type models. . .	25
3.3	Typical stress-strain relationship for Popovics (1973) type models.	28
3.4	Typical stress-strain relationship for confined and unconfined concrete. . .	41
3.5	Normalised lateral strain versus normalised axial strain.	42
3.6	Poisson's ratio for concrete (Rashid et al. 2002).	43
3.7	Normalised volumetric strain factor versus normalised axial strain factor (The "x" marked on the curves indicate peak stress points).	44
3.8	Normalised shear stress factor versus normalised shear strain factor.	46
3.9	Stress-strain curves for Grade 40 concrete.	47
3.10	Stress-strain curves for Grade 60 concrete.	48
3.11	Stress-strain curves for Grade 75 concrete.	48
3.12	Stress-strain curves for Grade 100 concrete.	49
3.13	Carbon fibre tensile test specimen.	51
3.14	Tensile stress-strain curve for carbon fibre composite.	51
3.15	Carbon fibre wrapped specimen.	52
3.16	Clip gauge system used to measure lateral strains.	53
3.17	Confinement action in FRP composites.	54
3.18	Stress-strain curves for Grade 30 concrete with 1 carbon fibre wrap.	55
3.19	Stress-strain curves for Grade 30 concrete with 3 carbon fibre wraps. . . .	55
3.20	Stress-strain curves for Grade 60 concrete with 1 carbon fibre wrap.	56
3.21	Stress-strain curves for Grade 60 concrete with 3 carbon fibre wraps. . . .	56
3.22	Stress-strain curves for Grade 100 concrete with 1 carbon fibre wrap. . . .	57
3.23	Stress-strain curves for Grade 100 concrete with 3 carbon fibre wraps. . . .	57

3.24	Procedure in drawing stress-strain curves for confined concrete (given ϵ_1 and f_c).	59
4.1	Confined concrete model proposed by Saatcioglu and Razvi (1992).	64
4.2	Lateral pressure and the strain gradient (Saatcioglu et al. 1995).	66
4.3	Details of column specimens.	67
4.4	Details of column specimens (Lloyd and Rangan 1995).	70
4.5	Mechanics of cover spalling.	71
4.6	Effectively confined core area of a square column.	73
4.7	Confining pressures for some common configurations.	74
4.8	Lateral confining pressure.	76
4.9	Procedure used in drawing moment-curvature curves for laterally confined concrete.	78
4.10	Combined ductility ratio in eccentrically loaded column.	80
4.11	Standard pin-ended column (Lloyd and Rangan 1995).	81
4.12	Load versus average strain + curvature \times eccentricity for 2L2030 and 2L2060 specimens.	83
4.13	Load versus average strain + curvature \times eccentricity 2L5030 and 2L50120 specimens.	84
4.14	Load versus average strain + curvature \times eccentricity 4L860 and 4L20120R specimens.	85
4.15	Load versus average strain + curvature \times eccentricity 4L5060 and 2M2030 specimens.	86
4.16	Load versus average strain + curvature \times eccentricity 2M5030 and 2M50120R specimens.	87
4.17	Load versus average strain + curvature \times eccentricity 4M5030 and 4F5030 specimens.	88
4.18	Comparison of moment-curvature relationships for C4-2 and C5-2 columns.	92
4.19	Comparison of moment-curvature relationships for C8-1 and C10-2 columns.	93
4.20	Moment-curvature relationships for series V specimen A.	95
4.21	Moment-curvature relationships for series V specimen B.	95
4.22	Moment-curvature relationships for series V specimen C.	96
4.23	Moment-curvature relationships for series VII specimen A.	96
4.24	Moment-curvature relationships for series VII specimen B.	97
4.25	Moment-curvature relationships for series VII specimen C.	97
4.26	Moment-curvature relationships for series XI specimen A.	98
4.27	Moment-curvature relationships for series XI specimen B.	98
4.28	Moment-curvature relationships for series XI specimen C.	99
5.1	Column-slab connection.	103

5.2	Details of specimens (Ospina and Alexander 1998).	106
5.3	Behaviour of joint concrete in an unloaded slab.	108
5.4	Behaviour of joint concrete in a loaded slab.	109
5.5	Stress-strain curves for unloaded slabs A1-A and A2-A.	111
5.6	Stress-strain curves for unloaded slabs A3-A and A4-A.	112
5.7	Stress-strain curves for loaded slabs A2C and A3B.	113
5.8	Stress-strain curves for loaded slabs A4B and A4C.	114
5.9	Effect of slab load on interior joint strength.	115
6.1	Stress-strain curve for cyclic loading of concrete.	118
6.2	Envelope curve for cyclic loading of concrete.	122
6.3	Stress-strain curves for unloading and reloading.	124
6.4	Stress-strain behaviour of concrete with cyclic loading (Park et al. 1972).	127
6.5	Proposed cyclic stress-strain curve for concrete in compression (Elmorsi et al. 1998).	128
6.6	Scheme of focal points model (Darwin and Pecknold 1977).	129
6.7	Model for plain concrete under cyclic load (Yankelevsky and Reinhardt 1987).	131
6.8	Damage due to loading cycle.	134
6.9	Control points for hysteresis loops (Darwin and Pecknold 1977).	140
6.10	Interpolation of reloading point for partial unloading.	141
6.11	Interpolation of plastic and envelope strains for partial reloading.	142
6.12	Hysteresis behaviour of steel.	144
7.1	Considered loading regimes.	150
7.2	Specimen before testing.	153
7.3	Tested specimens for uniaxial compressive strengths.	154
7.4	Schematic diagram of triaxial cell.	156
7.5	Photo of triaxial cell.	157
7.6	Schematic diagram of lateral strain measuring device.	159
7.7	Photo of lateral strain measuring device.	160
7.8	Schematic diagram of experimental setup.	160
7.9	Photo of experimental setup.	161
7.10	Comparison of average strain gauge and clip gauge readings.	166
7.11	User interface of the data acquisition program.	168
8.1	LVDT calibration.	171
8.2	Clip gauge calibration.	172
8.3	Unfiltered stress-strain curve.	173
8.4	Filtered stress-strain curve.	173
8.5	Tested specimens for Grade 40 concrete.	175
8.6	Grade 40 concrete with 4 MPa confining pressure.	176

8.7	Grade 40 concrete with 8 MPa confining pressure.	177
8.8	Grade 40 concrete with 12 MPa confining pressure.	178
8.9	Tested specimens for Grade 60 concrete.	180
8.10	Grade 60 concrete with 4 MPa confining pressure.	181
8.11	Grade 60 concrete with 8 MPa confining pressure.	182
8.12	Grade 60 concrete with 12 MPa confining pressure.	183
8.13	Tested specimens for Grade 80 concrete.	185
8.14	Grade 80 concrete with 4 MPa confining pressure.	186
8.15	Grade 80 concrete with 8 MPa confining pressure.	187
8.16	Grade 80 concrete with 12 MPa confining pressure.	188
8.17	Tested specimens for Grade 100 concrete.	190
8.18	Grade 100 concrete with 4 MPa confining pressure.	191
8.19	Grade 100 concrete with 8 MPa confining pressure.	192
8.20	Grade 100 concrete with 12 MPa confining pressure.	193
8.21	Comparison of monotonic and cyclic loading curves for 44 MPa concrete. .	195
8.22	Comparison of monotonic and cyclic loading curves for 58 MPa concrete. .	196
8.23	Comparison of monotonic and cyclic loading curves for 83 MPa concrete. .	197
8.24	Comparison of monotonic and cyclic loading curves for 106 MPa concrete. .	198
8.25	Behaviour of Poisson's ratio for 44 MPa concrete.	200
8.26	Behaviour of Poisson's ratio for 58 MPa concrete.	201
8.27	Behaviour of Poisson's ratio for 83 MPa concrete.	202
8.28	Behaviour of Poisson's ratio for 106 MPa concrete.	203
9.1	Poisson's ratio versus axial strain for monotonically increasing loads. . . .	210
9.2	Normalised total energy versus strain for unloading branches.	212
9.3	Normalised total energy versus strain for unloading branches.	213
9.4	Definitions used in energy approach.	214
9.5	Energy during unloading.	215
9.6	Dissipated energy during unloading.	216
9.7	Stress-strain state of a laterally confined concrete cylinder.	217
9.8	Mohr's circle for a stress/ strain field.	218
9.9	Failure sections in concrete under compression.	219
9.10	Shear stress factor versus shear strain factor for unloading branches of Grade 40 concrete.	219
9.11	Shear stress factor versus shear strain factor for unloading branches of Grade 60 concrete.	220
9.12	Shear stress factor versus shear strain factor for unloading branches of Grade 80 concrete.	220

9.13 Shear stress factor versus shear strain factor for unloading branches of Grade 100 concrete.	221
9.14 Key components in cyclic stress-strain model.	222
9.15 Shear stress factor versus shear strain factor for 72 unloading branches.	226
9.16 Normalised lateral strain versus normalised axial strain for 21 unloading curves in Grade 40 concrete.	228
9.17 Normalised lateral strain versus normalised axial strain for 22 unloading curves in Grade 60 concrete.	228
9.18 Normalised lateral strain versus normalised axial strain for 9 unloading curves in Grade 80 concrete.	229
9.19 Normalised lateral strain versus normalised axial strain for 20 unloading curves in Grade 100 concrete.	229
9.20 Shear stress factor versus shear strain factor for 65 reloading branches.	232
9.21 Normalised lateral strain versus normalised axial strain for 21 reloading curves in Grade 40 concrete.	232
9.22 Normalised lateral strain versus normalised axial strain for 8 reloading curves in Grade 60 concrete.	233
9.23 Normalised lateral strain versus normalised axial strain for 8 reloading curves in Grade 80 concrete.	233
9.24 Normalised lateral strain versus normalised axial strain for 18 reloading curves in Grade 100 concrete.	234
9.25 Variation of Poisson's ratio during hysteresis loops.	237
9.26 Procedure in drawing stress-strain curves for cyclically loaded concrete.	238
9.27 44 MPa with 4 MPa confining pressure.	239
9.28 44 MPa with 8 MPa confining pressure.	240
9.29 44 MPa with 12 MPa confining pressure.	241
9.30 58 MPa with 4 MPa confining pressure.	242
9.31 58 MPa with 8 MPa confining pressure.	243
9.32 58 MPa with 12 MPa confining pressure.	244
9.33 83 MPa with 4 MPa confining pressure.	245
9.34 83 MPa with 8 MPa confining pressure.	246
9.35 83 MPa with 12 MPa confining pressure.	247
9.36 106 MPa with 4 MPa confining pressure.	248
9.37 106 MPa with 8 MPa confining pressure.	249
9.38 106 MPa with 12 MPa confining pressure.	250
9.39 Model comparison with previous work (Desayi et al. 1979) for concrete with $f_c=22.3$ MPa.	251

9.40 Model comparison with previous work (Desayi et al. 1979) for concrete with $f_c=23$ MPa.	252
9.41 Model comparison with previous work (Desayi et al. 1979) for concrete with $f_c=17.8$ MPa.	252
9.42 Model comparison with previous work (Desayi et al. 1979) for concrete with $f_c=18.7$ MPa.	253
10.1 Column failures in Kobe 1995 earthquake (EQE 1995).	257
10.2 Section ductility parameters.	261
10.3 Basis for the column analysis.	266
10.4 Flowchart for the column analysis.	269
10.5 Structure of subroutines for the computer program.	270
10.6 User interface.	270
10.7 Loading history.	271
10.8 Convergence algorithm in finding axial load.	272
10.9 Storing unloading and reloading coordinates.	273
10.10 Axial load calculation.	275
10.11 "cc" values for each loading path in concrete.	276
10.12 Determination of stress in concrete from different loading paths.	277
10.13 Assigning the loading path for each slice of concrete.	278
10.14 "mm" values for each loading path in steel.	282
10.15 Assigning the loading path for each layer of steel.	283
10.16 Procedure used in calculating steel stresses.	284
10.17 Details of column specimens.	287
10.18 Typical column section used in the analysis.	288
10.19 Curvature and displacement relationships.	289
10.20 Comparison for C7010 column reported by Matamoros and Sozen (2003).	291
10.21 Comparison for C100B60N15 column reported by Legeron and Paultre (2000).	292
10.22 Comparison for C100B130N15 column reported by Legeron and Paultre (2000).	293
10.23 Comparison for C100B130N25 column reported by Legeron and Paultre (2000).	294
10.24 Comparison for C100B130N40 column reported by Legeron and Paultre (2000).	295
A.1 Loading regime 1 of Grade 40 concrete with 4 MPa confining pressure.	305
A.2 Loading regime 2 of Grade 40 concrete with 4 MPa confining pressure.	306
A.3 Loading regime 1 of Grade 40 concrete with 8 MPa confining pressure.	307
A.4 Loading regime 2 of Grade 40 concrete with 8 MPa confining pressure.	308
A.5 Loading regime 1 of Grade 40 concrete with 12 MPa confining pressure.	309

A.6	Loading regime 2 of Grade 40 concrete with 12 MPa confining pressure.	310
A.7	Loading regime 1 of Grade 60 concrete with 4 MPa confining pressure.	311
A.8	Loading regime 2 of Grade 60 concrete with 4 MPa confining pressure.	312
A.9	Loading regime 1 of Grade 60 concrete with 8 MPa confining pressure.	313
A.10	Loading regime 2 of Grade 60 concrete with 8 MPa confining pressure.	314
A.11	Loading regime 1 of Grade 60 concrete with 12 MPa confining pressure.	315
A.12	Loading regime 2 of Grade 60 concrete with 12 MPa confining pressure.	316
A.13	Loading regime 1 of Grade 80 concrete with 4 MPa confining pressure.	317
A.14	Loading regime 2 of Grade 80 concrete with 4 MPa confining pressure.	318
A.15	Loading regime 1 of Grade 80 concrete with 8 MPa confining pressure.	319
A.16	Loading regime 2 of Grade 80 concrete with 8 MPa confining pressure.	320
A.17	Loading regime 1 of Grade 80 concrete with 12 MPa confining pressure.	321
A.18	Loading regime 2 of Grade 80 concrete with 12 MPa confining pressure.	322
A.19	Loading regime 1 of Grade 100 concrete with 4 MPa confining pressure.	323
A.20	Loading regime 2 of Grade 100 concrete with 4 MPa confining pressure.	324
A.21	Loading regime 1 of Grade 100 concrete with 8 MPa confining pressure.	325
A.22	Loading regime 2 of Grade 100 concrete with 8 MPa confining pressure.	326
A.23	Loading regime 1 of Grade 100 concrete with 12 MPa confining pressure.	327
A.24	Loading regime 2 of Grade 100 concrete with 12 MPa confining pressure.	328

Abstract

The use of High Strength Concrete (HSC) in structures has significant technical and economical advantages. Its use however, demands additional care due to the decreased ductility compared to Normal Strength Concrete (NSC). Ductility improvements can be achieved by using adequate lateral confinement. Confining pressure exerted by the lateral reinforcement depends on the lateral dilation of concrete. Lateral dilation of HSC is less than that of NSC under similar stress conditions. Therefore effective confining pressure from the confining steel is reduced in HSC. Knowledge of the constitutive behaviour of HSC is essential to estimate the confining pressure required to provide a sufficient level of ductility.

Based on shear stress versus shear strain of concrete, a constitutive model is developed in this thesis for the behaviour of confined HSC subjected to monotonically increasing loads. The model is innovative in using the concepts of shear failure of concrete and is strain-based ensuring ease of application. Application of this novel constitutive model is demonstrated by establishing the behaviour of concentrically or eccentrically loaded confined HSC columns and column-slab joints. The comparisons of the results from this model with the experimental results show reasonably good correlation.

An experimental program was conducted as part of this study to establish the axial stress, axial strain and lateral strain relationships for confined HSC under cyclic loading. Four grades of concrete (Grade 40, 60, 80 and 100 MPa) were investigated with three levels of active lateral confinement (4, 8 and 12 MPa) and two loading regimes (with unloading strain as a variable and constant unloading strain and number of cycles as a variable). The cylindrical specimens (100 mm diameter and 200 mm high) were tested in a triaxial cell. A total of 24 tests were carried out.

Using the experimental results, the strain-based model developed for the behaviour of

laterally confined HSC subjected to monotonically increasing load has been further developed for cyclic axial compression. The concepts used in establishing a constitutive model for confined HSC under monotonically increasing load mentioned above were extended in implementing this model. The stress-strain curve for monotonically increasing loading of concrete forms the envelope curve for the ascending branch of the cyclically loaded HSC. However unlike in NSC, the descending branch of the envelope curve for HSC was found to be affected by the damage to concrete due to cyclic loading.

The constitutive model developed for cyclically loaded HSC can be utilised to estimate the required ductility to design structures against earthquake loadings. Poor column behaviour is one of the main reasons for most of the structural failures during recent earthquakes. Application of the constitutive model for cyclically loaded HSC is demonstrated by predicting moment-curvature relationships for HSC columns subjected to axial load and cyclic flexure. Analytical findings are in good agreement with the experimental results.

Several important observations are made during the analyses of the test results. Volumetric strain is zero at peak axial stress thus lateral strain at the peak axial stress is half of the corresponding axial strain. Unloading in the "initial elastic region" results in a decrease in the Poisson's ratio below the initial Poisson's ratio.

Both the constitutive models developed in this thesis are based on triaxial test results, which are conducted under well-controlled conditions, where direct measurements of axial and lateral strain have been possible. Ability to establish axial as well as lateral strain in confined concrete is a superior attribute of the proposed models. They are fundamentally more reliable and more likely to work for a wide range of column configurations and sizes than the models that are based on back-calculated results from reinforced column tests.

Acknowledgements

The author wishes to record her profound gratitude and deep appreciation for her main supervisor, Associate Professor J.G. Sanjayan for his invaluable support, constructive criticisms and continuous encouragement throughout her studies. Without his untiring effort, this work would not have been completed successfully. The author records her sincere gratitude and grateful appreciation to her associate supervisor, Dr. Sujeeva Setunge from RMIT University for her constant guidance, productive criticism, invaluable advice and the numerous support she extended to her right from the very beginning of her studies at Monash University. The kindness and flexibility shown towards the author by both supervisors are far beyond the expectations from a supervisor.

The author is grateful for Mr. Chris Powell, the resource manager, Mr. Graeme Rundle, the lab manager and the staff in the Civil Engineering Laboratory for the numerous support that was extended to her throughout her experimental program. Special thanks are due to Mr. Jeff Doddrell, Mr. Roger Doulis, Mr. Kevin and Mr. Alan Taylor for their invaluable assistance during the many problems encountered in the progress of the experiments.

Sincere gratitude is extended towards her colleagues in the Civil Engineering Department for the friendly environment she had throughout the study.

The author is eternally indebted to her beloved parents for their continuous encouragement, love, understanding and tremendous guidance which were the main driving forces to the success of her life. Sincere gratitude is extended for her two sisters for their love, numerous support, encouragement and patience.

Finally the author wishes to thank her loving husband, Dhammika for his endless support, continuous patience and unwavering love throughout this study. The moral support and the encouragement he gave her to recover from the recent sudden loss of her father is deeply appreciated.

List of publications from this study

Journal publications

1. Lokuge, Weena P., Sanjayan, G.J. and Setunge, Sujeeva, "Design of high strength concrete columns for ductility," *Concrete in Australia, Journal of the Concrete Institute of Australia*, 26(3), pp. 17-20, Sep-Nov, 2000.
2. Lokuge, Weena P., Setunge, Sujeeva and Sanjayan, G.J., "Modelling eccentrically loaded high-strength concrete columns," *Magazine of Concrete Research*, 55(4), pp. 331-341, August, 2003.
3. Lokuge, Weena P., Sanjayan, G.J. and Setunge, Sujeeva, "Triaxial test results of high strength concrete subjected to cyclic loading," *Magazine of Concrete Research*, 55(4), pp. 321-329, August, 2003.
4. Lokuge, Weena P., Sanjayan, G.J. and Setunge, Sujeeva, "Stress strain model for laterally confined concrete," *Journal of Materials in Civil Engineering, ASCE*, Approved for publication, 2003.
5. Lokuge, Weena P., Sanjayan, G.J. and Setunge, Sujeeva, "Constitutive model for confined high strength concrete subjected to cyclic loading," *Journal of Materials in Civil Engineering, ASCE*, Approved for publication, 2003.

Conference publications

6. Lokuge, Weena P., Setunge, Sujeeva and Sanjayan, G.J., "Lateral reinforcement requirement in high-strength concrete columns," *International Conference "Our World in Concrete and Structures"*, Singapore, pp. 411-417, August, 2000.

7. Lokuge, Weena P., Setunge, Sujeeva, P. Mendis and Sanjayan, G.J., "Prediction of Strength of Interior High-Strength Concrete Column-Slab Joints," *Proceedings of the 17th Australasian Conference on the Mechanics of Structures and Materials*, Queensland, Australia, pp. 185-190, June, 2002.
8. Lokuge, Weena P., Sanjayan, G.J. and Setunge, Sujeeva, "Stress strain relationship of high strength concrete subjected to cyclic loading," *International Association for Bridge and Structural Engineering Symposium*, Melbourne, Australia, Vol. 86, 9pp. (CD-ROM), September, 2002.

Acronyms and Symbols

A	constant defining parabolic transition curve (Equation 9.48)
A_{core}	area of core of section
A_{eff}	area of effectively confined core concrete
A_g	gross cross sectional area of a section
$A_{i,con}$	area of confined concrete in the i^{th} slice
$A_{i,uncon}$	area of unconfined concrete in the i^{th} slice
A_s	area of one leg of lateral reinforcement
$A_{s,j}$	total area of steel of the j^{th} layer
A_{sp}	total cross sectional area of lateral reinforcement
A_{st}	total longitudinal steel area
a	parameter in defining plastic strain
B	width of cross section
c	neutral axis depth from extreme compression side
cc	value used to differentiate loading path of concrete
D	a parameter added to fit the post peak shape of the concrete stress-strain curve (Candappa 2000)
D_c	combined ductility ratio
d	depth of cross section
d_1	distance to compression steel
d_2	distance to tension steel
d_i	distance to the i^{th} slice of concrete from the top
dr_m	distance to the m^{th} layer of longitudinal steel from the top
d_s	centre to centre distance between the transverse ties
E	energy at any stress and strain state
\bar{E}	normalised total energy

E_c	modulus of elasticity of concrete
E_{des}	deterioration rate
E_i	initial tangent modulus of concrete
EM	resultant moment
EN	resultant force
E_r	reloading point tangent modulus
E_s	secant value of Young's modulus of concrete
E_f	secant value of Young's modulus at peak stress of concrete
E_p	plastic modulus of steel
$E_{r,e}$	common return point tangent modulus
E_{rt}	averaged modulus of the reloading
$E_{r,o}$	reloading point tangent modulus
E_{sh}	strain hardening modulus of steel in the strain hardening region
E_{st}	modulus of elasticity of steel
E_{un}	unloading stiffness of concrete
E_{unt}	total energy at unloading point
e	eccentricity
F	horizontal cyclic load
F_i	force due to concrete in the i^{th} slice
F_{cc}	total force due to nn number of concrete slices
F_{cs}	total force due to m number of steel layers
$F_{su}(j)$	ultimate strength of steel in j^{th} layer
f_c	compressive strength of unconfined concrete
f_{cc}	peak axial stress of confined concrete
f'_{cc}	compressive strength of column concrete
f'_{ce}	effective compressive strength of column in column-slab joint
f_{cf}	hoop stress of the carbon fibre sheet
f_{cm}	mean value of compressive strength of concrete
f'_{cs}	compressive strength of slab concrete
$f_{i,con}$	stress due to confined concrete in the i^{th} slice
$f_{i,uncon}$	stress due to unconfined concrete in the i^{th} slice
f_l	confining pressure

f_{lc}	effective lateral confining pressure
f_s	steel stress
$f_{s,j}$	stress in the j^{th} layer of steel
f_{sy}	yield strength of reinforcing steel
$f_{sy}(j)$	yield strength of steel in j^{th} layer
f_t	tensile strength of concrete
$f_{un,s}$	stress at the unloading point of steel
g	strain parameter defining parabolic transition curve
$(\sqrt{J_2})_f$	square root of invariant at failure
k	constant defined in Equation (3.47)
k_e	coefficient of effectiveness ($k_e \leq 1$)
L	height of the column from base
L_e	effective length of the column
l_p	length of plastic hinge
M	moment in the critical section
m_1	shape parameter of the stress strain curve of steel
m	number of layers of longitudinal steel
m_1, m_2, m_3	concrete material parameters in Equation (3.61) which depends on the compressive strength
mm	value used to differentiate loading path of steel
N_ϕ	cumulative ductility ratio
n	number of cycles in cyclic loading of concrete
n_1	number of longitudinal steel bars in columns
n_2	number of carbon fibre sheets
n_3	number of lateral reinforcement legs in vertical cross section in spacing s
nn	number of horizontal slices considered in a section
P	axial load
P_{calc}	calculated axial load
P_m	maximum axial load
p	current loop in moment curvature analysis

q	concrete material parameter used to define unloading and reloading b. inches of concrete
R^2	correlation coefficient
r	modulus parameter
r_1	"Ramberg-Osgood" empirical parameter
s	spacing between lateral reinforcement
s_l	spacing of longitudinal reinforcement
s'	clear spacing between lateral reinforcement
t	thickness of a slice considered in column cross section
t_{cf}	thickness of a carbon fibre sheet
u	number of hysteresis loop
V	volume of concrete specimen
w_i	i^{th} clear distance between longitudinal bars
x	strain parameter
Z_m	slope of the straight line descending branch of stress-strain curve of confined concrete
β	non linearity index
β_l	stress point at which v^a deviates from a constant value
β_n	stress deterioration ratio in loading unloading cycle
γ_n	increasing ratio of plastic strain
γ_{max}	maximum shear strain
$\bar{\gamma}$	maximum shear strain factor
Δ	total flexural displacement of the tip
Δf_1	tip displacement due to rotation of plastic hinge
Δf_2	tip displacement due to bending of column
$\Delta \varepsilon(p)$	strain in current loop - strain in previous loop
δ	mid-height deflection of a slender column
ε_1	axial strain of concrete
ε_2	lateral strain of concrete
$\bar{\varepsilon}_1$	normalized axial strain factor
$\bar{\varepsilon}_2$	normalized lateral strain factor

ϵ_a	strain at the intersection of the initial tangent and the plastic unloading secant slopes
ϵ_{av}	average strain at the centroid of the section
ϵ_{co}	axial strain corresponding to peak uniaxial compressive strength
ϵ_{cc}	axial strain corresponding to peak axial stress of confined concrete
ϵ'_{cc}	lateral strain corresponding to peak axial stress of confined concrete
ϵ_i	strain of the i^{th} concrete slice
$\epsilon(i, p)$	strain of the i^{th} concrete slice in p^{th} loop
ϵ_j	strain of the j^{th} layer of steel
ϵ_{cu}	ultimate strain of concrete
ϵ_{pl}	plastic strain of concrete
ϵ_{re}	return point (reloading curve meets envelope curve) strain of concrete
ϵ_{ro}	strain at the reloading point of concrete
ϵ_{rp}	reloading strain for partial unloading and full reloading
ϵ_s	steel strain
ϵ_{ts}	tensile strain
ϵ_t	strain in extreme compression side
ϵ_{un}	strain at the unloading point of concrete
$\epsilon_{un}(i)$	strain at the unloading point of i^{th} slice of concrete
$\epsilon_{un,s}$	strain at the unloading point of steel
$\bar{\epsilon}_v$	normalized volumetric strain factor
$\epsilon_{v,max}$	maximum volumetric strain
ϵ_y	steel strain corresponding to yield strength
ϵ'	axial strain at the point where the shape of axial strain and lateral strain curves deviate
μ	displacement ductility factor
μ_ϕ	curvature ductility factor
ν^a	secant value of Poisson's ratio for the ascending branch
ν_d^a	secant value of Poisson's ratio for the descending branch
ν_f^a	secant value of Poisson's ratio at peak stress
ν_i^a	initial Poisson's ratio

ξ	average strain + curvature \times eccentricity
ξ_u	combined strain at the ultimate point
ξ_y	combined strain defined by 3/4 rule
ρ	density of concrete
ρ_s	lateral reinforcement ratio
σ_0	reference plastic stress of steel
$\sigma_1, \sigma_2, \sigma_3$	principal stresses (in this study $\sigma_1 \geq \sigma_2 = \sigma_3$, compression positive)
$\bar{\sigma}_1$	normalised stress
$\sigma(i, p)$	stress of the i^{th} concrete slice in p^{th} loop
σ_{lo}	lowest strain reached during partial unloading
σ_{new}	new axial stress reached at the end of reloading
σ_{re}	axial stress at the return point
σ_{ro}	concrete stress at the reloading point
σ_{un}	concrete stress at the unloading point
$\sigma_{un}(i)$	stress at the unloading point of i^{th} slice of concrete
τ_{max}	maximum shear stress
$\bar{\tau}$	maximum shear stress factor
ϕ	curvature
ϕ_{end}	curvature at the end of a loading cycle
ϕ_{start}	curvature at the beginning of a loading cycle
ϕ_u	curvature at the ultimate point
ϕ_y	curvature at the point in the ascending branch of the curve in which the moment is equal to 80% of the peak moment

Subscripts

<i>cp</i>	common point
<i>new</i>	new stress point in the reloading branch
<i>pl</i>	plastic strain point
<i>ro</i>	reloading point
<i>re</i>	returning point
<i>un</i>	unloading point
<i>mp</i>	maximum value at peak axial stress

Chapter 1

Introduction

The use of High Strength Concrete (HSC) in structural systems is increasing around the world due to economic and technical advantages it offers. Main advantages of HSC are its higher strength and stiffness per unit cost and higher strength per unit weight than those for Normal Strength Concrete (NSC). High load carrying capacity per unit weight has proven economic benefits in the construction of high-rise buildings and long span bridges. It offers excellent mechanical performance and durability. The use of HSC column sections in high-rise buildings, especially in lower stories, results in additional savings. Further it permits early removal of formwork thus increasing the speed of construction. In buildings, significant reduction in column sizes can be achieved by using HSC which ultimately result in economic benefits associated with increased floor area for rental.

As a result of ongoing progress in concrete technology, HSC is used in various other practical applications apart from buildings. In bridge design, the number of beams can be reduced and the loss of prestress due to creep in prestressed concrete is smaller if HSC is used. HSC is also used successfully in offshore platforms, maritime structures and piles. Often HSC is used not for its strength but for its superior durability in aggressive environments.

Reduction of ductility with the increase in concrete compressive strength is well known. The issue of ductility of concrete columns has become increasingly important with the introduction of HSC with compressive strengths from 50 to 100 MPa. This has led to many research programs worldwide to investigate methods of overcoming the problems of limited ductility. The strength and ductility improvements are important considerations in designing reinforced concrete columns especially in the areas requiring design for seismic loading.

Constitutive models for the behaviour of laterally confined concrete are widely available. They have been used in the modelling of the load-deformation characteristics of columns. In them, it is assumed that confining pressure applied by the lateral reinforcement corresponds to the yielding of the lateral reinforcement. However, the confining pressure depends on the lateral dilation of concrete. Therefore development of relationships between axial stress, axial strain and lateral strain for confined HSC is a timely concern.

The weight of the structures can be reduced with the use of HSC when compared to NSC. Since lighter structures attract less forces than heavier structures in an earthquake, the use of HSC can be beneficial in seismic regions. Behaviour of concrete (NSC or HSC) subjected to cyclic loading, needs to be known when a structural analysis is performed for earthquake loadings. Therefore it is imperative to develop a constitutive model for confined HSC subjected to cyclic axial compression.

1.1 Background

1.1.1 Definition of high strength concrete

There is no single definition of HSC. According to a study by Chan and Anson (1994), Grade 35 concrete was considered as high strength in 1950s, Grade 40 to 50 in 1960s and Grade 60 has been accepted as HSC since 1970s. ASTM defines Grade 41 and above as HSC while FIP/CEB (1990) defines Grade 60 concrete for the same.

In Australia, HSC is defined as concrete with a characteristic compressive strength from 50 MPa to 120 MPa (Hadi and Ai-samaraie 2001). In Europe and North America the lower strength limit is 60 MPa and 42 MPa respectively (Diniz and Frangopol 1997). In general, concrete of strength greater than 40 MPa is considered to be HSC in the southeast asian region. Grade 80 concrete has been used in Asia for high-rise buildings (Rashid et al. 2002). However, in areas where 60 MPa concrete is used extensively, the compressive strengths in the range from 80 to 140 MPa are considered to be HSC.

Throughout this study, the lower limit of HSC is used as the 28-day characteristic compressive strength of 50 MPa. Generally for concrete with uniaxial compressive strength greater than 50 MPa, special admixtures are required. As a result that concrete has a different class of material. Therefore the definition for the lower limit of HSC is pertinent.

1.1.2 Applications

In the 1960s, Grade 60 concrete was used on tall buildings such as Water Place in Chicago (Chan and Anson 1994). Seattle and Washington, which are among the regions of high seismicity in United States, used HSC in many structures (Ghosh 1997). In late 1980s in Seattle, the First Pacific Centre utilised concrete with compressive strength of 115 MPa (Laogan and Elnashai 1999). Two Union Square used 97 MPa in-situ concrete in its columns and the compressive strength increased to 131 MPa at the age of one year (Ghosh 1997). Ghosh (1997) reported that although Two Union Square is said to have the highest strength of any in-situ concrete ever made, the First Pacific Centre achieved even higher compressive strength in one year. Laogan and Elnashai (1999) documented that Two Prudential Plaza (281 m) and South Wacker Drive (295 m), both located in Chicago, used a mix with compressive strength of 83 MPa. Chan and Anson (1994) reported that the 378 m high Central Plaza used HSC of Grade 60. An example for the highly developed city centres with high-rise structures using high strength materials is Chicago, Illinois where the development of the high strength followed the trend shown in Table 1.1 (Laogan and Elnashai 1999).

Table 1.1: Development of concrete strength in Chicago (Laogan and Elnashai 1999).

Year	Building name	Strength (MPa)
1962	Outer Drive East	41
1965	Lake Point Tower	52
1972	Mid-Continental Plaza	62
1976	River Plaza	76
1982	Chicago Mercantile	96
1988	Construction Tech. Labs	117

HSC is used in many parts of the world apart from the United States. Melbourne central building in Australia used 60-65 MPa concrete (Lloyd and Rangan 1993). Rialto tower in Melbourne and R & I tower in Perth are some other examples of HSC applications in Australia. Two uses of HSC for tall buildings in China, The New Century Hotel and Sichuan Mansion, were documented by Hu and Zhu (1994). Both buildings used Grade 60 concrete. The BfG building in Frankfurt (186 m) used concrete of 85 MPa

compressive strength (Laogan and Elnashai 1999). The 1,483 feet tall Petronas tower in Kuala Lumpur, Malaysia, the tallest building in the world, utilised Grade 80 concrete.

Ghosh (1997) stated the widespread applications of HSC (compressive strengths greater than 40 MPa) in buildings in high seismic regions in the United States. However, the use of HSC is still limited in many other seismic regions such as Southern California (Martirosyan and Xiao 2001).

Despite the lack of design rules for HSC in the design standards, HSC has been extensively used in the construction projects all over the world. Present design methods are based on the design specifications for NSC, which are not suitable enough for HSC specially in seismic regions. The design of reinforced concrete columns is based on a rectangular stress block which is assumed to represent the actual compressive stresses in concrete. It has a uniform stress intensity of $0.85f_c$ and a depth less than neutral axis depth. Many researchers (Rangan 1991; Rangan 1998; Attard and Stewart 1998) have modified this stress block to extend its applicability in the design of HSC columns. However, the design rules may need further modifications for HSC to be used in earthquake regions.

1.2 Research significance and project objectives

Poor column behaviour in inelastic deformation was the cause for most of the structural failures due to earthquakes. When a structure is analysed for earthquake loadings, it is necessary to regard the effect of cyclic lateral forces on the structure. Therefore a thorough knowledge of the material behaviour of the constituents (such as concrete and steel) subjected to cyclic loading is of great importance.

There are experimental studies reported in the literature for the behaviour of unconfined (Sinha et al. 1964; Karsan and Jirsa 1969; Desayi et al. 1979) or confined (Desayi et al. 1979; Shah et al. 1983; Mander et al. 1988a; Watanabe and Muguruma 1988; Sakai and Kawashima 2000) NSC (20-49 MPa) subjected to cyclic axial compression. No experimental studies as such has been reported for HSC in the literature. The existing stress-strain models for the cyclic behaviour of confined NSC are based on column tests. Concrete is passively confined in these tests and several assumptions are used for the effectiveness of the confinement. Instead of using passive confinement, as in the case of

column tests, if active confining pressure is applied, then the pressure can be measured accurately. Therefore a suitable experimental program needs to be conducted to record the axial stress, axial strain and lateral strain for HSC subjected to cyclic loading.

The available constitutive models for NSC, are capable of predicting only the axial stress versus axial strain relationships. However, the confinement provided by lateral steel reinforcement depends on the lateral dilation of concrete. Therefore it is a timely concern to develop a complete deformational behaviour including both axial and lateral strains of laterally confined HSC with cyclic axial compression.

It is widely believed among the researchers (Karsan and Jirsa 1969; Desayi et al. 1979; Mander et al. 1988b; Cheong and Perry 1993) that the stress-strain curve corresponding to monotonically increasing loads, forms the envelope curve for cyclic loading. Therefore envelope curve plays an important role in the stress-strain curve for cyclic loading. A detailed study of the behaviour of HSC subjected to monotonically increasing loads was carried out first before the cyclic loading was investigated in this thesis.

1.2.1 Objectives of the thesis

The main objective of the thesis is to develop constitutive models for the behavior of confined HSC subjected to

- Monotonically increasing loads
- Cyclic loads.

The specific research aims are as follows:

Monotonically increasing loads

- To investigate how the ductility can be improved in HSC using lateral confinement
- To develop a strain-based constitutive model for the behaviour of actively confined HSC
- To apply and verify the model in column analysis
- To apply and verify the model in column-slab joint analysis

Cyclic loads

- To conduct an experimental program to measure the axial stress, axial strain and lateral strain of HSC confined in a triaxial cell
- To use the experimental results to develop a constitutive model for actively confined HSC
- To validate the model in column analysis

1.3 Structure of the thesis

Major advantages of using HSC in structural systems are described in this current chapter. The two main parts of the investigations presented in this thesis are the development of constitutive models for confined HSC subjected to monotonically increasing and cyclic loadings. Chapters 2 to 5 deals with monotonically increasing loads. Chapters 6 to 10 deals with cyclic loads. A chapter by chapter summary of the thesis follows.

1.3.1 Monotonically increasing loads

- Chapter 2 demonstrates a method to calculate the load-deformation or moment-curvature curves of eccentrically loaded columns. Using an existing stress-strain model, it illustrates that the low ductility levels observed in the stress-strain curves are translated into low ductility in column behaviour. Further, the use of confinement to improve the ductility of columns is demonstrated with this model. The examples provided in this chapter form the justification to investigate confinement as a means of improving ductility of columns.
- Chapter 3 reviews the existing constitutive models developed in the past for the behaviour of confined HSC subjected to monotonically increasing loading. Having identified the gaps in knowledge in these models, a novel approach is proposed to develop a model for the stress-strain relationship of HSC subjected to lateral confinement. Previously reported experimental results for circular HSC columns with passive confinement were used to verify the model.

- Chapter 4 uses the constitutive model proposed in Chapter 3 in developing a methodology for the load-deformation behaviour of eccentrically loaded HSC columns. The analytical work thus obtained are compared with the experimental observations reported in the literature. Further, it is demonstrated that the model proposed in Chapter 3 is superior to the current models in predicting the behaviour of eccentrically loaded HSC columns.
- Chapter 5 demonstrates another application of the constitutive model proposed in Chapter 3. It is used to model the behaviour of the weaker layer of slab concrete within an interior high-strength concrete column. The model is proven to be giving satisfactory comparisons with the experimental observations reported for unloaded and loaded slabs.

1.3.2 Cyclic loads

- Chapter 6 presents a literature review of the previous work on the behaviour of unconfined and confined concrete as well as reinforcing steel subjected to cyclic loading. Based on the review, research significance in establishing a constitutive model for confined HSC under cyclic loading is highlighted.
- Chapter 7 describes the experimental program carried out to obtain the axial stress versus axial and lateral strain relationships. The development of the triaxial testing equipment, problems encountered in the tests, measures taken to overcome them and an outline of the experimental procedure carried out are explained in detail.
- Chapter 8 presents the results obtained from the experimental program described in Chapter 7.
- Chapter 9 presents a constitutive model developed for confined HSC subjected to cyclic loading, based on the experimental results reported in Chapter 8. Chapter 9 also presents various attempts made by the author to develop this model by different approaches.
- Chapter 10 presents the previous work for the experimental and analytical behaviour of confined concrete columns subjected to constant axial load and lateral load reversals. An analytical procedure is developed to calculate the behaviour of HSC

columns subjected to combined axial load and cyclic flexure. This chapter describes a computer program to implement this procedure. The model proposed in Chapter 9 is validated by comparing it with some of the reported experimental results of confined HSC columns under axial load and cyclic flexure.

- Chapter 11 presents the conclusions and suggestions for further research work.

1.4 Contributions to knowledge

The research work reported in this thesis makes several contributions to the field of structural behaviour of HSC and its applications. These are listed below:

- A comprehensive review of the constitutive models for concrete subjected to monotonically increasing and cyclic loading.
- A novel constitutive model based on the shear failure of concrete for HSC subjected to monotonically increasing loading. The model can establish the axial stress, axial strain and lateral strain relationships for HSC. It can be applied to concrete with active as well as passive confinement.
- An analytical procedure for using the constitutive model to predict the behaviour of laterally confined HSC columns subjected to eccentric static loading.
- An analytical procedure for establishing the behaviour of reinforced concrete column-slab interface when a weaker layer of slab concrete is embedded in a HSC column, based on the proposed constitutive model.
- Experimental results for the axial stress, axial strain and lateral strain relationships for confined HSC subjected to cyclic loading.
- A novel strain-based constitutive model for confined HSC subjected to cyclic loading. This model can be applied to concrete with active as well as passive confinement.
- A computational method based on the constitutive model for the analysis of columns subjected to axial load and cyclic lateral loads.

1.4.1 Important observations

It is worth noting the following observations from the experimental results reported in this thesis.

- When confined concrete is stressed, initially it contracts (reducing in volume). After a certain stress, it starts to expand (increasing in volume). The maximum volumetric strain occurs at this point where the contraction turns into expansion. This point occurs at an axial strain of $0.5\varepsilon_{cc}$ for 40 MPa concrete and $0.7\varepsilon_{cc}$ for 100 MPa concrete; where ε_{cc} is the axial strain at peak axial stress.
- At the time of peak axial stress, the volume of concrete is back to its original unloaded volume. That is, the volumetric strain is observed to be back to zero at peak axial stress. This means that the magnitude of lateral strain at peak axial stress is half of corresponding axial strain. This is a very useful observation for constitutive models which has not been reported in the literature.
- It is reported in the literature that the monotonically increasing loading curve forms an envelope of curves for cyclic loading for unconfined and confined NSC. From the results of the experimental program carried out by the author, it is observed that this is valid only in the ascending branch of the stress-strain curves of HSC and not valid for the descending branch of HSC. Descending branch of the envelope curve has to be modified by scaling down the corresponding stresses for HSC.
- Poisson's ratio is constant in the initial elastic region, and rapidly increases when loaded beyond this region.
- When unloading occurs in the initial elastic region, the Poisson's ratio decreases and increases back to the same value when reloading occurs. The proposed model is capable of modelling this decreasing phenomenon of Poisson's ratio.

Chapter 2

MONOTONICALLY INCREASING LOADS:

Lateral reinforcement requirement in high strength concrete columns using existing model

2.1 Introduction

High strength concrete (HSC) can lead to significant cost savings in columns. One major concern with HSC columns is an increased brittleness compared to normal strength concrete (NSC). It is well established that the ductility of HSC columns can be increased by confinement of the core of the column using lateral steel reinforcement. However, the lateral dilation of concrete under axial load has been observed to be less in HSC compared to that of NSC, which may cause a reduction in effectiveness of lateral steel when used in HSC columns.

This chapter examines the available ductility in HSC columns and compares them with NSC columns. A numerical method developed to establish the load-deformation characteristics of eccentrically loaded columns is presented. The method uses a widely accepted stress-strain curve for concrete subjected to lateral confinement. Using an example of a typically reinforced 100 MPa column, it demonstrates how ductility of a column can be estimated. The example also demonstrates that by increasing the lateral confinement, the available ductility can be increased. By comparison with a typical 40 MPa reinforced

concrete column, the example presents a method to estimate the required lateral reinforcement for a 100 MPa column for the same level of ductility available in a 40 MPa column.

However, in the modelling of the load-deformation characteristics of column, it is assumed that the confining pressure corresponds to the yielding of lateral confining steel. In reality, confining pressure increases with the lateral dilation (strain) of concrete. Therefore a constitutive model for concrete including lateral strains is necessary to establish the load-deformation characteristics of column accurately.

The outcomes of this chapter are published in Lokuge et al. (2000a) and Lokuge et al. (2000b).

2.2 Ductility

In order to study the ductility of columns, it is important to define the term ductility and how it will be measured. Ductility is the ability of the structure or structural member to undergo substantial deformations without losing the capacity to resist loads.

Ductility is an essential characteristic of a well designed structure. Present design methods for reinforced concrete members involve an elastic analysis of structures to determine the maximum design actions followed by an ultimate strength calculation for the section using the full-range stress-strain curve of the material. The actual behaviour of structures does not exactly match the model on which the design is based. Ductility is the characteristic of the structures which enables the structure to redistribute the forces in the structures so that the design load capacity can be reached without any premature local failures. If the reinforced concrete section is subjected predominantly to a bending moment, a redistribution of bending moment is allowed depending on the available ductility in the section. For the members subjected to predominantly compressive forces and small bending moments (columns), design includes allowance for secondary bending moments by increasing the bending moment determined from an elastic analysis. In these members, re-distribution of bending moment is not allowed and the failure is expected to be fairly brittle. Lateral confinement is expected to improve the failure to a fairly ductile mode.

2.2.1 Ductility improvement

From the recent research work reported (Lloyd and Rangan 1993; Azizinamini 1995; Biolzi et al. 1997; Liu et al. 1998), it is evident that ductility improvement in HSC has been a major issue. The ductility level is important as it safeguards the structure against unforeseen overloading (Hadi 2001). The traditional method used to overcome this effect is to have proper confining reinforcement. Using high strength steel as the confining material will further increase the reaction force for the lateral dilation of HSC columns thus increasing the strength and ductility (Hadi and Ai-samaraie 2001; Han et al. 2003). Hadi and Ai-samaraie (2001) tested HSC columns with helical reinforcement and investigated the effect of pitch size and the distribution of longitudinal reinforcement. They concluded that the smaller the pitch size the larger the ductility of the HSC columns which was also consistent with the findings of Razvi and Saatcioglu (1994).

Current Australian design standard for concrete structures (AS3600 2001) gives the requirement of lateral steel in the form of the size of lateral confining steel, the configuration of confining steel in the section and the spacing of confining steel. For HSC columns such design guidelines are not available.

2.2.2 Measure of ductility

There is no consensus on the best method of measuring ductility. Most widely accepted definition of ductility is the ratio of curvature of the section at the end and the beginning of the plastic plateau of the load-curvature curve. The definition has been modified sometimes as the ratio of curvature corresponding to 80% of the load capacity on the descending portion of the load-curvature curve and the curvature corresponding to the 80% of load capacity on the ascending portion of the load-curvature curve. The second definition is more indicative of the softening slope of the load-curvature curve than the first definition. However, an accompanied reduction in load capacity to $0.8P_m$ (Figure 2.1) is used with the second definition of ductility. Ductility factor (μ) (Figure 2.1) is defined as,

$$\mu = \frac{\phi_u}{\phi_y} \quad (2.1)$$

where, ϕ_u is the curvature at the ultimate point which is defined as the point in the descending branch of the curve in which the load is equal to 80% of the peak load (Joen

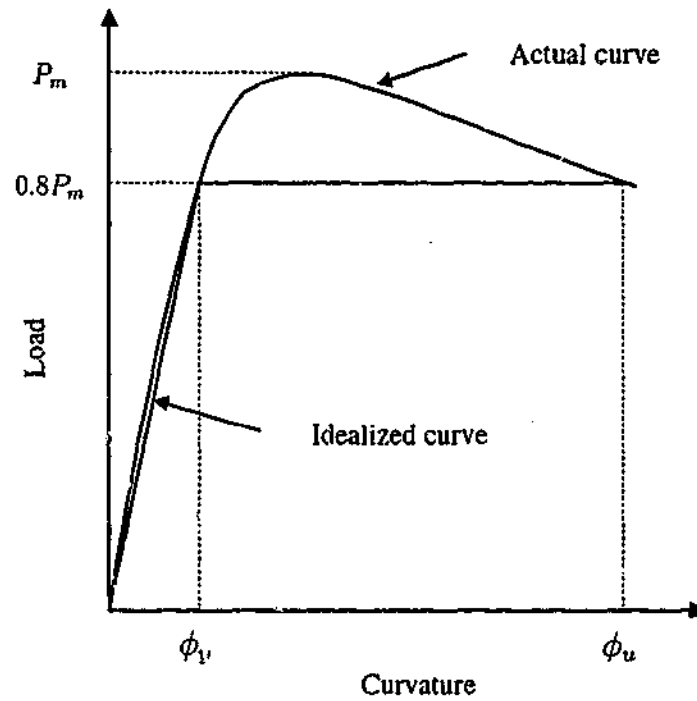


Figure 2.1: Load versus curvature relationship with ultimate and yielding points.

and Park 1990) and ϕ_y is the curvature at the point in the ascending branch of the curve in which the load is equal to 80% of the peak load. P_m is the maximum load reached in the load-curvature curve.

This definition is used in this study to compare ductility of NSC and HSC columns.

2.3 Axial load versus curvature relationship

Force versus deformation characteristics of an eccentrically loaded column can either be described by axial force versus axial deformation curve or axial force versus curvature curve. The curvature is the result of the moment created by the eccentricity. The axial force versus curvature relationship is chosen to estimate the ductility, because the curvature is the deformation more likely to be associated with redistribution of loads in a structure than the axial deformation.

The following sections describe the method involved in calculating this relationship.

2.3.1 Stress-strain model for concrete proposed by Mander et al. (1988b)

There are several models reported in the literature to illustrate the stress-strain behaviour of concrete with passive confinement. Among them, the one proposed by Mander et al. (1988b) has several advantages. They proposed a strain-based model for concrete confined by transverse reinforcement. It has one continuous function for both ascending and descending branches. It can be applied to any general type of cross section such as circular or rectangular. The model has been found to be useful in the development of full-range moment-curvature behaviour of HSC flexural members with a reasonable accuracy (Setunge et al. 1994; Mendis et al. 2000). Because of "it's" wide acceptance for NSC, Mander et al. (1988b) model has been used here to develop the analytical procedure for predicting the behaviour of eccentrically loaded, laterally confined columns. It is believed that once the analytical procedure is established, this model can be replaced by complex constitutive models.

For a slow strain rate and monotonic loading, the longitudinal compressive stress σ_1 is given in terms of f_{cc} , maximum stress of confined concrete, x , strain parameter and r , modulus parameter,

$$\sigma_1 = \frac{f_{cc} x r}{r - 1 + x^r} \quad (2.2)$$

Strain parameter x is given by,

$$x = \frac{\varepsilon_1}{\varepsilon_{cc}} \quad (2.3)$$

where,

$$\varepsilon_{cc} = \varepsilon_{co} \left[1 + 5 \left(\frac{f_{cc}}{f_c} - 1 \right) \right] \quad (2.4)$$

ε_1 is longitudinal compressive strain, f_c is unconfined concrete strength, ε_{cc} is strain at maximum concrete stress (f_{cc}) and ε_{co} is strain corresponding to the unconfined concrete strength, assumed as 0.002. Modulus parameter r is given in terms of E_c , modulus of elasticity of concrete and E_f , secant modulus of confined concrete at maximum stress,

$$r = \frac{E_c}{E_c - E_f} \quad (2.5)$$

where,

$$E_c = 5000 \sqrt{f_c} \text{ MPa} \quad (2.6)$$

and

$$E_f = \frac{f_{cc}}{\epsilon_{cc}} \quad (2.7)$$

Peak stress of confined concrete (f_{cc}) is defined as,

$$f_{cc} = f_c \left(-1.254 + 2.254 \sqrt{1 + \frac{7.94 f_{le}}{f_c}} - 2 \frac{f_{le}}{f_c} \right) \quad (2.8)$$

f_{le} is the effective lateral confining pressure and is given by,

$$f_{le} = \frac{A_{sp} f_{sy}}{s d_s} \quad (2.9)$$

where A_{sp} is the total area of lateral reinforcement, f_{sy} is the yield strength of lateral reinforcement, s is the spacing of lateral reinforcement and d_s is the distance from centre-to-centre of the lateral reinforcement.

Further details of this stress-strain model for concrete can be found in Mander et al. (1988b).

2.3.2 Stress-strain model for steel

The relationship between the steel stress, f_s and steel strain, ϵ_s is,

$$f_s = \begin{cases} E_{st} \epsilon_s & \text{if } 0 \leq \epsilon_s \leq \epsilon_y, \\ f_{sy} & \text{if } \epsilon_s > \epsilon_y \end{cases} \quad (2.10)$$

where E_{st} is the modulus of elasticity of steel, f_{sy} is the yield strength of steel and ϵ_y is the corresponding steel strain.

2.3.3 Load-curvature analysis

Load-curvature relations for rectangular columns subjected to combined axial load and flexure are obtained using the following assumptions:

- Plane sections remain plane after bending.
- Perfect bond between the longitudinal steel and the concrete.
- Concrete does not resist any tensile force.

For the purpose of the analysis, the cross section of the column was divided into a number of slices. In order to calculate points on the load-curvature curve (P_m, ϕ_m), for the specified eccentricity (e^*), the strain on the extreme compression side (ϵ_t) was varied through the entire possible range of values, and the corresponding P_m and ϕ_m values were calculated. For each value of ϵ_t , an iterative procedure was used to calculate the corresponding P_m and ϕ_m . The iterative procedure involved starting with an assumed value of ϕ_m and calculating the corresponding P_m and the eccentricity. The iteration was continued until the calculated eccentricity matched the specified eccentricity with a certain tolerance.

The following equation should be satisfied for equilibrium (Figure 2.2):

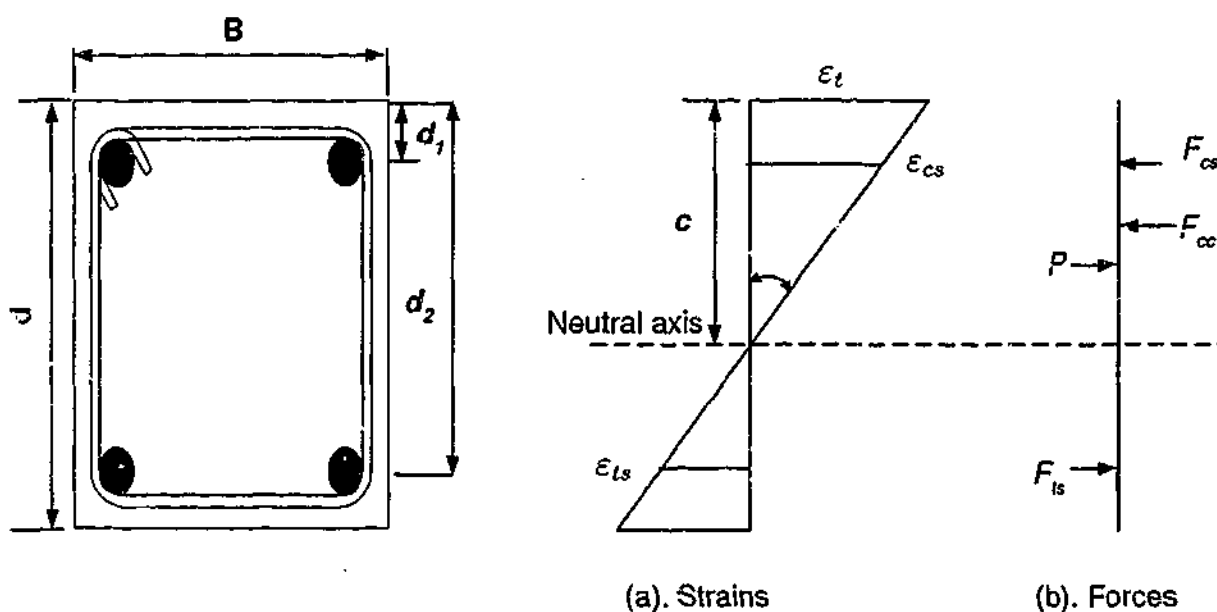


Figure 2.2: Cross section analysis.

$$P = \sum_{i=1}^{n_c} f_{ci} A_{ci} + f_{cs} A_{cs} - f_{ts} A_{ts}. \quad (2.11)$$

A_{cs} and A_{ts} are area of compression and tension steel respectively, A_{ci} is area of i^{th} concrete slice, f_{ci} is stress in i^{th} concrete slice and n_c is the number of concrete slices in compression side. f_{cs} and f_{ts} are the stresses in compression and tension steel respectively which can be calculated using Equation (2.10) with the use of corresponding strains as given below:

$$\epsilon_{cs} = \frac{\epsilon_t}{c} (c - d_1) \quad (2.12)$$

and

$$\epsilon_{ts} = \frac{\epsilon_t}{c}(d_2 - c) \quad (2.13)$$

where, c is the neutral axis depth from extreme compression side, d_1 is the distance to compression steel and d_2 is the distance to tension steel.

For moment equilibrium (Figure 2.2),

$$P(e + d/2 - d_1) = M = \left(\sum_{i=1}^{n_c} f_{ci} A_{ci} \right) (d_2 - c - n) + f_{cs} A_{cs} (d_2 - d_1) \quad (2.14)$$

where, d is the depth of the considered section and n is the distance from the neutral axis to the place at which the resulting concrete compressive force acts and is given by,

$$n = \frac{\sum_{i=1}^{n_c} f_{ci} A_{ci} y_{ci}}{\sum_{i=1}^{n_c} f_{ci} A_{ci}} \quad (2.15)$$

where, y_{ci} is the distance from the neutral axis to the centroid of the i^{th} concrete slice.

Simplex method was used as a way of organising the procedure so that a series of combinations was tried until calculated e equals the assumed minimum eccentricity e^* with a certain tolerance. MATLAB software was used in implementing this. The method is explained in a step by step procedure below.

step 1 set the initial value of ϵ_t

step 2 $st = \epsilon_t / 2$

step 3 calculate e

step 4 if $|e - e^*| < \text{tolerance}$ stop

step 5 if $e > e^*$, $\epsilon_t = \epsilon_t + st$ else $\epsilon_t = \epsilon_t - st$

step 6 $st = st / 2$ go to step 3

2.4 Example

The cross section details of the selected column are given in Figure 2.3. Compressive strengths of 40 MPa for NSC and 100 MPa for HSC were used in the calculations. Grade 300 and 400 of steel were used for transverse and longitudinal steel respectively. The column was assumed to be loaded at its minimum eccentricity of 25 mm (AS3600 2001)

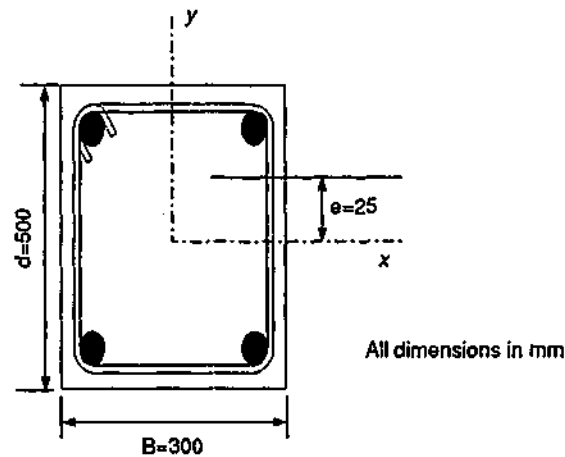


Figure 2.3: Section details.

from the centre line of the specimen towards y direction. Distance to the centre line of either the compressive or tensile steel from the face of the specimen (d_1) was taken as 50 mm. Diameter of longitudinal steel was taken as 32 mm.

2.4.1 Results

Initially the load-curvature curves were obtained as in Figure 2.4, with 10 mm diameter stirrups at 300 mm (AS3600 2001 code minimum spacing) spacing for both NSC (40 MPa) and HSC (100 MPa). NSC column shows a fairly ductile behaviour than the HSC column. Ductility factors were calculated using Equation (2.1). The values obtained for 40 MPa and 100 MPa columns were 5.8 and 1.9 respectively.

It is widely accepted that the ductility in HSC columns can be improved by increasing the lateral confining pressure using proper confinement. According to Equation (2.9), the lateral confining pressure can be increased by reducing the spacing of the stirrups or increasing the diameter of the stirrups or using high yield strength lateral steel.

The level of confinement of 100 MPa column was increased until the ductility of this column matched the 40 MPa column with confinement mentioned above (10 mm diameter stirrups at 300 mm spacing). The level of confinement needed in 100 MPa column was found to be either,

- 12 mm stirrups at 48 mm spacing or
- 10 mm stirrups of 500 MPa yield strength at 77 mm spacing.

The corresponding curves are shown in Figure 2.5.

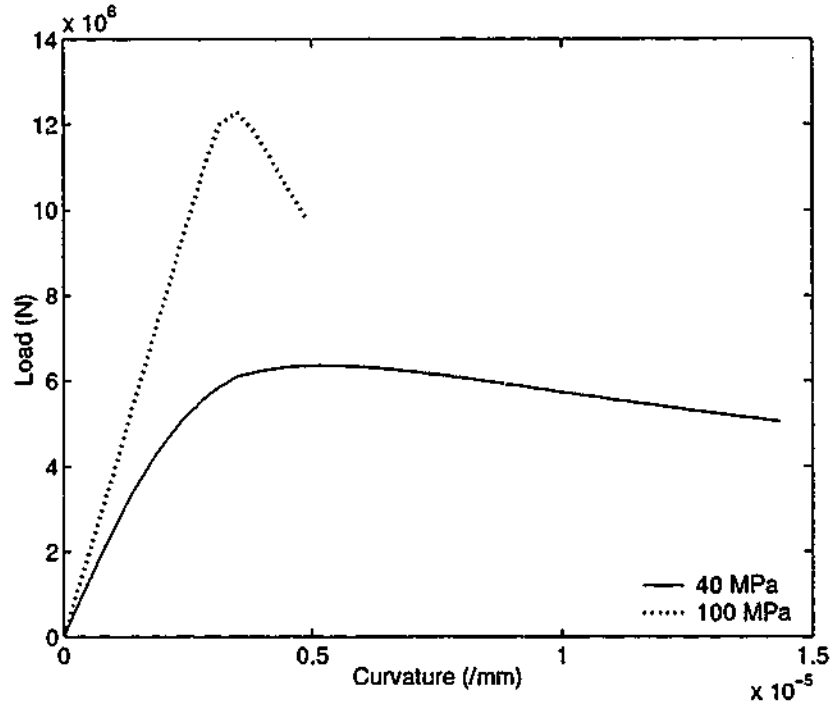


Figure 2.4: Load-curvature curve for 40 MPa and 100 MPa with same stirrup spacing (300 mm).

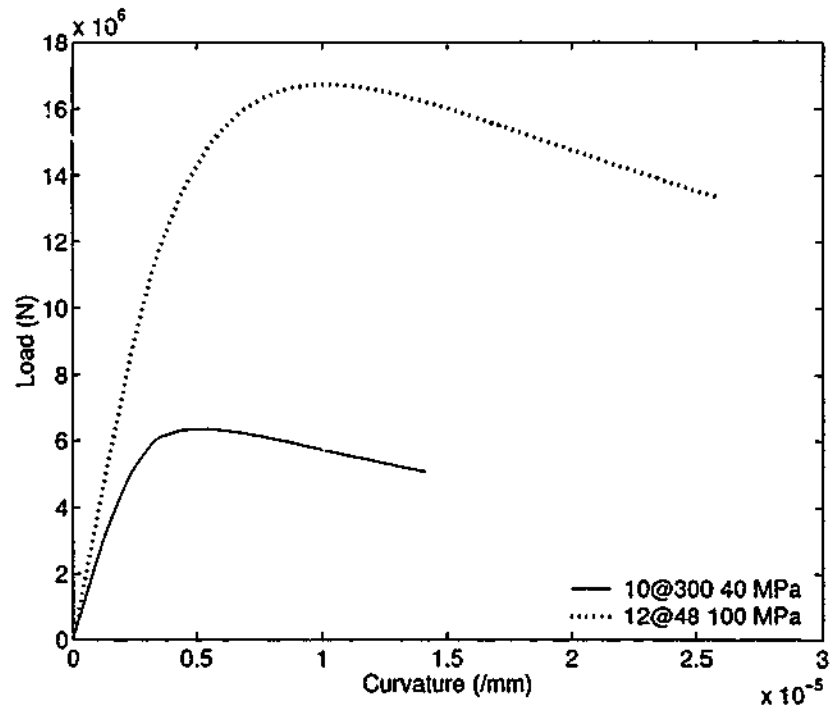


Figure 2.5: Load-curvature curve for 40 MPa and 100 MPa with same ductility 5.8.

2.5 Conclusions

Work reported herein outlines a numerical procedure for the load-curvature behaviour of eccentrically loaded columns.

- Analysis performed in this chapter clearly indicates that a significant reduction in ductility is possible with increase in compressive strength of concrete.
- Ductility of the HSC column can be increased to that of the NSC column by increasing the diameter of confining steel, reducing the spacing or using high yield strength steel as the confining reinforcement.
- In this work, the confining pressure provided by the lateral confining steel is calculated assuming that confining steel yields before the maximum stress of the column (Equation 2.9). However, in reality, the stress in lateral steel will be increased gradually with the increase in axial force in the member and the corresponding lateral dilation. Therefore for any axial load before it reaches its maximum, if the lateral dilation of concrete is known, the confining pressure can be calculated using the corresponding stress in confining steel.
- In order to develop an understanding of the actual behaviour of the column, a constitutive model for confined HSC, which is capable of predicting both axial and lateral stress-strain behaviour is needed.
- Upon developing a constitutive model, the analytical procedure developed in this chapter can be used to predict ductility.

Chapter 3

MONOTONICALLY INCREASING LOADS:

Development of a constitutive model for confined concrete

3.1 Introduction

The traditional method of improving ductility of columns by lateral confinement with steel reinforcement has been found to be less effective in high strength concrete (HSC) due to a reduction in lateral strains observed under axial load. The reduced effectiveness of the confining steel combined with increased brittleness of HSC raised concerns about the ductility of HSC columns and has led to a number of research programs in the field (Martinez et al. 1984; Pessiki and Fieroni 1997). However, there is no general agreement about the amount of lateral steel required in HSC columns to provide a required level of ductility.

The experimental studies reported so far, covered the behaviour of small-scale circular or square columns with a limited configuration of steel reinforcements, tested under laboratory conditions. One disadvantage of these types of experiments is that the value of the minor principal stresses cannot be controlled, since the confinement provided by lateral steel is passive. Passive confinement (using lateral reinforcement such as spirals, ties, steel tubes or other form of material like carbon fibre) depends on lateral dilation of the concrete under axial load and the stress-strain relationship of the confining material. Most of the existing models for the stress-strain behaviour of confined concrete are based

on column tests. Several assumptions have to be made in these experiments to calculate the effective confinement stress provided by the steel at various stages of the loading. In the previous studies as well as in the column analysis reported in the previous chapter, it is assumed that the confining pressure corresponds to the yielding of the lateral reinforcement. However, the confining pressure applied by the lateral reinforcement is a function of the lateral strain of concrete.

Candappa (2000) conducted an experimental program to investigate the complete axial stress, axial strain, lateral strain behaviour of HSC using active confinement. In active confinement, the confining pressure is applied directly on the specimen without relying on the lateral strain to induce the confining stress. Therefore, the confining pressure can be independently controlled and accurately known at any time during the tests.

This chapter surveys the existing stress-strain models for the behaviour of unconfined and confined NSC. It then identifies the necessity of developing axial stress, axial strain and lateral strain relationships for confined HSC. A novel approach based on shear failure of concrete is utilised in the model formulation. It is based on the experimental results for concrete with active confinement reported by Candappa (2000).

Subsequently, an iterative procedure for modelling columns subjected to passive confinement is developed. The chapter concludes with a comparison of model predictions with the experimental results for HSC confined by carbon fibre wraps.

The results presented in this chapter will be published in Lokuge et al. (accepted for publication in 2003 by *Journal of Materials in Civil Engineering*, ASCE).

3.2 Existing stress-strain models

Based on the test results, various stress-strain models for confined concrete have been proposed by many researchers, such as Sheikh and Uzumeri (1982), Mander et al. (1988b) and Cusson and Paultre (1995). Existing stress-strain models for confined, unconfined NSC as well as HSC can be divided into three broad categories with few exemptions. One group of researchers used a form of equation proposed by Sargin et al. (1971) (Table 3.1). Another group of researchers proposed a second order parabola for the ascending branch and a straight line for the descending branch and their studies were based on equations proposed by Kent and Park (1971) (Table 3.2). The other group developed stress-strain

relationships based on equations suggested by Popovics (1973) (Table 3.3). In all these models, selected parameters were included in the stress-strain curves and then they were calibrated using the test results.

3.2.1 Sargin et al. (1971) type models

The first group of researchers used a form of equation proposed by Sargin et al. (1971) for the behaviour of concrete. The stress-strain curve for unconfined and confined concrete has the general shape as shown in Figure 3.1. Various versions of this form of equation

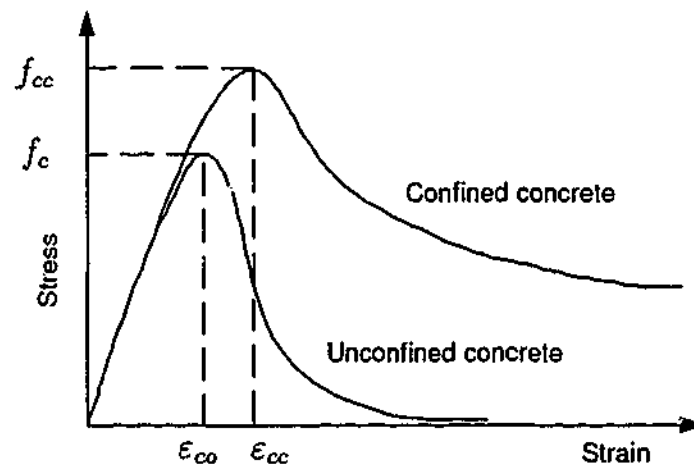


Figure 3.1: Typical stress-strain relationship for Sargin et al. (1971) type models.

were proposed by many researchers for the stress-strain curves of unconfined and confined concrete (Table 3.1). In these equations, f_l is the confining pressure, (σ_1, ϵ_1) are the coordinates of any point in the stress strain curve, ϵ_{co} is the peak axial strain of unconfined concrete strength, f_c , ϵ_{cc} is the peak axial strain of confined concrete strength, f_{cc} , E_c is the elastic modulus of concrete, E_i is the initial tangent modulus and E_f is the secant modulus of concrete measured at peak stress.

Wang et al. (1978) used a similar form of an equation but the parameters were different for ascending branch and the descending branch. Ahmad and Shah (1982) proposed another version of the same form of equation for concrete confined by steel reinforcement. Ahmad and Mallare (1994) performed a comparative study of the available models for concrete confined by circular spirals. They concluded that the model predictions by Ahmad and Shah (1982) were in close agreement with the experimental results for wider range of concrete (26-68 MPa). Later El-Dash and Ahmad (1995) and Attard and Setunge

Table 3.1: Stress-strain models for confined concrete based on Sargin et al. (1971).

Researcher	$Y = \frac{AX + (D-1)X^2}{1 + (A-2)X + DX^2}$	
	A	D
Sargin et al. (1971)	$E_c \varepsilon_{co} / k f_c$	$0.65 - 7.25 f_c \times 10^{-3}$
Wang et al. (1978)	Different parameters for ascending and descending branches	
Ahmad and Shah (1982)	E_i / E_f	$1.111 + 0.876A - 4.0883 \frac{\tau_{oct}}{f_c}$
El-Dash and Ahmad (1995)	E_c / E_f	$\frac{16.5}{\sqrt{f_c}} \left(\frac{f_l}{(s/d)} \right)^{0.33}$
Attard and Setunge (1996)	$\frac{E_i \varepsilon_{cc}}{f_{cc}}$	$\frac{(A-1)^2}{\alpha \left(1 - \frac{f_l}{f_{cc}}\right)} + \frac{A^2(1-\alpha)}{\alpha^2 \frac{f_l}{f_{cc}} \left(1 - \frac{f_l}{f_{cc}}\right)}$
Assa et al. (2001a)	$\frac{E_c \varepsilon_{cc}}{f_{cc}}$	$\frac{(\varepsilon_{80}/\varepsilon_{cc})^2 - (0.2A + 1.6)(\varepsilon_{80}/\varepsilon_{cc}) + 0.8}{0.2(\varepsilon_{80}/\varepsilon_{cc})^2}$

(1996) modified this form of equation and calibrated the model parameters by using confined and unconfined HSC. Attard and Setunge (1996) model was shown to be applicable for a wide range of concrete strengths (20-130 MPa). Peak stress, strain at peak stress, elastic modulus and the stress and strain at the inflection point on the descending curve were required to establish the stress-strain curves for unconfined concrete. For confined concrete, stress and strain at one other point on the descending curve was additionally required.

Assa et al. (2001a) proposed stress-strain relationships, using two parameters and validated it using test results for confined concrete with a strength range of 20-90 MPa. They first developed this for spirally confined columns and then extended to concrete confined by rectangular ties (Assa et al. 2001b). The most recent version of the model proposed by Sargin et al. (1971), is the one developed by Assa et al. (2001a). A summary of that model is presented here. The generic equation for stress-strain behaviour of confined concrete (for ascending and descending) proposed by Sargin et al. (1971) is as follows:

$$Y = \frac{AX + BX^2}{1 + CX + DX^2} \quad (3.1)$$

$Y = \sigma_1/f_{cc}$ and $X = \epsilon_1/\epsilon_{cc}$ and the model parameters are given as,

$$A = \frac{E_i \epsilon_{cc}}{f_{cc}}$$

$$B = \frac{(\epsilon_{80}/\epsilon_{cc})^2 - (0.2\alpha + 1.6)(\epsilon_{80}/\epsilon_{cc}) + 0.8}{0.2(\epsilon_{80}/\epsilon_{cc})^2} - 1 \quad (3.2)$$

$$C = (A - 2)$$

$$D = (B + 1)$$

where σ_1 and ϵ_1 are the axial stress and strain, ϵ_{cc} is the axial strain corresponding to the peak stress of confined concrete (f_{cc}), ϵ_{80} is the axial strain of confined concrete at $0.8f_{cc}$ on descending branch and E_i is the initial tangent modulus. It is proposed by Assa et al. (2001a) as,

$$E_i = 4700\sqrt{f_c} \quad (3.3)$$

Parameter A controls the stiffness of the ascending branch and B controls the slope of the descending branch.

3.2.2 Kent and Park (1971) type models

The model proposed by Kent and Park (1971) was the basis of the second group of researchers in predicting the behaviour of concrete. Kent and Park (1971) suggested a second-degree parabola for the ascending branch (independent of the confinement) and a linear descending branch (depending on the confinement) as shown in Figure 3.2 for concrete confined by rectangular hoops.

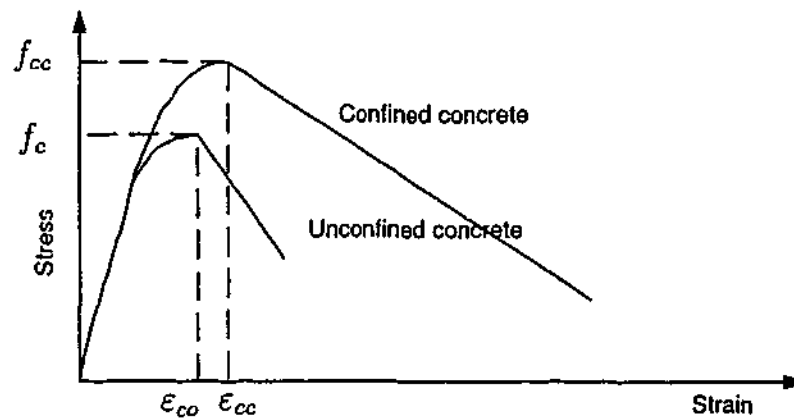


Figure 3.2: Typical stress-strain relationship for Kent and Park (1971) type models.

A number of models reported in the literature either used the similar equations or modified these equations as shown in Table 3.2. In these equations, (σ_1, ϵ_1) are the

coordinates of any point in the stress strain curve, ϵ_{co} is the peak axial strain of unconfined concrete strength, f_c , ϵ_{cc} is the peak axial strain of confined concrete strength, f_{cc} and Z_m is the slope of the descending branch.

Table 3.2: Stress-strain models for confined concrete based on Kent and Park (1971).

Researcher	Ascending branch (σ_1)	Descending branch (σ_1)
Kent and Park (1971)	$f_{cc} \left[2 \left(\frac{\epsilon_1}{0.002} \right) - \left(\frac{\epsilon_1}{0.002} \right)^2 \right]$	$f_{cc}[1 - Z_m(\epsilon_1 - 0.002)]$
Sheikh and Uzumeri (1982)	$K f_c \left[2 \left(\frac{\epsilon_1}{\epsilon_{cc}} \right) - \left(\frac{\epsilon_1}{\epsilon_{cc}} \right)^2 \right]$	$f_{cc}[1 - Z_m(\epsilon_1 - \epsilon_{cc})]$
Park et al. (1982)	$K f_c \left[2 \left(\frac{\epsilon_1}{0.002K} \right) - \left(\frac{\epsilon_1}{0.002K} \right)^2 \right]$	$K f_c[1 - Z_m(\epsilon_1 - 0.002K)]$
Scott et al. (1982)	same as Park et al. (1982)	
Samra (1990)	same as Kent and Park (1971)	
Saatcioglu and Razvi (1992)	$f_{cc} \left[2 \left(\frac{\epsilon_1}{\epsilon_{cc}} \right) - \left(\frac{\epsilon_1}{\epsilon_{cc}} \right)^2 \right]^{1/(1+2K)}$	$f_{cc}[1 - Z_m(\epsilon_1 - \epsilon_{cc})]$
Saatcioglu et al. (1995)	same as Saatcioglu and Razvi (1992)	
Razvi and Saatcioglu (1999)	$\frac{f_{cc} x^r}{r - 1 - x^r}$	$f_{cc}[1 - Z_m(\epsilon_1 - \epsilon_{cc})]$
Mendis et al. (2000)	$K f_c \left[2 \left(\frac{\epsilon_1}{\epsilon_{cc}} \right) - \left(\frac{\epsilon_1}{\epsilon_{cc}} \right)^2 \right]$	$K f_c[1 - Z_m(\epsilon_1 - \epsilon_{cc})]$
Shah et al. (1983)	$f_{cc} \left[1 - \left(1 - \frac{\epsilon_1}{\epsilon_{cc}} \right)^4 \right]$	$f_{cc} e^{-k(\epsilon_1 - \epsilon_{cc})^{1.15}}$

Park et al. (1982) modified this model by including strength and strain increase due to the confinement. Scott et al. (1982) and Sheikh and Uzumeri (1982) also used a similar kind of equation for parabolic ascending branch and linear descending branch and it was validated for NSC. Samra (1990) used the model proposed by Kent and Park (1971) and developed a new approach for the behaviour of confined concrete. They showed that the new approach is more realistic than the ACI Building Code for detailing columns for ductility.

Saatcioglu and Razvi (1992) suggested an analytical model for confined NSC and validated it for circular, square and rectilinear columns. This model consists of a parabolic ascending branch, linear descending branch and a constant residual strength. Ascending branch was a modified version of Hognestad et al. (1955)'s curve. The model proposed by Saatcioglu and Razvi (1992) is presented here.

$$\sigma_1 = f_{cc} \left[2 \left(\frac{\varepsilon_{cc}}{\varepsilon_{co}} \right) - \left(\frac{\varepsilon_{cc}}{\varepsilon_{co}} \right)^2 \right]^{1/(1+2K)} \quad \text{if } \sigma_1 \leq f_{cc} \quad (3.4)$$

σ_1 is the axial stress at axial strain level ε_1 and f_{cc} is the peak axial stress and the corresponding axial strain is ε_{cc} of confined concrete, and parameter K is defined by,

$$K = \frac{6.7 f_1^{0.83}}{f_c} \quad (3.5)$$

Application of this model was confirmed for NSC and it overestimated the initial modulus of elasticity when applied to HSC (Razvi and Saatcioglu 1999). Therefore a relationship first proposed by Popovics (1973) and later used by Mander et al. (1988b) for NSC was used by Cusson and Paultre (1995) and Razvi and Saatcioglu (1999) for HSC. Mendis et al. (2000) later modified Scott et al. (1982) model for the behaviour of normal and high strength confined concrete.

Shah et al. (1983) developed a stress-strain equation for confined concrete in an attempt to observe the envelope curve of cyclically loaded columns. They pointed out that Kent and Park (1971) model has a discontinuity between the ascending and the descending branches and using a linear relationship for the descending branch is not accurate. By noting that the curve proposed by Sargin et al. (1971) does not give good descending branches for unconfined concrete, Shah et al. (1983) proposed a different form of equation for the ascending branch and an exponential equation for the descending branch.

3.2.3 Popovics (1973) type models

The third group of researchers developed stress-strain curves for concrete based on an equation suggested by Popovics (1973). The typical stress-strain curves for unconfined and confined concrete are shown in Figure 3.3.

Table 3.3 shows a summary of the modifications made by other researchers for Popovics (1973) model. In these models, $(\sigma_1, \varepsilon_1)$ are the coordinates of any point in the stress strain

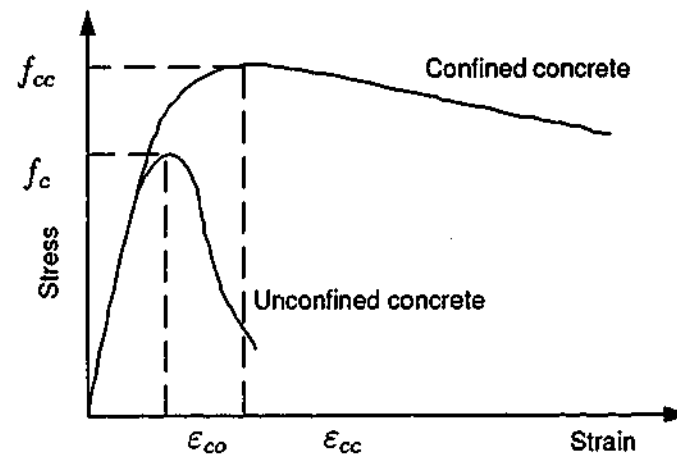


Figure 3.3: Typical stress-strain relationship for Popovics (1973) type models.

curve, ϵ_{co} is the peak axial strain of unconfined concrete strength, f_c , ϵ_{cc} is the peak axial strain of confined concrete strength, f_{cc} , x is the strain parameter and r is the modulus parameter.

Carreira and Chu (1985) proposed a model for plain concrete in compression. Mander et al. (1988b) developed a similar relationship which was extended to establish the stress-strain curves for confined concrete subjected to cyclic loading. The major difference between Popovics (1973) type model and the other reported models is that it has one continuous function for both ascending and descending branches. The ascending branch of Cusson and Paultre (1995) model is a relationship originally proposed by Popovics (1973) and the descending branch proposed was a modified version of Fafitis and Shah (1985). The model was proven to be valid from the experimental studies carried out for a wide range of concrete (60 to 120 MPa). The ascending branch of Chung et al. (2002) and Han et al. (2003) models was similar to that proposed by Cusson and Paultre (1995), but the descending branch was a straight line.

Wee et al. (1996) proposed a modified version of Carreira and Chu (1985) model noting that Wang et al. (1978) model is complicated for routine use and that Carreira and Chu (1985) model does not represent the descending branch of the curve for a wider range of concrete strength. For the ascending branch of the stress-strain curves, Wee et al. (1996) used the equation proposed by Carreira and Chu (1985) but for modelling the descending branch, two correction factors were introduced. Hsu and Hsu (1994) used

Table 3.3: Stress-strain models for confined concrete based on Popovics (1973).

Researcher	Ascending branch (σ_1)	Descending branch (σ_1)
Popovics (1973)	$f_c \frac{\varepsilon_1}{\varepsilon_{co}} \left(\frac{n}{n-1 + (\varepsilon_1/\varepsilon_{co})^n} \right)$	
Carreira and Chu (1985)	$\frac{f_{cc}(\varepsilon_1/\varepsilon_{co})^\beta}{\beta - 1 + (\varepsilon_1/\varepsilon_{co})^\beta}$	
Mander et al. (1988b)	$\frac{f_{cc}(\varepsilon_1/\varepsilon_{co})^r}{r - 1 + (\varepsilon_1/\varepsilon_{co})^r}$	
Hsu and Hsu (1994)	$\frac{f_{cc}n(\varepsilon_1/\varepsilon_{co})^\beta}{n\beta - 1 + (\varepsilon_1/\varepsilon_{co})^{n\beta}}$	$0.3f_{cc}e^{-0.8((\varepsilon_1/\varepsilon_{co}) - x_d)^{0.5}}$
Cusson and Paultre (1995)	$f_{cc} \left[\frac{k(\varepsilon_1/\varepsilon_{cc})}{k-1 + (\varepsilon_1/\varepsilon_{cc})^k} \right]$	$f_{cc}e^{k_1(\varepsilon_1 - \varepsilon_{cc})^{k_2}}$
Wee et al. (1996)	$\frac{f_{cc}(\varepsilon_1/\varepsilon_{co})^\beta}{\beta - 1 + (\varepsilon_1/\varepsilon_{co})^\beta}$	$\frac{k_1 f_{cc}(\varepsilon_1/\varepsilon_{co})^\beta}{k_1\beta - 1 + (\varepsilon_1/\varepsilon_{co})^{k_2\beta}}$
Hoshikuma et al. (1997)	$E_c \varepsilon_1 \left[1 - \frac{1}{n} \left(\frac{\varepsilon_1}{\varepsilon_{cc}} \right)^{n-1} \right]$	$f_{cc} - E_{des}(\varepsilon_u - \varepsilon_{cc})$
Martirosyan and Xiao (2001)	$\frac{f_{cc}(\varepsilon_1/\varepsilon_{co})^r}{r - 1 + (\varepsilon_1/\varepsilon_{co})^{k_3r}}$	
Chung et al. (2002)	$f_{cc} \left[\frac{k(\varepsilon_1/\varepsilon_{cc})}{k-1 + (\varepsilon_1/\varepsilon_{cc})^k} \right]$	$f_{cc} + \frac{0.15f_{cc}}{\varepsilon_{85} - \varepsilon_{cc}}(\varepsilon_{cc} - \varepsilon_1)$

a modified version of Carreira and Chu (1985) model for the ascending branch and an exponential function for the descending branch. Later Mansur et al. (1997) used the same equations as Wee et al. (1996) and concluded that they give good agreement for the stress-strain response of high strength plain and fibre concrete.

Hoshikuma et al. (1997) developed a new model after observing that a second order parabola for the ascending branch can reflect only three boundary conditions of the four boundary conditions which should be reflected by the ascending branch of the stress-strain curves. In that model, ascending branch is given by,

$$\sigma_1 = E_c \varepsilon_1 \left[1 - \frac{1}{n} \left(\frac{\varepsilon_1}{\varepsilon_{cc}} \right)^{n-1} \right] \quad (3.6)$$

where ε_1 and σ_1 are the axial strain and axial stress respectively, E_c is the modulus of

elasticity of concrete and

$$n = \frac{E_c \varepsilon_{cc}}{E_c \varepsilon_{cc} - f_{cc}} \quad (3.7)$$

where $(f_{cc}, \varepsilon_{cc})$ is the peak point. The descending branch is given by,

$$\sigma_1 = f_{cc} - E_{des}(\varepsilon_{cu} - \varepsilon_{cc}) \quad (3.8)$$

where E_{des} is the deterioration rate and ε_{cu} is the ultimate strain.

Martirossyan and Xiao (2001) tested fifteen HSC columns (compressive strength 69 MPa) under concentric compression. Further they prepared a database of eighty six axial compression test data, carried out by different researchers. Thirty seven of the specimens had high strength lateral reinforcement having yield strength of 690 to 1380 MPa. Compressive strengths of concrete had a wide range of 40 to 140 MPa. Based on the extensive analysis of the data, Martirossyan and Xiao (2001) proposed a constitutive model for HSC columns. It is a modified version of Mander et al. (1988b) model which was originally proposed by Popovics (1973). Studies by Martirossyan and Xiao (2001) showed that widely used equation originally proposed by Popovics (1973) may yield inaccurate results for the descending part of the curve and modified that equation as follows:

$$f_c = \frac{f_{cc} x^r}{r - 1 - x^{k_3 r}} \quad (3.9)$$

Strain parameter x is given by,

$$x = \frac{\varepsilon_1}{\varepsilon_{cc}} \quad (3.10)$$

Modulus parameter r is defined by using E_{50} , instead of E_c used by Mander et al. (1988b) and E_f is defined similar to previous researchers (Mander et al. 1988b).

$$r = \frac{E_{50}}{E_{50} - E_f} \quad (3.11)$$

The new term E_{50} controls the stiffness of ascending branch and makes it more accurate than the term E_c . It is defined as,

$$E_{50} = 3820 \times k_2 \times \sqrt{f_c} \quad (3.12)$$

and coefficient k_2 is calculated as,

$$k_2 = \left(\frac{f_{yeff}}{f_{sy}} \right)^{0.2} \quad (3.13)$$

The coefficient k_3 in Equation (3.9) controls the descending branch of the stress-strain curve and given by,

$$k_3 = \begin{cases} 1 & \text{for } 0 \leq \epsilon_1 \leq \epsilon_{cc}, \\ \frac{\ln \left[1 - r + \frac{1.25\epsilon_{cu} \leq r}{\epsilon_{cc}} \right]}{r \leq \ln \left[\frac{\epsilon_{cu}}{\epsilon_{cc}} \right]} & \text{for } \epsilon_{cc} \leq \epsilon_1 \leq \epsilon_{cu}. \end{cases} \quad (3.14)$$

Martirosyan and Xiao (2001) reported that above stress-strain relationships provide satisfactory comparisons with the available experimental results.

Using a strain and stress ratio Desayi et al. (1979) reported stress-strain curve for concrete under monotonic loading.

$$\sigma_1 = \frac{E_c \epsilon_1}{Dr(2)} \quad (3.15)$$

where,

$$Dr(2) = 1 + \left[\frac{1 - 2k\beta + k\beta^2}{k(\beta - 1)^2} \frac{E_c}{E'_c} - \frac{2\beta + 1}{\beta} \right] + \left[\frac{\beta + 2}{\beta} - \frac{2(1 - k)}{k(\beta - 1)^2} \frac{E_c}{E'_c} \right] \left(\frac{\epsilon_1}{\epsilon_{cc}} \right)^2 + \left[\frac{1 - k}{k(\beta - 1)^2} \frac{E_c}{E'_c} - \frac{1}{\beta} \right] \left(\frac{\epsilon_1}{\epsilon_{cc}} \right)^3. \quad (3.16)$$

3.2.4 Models capable of predicting lateral strain

Ottosen (1979) proposed a model based on nonlinear elasticity where the secant values of Young's modulus (E_s) and Poisson's ratio (ν^a) are changed accordingly. However, Ottosen (1979) model gives the parameter values only for the ascending branch of the stress-strain curves. It has the capability of modelling axial stress, axial strain and lateral strain behaviour. Candappa (2000) used Ottosen (1979) model and developed a stress-based model which was proven to be valid for HSC. Candappa (2000) model is presented here in detail as it is the only available model which can predict lateral strains as well. The model proposed for concrete confined by square transverse ties, includes the basic nonlinear elastic relationships,

$$\begin{aligned} \epsilon_1 &= \frac{\sigma_1 - \nu^a(f_l + f_l)}{E_s} \\ \epsilon_2 &= \frac{f_l - \nu^a(f_l + \sigma_1)}{E_s} \end{aligned} \quad (3.17)$$

where, σ_1 is the axial stress, f_l is the effective lateral confining pressure, E_s is secant value of Young's modulus, $\varepsilon_1, \varepsilon_2$ are axial and lateral strains respectively. ν_a is secant value of Poisson's ratio for the ascending branch. It is defined as,

$$\nu^a = \begin{cases} \nu_i^a & \text{if } \beta \leq \beta_l, \\ \nu_f^a - \nu_i^a \sqrt{1 - \left(\frac{\beta - \beta_l}{1 - \beta}\right)^2} & \text{if } \beta > \beta_l. \end{cases} \quad (3.18)$$

Non linearity index β is defined as,

$$\beta = \frac{\sigma_1}{f_{cc}} \quad (3.19)$$

where, f_{cc} being the peak stress of confined concrete.

$$\beta_l = \begin{cases} 0.7 & f_c \leq 40 \text{ MPa}, \\ 0.7 + 0.005(f_c - 40) & 40 \text{ MPa} < f_c \leq 60 \text{ MPa}, \\ 0.8 & f_c > 60 \text{ MPa}. \end{cases} \quad (3.20)$$

f_c being the strength of unconfined concrete, ν_i^a is the initial Poisson's ratio and ν_f^a is the secant value of Poisson's ratio at peak stress.

$$\nu_i^a = \begin{cases} 8 \times 10^{-6}(f_c)^2 + 0.0002f_c + 0.138 & \text{active confinement,} \\ 0.15 & \text{passive confinement,} \end{cases} \quad (3.21)$$

$$\nu_f^a = 0.5.$$

Secant value of Poisson's ratio for the descending branch (ν_d^a) is expressed as,

$$\nu_d^a = \begin{cases} 0.5 + 1.29\sqrt{(1 - \beta)} & \text{active confinement,} \\ 0.5 + 2.43\sqrt{(1 - \beta)} & \text{passive confinement.} \end{cases} \quad (3.22)$$

Secant value of Young's modulus (E_s) is defined as,

$$E_s = \frac{1/2}{E_i} - \beta \left(\frac{1}{2}E_i - E_f \right) \pm \sqrt{\left[\frac{1/2}{E_i} - \beta \left(\frac{1}{2}E_i - E_f \right) \right]^2 + E_f^2 \beta [D(1 - \beta) - 1]} \quad (3.23)$$

where, E_i is the initial tangent modulus of concrete, E_f is the secant value of Young's modulus at peak stress which is defined as,

$$E_f = \frac{E_c}{1 + 2.5 \frac{E_0}{E_c} \left(\frac{(\sqrt{J_2})_f}{f_c} - \frac{1}{\sqrt{3}} \right)}. \quad (3.24)$$

E_0 and E_c being the initial and peak uniaxial secant value of Young's modulus respectively and $(\sqrt{J_2})_f$ is the square root of invariant at failure. D is a parameter added to fit the post peak shape of the curve and defined as,

$$D = -31 \left(\frac{f_l}{f_c} \right)^2 + 19.3 \left(\frac{f_l}{f_c} \right) - 0.1. \quad (3.25)$$

Further details can be found in Candappa (2000).

3.2.5 Axial strain at peak axial stress (ϵ_{cc})

Several expressions for the axial strain at peak axial stress are available in the literature. They are based on the relevant experimental results for confined NSC and HSC. Many of the researchers defined ϵ_{cc} using the peak axial stress, uniaxial strength and axial strain corresponding to uniaxial strength. Mander et al. (1988b) proposed

$$\epsilon_{cc} = \epsilon_{co} \left[1 + 5 \left(\frac{f_{cc}}{f_c} - 1 \right) \right] \quad (3.26)$$

where f_{cc} and f_c are the compressive strength of confined and unconfined concrete respectively and ϵ_{co} is the strain at peak stress (f_c) of unconfined concrete. Martirosyan and Xiao (2001) modified Mander et al. (1988b) equation by introducing a new parameter, k_1 ,

$$\epsilon_{cc} = \epsilon_{co} \left[1 + k_1 \left(\frac{f_{cc}}{f_c} - 1 \right) \right] \quad (3.27)$$

where coefficient k_1 depends on the concrete strength (f_c), lateral steel yield strength (f_{sy}) and lateral reinforcement ratio (ρ_s).

$$k_1 = 5 + 1.3 \times \rho_s \frac{f_{sy}}{f_c}. \quad (3.28)$$

Unconfined concrete peak strain (ϵ_{co}) was defined as follows:

$$\epsilon_{co} = \frac{0.9(f_c)^{0.27}}{1000}. \quad (3.29)$$

Issa and Tobaa (1984) proposed an expression using high strengths (83 MPa) which has a similar form of Equation (3.26). The major difference in this expression is that it includes the confining pressure.

$$\frac{\epsilon_{cc}}{\epsilon_{co}} = 1 + k_2 \frac{f_l}{f_c} \quad k_2 = c \left(\frac{f_l}{f_c} \right)^d. \quad (3.30)$$

c and d are material parameters. A similar approach was taken by Saatcioglu and Razvi (1992),

$$\varepsilon_{cc} = \varepsilon_{co} \left[1 + 5 \left(\frac{6.7 f_l^{0.83}}{f_c} \right) \right], \quad (3.31)$$

and Assa et al. (2001a),

$$\frac{\varepsilon_{cc}}{\varepsilon_{co}} = 1 + 21.5 \left(\frac{f_l}{f_c} \right) \quad (3.32)$$

in defining axial strain at peak axial stress. Cusson and Paultre (1995) proposed an expression for ε_{cc} using an effective confinement index (f_{le}),

$$\varepsilon_{cc} = \varepsilon_{co} + 0.21 \left(\frac{f_{le}}{f_c} \right)^{1.7}. \quad (3.33)$$

A similar form of equation was proposed by El-Dash and Ahmad (1995) as,

$$\varepsilon_{cc} = \varepsilon_{co} + k_2 \frac{f_l}{f_c} \quad (3.34)$$

where k_2 is a function of unconfined concrete strength and the diameter and spacing of the transverse reinforcements.

Hoshikuma et al. (1997) defined strain corresponding to peak axial stress for circular sections and square sections separately.

$$\varepsilon_{cc} = \begin{cases} 0.00218 + 0.0332 \frac{\rho_s f_{sy}}{f_c}, & \text{for circular sections;} \\ 0.00245 + 0.0122 \frac{\rho_s f_{sy}}{f_c}, & \text{for square sections.} \end{cases} \quad (3.35)$$

ρ_s is the volumetric ratio of steel and f_{sy} is the yield strength of lateral reinforcement. Shah et al. (1983) first proposed,

$$\varepsilon_{cc} = 1.491 \times 10^{-8} f_c + 0.296 \frac{f_{le}}{f_c} + 0.00195 \quad (3.36)$$

and later Diniz and Frangopol (1997) used it in confined HSC. This is not a function of ε_{co} , strain at peak stress of unconfined concrete.

Setunge (1993) and Attard and Setunge (1996) suggested equations for axial strain corresponding to peak axial stress ε_{cc} ,

$$\frac{\varepsilon_{cc}}{\varepsilon_{co}} = 1 + (17 - 0.06 f_c) \left(\frac{f_l}{f_c} \right) \quad (3.37)$$

where f_l is the confining pressure and ε_{co} is the axial strain corresponding to peak uniaxial compressive strength (generally assumed to be 0.002).

In this study Equation (3.37) is used to define the axial strain corresponding to peak axial stress (f_{cc}), which is determined by Equation (3.46) in the next section.

3.2.6 Peak axial stress for confined concrete (f_{cc})

Many researchers defined the peak axial stress for confined concrete using uniaxial concrete strength and confining pressure. Shah et al. (1983) suggested,

$$f_{cc} = f_c + \left(1.15 + \frac{2100}{f_c}\right) f_l \quad \text{kPa} \quad (3.38)$$

where f_c is the unconfined concrete strength and f_l is the confining pressure. Diniz and Frangopol (1997) also used the same equation.

Saatcioglu and Razvi (1992) proposed a different form of equation as follows:

$$f_{cc} = f_c + 6.7 f_l^{0.83}. \quad (3.39)$$

A similar form of equation was suggested by Cusson and Paultre (1995),

$$\frac{f_{cc}}{f_c} = 1.0 + 2.1 \left(\frac{f_l}{f_c}\right)^{0.7}, \quad (3.40)$$

Assa et al. (2001a)

$$f_{cc} = f_c \left(1 + 3.36 \frac{f_l}{f_c}\right), \quad (3.41)$$

and Martirosyan and Xiao (2001)

$$f_{cc} = f_c + 3.96 f_l. \quad (3.42)$$

Issa and Tobaa (1994) defined similar form of an equation proposed by Saatcioglu and Razvi (1992) but the parameters involved were obtained using high strengths (upto 83 MPa).

$$\frac{f_{cc}}{f_c} = 1 + k_1 \frac{f_l}{f_c}. \quad (3.43)$$

k_1 was given as,

$$k_1 = \frac{1}{a + b \sqrt{\frac{f_l}{f_c}}}. \quad (3.44)$$

El-Dash and Ahmad (1995) suggested a similar equation as Equation (3.43). However in their study, k_1 is a function of unconfined concrete strength, diameter and yield strength of lateral reinforcement and volumetric ratio. k_1 was based on the experimental results of several other researchers (Mander et al. 1988b; Ahmad and Shah 1982; Issa and Tobaa 1994; Martinez et al. 1984).

Hoshikuma et al. (1997) defined peak axial stress for circular sections and square sections separately.

$$\frac{f_{cc}}{f_c} = \begin{cases} 1.0 + 3.83 \frac{\rho_s f_{sy}}{f_c}, & \text{for circular sections;} \\ 1.0 + 0.73 \frac{\rho_s f_{sy}}{f_c}, & \text{for square sections,} \end{cases} \quad (3.45)$$

where ρ_s is the volumetric ratio of steel and f_{sy} is the yield strength of lateral reinforcement.

Peak axial stress for confined concrete (f_{cc}) was defined by Attard and Setunge (1996) as,

$$\frac{f_{cc}}{f_c} = \left(\frac{f_l}{f_t} + 1 \right)^k \quad (3.46)$$

where k is a constant given by,

$$k = 1.25 \left(1 + 0.062 \frac{f_l}{f_c} \right) (f_c)^{-0.21} \quad (3.47)$$

and f_t is the tensile strength. As silica fume was not used in this project tensile strength is given by,

$$f_t = 0.9 \times 0.32 (f_c)^{0.67}. \quad (3.48)$$

In this study equation proposed by Attard and Setunge (1996) is used as the peak axial stress of confined concrete.

3.2.7 Experimental investigations on high strength concrete

Martirosyan and Xiao (2001) conducted an experimental program to establish the response of HSC columns, confined with steel spirals and subjected to short term compressive loadings. The main variables considered were compressive strength of concrete, amount of confinement and specimen size. They concluded that compressive strength and strain at maximum stress of normal weight and light weight spirally reinforced columns increase with increase in confinement stress irrespective of the concrete strength. Liu et al. (2000) tested twelve HSC columns (60 to 96 MPa compressive strength) under axial compression to study the effect of concrete strength, tie spacing or the pitch of the spiral, the diameter of the tie or spiral reinforcement and the cover to the ties.

3.3 Damage models for concrete

An elastoplastic constitutive model for damaged concrete materials based on a thermo-mechanically consistent mechanical model was proposed by Peng et al. (1997). Since the concrete is generally subjected to triaxial loading, the coupling between volumetric and deviatoric responses were considered in the model formulation. The effect of hydrostatic stress on the inelastic deviatoric deformation was considered as follows:

- Hydrostatic stress is introduced into the stiffness of the springs and the damping coefficients of the dashpot-like blocks.

Proposed model has been validated by comparing with the experimental results of concrete subjected to triaxial stress histories with cyclic loading and unloading.

3.4 Effect of strain rate on stress-strain behaviour

In severe earthquake ground motions, cyclic loading with high strain rates is imposed on structures. Behaviour of HSC loaded with high strain rates, such as those that would resemble the earthquake ground motions, has been studied by only a few researchers in the literature (Fu et al. 1991a; Fu et al. 1991b; Bing et al. 2000). Bing et al. (2000) conducted an experimental program to investigate the behaviour of short columns subjected to concentric loads at different strain rates. Thirty reinforced concrete columns (240 mm diameter circular or 240 mm square and 720 mm high) with different confining reinforcement configurations, yield strengths of confining reinforcements and concrete compressive strengths were investigated. Stress-strain curves for confined HSC loaded at high strain rates were proposed and compared with the same for NSC. Bing et al. (2000) concluded that high strain rates seem to have a less effect on stress-strain relationships of HSC than on NSC.

3.5 Gaps in knowledge

Most of the constitutive models available in the literature for monotonically increasing loading are for NSC. Only a few researchers (Martirosyan and Xiao 2001; Liu et al. 2000) reported this behaviour for HSC. For both NSC and HSC, the reported models are

based on column test results which need assumptions about the confinement effectiveness. None of the above models recorded the volumetric strain of concrete. Furthermore in load-deflection analysis of columns, lateral confining pressure was suggested to be corresponding to the yield strength of steel. However, use of steel yield strength in these models predicted unconservative results (Sheikh and Yeh 1992). In reality, the confining pressure or the stress in lateral reinforcement increases gradually with lateral dilation of concrete until the confining steel yields, after this point, the confining pressure remains constant (neglecting strain hardening). Therefore the behaviour of confined concrete can be established accurately if the lateral dilation of concrete is known.

The only exception to all these models is the constitutive model proposed by Candappa (2000) for confined HSC subjected to monotonically increasing load. It is based on the triaxial tests which are conducted under well controlled lateral confinement. It has the capability of establishing axial stress, axial strain as well as lateral strains. However, it is a stress-based model and involves iteration procedure when applied to passively confined concrete. Due to the complexity of that model and further the inability to extend that model for the cyclic behaviour of concrete, led the author to develop another constitutive model for HSC using the experimental triaxial test results of Candappa (2000). The formulation of the model is presented in the next section.

3.6 Model formulation

The model formulation is based on the experimental results reported by Candappa (2000), which were obtained under active lateral confinement.

3.6.1 Experimental results

Candappa et al. (2001) used four grades of concrete (40, 60, 75 and 100 MPa) and three confining pressures (4, 8 and 12 MPa) as test variables in the experimental program. Since the tests were performed in duplicate, a total of 24 tests have been reported. Further details of the experimental program can be found in Candappa et al. (1999), Candappa (2000) and Candappa et al. (2001). However, for the convenience of the reader, a brief outline of the experimental set up and procedures are presented here.

Cylindrical specimens (98 mm diameter and 200 mm high) were prepared according to

AS1012, Part 2 (2000) and cured according to AS1012, Part 8 (2000). Having both ends properly ground, pores filled with plaster, two strain gauges were placed longitudinally in two diametrically opposite sides. Similarly, another two strain gauges were placed laterally at the middle third in two diametrically opposite sides. The specimen thus prepared was then accommodated in a triaxial cell. Details of the triaxial cell are explained later in Chapter 7. The required pressure was applied to the specimen using oil through a flexible polyurethane membrane. A bleed valve was utilised to maintain the required confining pressure.

The two strain gauges placed longitudinally were used to measure the axial deformations. Since the strain gauge readings are unreliable after reaching the peak strength, Linear Variable Displacement Transducers (LVDTs) were also used to measure the axial deformation of concrete. In all the experimental curves, axial strains were verified using these two methods of measurements. Similarly, lateral strains were also measured by strain gauges as well as clip gauge.

3.6.2 Basis of model formulation

The proposed model formulation has several novel key aspects, based on following observations.

- Lateral strain versus axial strain relationship:
 - Normalised lateral strains were plotted against normalised axial strains for all four concrete strengths and for all confining pressures. It is clearly seen that for a particular concrete strength, these curves have a similarity in the shape irrespective of the confining pressure applied. The gradient of these curves is directly related to an important parameter, Poisson's ratio.
- Shear stress versus shear strain relationship:
 - In an attempt to develop a stress-strain model, normalised shear stress versus normalised shear strain were plotted. Further analysis indicated that these curves coincide for a particular concrete compressive strength with different confining pressures. This observation is consistent with the theory that concrete failure is a shear type failure (Nielsen 1999).

- At the peak axial stress volumetric strain becomes zero:
 - Volumetric strain is an important factor, especially when lateral confinement is involved. Normalised volumetric strain versus normalised axial strain curves have a similar shape. The author found that the volumetric strain is close to zero at peak axial stress.

The model requires the uniaxial compressive strength of concrete, f_c , as an input variable. Corresponding axial strain ε_{co} is assumed to be 0.002 and can be made as input variable if required. The strain-based model is formulated based on theory of shear failure with three relationships as follows:

1. Relationship between peak axial stress, corresponding axial strain and lateral strain
2. Relationship between axial strain and lateral strain
3. Relationship between shear stress and shear strain which is used to find a relationship between axial stress, axial strain and lateral strain

In the reported studies so far, a second order parabolic curve, or a form of an equation was proposed for the ascending branch of the stress-strain curves of confined concrete. For the descending branch, previous researchers proposed a linear relationship or an exponential function. However in some models, at the peak point the peak stress calculated using ascending branch and descending branch were incompatible. Some models were unable to establish the behaviour of HSC. They are important issues in establishing behaviour of confined HSC. The author proposes complete stress-strain curves based on a basic theory of shear failure of concrete. At the peak stress, the ascending and descending branches are compatible. The proposed stress-strain relationship consists of different exponential functions for ascending branch and descending branch for unconfined and confined concrete as illustrated in Figure 3.4.

3.6.3 Developing a relationship between axial strain and lateral strain

In order to find a relationship between axial strain and lateral strain, the curves shown in Figure 3.5 were developed based on experimental results reported by Candappa (2000). Each line in these graphs represents average of two test results.

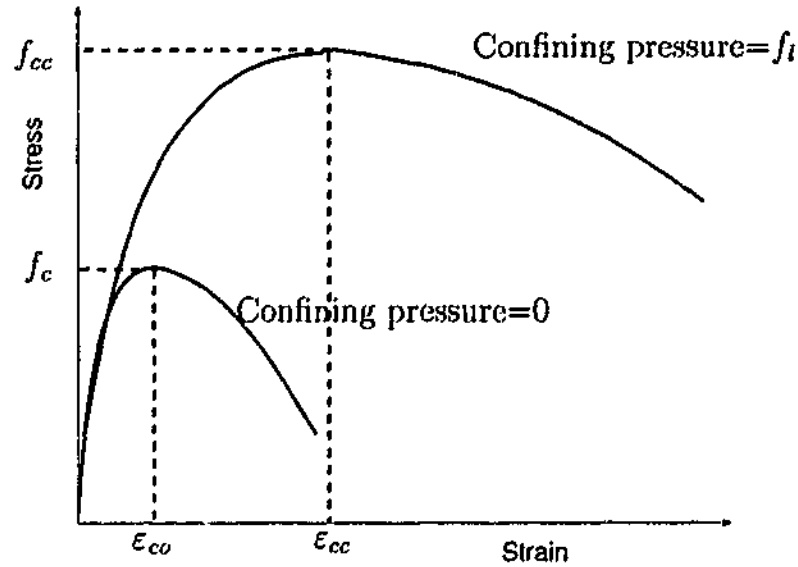


Figure 3.4: Typical stress-strain relationship for confined and unconfined concrete.

The curves are for normalised lateral strain (with respect to lateral strain at peak stress), $\bar{\epsilon}_2$ versus normalised axial strain (with respect to axial strain at peak stress), $\bar{\epsilon}_1$.

$$\bar{\epsilon}_2 = \frac{\epsilon_2}{\epsilon'_{cc}} \quad \text{and} \quad \bar{\epsilon}_1 = \frac{\epsilon_1}{\epsilon_{cc}} \quad (3.49)$$

ϵ_1 and ϵ_2 are axial and lateral strains respectively, ϵ_{cc} is the axial strain corresponding to peak axial stress and ϵ'_{cc} is the corresponding lateral strain. The gradient of these curves will be related to the Poisson's ratio. It will be a constant at the beginning and increases gradually. Therefore the observed behavior can be approximated by a pair wise equation.

$$\frac{\epsilon_2}{\epsilon'_{cc}} = \begin{cases} \nu'_i \left(\frac{\epsilon_1}{\epsilon_{cc}} \right) & \text{if } \epsilon_1 \leq \epsilon' \\ \left(\frac{\epsilon_1}{\epsilon_{cc}} \right)^{m_1} & \text{if } \epsilon_1 > \epsilon' \end{cases} \quad (3.50)$$

ν'_i is the initial Poisson's ratio, m_1 is a material parameter which depends on the uniaxial concrete strength. The value of m_1 for each concrete strength was found using the best-fit curves and summarised in Table 3.4.

$$m_1 = 0.0177f_c + 1.2818 \quad (3.51)$$

ϵ' can be obtained by equating the right hand side of Equation (3.50). Rashid et al. (2002) reported experimental values of Poisson's ratio of concretes in the elastic region from the available data in the literature (Figure 3.6).

Based on these data, the initial Poisson's ratio for HSC seems to be marginally higher than those for NSC. Rashid et al. (2002) found that Poisson's ratio changes from 0.15 to

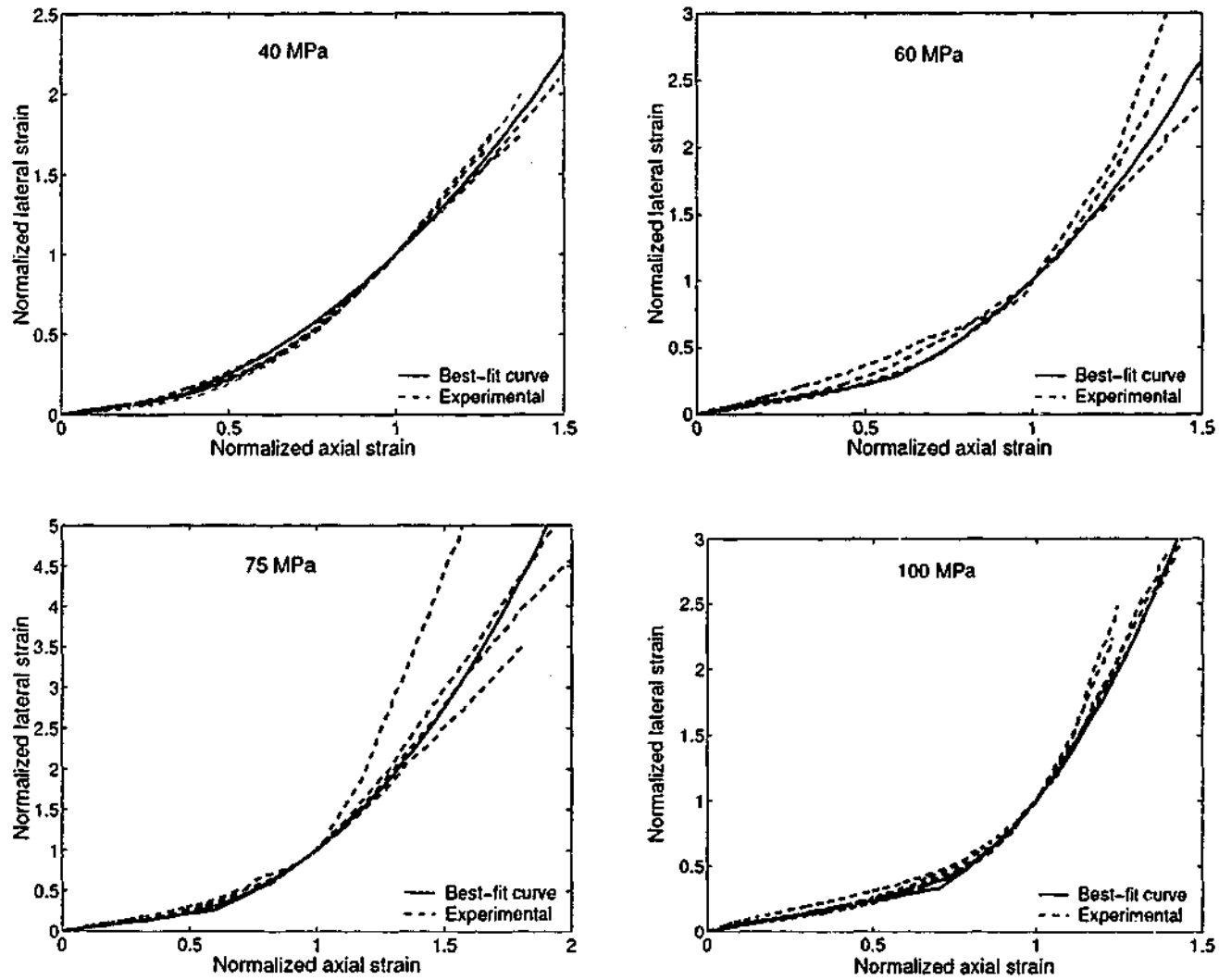


Figure 3.5: Normalised lateral strain versus normalised axial strain.

0.25 and an average value of 0.2 was justified for a compressive strength range of 20 120 MPa. Initial Poisson's ratio (ν_i^0) is defined by Candappa (2000).

$$\nu_i^0 = 0.15. \quad (3.52)$$

In this study Equation (3.52) is used for the initial Poisson's ratio. Therefore if axial strain (ϵ_{cc}) and lateral strain (ϵ'_{cc}) corresponding to peak axial stress can be expressed, the relationship between axial strain and lateral strain at any stress-strain state is fully defined by Equation (3.50).

Table 3.4: Material parameters in Equations (3.50) and (3.61).

Parameter	40	60	75	100	General equation	R^2
m_1	2.0	2.4	2.5	3.1	$0.0177f_c + 1.2818$	0.9717
m_2	6.0	5.3	4.4	3.5	$-0.0427f_c + 7.7381$	0.9899
m_3	-0.020	-0.025	-0.030	-0.040	$-0.0003f_c - 0.0057$	0.9873

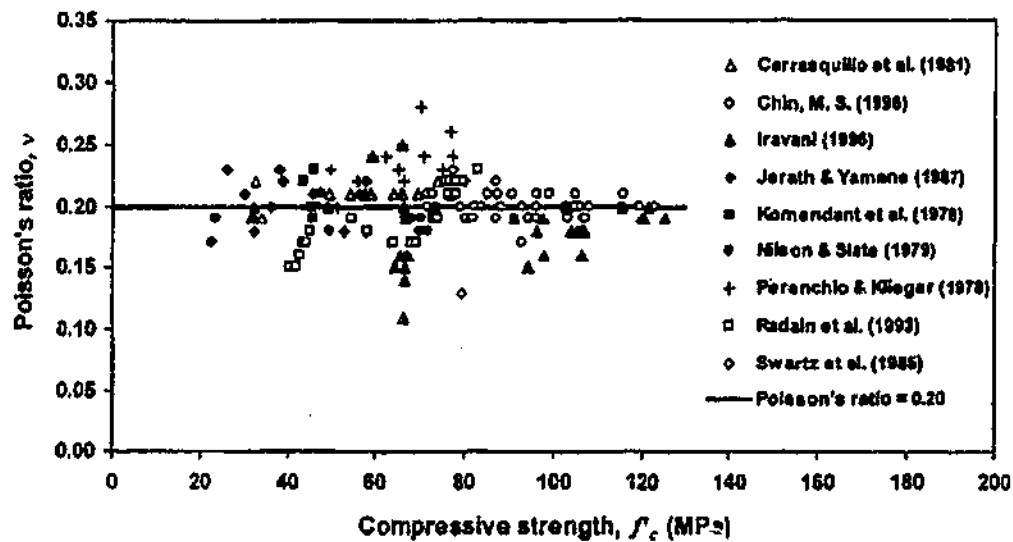


Figure 3.6: Poisson's ratio for concrete (Rashid et al. 2002).

3.6.4 Lateral strain at peak axial stress (ϵ'_{cc})

In order to find a relationship between axial and lateral strain at peak axial stress, normalised volumetric strain factor ($\bar{\epsilon}_v$) versus normalised axial strain factor ($\bar{\epsilon}_1$) graphs were plotted for all grades of concrete and all confining pressures. Normalised volumetric strain factor ($\bar{\epsilon}_v$) is defined as,

$$\bar{\epsilon}_v = \frac{\epsilon_v}{\epsilon_{v,max}} = \frac{\epsilon_1 + 2\epsilon_2}{\epsilon_{v,max}} \quad (3.53)$$

where $\epsilon_{v,max}$ is the maximum volumetric strain.

Normalised axial strain factor ($\bar{\epsilon}_1$) is the same defined in Equation (3.49). The curves are shown in Figure 3.7. The normalised volumetric strain factors and axial strain factors corresponding to the peak point are marked as a "x" in each curve. It is clearly seen that there is a similarity in all the curves irrespective of concrete strength or confining pressure. Initially volumetric strain increases gradually and then starts decreasing. That is, with the increasing axial stress, the concrete first contracts and then gradually it expands. At a

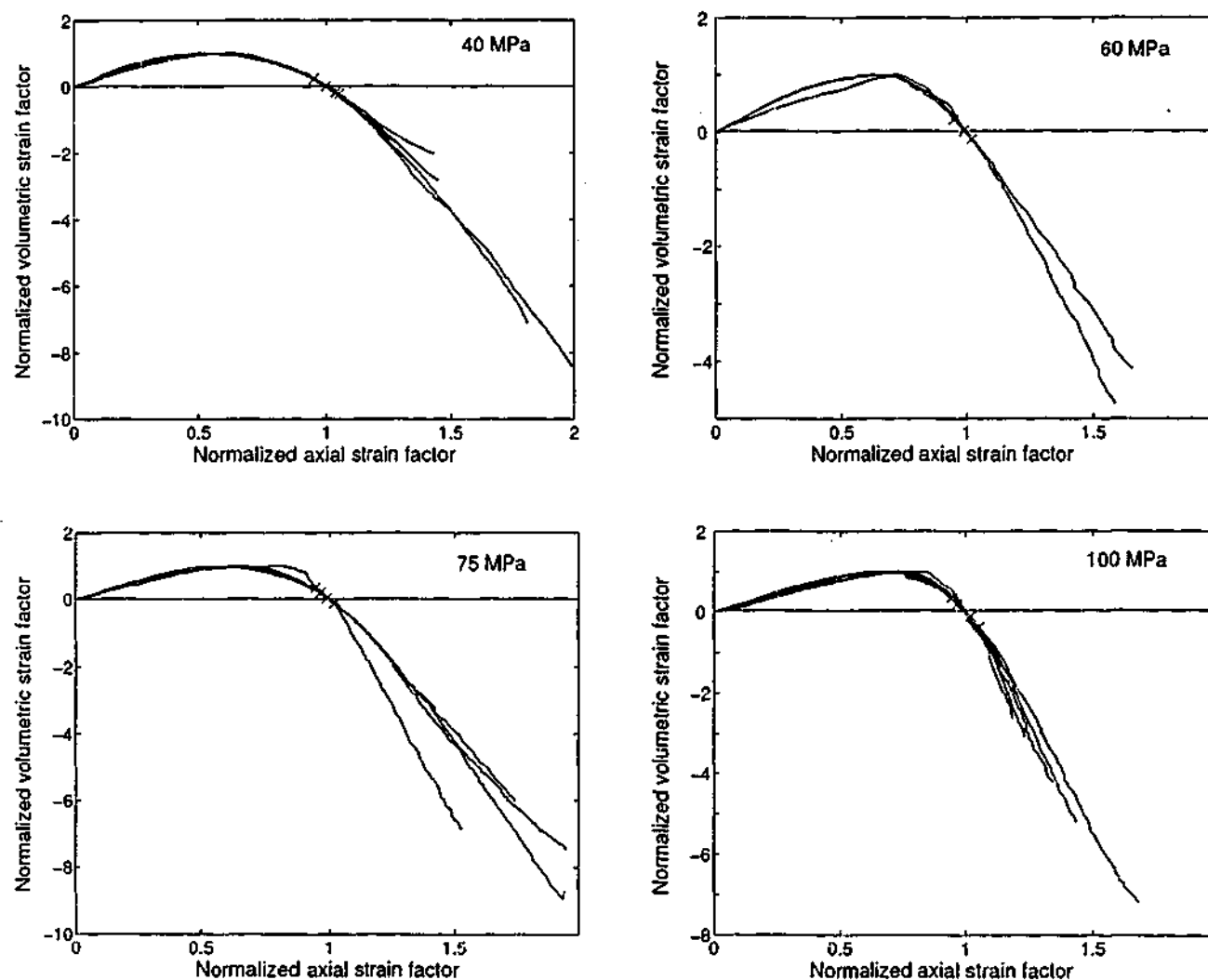


Figure 3.7: Normalised volumetric strain factor versus normalised axial strain factor (The "x" marked on the curves indicate peak stress points).

particular point the contraction changes to expansion. At this point the volumetric strain is maximum. This maximum value ($\epsilon_{v,max}$) is approximately close to the point where axial strain is half of that at the peak axial stress. However, this point changes with the concrete strength and for the concrete (40, 60, 75 and 100 MPa) considered in this study, volumetric strain becomes maximum when 0.5, 0.6, 0.63 and 0.7 of the respective axial strain at peak stress.

It is interesting to note that there is a point where volumetric strain changes its sign. That is, at this point the volume of concrete comes back to its original volume. When the experimental data are carefully analysed for the peak axial stress, it is observed that volumetric strain becomes zero when peak axial stress is reached. Normalized volumetric

strain factor and axial strain factor corresponding to the peak stress is marked as "x" in each curve in Figure 3.7. Therefore at peak stress,

$$\bar{\epsilon}_v = \frac{\epsilon_1 + 2\epsilon_2}{\epsilon_{v,max}} = 0, \quad (3.54)$$

and

$$\epsilon_{cc} = 2\epsilon'_{cc}. \quad (3.55)$$

By introducing Poisson's ratio, Equation (3.55) can be written as,

$$\nu_f^a = 0.5 \quad (3.56)$$

where ν_f^a is the secant value of Poisson's ratio at peak stress. This has been addressed in the literature by few researchers (Ottosen 1979; Madas and Elnashai 1992; Dahl 1992; Cusson and Paultre 1995; Candappa et al. 2001). Ottosen (1979) suggested a value of 0.36 for ν_f^a and his study is said to be valid up until failure. He further stated that secant value of Poisson's ratio must always be less than 0.5. Madas and Elnashai (1992) proposed that Poisson's ratio can reach and exceed the value of 0.5 at high compressive stresses near failure. Dahl (1992) proposed 0.5 for ν_f^a for triaxial tests and later Cusson and Paultre (1995) and Candappa et al. (2001) found that it is approximately 0.5. Based on the experimental results by Candappa (2000) and observing the volumetric behaviour for both normal and high strength concrete (Figure 3.7), it can be confirmed that secant value of Poisson's ratio at peak stress is 0.5.

3.6.5 Relationship between axial stress, axial strain and lateral strain

Maximum shear stress (τ_{max}) and maximum shear strain (γ_{max}) are defined as,

$$\tau_{max} = \frac{\sigma_1 - f_l}{2} \quad \text{and} \quad \gamma_{max} = \frac{\epsilon_1 + \epsilon_2}{2} \quad (3.57)$$

where σ_1 is the axial stress, f_l is the lateral stress (confining pressure), ϵ_1 is the axial strain and ϵ_2 is the lateral strain. Shear stress factor is defined as,

$$\bar{\tau} = \frac{\text{maximum shear stress}}{\text{maximum shear stress at peak}} = \frac{\tau_{max}}{\tau_{mp}}. \quad (3.58)$$

Similarly shear strain factor is defined as,

$$\bar{\gamma} = \frac{\text{maximum shear strain}}{\text{maximum shear strain at peak}} = \frac{\gamma_{max}}{\gamma_{mp}}. \quad (3.59)$$

Shear stress factor (Equation 3.58) against shear strain factor (Equation 3.59) graphs were plotted for all the grades of concrete and for all confining pressures. They are shown in Figure 3.8. The relationship between these factors can be approximated by the following

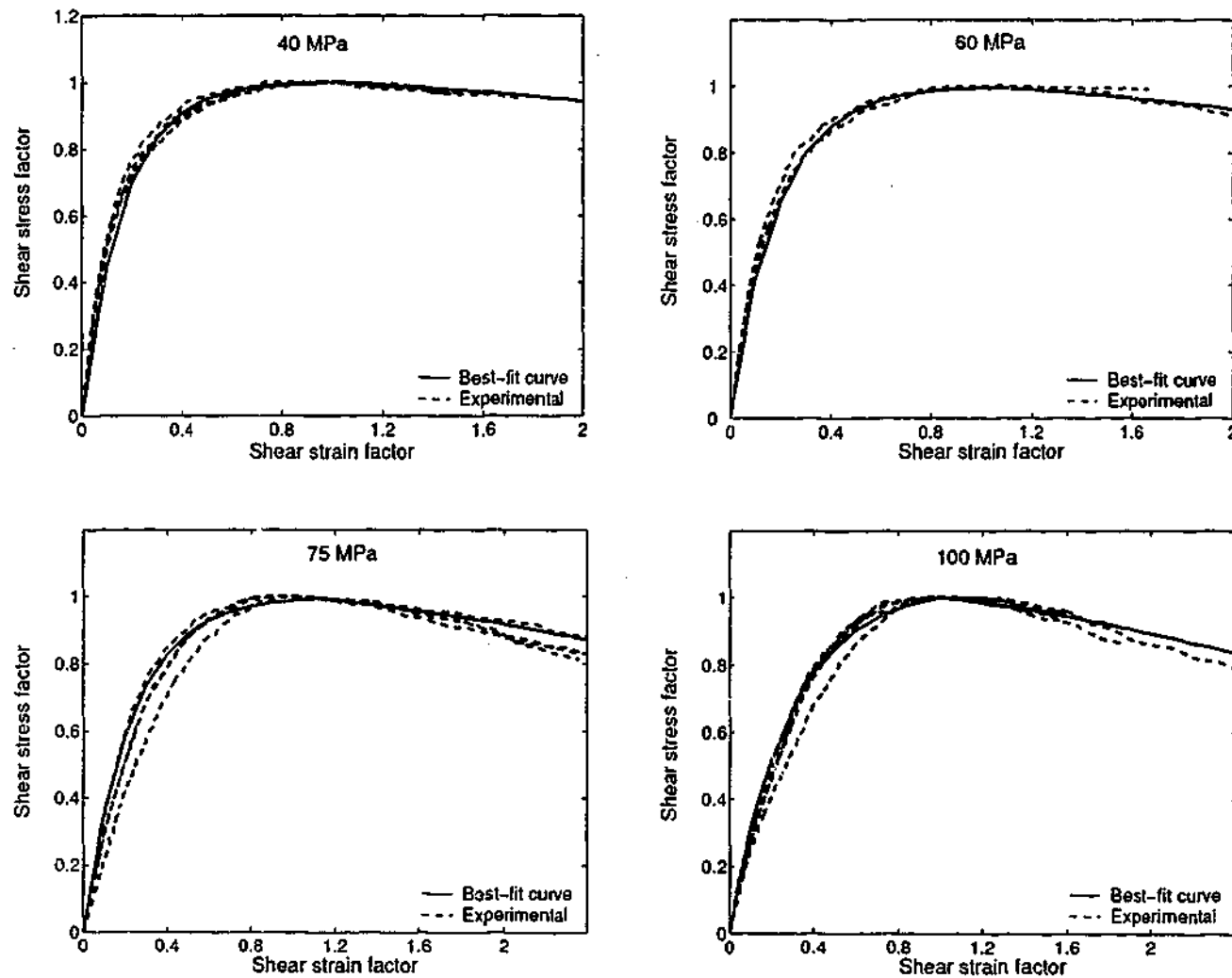


Figure 3.8: Normalised shear stress factor versus normalised shear strain factor.

exponential functions,

$$\bar{\tau} = \begin{cases} (1 - e^{-m_2 \bar{\gamma}}) & \text{before peak} \\ e^{m_3 \bar{\gamma}^2} - m_3 & \text{after peak} \end{cases} \quad (3.60)$$

where m_2 and m_3 are material parameters. They depend on the uniaxial concrete strength. Their values for each concrete strength were found using the best-fit curves and summarised in Table 3.4. Substituting shear stress ($\bar{\tau}$) and shear strain factors ($\bar{\gamma}$) in terms of axial stress (σ_1), axial strain (ϵ_1), lateral strain (ϵ_2), maximum shear stress at peak (τ_{mp}) and maximum shear strain at peak (γ_{mp}), complete deformational behaviour

of concrete can be expressed as,

$$\sigma_1 = \begin{cases} 2\tau_{mp}(1 - e^{-m_2(\frac{\epsilon_1 + \epsilon_2}{2\tau_{mp}})}) + f_l & \text{before peak} \\ 2\tau_{mp}(e^{m_3(\frac{\epsilon_1 + \epsilon_2}{2\tau_{mp}})^2} - m_3) + f_l & \text{after peak.} \end{cases} \quad (3.61)$$

Thus, having established the axial strain and lateral strain relationship and shear strain factor and shear stress factor relationship, the actual stress versus strain curves for the different specimens under various confining stresses are computed and compared to experimental results. The curves for Grade 40, 60, 75 and 100 concrete are shown in Figures 3.9-3.12 respectively. Each figure includes 3 sets of results for the three different confining pressures applied (4, 8 and 12 MPa). Due to the lack of experimental data for the behaviour of actively confined HSC columns, it is unable to apply the model for a similar situation.

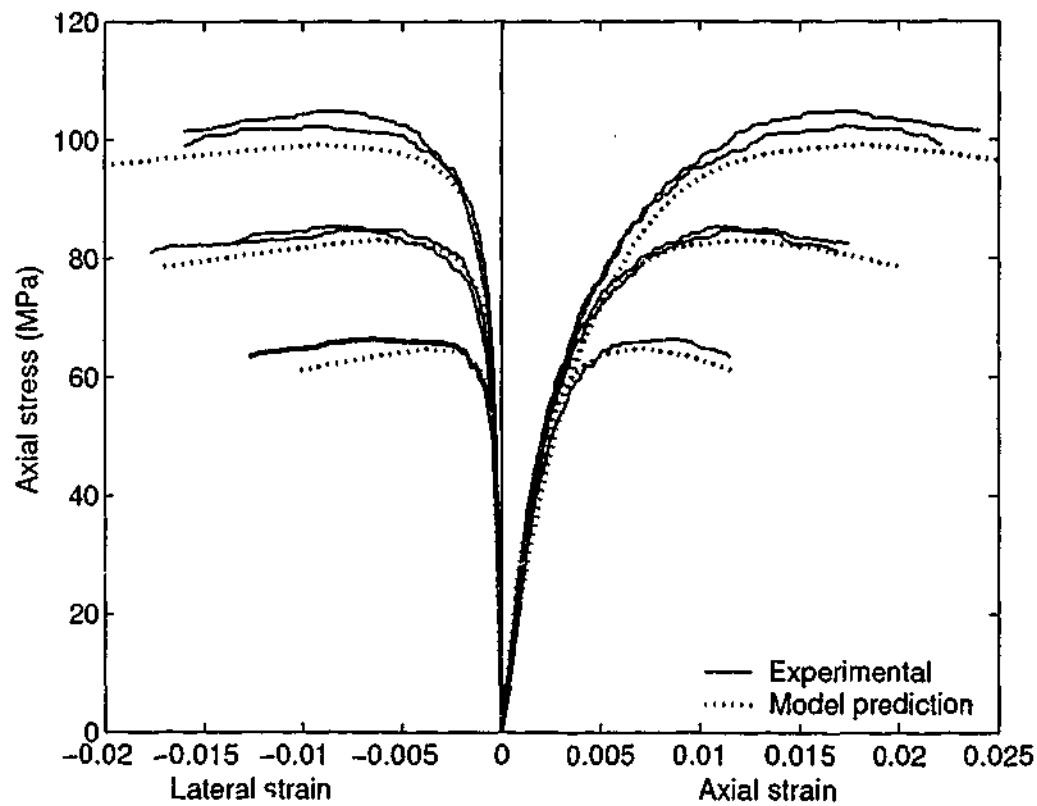


Figure 3.9: Stress-strain curves for Grade 40 concrete.

The model developed in this chapter is based on experimental results for HSC subjected to active lateral confinement and monotonically increasing axial load. However, it can easily be extended to predict the performance of passively confined HSC columns as shown below.

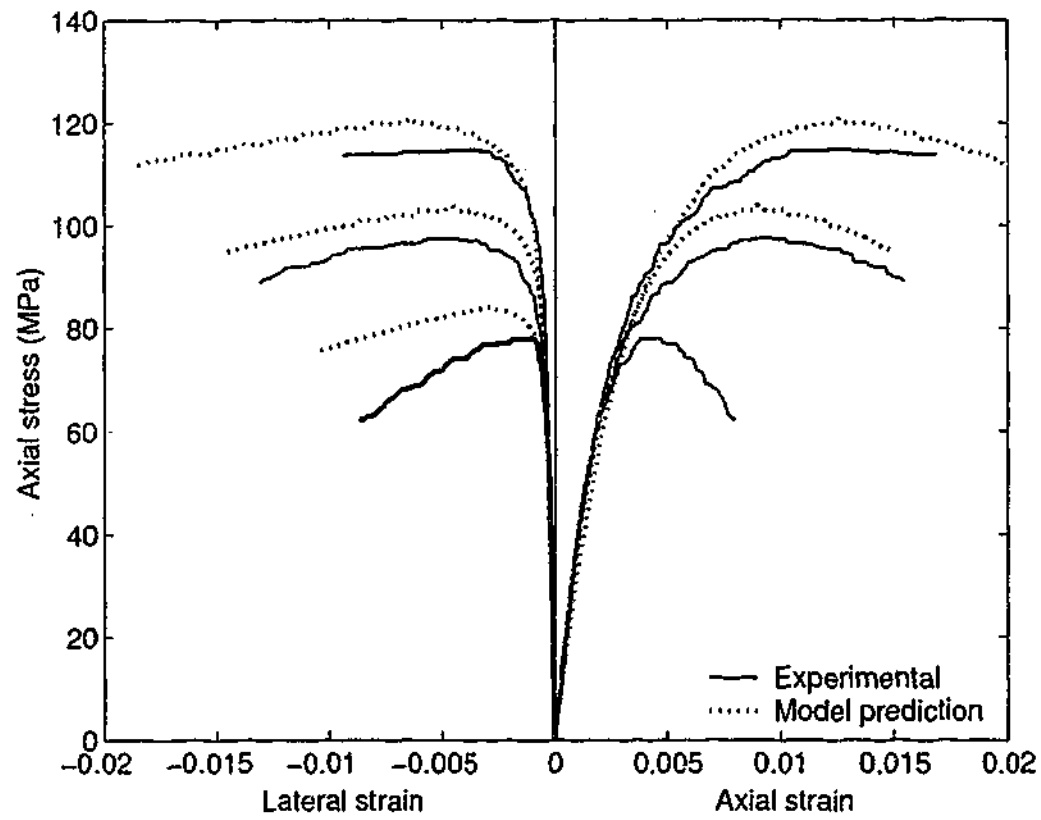


Figure 3.10: Stress-strain curves for Grade 60 concrete.

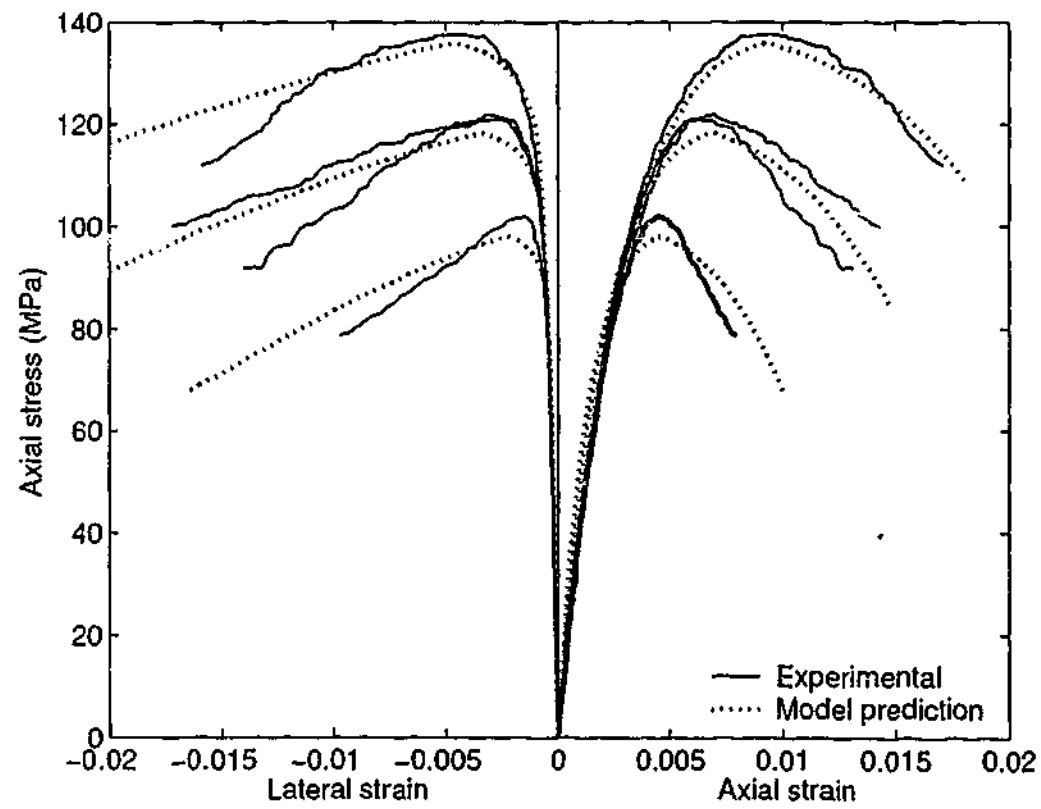


Figure 3.11: Stress-strain curves for Grade 75 concrete.

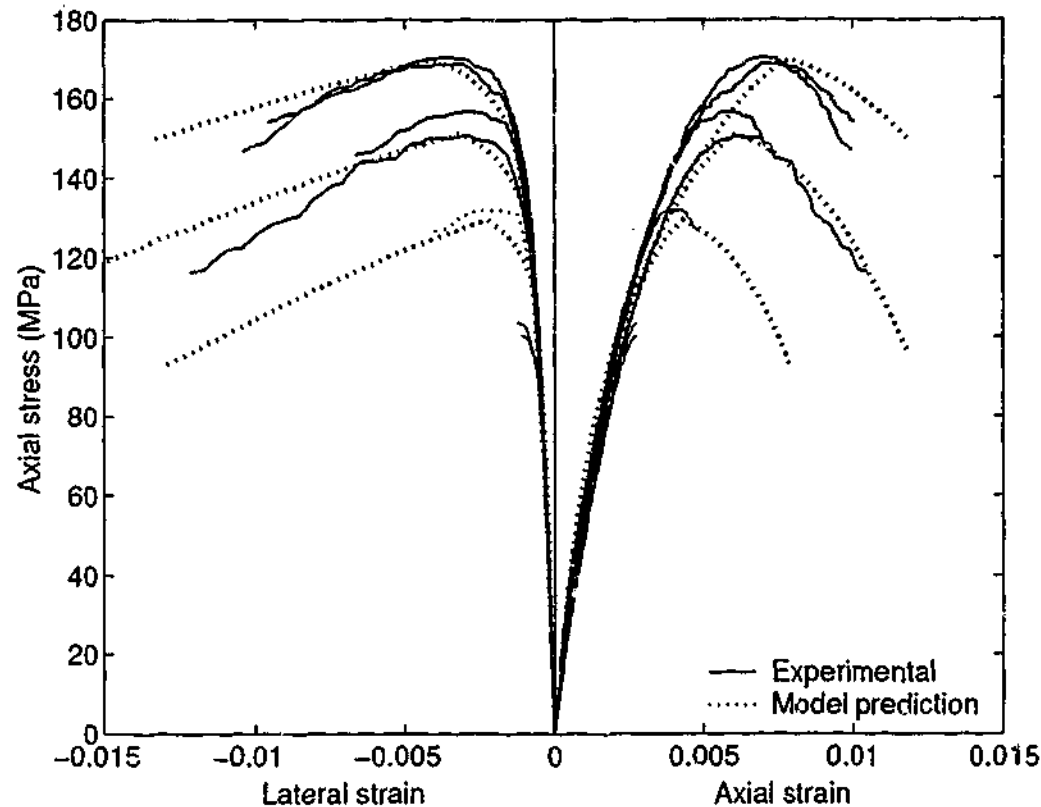


Figure 3.12: Stress-strain curves for Grade 100 concrete.

3.7 Model application in columns with passive confinement

In the literature, many experimental results on cylindrical concrete columns subjected to passive confinement are available. Such studies are based on concrete confined by spirals and hoops (Ahmad and Shah 1982; Martinez et al. 1984; Pessiki and Pieroni 1997), rectilinear ties (Sargin 1971; Sheikh and Uzumeri 1980; Cusson and Paultre 1995) and concrete filled steel tubular columns (Shams and Saadeghvaziri 1997). In the last two decades, the use of fibre reinforced polymer composites as the method of confinement has been gaining increasing popularity. Experimental results on cylindrical columns confined by fibre reinforced plastic sheets would be ideal for verification of the proposed model in this chapter. From the many available experimental results, it was decided to use the experimental results reported by Candappa (2000), who used carbon fibre reinforced plastic sheets as the method of confinement. There were two reasons for this selection.

- The complete experimental data in electronic form was easily available for the author

- Candappa (2000) reported axial stress, axial strain and lateral strain relationships

Since the experimental program carried out by Candappa (2000) has not been published elsewhere, it is described here in detail.

3.7.1 Experimental program

The main aim of the experimental program was to study the behaviour of confined HSC columns with monotonically increasing loads. The confinement was provided using carbon fibre wraps. There were two test variables, namely the compressive strength of concrete and the level of confinement provided. Three compressive strengths (30, 60 and 100 MPa) and three levels of confinement (1, 2 and 3 wraps) were investigated. Tests were performed in duplicate for each wrapping configuration and each compressive strength. All together 18 specimens were tested in the experimental program.

Details of concrete mixes

Concrete mix proportions for the carbon fibre wrapped testing program are given in Table 3.5.

Table 3.5: Mix proportions for carbon fibre wrapped specimens.

Material (for 1 m ³)	CF30	CF60	CF100
Cement (kg)	305	360	500
Water (kg)	150	180	140
Coarse aggregate (kg)	1500	1130	1340
Fine aggregate (kg)	806	830	520
Superplasticiser (kg)	-	-	8.7
W/C ratio	0.7	0.5	0.3
Slump (mm)	100	100	150

Table 3.6 gives the 28-day strengths and the strength and the age at time of testing for all three grades of concrete.

Properties of fibre wraps

Tensile test specimens were prepared in order to determine the stress-strain properties of the fibre composites. The prepared tensile test specimen is shown in Figure 3.13. The

Table 3.6: Uniaxial strengths (specimens to be wrapped by carbon fibre).

	CF30	CF60	CF100
28-day strength (MPa)	20.31	60.95	94.18
Strength at testing (MPa)	28.90	66.03	101.86
Age at testing (days)	78	96	119



Figure 3.13: Carbon fibre tensile test specimen.

tensile stress-strain curves obtained for carbon fibre composites are linear until failure. They are shown in Figure 3.14. The average tensile strength of carbon fibre composites was 741.3 MPa (standard deviation of 72 MPa) and the average Young's modulus was 101,920 MPa (standard deviation of 5830 MPa).

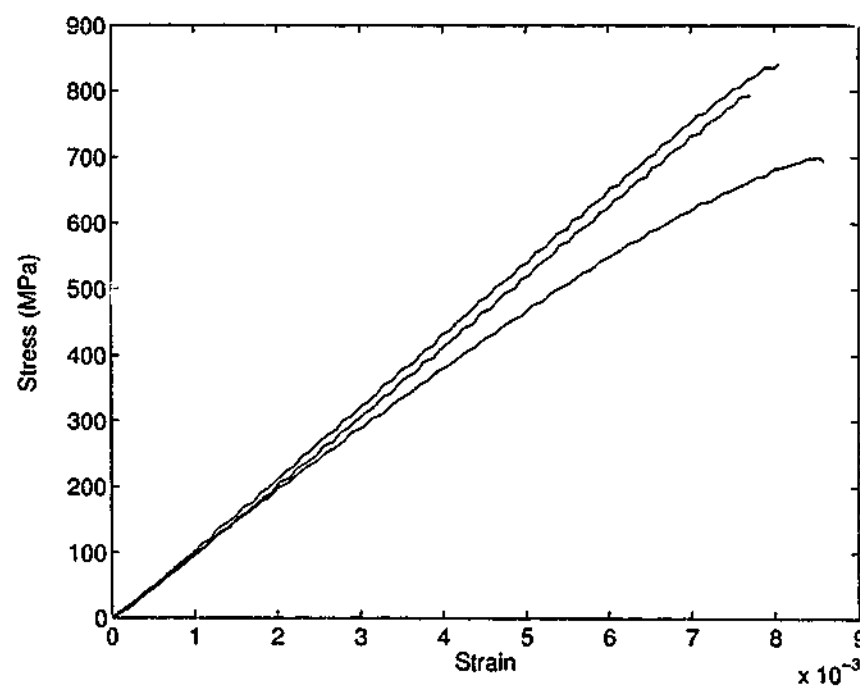


Figure 3.14: Tensile stress-strain curve for carbon fibre composite.

Specimen preparation

Specimen preparation method plays an important role in fibre wrapped concrete. The method used by Candappa (2000) is described here in detail.

The cylindrical specimens (150 mm diameter and 300 mm high) were allowed to air dry for about a week after taking out from the curing bath. They were then sand blasted to remove any loose particles and the dust was wiped off thoroughly. Any surface pores were filled with a quick setting filler. Having applied an epoxy-based primer onto the concrete surface, it was allowed to cure overnight. Before fibre wrapping, the concrete specimen surface was slightly sanded.

The required length of fibre wrap was cut with an allowance of 30 mm for overlapping. Laminating resin of equal mass as the weight of the fibre wrap was applied on the surface of the fibre wrap using a soft brush. Distributing laminating resin and squeezing any excess resin out was performed using a bubble breaker. The composite fibre was then wrapped tightly around concrete specimen and allowed to cure for two weeks. All the specimens were prepared using this method and one such specimen is shown in Figure 3.15. The concrete specimens were wrapped in one, two or three layers of carbon fibre composite.

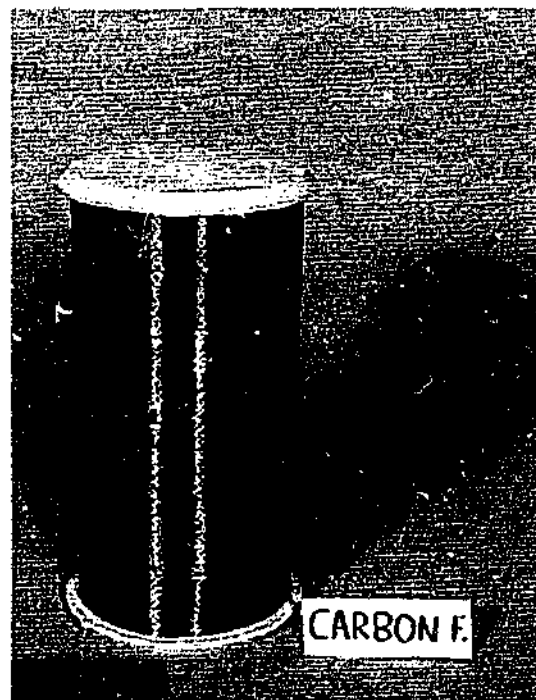


Figure 3.15: Carbon fibre wrapped specimen.

Test procedure

The fibre wrapped specimens were then tested in a compression testing machine which was set to displacement control at the rate of 0.25 mm vertical displacement per minute. LVDTs were used to measure the axial deformations. The clip gauge used to measure the lateral deformations in actively confined concrete was modified to measure the lateral strains in passively confined concrete columns. A custom made chain was wrapped around the specimen and connected to the arms of the clip gauge. The clip gauge system is shown in Figure 3.16.

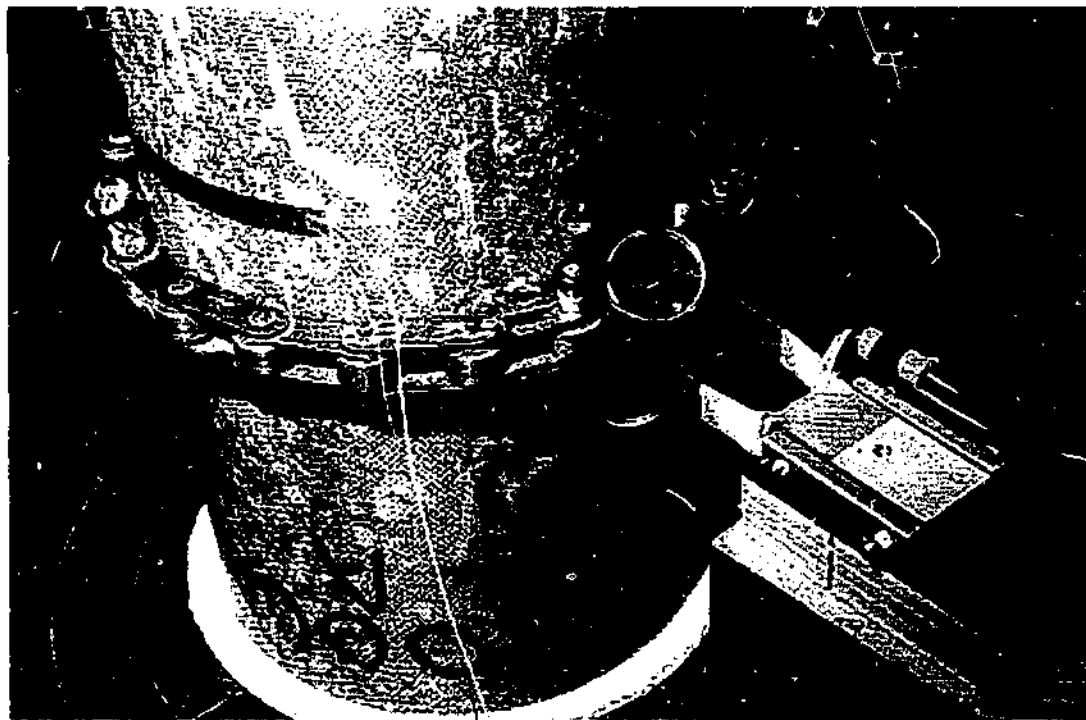


Figure 3.16: Clip gauge system used to measure lateral strains.

Confining pressure

The confining pressure exerted by the fibre reinforced plastic sheets on the concrete core is of passive type. As the axial stress increases, the corresponding lateral strain in concrete increases and a tensile hoop stress is developed in the confining sheets which is balanced by the uniform radial pressure due to the lateral expansion of concrete (Figure 3.17).

Confining pressure can then be found by the equilibrium of forces.

$$f_l \times d_s = f_{cf} n_2 t_{cf} \quad (3.62)$$

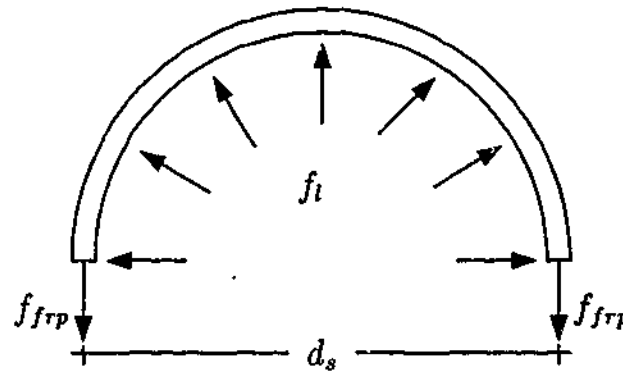


Figure 3.17: Confinement action in FRP composites.

f_l is the confining pressure, d_s is the diameter of the cylinder, f_{cf} is the hoop stress of the carbon fibre sheet, n_2 is the number of sheets and t_{cf} is the thickness of a sheet. Therefore confining pressure is given as,

$$f_l = \frac{f_{cf} n_2 t_{cf}}{d_s} \quad (3.63)$$

The hoop strength of the carbon wrap was assumed to be the tensile strength of the carbon fibre composite (741.3 MPa). The diameter of the specimen was 150 mm and the thickness of one layer of carbon fibre was 0.24 mm. It resulted in the following maximum pressures.

- 1 Wrap: 2.37 MPa
- 2 Wraps: 4.74 MPa
- 3 Wraps: 7.11 MPa

3.7.2 Results

The constitutive model for HSC presented in this chapter (Section 3.6), is applied to obtain the behaviour of carbon fibre wrapped concrete columns. The analytical findings are compared with the experimental results outlined above. Comparisons are shown in Figures 3.18-3.23.

3.7.3 Discussion

The general shapes of the stress-strain curves obtained for carbon fibre wrapped columns are significantly different to the curves for concrete confined by lateral steel reinforcement. Continuously increasing stress versus strain curves can be seen for all specimens except

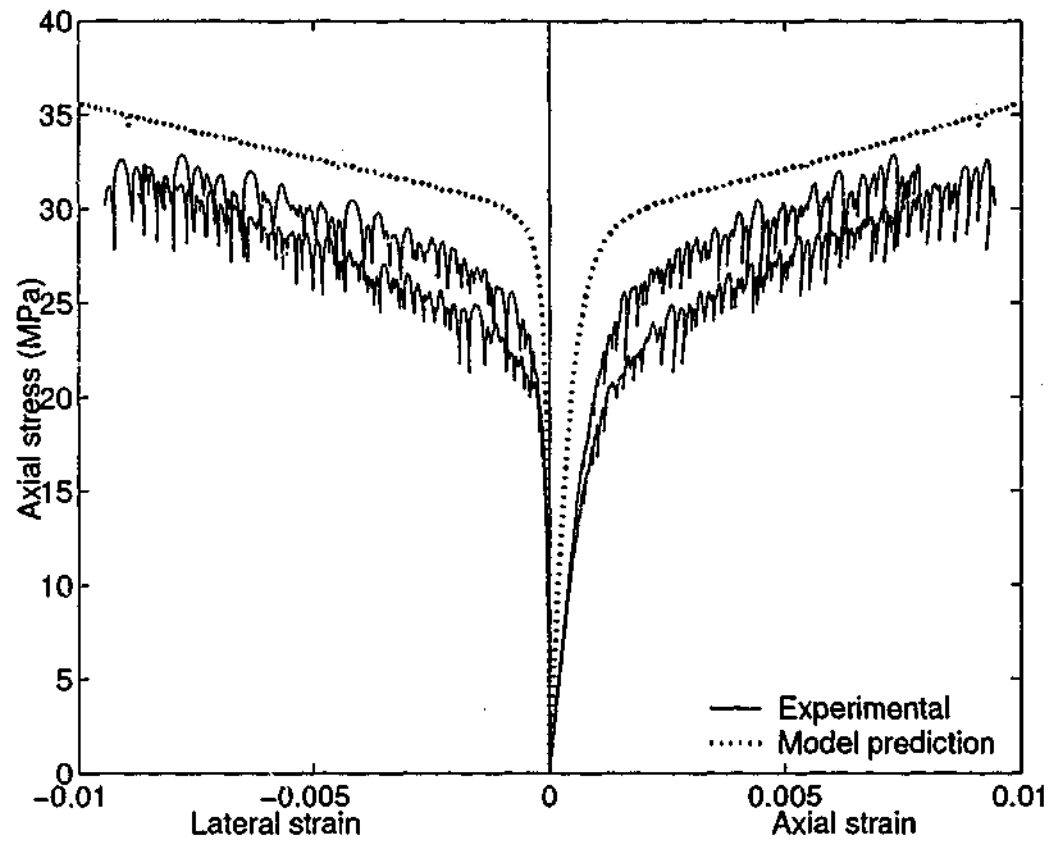


Figure 3.18: Stress-strain curves for Grade 30 concrete with 1 carbon fibre wrap.

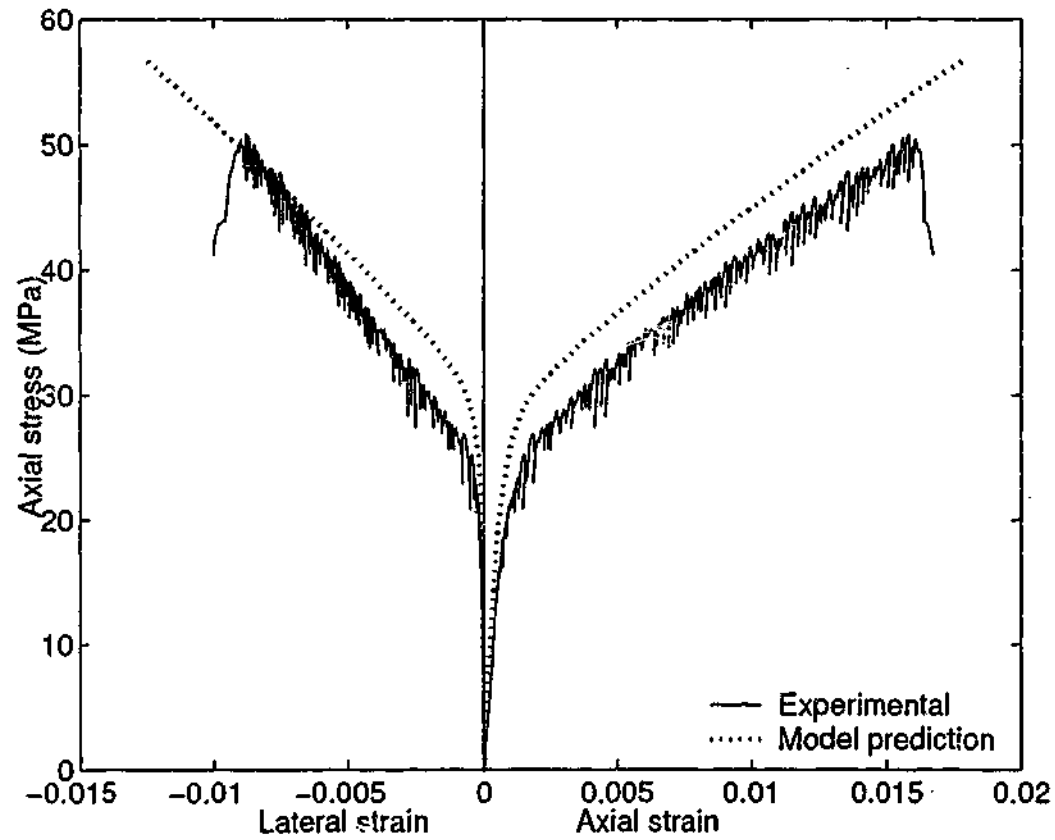


Figure 3.19: Stress-strain curves for Grade 30 concrete with 3 carbon fibre wraps.

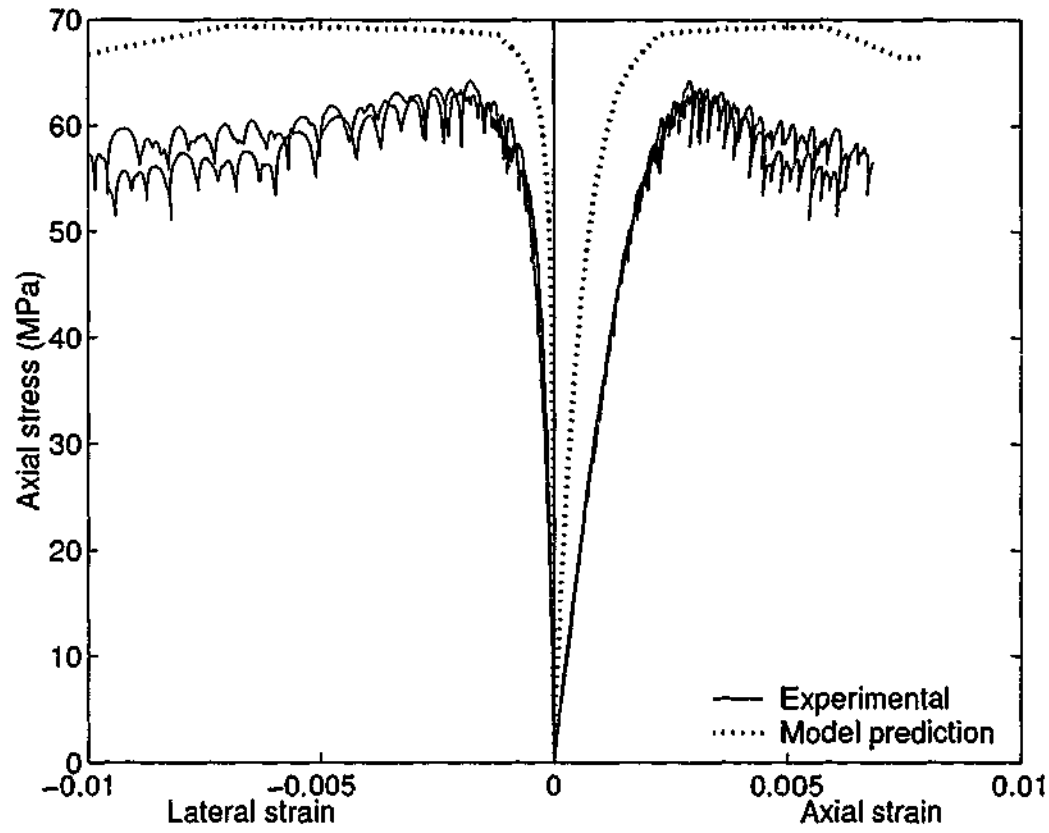


Figure 3.20: Stress-strain curves for Grade 60 concrete with 1 carbon fibre wrap.

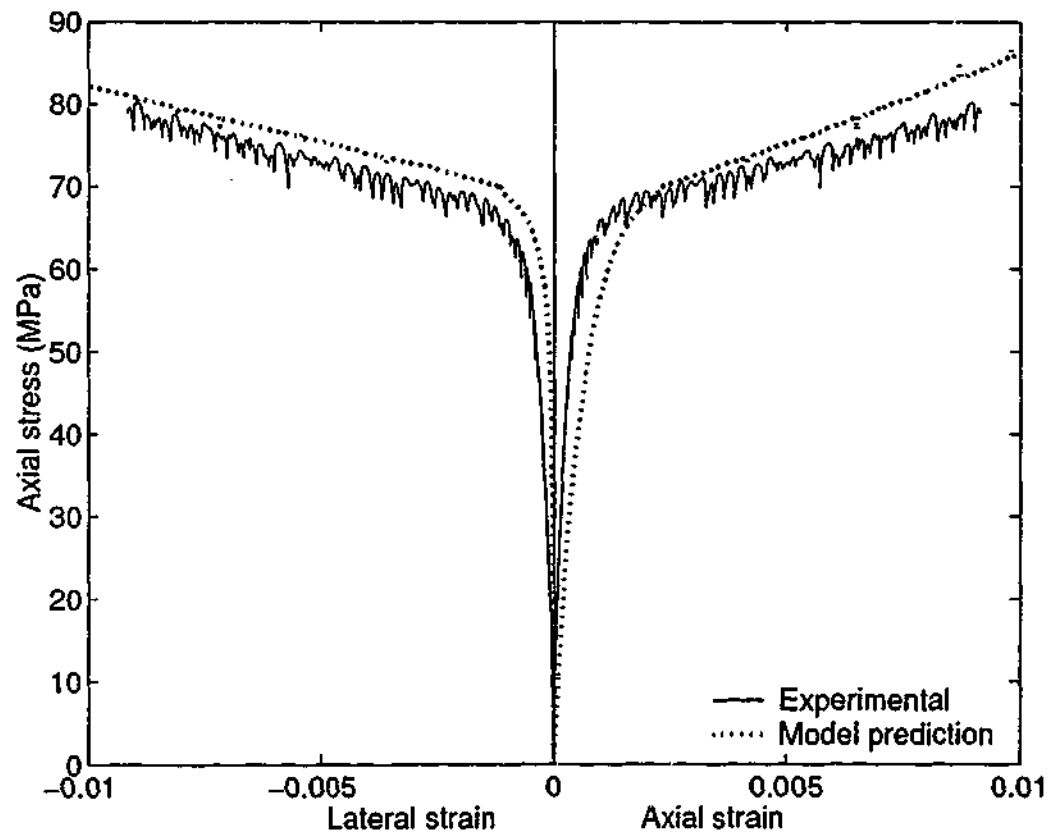


Figure 3.21: Stress-strain curves for Grade 60 concrete with 3 carbon fibre wraps.

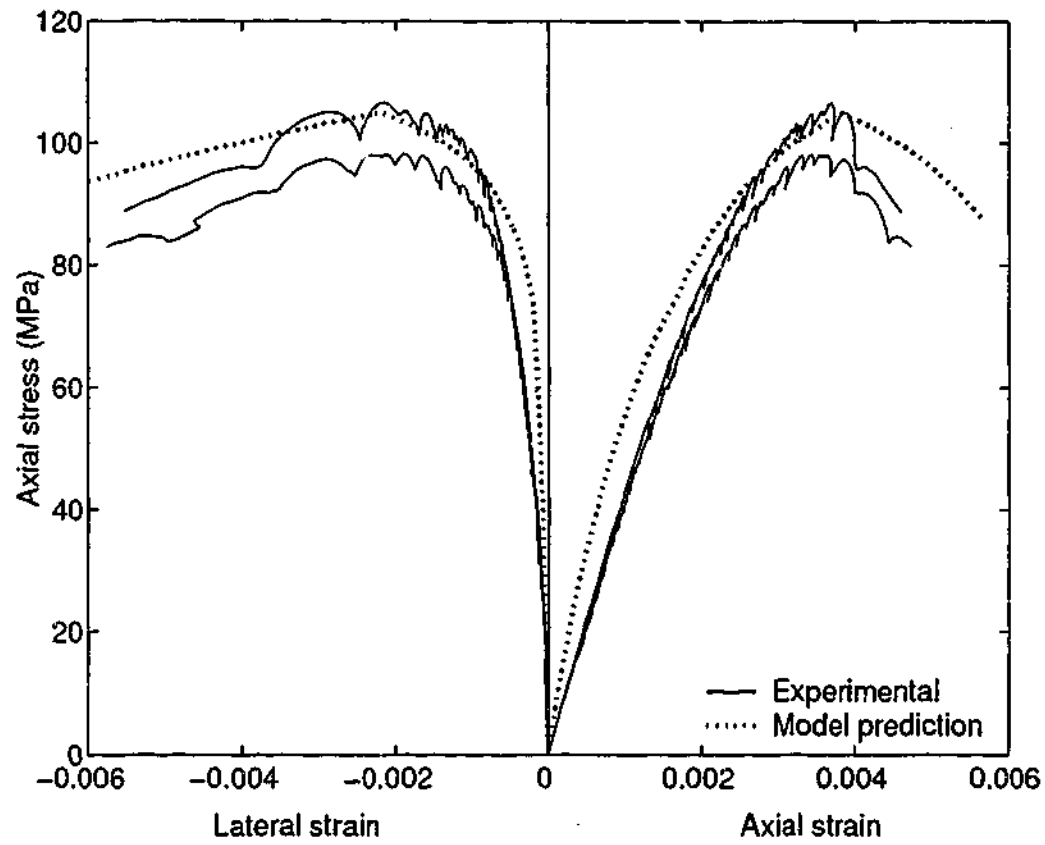


Figure 3.22: Stress-strain curves for Grade 100 concrete with 1 carbon fibre wrap.

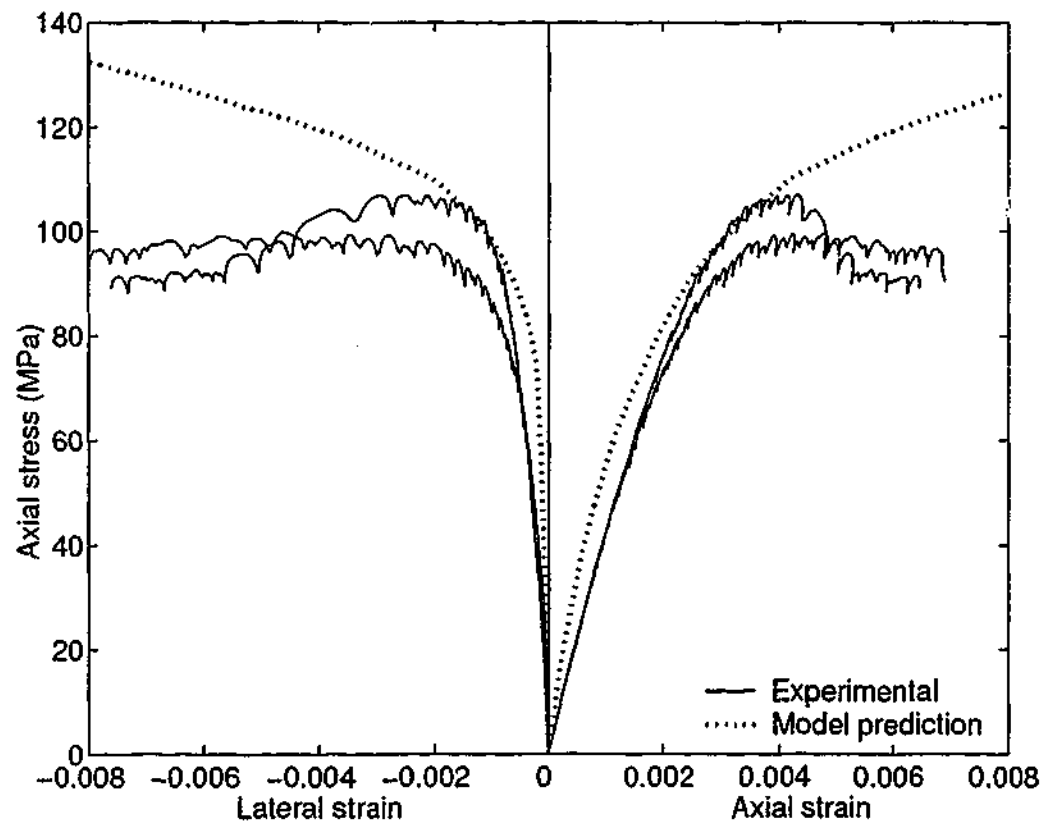


Figure 3.23: Stress-strain curves for Grade 100 concrete with 3 carbon fibre wraps.

Grade 60 and 100 concrete with 1 wrap (Figures 3.20 and 3.22). This behaviour is due to the linear behaviour (without any yield points) of carbon fibre composites. After the initial linearly elastic phase, steel displays a yielding plateau. Therefore after reaching the maximum stress corresponding to yielding, the confining pressure remains constant.

When high confining pressure is applied to HSC (100 MPa concrete with 3 carbon fibre wrap), there may be bond failure (bond between concrete and carbon fibre). However, in the model prediction it is assumed a perfect bond between concrete and carbon fibre. This may be the reason for the difference in model prediction and the experimental curve for 100 MPa concrete with 3 carbon fibre wraps (Figure 3.23). Apart from this, all the other specimens are in good agreement with the model predictions.

All three grades of concrete specimens show a ductility improvement with the increasing level of confinement.

Many researchers (Lorenzis 2001) have noted that the strain measured in the confining FRP at rupture is in many cases lower than the ultimate strain of FRP tested for tensile strength. The recorded hoop strains corresponding to rupture had a range of 50 to 80% of the failure strain obtained in the tensile tests (Xiao and Wu 2000). This phenomenon considerably affects the accuracy of the model.

3.8 Conclusions

The following conclusions can be drawn from the work reported in this chapter.

1. The proposed stress-strain model for confined concrete is summarised as shown in Figure 3.24.
2. Volumetric strain is close to zero at peak axial stress. Thus it can be concluded that the lateral strain at peak axial stress is half of axial strain at the same point (i.e. $\epsilon_2 = 0.5\epsilon_1$ when $\sigma_1 = f_{cc}$). ϵ_1 and ϵ_2 are axial and lateral strains, σ_1 is the axial stress and f_{cc} is the peak stress of confined concrete.
3. Volumetric strain reaches its maximum value at the axial strain, $q\epsilon_{cc}$, where parameter q is approximately 0.5 for 40 MPa and increases with increasing concrete strength to a value of 0.7 for 100 MPa.

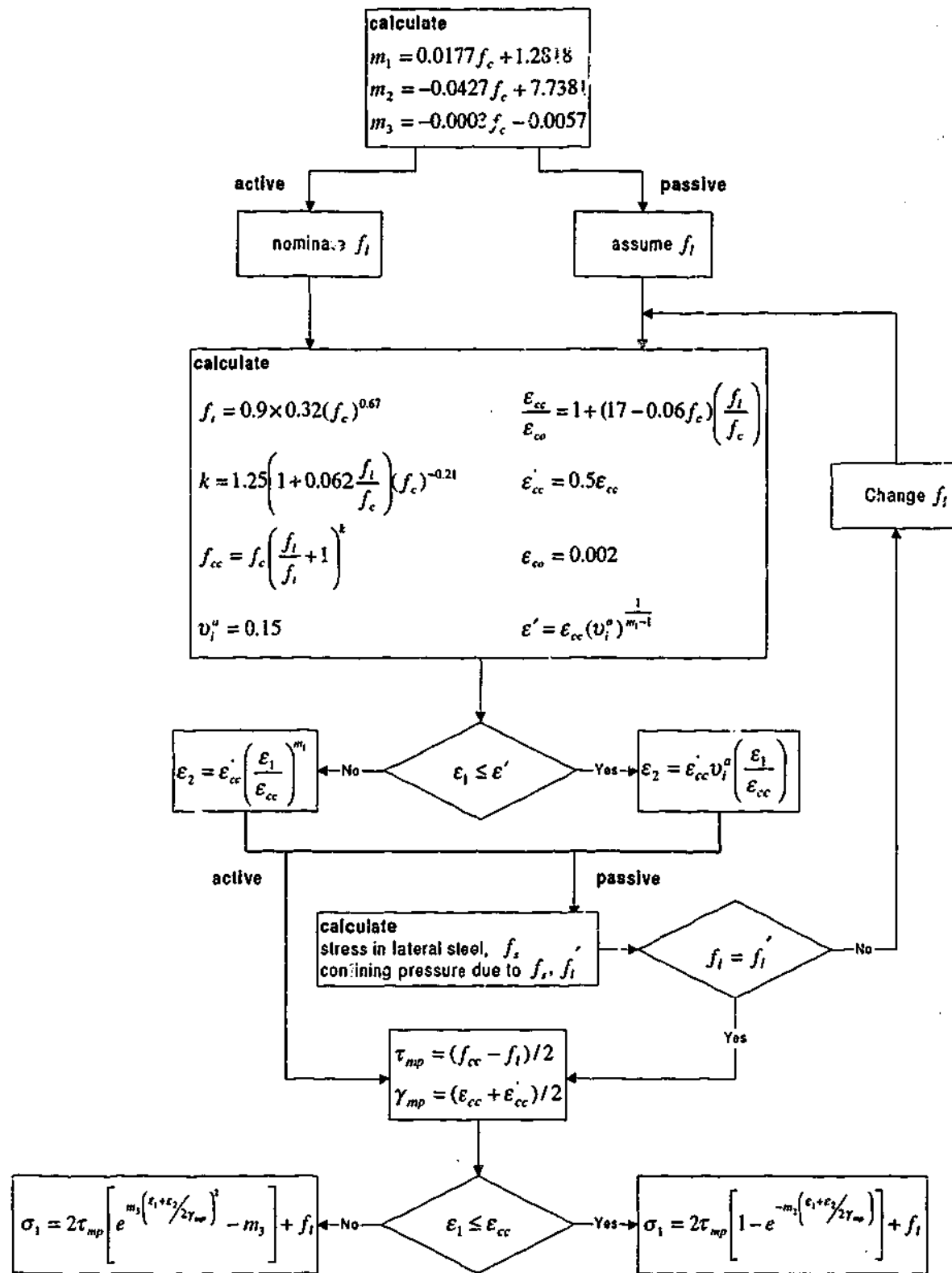


Figure 3.24: Procedure in drawing stress-strain curves for confined concrete (given ϵ_1 and f_c).

4. The proposed strain-based stress-strain model is a new approach in establishing the behaviour of confined HSC.
5. The constitutive model for confined concrete subjected to concentric monotonically increasing loading developed in this chapter is extended to establish the complete stress-strain curves for HSC with passive confinement. It is proven to be generally in close agreement with the experimental test results for concrete confined by carbon fibre wraps.

Chapter 4

MONOTONICALLY INCREASING LOADS:

Development of load-deformation characteristics of columns

4.1 Introduction

The analysis method for concrete columns subjected to concentric or eccentric axial loads can be found in standard text books (Warner et al. 1998). The standard method of column analysis does not explicitly take into account of the effect of confining reinforcement when the column is subjected to eccentric loading. This type of analysis is the subject of this chapter.

Based on the constitutive model for confined concrete subjected to monotonically increasing loading presented in Chapter 3, an analytical method is developed in this chapter for the behaviour of laterally confined concrete columns subjected to eccentric static loading. The method incorporates the effect of strain gradient on the lateral confining pressure exerted by transverse reinforcement. It includes modifications for coefficient of effectiveness. Analysis proposed here is verified using the experimental results reported in the literature for short columns (Attard and Foster 1995; Foster and Attard 1997; Saatcioglu et al. 1995) and for slender columns (Lloyd and Rangan 1995; Lloyd and Rangan 1996). Experimental results for normal, medium and high strength concrete were used. By including the effects of confinement, the analytical procedure described in this chapter provides a better tool for column analysis than the use of stress block for concrete under

a strain gradient.

The results presented in this chapter has been published in Lokuge et al. (2003d).

4.2 Previous work on eccentrically loaded columns

The experimental investigations on eccentrically loaded normal and high strength concrete columns can be divided into two broad categories. Some researchers (Attard and Foster 1995; Saatcioglu et al. 1995; Foster and Attard 1997; Xie et al. 1997) used short columns. With the use of HSC in building systems, the resulting reduction in column sizes leads to investigations of the slenderness effect on the column behaviour (Rangan 1991). As a result, a few researchers (Lloyd and Rangan 1996; Ibrahim and MacGregor 1996; Claeson and Gylltoft 1998) used full scale slender columns in analysing eccentrically loaded columns.

Saatcioglu et al. (1995) tested 12 NSC square short columns (25-35 MPa). They concluded that the strength and deformability of eccentrically loaded columns can be improved with the use of well-distributed longitudinal reinforcements and closely spaced lateral reinforcements. Foster and Attard (1997) tested 36 HSC square short columns (40-88 MPa). They argued that the ductility measurement for eccentrically loaded columns should be based on the applied load versus (average strain + curvature \times eccentricity) curves. They concluded that the experimental ultimate strength of HSC columns compared reasonably well with the predictions based on AS3600 (2001) rectangular stress block. Later Xie et al. (1997) presented a parametric study for 21 rectangular short concrete columns (37.5-75 MPa). The study was based on an elasto-plastic three dimensional finite element model. They concluded that the rectangular stress block in the ACI 318-89 Code overestimates the flexural strength of eccentrically loaded HSC columns.

Ibrahim and MacGregor (1996) reported test results for 20 high strength (60 to 90 MPa) and ultra high strength (115 to 130 MPa) concrete columns subjected to axial loads with small eccentricities. They investigated the behaviour of plain concrete using rectangular and triangular columns. They observed that the columns with triangular cross sections exhibited more ductile behaviour than those with rectangular cross sections. Xie et al. (1996) used 4 rectangular columns tested by Ibrahim and MacGregor (1996) in a finite element model comparison. Xie et al. (1996) concluded that well-confined concrete

columns showed a more ductile behaviour than the poorly-confined concrete columns.

Lloyd and Rangan (1995) tested 36 slender HSC columns (58-97 MPa) having rectangular and square cross sections under three different levels of axial load eccentricities. They concluded that increasing the level of eccentricity resulted in a decrease in the failure load. Furthermore, they observed that for columns with high load eccentricities, the lateral reinforcement was sufficient to provide some ductility whereas for columns with low load eccentricities, the lateral reinforcement was insufficient to provide a reasonable ductility.

Claeson and Gylltoft (1998) tested 12 full scale slender square confined HSC columns (43-93 MPa) under eccentric loading. They compared the test results with the analytical findings using a finite element analysis. They observed that an increase in eccentricity will result in a more rapid decrease in strength of HSC columns than that of NSC columns.

Samra et al. (1996) studied the available ductility of spirally confined reinforced concrete columns subjected to eccentric loading. Their analysis method used the stress-strain relationships proposed by Mander et al. (1988b) for confined concrete. Based on the analytical findings they emphasised the need to include the effect of eccentricity of the applied axial load in calculating the required amount of transverse reinforcement to provide sufficient level of ductility.

Although many research work have been reported in the literature about eccentric loading of confined concrete columns, there exists a controversial issue about the effect of strain gradient. One group of researchers (Hognestad et al. 1955, Karsan and Jirsa 1970) has shown that the use of stress-strain models developed for columns loaded in concentric compression can be used to model the behaviour of eccentrically loaded columns. However, Sargin et al. (1971) observed that the stress-strain relationship of concrete under a strain gradient is different to that of uniform compression. They developed stress-strain models specifically for the flexural stress block under a strain gradient.

Saatcioglu et al. (1995) noted the effect of strain gradient in the section on the confinement provided by the lateral steel, which in turn affects the concrete stress at a given section. Their model is described here in detail.

4.2.1 Analytical model used by Saatcioglu et al. (1995)

Saatcioglu et al. (1995) used the confined concrete model proposed by Saatcioglu and Razvi (1992) for concentric loading as shown in Figure 4.1. The axial stress in the as-

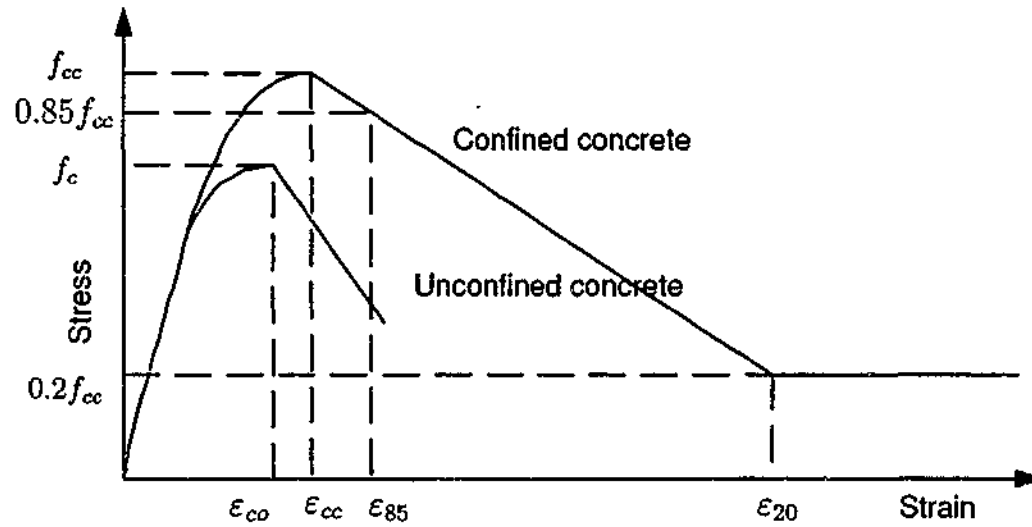


Figure 4.1: Confined concrete model proposed by Saatcioglu and Razvi (1992).

cending branch is given by,

$$\sigma_1 = f_{cc} \left[2 \left(\frac{\epsilon_1}{\epsilon_{cc}} \right) - \left(\frac{\epsilon_1}{\epsilon_{cc}} \right)^2 \right]^{1/(1+2K)} \quad (4.1)$$

where, ϵ_{cc} is the axial strain corresponding to peak stress of confined concrete, σ_1 is the axial stress and ϵ_1 is the axial strain. f_{cc} is the peak stress of confined concrete.

$$f_{cc} = f_c + k_1 f_{le} \quad (4.2)$$

f_c is the uniaxial strength of concrete and k_1 is a parameter defined as,

$$k_1 = 6.7(f_{le})^{-0.17} \quad (4.3)$$

f_{le} is the equivalent uniform pressure,

$$f_{le} = k_2 f_l \quad (4.4)$$

where, f_l is the average pressure and k_2 is a parameter defined as,

$$k_2 = 0.26 \sqrt{\left(\frac{d_s}{s} \right) \left(\frac{d_s}{s_l} \right) \left(\frac{1}{f_l} \right)} \leq 1.0 \quad (4.5)$$

s is the spacing of the lateral reinforcement in longitudinal direction, s_l is the spacing of the longitudinal reinforcement and d_s is the core dimension measured centre-to-centre of the perimeter hoops. Average pressure (f_l) is defined as,

$$f_l = \frac{\sum A_s f_{sy} \sin \alpha}{s d_s} \quad (4.6)$$

where, α is the angle between the leg of transverse reinforcement and the column side crossed by the same leg, A_s is the area of one leg of the lateral reinforcement and f_{sy} is the yield strength of lateral reinforcement. The axial strain corresponding to peak axial stress is defined as,

$$\epsilon_{cc} = \epsilon_{co}(1 + 5K); \quad K = \frac{k_1 f_{le}}{f_c} \quad (4.7)$$

where, ϵ_{co} is the axial strain corresponding to uniaxial strength of concrete.

The descending branch is defined using the axial strain corresponding to axial stress of 85% of peak stress (f_{cc}).

$$\epsilon_{85} = 260\rho\epsilon_{cc} + \epsilon_{085}; \quad \rho = \frac{\sum A_s}{s(d_{sx} + d_{sy})} \quad (4.8)$$

d_{sx} and d_{sy} are core dimensions in x and y directions respectively.

The effect of strain gradient was incorporated into this model by using an equivalent uniform pressure (f_{le}) and average pressure (f_l). However, by arguing that the difference in confining pressures does not affect the behaviour of the column considerably, Saatcioglu et al. (1995) used an average confining pressure in establishing the stress-strain behaviour of concrete (Figure 4.2).

Each of the empirical formula recommended by different researchers was based on a particular series of tests. The applicability of these formulas to a general case is often not well established. Therefore in this chapter, an analytically based method is proposed for the estimation of the behaviour of columns subjected to eccentrically loads. The methodology incorporates the effect of strain gradient.

4.3 Experimental program

The results from the model proposed in this chapter are compared with the experimental results for short HSC columns (Foster and Attard 1997), short NSC columns (Saatcioglu et al. 1995) as well as slender HSC columns (Lloyd and Rangan 1995). The details of each of the experimental program are presented here.

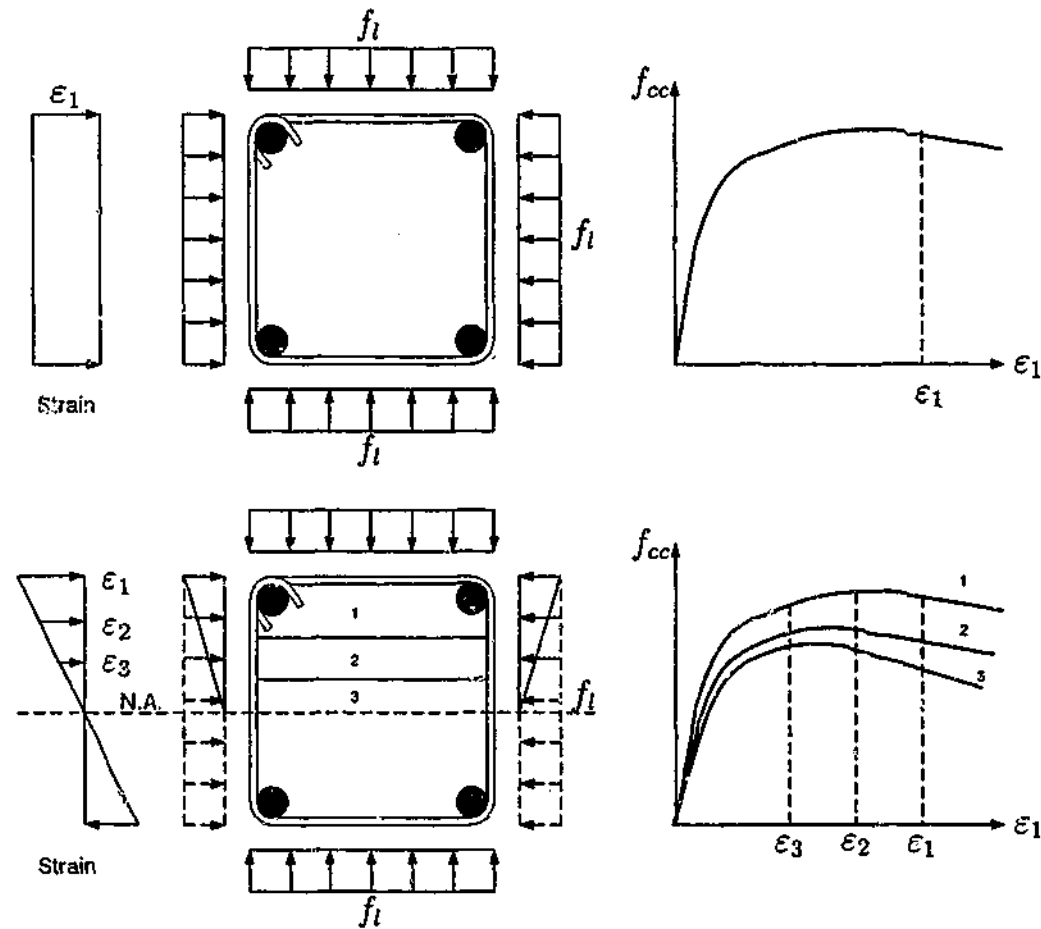


Figure 4.2: Lateral pressure and the strain gradient (Saatcioglu et al. 1995).

4.3.1 Short column tests

Foster and Attard (1997) reports investigation of 68 end-haunched square columns (150 mm). But the detailed research report shows curves for only 50 columns. The specimens were categorised as “L”, “M” and “H” (low, medium and high strength) according to the strength at the time of testing. In their study, strengths in the range 40 to 56 MPa was considered as low strength, 75 MPa as medium strength and 90 MPa as HSC. However in the study reported in this thesis, compressive strengths over 50 MPa are considered as HSC. Therefore almost all “Medium-strength” and “High-strength” series and some of “Low-strength” series of Foster and Attard (1997) study are considered to be HSC columns in this study. Designated name for each specimen relates to the strength, reinforcement arrangement, eccentricity and the spacing of lateral reinforcement. For example, specimen 2M20-60 has 2% longitudinal reinforcement, medium strength concrete, an eccentricity of 20 mm and a centre-to-centre tie spacing of 60 mm. The dimensions and details of the reinforcement arrangements for the tested columns are given in Table 4.1 and Figure 4.3.

Table 4.1: Details of column specimens (Foster and Attard 1995).

Specimen	f_c (MPa)	Cover (mm)	A in Fig.4.3 (mm)	Eccentricity at peak load (mm)	Tie reinforcement
2L20-30	40	10	101	24.8	R6-1
2L20-60	43	12	97	26.2	R6-1
2L50-30	40	12	97	59	R6-1
2L50-120	40	14	93	59	R6-1
4L8-60	43	9	102	14	R6-1
4L20-120R	53	13	95	26	R6-2
4L50-60	40	9	102	58	R6-1
2M20-30	74	10	100	26	R6-1
2M50-30	74	11	98	59.5	R6-1
2M50-120R	73	10	100	63.2	R6-1
4M50-30	74	18	85	59.5	R6-2
4H50-30	88	11	99	60.5	R6-1

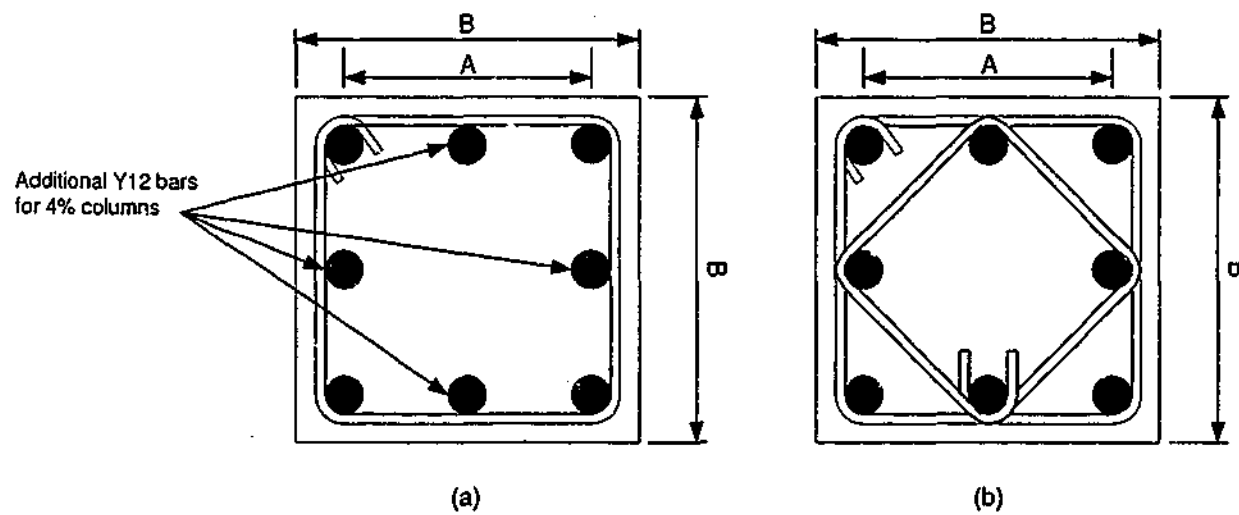


Figure 4.3: Details of column specimens.

Dimension B was 150 mm in Foster and Attard (1997) study. Dimension A for each specimen is given in Table 4.1. A number of low and medium strength columns were tested in a Baldwin 2000 kN displacement controlled testing machine. It was observed that testing machine did not have the stiffness required to obtain the descending curve for medium strength concrete. Therefore testing was later moved onto fabricated stiff testing frame. Loading was either stopped or decreased to make sure the lateral displacement stability. By doing this, it was possible to obtain the descending branches for a number of the medium strength and some of the high strength columns. A very slow loading rate was used.

Saatcioglu et al. (1995) conducted an experimental program for 12 square columns (210 mm) with two different levels of end eccentricities, 60 and 75 mm and two different spacings, 50 and 100 mm. The tested specimens had compressive strengths in the range of 25-35 MPa. Details of the specimens are given in Table 4.2 and Figure 4.3 (a) and (b). Dimension B was 210 mm in their study. Cover and dimension A for all the specimens were 12.5 mm and 160 mm respectively. Columns were tested in a Tinius Olson universal testing machine. Monotonically increasing compression was used at a constant end eccentricity. Experiment was terminated when a significant strength decay was reported indicating failure. They compared experimental observations with their analytical findings, in which the effect of strain gradient was included.

Table 4.2: Details of column specimens (Saatcioglu et al. 1995).

Specimen	f_c (MPa)	Tie reinforcement	Spacing (mm)	End eccentricity (mm)
C4-2	35	Fig.4.3(a)	50	75
C5-2	35	Fig.4.3(b)	50	75
C8-1	25.3	Fig.4.3(b)	100	60
C10-2	27.4	Fig.4.3(a)	100	75

In this study, the experimental results presented by Foster and Attard (1997) were selected for comparison with the model predictions, because they tested HSC columns and reported lateral strains in concrete as well. No other column tests reported lateral displacements. Therefore by selecting the experiments carried out by Foster and Attard (1997), experimental lateral strains could be compared with the lateral strains estimated.

Further, the report obtained by the author from Foster and Attard (1997) had complete information about the results, compared to other published papers which only had condensed and limited information.

Low strength concrete columns tested by Saatcioglu et al. (1995) were also compared with the analytical procedure proposed in this study.

The analytical method developed by Saatcioglu et al. (1995) and presented in Section 4.2.1 for eccentrically loaded short columns, is also utilised to compare the experimental results of Foster and Attard (1997) and Saatcioglu et al. (1995).

4.3.2 Slender column tests

Lloyd and Rangan (1996) tested slender concrete columns subjected to eccentric loads. HSC was used in the tested columns. Detailed information about the experimental results in a research report (Lloyd and Rangan 1995) was made available. Therefore, in order to extend the model comparisons for slender concrete columns, the experimental results reported by Lloyd and Rangan (1996) were used.

Lloyd and Rangan (1996) tested 36 eccentrically loaded slender columns. Twelve test series were considered in their experimental program. Column cross sections and the reinforcement configuration were the test variables in each test series. Each series had 3 specimens differing from one another only by the eccentricity. Column cross sections were either 175×175 mm or 300×100 mm. The spacing of the lateral steel was 60 mm for all specimens. Three different levels of eccentricities 15, 50 and 65 mm were used. The tested specimens had compressive strengths in the range 58-97 MPa. From the 36 test results, only square columns have been selected in this study. Details of the specimens are given in Table 4.3 and Figure 4.4 (a) and (b).

Dimension B was 175 mm in their study. Cover and dimension A for all the specimens were 12.5 mm and 160 mm respectively. These columns were loaded at a rate of 350 N/min until failure. Load and the mid-height deflection were recorded for each tested specimen. The effective length of the columns used in the analysis was 1680 mm.

Table 4.3: Details of column specimens (Lloyd and Rangan 1995).

Specimen	f_c (MPa)	Tie reinforcement	Eccentricity (mm)
VA	92	Fig.4.4(a)	15
VB	92	Fig.4.4(a)	50
VC	92	Fig.4.4(a)	65
VIIA	92	Fig.4.4(b)	15
VIIB	92	Fig.4.4(b)	50
VIIC	92	Fig.4.4(b)	65
XIA	97	Fig.4.4(b)	15
XIB	97	Fig.4.4(b)	50
XIC	97	Fig.4.4(b)	65

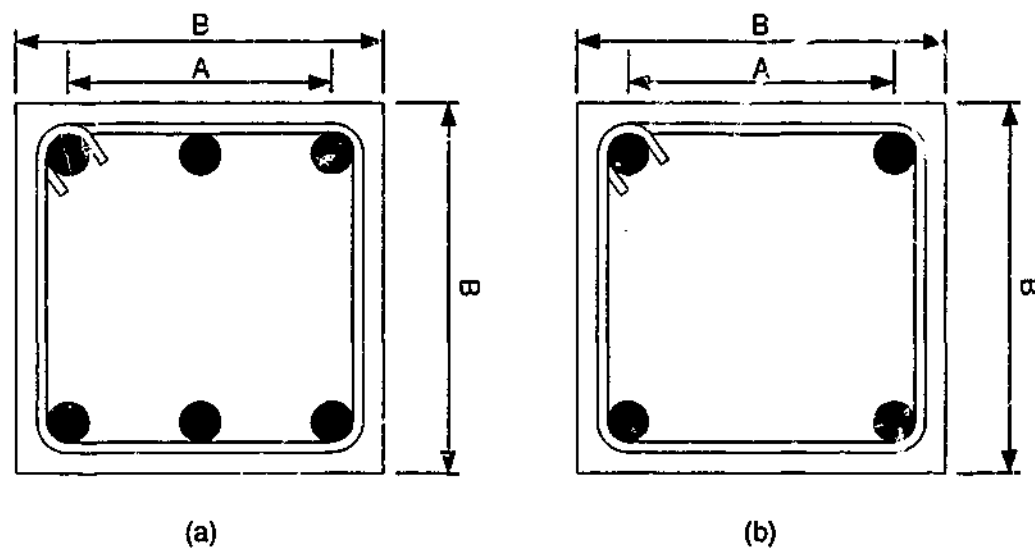


Figure 4.4: Details of column specimens (Lloyd and Rangan 1995).

4.4 Stress-strain model for concrete

The constitutive model for HSC under monotonically increasing load, developed by the author and presented in the previous chapter is utilised to establish the behaviour of columns under eccentric loading.

4.4.1 Cover concrete

In analytical modelling of column behaviour, treatment of cover concrete needs careful consideration. If the uniaxial stress-strain curve for HSC is used, cover concrete ceases to be effective after the peak stress in uniaxial compression. Tests on conventional strength concrete columns by Sheikh and Uzumeri (1980) suggest that the cover continues to carry

some load even after the peak compressive stress is attained. Experimental studies on HSC columns by Cusson and Paultre (1995) suggest that cover spalls suddenly with about 10-15% loss in the peak load. Candappa (2000) incorporated the effect of cover concrete carrying some load after spalling in his model. Recently Liu et al. (2000) conducted an experimental program giving particular emphasis to the issue of early spalling of the concrete cover. Their study showed that the longitudinal reinforcement yielded at the spalling load and further induce cover spalling due to circumferential expansion of the bars. But at the time of cover spalling, they found that the confining reinforcement had not yielded. After cover spalled off, micro cracking of the core leads to expansion of the core and activation of the confinement provided by the transverse ties. It will reach a second peak load when the tie or spiral steel yields which incurs the maximum confining pressure application to the core concrete. Figure 4.5 shows the mechanics of cover spalling. Foster et al. (1998) showed that cracking occurs at the cover-core interface as a result of the triaxial stress condition due to the confinement of the core. They further showed that the interface cracking occurs regardless of the concrete strength.

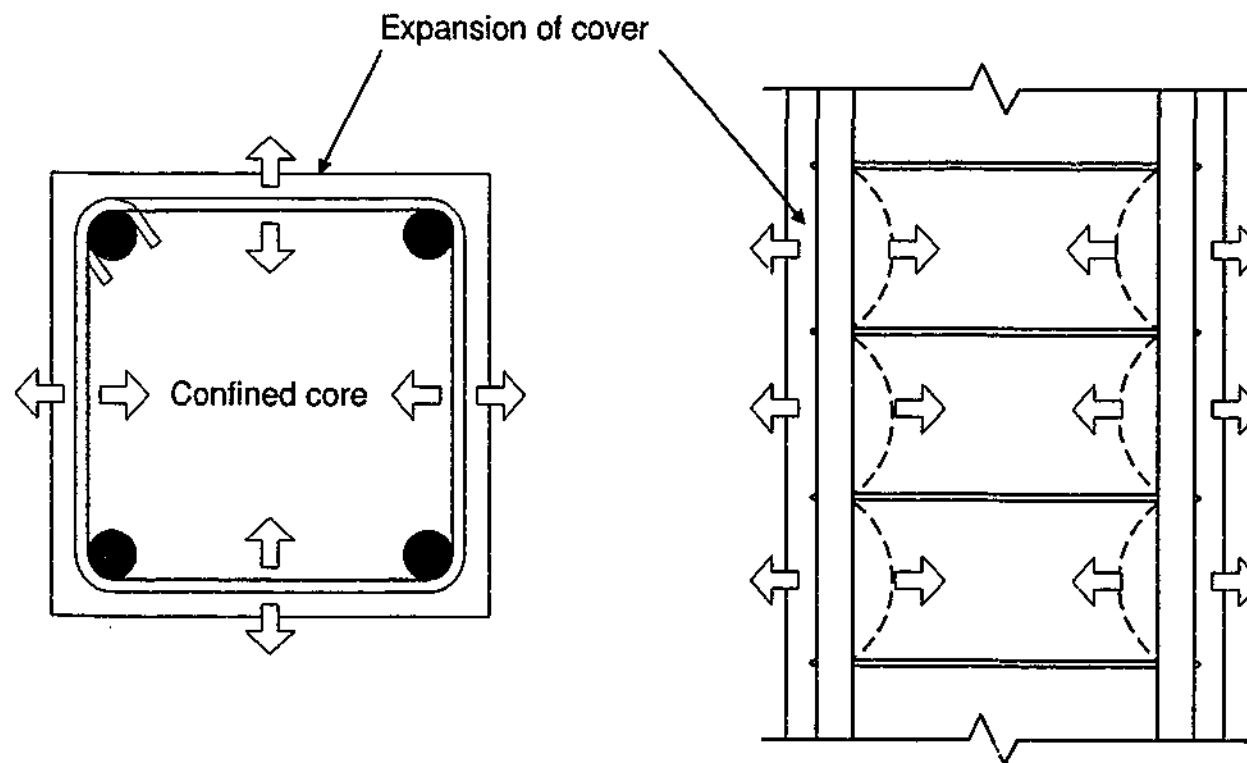


Figure 4.5: Mechanics of cover spalling.

4.4.2 Effective lateral confining pressure

After the cover concrete spalls off, the confining restraint provided by the ties is activated. With the increasing load, this confining pressure increases gradually upto a maximum value, which corresponds to the yielding of the ties. As shown by many researchers in the literature (Sheikh and Yeh 1992; Mander et al. 1988b; Cusson and Paultre 1995), confining pressure provided by the ties dissipates between the longitudinal bars in the plane of cross section of the specimen and between the ties in the longitudinal direction. As a result, only a portion of the core area is effectively confined. Therefore,

$$A_{eff} = k_e A_{core} \quad (4.9)$$

where A_{eff} is effectively confined core area, k_e is coefficient of effectiveness, $k_e \leq 1$ and A_{core} is the area of core (normally defined as the area enclosed by the perimeter of the centreline of ties). The effective confining pressure f_{le} is given by,

$$f_{le} = k_e f_l \quad (4.10)$$

where f_l is the lateral pressure from lateral reinforcement assuming uniform distribution over the surface of the concrete core.

There have been different definitions for coefficient of effectiveness (k_e) reported in literature. Confining pressure distribution is assumed to be a parabolic arch between the longitudinal bars as well as between the transverse ties, with initial tangent at 45° . For a square column, coefficient of effectiveness at the tie level (k_{e1}) can be expressed as,

$$k_{e1} = 1 - \frac{\sum_{i=1}^n w_i^2}{6d_s^2} - \frac{A_{st}}{d_s^2} \quad (4.11)$$

where w_i is the i^{th} clear distance between longitudinal bars, n is the number of longitudinal bars, d_s is versus distance between the transverse ties and A_{st} is cross-sectional area of total longitudinal steel. Coefficient of effectiveness is at its minimum at the tie level; then it gradually increases in the longitudinal direction upto the midway between ties (Figure 4.6). Coefficient of effectiveness midway between transverse ties (k_{e2}) can be expressed as,

$$k_{e2} = \left(1 - \frac{s'}{2d_s}\right)^2 \quad (4.12)$$

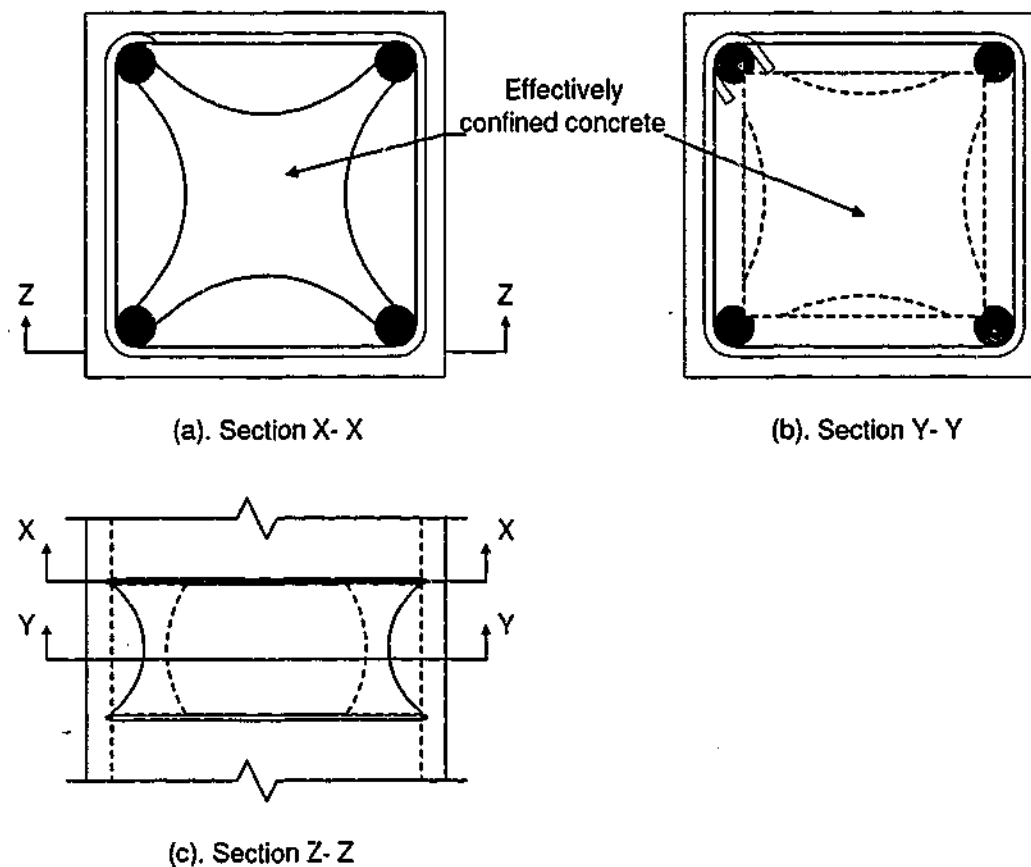


Figure 4.6: Effectively confined core area of a square column.

where s' is the clear spacing between ties. k_{e2} is at its minimum at midway between the ties; then it gradually increases in the longitudinal direction towards the tie level.

Different suggestions are reported in the literature for the effectiveness in confining concrete, which will dominate the strength of the concrete column after spalling. Following the concept proposed by Sheikh and Uzumeri (1982), researchers have proposed expressions for confining effect which are similar to Equations (4.11) and (4.12) (Cusson and Paultre 1995; Assa and Nishiyama 1998) or a combination of those two equations (Mander et al. 1988b; Cusson and Paultre 1995; Foster et al. 1998). Attard and Foster (1995) suggested that confining pressure would be dominated by the larger of the values given by Equations (4.11) and (4.12). It is proposed that confining effect will be governed by either the spacing and number of longitudinal bars or the spacing of the transverse ties.

Considering the equilibrium of half of the spiral or tie, the confining pressure exerted by the reinforcement at yield is given by,

$$f_l = \frac{2f_{sy}A_s}{sd_s} \quad (4.13)$$

where A_s is the cross sectional area of one lateral reinforcement, s is the clear vertical distance between the steel reinforcement, d_s is the diameter of the circular hoop or versus distance of the steel reinforcement in square columns and f_{sy} is the yield strength of reinforcement.

Mander et al. (1988a) reported that configuration of the transverse reinforcement has an effect on the confinement effectiveness coefficient. It varies in the range of 0.4-0.7 for the rectangular walls and 0.89-1.0 for circular columns. Confining pressures for some common configurations are shown in Figure 4.7. There are several exceptions to the normally used equation for calculation of confining pressure (Equation 4.13).

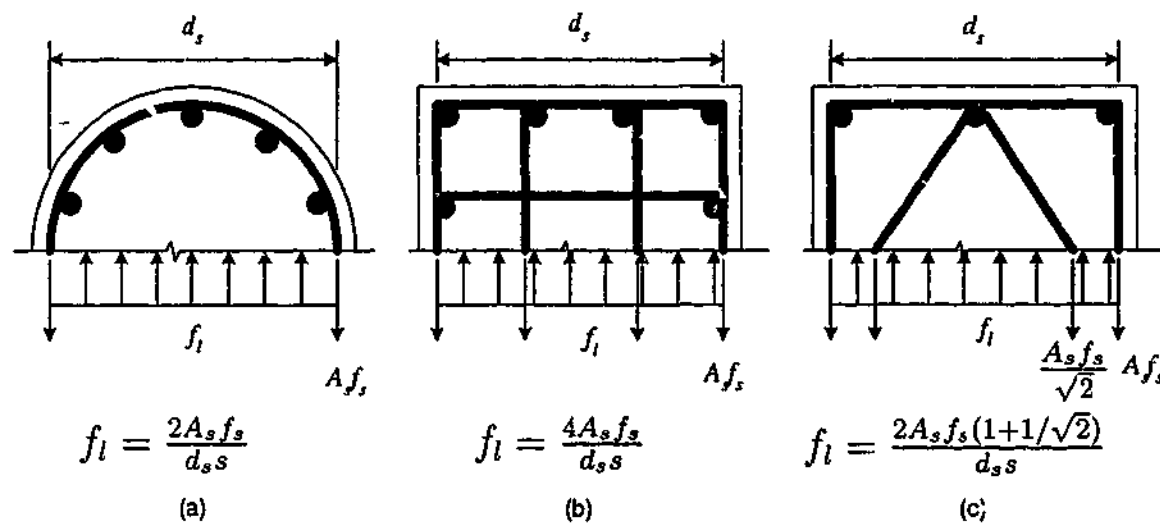


Figure 4.7: Confining pressures for some common configurations.

Assa and Nishiyama (1998b) defined the confining effect of the transverse reinforcement in a different way as follows:

$$f_l = \frac{\rho_s f_{sy}}{f_{cc}} \left(-0.7 \frac{s}{b} \right) k_e k_n. \quad (4.14)$$

ρ_s is the volumetric ratio of transverse reinforcement, s is the spacing of transverse reinforcement measured from versus, b is the least dimension of cross section, f_{sy} is the yield strength of transverse reinforcement and k_e and k_n are the confinement effectiveness factors. k_e represents the configuration of transverse and longitudinal reinforcements.

$$k_e = 1 - \frac{\sum_{i=1}^n w_i^2}{6d_s^2} \quad (4.15)$$

w_i is the i^{th} clear distance between longitudinal bars, n is the number of longitudinal bars and d_s is versus distance between the transverse ties. k_n represents the confinement

effectiveness due to the presence of strain gradient along the section depth. The coefficient is related to the applied axial load (N) and is given by,

$$k_n = \left(0.2 + 0.8 \frac{N}{f_{cc} d_s^2} \right). \quad (4.16)$$

k_n ranges from 0.2 for beams and 1.0 for columns with concentric axial compression.

Martirosyan and Xiao (2001) defined the confining pressure as,

$$f_l = \rho_s f_{yeff}. \quad (4.17)$$

ρ_s is the lateral reinforcement ratio defined as,

$$\rho_s = \frac{n_3 A_s}{d_s s} \quad (4.18)$$

where A_s is the area of one leg of lateral reinforcement, d_s is the diameter of the perimeter hoops, n_3 is the number of lateral reinforcement legs in the vertical cross section in spacing s and f_{yeff} is the effective stress of confining steel at maximum compressive strength of HSC column.

$$f_{yeff} = \min(f_{sy}, f_{ye}). \quad (4.19)$$

f_{sy} is the yield strength of lateral reinforcement. f_{ye} is calculated as follows:

$$f_{ye} = 80 \times \left(\frac{1}{\rho_s} \times \frac{f_{sy}}{f_c} \right)^{0.26}. \quad (4.20)$$

This confining pressure calculation is contrary to the conventionally accepted approach that the confining pressure at peak strength is related to the steel yield strength.

There will be no confining effect in the ascending branch of the load-curvature curve ($k_e = 1$) and it will be activated after spalling. In the descending branch of the curve, there will be a point where the transverse steel yields ($k_e = k_e^*$). Beyond that point in the descending branch, there will be a uniform confining pressure applied by the transverse steel. Between spalling and the time of yielding of transverse steel, coefficient of effectiveness is assumed to be varying between 1 and k_e^* . In this study it was decided that smaller of the values given by Equations (4.11) and (4.12) will give the most suitable indication of the confinement effectiveness.

4.4.3 Effect of strain gradient

Effect of strain gradient has to be included in the stress-strain model for confined concrete columns as it is basically developed based on the tests on concentrically loaded columns. If the cross section of the column is divided into a number of slices, the lateral strain in each slice is varied when there is a strain gradient (Figure 4.8).

For a particular axial strain distribution, the lateral strains in each slice can be calculated using the constitutive model for concrete. Using the summation of the original and final lengths of all the strips (Figure 4.8), the average strain in transverse reinforcement can be estimated. The corresponding confining pressure exerted by the ties is then calculated using the stress-strain curve for steel. Confining pressure increases with the increasing lateral dilation of concrete and reaches a maximum corresponding to the yield of transverse reinforcement.

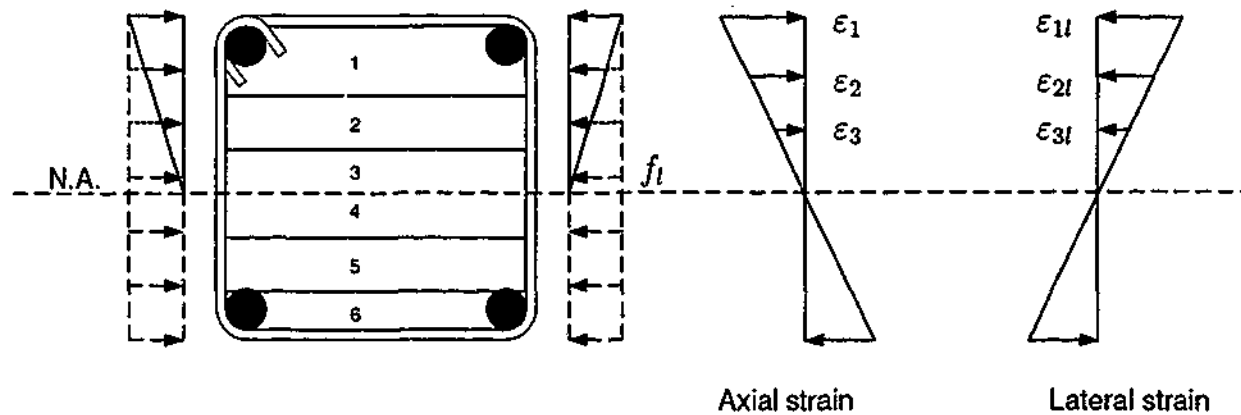


Figure 4.8: Lateral confining pressure.

4.5 Stress-strain model for steel

Poh (1997) has defined the relationship between steel stress (f_s) and steel strain (ϵ_s) as,

$$f_s = \frac{(E_{st} - E_p)\epsilon_s}{\left(1 + \left|\frac{(E_{st} - E_p)\epsilon_s}{\sigma_0}\right|^{m_1}\right)^{\frac{1}{m}}} + E_p\epsilon_s \quad (4.21)$$

where, E_{st} is modulus of elasticity of steel, E_p is plastic modulus, σ_0 is a reference plastic stress and m_1 is the shape parameter of the stress-strain curve. When establishing the load-curvature curves of Attard and Foster (1995) and Saatcioglu et al. (1995), these

parameters are changed in order to get the same experimental stress-strain curves for steel obtained by each of them.

Lloyd and Rangan (1995) assumed an idealised elasto-plastic stress-strain relationship for steel as follows:

$$f_s = \begin{cases} E_{st}\epsilon_s & \text{if } 0 \leq \epsilon_s \leq \epsilon_y, \\ f_{sy} & \text{if } \epsilon_s > \epsilon_y \end{cases} \quad (4.22)$$

where f_s is the steel stress, ϵ_s is the steel strain, E_{st} is the modulus of elasticity of steel, f_{sy} is the yield strength of steel and ϵ_y is the corresponding steel strain.

4.6 Load-deformation analysis

Load-deformation relations for square columns subjected to combined axial load and flexure are obtained assuming that the plane sections remain plane after bending. Perfect bond between the longitudinal steel and the concrete is assumed. Thus it is possible to get the strain of the longitudinal steel as that of the surrounding concrete at the same distance from the neutral axis. In the tensile zone of the cross section, it is assumed that only tension steel resists the tensile forces and concrete does not resist any tensile force. The stress-strain relationship for concrete is assumed to be as described in Chapter 3. Equations (4.21) and (4.22) are used for the stress-strain curve for steel.

The cross section is discretised into a number of slices. Each slice is composed of either cover concrete only or cover and core concrete. With the assigned strain distribution, which is defined by curvature (ϕ_m) and strain in extreme compression side (ϵ_t), stresses in cover concrete in each slice and in each layer of reinforcement are calculated using corresponding stress-strain curves. Stress calculation in core concrete requires the estimation of the confining pressure exerted by the lateral reinforcement due to lateral dilation of concrete. Method described in Section 4.4.3 is adopted in doing this. Therefore stress in core concrete is calculated using this confining pressure in the stress-strain curve for confined concrete.

In order to calculate points on the load-curvature curve (P_m, ϕ_m) for a specified eccentricity (e^*), the strain on the extreme compression side is iterated to satisfy the condition, $|e_{specified}(e^*) - e_{calculated}| \leq \text{tolerance}$. The procedure used in establishing moment-curvature relationships is summarised in Figure 4.9.

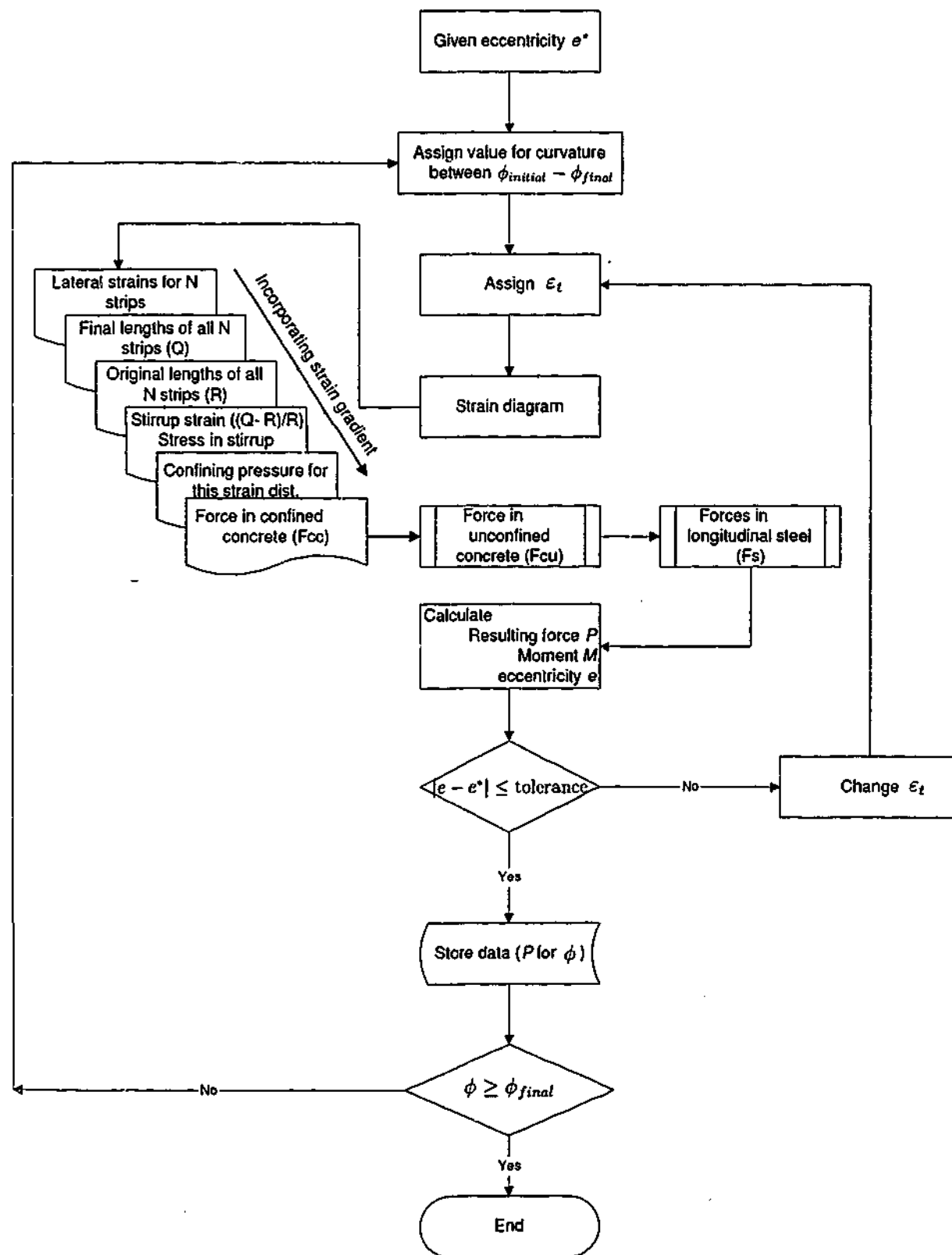


Figure 4.9: Procedure used in drawing moment-curvature curves for laterally confined concrete.

According to the experiments carried out by Attard and Foster (1995), eccentricity at peak load is always higher than initial eccentricity (Table 4.1). This happened due to the lateral deflections of the specimens near failure. Therefore in the analysis of the columns reported by them it is assumed that eccentricity varies linearly from the initial eccentricity to the eccentricity at peak load and then remains constant. In both the column test series conducted by Saatcioglu et al. (1995) and Lloyd and Rangan (1995), the specified level of eccentricity was maintained throughout the experiments.

4.6.1 Ductility measurement

Ductility of the columns tested by Attard and Foster (1995) were evaluated using the two definitions given below.

1. Commonly used definition for ductility factor is the ratio of curvature corresponding to 80% of the moment capacity on the descending portion of the moment-curvature curve and the curvature corresponding to 80% of moment capacity on the ascending portion of the moment-curvature curve. It is described in Section 2.2.2 in Chapter 2.
2. Foster and Attard (1997) suggested a definition for combined ductility ratio by considering the work done by a force applied at an eccentricity. It used P versus ξ curve (Figure 4.10). P is the load applied and ξ is (average strain (ϵ_{av}) + curvature \times eccentricity). ϵ_{av} is the average strain at the centroid of the section. Combined ductility ratio (D_c) (Figures 4.10) is defined as,

$$D_c = \frac{\xi_u}{\xi_y} \quad (4.23)$$

where, ξ_u is the combined strain at the ultimate point which is defined as the point in the descending branch of the curve in which the load is equal to 85% of the peak load. ξ_y is defined by the 3/4 rule as shown in Figure 4.10.

4.6.2 Analysis of slender columns

An equivalent standard pin-ended column as shown in Figure 4.11 can be used in analysing slender concrete columns (Lloyd and Rangan 1995). The procedure used to obtain the

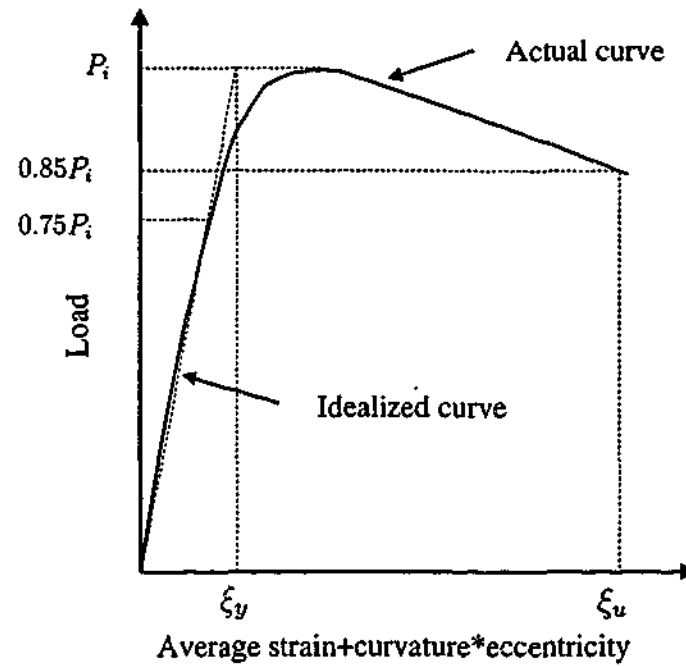


Figure 4.10: Combined ductility ratio in eccentrically loaded column.

mid-height deflection is the one reported by Rangan (1990). It is described here in detail.

The moment at mid-height of the column, M is,

$$M = P(e + \delta) \quad (4.24)$$

where δ is the mid-height deflection of the column and e is the eccentricity of the applied load, P . In order to use the procedure explained earlier in this section (Figure 4.9), it is necessary to find the mid-height deflection. In doing that, the deflected shape, $v(x)$ is assumed to be represented by a sine function as follows:

$$v(x) = \delta \sin \left(\frac{x\pi}{L_e} \right) \quad (4.25)$$

where, L_e is the effective length of the column. Thus the curvature is given by,

$$\begin{aligned} \phi(x) &= \frac{d^2v}{dx^2} \\ &= \frac{\pi^2}{L_e^2} \delta \sin \left(\frac{x\pi}{L_e} \right). \end{aligned} \quad (4.26)$$

At mid-height, $x = L_e/2$. Therefore,

$$\phi \left(\frac{L_e}{2} \right) = \frac{\pi^2}{L_e^2} \delta. \quad (4.27)$$

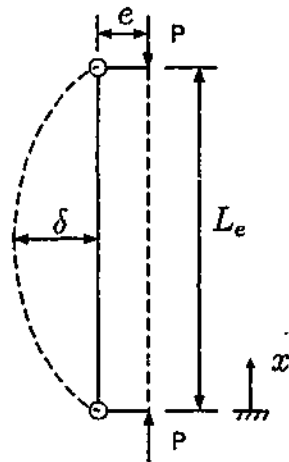


Figure 4.11: Standard pin-ended column (Lloyd and Rangan 1995).

Mid-height deflection, δ obtained from Equation (4.27) can thus be substituted in Equation (4.24) to calculate e , which is then compared with the specified value. The iteration is then performed until the calculated e value and the specified value converge. The procedure described in Figure 4.9 can now be used for the analysis of slender concrete columns.

Load-deformation analysis described in Figure 4.9 was conducted for eccentrically loaded column results made available in the literature. These are:

1. high and normal strength concrete short columns (Attard and Foster 1995),
2. NSC short columns (Saatcioglu et al. 1995), and
3. slender HSC columns (Lloyd and Rangan 1995).

4.7 Analytical findings

4.7.1 Comparison with experimental results of Attard and Foster (1995)

Attard and Foster (1995) investigated 68 square specimens but only 30 had the complete ascending and descending branches. They have stated that this happened due to the limitations of the experiment. Therefore in the present study, only those 30 experimental observations were compared with the analysis results. Among the 30 tests, 6 of the results showed no variation of experimental stress-strain curves with the variation of spacing of lateral reinforcement, when the longitudinal reinforcement details and the eccentricity were kept constant. There is obviously some faulty in these experimental results. Therefore these six tests also were not included in the analysis for comparisons. Consequently experimental results of 24 specimens were compared with analytical results. The comparisons are shown only for 12 specimens. But the reliability of the analysis was assessed using 24 specimens. The 12 comparisons shown here were selected to be representative of the sample in terms of the eccentricity, strength etc. rather than on the basis of the agreement between the analytical and experimental results.

Saatcioglu et al. (1995) developed an analytical method for the behaviour of eccentrically loaded confined concrete columns. The method was based on confined concrete model proposed by Saatcioglu and Razvi (1992) for concentrically loaded columns. The model is described in detail in Section 4.2.1. Analytical model for confined concrete was based on average confining pressure and the descending branch was a straight line. They reported same rate of strength decay after the peak load regardless of the reinforcement arrangement. It incorporated the significance of strain gradient in their analysis for eccentrically loaded columns. Therefore their procedure is also used in this study to compare the experimental results.

Figures 4.12-4.17 show the experimental load versus (average strain + curvature \times eccentricity) curves for the eccentrically loaded columns reported by Attard and Foster (1995). Predicted behaviour using Saatcioglu et al. (1995) method and the analytical procedure described in this chapter is also presented in these figures.

Experimental and computed peak load and ductility values are given in Table 4.4 and Table 4.5 respectively. A quantitative comparison has been done in terms of peak load

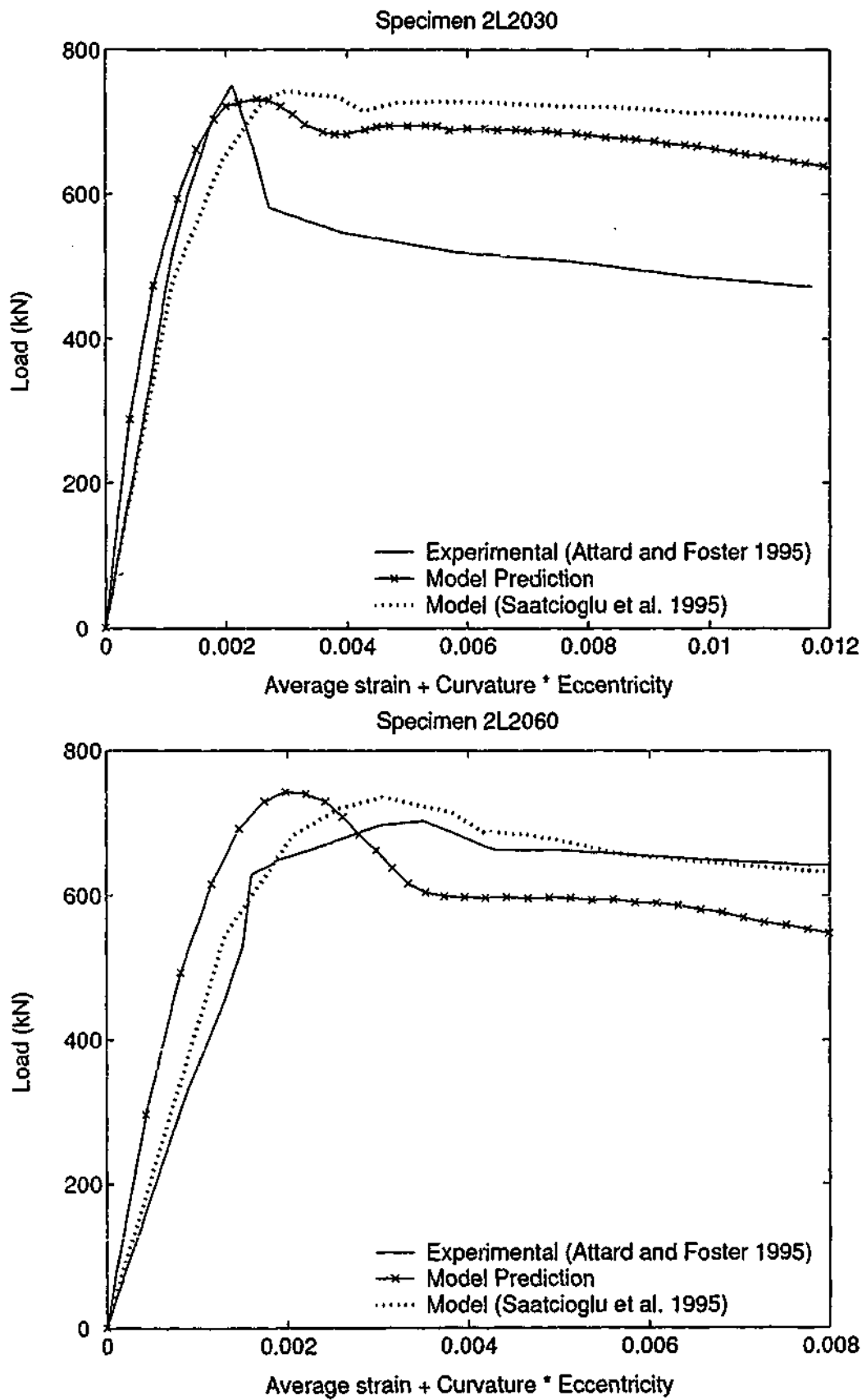


Figure 4.12: Load versus average strain + curvature × eccentricity for 2L2030 and 2L2060 specimens.

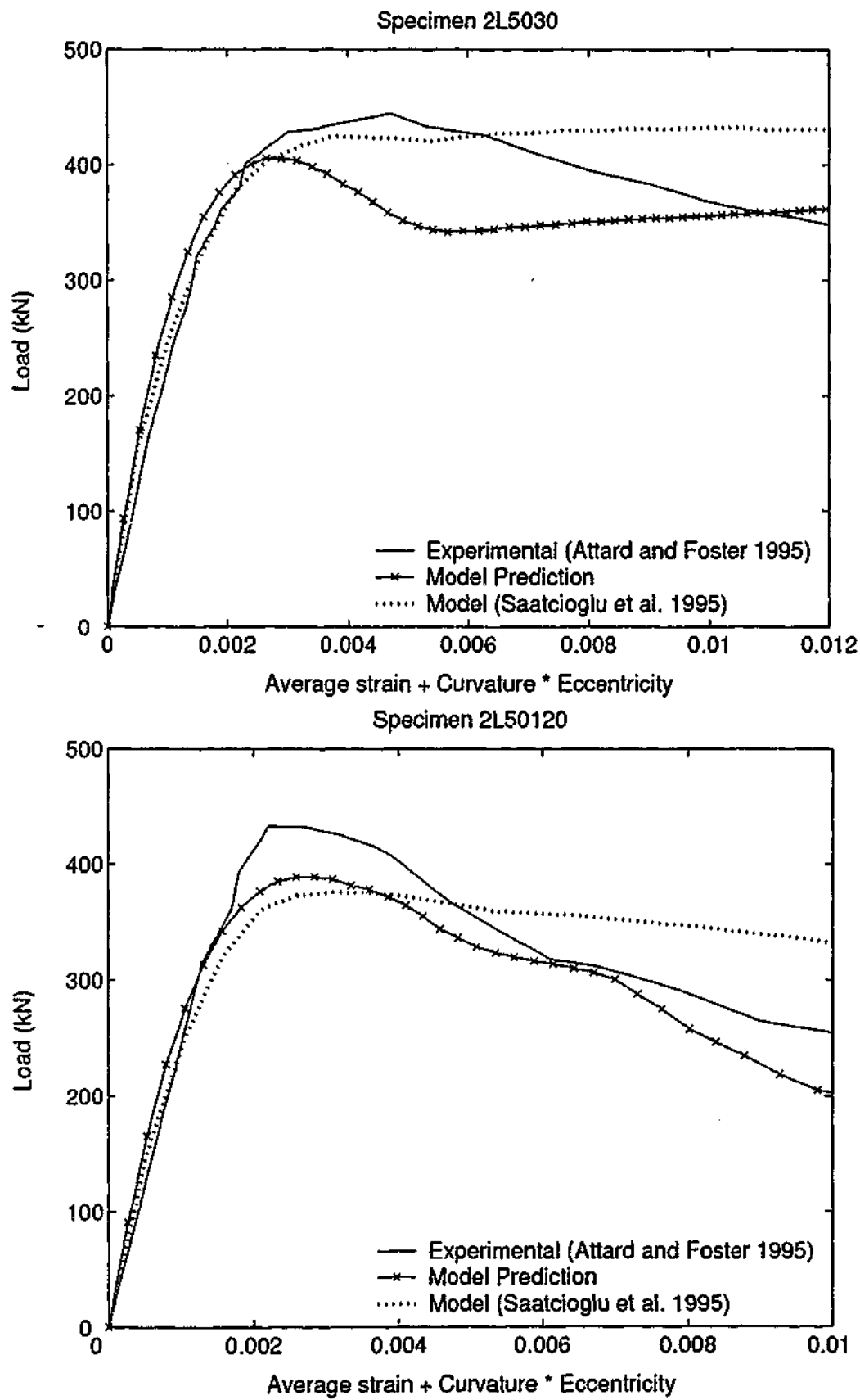


Figure 4.13: Load versus average strain + curvature \times eccentricity 2L5030 and 2L50120 specimens.

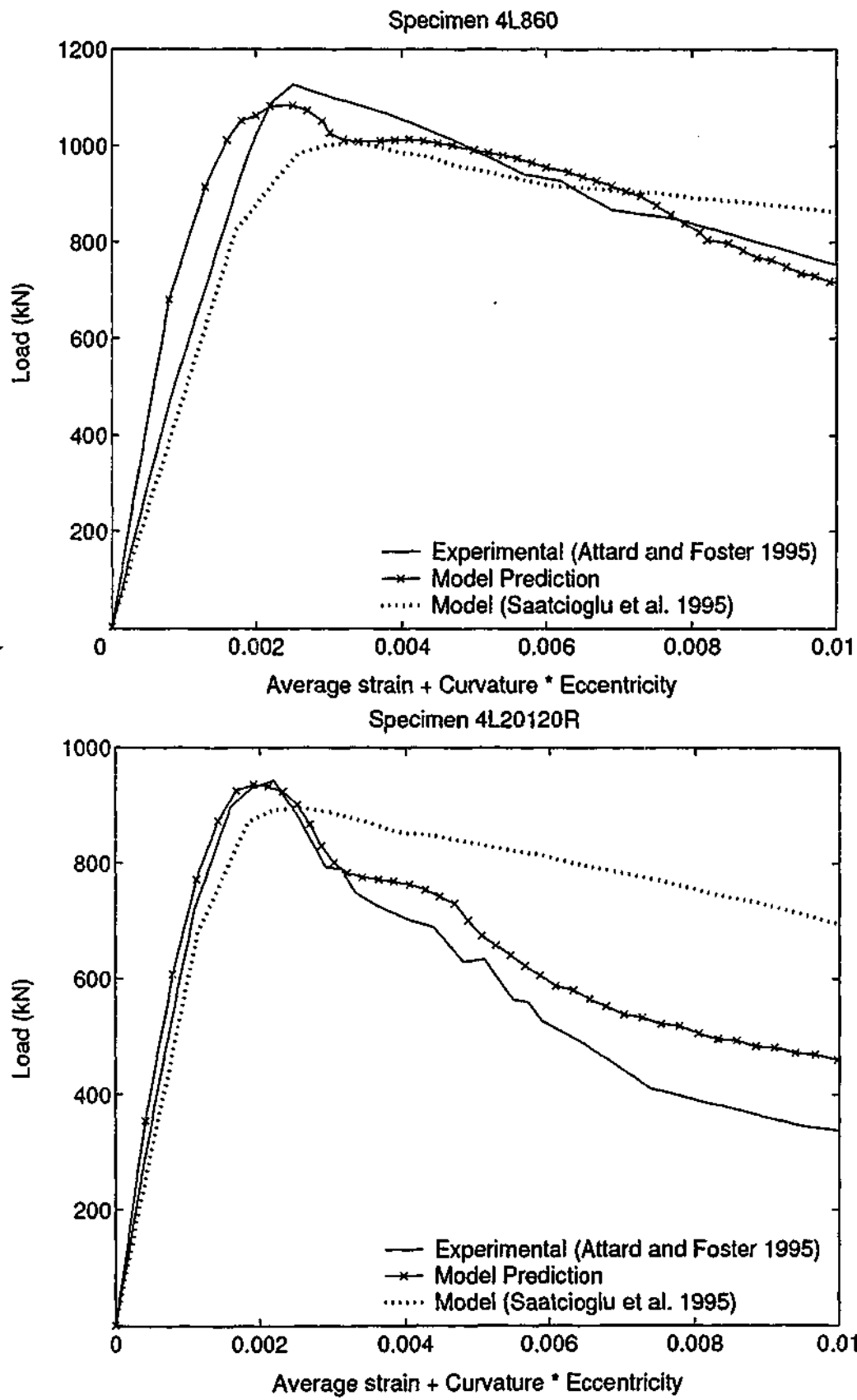


Figure 4.14: Load versus average strain + curvature \times eccentricity 4L860 and 4L20120R specimens.

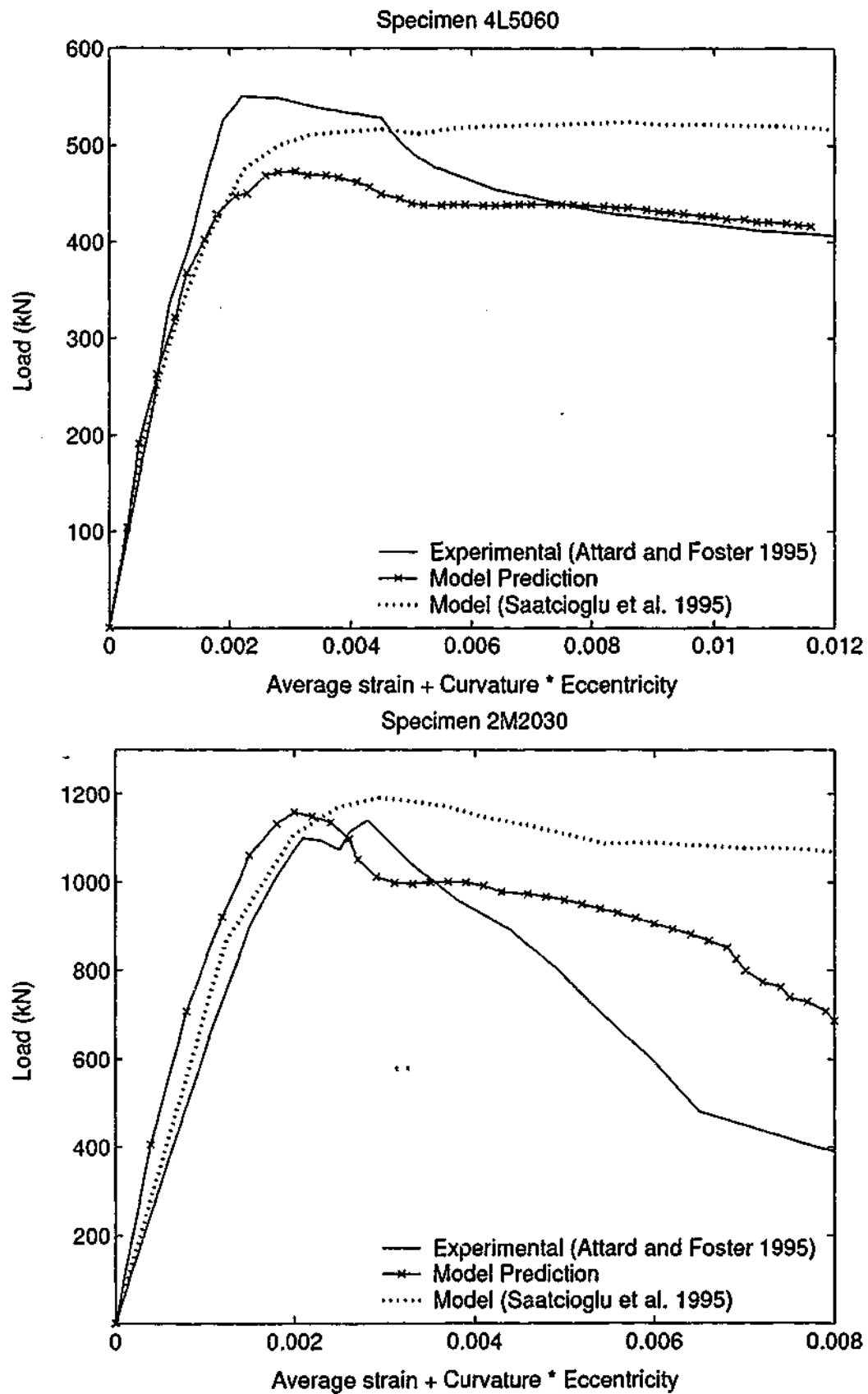


Figure 4.15: Load versus average strain + curvature \times eccentricity 4L5060 and 2M2030 specimens.

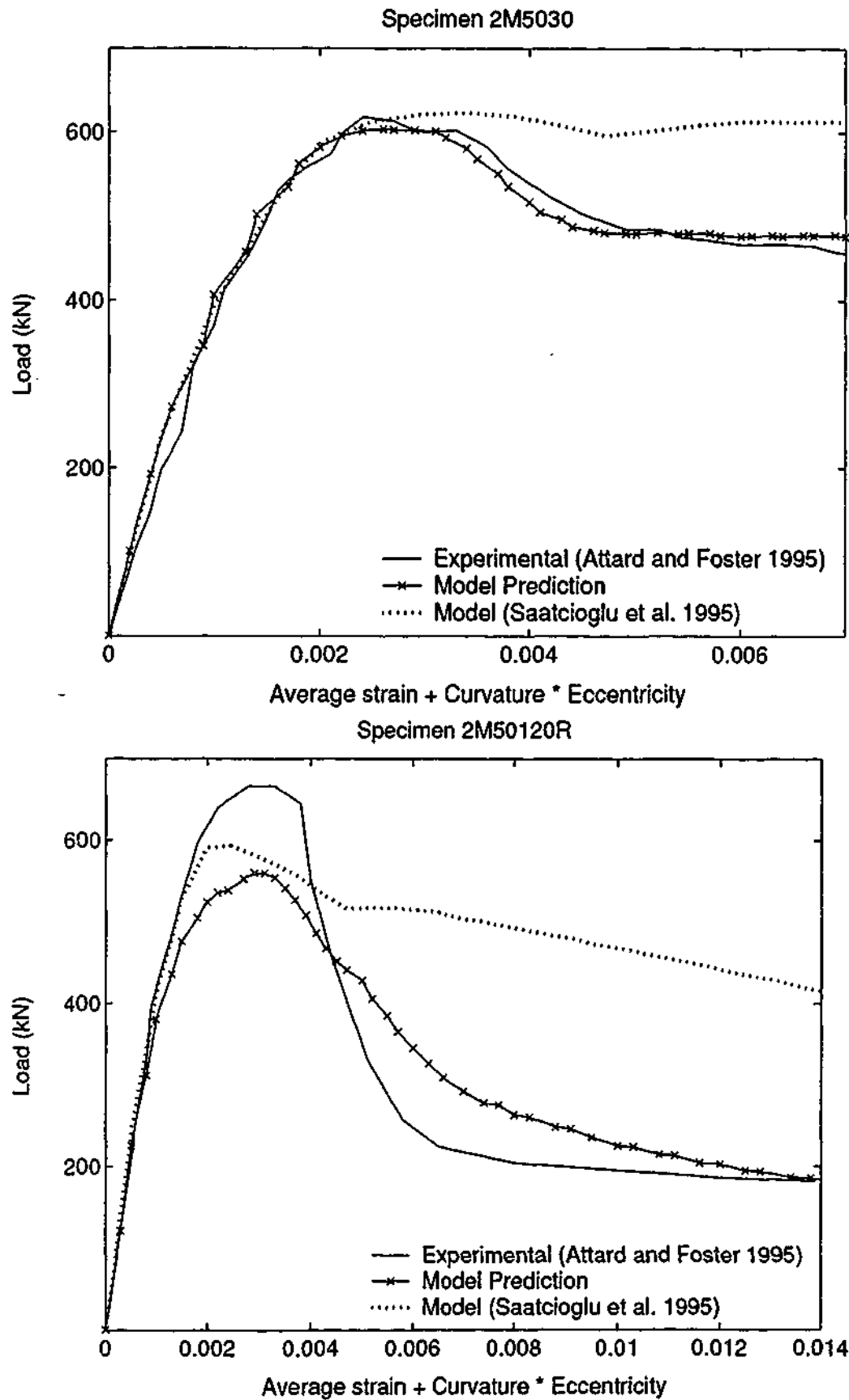


Figure 4.16: Load versus average strain + curvature \times eccentricity 2M5030 and 2M50120R specimens.

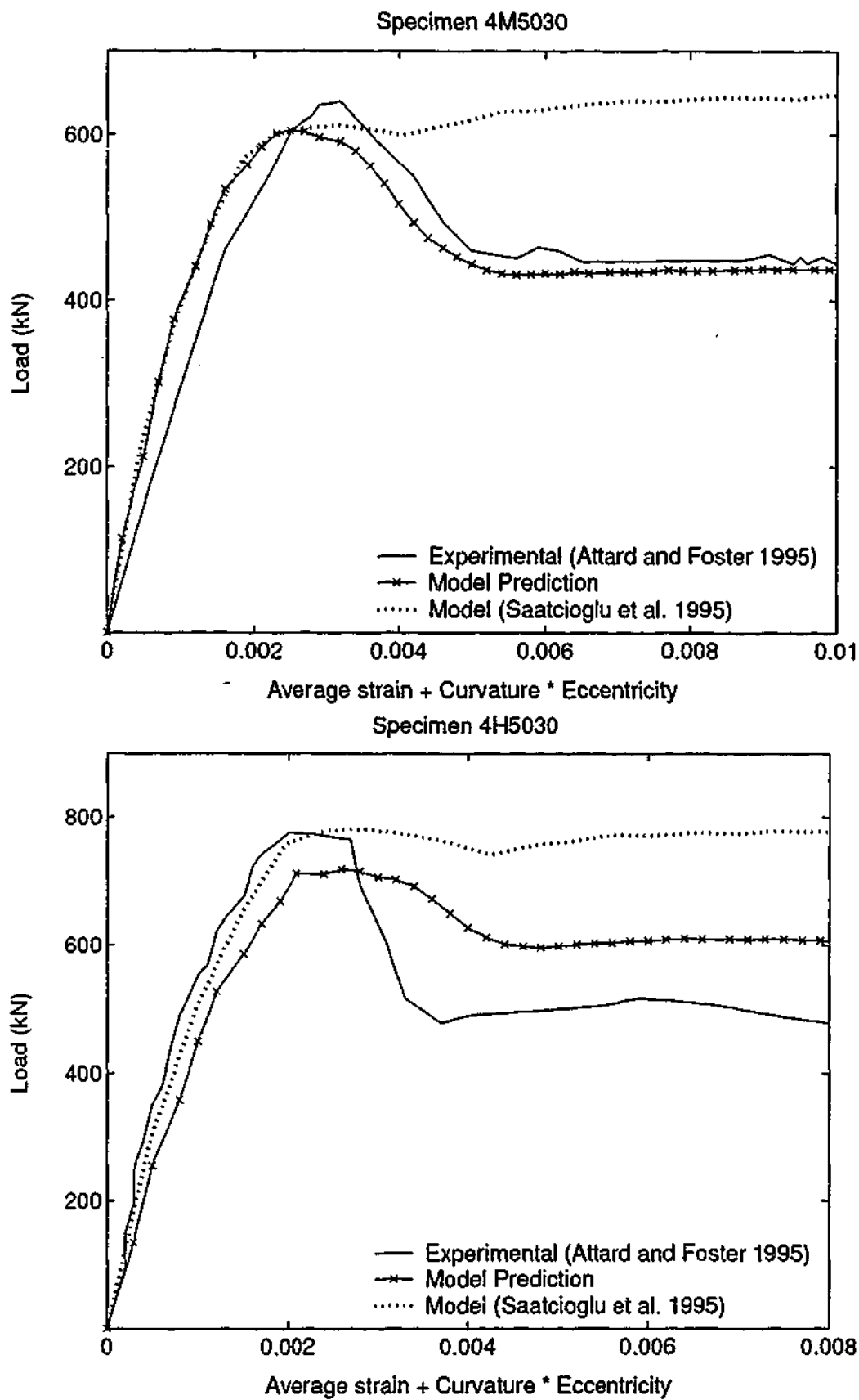


Figure 4.17: Load versus average strain + curvature \times eccentricity 4M5030 and 4H5030 specimens.

and ductility levels (Tables 4.4 and 4.5). It is evident that the methodology adopted by Saatcioglu et al. (1995) gives a reasonable prediction for experimental load-deformation curves of low strength concrete columns whereas analytical behaviour for high and medium strength concrete columns gives much higher ductility than the experimental values (Figures 4.12-4.17). This can be attributed to the inadequacy of accounting for the reduction of lateral dilation under axial load with increase in compressive strength, when using an average confining pressure as done by Saatcioglu et al. (1995). The average confining pressure corresponds to the yielding of transverse reinforcement. But in reality, confining pressure changes with the increasing lateral dilation of concrete and finally reaches a maximum value.

Table 4.4: Peak loads of eccentrically loaded reinforced concrete columns reported by Attard and Foster (1995).

Specimen	f_c (MPa)	Peak load (kN)		
		Experimental	Proposed model	Analytical Saatcioglu et al. (1995)
2L20-30	40	750	732	743
2L20-60	43	700	742	735
2L50-30	40	440	405	433
2L50-120	40	440	392	376
4L8-60	43	1150	1083	1006
4L20-120R	53	945	936	894
4L50-60	40	550	485	524
2M20-30	74	1160	1158	1190
2M50-30	74	630	603	623
2M50-120R	73	672	560	593
4M50-30	74	656	604	647
4H50-30	88	780	718	781

From Figures 4.12-4.17, it can generally be observed that the experimental curves and analytical curves match well in terms of peak load, shape of the curve and ductility for most of the medium strength concrete. However, the experimental behaviour of the one HSC column does not agree well with the analytical behaviour. It is noted that the reported experimental curve has a straight portion just after the peak stress, which may

indicate that the loading machine has been unable to follow the specimen for a short while. In such a situation, loss of some data points may lead to a sharp change in direction of the measured load strain curves. With the increasing eccentricity, the strength of concrete columns decreases. This decrease in strength is higher for HSC (columns 2M2030 and 2M5030) than that for NSC (columns 2L2030 and 2L5030).

Table 4.5: Ductility of eccentrically loaded reinforced concrete columns reported by Attard and Foster (1995).

Specimen	f_c (MPa)	Combined ductility *			Ductility †	
		Experimental	Analytical		Proposed model	Saatcioglu et al. (1995)
			Proposed model	Saatcioglu et al. (1995)		
2L20-30	40	1.50	2.61	2.8	3.91	4.2
2L20-60	43	3.95	3.17	2.6	2.41	3.6
2L50-30	40	4.36	3.65	2.4	2.8	3.2
2L50-120	40	2.76	2.79	2.3	4.15	3.1
4L8-60	43	2.5	4.77	2.7	6.48	5.2
4L20-120R	53	1.86	2.41	3.4	3.93	5.8
4L50-60	40	3.26	4.25	2.3	6.74	3.1
2M20-30	74	2.00	1.99	2.9	2.53	5.8
2M50-30	74	2.45	2.32	2.1	2.94	2.8
2M50-120R	73	2.09	2.48	1.8	3.14	2.3
4M50-30	74	1.72	2.32	2.0	2.94	2.6
4H50-30	88	2.06	2.04	1.8	2.51	2.3

* Definition No.1, Section 4.6.1

† Definition No.2, Section 4.6.1

4.7.2 Comparison with experimental results of Saatcioglu et al. (1995)

Saatcioglu et al. (1995) tested 12 eccentrically loaded columns. Figures 4.18 and 4.19 show the moment-curvature curves for the selected specimens from the 12 column tests conducted by Saatcioglu et al. (1995). The figures include the experimental curves reported by them and the analytical curves predicted by using two different methods namely, (1). method proposed by Saatcioglu et al. (1995) and (2). method proposed in this chapter.

Comparison of analytical findings and experimental results of Saatcioglu et al. (1995) column tests validates their proposed model for NSC. However, when that analytical method is applied for the medium and high strength concrete columns of Attard and Foster (1995), the predicted curves show a more ductile behaviour than the experimental curves.

The analytical findings using the method developed in this chapter are in reasonable agreement with the experimental results for eccentrically loaded NSC as well as HSC short columns.

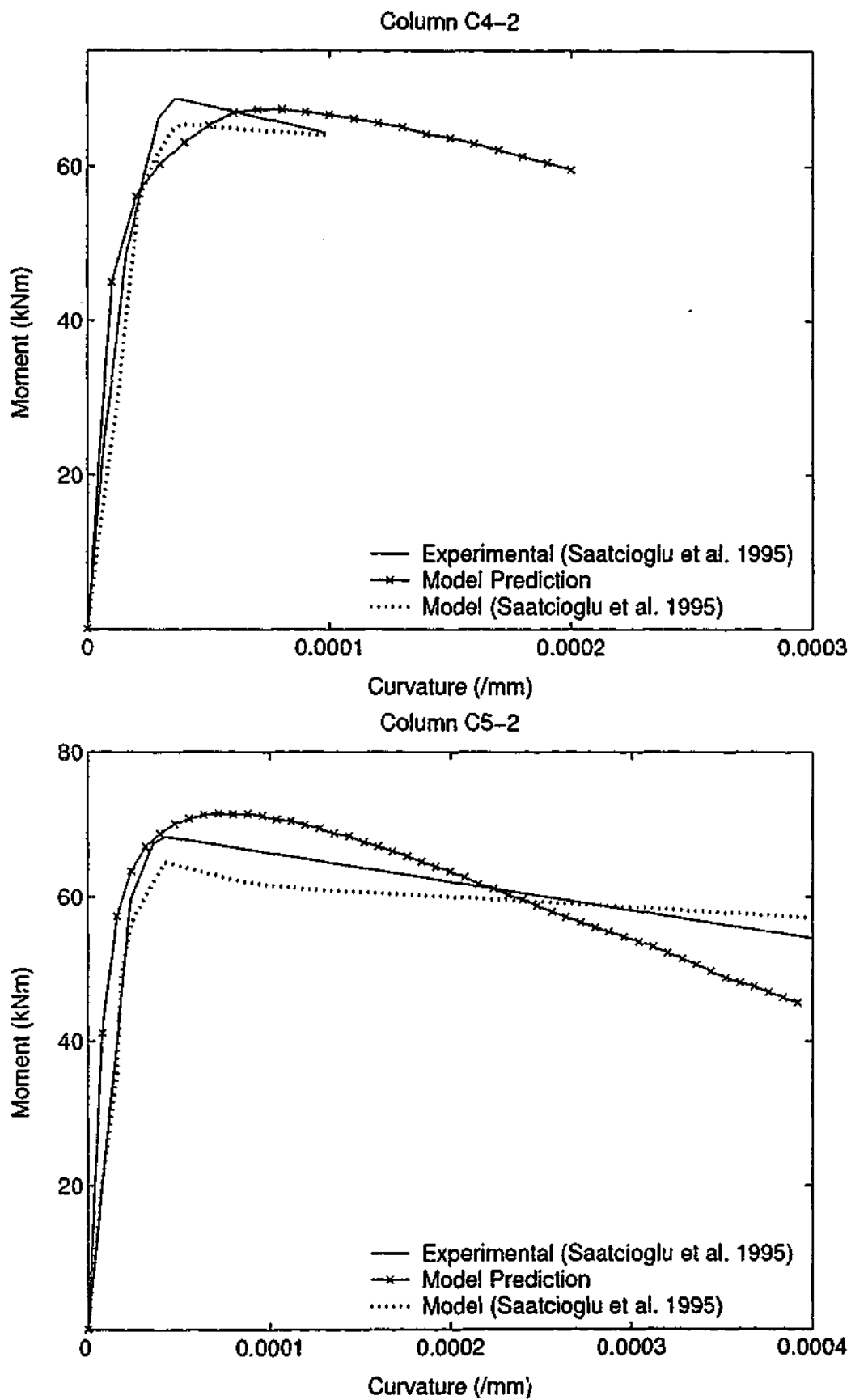


Figure 4.18: Comparison of moment-curvature relationships for C4-2 and C5-2 columns.

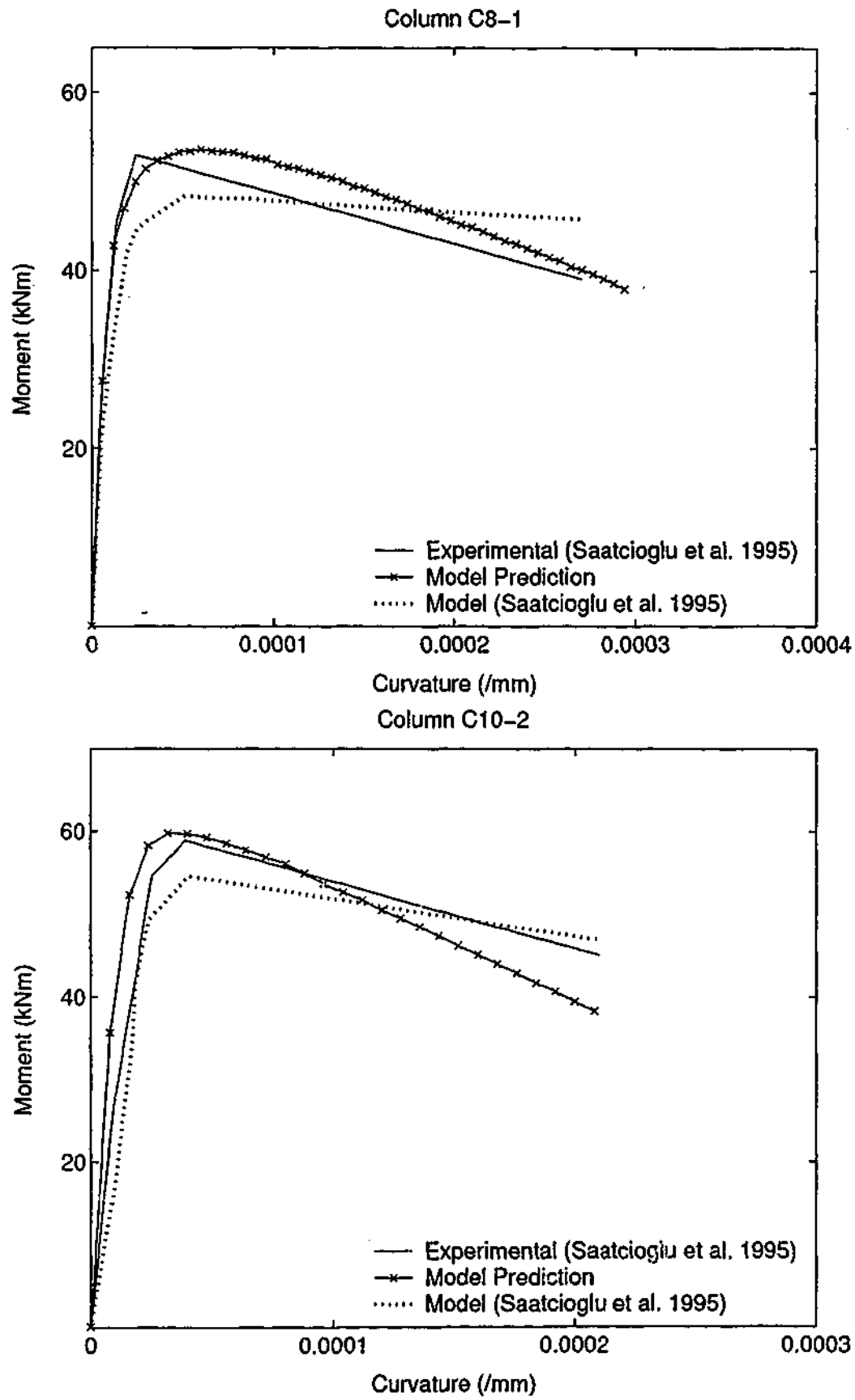


Figure 4.19: Comparison of moment-curvature relationships for C8-1 and C10-2 columns.

4.7.3 Comparison with experimental results of Lloyd and Rangan (1995)

From the 36 slender columns tested by Lloyd and Rangan (1995), 9 square columns have been selected to compare with the model predictions. The experimental and the computed peak loads and deflections at peak load are shown in Table 4.6. Moment-curvature relationships for all the slender columns considered in this study are shown in Figures 4.20-4.28.

Table 4.6: Peak loads of eccentrically loaded reinforced concrete columns reported by Lloyd and Rangan (1995).

Specimen	f_c (MPa)	Peak load (kN)		Deflection at Peak load (mm)	
		Experimental	Analytical	Experimental	Analytical
VA	92	1693	2160	6.2	4.6
VB	92	1013	1151	9.7	8.0
VC	92	795	838	12.3	11.4
VIIA	92	1733	2104	7.6	4.6
VIIB	92	906	1058	11.1	8.6
VIIC	92	663	719	15.4	12.0
XIA	97	1928	2188	5.6	4.6
XIB	97	965	1104	10.7	8.6
XIC	97	748	737	13.9	11.4

The analytical procedure was capable of predicting the ascending branch as well as the descending branch for all the curves whereas it is observed that the experimental curves are only for the ascending branch. Lloyd and Rangan (1995) commented that the descending branches of the curves were difficult to measure and it may be due to the stiffness of the testing machine.

Model predictions are in reasonable agreement for the low curvature values. However, it is impossible for the author to make a judgement about the descending branches of the curves. The predicted peak load is always higher than that in the experimental results (Table 4.6). On the other hand predicted deflections at peak loads are always lower than those in the experimental results. These discrepancies between the experimental results

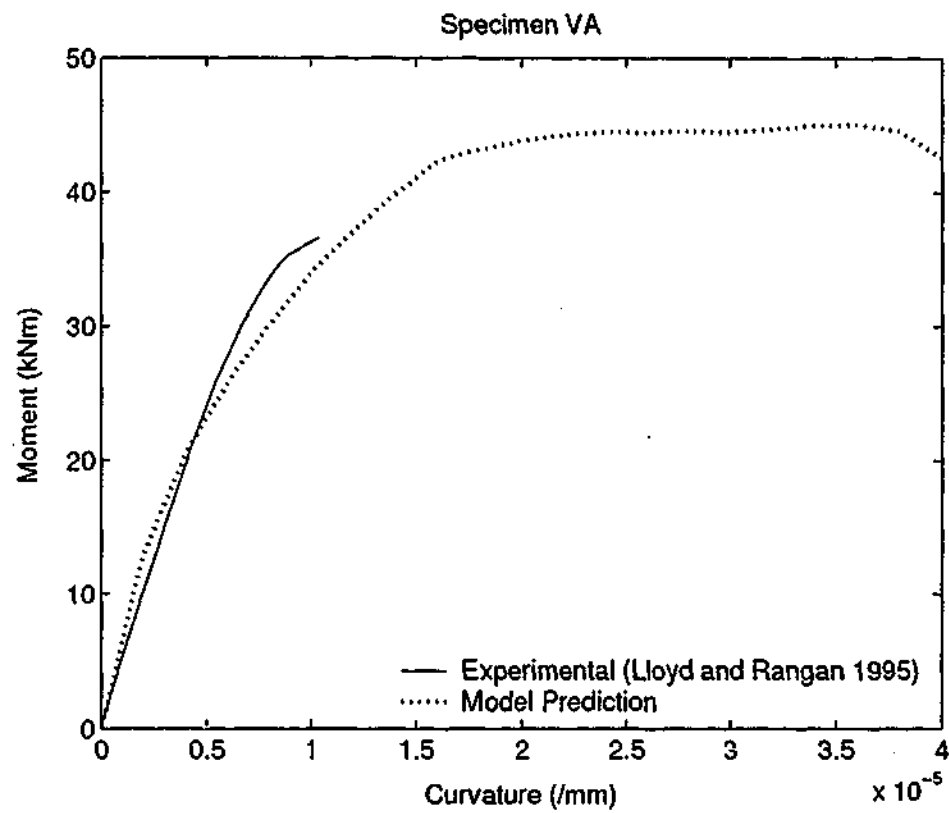


Figure 4.20: Moment-curvature relationships for series V specimen A.

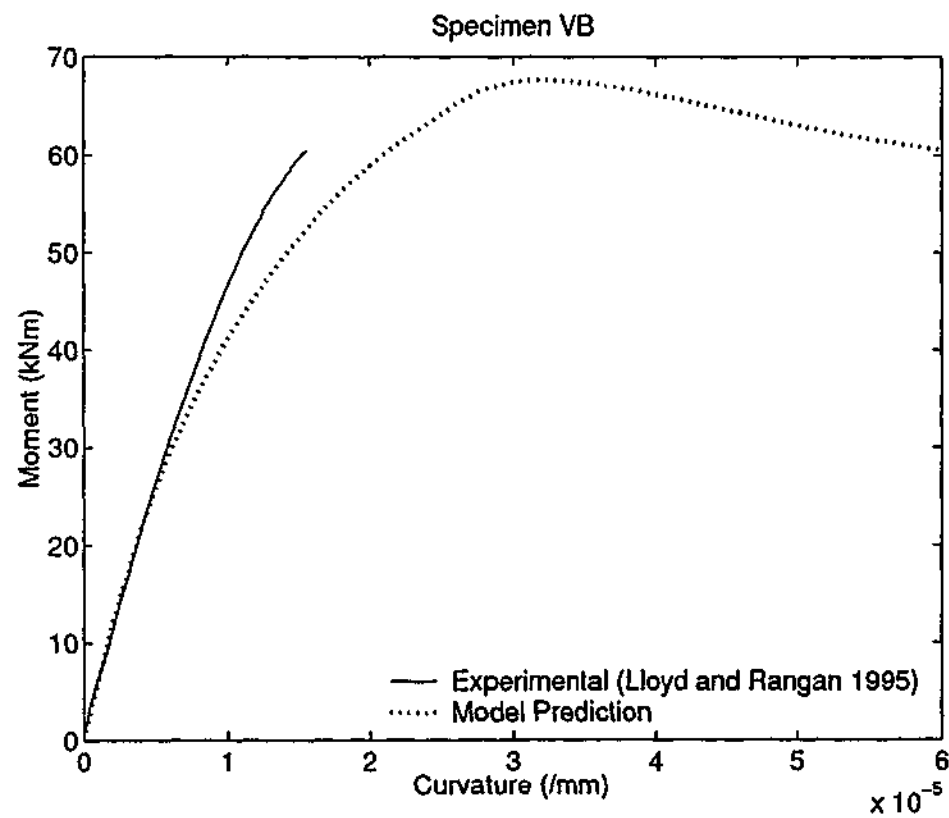


Figure 4.21: Moment-curvature relationships for series V specimen B.

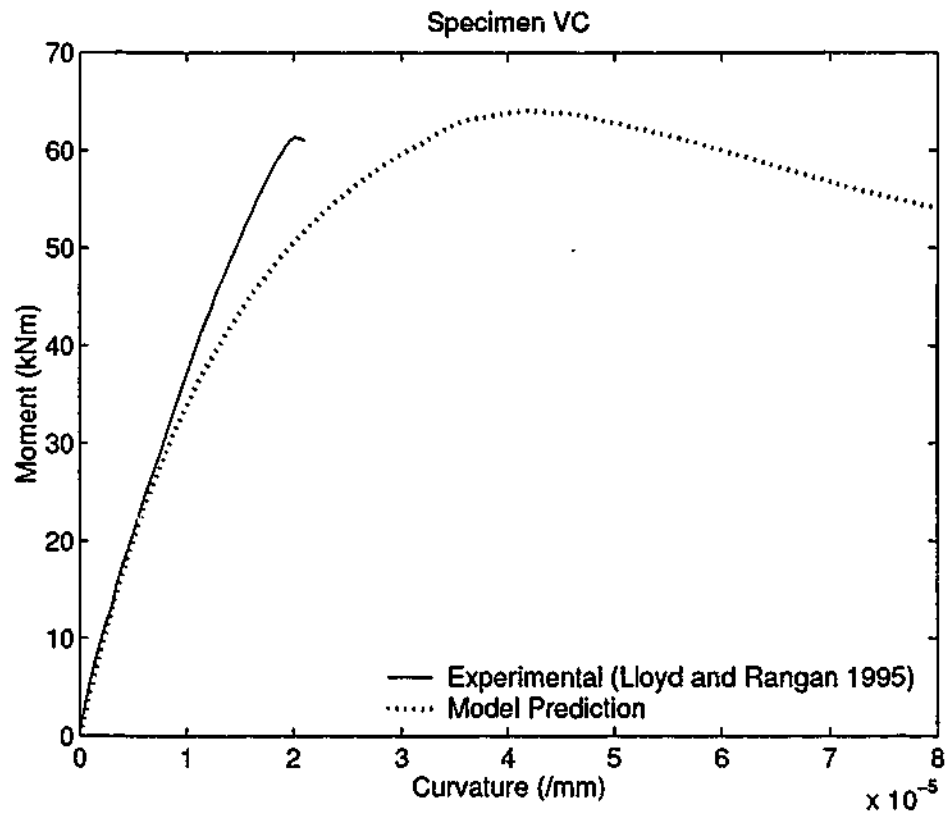


Figure 4.22: Moment-curvature relationships for series V specimen C.

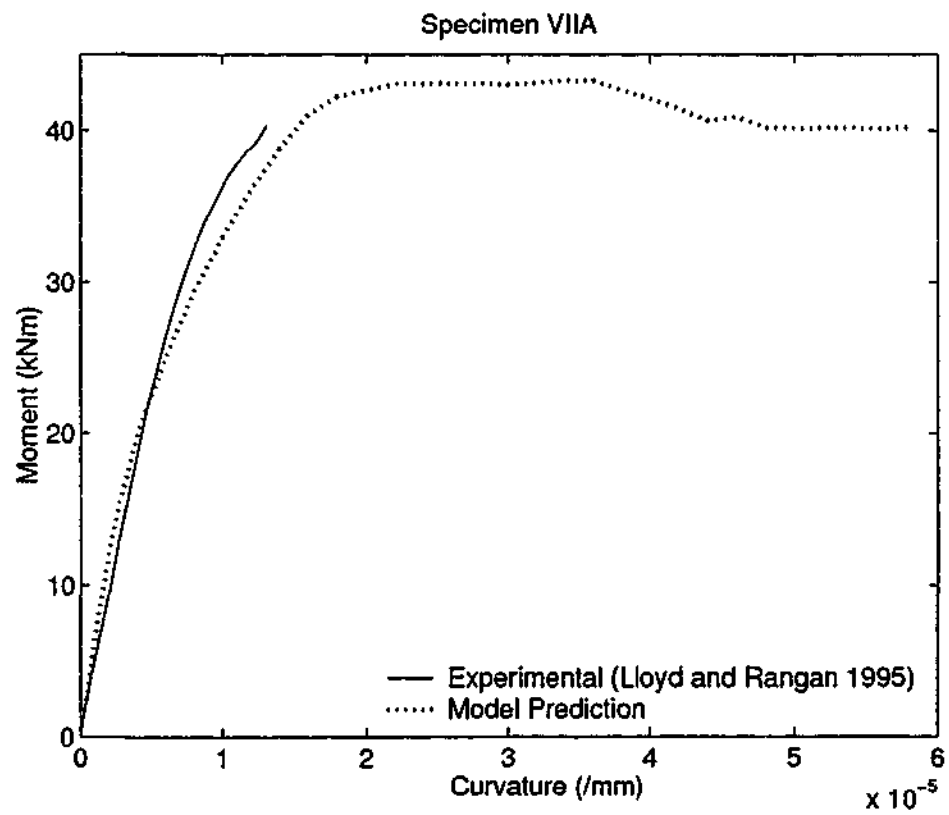


Figure 4.23: Moment-curvature relationships for series VII specimen A.

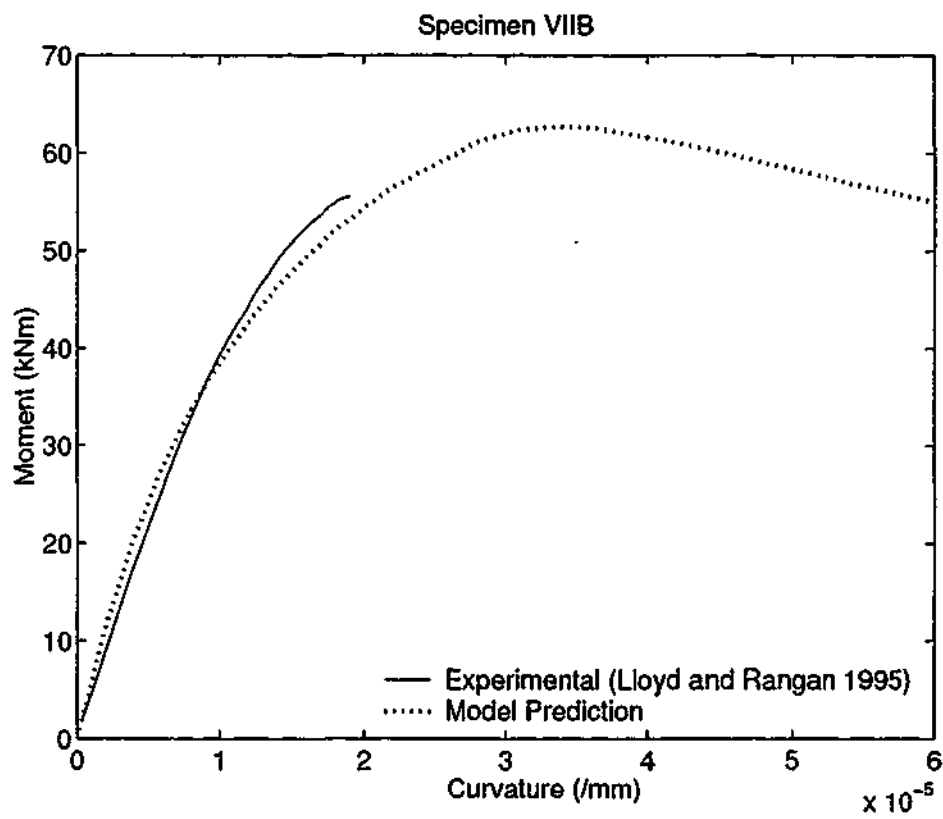


Figure 4.24: Moment-curvature relationships for series VII specimen B.

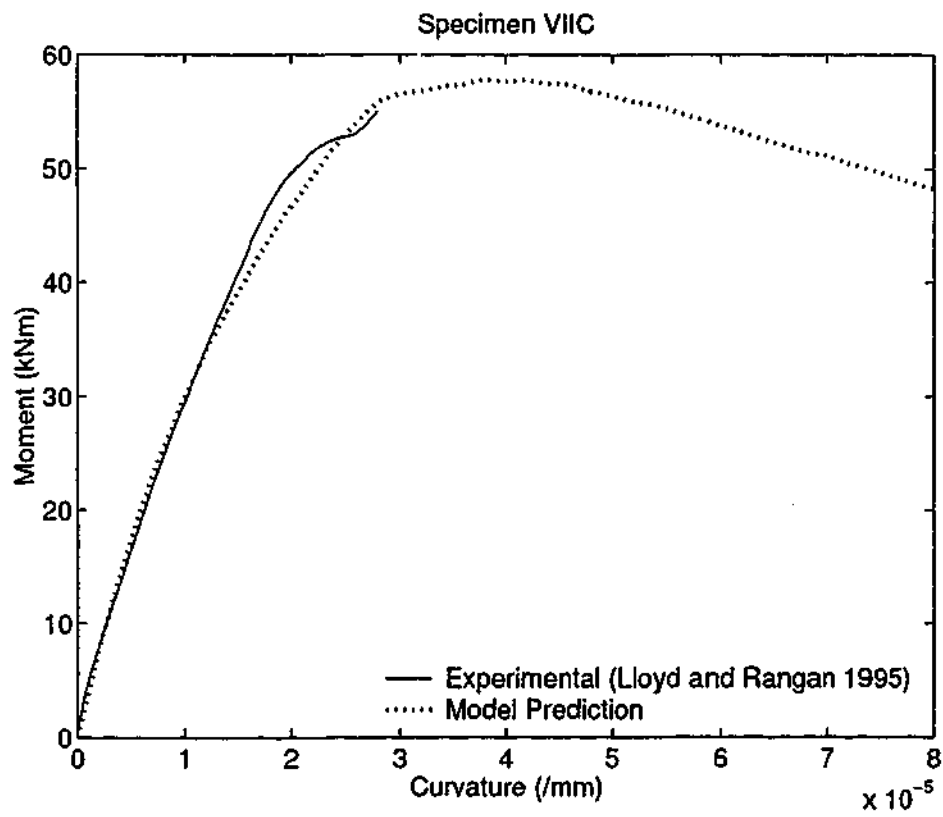


Figure 4.25: Moment-curvature relationships for series VII specimen C.

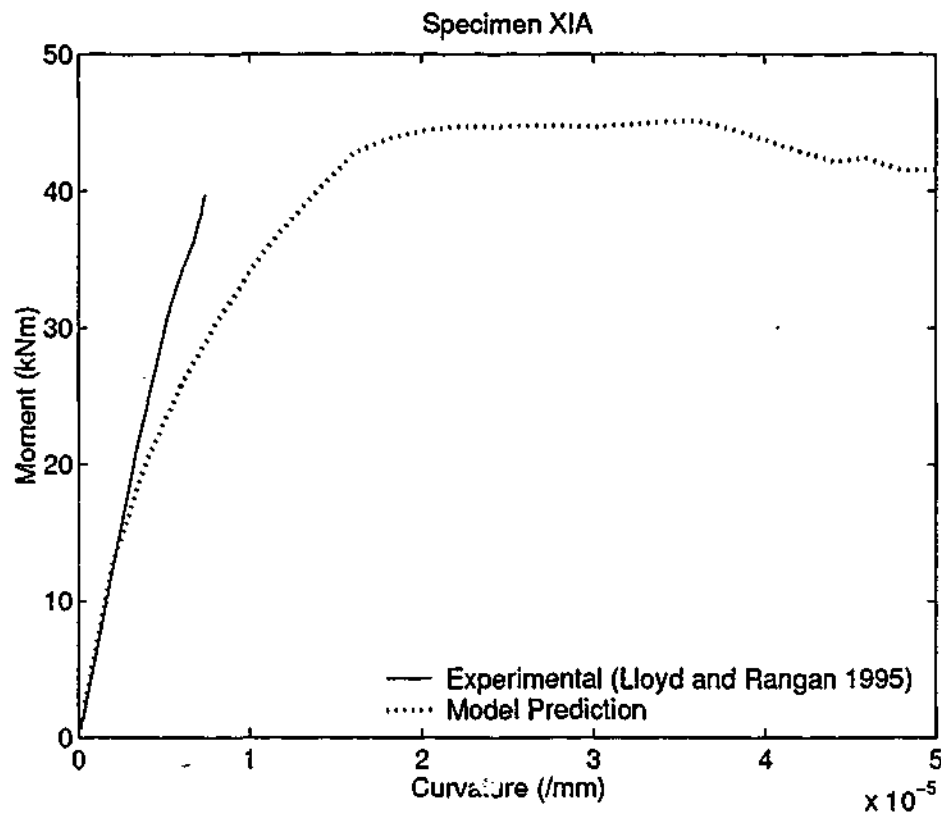


Figure 4.26: Moment-curvature relationships for series XI specimen A.

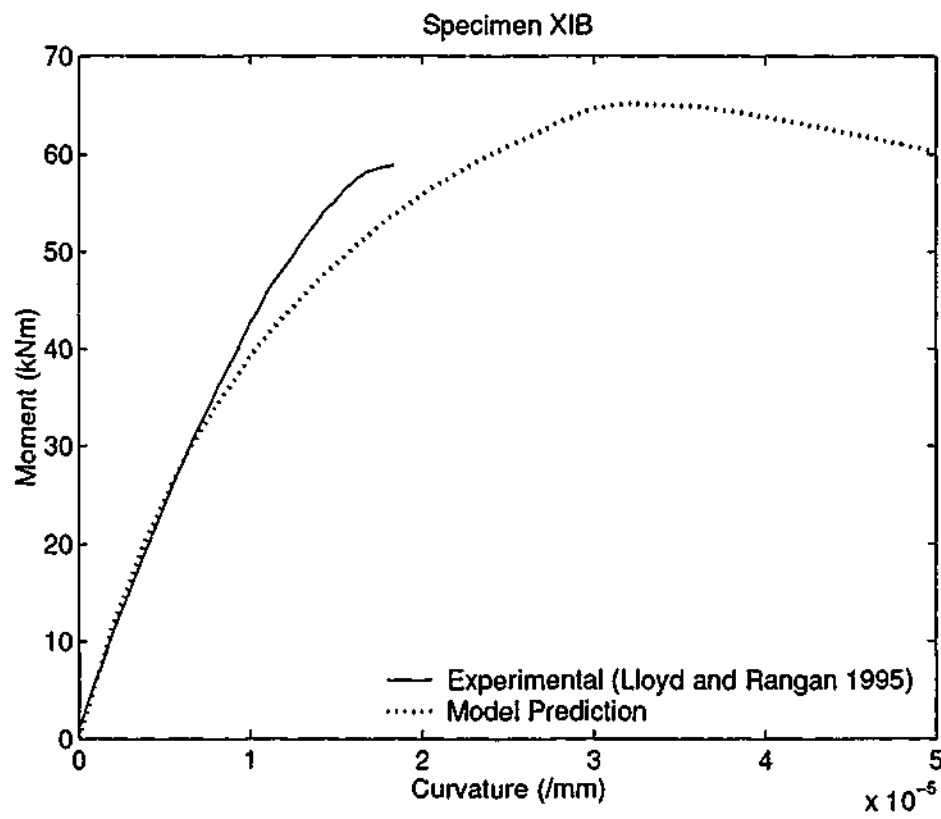


Figure 4.27: Moment-curvature relationships for series XI specimen B.

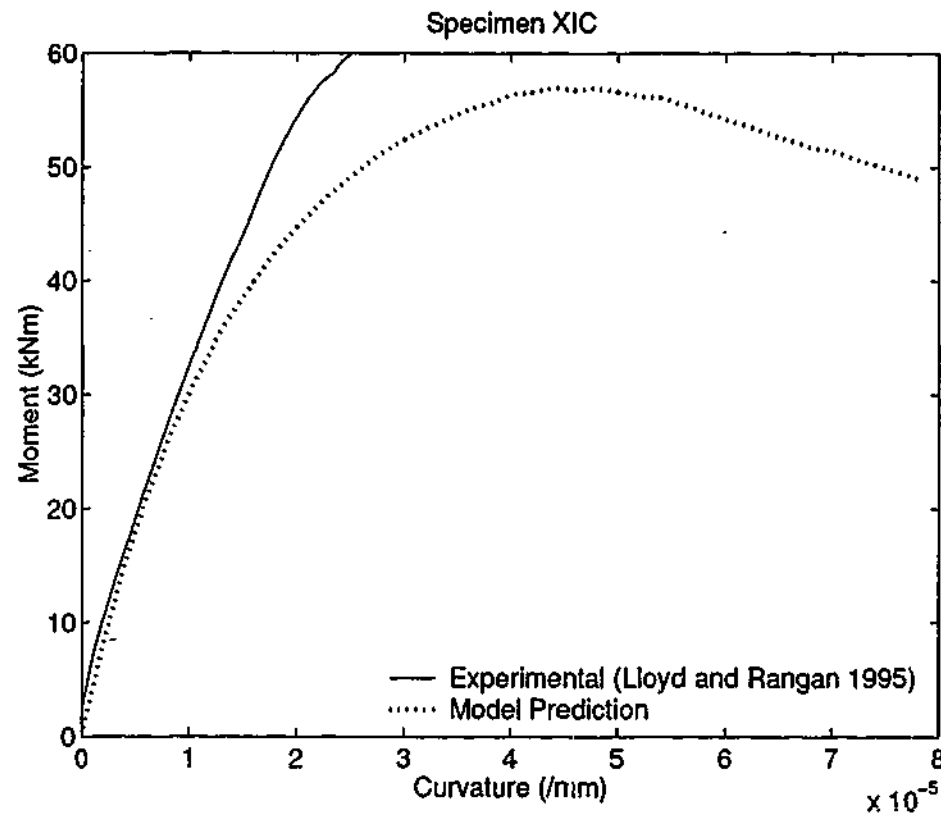


Figure 4.28: Moment-curvature relationships for series XI specimen C.

and the model predictions may be due to the assumed sine wave function for the deflected shape of the column.

4.8 Conclusions

The proposed analytical procedure to model load-deformation behaviour of eccentrically loaded NSC and HSC short columns compares well with the experimental results reported by Attard and Foster (1995) and Saatcioglu et al. (1995). However, the model predictions do not compare well for the slender columns tested by Lloyd and Rangan (1995). The conclusions resulted from this chapter are summarised as follows:

- The stress-strain model developed in the previous chapter is effective in the analysis of eccentrically loaded columns, as it reflects both axial and lateral strain of confined concrete.
- Proposed analytical procedure is more realistic than the previous methods where confinement effectiveness is estimated by assuming an effective area of confinement.

Proposed method uses the confining pressure applied by lateral steel which changes with lateral dilation of concrete.

- With the increasing eccentricity, the strength of HSC columns decreases more rapidly than that of NSC.
- Proposed analytical procedure is proven to be valid for NSC and HSC short columns.
- The proposed analysis has both of academic interest and practical implications. The academic interest is mainly to develop a constitutive model based on triaxial tests, which are fundamentally more solid than models that are back calculated from columns tests. The practical implications are that this model, based on triaxial tests, is more likely to work for a wide range of columns configurations and sizes than the models back calculated from columns tests, which may not work for columns which are significantly different from the original test configurations.
- Proposed analytical method does not provide good agreement with the experimental results for slender columns. The results of slender columns not only depend on the moment-curvature of cross section, but also on curvature-deflection relationship of the column. The simplified sine-curve relationship is likely to have contributed to the lack of good agreement between the results. Therefore it may be necessary to consider the assumption about the deflected shape of the column.

In the columns considered in this study, lateral reinforcement has been used as the method of confinement. However, the proposed methodology can also be used for eccentrically loaded HSC columns with different methods of lateral confinement such as steel tubes and FRP composites. Behaviour of column-slab joints where joint concrete is confined by surrounding slab concrete is another potential application of the constitutive model.

Chapter 5

MONOTONICALLY INCREASING LOADS:

Application of the constitutive model to estimate the strength of high strength concrete column-slab joints

5.1 Introduction

In high-rise buildings a significant cost saving can be achieved with the use of high strength concrete in columns and normal strength concrete in slabs. Since the column load has to transfer through a weaker layer of slab concrete, the compressive strength of concrete to be used in design of the column is an important issue. It is termed as the "effective column strength". It is the uniaxial cylinder strength of hypothetical joint concrete which has the combined characteristics of slab and column concrete. Reported experimental works to date indicate that the effective strength of an interior column is greater than the strength of slab concrete due to the confinement provided by the surrounding slab concrete. It is also established that at larger ratios of concrete compressive strengths of column and slab, the effective strength of the column is less than the compressive strength of the column. The triaxial constitutive model developed for high and normal strength concrete in Chapter 3 is used in this chapter to model the behaviour of the weaker layer of slab concrete within an interior HSC column.

Using an iterative procedure to estimate the confining pressure applied by the surrounding slab on column concrete, the stress-strain behaviour and failure stress of the

slab layer within the column can be established. The analytical findings are compared with the reported experimental work. When the slab is loaded, taking the stress gradient applied on the column into account in calculating the confining pressure, a better estimate of the failure stress can be obtained.

The outcomes of this chapter are published in Lokuge et al. (2002b).

5.2 Background

In present day construction of multi-storey reinforced concrete buildings, considerable economy may be achieved by designing the columns with HSC ($f_c > 50$ MPa) and the floor slabs with NSC. The preferred construction technique for such buildings is to cast the columns up to the soffit of the slab they will support and then to cast a continuous slab. The columns of the next storey are then cast, resulting in a layer of slab concrete intersecting the HSC columns at each floor level. The axial load on a column must therefore transverse a layer of weaker floor concrete. Under some circumstances, this layer may cause a decrease in the load carrying capacity of the column. Therefore it is difficult to estimate the compressive strength that should be used in the design of the column.

Current design practices in Australia and overseas in respect to the transmission of column loads through slabs consist of three approaches. The first approach, commonly referred to as "puddling", involves placing column concrete within the joint region and then designing the joint based on the cylinder strength of the column concrete. This method carries with it unwanted logistical problems as two different grades of concrete are required to cast the slab, thus extensive planning and a high level of on-site supervision is required. Some designers avoid the difficulties associated with puddling by opting to cast the entire slab with HSC, even though there is no need for the extra strength or the additional associated costs which may lead to an overall less economical building design.

The second approach is based on an assumption that the strength of column concrete is the same as the uniaxial strength of slab concrete, with the addition of vertical and lateral reinforcement to the joint region.

The third provision is to design the column using an "effective" concrete strength, f'_{ce} , which is equal to or greater than the slab concrete strength, f'_{cs} , but limited by the

column concrete strength, f'_{cc} . The value of effective concrete strength of the column-slab joint has been found by previous researchers to be predominantly dependant on the ratio of column concrete strength to slab concrete strength, the aspect ratio of the joint, i.e., the ratio of slab thickness to column side dimension, and the degree of lateral confinement offered to the joint region by the surrounding slab which will differ for each of the three types of columns: interior, edge and corner (Figure 5.1).

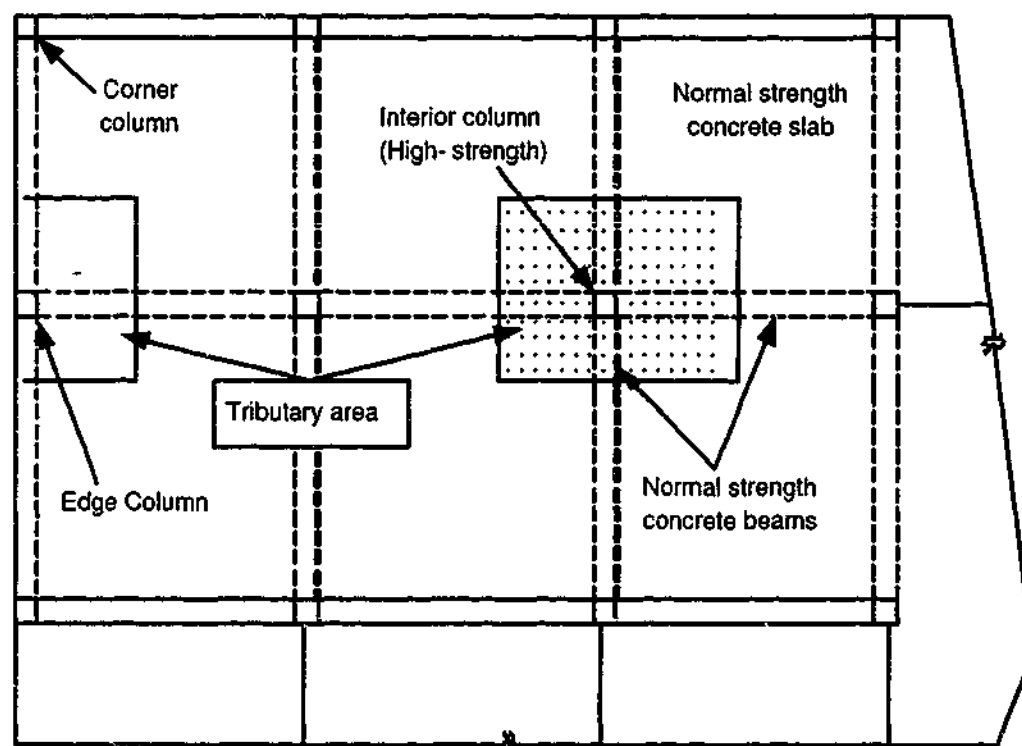


Figure 5.1: Column-slab connection.

5.2.1 Reported work on the behaviour of column-slab joints

A summary of previous research on transmission of column axial loads through weaker slabs are given in Table 5.1. As seen from Table 5.1, investigations on transmission of HSC column loads through NSC slabs, both locally and internationally have been very limited.

Based on the test results of Bianchini et al. (1961), the American Concrete Institute Code 318 (1999) has defined equations for the effective strength of interior and edge columns. These are given in Table 5.2. These provisions have not been revised for more than 30 years. Except these three Codes mentioned above, none of the other major codes cover transmission of axial loads through a weaker layer.

Table 5.1: A summary of previous research.

Investigators	Range of f'_{cc} (MPa)	Range of f'_{cs} (MPa)	Comments
Bianchini et al. (1961)	23 to 51	13 to 22	Tested 11 column-slab joint specimens without beams. Tested 3 column-beam joint specimens.
Gamble and Klinar (1991)	72 to 97	17 to 43	Tested 6 column-slab joint specimens.
Kayani (1992)	-	-	A design equation was proposed based on the available test data for interior column-slab joint specimens.
Siao (1994)	24.4 to 29.6 ¹	39.4 to 50.4 ²	Tested 6 column-beam specimens.
Ospina and Alexander (1997)	89 to 120	15 to 46	A total of 12 column-slab joint specimens were tested. Investigated the effect of the aspect ratio h/c , where h = the slab thickness and c = column dimension.
McHarg (2000)	80.7 to 85.7	30 to 39 or 33.4 to 41.5 ³	Tested 6 column-slab specimens. Steel fibre reinforced concrete was used in four of six slab column specimens.

Notes:

1 and 2: cube strength of concrete

3: compressive strength of slab concrete with fibres

Table 5.2: Provisions of design codes.

Interior Columns	
ACI 318 (1999)	if $f'_{cc}/f'_{cs} \leq 1.4$; $f'_{ce} = f'_{cc}$ if $f'_{cc}/f'_{cs} \geq 1.4$; $f'_{ce} = 0.75f'_{cc} + 0.35f'_{cs}$
CSA A23.3 (1994)	if $f'_{cc}/f'_{cs} \leq 1.4$; $f'_{ce} = f'_{cc}$ if $f'_{cc}/f'_{cs} \geq 1.4$; $f'_{ce} = 0.25f'_{cc} + 1.05f'_{cs}$
AS3600 (2001)	if $f'_{cc}/f'_{cs} \leq 2.0$; $f'_{ce} = f'_{cc}$

It is important to note that AS3600 (2001) adopts a critical f'_{cc}/f'_{cs} ratio of 2, which exceeds the commonly accepted value amongst previous investigators and other codes of 1.4. Some work conducted at the University of Alberta (Ospina and Alexander 1998) on HSC column-slab joints and at the University of Melbourne (Portella et al. 1999) on corner HSC column-slab joints have shown that the recommendations given in the American Concrete Code, ACI 318 (1999) and the Australian Concrete Structures Code, AS3600 (2001) are unconservative. Therefore urgent attention is required to address and resolve this important issue.

The results of an analytical procedure to model the concrete in the column-slab interface accounting for the confinement provided by the slab concrete are presented in this chapter. The method uses the triaxial constitutive model developed for confined concrete and an analytical iterative procedure to estimate the actual confinement provided by the slab concrete.

5.3 Experimental program

Ospina and Alexander (1997) tested thirty specimens, in four series to observe the behaviour of reinforced concrete column-slab joints. Eight interior column-slab connections have been selected in this study. The constitutive model developed in Chapter 3 is used to analyse the joint concrete behaviour.

Details of the tested interior column specimens are shown in Table 5.3 and Figure 5.2. Dimensions a , b and c are 1380, 1100 and 200 mm respectively for all specimens. Table 5.3 also shows the uniaxial compressive strengths of slab and column concrete separately. The

Table 5.3: Details of the specimens.

Specimen	h in Fig.5.2 (mm)	Slab load (kN)	Concrete strength (MPa)	
			Column	Slab
A1-A	100	0	105	40
A2-A	100	0	112	46
A3-A	150	0	89	25
A4-A	150	0	106	23
A2-C	100	86	112	46
A3-B	150	100	89	25
A4-B	150	93.2	106	23
A4-C	150	135.2	106	23

slab loads given in the Table 5.3 is the total slab load. It is reported that the dimensions of the slabs are selected so that the location and the magnitude of the applied slab load, will result in moments and shear forces at column face representing a prototype joint.

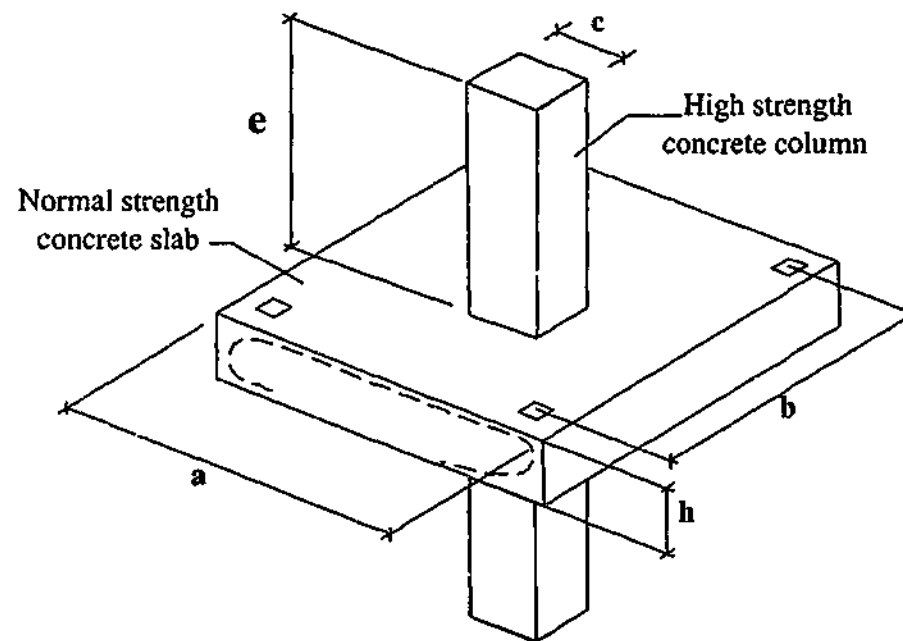


Figure 5.2: Details of specimens (Ospina and Alexander 1998).

5.4 Application of the constitutive model for the confined column-slab interface

When the axial load on column is increased, the slab concrete will apply a confining pressure on the joint concrete as a reaction for the expansion of the joint concrete. The estimation of the confining pressure depends on the lateral expansion (strain) of joint concrete. Therefore the stress-strain model for joint concrete should have the capability of predicting the lateral strains as well, in order to find the confining pressure from the slab concrete accurately. The constitutive model developed in Chapter 3 is used in this chapter to model the behaviour of column-slab joint as it can establish axial stress, axial and lateral strain relationships.

5.5 Analytical procedure

The layer of weaker slab concrete at the column-slab interface is considered as plain concrete laterally confined by surrounding slab concrete. When the axial load of the column increased, the concrete at the interface will try to expand and will be resisted by the surrounding slab concrete. If the slab is not loaded, the confinement provided by the slab concrete will be approximately uniform whereas in a loaded slab the confining pressure will change with the strain gradient in the slab due to bending moment. The two scenarios are considered separately and are described below.

5.5.1 Unloaded slab

When a column load is applied, there will be a lateral expansion of the joint concrete, which is restrained by the surrounding slab concrete. Therefore the slab concrete provides a passive confining pressure to the joint concrete. Figure 5.3 illustrates this for a column-slab joint with unloaded slab. For this case, the confining pressure is distributed uniformly over the height of the joint. For a particular axial strain of joint concrete, the lateral expansion can be estimated using the constitutive model described in Chapter 3. Using an iterative procedure, the actual confining pressure applied on the joint concrete by the slab concrete can be calculated. Joint concrete is analysed using this confining pressure in the constitutive model. Thus the axial column stress corresponding to the particular axial strain can be deduced. The confining pressure applied by the surrounding concrete

increases gradually. However, once the slab concrete cracks, the confining pressure applied on the joint concrete by the slab will either remain same or reduce. Ospina and Alexander (1997) reports that the slab cracked when the stress on column is about 60% of the peak stress. Therefore in this study, it is assumed that the confining pressure will not increase after the joint concrete has reached 60% of the peak stress.

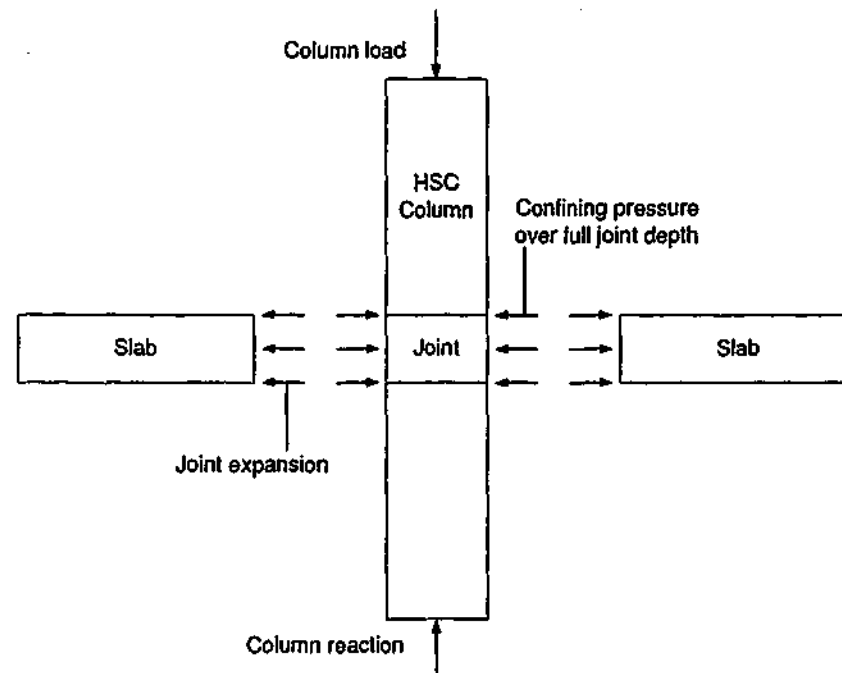


Figure 5.3: Behaviour of joint concrete in an unloaded slab.

5.5.2 Loaded slab

Stress-strain relations for square columns subjected to combined axial load and flexure are obtained assuming that plane sections remain plane after bending. Perfect bond between steel and concrete is assumed thus it is possible to get the strain of steel as that of the surrounding concrete. It is assumed that the concrete does not resist any tensile force.

The point slab load is applied at the beginning of the test and held constant throughout the progress of the experiments, while the column load is increased to failure. When the slab is loaded, bending of the slab places the top region of the joint in tension and the bottom region in compression as shown in Figure 5.4. Therefore the joint concrete above neutral axis of bending is not confined by the surrounding concrete, whilst concrete below the neutral axis is actively confined by the slab concrete. In addition to this active confinement, the slab concrete applies a passive confinement on joint concrete. This is

due to the lateral expansion of joint concrete due to the increasing column load.

The joint concrete is divided into a number of horizontal slices through slab thickness for the modelling purpose. Each slice is subjected to constant axial strain due to the column load. Same as for unloaded slabs, there will be a lateral expansion, which ultimately results in a confining pressure application on this joint concrete. This confining pressure is further increased by the effect due to bending of the slab. Due to the bending of the slab, the bottom portion of the joint will be under compression. This results in a compressive force (confining pressure) application on the joint concrete by the surrounding slab. Joint concrete is analysed with this added confining pressure and stress-strain relationship is established. It is assumed that the confining pressure will not increase beyond that corresponding to 50-60% of the peak stress of joint concrete.

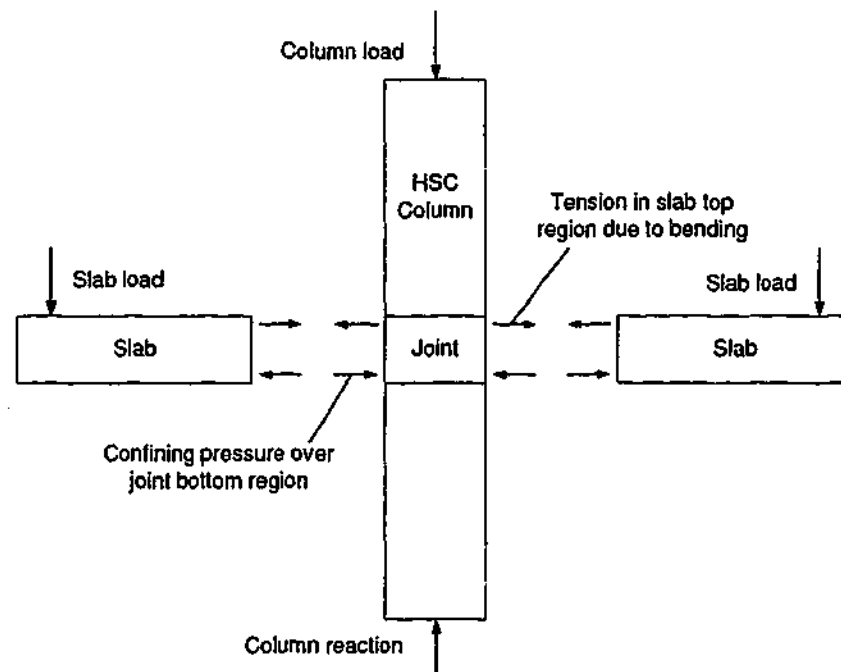


Figure 5.4: Behaviour of joint concrete in a loaded slab.

5.6 Comparison of the model predictions with reported experimental results

Ospina and Alexander (1998) reported experimental results for the behaviour of twenty interior column-slab joints. It consisted of two series. Series "A" had 12 interior sandwich plate specimens and the aim of that series was to study the effect of slab loading on the

joint compressive strength. Eight test specimens from series "A" have been considered in this study which represent a sample of different slab loads, different slab and column strengths. Model predictions are compared with the experimental observations reported by Ospina and Alexander (1998). Figures 5.5-5.8 show the comparisons as stress in the joint in the vertical direction versus column strain through slab for unloaded and loaded slabs.

As shown in Figures 5.5 and 5.6, analytical findings are in close agreement with the experimental observations for unloaded slabs. Ascending branch of specimen A4-A deviates from that of the experimental curve. It is observed that the experimental and the predicted curves match well in terms of the shape and peak load. The only discrepancy observed is that steeper ascending branch shown in all the predicted curves. A possible reason for this may be the assumption made about the cracking stage. That is, in this study, it is assumed that the slab concrete cracks before the joint concrete reaches its peak. After this point, the confining pressure exerted by the surrounding slab concrete will not increase.

The model comparisons with the experimental observations for loaded slabs are shown in Figure 5.7 and Figure 5.8. Effect of slab load can be analysed, if the specimens A4-A, A4-B and A4-C are considered (Figure 5.9), where the slab load increases gradually. The higher the slab load is, the lower the peak stress and the strain at peak stress. This shows that even with a high slab load, the joint benefits from some confinement. However, the confining pressure reduces with the increase in slab load.

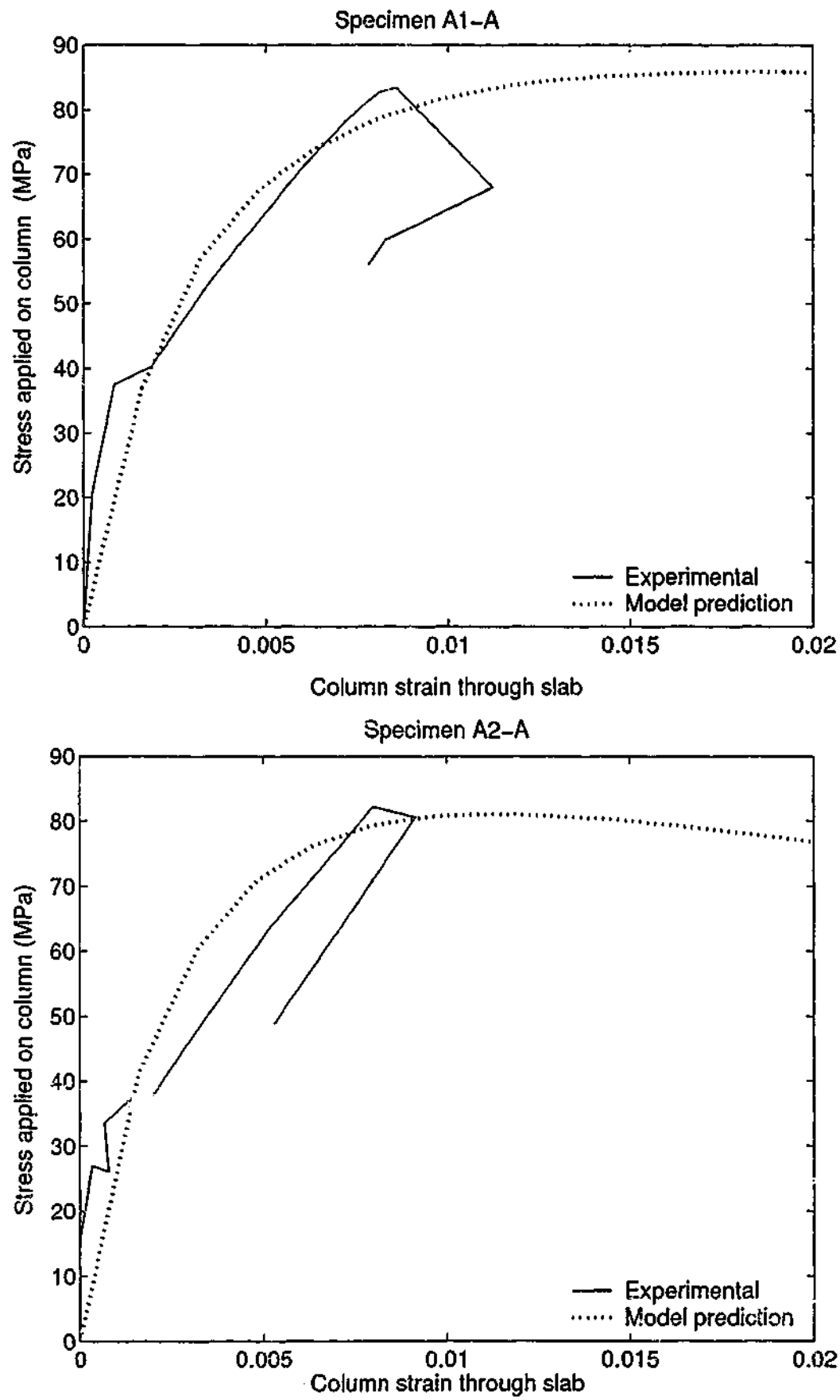


Figure 5.5: Stress-strain curves for unloaded slabs A1-A and A2-A.

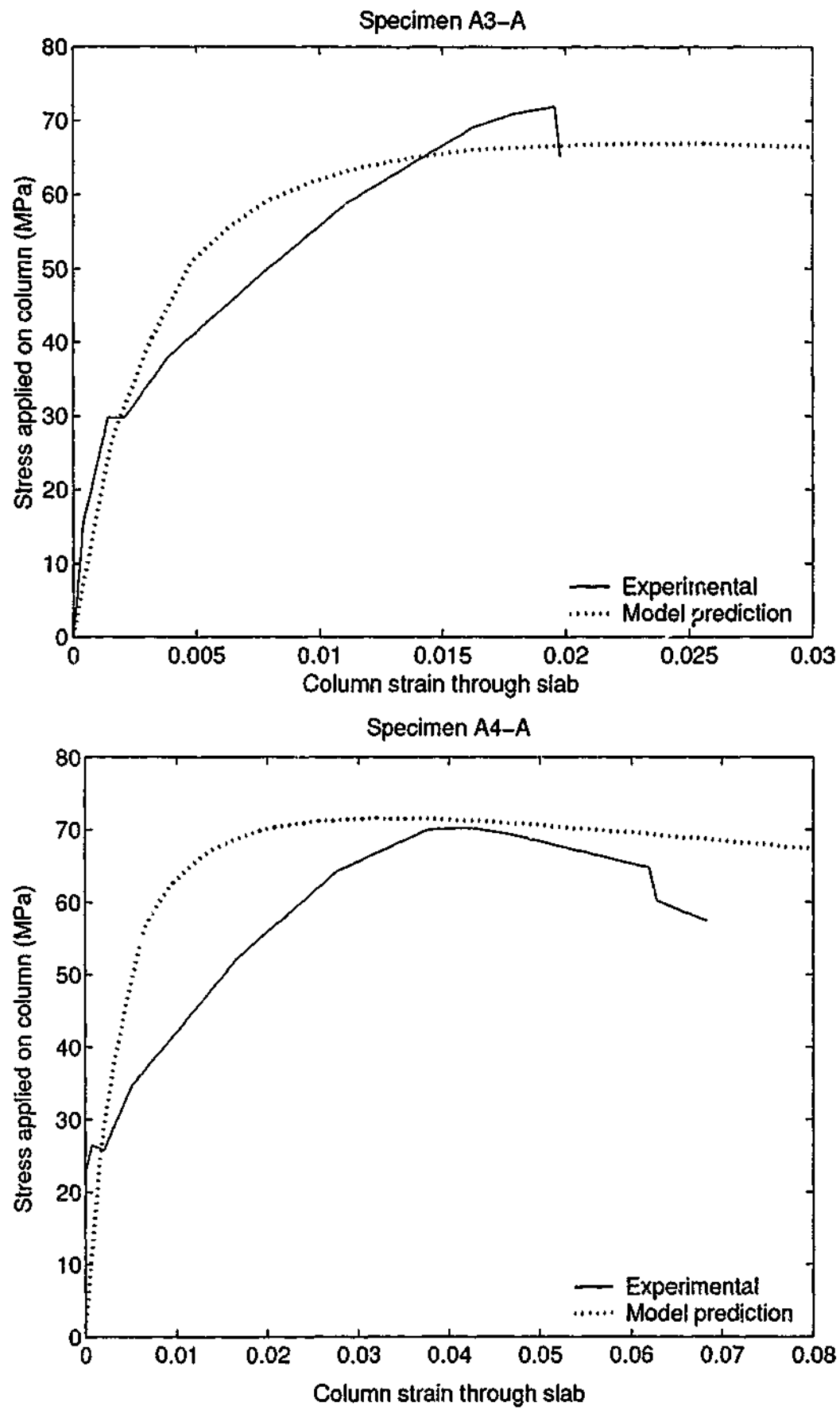


Figure 5.6: Stress-strain curves for unloaded slabs A3-A and A4-A.

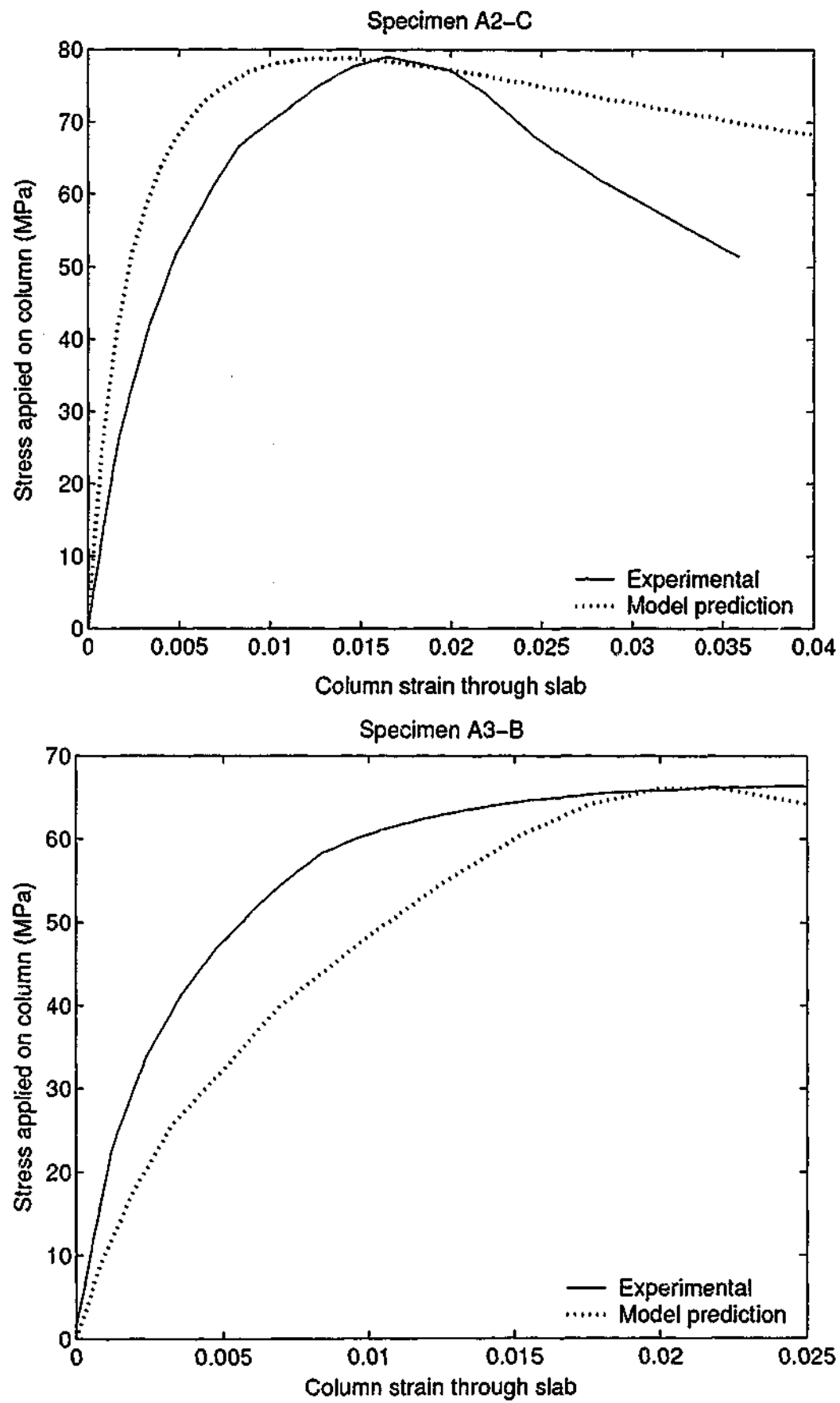


Figure 5.7: Stress-strain curves for loaded slabs A2C and A3B.

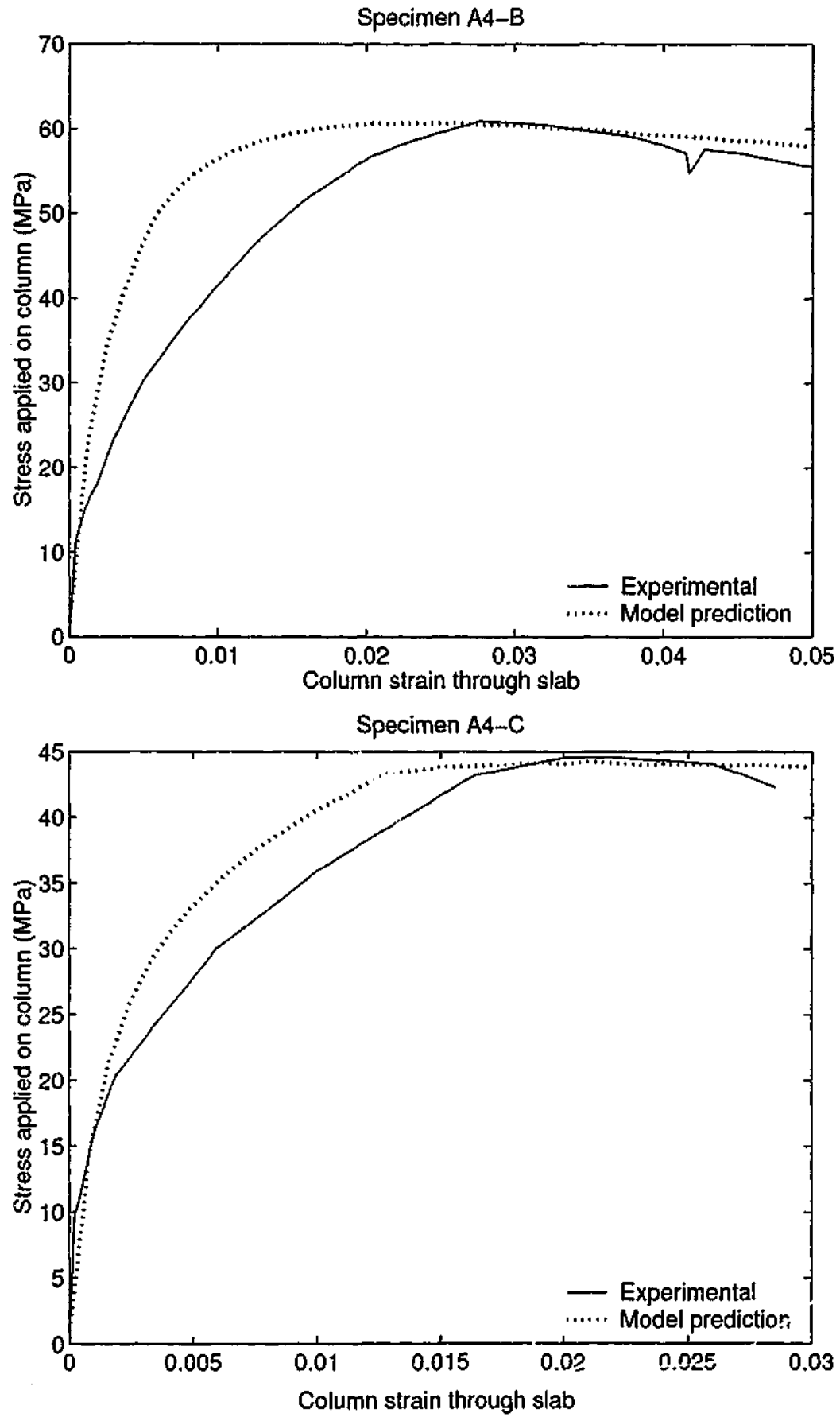


Figure 5.8: Stress-strain curves for loaded slabs A4B and A4C.

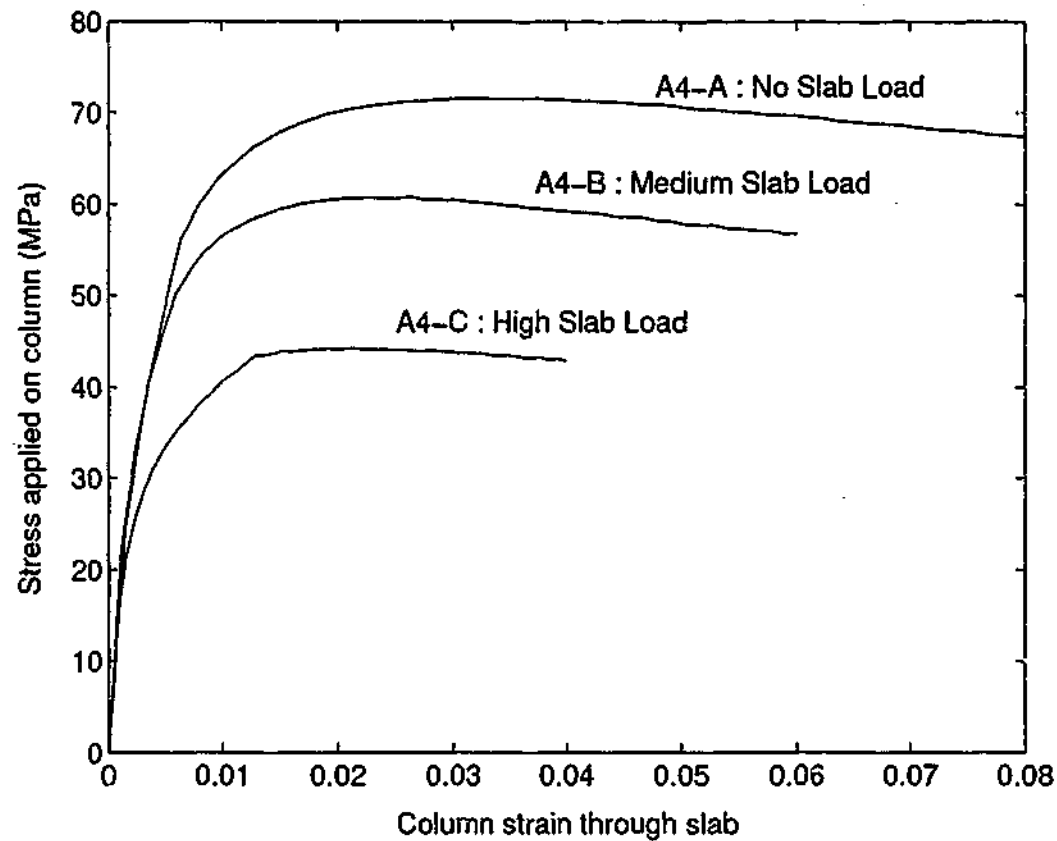


Figure 5.9: Effect of slab load on interior joint strength.

5.7 Conclusions

The analytical method developed is shown to predict the behaviour of reinforced concrete column-slab interface when a weaker layer of slab concrete is embedded in a HSC column. Several conclusions are drawn from this analysis.

- The stress-strain model developed in Chapter 3 is effective in structural analysis of column-slab joints, as it reflects lateral strain of confined concrete. Thus the confining pressure exerted by the surrounding slab concrete can be accurately estimated.
- The developed method is shown to give good comparisons in modelling the behaviour column-slab joint of interior columns with or without slab load.
- When the slab load is increased, the maximum compressive strength is decreased.
- In the analytical procedure presented it is assumed that
 - slab concrete cracks before column concrete reaches its maximum strength and

- confining pressure applied by the surrounding slab concrete after this cracking stage will remain the same.

However, these assumptions need careful investigations to develop the analytical procedure further.

- Modelling the behaviour of reinforced concrete column-slab joint when a weaker layer of slab concrete is embedded in a HSC column, is an issue, which has previously only been addressed by empirical methods. It is advantageous to use analytical methods, such as the one presented in this chapter, to estimate the strength of column-slab joint because they would be applicable to a wide range of situations than the empirical methods presented in Table 5.2.

Chapter 6

CYCLIC LOADS: Previous works on constitutive models of concrete and steel

6.1 Introduction

The first part of this thesis, from Chapters 2-5 focused on the behaviour of high strength concrete (HSC) under monotonically increasing loads. The second part of the thesis extends the underlying concept of the constitutive model presented in Chapter 3, to develop a model for the cyclic behaviour of confined HSC. This chapter describes the previous research work for the behaviour of unconfined and confined normal strength concrete (NSC) and confining steel subjected to cyclic loading.

During an earthquake, the structures are subjected to cyclic lateral forces. In performing a structural analysis in a seismic region, the effect of earthquake loadings on the structure needs to be analysed. Therefore understanding of the behaviour of concrete and confining material (typically steel) subjected to cyclic loading is necessary in such analysis. The stress-strain relationships for concrete under cyclic loading have been studied from well over four decades. The experimental studies for the behaviour of unconfined NSC subjected to cyclic axial compression by Sinha et al. (1964), Karsan and Jirsa (1969) and Desayi et al. (1979) were the first ones to be published. Similar studies were reported for confined NSC (20-49 MPa) by Desayi et al. (1979), Shah et al. (1983), Mander et al. (1988a), Watanabe and Muguruma (1988) and Sakai and Kawashima (2000).

The stress-strain curve for both confined and unconfined concrete subjected to cyclic loading has a general shape as shown in Figure 6.1. It consists of several key components.

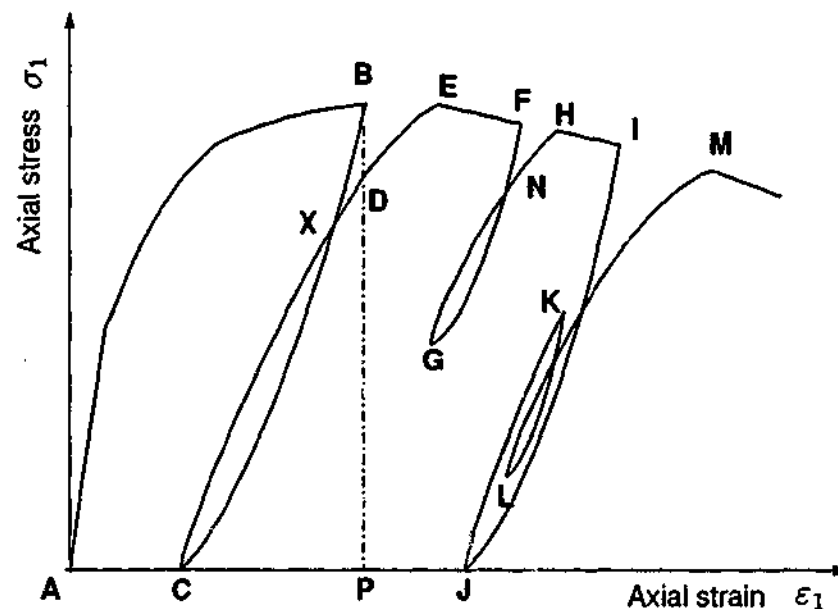


Figure 6.1: Stress-strain curve for cyclic loading of concrete.

Terminology and the description for each component or point of the stress-strain curve (Figure 6.1) are tabulated in Table 6.1.

The envelope curve for cyclic loading of concrete is "ABEFHIM". It is well accepted among the research community that the stress-strain curve corresponding to monotonically increasing load forms the envelope curve for cyclic loading. Unloading curve (BC) represents the behaviour of concrete during unloading and it initiates from the unloading point (B). Unloading stress and unloading strain are the coordinates of this point (B). The unloading may proceed upto point "C", where the axial stress becomes zero. This point is called the residual strain, non-recoverable strain or the *plastic strain*. If unloading reaches the plastic strain point, it is called the full unloading (BC and IJ). In the progress of unloading, if reloading initiates before unloading curve reaches the plastic strain, it is called partial unloading (FG and KL).

Reloading curve (CDE) represents the behaviour of concrete during reloading. It initiates from the reloading point (C) and reaches the envelope curve at point "E" which is named as return point (E,H and M). The coordinates of the last point of unloading curve or the first point of reloading curve (C,G,J and L), are termed as reloading stress and reloading strain. In the case of full unloading, reloading point is the same as plastic strain point (C and J). If reloading reaches the envelope curve, it is called full reloading (CDE,GNH and LM). If another unloading starts before it reaches the envelope curve, it

Table 6.1: Terminology used in the stress-strain curve for cyclic loading of concrete.

Component or point	Terminology and description
ABEFHIM	Envelope curve
B,F,I,K	Unloading point
AC	Plastic strain (strain at C)
AJ	Plastic strain (strain at J)
BC,FG,IJ,KL	Unloading curve
C,G,J,L	Reloading point
CDE,GNH,JK,LM	Reloading curve
BD	Damage due to cycle BCD
FN	Damage due to cycle FGN
E,H,M	Return point
BC,IJ	Full unloading
FG,KL	Partial unloading
CDE,GNH,LM	Full reloading
JK	Partial reloading
X	Common point

is called partial reloading (JK). In a particular loading cycle in concrete (BCDE), during reloading, the stress corresponding to the unloading strain (PD) is always lower than the initial unloading stress (PB). This loss of stress is termed as deterioration or damage in concrete due to loading cycle (BD).

Several different definitions have been reported in the literature for the above explained key components of the stress-strain curves for unconfined as well as confined NSC subjected to cyclic loading. This chapter describes the experimental programs and different definitions for those key components namely, envelope curve, unloading curve, reloading curve, plastic strain point and the damage in concrete due to each cycle. It finally identifies the need for a simple constitutive model for confined HSC subjected to cyclic loading.

6.2 Previous work on models for cyclic loading of concrete

Experimental programs to study the constitutive behaviour of unconfined or confined NSC subjected to cyclic loading date back to the early 1960s. Major objectives of these experimental programs can be summarised as follows:

- To compare the stress-strain curve for monotonically increasing load and the envelope curve for cyclic loading of concrete.
- To find the behaviour of unloading and reloading curves.
- To estimate the plastic strain.
- To estimate the damage in concrete due to each cycle of loading.

6.2.1 Experimental work

Unconfined concrete

The research works for cyclic loading of unconfined concrete were published before that for confined concrete. Sinha et al. (1964) found that the response of concrete to loading and unloading cycles has not been reported in the literature. As a result, they conducted an experimental program on twenty four 6 × 12-in cylinders of 28 MPa compressive strength and twelve 3 × 6-in cylinders of 25 and 20 MPa compressive strengths. Studying the behaviour of plain concrete under cyclic loading was the aim of the experimental investigation. There were several points of interest.

1. Shape of the unloading and reloading curves for different loading histories and the possibility of representing them as a family of curves
2. A comparison of the monotonic loading curve with the envelope curve obtained from the cyclic loading of concrete
3. Investigation of the uniqueness of stress-strain relationships

Similar to Sinha et al. (1964), Karsan and Jirsa (1969) tested 46 short rectangular columns subjected to cyclic loading to establish stress-strain curves for plain concrete. Later Desayi et al. (1979) also conducted few cyclic loading tests on unconfined concrete for the purpose

of comparison with confined concrete. Instead of the circular, square or rectangular cross sections of the specimens as carried out by other researchers, Zhang et al. (1984) tested 58 prismatic concrete specimens ($10 \times 10 \times 30$ cm). The compressive strengths used were 50 and 30 MPa and they were tested under three different loading conditions; monotonic loading, cyclic loading with equal strain increments and repeated cycles of loading in each strain increment.

Confined concrete

The experimental programs were then extended to observe the behaviour of confined concrete subjected to cyclic loading. Desayi et al. (1979) performed repeated loading tests on 150 mm diameter \times 300 mm high concrete cylinders with 13-23 MPa compressive strength and circular steel spirals confining the concrete. The loading and unloading was performed for 6 to 10 cycles increasing the unloading strain at each cycle until the load reached 70% of the maximum load after reaching the peak. In their experimental program, it was decided to have 2-3 cycles before peak stress, 1 or 2 cycles near peak and 2-3 cycles in the descending branch after the peak stress. Sakai and Kawashima (2000) tested larger confined concrete cylinders (600 mm high and 200 mm in diameter) than those used by Desayi et al. (1979). The compressive strengths considered varied from 23 to 36.7 MPa while the volumetric ratio varied from 0.67 to 2.67%. The specimens were subjected to uniaxial loading under displacement control. Otter and Naaman (1988) tested 32 cylindrical specimens of fibre reinforced concrete. The compressive strengths had a range of 25-46 MPa.

Based on these experimental programs, several definitions were proposed for the key components shown in Figure 6.1. They are explained in detail in the following sections.

6.3 Envelope curve

A definition of the envelope curve is given in Figure 6.1 and Section 6.1. Sinha et al. (1964) were the first group of researchers to publish research work about the envelope curve. Their definition is shown in Figure 6.2. They defined it as the locus of broken lines connecting the start of unloading curve (B or F) and the end of reloading curve (E or H). Desayi et al. (1979) and Shah et al. (1983) superimposed stress-strain curves for monotonically increasing load onto those for cyclic loading of concrete for comparison.

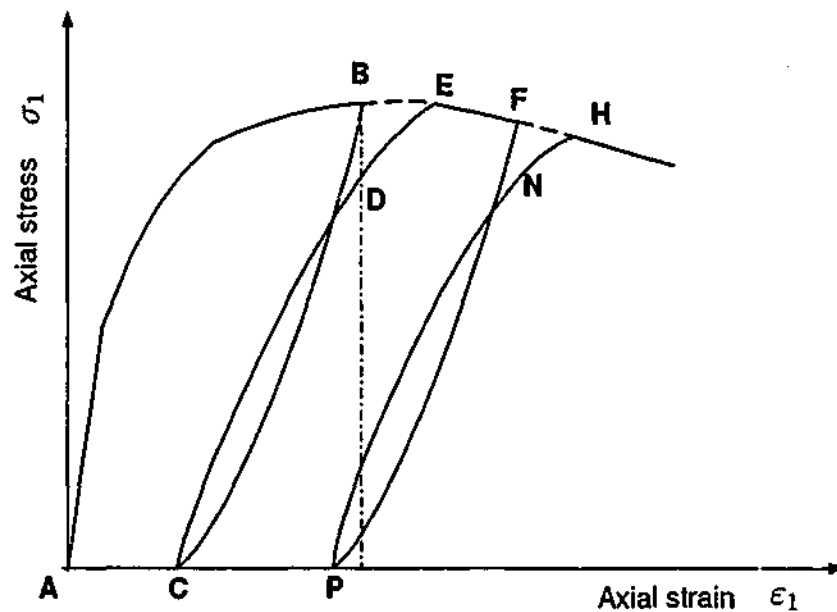


Figure 6.2: Envelope curve for cyclic loading of concrete.

From the previously published research programs, the envelope curve was defined as the stress-strain curve obtained under monotonically increasing load to failure for unconfined concrete (Karsan and Jirsa 1969; Desayi et al. 1979; Perry and Cheong 1991) as well as for confined concrete (Karsan and Jirsa 1969; Desayi et al. 1979; Maher and Darwin 1980; Shah et al. 1983; Zhang et al. 1984; Yankelevsky and Reinhardt 1987; Mander et al. 1988b; Otter and Naaman 1988; Cheong and Perry 1993).

6.4 Plastic strain

The definition of plastic strain is provided in Figure 6.1 and in Section 6.1. However, different estimations of plastic strain are available in the literature. They are presented here in detail.

6.4.1 Plastic strain based on unloading strain only

The plastic strain was considered to be a function of the unloading strain by many researchers (Karsan and Jirsa 1969; Darwin and Pecknold 1977; Maher and Darwin 1980; Zhang et al. 1984). Darwin and Pecknold (1977) established an empirical relationship between the unloading strain in the envelope curve (ϵ_{un}), and the plastic strain (ϵ_{pl}), as follows:

$$\frac{\epsilon_{pl}}{\epsilon_{cu}} = 0.145 \left(\frac{\epsilon_{un}}{\epsilon_{cu}} \right)^2 + 0.13 \left(\frac{\epsilon_{un}}{\epsilon_{cu}} \right). \quad (6.1)$$

ϵ_{cu} is the ultimate strain in concrete. Similar power function was introduced by Zhang et al. (1984) for the plastic strain (ϵ_{pl}) as follows:

$$X_p = GX_{un}^H \quad (6.2)$$

$$X_p = \frac{\epsilon_{pl}}{\epsilon_{cc}} \quad \text{and} \quad X_{un} = \frac{\epsilon_{un}}{\epsilon_{cc}} \quad (6.3)$$

ϵ_{cc} is the axial strain corresponding to peak stress, G and H are material parameters.

Otter and Naaman (1989) suggested that plastic strain for plain and fibre reinforced concrete is a function of unloading strain. It was approximated by a generalised exponential expression as shown in the Equation (6.4).

$$\frac{\epsilon_{pl}}{\epsilon_{cc}} = \frac{\epsilon_{un}}{\epsilon_{cc}} - k_u \left(1 - e^{-\frac{\epsilon_{un}}{k_u \epsilon_{cc}}} \right) \quad (6.4)$$

ϵ_{pl} is the plastic strain, ϵ_{un} is the unloading strain, ϵ_{cc} is the strain at the peak stress of monotonic curve and k_u is an unloading constant which was estimated to be 0.8.

6.4.2 Plastic strain based on unloading stress and strain

Mander et al. (1988b) defined the plastic strain, ϵ_{pl} based on the coordinates at the unloading point ($\epsilon_{un}, \sigma_{un}$), in order to establish the unloading curve from the compressive loading curve. The procedure used by them is similar for both confined and unconfined concrete. According to their study, the plastic strain (ϵ_{pl}) depends on the strain ϵ_a at the intersection of the initial tangent and the plastic unloading secant slopes (Figure 6.3).

$$\epsilon_a = a \sqrt{\epsilon_{un} \epsilon_{cc}} \quad (6.5)$$

The value of a will be,

$$a = \frac{\epsilon_{cc}}{\epsilon_{cc} + \epsilon_{un}} \quad \text{or} \quad \frac{0.09 \epsilon_{un}}{\epsilon_{cc}}, \quad \text{whichever is greater.} \quad (6.6)$$

ϵ_{cc} is the axial strain corresponding to peak axial stress. Plastic strain on the secant line between ϵ_a and ϵ_{un} is given by,

$$\epsilon_{pl} = \frac{(\epsilon_{un} + \epsilon_a) \sigma_{un}}{(\sigma_{un} + E_c \epsilon_a)} \quad (6.7)$$

where, σ_{un} is the axial stress at unloading point and E_c is the modulus of elasticity of concrete.

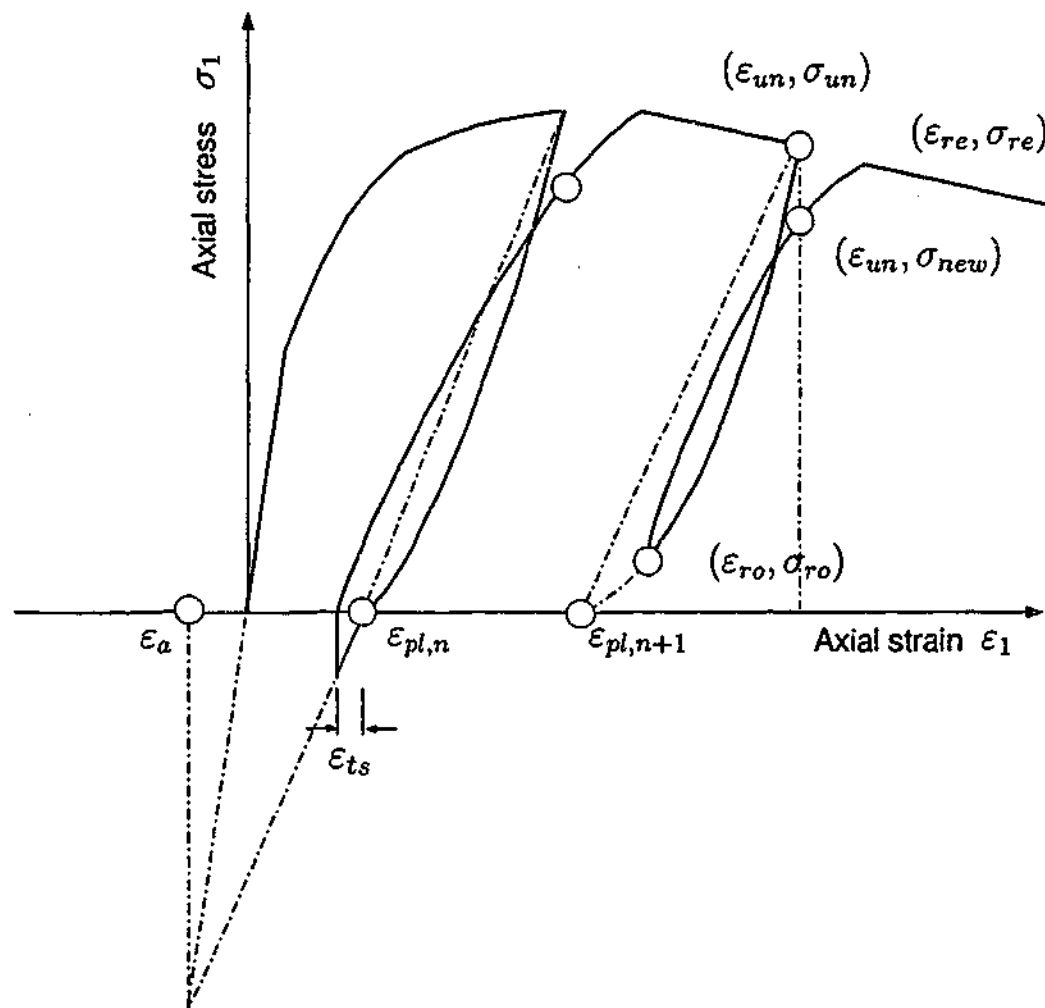


Figure 6.3: Stress-strain curves for unloading and reloading.

6.4.3 Plastic strain based on unloading strain and number of cycles

Sakai and Kawashima (2000) defined the plastic strain in a different way by arguing that it increases as the number of cycles increases. They defined the term $\epsilon_{pl,n}$ for plastic strain after n cycles. For the first cycle ($n=1$) it is given by,

$$\epsilon_{pl,n} = \begin{cases} 0 & \text{if } 0 \leq \epsilon_{un} \leq 0.001, \\ 0.40(\epsilon_{un} - 0.001) & \text{if } 0.001 \leq \epsilon_{un} \leq 0.0035, \\ 0.94(\epsilon_{un} - 0.00245) & \text{if } 0.0035 \leq \epsilon_{un} \leq 0.03. \end{cases} \quad (6.8)$$

For two consecutive loading cycles from the same unloading point there are two different corresponding plastic strains ($\epsilon_{pl,n-1}$ and $\epsilon_{pl,n}$). A relationship between these two plastic strain and the unloading strain (ϵ_{un}), is termed as increasing ratio of plastic strain (γ_n).

It is given as,

$$\gamma_n = \frac{\varepsilon_{un} - \varepsilon_{pl,n}}{\varepsilon_{un} - \varepsilon_{pl,n-1}} \quad (6.9)$$

where,

$$\gamma_n = \begin{cases} 0.945 & \text{if } n = 2 \\ 0.965 + 0.005(n - 3) & \text{if } n \geq 3 \end{cases} \quad (6.10)$$

and n is the number of cycles.

6.4.4 Summary of plastic strain works

Majority of the researchers defined plastic strain using only the unloading strain (Karsan and Jirsa 1969; Darwin and Pecknold 1977; Maher and Darwin 1980; Zhang et al. 1984). Few others (Mander et al. 1988b; Sakai and Kawashima 2000) defined plastic strain using unloading stress or the number of cycles together with the unloading strain. If plastic strain depends only on the unloading strain, there cannot be different plastic strains corresponding to many cycles originating from the same unloading strain. In this sense, plastic strain based on unloading strain and stress and/ or unloading strain and number of cycles seem to be more realistic than that based on only the unloading strain. As a summary, plastic strain depends on the the following parameters.

- Unloading stress and strain
- Number of cycles.

6.5 Unloading curve

The shape of the unloading curve is normally characterised by its concavity and single curvature. The mathematical expressions used to describe unloading curve include parabolic (Sinha et al. 1964; Karsan and Jirsa 1969; Sakai and Kawashima 2000), bilinear (Park et al. 1972; Elmorsi et al. 1998), trilinear (Darwin and Pecknold 1976; Yankelevsky and Reinhardt 1987), power (Zhang et al. 1984) functions, combined linear and parabolic functions (Watanabe and Muguruma 1988) and combined linear and power functions (Otter and Naaman 1989). Each of these proposed types are discussed in detail in the following sections.

6.5.1 Unloading curve as a parabolic function

Sinha et al. (1964) defined unloading curve as a different curve which will be traced in the stress-strain plane when the strain was decreased from a value above the elastic limit of concrete. A set of unloading curves were obtained by varying the strain at the unloading point. It was found that this set can be represented by a mathematical family of curves named as "family of unloading curves". The family of unloading curves obtained from the experimental program could be approximated by a second order curve as shown in Equation (6.11).

$$\sigma_1 + H = \frac{J}{X}(\varepsilon_1 - X)^2 \quad (6.11)$$

H and J are experimental constants, $(\varepsilon_1, \sigma_1)$ are the coordinates of any point in the unloading curve and X is a parameter which is different for different members of the family. For an unloading curve passing through a known point (ε, σ) , these coordinates are substituted in Equation (6.11) to determine the value of the parameter X .

$$X = \varepsilon + \frac{\sigma + H}{2J} - \sqrt{\left(\varepsilon + \frac{\sigma + H}{2J}\right)^2 - \varepsilon^2}. \quad (6.12)$$

However, the known point (ε, σ) was not clearly defined by Sinha et al. (1964). It may be the unloading point or the plastic strain point. Unloading curves obtained from the above equations compared reasonably well with the experimental results.

Similar to Sinha et al. (1964), a second degree parabola was selected by Karsan and Jirsa (1969) to represent unloading curve. The findings of Karsan and Jirsa (1969) study was that the shape of the loading and unloading curve is a function of plastic strain ratio. The coordinates of the unloading point at the envelope curve $(\varepsilon_{un}, \sigma_{un})$, the common point $(\varepsilon_{cp}, \sigma_{cp})$ and the plastic strain point $(\varepsilon_{pl}, 0)$ defined the second degree parabola for unloading curve.

A novel method was adopted by Sakai and Kawashima (2000) in defining the unloading curve. They first obtained a relationship between normalised stress $(\bar{\sigma}_1)$ and normalised strain $(\bar{\varepsilon}_1)$.

$$\bar{\sigma}_1 = \frac{\sigma_1}{\sigma_{un}} \quad \bar{\varepsilon}_1 = \frac{\varepsilon_1 - \varepsilon_{pl}}{\varepsilon_{un} - \varepsilon_{pl}}. \quad (6.13)$$

σ_1 and ε_1 are axial stress and strain respectively, $(\sigma_{un}, \varepsilon_{un})$ are the coordinates of the unloading point and ε_{pl} is the corresponding plastic strain. Therefore for an assigned

axial strain, ϵ_1 , axial stress for unloading curves is given by,

$$\sigma_1 = \sigma_{un} \left(\frac{\epsilon_1 - \epsilon_{pl}}{\epsilon_{un} - \epsilon_{pl}} \right)^2 \quad (6.14)$$

using the plastic strain defined in Equation (6.8).

A combination of a parabolic function and a straight line was used as the unloading curve by Watanabe and Muguruma (1988). In their study, unloading curve is a straight line until it intersects common point of the unloading and reloading curves and after that it is a parabola.

6.5.2 Unloading curve as a bilinear function

Park et al. (1972) used the idealised behaviour shown in Figure 6.4 for repeated loading of concrete. At the beginning of unloading, it is assumed that 0.75 of the previous stress is lost without a decrease in strain and then it follows a linear path with a slope of $0.25E_c$. E_c is the tangent modulus of concrete. It is noted that the average slope of the idealised loop is parallel to the initial tangent modulus of the stress-strain curve.

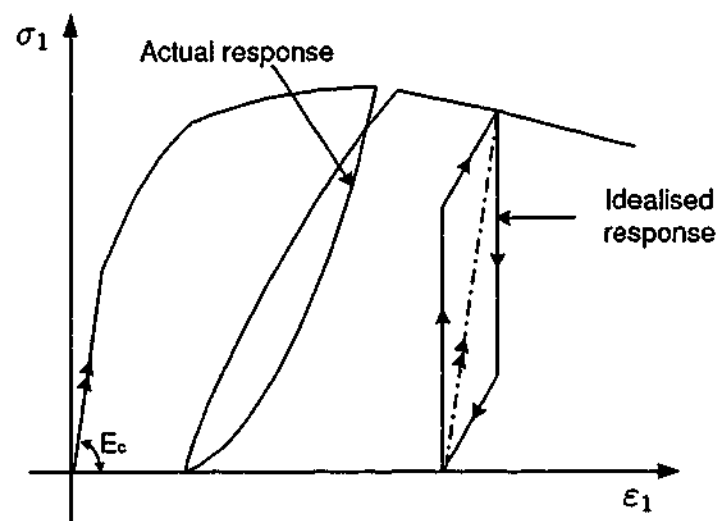


Figure 6.4: Stress-strain behaviour of concrete with cyclic loading (Park et al. 1972).

A different form of bilinear unloading curve was proposed by Elmorsi et al. (1998). They defined the typical stress-strain relationship for cyclic compression of reinforced concrete as shown in Figure 6.5. It is based on the findings of previous experimental and analytical studies. The unloading curve is composed of two regions, initial unloading region and the zero stiffness region. The initial unloading region is a straight line which

starts from unloading point $(\epsilon_{un}, \sigma_{un})$ and has a slope of E_{un} . The unloading stiffness, E_{un} is defined in terms of unloading strain and the strain at the peak stress as given in Equation (6.15).

$$\frac{E_{un}}{E_c} = 1 - 0.3 \left(\frac{\epsilon_{un}}{\epsilon_{cc}} - 1 \right) \quad (6.15)$$

E_c is the tangent modulus of elasticity of concrete and is given by,

$$E_c \geq E_{un} \leq 0.25E_c. \quad (6.16)$$

According to the studies by Elmorsi et al. (1998), the initial unloading region ends, when concrete stress becomes zero. This zero stress is then continued until another reloading initiates.

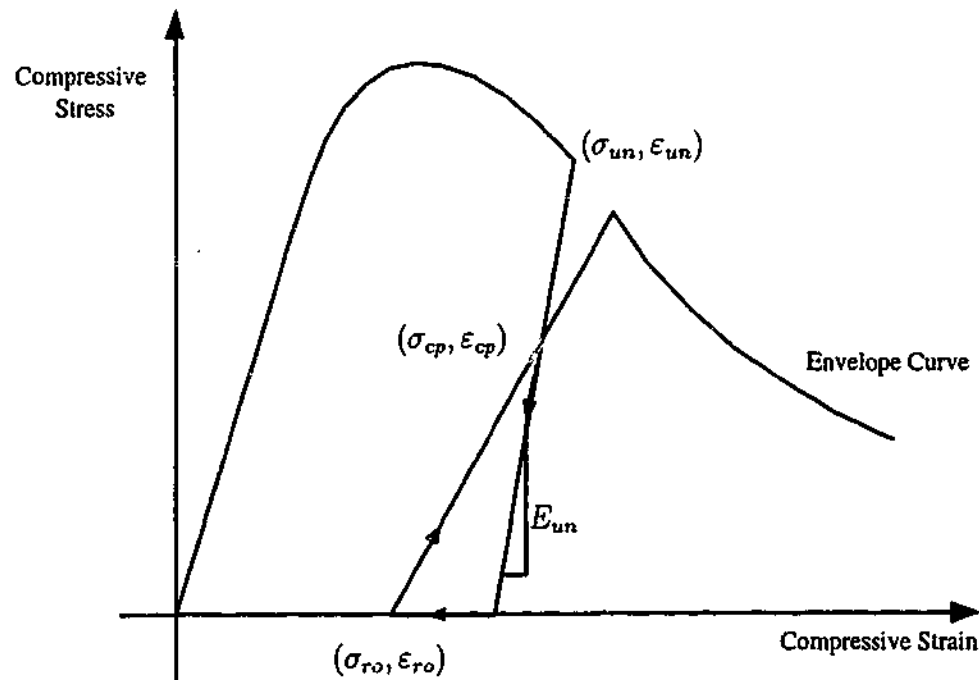


Figure 6.5: Proposed cyclic stress-strain curve for concrete in compression (Elmorsi et al. 1998).

6.5.3 Unloading curve as a trilinear function

Darwin and Pecknold (1977) showed that a model developed to simulate the cyclic response of concrete should be capable of accounting for strength degradation, stiffness degradation and hysteretic behaviour under loading cycles. The proposed model was based on the experimental data on uniaxial loading of Karsan and Jirsa (1969). Typical hysteresis curve for the proposed model is shown in Figure 6.6.

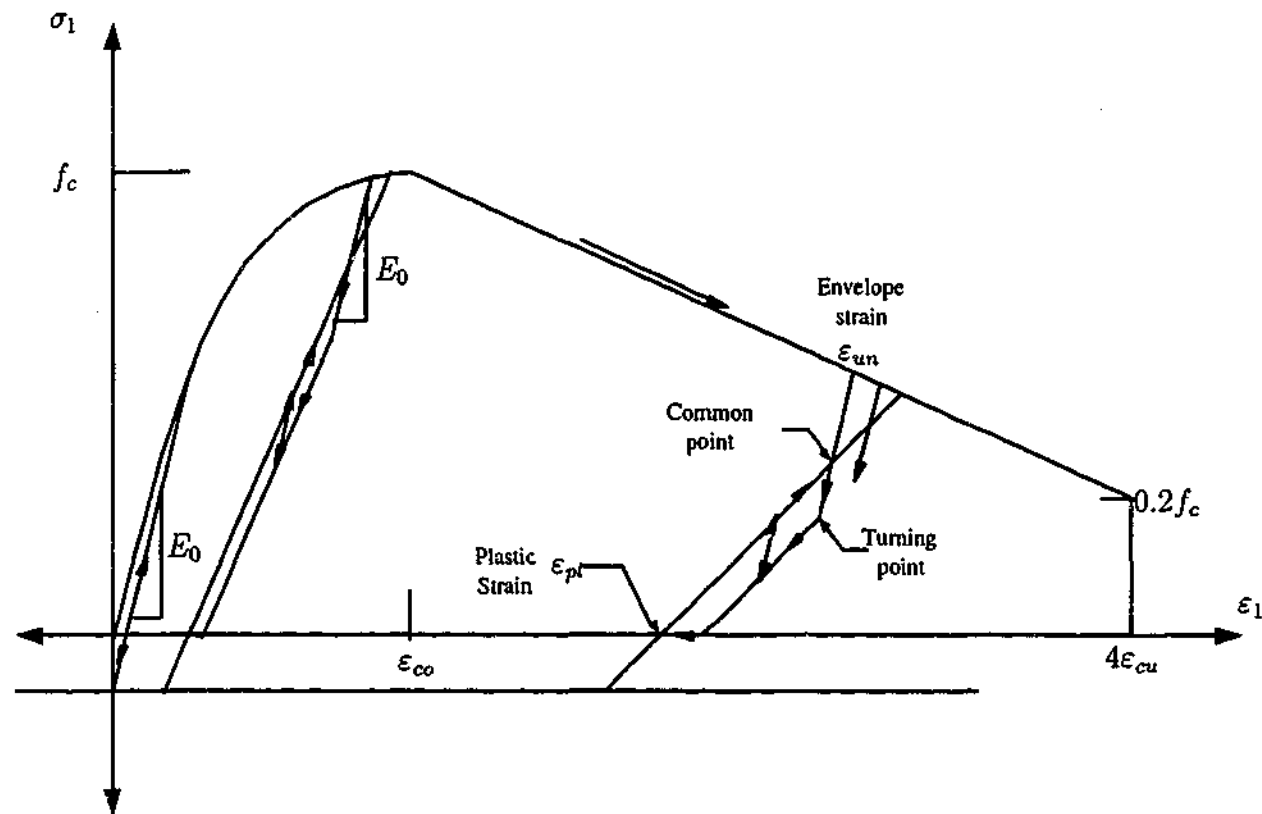


Figure 6.6: Scheme of focal points model (Darwin and Pecknold 1977).

Straight lines are used for hysteresis loops. The size and shape of the loops were based on several of the findings of Karsan and Jirsa (1969). At high uniaxial strains, Darwin and Pecknold (1977) approximated the unloading curve by three straight lines: the first with slope E_0 , the second parallel to the reloading line; and the third with zero slope. The unloading curves initially follow the line with slope E_0 between the parallel unloading and reloading lines. However in the model explanations of Darwin and Pecknold (1977), it is not clear what should be the slope of these parallel unloading and reloading lines.

Another form of a trilinear unloading curve was proposed by Yankelevsky and Reinhardt (1987). They introduced several geometrical points in the uniaxial stress-strain plane in order to define the unloading and reloading curves. The unloading curve is concave from the unloading point and has a high stiffness. With the progress of unloading, the slope of the unloading curve decreases gradually at low stress levels. A non dimensional uniaxial stress-strain coordinate system was defined. The non-dimensional stress coordinate in compression was defined as,

$$U = \frac{\sigma_1}{f_c} \quad (6.17)$$

where σ_1 is the stress and f_c is the compressive strength of concrete. The non-dimensional strain coordinate in compression was defined as,

$$S = \frac{\epsilon_1}{\epsilon_{cc}} \quad (6.18)$$

where ϵ_1 is the axial strain and ϵ_{cc} is the strain corresponding to the peak stress in envelope curve. In this coordinate system, the envelope curve is plotted having peak point coordinates (1,1). As shown in Figure 6.7, the focal points E, F, G, H and I are placed along the tangent at the origin to the envelope curve with the following coordinates.

$$U_E = -3.0 \times U_{max} \quad (6.19)$$

$$U_F = -U_{max} \quad (6.20)$$

$$U_G = -0.75 \times U_{max} \quad (6.21)$$

$$U_H = -0.47 \times U_{max} \quad (6.22)$$

$$U_I = -0.2 \times U_{max} \quad (6.23)$$

The coordinates of focal point J are

$$S_J = -1.0; \quad U_J = 0 \quad (6.24)$$

For a given unloading point, the following procedure is used to obtain the stress-strain relationships.

1. Connect the unloading point $A(S, U)$ and the focal point F by a straight line. The line intersects the non-dimensional strain axis at point $B(S_B, 0)$. S_B corresponds to the plastic strain of that particular cycle.
2. Line connecting the focal point G and known point B intersects at point $C(S, U_C)$ with a vertical line. Point C is the intersection point of the unloading and reloading curves.
3. Line connecting the focal point E with the known point C intersects at point D with the line connecting focal points I and B. Three parts of the unloading branch is now determined as AC-CD-DB and the initial region of the reloading branch is also known, BC.

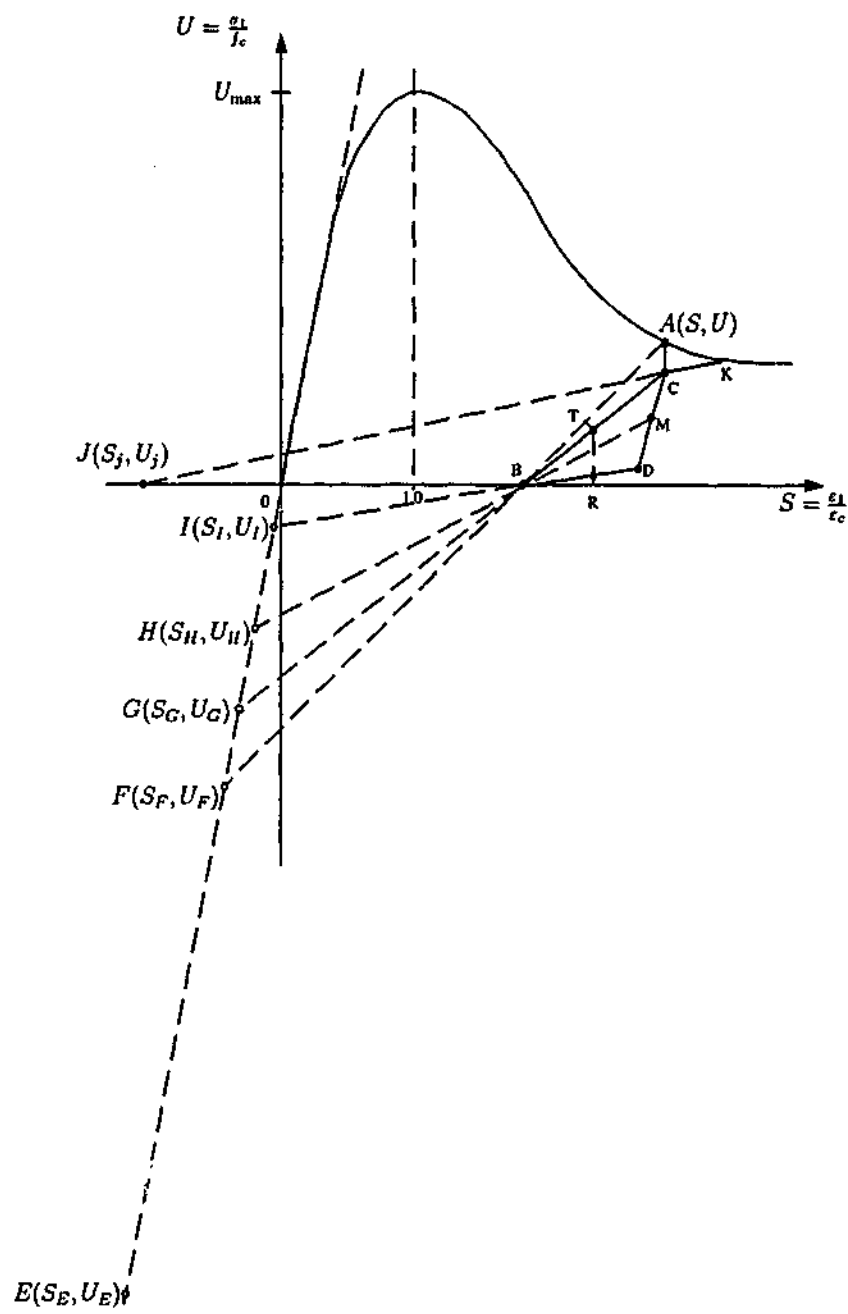


Figure 6.7: Model for plain concrete under cyclic load (Yankelevsky and Reinhardt 1987).

4. To complete the reloading curve, remaining part CK is obtained by connecting focal point J and common point C. K is the intersection point with the envelope curve.

This graphical method was represented by a mathematical formulation in their study.

6.5.4 Unloading curve as a power function

Zhang et al. (1984) defined the unloading curve using the plastic strain explained earlier in Equation (6.2).

$$\frac{\sigma_1}{\sigma_{un}} = \left(\frac{\epsilon_1 - \epsilon_{pl}}{\epsilon_{un} - \epsilon_{pl}} \right)^n \quad (6.25)$$

(ϵ_1, σ_1) is any strain and stress level in unloading curve. n can be obtained from,

$$n = 1 + \sqrt{X_{un}} \quad (6.26)$$

where, X_{un} is defined in Equation (6.3).

A similar kind of power equation was combined with a linear function by Otter and Naaman (1989) to form a general polynomial for the unloading curve.

$$\frac{\sigma_1}{\sigma_{un}} = (1 - p) \left(\frac{\epsilon_1 - \epsilon_{pl}}{\epsilon_{un} - \epsilon_{pl}} \right) + p \left(\frac{\epsilon_1 - \epsilon_{pl}}{\epsilon_{un} - \epsilon_{pl}} \right)^{n_{uc}} \quad (6.27)$$

(σ_1, ϵ_1) is any point in the unloading curve, $(\sigma_{un}, \epsilon_{un})$ is the unloading point, ϵ_{pl} is the plastic strain, p and n_{uc} are the unloading curve parameters and approximated as 0.9 and 3 respectively.

6.5.5 Unloading curve as a modified form of ascending branch of monotonic loading curve

A different approach was taken by Desayi et al. (1979) and Mander et al. (1988b) in defining equations for the stress-strain curves of repeated loading tests. They observed a similarity between the unloading curve and the ascending branch of the monotonically increasing loading curve.

The equations proposed by Desayi et al. (1979) were based on the stress ratio (F) and strain ratio (S) defined as,

$$F = \frac{\sigma_1}{f_{cc}} \quad \text{and} \quad S = \frac{\epsilon_1}{\epsilon_{cc}} \quad (6.28)$$

where (ϵ_1, σ_1) is the strain and stress at any stress level and (ϵ_{cc}, f_{cc}) is the peak point coordinates of confined concrete. Curves were plotted for the unloading $F - S$ values. It

was found that the general shape of the unloading $F - S$ curve is similar to the rising branch of the monotonic loading curve. The unloading curve is defined by using the initial slope of the unloading curve, plastic strain and an intermediate point on the unloading curve. The unloading curve is thus defined as,

$$\sigma_1 = \sigma_{un} - \frac{E_{un}(\epsilon_{un} - \epsilon_{pl})^2 \sigma_{un}(\epsilon_{un} - \epsilon_1)}{Dr(3)} \quad (6.29)$$

where,

$$\begin{aligned} Dr(3) = & (\epsilon_{un} - \epsilon_{pl})^2 \sigma_{un} \\ & + [(1.353E_{un}(\epsilon_{un} - \epsilon_{pl})^2 - 3\sigma_{un}(\epsilon_{un} - \epsilon_{pl}))](\epsilon_{un} - \epsilon_1) \\ & + [2\sigma_{un} - 0.353E_{un}(\epsilon_{un} - \epsilon_{pl})](\epsilon_{un} - \epsilon_{pl})^2 \end{aligned} \quad (6.30)$$

and

$$E_{un} = f_{cc}/(0.033\epsilon_{cc} + 0.06\epsilon_{un}) \quad (6.31)$$

(σ_1, ϵ_1) is the stress and strain at any point in the unloading branch, $(\sigma_{un}, \epsilon_{un})$ is the stress and strain at the onset of unloading, (f_{cc}, ϵ_{cc}) is the peak axial stress and corresponding axial strain and ϵ_{pl} is the plastic strain.

A similar concept was used by Mander et al. (1988b) in defining the unloading curve. In their study, it is a modified form of the ascending branch of the stress-strain curve corresponding to monotonically increasing load. The unloading curve was based on the plastic strain defined in Equation (6.7).

$$\sigma_1 = \sigma_{un} - \frac{\sigma_{un}x_{un}r_{un}}{r_{un} - 1 + x_{un}^{r_{un}}} \quad (6.32)$$

x_{un} and r_{un} are given by,

$$r_{un} = \frac{E_{un}}{E_{un} - E_{sec}} \quad (6.33)$$

where,

$$E_{sec} = \frac{\sigma_{un}}{\epsilon_{un} - \epsilon_{pl}} \quad (6.34)$$

and

$$x_{un} = \frac{\epsilon_1 - \epsilon_{un}}{\epsilon_{pl} - \epsilon_{un}} \quad (6.35)$$

E_{un} is the initial modulus of elasticity at the onset of unloading and given by,

$$E_{un} = \left(\frac{\sigma_{un}}{f_c}\right) \left(\frac{\epsilon_{cc}}{\epsilon_{un}}\right)^{0.5} E_c \quad (6.36)$$

6.5.6 Summary of models for unloading curve

The unloading curve of unconfined and confined NSC is defined in many simple equations (parabolic, bilinear and trilinear) and complex equations (power). An interesting approach was used by few researchers, who found a similarity in the shape of the unloading curve and the ascending branch of the monotonically increasing loading curve for concrete. The parameters defining the unloading curve can be summarised as follows:

- Unloading point
- Common point
- Reloading point or plastic strain point

6.6 Damage due to each cycle

When concrete is unloaded from the point $(\sigma_{un}, \epsilon_{un})$ and reloaded again, in the reloading curve the stress value corresponding to unloading strain is always lower than the unloading stress (σ_{un}) . This stress loss is called damage due to this loading cycle and this is illustrated in Figure 6.8.

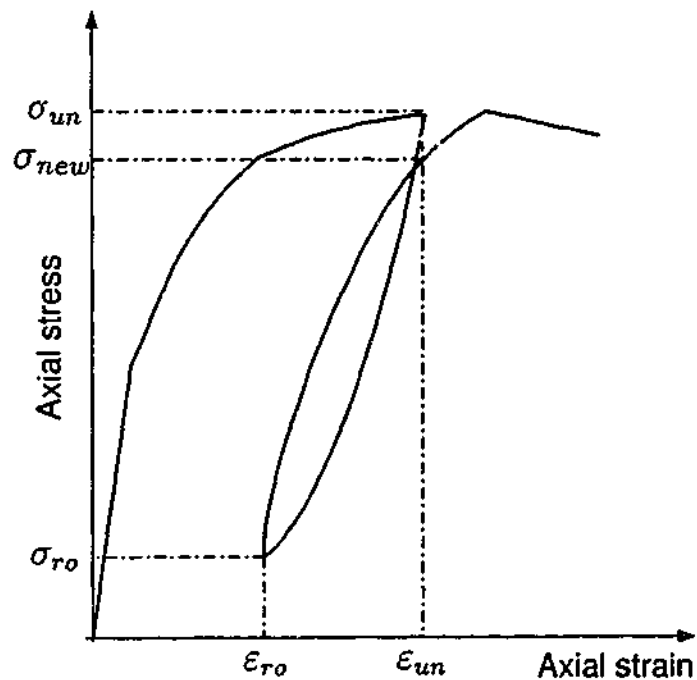


Figure 6.8: Damage due to loading cycle.

Mander et al. (1988b) defined the damage in concrete in terms of the unloading stress (σ_{un}) and reloading stress (σ_{ro}).

$$\sigma_{new} = 0.92\sigma_{un} + 0.08\sigma_{ro}. \quad (6.37)$$

σ_{new} is the new stress level reached at the end of reloading. In order to estimate the deterioration of stress at unloading strain, ϵ_{un} after unloading and reloading, a stress deterioration ratio, β_n was introduced by Sakai and Kawashima (2000) as given below:

$$\beta_n = \frac{\sigma_{new}}{\sigma_{un}}. \quad (6.38)$$

σ_{un} is the unloading stress and σ_{new} is the new return stress. Deterioration ratio depends on the number of cycles, n and unloading strain, ϵ_{un} . If $1 \leq n \leq 2$, then

$$\beta_n = \begin{cases} 1 & \text{if } 0 \leq \epsilon_{un} \leq 0.001 \\ 1 - (10n + 22)(\epsilon_{un} - 0.001) & \text{if } 0.001 \leq \epsilon_{un} \leq 0.0035 \\ 0.92 + 0.025(n - 1) & \text{if } 0.0035 \leq \epsilon_{un} \leq 0.03. \end{cases} \quad (6.39)$$

If $n \geq 3$, then

$$\beta_n = \begin{cases} 1 & \text{if } 0 \leq \epsilon_{un} \leq 0.001 \\ 1 - (2n + 8)(\epsilon_{un} - 0.001) & \text{if } 0.001 \leq \epsilon_{un} \leq 0.0035 \\ 0.965 + 0.005(n - 3) & \text{if } 0.0035 \leq \epsilon_{un} \leq 0.03. \end{cases} \quad (6.40)$$

In summary, the damage due to each unloading reloading cycle has been termed as a function of unloading stress and reloading stress (Mander et al. 1988b) or as a function of unloading strain and the number of cycles (Sakai and Kawashima 2000).

6.7 Reloading curve

The shape of the reloading curve is more complex than that of the unloading curve. Existing models use straight line (Sinha et al. 1964; Darwin and Pecknold 1976; Aoyama and Noguchi 1979; Yankelevsky and Reinhardt 1987; Otter and Naaman 1989; Elmorsi et al. 1998), bilinear (Park et al. 1972; Yankelevsky and Reinhardt 1987), parabolic (Karsan and Jirsa 1969; Desayi et al. 1979), combination of a straight line and a parabolic function (Mander et al. 1988b; Watanabe and Muguruma 1988; Sakai and Kawashima 2000) and a power function (Zhang et al. 1984). Each type is discussed in detail in the following sections.

6.7.1 Reloading curve as a straight line

Sinha et al. (1964) reported that after unloading, if the strain is increased then another curve is traced in the stress-strain plane which will be called as a reloading curve as described in Figure 6.1. Due to the hysteresis effect, reloading curve is different from the unloading curve. Reloading curves starting from different stages of unloading forms a set of reloading curves. If this set of reloading curves can be represented by a mathematical family of curves it is called "family of reloading curves" by Sinha et al. (1964). From the experimental results, the family of reloading curves could be represented by straight lines as follows:

$$\sigma_1 + K = Y(\epsilon_1 + L). \quad (6.41)$$

K and L are experimental constants and Y is a parameter which could be found similar to parameter X in Equation (6.11).

$$Y = \frac{\sigma + K}{\epsilon + L}. \quad (6.42)$$

By comparing with the experimental results, Sinha et al. (1964) concluded that the analytical curves are sufficiently realistic.

Both Darwin and Pecknold (1977) and Yankelevsky and Reinhardt (1987) approximated the reloading curve by a straight line from the plastic strain ($\epsilon_{pl}, 0$) point through the common point. Same idea was supported by Elmorsi et al. (1998) and replaced the plastic strain point by the general reloading point ($\epsilon_{ro}, \sigma_{ro}$). In the proposed model, common point ($\epsilon_{cp}, \sigma_{cp}$) is assumed to be the intersection of the initial unloading curve and the reloading curve and σ_{cp} is assumed to be $0.7\sigma_{un}$. In their study, reloading point or the plastic strain point and common point were used in defining the reloading curve.

Instead of the common point used by Darwin and Pecknold (1977), Yankelevsky and Reinhardt (1987) and Elmorsi et al. (1998), return point coordinates were used by Otter and Naaman (1989) in defining the reloading curve. Otter and Naaman (1989) selected a linear expression for the reloading curve by arguing that it provides a good approximation to the actual behaviour and it is a continuous function throughout. It is given by,

$$\frac{\sigma_1}{\sigma_{re}} = \left(\frac{\epsilon_1 - \epsilon_{re}}{\epsilon_{re} - \epsilon_{pl}} \right) \quad (6.43)$$

where (σ_1, ϵ_1) is any point in the reloading curve, $(\sigma_{re}, \epsilon_{re})$ is the return point (ie. point at which the reloading curve reaches the envelope curve) and ϵ_{pl} is the plastic strain. Otter

and Naaman (1989) defined the return point as a function of unloading strain as shown in Equation (6.44).

$$\frac{\epsilon_{re}}{\epsilon_{cc}} = \frac{\epsilon_{un}}{\epsilon_{cc}} + k_r. \quad (6.44)$$

ϵ_{re} is the return strain, ϵ_{cc} is the strain at the peak stress of monotonic curve and constant k_r can be taken as 0.1 for both plain and fibre-reinforced concrete.

6.7.2 Reloading curve as a parabolic function

Karsan and Jirsa (1969) defined a second degree parabola for reloading curve using the coordinates of the reloading point $(\epsilon_{pl}, 0)$, the common point $(\epsilon_{cp}, \sigma_{cp})$ and the point at which the reloading curve reaches the envelope curve $(\epsilon_{re}, \sigma_{re})$.

Desayi et al. (1979) defined the reloading branch using stress ratio (F) and strain ratio (S) defined in Equation (6.28). It starts from the plastic strain of the previous unloading, intersects the unloading branch and meets the envelope curve. $F - S$ curve for reloading was approximated by a second degree parabola. The reloading curve was defined by using the initial slope of the reloading curve and an intermediate point on the reloading curve. It was thus defined as,

$$\sigma_1 = \left[\frac{0.8\sigma_{un} - E_{rl}(\epsilon_{un} - \epsilon_{pl})}{(\epsilon_{un} - \epsilon_{pl})^2} \right] \times (\epsilon_1 - \epsilon_{pl})^2 + E_{rl}(\epsilon_1 - \epsilon_{pl}) \quad (6.45)$$

where,

$$E_{rl} = E_c f_{cc} / (f_{cc} + 0.5 E_c \epsilon_{un}). \quad (6.46)$$

6.7.3 Reloading curve as a combination of straight line and a parabolic function

Mander et al. (1988b) reported that the coordinates of the reloading point $(\epsilon_{ro}, \sigma_{ro})$ may be from either the unloading curve or from the cracked state where $\epsilon_{ro} = (\epsilon_{pl} - \epsilon_{ts})$ and $\sigma_{ro} = 0$ as shown in Figure 6.3. ϵ_{ts} is the tensile strain and is given by,

$$\epsilon_{ts} = \frac{f_t}{E_i}. \quad (6.47)$$

A linear stress-strain relationship which accounts for the degradation due to cyclic behaviour is assumed between reloading strain and unloading strain,

$$\sigma_1 = \sigma_{ro} + E_r(\epsilon_1 - \epsilon_{ro}) \quad (6.48)$$

to a revised stress magnitude which is denoted by σ_{new} , defined in Equations (6.37) and,

$$E_r = \frac{\sigma_{ro} - \sigma_{new}}{\epsilon_{ro} - \epsilon_{un}} \quad (6.49)$$

Mander et al. (1988b) introduced a parabolic transition curve between the linear reloading relation and the monotonic stress-strain curve return coordinates $(\epsilon_{re}, \sigma_{re})$. The common return strain is given by,

$$\epsilon_{re} = \epsilon_{un} + \frac{(\sigma_{un} - \sigma_{new}) \times \left(2 + \frac{f_{cc}}{f_c}\right)}{E_r} \quad (6.50)$$

Parabolic transition curve is defined as,

$$\sigma_1 = \sigma_{re} + E_{re}x + Ag^2 \quad (6.51)$$

where,

$$g = \epsilon_1 - \epsilon_{re}, \quad (6.52)$$

$$A = \frac{(\sigma_{new} - \sigma_{re}) - E_r(\epsilon_{un} - \epsilon_{re})}{(\epsilon_{un} - \epsilon_{re})^2}, \quad (6.53)$$

E_{re} and σ_{re} are the common return point tangent modulus and the stress calculated using return strain, ϵ_{re} using the monotonic stress-strain curve.

Sakai and Kawashima (2000) defined the axial stress for reloading curves for an assigned axial strain, ϵ_1 as,

$$\sigma_1 = \begin{cases} 2.5\sigma_{un} \left(\frac{\epsilon_1 - \epsilon_{pl,n}}{\epsilon_{un} - \epsilon_{pl,n}} \right)^2 & \text{if } 0 \leq \bar{\epsilon}_1 \leq 0.2 \\ E_{rl}(\epsilon_1 - \epsilon_{un}) + \sigma_{new} & \text{if } 0.2 \leq \bar{\epsilon}_1 \leq 1.0 \end{cases} \quad (6.54)$$

where $\epsilon_{pl,n}$ is the plastic strain in cycle n . $\bar{\epsilon}_1$ is the normalised strain defined in Equation (6.13) and E_{rl} is the averaged modulus of the reloading and given by,

$$E_{rl} = \frac{\sigma_{new} - 0.1\sigma_{un}}{0.8(\epsilon_{un} - \epsilon_{pl,n})} \quad (6.55)$$

Watanabe and Muguruma (1988) used a combined parabola and a straight line to define the reloading curve. According to their study, reloading curve is a straight line until it meets the common point and from that point it is a parabola till it intersects monotonic curve.

6.7.4 Reloading curve as a power function

Zhang et al. (1979) defined the reloading curve from zero stress $(\epsilon_{pl}, 0)$ to a tangent point $(\epsilon_{re}, \sigma_{re})$ to the envelope curve. The relationship between ϵ_{re} and ϵ_{pl} was proposed as,

$$X_{re} = LX_p^M \quad (6.56)$$

where

$$X_{re} = \frac{\epsilon_{re}}{\epsilon_{cc}} \quad \text{and} \quad X_p = \frac{\epsilon_{pl}}{\epsilon_{cc}}. \quad (6.57)$$

L and M are material parameters. Reloading curve was thus defined as,

$$\frac{\sigma_1}{\sigma_{re}} = \left(\frac{\epsilon_1 - \epsilon_{pl}}{\epsilon_{re} - \epsilon_{pl}} \right)^{1.2}. \quad (6.58)$$

(ϵ_1, σ_1) is any strain and stress level in reloading curve.

6.7.5 Common points

From the experimental results of Sinha et al. (1964) it is concluded that the stress-strain relationship for concrete under repeated loading histories has a band of points which are defined as the point of intersection of the unloading curve and the reloading curve. Stresses above the common point curve result in additional strains while strains below common point curve result in a loop of stress and strain during a loading/unloading cycle. This idea was supported by Karsan and Jirsa (1969) using the tests results of 46 rectangular short columns. For the model developed by Darwin and Pecknold (1977), this band of points was reduced to a single curve called locus of common points (Figure 6.9). The number of cycles to failure was said to be controlled by the location of the common points with respect to envelope curve. When the locus of the common points was lowered, fewer cycles are needed to intersect the same stress level in envelope curve. Watanabe and Muguruma (1988) proposed a hysteresis model for cyclic loading, defining a common point curve by scaling down the monotonic curve by 0.9 times about stress and strain axes.

Darwin and Pecknold (1977) reported that the energy dissipation in each cycle is controlled by the location of the turning point. The lower the turning point is the higher the energy dissipated per cycle. They pointed out that the model dissipates less energy than it is for real specimen for low strains which is a common defect of many hysteresis models and higher energy for higher strains.

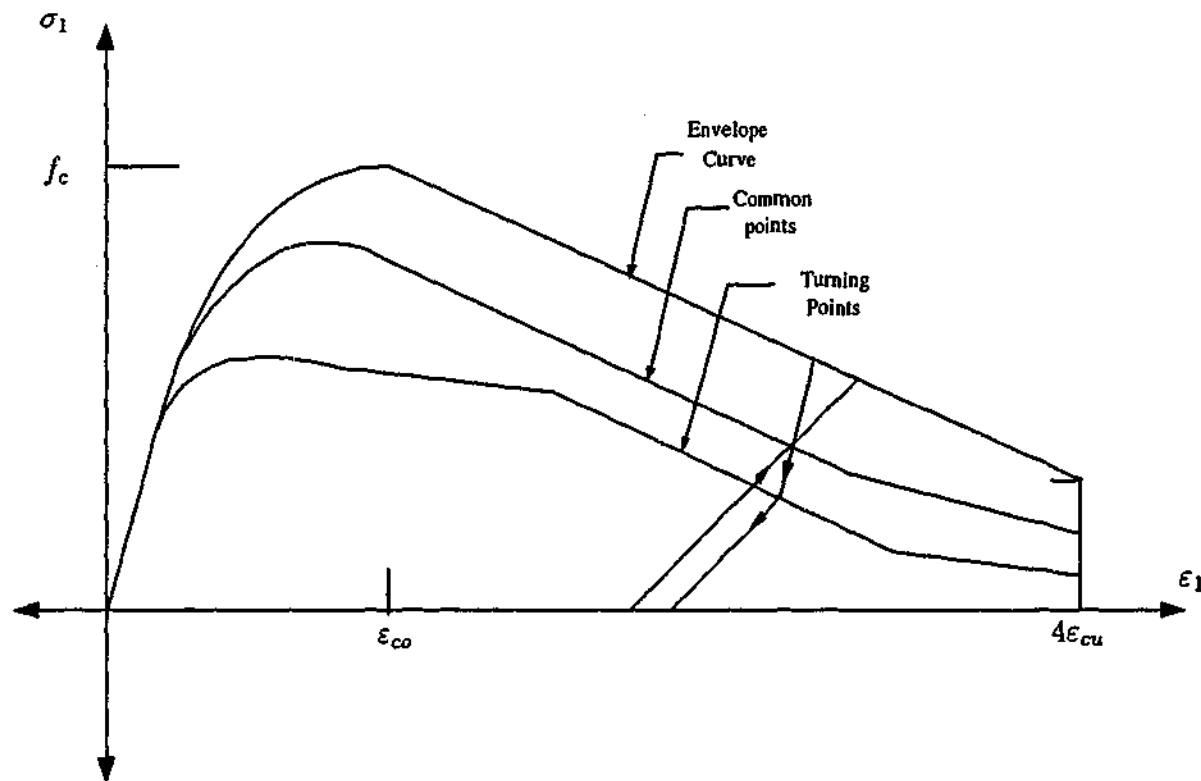


Figure 6.9: Control points for hysteresis loops (Darwin and Pecknold 1977).

6.7.6 Summary of the models for reloading curve

According to all the reported stress-strain curves for the reloading curve for NSC, there are several points of interest in defining the reloading curve. They are,

- Plastic strain
- Reloading point
- Return point
- Unloading point
- Common point

6.8 Partial unloading and reloading

Otter and Naaman (1989) discussed the response of concrete to random load histories by considering partial unloading and reloading.

6.8.1 Location of reloading point for partial unloading

The actual reloading strain for partial unloading with full reloading is a function of the amount of unloading. An interpolation function is proposed for the actual reloading strain (Figure 6.10),

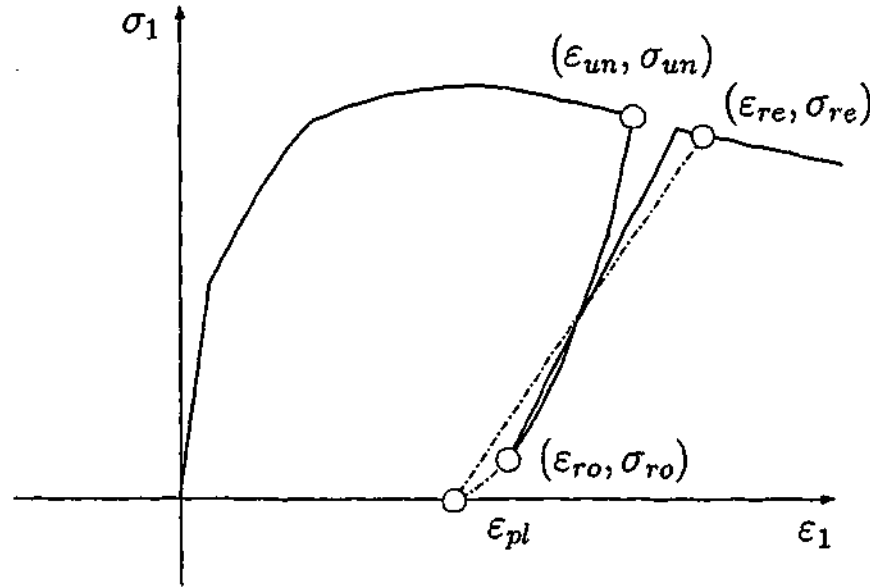


Figure 6.10: Interpolation of reloading point for partial unloading.

$$\epsilon_{rp} = \epsilon_{un} + (\epsilon_{ro} - \epsilon_{un}) \left(\frac{\sigma_{un} - \sigma_{ro}}{\sigma_{un}} \right)^{n_{pu}} \quad (6.59)$$

ϵ_{rp} is the reloading strain for partial unloading and full reloading, ϵ_{ro} is the reloading strain for full unloading and reloading, σ_{ro} is the lowest strain reached during unloading and n_{pu} is the partial unloading parameter. Consider the example shown in Figure 6.11 of a specimen, which had a previous loading up to point A, but now fully unloaded up to point B. If it is fully reloaded and unloaded, it will follow the path BCD. The following expression is proposed for the new envelope unloading point,

$$\epsilon_{unew} = \epsilon_{uold} + (\epsilon_{re} - \epsilon_{uold}) \left(\frac{\sigma_{hi} - \sigma_{ro}}{\sigma_{re} - \sigma_{ro}} \right)^{n_{pu}} \quad (6.60)$$

where ϵ_{uold} and ϵ_{unew} are the old and new values of the envelope unloading strain ϵ_{un} , $(\epsilon_{re}, \sigma_{re})$ is the return point on the envelope curve if full reloading occurred, σ_{hi} is the highest stress level attained during reloading, σ_{ro} is the stress at which reloading began and n_{rp} is the partial reloading parameter.

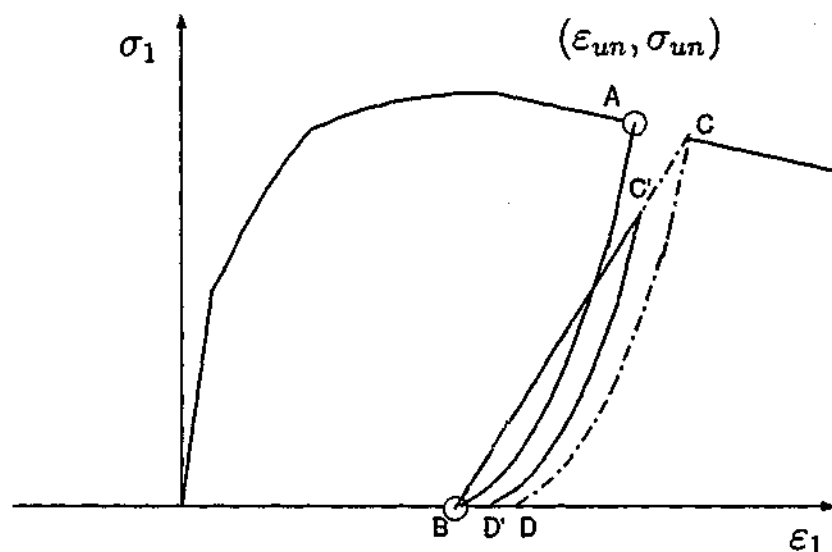


Figure 6.11: Interpolation of plastic and envelope strains for partial reloading.

6.9 Unloading/reloading cycles in the elastic region

Darwin and Pecknold (1977) defined at low uniaxial strains (in the elastic region) reloading follows a single line with a slope of E_i , tangent modulus of elasticity at zero stress. This idea was supported by Elmorsi et al. (1998) who proposed that if the reloading occurs in the initial unloading region, it follows the same unloading curve until it meets the envelope curve. They did not comment on the slope of the unloading or reloading curves. However, they defined the initial unloading region which is the same as the elastic region defined by Darwin and Pecknold (1977). The initial unloading region terminates when the stress reaches zero during unloading and then continues with zero slope and zero stress level upto the origin.

6.10 Validation of the models

Some of the models reported in the literature for cyclic loading of concrete have been validated using either the previously published or new experimental results.

Model proposed by Yankelevsky and Reinhardt (1987) was compared with several uniaxial cyclic tests carried out by previous researchers and shown to have a good agreement. Similarly, the model proposed by Elmorsi et al. (1998) was compared with the experimental results of Karsan and Jirsa (1969) and they concluded that although the model is quite simple it compares fairly well with the experimental results.

Darwin and Pecknold (1976) presented numerical solutions for two shear panels tested by previous researchers and concluded that proposed model agrees well with the experimental results. They further presented model comparisons for a shear wall-frame system loaded monotonically and a shear wall loaded cyclically. Desayi et al. (1979) concluded that the proposed model for the cyclic loading of confined concrete represented the experimental curves satisfactorily. Thirty one nearly full size reinforced concrete short columns of circular, square or rectangular wall cross section and with different configurations of lateral and longitudinal steel were tested by Mander et al. (1988a) in order to validate the proposed stress-strain model for confined concrete (Mander et al. 1988b).

6.11 Previous work on models for cyclic loading of reinforcing steel

In the literature, several models have been used to depict the Bauschinger effect in cyclic loading of steel, by using the Ramberg-Osgood or Menegotto-Pinto relationships (Dodd and Restrepo-posada 1995). Ramberg-Osgood relationships were used by Park et al. (1972) and Lim (1986). Dodd and Restrepo-posada (1995) proposed a closed form relationship for any set of end conditions for steel behaviour under cyclic loading. Kwan and Billington (2001) pointed out that a model for steel can have a significant influence on the hysteresis behaviour of structural elements. Not having the Bauschinger effect in steel constitutive model can lead to an overestimating energy capacity.

The hysteresis model used for steel stress-strain behaviour has a general shape shown in Figure 6.12. Loading prior to any unloading follows the monotonic loading curve with slopes of E_{st} , modulus of elasticity of steel in the elastic region, 0 modulus of elasticity in the plastic region and E_{sh} , strain hardening modulus in the strain hardening region. Unloading path follows the initial elastic slope, E_{st} . During unloading, after first yield excursion, the curve becomes non linear due to Bauschinger effect. Reloading after non linear unloading follows the initial elastic slope and it becomes non linear again.

The non linear unloading and reloading parts of the steel stress-strain curves are represented by the Ramberg-Osgood relationship as follows:

$$\epsilon_s - \epsilon_{si} = \frac{f_s}{E_{st}} \left(1 + \left| \frac{f_s}{f_{ch}} \right|^{r_1-1} \right). \quad (6.61)$$

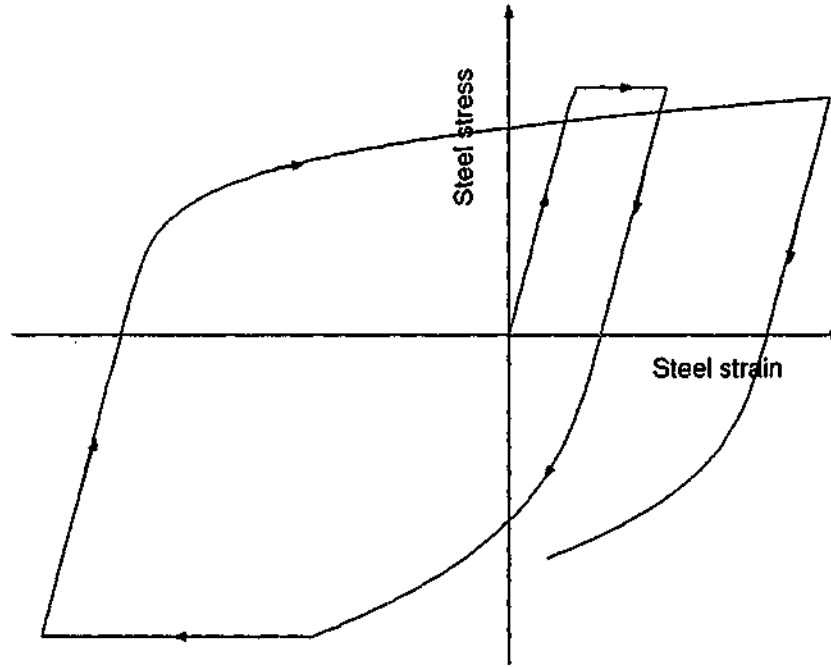


Figure 6.12: Hysteresis behaviour of steel.

ε_s is the steel strain, ε_{si} is the steel strain at the beginning of loading run, f_s is steel stress, E_{st} is steel modulus of elasticity, r_1 is "Ramberg-Osgood" empirical parameter and f_{ch} is defined by,

$$f_{ch} = f_{sy} \left[\frac{0.744}{\ln(1 + 1000\varepsilon_{ip})} - \frac{0.071}{1 - \exp(1000\varepsilon_{ip})} + 0.241 \right] \quad (6.62)$$

where f_{sy} is the yield stress of steel and ε_{ip} is the plastic strain produced in previous loading run.

If first yield occurs at $n = 0$, then $n = 1$ is the first post yield stress reversal, $n = 2$ is the second post yield reversal ... etc. "Ramberg-Osgood" parameter is defined for "odd" and "even" cycles separately. "odd" cycles are odd numbered loading runs ($n = 1, 3, 5, \dots$) and "even" cycles are even numbered loading runs ($n = 2, 4, 6, \dots$). Ramberg-Osgood parameter is different for odd and even cycles and are given as follows:

$$r_{odi} = \frac{4.489}{\ln(n + 1)} - \frac{6.026}{\exp(n) - 1} + 0.297 \quad (6.63)$$

and

$$r_{even} = \frac{2.197}{\ln(n + 1)} - \frac{0.469}{\exp(n) - 1} + 3.043. \quad (6.64)$$

Since the investigation of the behaviour of steel subjected to cyclic loading is beyond the scope of this study, it was decided to approximate it by the Ramberg-Osgood relationship.

6.12 Conclusions

A number of experimental programs have been carried out for the behaviour of unconfined and confined NSC subjected to cyclic axial compression. Based on the results, envelope curve, unloading curve, reloading curve, plastic strain and deterioration in axial stress due to each cycle have been empirically proposed. They provide a good understanding and the background information necessary to model the cyclic behaviour of unconfined and confined NSC. However, the reported research works to-date do not address the following issues:

- High strength concrete
None of the experimental programs carried out so far has considered the behaviour of unconfined or confined HSC subjected to cyclic loading.
- Lateral strain
 - All the published models established axial stress, axial strain relationship for unconfined and confined NSC subjected to cyclic axial compression. None of them was capable of modelling the lateral dilation (strain) of concrete which is essential in the confining pressure calculations, especially in HSC where lateral dilation is expected to be less.
 - None of the reported research work has addressed the effect of unloading on lateral confining steel and the resulting effect on the behaviour of confined HSC columns.

The issues which need to be carefully investigated for the behaviour of unconfined or confined HSC subjected to cyclic axial compression are as follows:

- Validity of using the stress-strain curve for monotonically increasing load as the envelope curve for cyclic loading.
- When unloaded in the elastic region, whether the unloading curve and the reloading curve follows the same straight line as in the case for NSC.
- The validity of extrapolating stress-strain curves from column test results.
The stress-strain models were back calculated from the column results and therefore subjected to many assumptions about the effectiveness of the confinement.

- Complexity of using the stress-strain models for analysing reinforced concrete structures.

Elmorsi et al. (1998) have pointed out that most of the previous analytical models for cyclic loading of concrete give better comparisons in element level but their use is limited due to the complexity in analysing actual reinforced concrete structures.

As shown in Chapters 3-5, fundamental constitutive model for confined concrete developed based on tests with controlled active confinement is extremely powerful in predicting the behaviour of confined HSC subjected to monotonic loading. It is hypothesised that a similar approach would lead to a good understanding of the behaviour of HSC columns under cyclic loading. Such a constitutive model can be used in conjunction with hysteresis behaviour of confining steel to give a realistic prediction of the behaviour of laterally confined HSC column under cyclic loading.

Chapter 7

CYCLIC LOADS: Experimental program

7.1 Introduction

As identified at the conclusions of the previous chapter, there is a significant gap in knowledge about the behaviour of laterally confined HSC subjected to cyclic loading. Whilst column tests on NSC give an insight to the general behaviour, fundamental material behaviour and specially the change in lateral or volumetric strains of concrete under cyclic loading is poorly understood. The experimental program developed by the author addresses this gap in knowledge.

This chapter describes a testing program carried out to obtain relationships between axial stress, axial strain and lateral strain for HSC under cyclic loading and subjected to constant lateral confining pressures. Compressive strengths of concrete tested were 44, 58, 83 and 106 MPa. Uniform confining pressures applied were 4, 8 and 12 MPa. An introduction of the triaxial testing equipment which accommodates the specimen, an in-house built clip gauge that is used to measure the lateral strain, experimental set up, problems encountered in the trial tests, measures taken to overcome them and an outline of the experimental procedure carried out are explained in detail in this chapter.

The experimental findings which resulted from this chapter are published in two research papers, Lokuge et al. (2002a) and Lokuge et al. (2003c).

7.2 Test variables

The major variables investigated were the compressive strength of concrete, the confining pressures maintained on the specimen and the two different loading regimes.

7.2.1 Compressive strength

Four compressive strengths were used as testing variables, which demonstrate the behaviour of a range of HSC (Grade 60, 80 and 100) and Grade 40 was also used for comparison with NSC. The four compressive strength grades of concrete were designated as Grade 40, Grade 60, Grade 80 and Grade 100 and they resulted in compressive strengths of 44, 58, 83 and 106 MPa respectively.

7.2.2 Confining pressure

A review of available literature on experimental studies of confined NSC and HSC was conducted to make a decision about the range of confining pressures. For the reported column tests, an equivalent confining pressure was calculated using the method suggested by Mander et al. (1988b) which is similar to that proposed by Sheikh and Uzumeri (1980). The calculated equivalent confining pressure can be divided by the strength of concrete under uniaxial compression to obtain the normalised confining pressure. Candappa (2000) conducted triaxial tests on confined HSC using 4, 8 and 12 MPa confining pressures. Majority of the column tests reported in the literature were passively confined. However, a few studies have been conducted on column tests using active confinement.

Active confinement versus passive confinement

Where testing of laterally confined concrete is concerned, researchers tend to have a preference in using passive confinement such as spiral reinforcement in columns. The advantage of these kinds of column tests is that the specimens need not to be accommodated in a Hoek type triaxial cell to apply confining pressure. As a result, measurement of strains is straight forward in these tests. The disadvantage of using passive confinement is that the stress-strain models have to be back calculated from the column test results and therefore subjected to many assumptions. Constitutive models based on column tests use an

estimate of the level of confinement. In tests with active confining pressure, level of confinement is determined by the test and is accurately known. The confinement provided by spirals or ties (in passive confinement) is not uniform and hence an effective confinement area has to be assumed. In active tests the entire test specimen is uniformly confined. In this sense, the triaxial tests presented in this chapter are "pure" as they directly measure the behavior of confined concrete. Constitutive models based on active tests tend to be more repeatable and less case dependent than models based on passive test results.

Therefore it was decided to use 4, 8 and 12 MPa as the confining pressures. They were selected to be consistent with Candappa (2000), so that cyclic loading results can be compared with Candappa (2000)'s monotonic loading results. The confining pressures applied are significantly higher than the pressures experienced in many columns found in practice. The experimental program is aimed to study the effect of confining pressure on ductility, rather than to repeat the current practice that is usually inadequate to provide sufficient ductility.

7.2.3 Loading regime

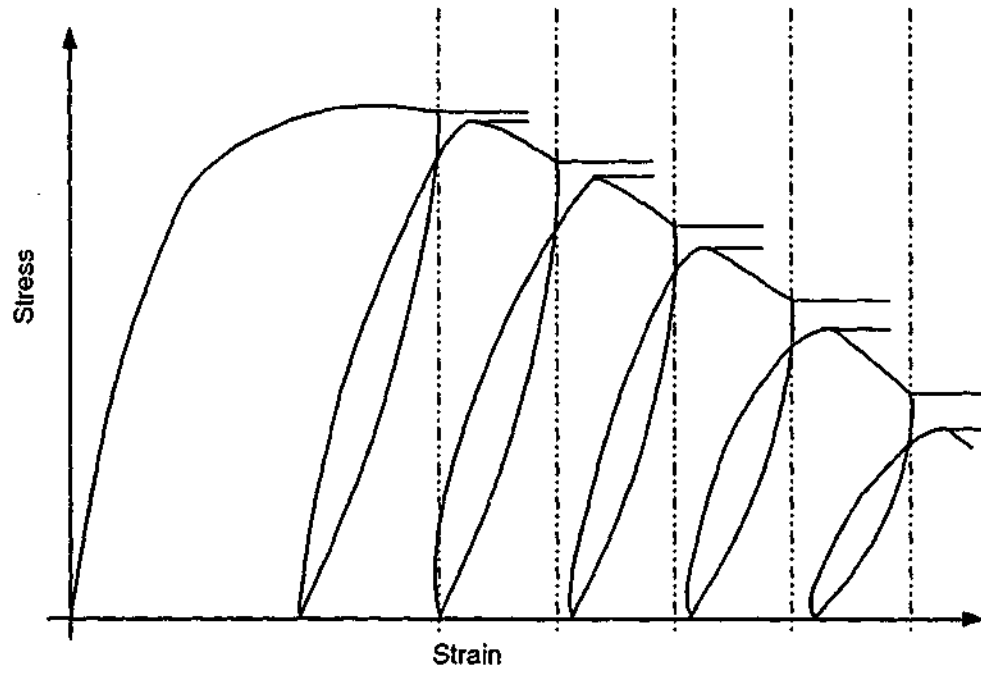
For a particular strength and confining pressure, 2 different loading regimes were adopted. One loading regime consisted of 3 to 4 cycles of loading at different unloading points before and after the peak stress (Figure 7.1(a)). The other loading regime consisted of a large number of cycles at the same unloading strain (Figure 7.1 (b)).

7.3 Concrete mixes and specimen preparation

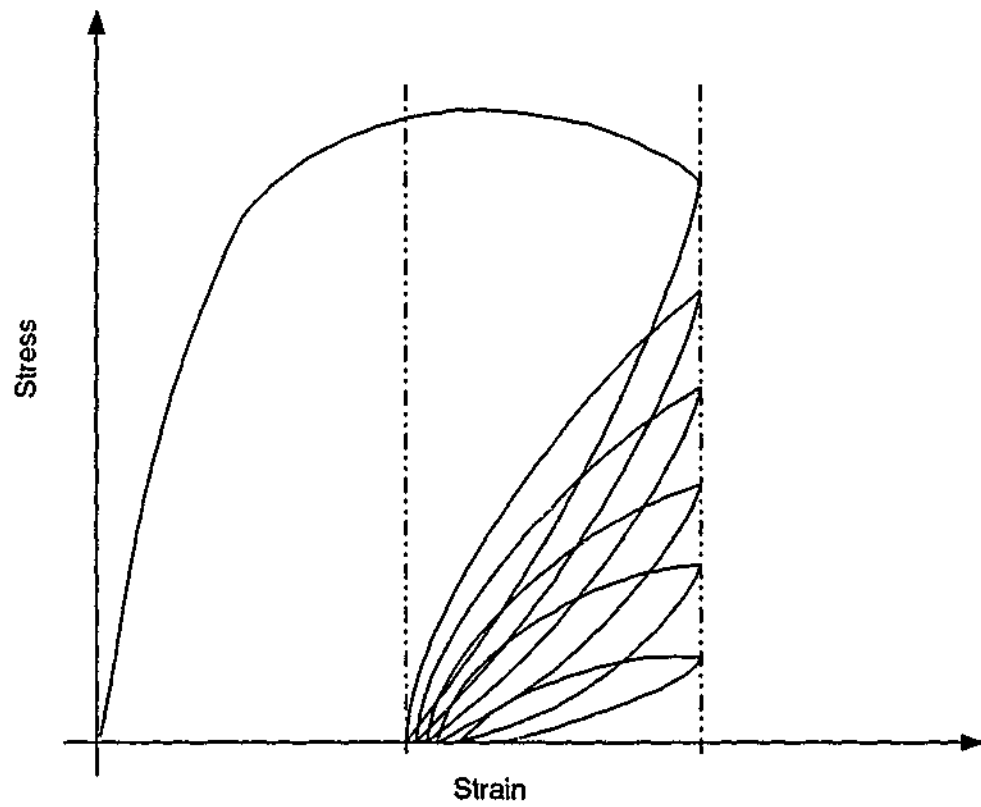
7.3.1 Details of concrete mixes

General purpose Portland cement (Type GP) is used in the laboratories by previous researchers (Candappa 2000) as well as in majority of the construction projects in producing HSC. Therefore Type GP Portland cement was selected for all mixes. Fine aggregate used had a fineness modulus of 2.9 and crushed basalt of maximum aggregate size of 14 mm was used as coarse aggregate. Gradings of the fine and coarse aggregate are presented in Table 7.1.

Superplasticiser (Rheobuild) was also used in Grade 80 and Grade 100 concrete. In a concrete mix design, the ingredients have to be proportioned optimally and economically



(a). Loading Regime 1



(b). Loading Regime 2

Figure 7.1: Considered loading regimes.

Table 7.1: Gradings of fine and coarse aggregate.

Aggregate type	Sieve size (mm)	% passing
Coarse aggregate	19	100
	12.7	88
	9.5	38
	4.76	1
Fine aggregate	4.75	100
	2.36	96
	1.18	77
	0.600	56
	0.300	40
	0.150	12
	0.075	1

to produce concrete with required strength and workability. Mix proportions for each grade of concrete is given in Table 7.2.

Table 7.2: Mix proportions.

Material (for 1 m ³)	U40	U60	U80	U100
Cement (kg)	300	360	400	550
Water (kg)	150	180	140	138
Coarse aggregate (kg)	1307	1266	1292	1243
Fine aggregate (kg)	690	645	633	621
Superplasticiser (kg)	-	-	2.2	8.7
W/C ratio	0.5	0.5	0.45	0.3
Slump (mm)	100	100	100	150

7.3.2 Specimen preparation

A pan type mixer with a capacity of 0.08 m³ was used to prepare all the concrete mixes. Inside surface of the pan was properly moistened before mixing commenced, so that water from the concrete mixture does not get absorbed by the pan. The steps involved in preparing the concrete mixes are described below, which are according to AS1012, Part 2 (2000).

(a) A sample of fine aggregate and coarse aggregate were dried for 24 hours to find out

the moisture content.

- (b) Water content was adjusted by taking into account the moisture content
- (c) Fine aggregate and the coarse aggregate were mixed for half a minute in the mixer.
- (d) Cement was then added to the aggregate and mixed for 2 minutes. Water and the Superplasticiser were added within the first minute.
- (e) Allowed to rest for 2 minutes.
- (f) Mixed again for another 2 minutes.
- (g) A standard slump test was performed within the next 3 minutes to make sure achieving the expected slump. The slump test was carried out according to AS1012, Part 3 (2000).

Steel moulds (100 × 200 mm cylinders) were used to cast all specimens. The size of the specimens cast was 98 mm × 200 mm. The 98 mm diameter of the specimen was obtained by inserting a 1 mm thick sheet of plastic sleeve in a 100 mm diameter mould. The ratio of the height and the average diameter of the specimen was in accordance with that proposed in AS1012, Part 8 (2000). This reduction in the diameter eased the removal of the tested specimens from the membrane in triaxial testing. The cylinders were filled in three layers while being placed on a variable speed vibrating table. The tops of the cylinders were smoothed with a trowel. The specimens were covered with a polythene sheet to minimise the loss of moisture from the specimen. The specimens were de-moulded in 24 hours after casting and placed under standard moist-curing conditions (23°C) according to AS1012, Part 8 (2000).

Two different end preparation methods were used in these tests. The cylinders to be tested for 28-day compressive strengths were capped using sulphur and the cap was more than 2 hours old at the time of testing (AS1012 Part 9, 2000). The cylinders to be tested in the triaxial cell had to be ground properly at both ends to obtain a smooth surface. The grinding was done at a location away from the laboratory using a commercial steel polishing machine. Therefore drying of cylinders could not be prevented during transportation to the grinder. All cylinders used in triaxial tests were air dried one week before being tested. Any loose particles in the curved surface of the cylinders

were removed using sand blasting. The specimen pores were filled with casting plaster to prevent membrane damage. The diameter of the specimen was measured. Two strain gauges of 67 mm gauge length were fixed at the middle third of the height of the specimen longitudinally in two diametrically opposite sides. Similarly another two strain gauges were placed laterally at the middle third in two diametrically opposite sides. All specimens were prepared according to these procedures and one such specimen ready to be tested is shown in Figure 7.2.

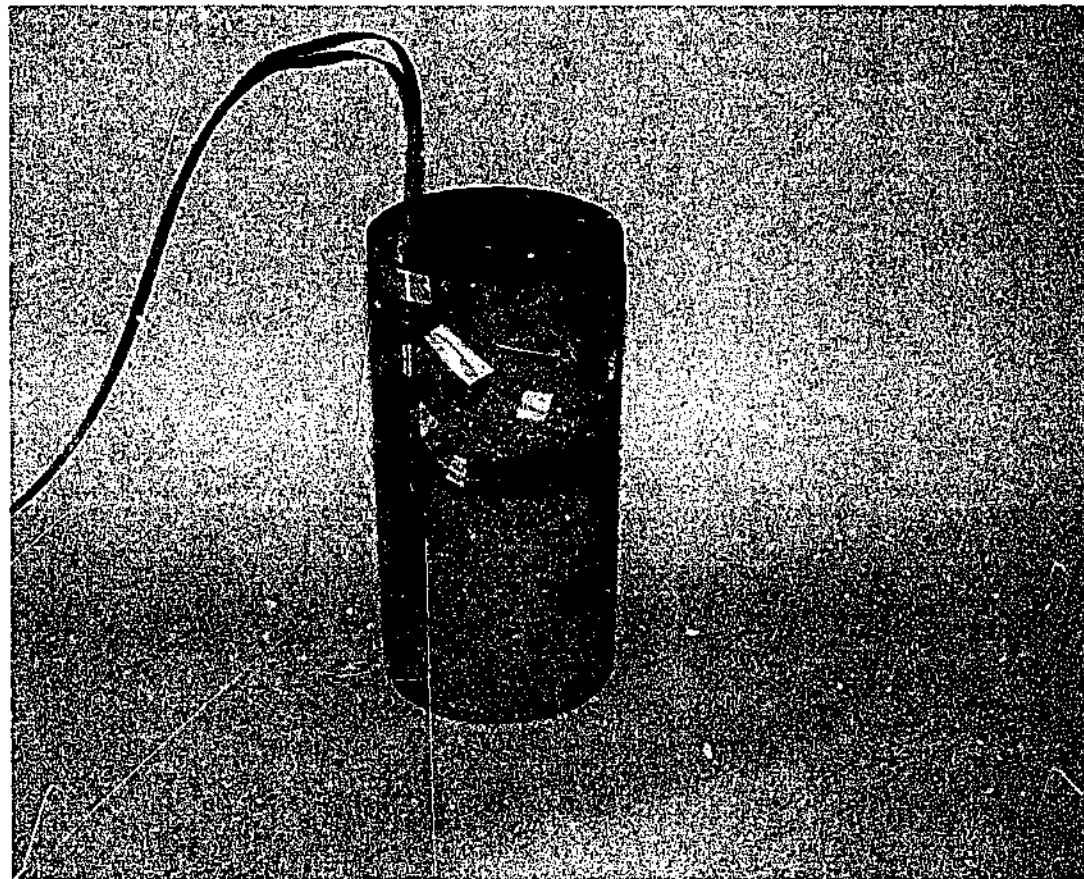


Figure 7.2: Specimen before testing.

7.3.3 Uniaxial compressive strengths

Table 7.3 gives the 28-day strengths and the strength and the age at time of testing for all grades of concrete.

Figure 7.3 shows the tested NSC and HSC specimens for the uniaxial compressive strengths.

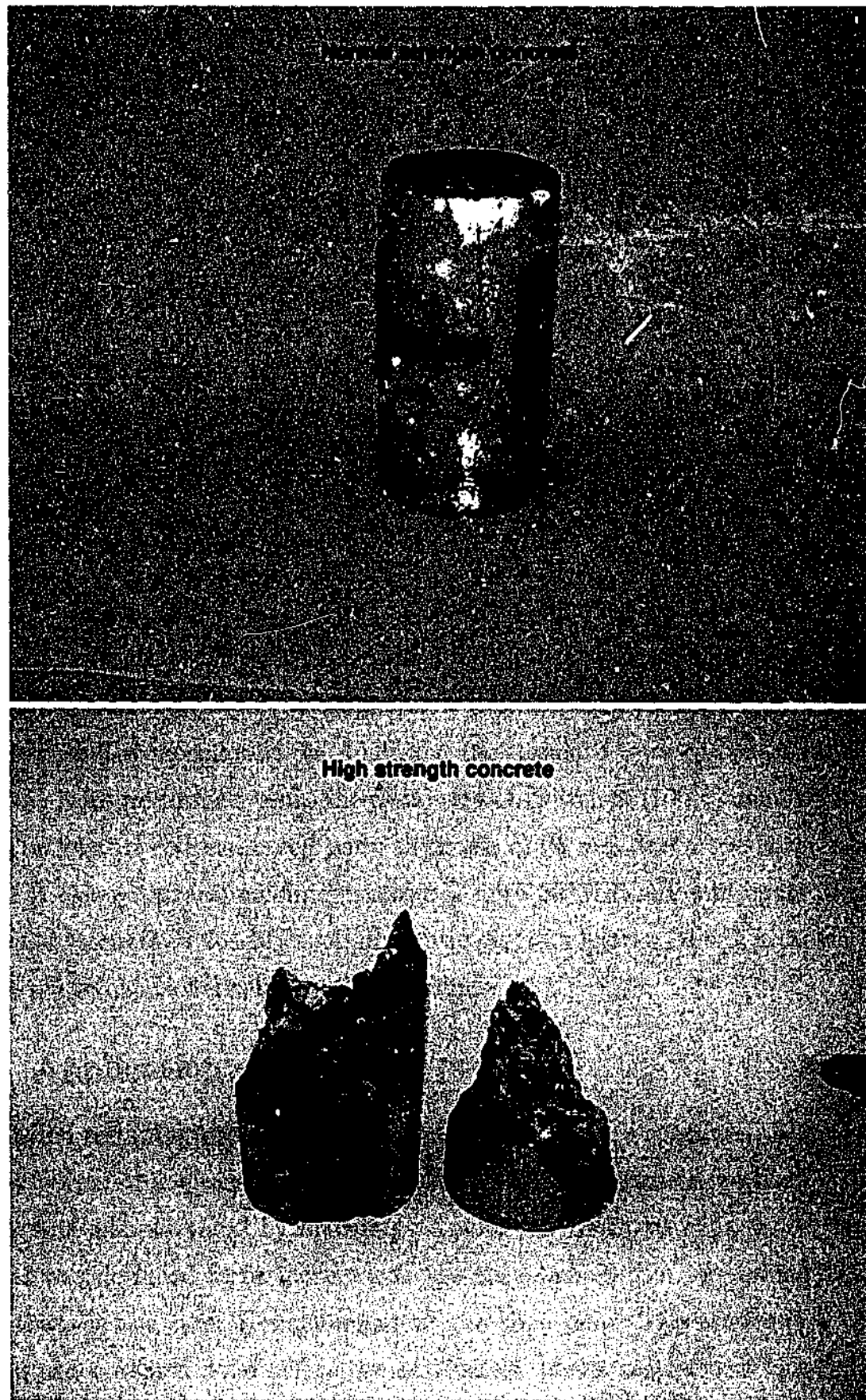


Figure 7.3: Tested specimens for uniaxial compressive strengths.

Table 7.3: Uniaxial strengths at 28 days and at time of testing.

	U40	U60	U80	U100
28-day strength (MPa)	35.8	48.7	79.8	101.4
Strength at testing (MPa)	43.6	57.5	83.0	105.9
Age at testing (days)	150	158	113	91

7.4 The test equipment

This section describes triaxial testing equipment used in the cyclic loading experiments. It then gives a detailed description of the methods used to measure the strains including the clip gauge, an in house built lateral strain measuring device.

7.4.1 Triaxial cell

The set-up constitutes a triaxial cell, which can accommodate a 98 mm diameter and 200 mm high concrete cylinder encased in a polyurethane membrane. These dimensions are consistent with the widely accepted view that larger specimens better simulate the behaviour of full-scale columns. In Australia, the standard tests on compressive strength of concrete were performed using the same size of cylinders (100 diameter and 200 mm high). The triaxial cell had a cell body thickness of 25 mm and a top cover thickness of 30 mm. It can withstand confining pressures upto 30 MPa. It was made of mild steel with a yield strength of 250 MPa. A schematic diagram of triaxial cell is shown in Figure 7.4. The photo of triaxial cell is shown in Figure 7.5.

7.4.2 Application of confining pressure

The required confining pressure was applied to the concrete specimen using oil through a flexible polyurethane membrane (Figure 7.4). The prefabricated membrane was 2 mm thick. It was manufactured by machining a solid polyurethane cylinder to the required shape. It was designed to fit loosely over the specimen so that membrane did not contribute towards the lateral confinement of the specimen. The application of the full confining pressure was done before the application of the axial stress. An Enerpac hydraulic pump was used to apply confining pressure. Maintaining a constant confining pressure during loading and unloading was achieved by connecting a precharged pressure

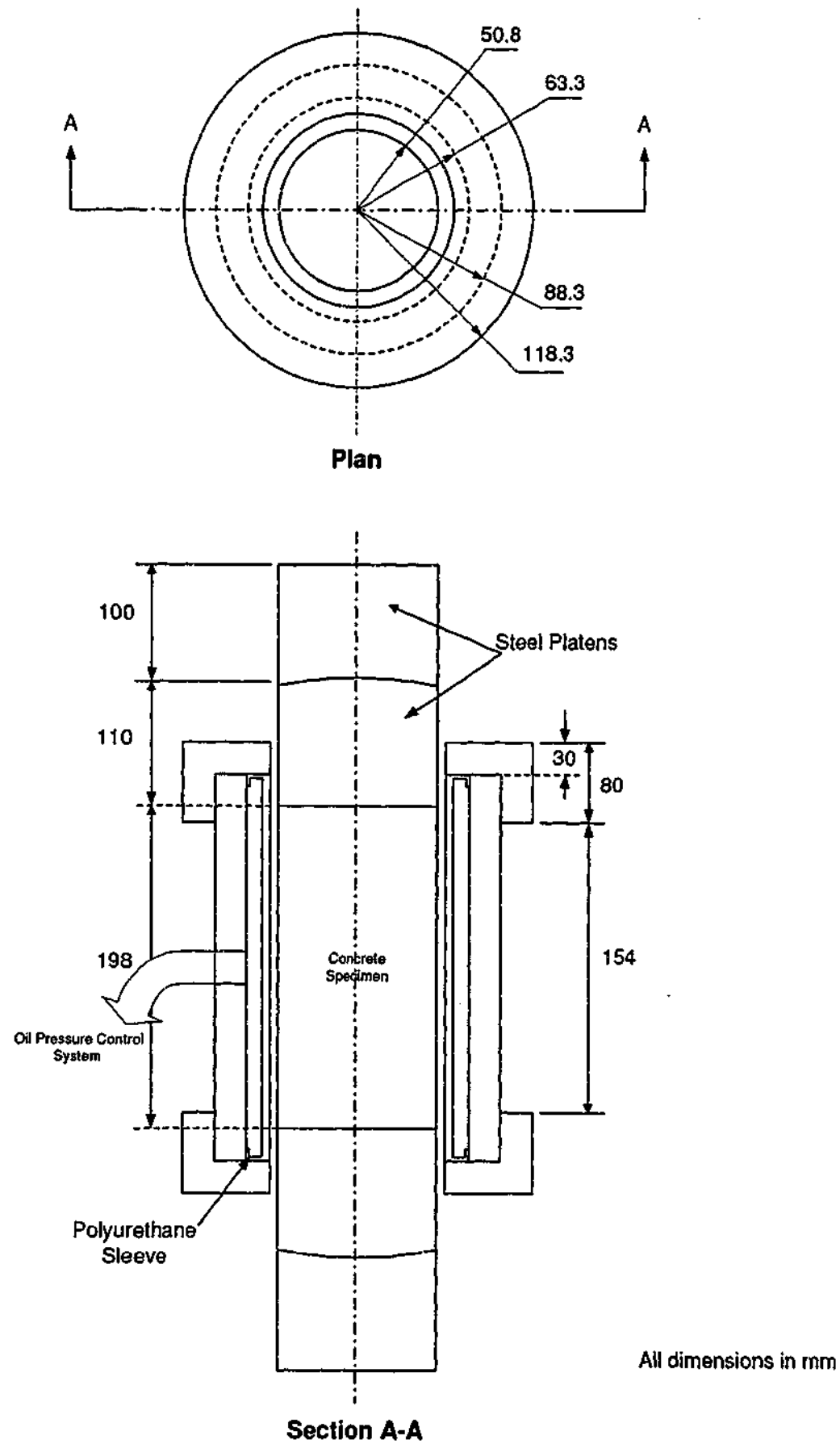


Figure 7.4: Schematic diagram of triaxial cell.

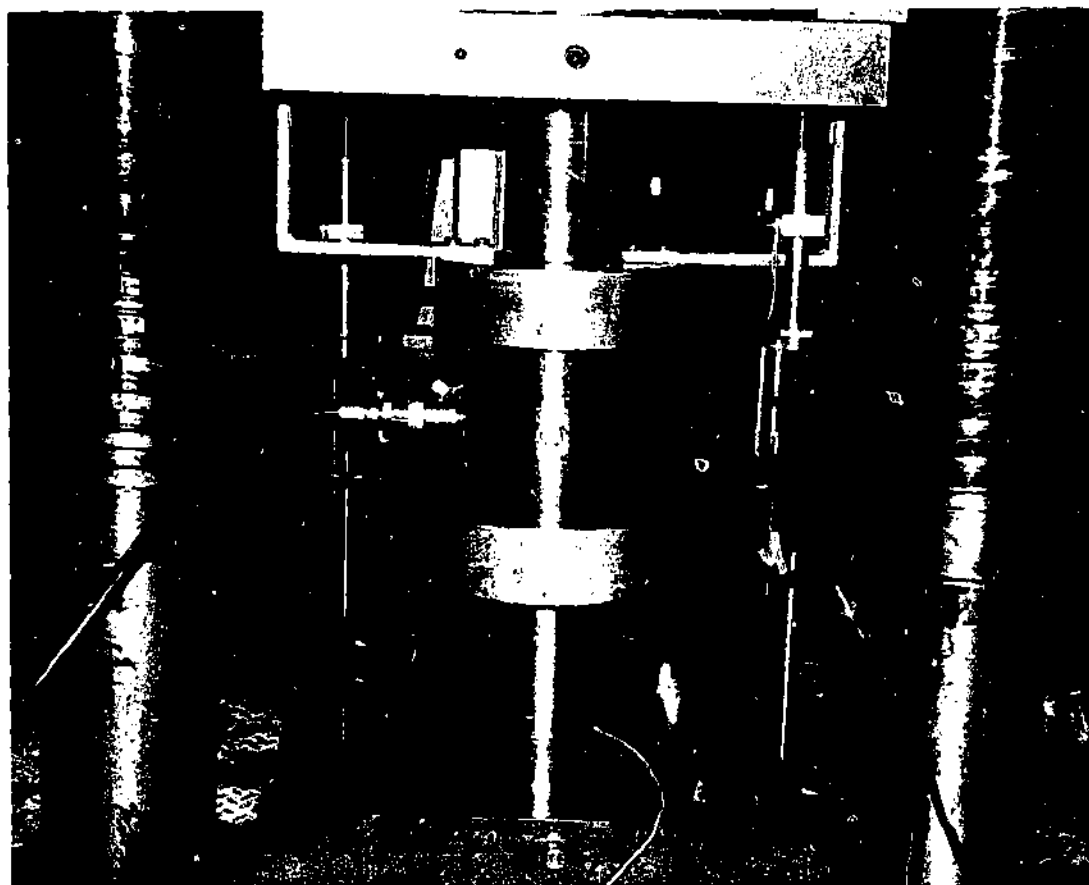


Figure 7.5: Photo of triaxial cell.

accumulator to the system.

7.4.3 Measurement of axial and lateral strains

Linear Variable Displacement Transducers (LVDTs) were used to measure the axial deformation of concrete. They are relatively easy to set up and can be reused after testing. They can also be used to measure the descending branch of the stress-strain curves. However, this method required the calibrations for the loading components as LVDTs would measure the platen to platen displacement. The method used in this experimental program was to use two LVDTs placed diametrically opposite to measure the axial strain between platens. Although LVDTs were used to measure axial strain, each tested sample had two strain gauges mounted across a diameter to verify the LVDT readings until the peak stress was achieved. After the peak stress, the strain gauge readings were unreliable.

A strain measuring system developed in-house (clip gauge), which constitutes a piano wire connected to two strain gauged arms was used to monitor the lateral strains during cyclic loading. The wire was attached around the concrete specimen, touching at stud

points penetrating the membrane. The strain measuring system was designed to function while immersed in fluid under pressure. A schematic diagram of this device is shown in Figure 7.6 together with a photo in Figure 7.7. The accuracy of the lateral strain measurement was confirmed using lateral strain gauges fixed to concrete until the strain gauges reached their limits.

7.5 Experimental setup

The specimens were prepared by grinding both ends flat and parallel and filling out any holes on the surface so that they do not damage the membrane. The specimen was then accommodated in the triaxial cell. The cell was mounted between the platens of the compressive testing machine by using two steel arms. The cell was connected to the hydraulic pump through a hole in the middle of the cell body, which was used to apply the confining pressure. A precharged pressure accumulator connected parallel with this was utilised to maintain the required confining pressure. A servo-controlled Amsler Compression Testing Machine, which has a maximum load capacity of 5000 kN, was used to provide the axial load. The compressive load was applied using two spherically seated cylindrical loading blocks that were designed to fit either end of the triaxial cell. The advantage of the testing method was the ability to do several tests at one setting. A commercially available data logging system named "Data Taker, DT100" was used as the data acquisition system, which required a host computer for entering commands, reading the returned data and for managing the output channels. Experimental setup is shown as a schematic diagram in Figure 7.8 and a photo in Figure 7.9.

7.6 Test procedure

Once the triaxial cell was in place in the 5000 kN capacity hydraulically operated Amsler testing machine, a small vertical load was applied to make sure the cell was secured, before applying confining pressure. The testing machine was then set to displacement control at the rate of 0.125 mm vertical displacement per minute. The full confining pressure was applied at the very beginning and maintained constant while the axial load was increased and decreased through the loading unloading cycles. It is hypothesised that the major parameters influencing the load-deformation behaviour under cyclic loading are

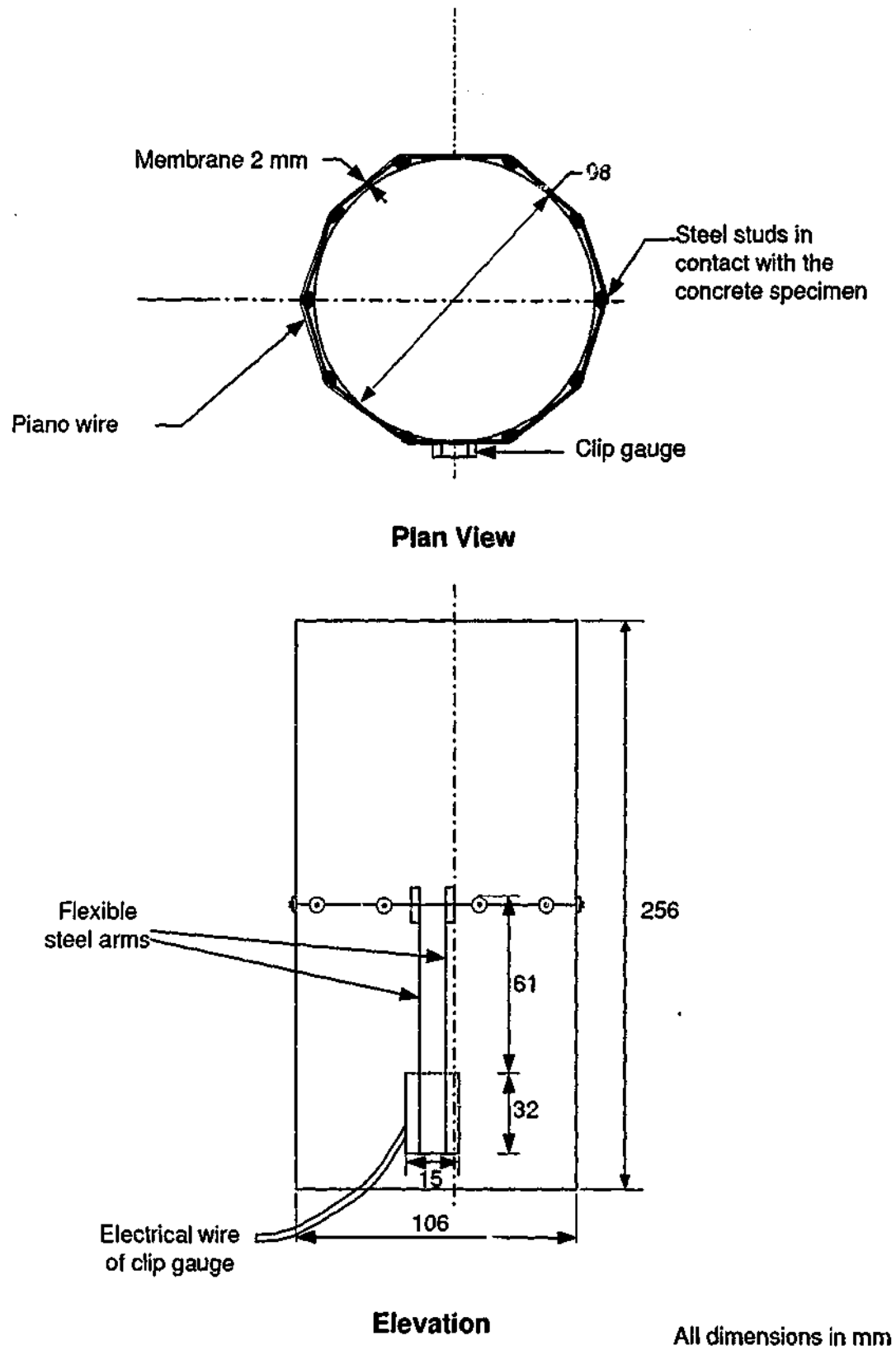


Figure 7.6: Schematic diagram of lateral strain measuring device.



Figure 7.7: Photo of lateral strain measuring device.

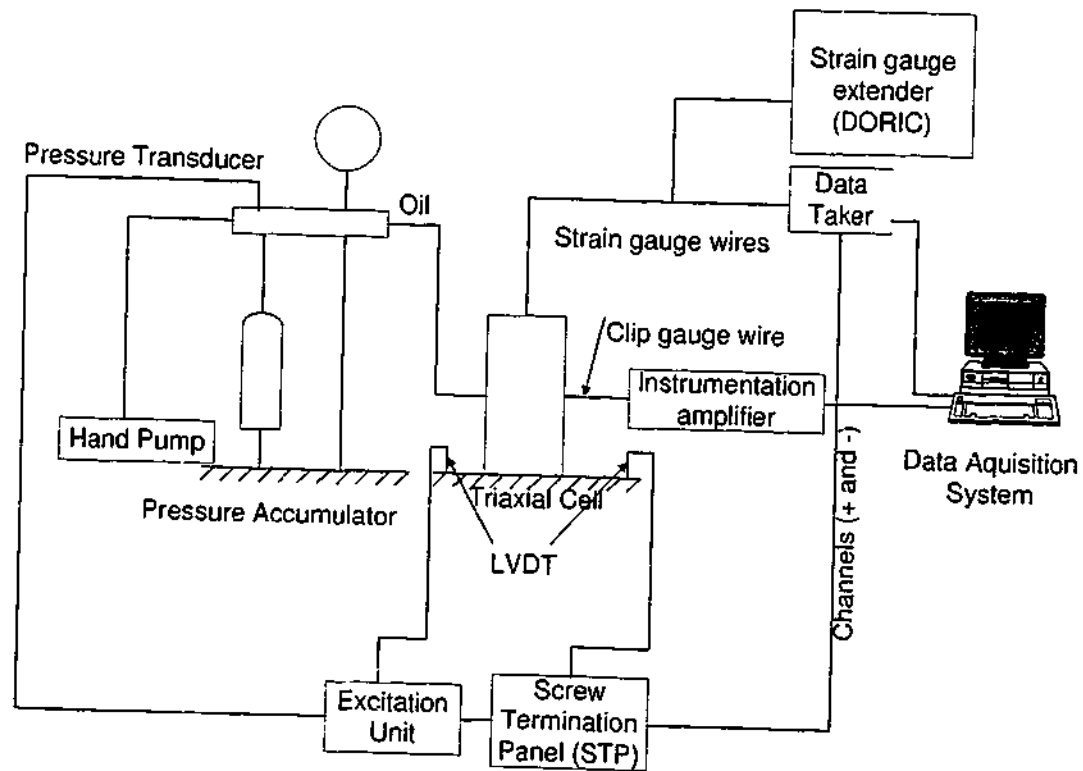


Figure 7.8: Schematic diagram of experimental setup.

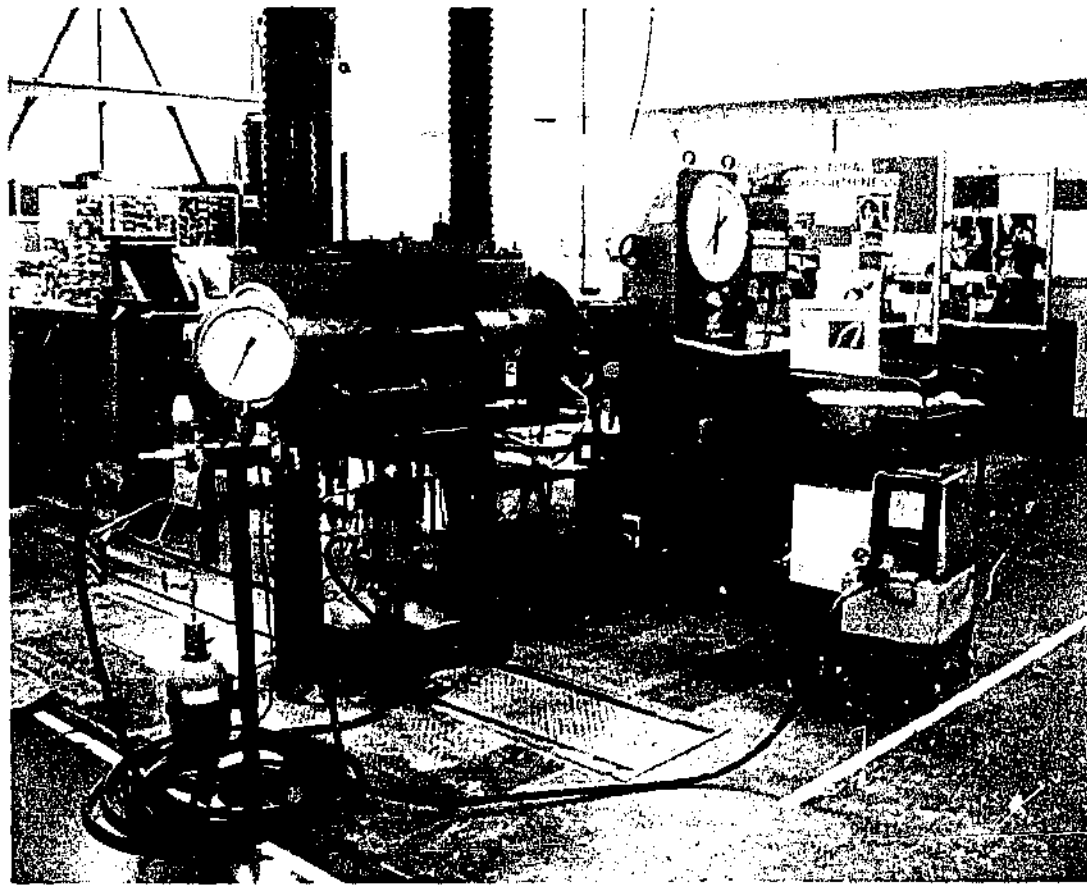


Figure 7.9: Photo of experimental setup.

loading and unloading stiffness in the directions of major and minor principle stresses. An initial experimental program was planned based on this hypothesis. The effect of the rate of loading was not considered in this test program. Several parameters were aimed to be studied in this experimental program. They were the change in ductility with confining pressure, the stress reduction in each hysteresis loop, the thickness of the loops and Poisson's ratio.

The experimental program included four grades of concrete, three different confining pressures applied and two loading regimes. After the uniaxial compressive strength was determined, the peak axial stress for a particular strength with known confining pressure was calculated using equations presented in Chapter 3 (Section 3.2.6). The expected unloading points are shown in Tables 7.4-7.7.

7.7 Trial tests

In order to identify any problems with either the testing equipment or the methodology, trial tests were performed on Grade 80 concrete specimens. The specimens were tested for

Table 7.4: Planning of testing for Grade 40 (44 MPa) concrete.

Confining pressure (MPa)	Expected peak load (kN)	Loading Regime 1		Loading Regime 2	
4	534	Ascending branch			
		Cycle	Unloading load	Cycle	Unloading load
		1	250	1	250
		2	520	2	520
		Descending branch			
		Cycle	Unloading load	Cycle	Unloading load
		3	530	3	520
		4	520		
		5	510		
		8	668	Ascending branch	
Cycle	Unloading load			Cycle	Unloading load
1	350			1	350
Descending branch					
Cycle	Unloading load			Cycle	Unloading load
2	655			2	655
3	650				
4	640				
5	630				
6	610				
12	815	Ascending branch			
		Cycle	Unloading load	Cycle	Unloading load
		1	400	1	400
		Descending branch			
		Cycle	Unloading load	Cycle	Unloading load
		2	800	2	655
		3	790		
		4	780		
		5	770		

Table 7.5: Planning of testing for Grade 60 (58 MPa) concrete.

Confining pressure (MPa)	Expected peak load (kN)	Loading Regime 1		Loading Regime 2	
4	630	Ascending branch			
		Cycle	Unloading load	Cycle	Unloading load
		1	300	1	300
		Descending branch			
		Cycle	Unloading load	Cycle	Unloading load
		2	615	2	615
		3	600		
		4	580		
8	760	Ascending branch			
		Cycle	Unloading load	Cycle	Unloading load
		1	380	1	380
		Descending branch			
		Cycle	Unloading load	Cycle	Unloading load
		2	750	2	750
		3	730		
		4	700		
12	840	Ascending branch			
		Cycle	Unloading load	Cycle	Unloading load
		1	450	1	450
		Descending branch			
		Cycle	Unloading load	Cycle	Unloading load
		2	835	2	835
		3	815		
		4	780		
	750				

Table 7.6: Planning of testing for Grade 80 (83 MPa) concrete.

Confining pressure (MPa)	Expected peak load (kN)	Loading Regime 1		Loading Regime 2	
4	824	Ascending branch			
		Cycle	Unloading load	Cycle	Unloading load
		1	420	1	420
		Descending branch			
		Cycle	Unloading load	Cycle	Unloading load
		2	800	2	800
		3	780		
		4	740		
8	982	Ascending branch			
		Cycle	Unloading load	Cycle	Unloading load
		1	550	1	550
		Descending branch			
		Cycle	Unloading load	Cycle	Unloading load
		2	975	2	655
		3	950		
		4	925		
		5	900		
		12	1120	Ascending branch	
Cycle	Unloading load			Cycle	Unloading load
1	600			1	600
Descending branch					
Cycle	Unloading load			Cycle	Unloading load
2	1115			2	1115
3	1080				
4	1050				
5	1000				

Table 7.7: Planning of testing for Grade 100 (106 MPa) concrete.

Confining pressure (MPa)	Expected peak load (kN)	Loading Regime 1		Loading Regime 2	
4	990	Ascending branch			
		Cycle	Unloading load	Cycle	Unloading load
		1	500	1	500
		Descending branch			
		Cycle	Unloading load	Cycle	Unloading load
		2	900	2	900
		3	800		
		4	700		
8	1155	Ascending branch			
		Cycle	Unloading load	Cycle	Unloading load
		1	600	1	600
		Descending branch			
		Cycle	Unloading load	Cycle	Unloading load
		2	1150	2	1150
		3	1000		
		4	800		
12	1295	Ascending branch			
		Cycle	Unloading load	Cycle	Unloading load
		1	680	1	700
		2	700	1	
		3	1000	1	
		Descending branch			
		Cycle	Unloading load	Cycle	Unloading load
		4	1295	2	1290
5	1220				

28-day compressive strength. Initially, the monotonically increasing axial compression test for one specimen was conducted to ensure that the systems work well. Then two specimens were tested with cyclic axial loading while it was subjected to lateral confinement. In these preliminary tests, the axial strain was measured by using strain gauges and LVDTs; and for measuring lateral strains, strain gauges and the in-house built clip gauge system were used.

A good comparison was observed between the average strain gauge readings and the clip gauge reading until the peak stress (Figure 7.10). The two readings start to separate after the peak point indicating the failure of strain gauges. Therefore it was decided to use LVDTs and strain gauges for axial strain measurement and clip gauge and strain gauges for lateral strain measurement. As explained below a number of problems were identified and corrected before proceeding with the major triaxial testing program.

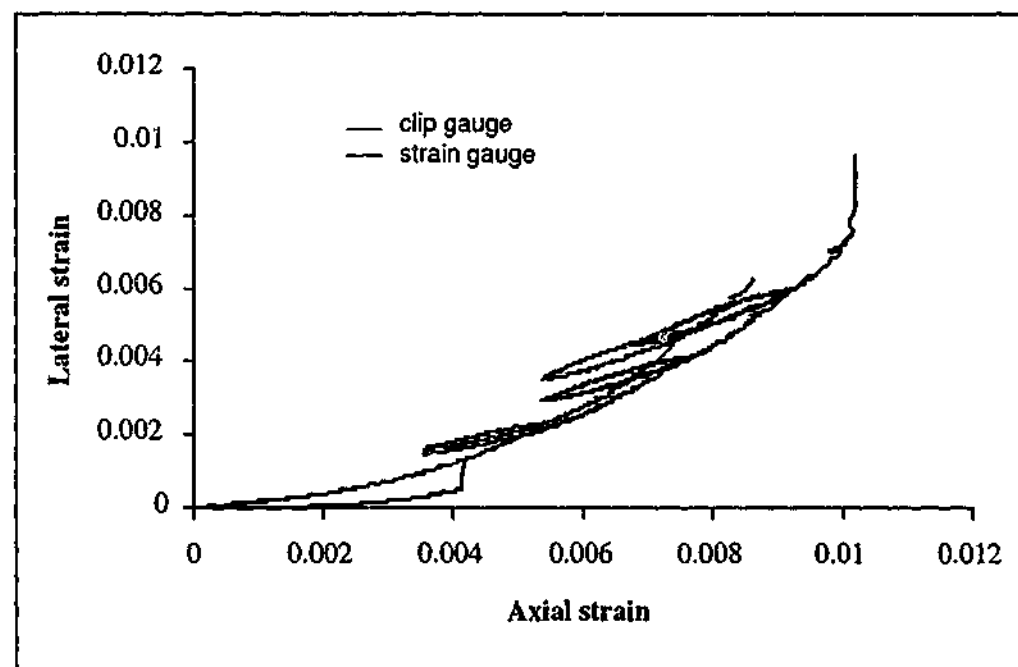


Figure 7.10: Comparison of average strain gauge and clip gauge readings.

7.7.1 Problems encountered

- Preparing Grade 100 concrete

The first trial mix was tested and the required 28-day compressive strength could not be obtained. A second trial mix was prepared with the required amount of coarse and fine aggregate sealed the day before, to minimise moisture loss. Using

this mix, required 28-day compressive strength could not be achieved. Therefore another trial mix was prepared and the compressive strengths were measured at days 1, 3, 7, 14, 21 and 28. It was observed that the compressive strength at day 1 of this mix was as high as 73 MPa but it was about 92 MPa in 28 days. Therefore it was decided that the concrete mixes were of high early strength type. This is likely due to the variation in the cement supply in cold and hot weather. The cement suppliers informed that the Type GP cement supplied in winter is of high early strength type to avoid construction delays.

- Maintaining constant pressure

There was a fluctuation in confining pressure during unloading and reloading due to the lateral expansion and contraction of the specimen. A precharged pressure accumulator was used to overcome this difficulty. It allowed keeping the oil pressure at a constant value throughout the experiments.

- Lack of smoothness in the stress-strain curves

The compression testing machine (Amsler) caused this problem. The proportional gain setting of the machine was determined by the stiffness of the test specimen. The gain value is normally set for a specimen based on its elastic stiffness. However, when the test progresses into the inelastic regions, the gain values do not match the change in the stiffness of the test specimen. This causes load fluctuations prominently visible after the peak stress is reached. Therefore in these experiments it was decided to change the gain value during the progress of the experiments in order to minimise the lack of smoothness in the stress-strain curves. A certain level of experience was needed to perform this exercise which was obtained by trial and error.

- Stopping test before the specimen fails

In the trial test conducted for cyclic axial compression, the tested specimen did not have any cracks. When the data was carefully analysed it was realised that the unloading reloading cycles were carried out only before the peak stress. Therefore it was arranged to plot the axial stress and axial strain curve during the test in order to make sure that unloading was done from the descending branch as well. A photo of this user interface of the data acquisition program is shown in Figure 7.11.

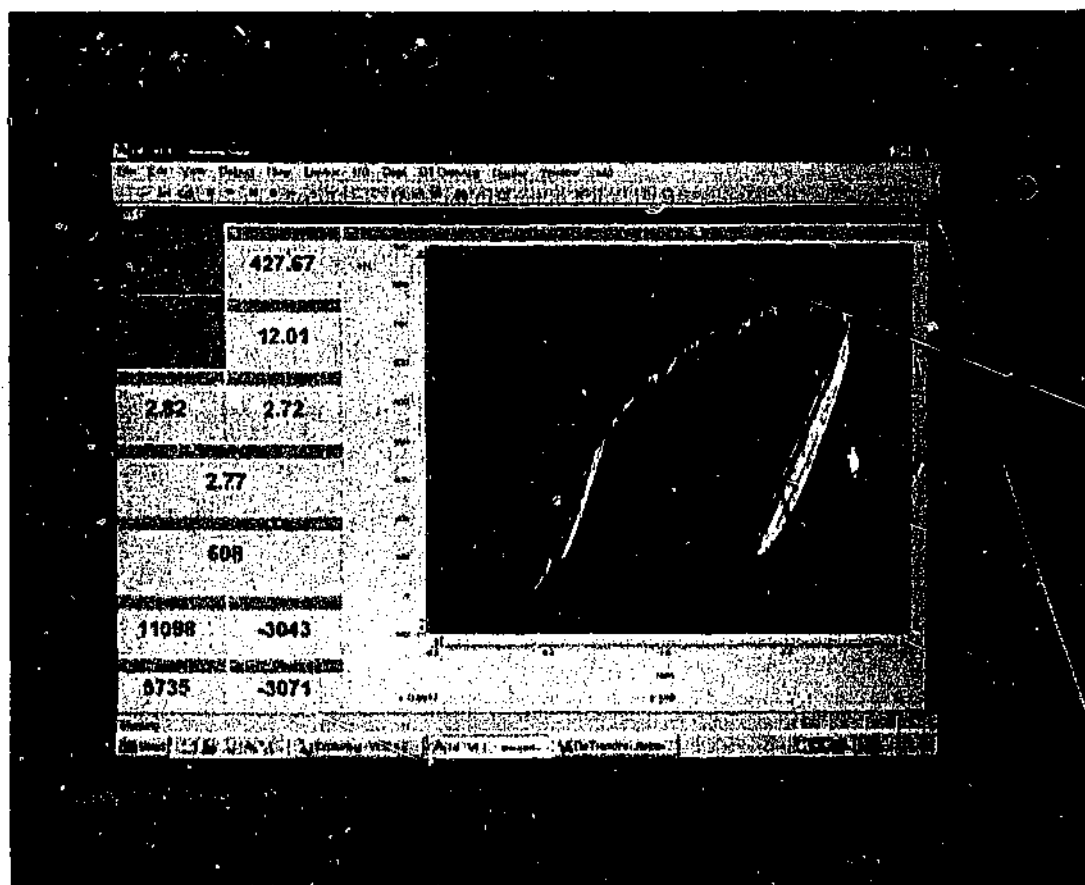


Figure 7.11: User interface of the data acquisition program.

- Strain gauges becoming dead when confining pressure is applied

Initially when the confining pressure was applied, all the strain gauges become dead and once the confining pressure was released, the strain gauges were normal. A coat of insulation was applied over the surface of the pasted strain gauges as a remedial measure. Furthermore, testing of a specimen was conducted after about 3-5 days of strain gauge fixing. These two methods were used to overcome this difficulty.

7.8 Conclusions

- Measurements of axial stress, axial strain and lateral strain in cyclically loaded concrete specimens were successfully completed in this experimental program.
- There were number of problems encountered in the experimental program, and all of them were systematically overcome.
- The strain measurements were compared using alternative methods of measurements. These comparisons confirmed the results and provided confidence in the

methods.

- The experimental procedures, including test specimen preparation and test method and measurement system, were carefully developed and systematically tested to ensure that the results obtained are very reliable and repeatable.
- Envelope curves were compared with the experimental curves of Candappa (2000) for monotonically increasing loads, to ensure that the results are of correct order.

Chapter 8

CYCLIC LOADS: Experimental results and analysis

8.1 Introduction

The raw data obtained in the previous chapter had to be processed and filtered in order to get smooth curves for the constitutive behaviour of confined HSC subjected to cyclic loading. In this chapter, first the calibrations of the instruments are described. Then the experimental results are presented and the effects of cyclic loading and confinement on the constitutive behaviour of HSC are described. Finally several observations about using monotonic loading curve as the envelope curve, ductility, stress loss due to hysteresis loops and Poisson's ratio are presented.

8.2 Calibrations

A number of calibrations were performed to interpret the experimental data correctly. The important ones are calibration of LVDTs and the lateral strain measuring device, clip gauge. The use of LVDTs required another calibration accounting for the compliance of all the loading components including the loading machine that influences the LVDT readings.

8.2.1 Calibration of LVDTs

A purpose built LVDT calibrating instrument was used in doing this. LVDT was connected to the output channel as well to record the readings. The readings were in milli volts. The instrument had a micrometer from which it was possible to give a known

displacement to the LVDT. The readings from the output channels of the LVDT were recorded with a known displacement starting from 0.5 upto 10 mm with an increment of 0.5 mm. Three sets of readings were taken at the same displacement. A graph was plotted for the actual displacement versus the relative average of these readings (Figure 8.1). The best-fit curve was found for these data points with a correlation factor of 0.999996. The second LVDT was also calibrated using the same method. LVDTs were setup to mea-

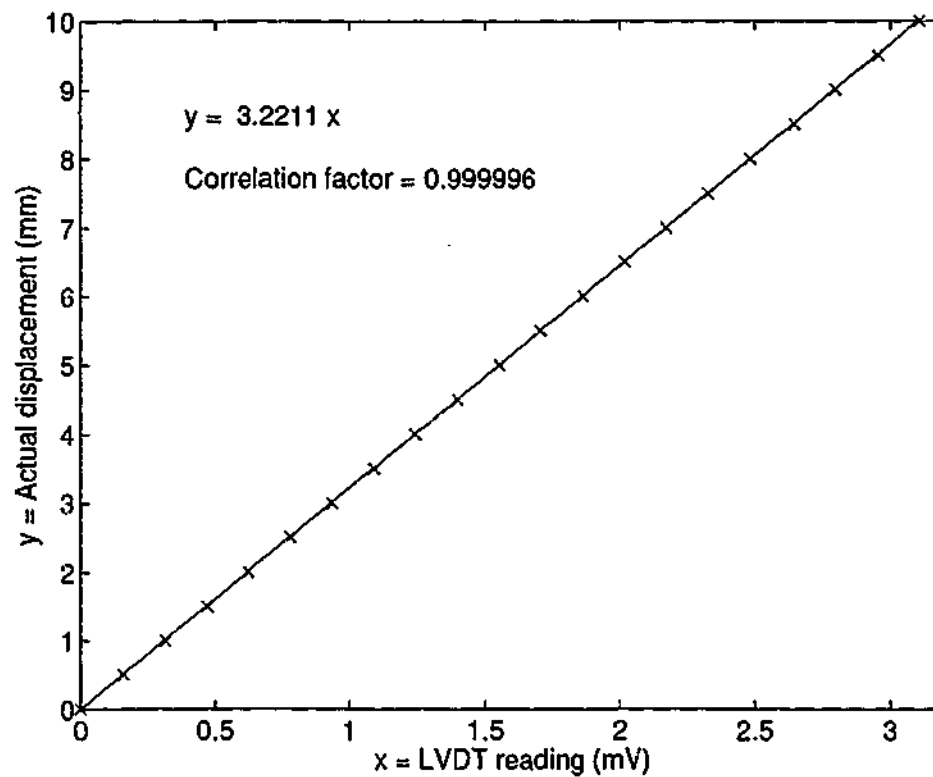


Figure 8.1: LVDT calibration.

sure the platen-to-platen displacement whereas the interest of this experimental program was to find axial displacement in concrete specimen. Therefore careful calibrations for all the loading components that influence the LVDT readings were necessary. Deformations of the four spherically seated loading blocks will affect the LVDT readings. The compliance of the loading blocks was determined by placing them in series without the specimen and obtaining the load-deformation curve. It was used to make adjustments for the contribution of the loading blocks to the actual axial strain readings.

8.2.2 Calibration of clip gauge

Extensometer calibrator was used in clip gauge calibration. Clip gauge was first connected to the instrumentation amplifier and checked whether it recorded strains other than the

direct strain. Known displacement was given to the clip gauge starting from 0 upto 0.2 inches in steps of 0.025 inches and the output readings were recorded from the output channels. Three sets of readings were taken for the same. A graph was plotted for the actual displacement versus the relative average of these readings (Figure 8.2). The best-fit curve was found for these data points with a correlation factor of 0.99988.

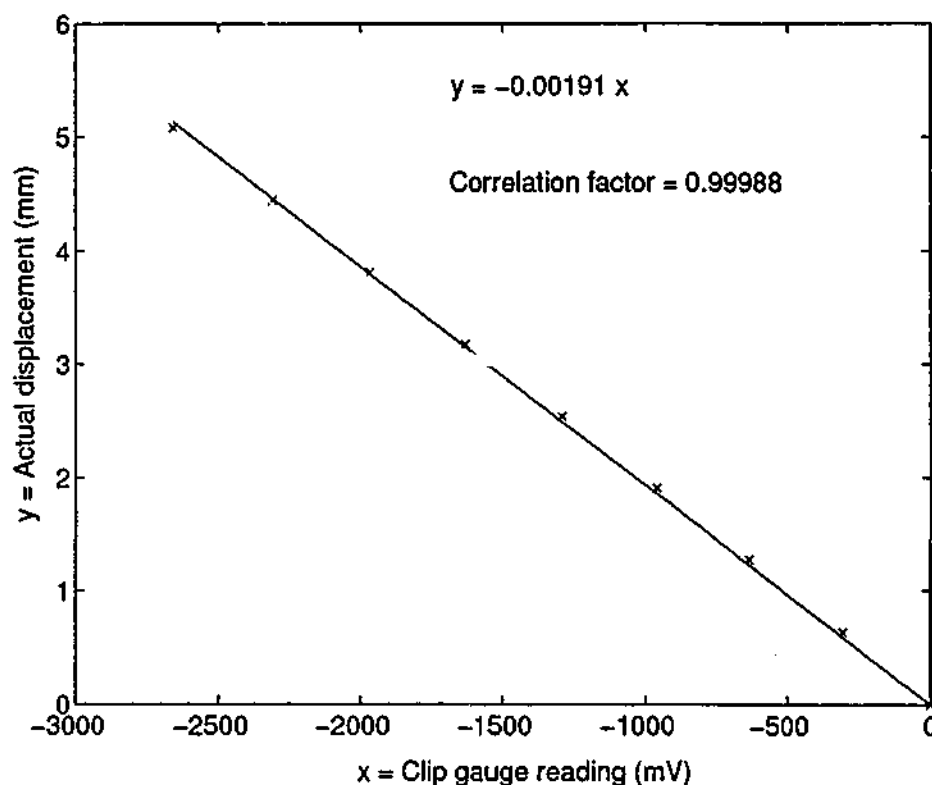


Figure 8.2: Clip gauge calibration.

8.3 Experimental results

Typical stress-strain curve obtained in the experiments is shown in Figure 8.3. It can be observed that these curves lack smoothness and difficult to read. This is due to the fluctuations caused by Amsler testing machine under displacement control. Therefore it was decided to remove the small cycles caused by the test machine. By filtering the results, stress-strain curve obtained as shown in Figure 8.4 becomes more readable than the unfiltered curves.

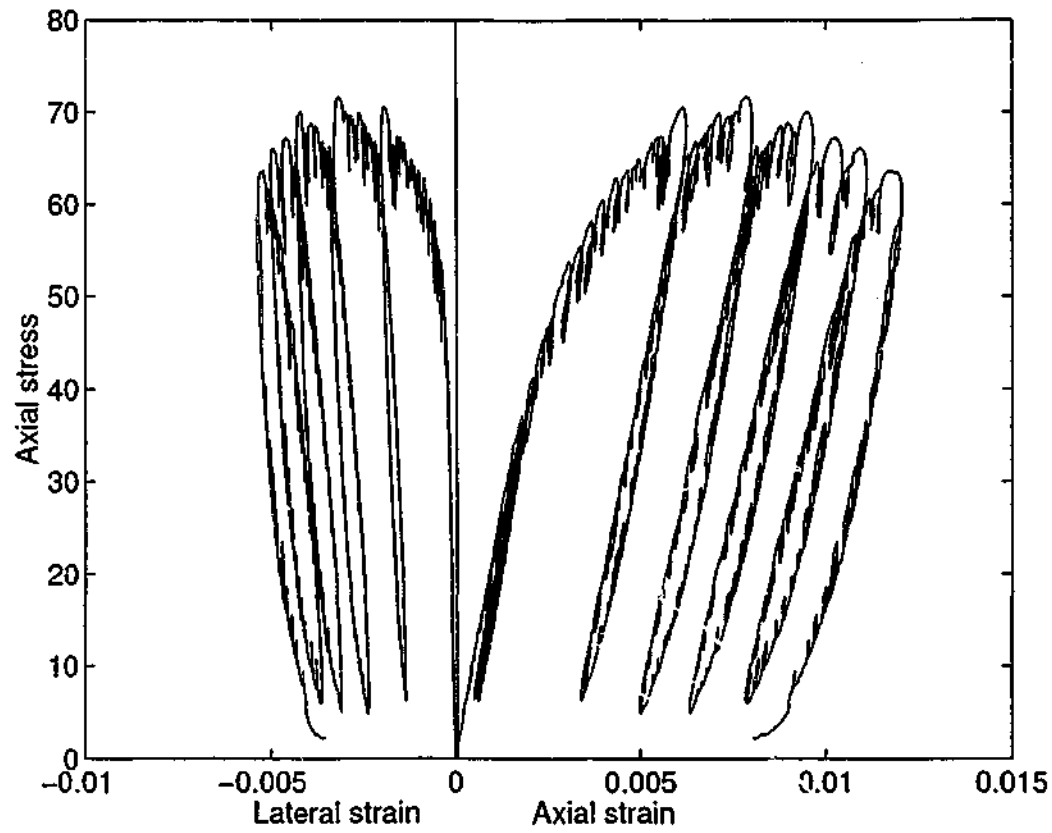


Figure 8.3: Unfiltered stress-strain curve.

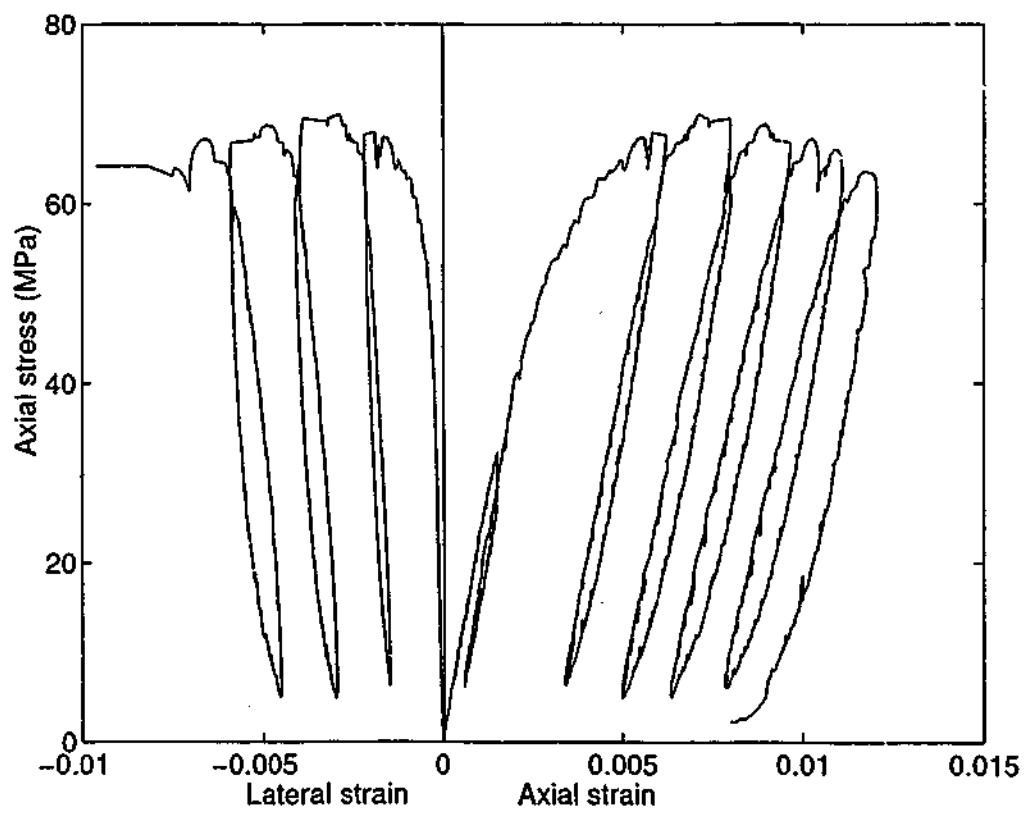


Figure 8.4: Filtered stress-strain curve.

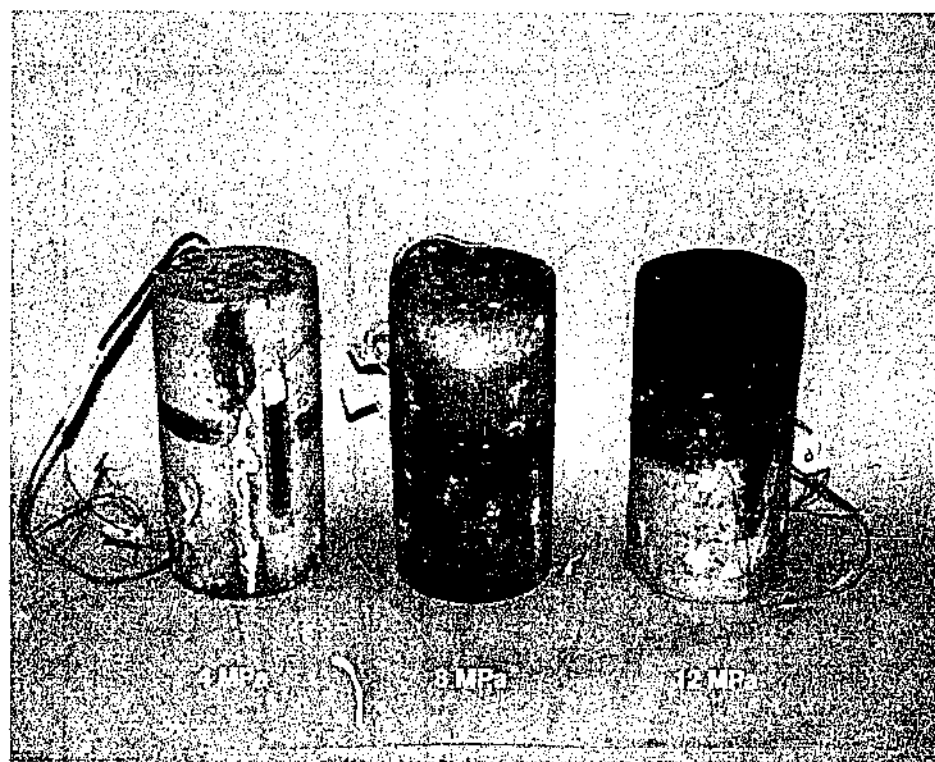
8.3.1 Grade 40 test series

Grade 40 concrete specimens at the end of testing are shown in Figure 8.5. The tests were terminated once 2-3 cycles could be established in the descending curve. Therefore Grade 40 test specimens appear to be undamaged.

The axial stress-axial strain and axial stress-lateral strain curves for Grade 40 concrete are shown in Figures 8.6-8.8 for both Loading Regimes 1 and 2. It is apparent from the figures that significant strength gains has been achieved with the increasing lateral confinement. Each 4 MPa increment in the lateral confinement has increased the peak strength by 15-20 MPa. Axial strain corresponding to the peak axial stress, increases with the increasing lateral confinement. Grade 40 concrete shows a good ductility for all the three confinement levels.

In Loading Regime 1 of the experiments, it can be observed that after each cycle, the curves do not return to the original unloading point. This loss of stress is termed here as damage. The curves for Loading Regime 1, show that this damage varies for different unloading points (stress and strain) and the cycle number. However the curves for Loading Regime 1, depict that the damage cannot be a function of the unloading strain only.

The thickness of each cycles seems to be increasing with the progressing of unloading and reloading. In the "initial elastic region", reloading curve follows the same unloading curve and this seems to be a straight line. This observation can be made only in the axial stress-lateral strain relationships. However in the axial stress-axial strain relationships, it can be observed that in the "initial elastic region" unloading and reloading cycles follow different loading paths.



(a). Loading Regime 1



(b). Loading Regime 2

Figure 8.5: Tested specimens for Grade 40 concrete.

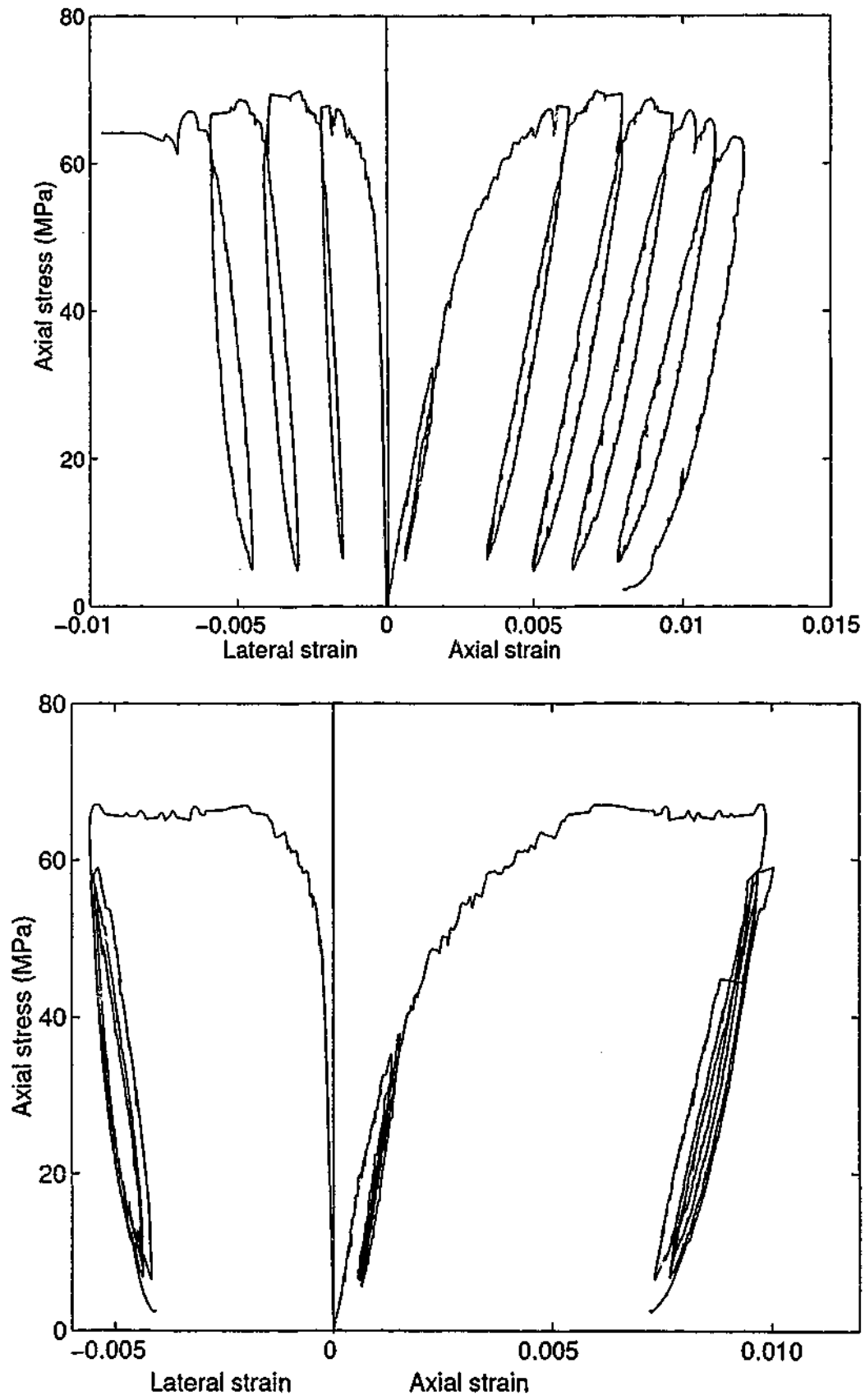


Figure 8.6: Grade 40 concrete with 4 MPa confining pressure.

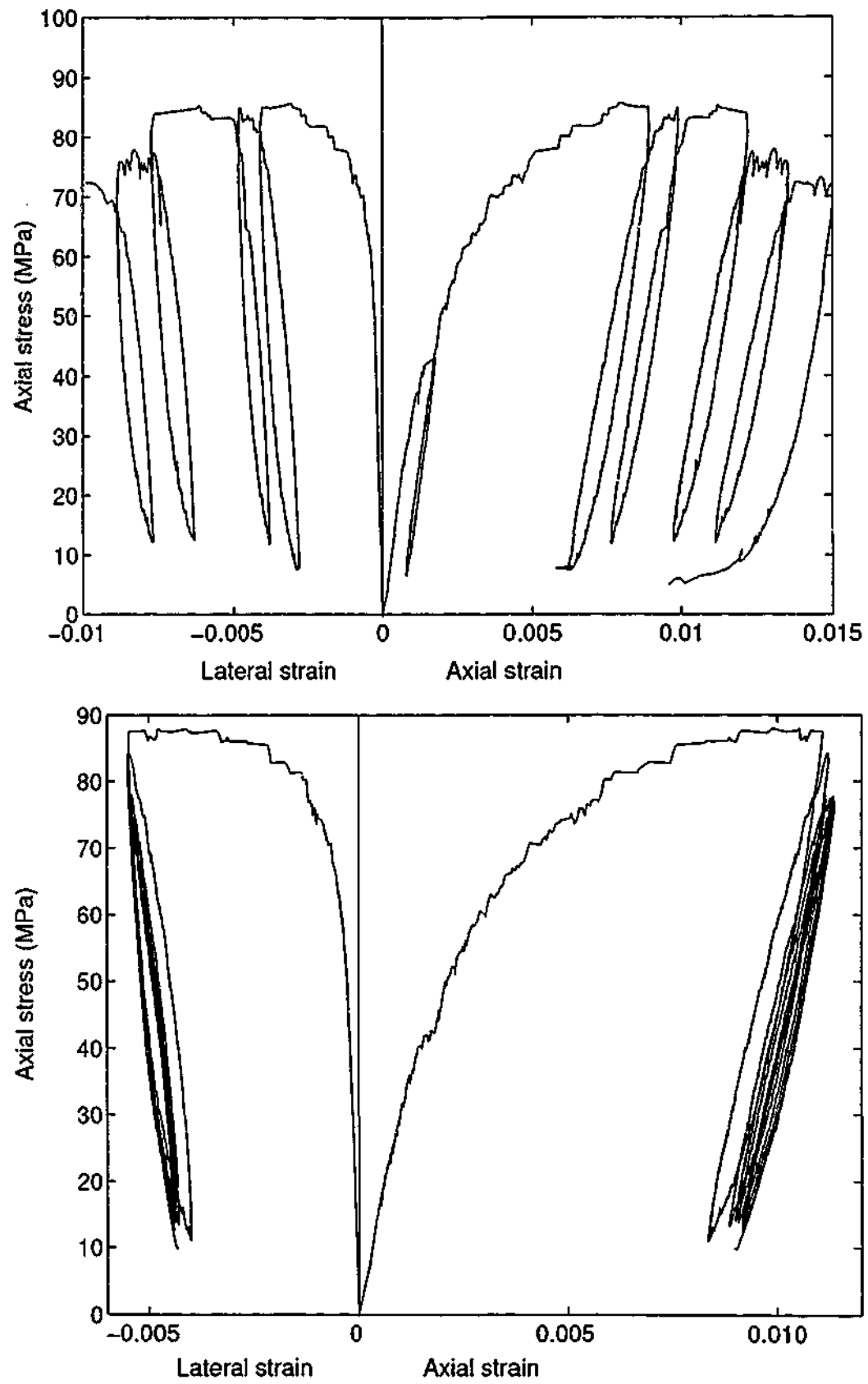


Figure 8.7: Grade 40 concrete with 8 MPa confining pressure.

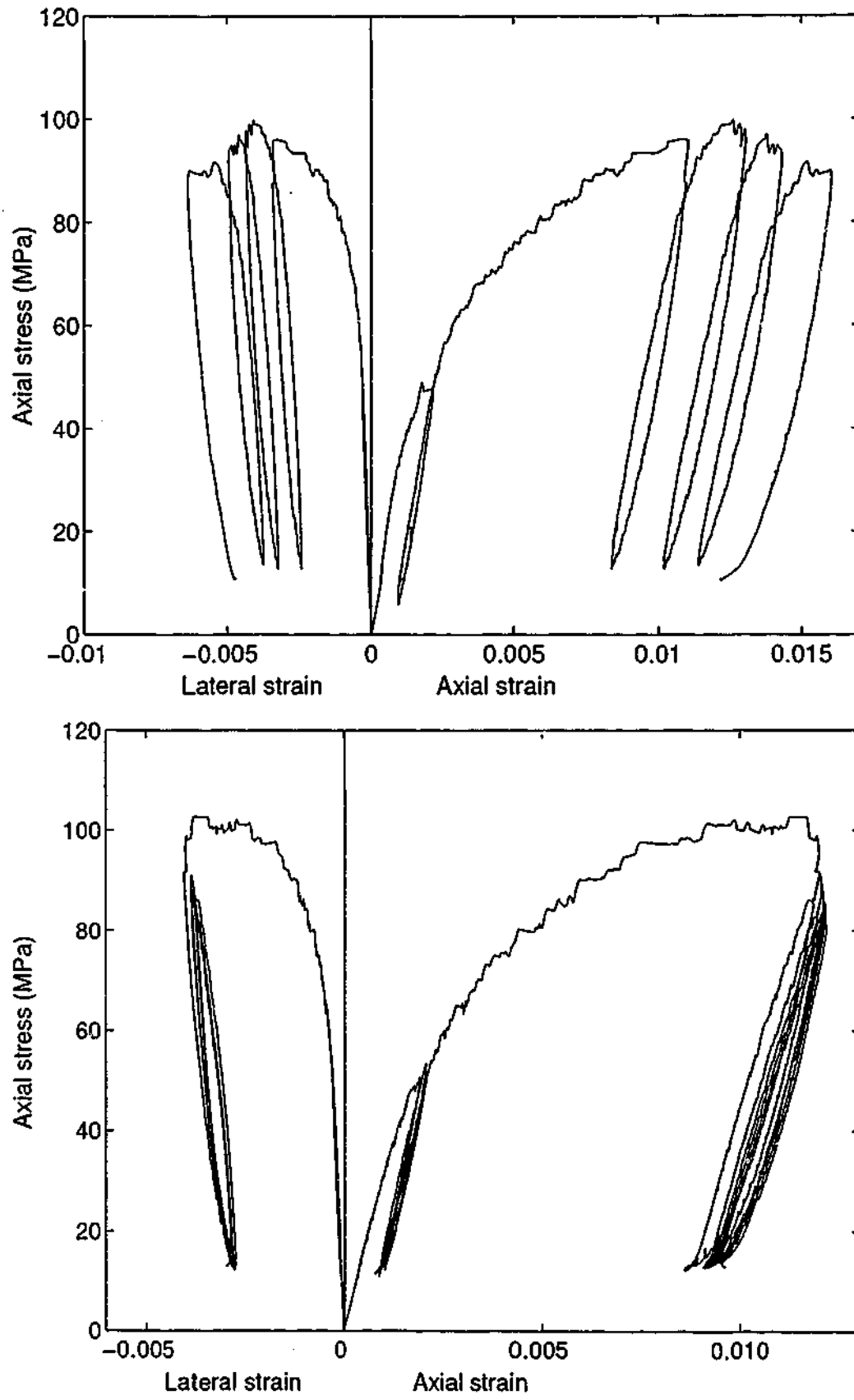


Figure 8.8: Grade 40 concrete with 12 MPa confining pressure.

8.3.2 Grade 60 test series

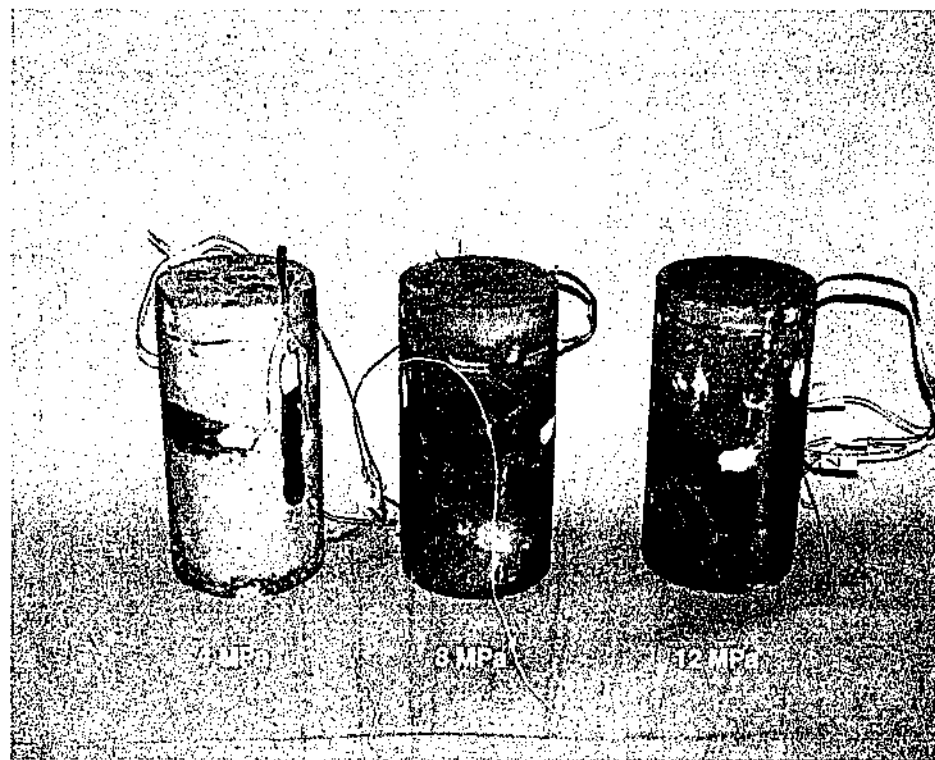
Figure 8.9 shows the tested Grade 60 concrete specimens. Except minor cracks, Grade 60 test specimens appear to be undamaged.

Figures 8.10-8.12 show the axial stress-axial strain and axial stress-lateral strain curves for Grade 60 concrete. The increase in peak strength is proportional to the level of confinement. Similar to Grade 40 concrete, 4 MPa increase in the lateral confinement has increased the peak strength by 15-20 MPa. Axial strain corresponding to the peak axial stress, increases with the increasing lateral confinement.

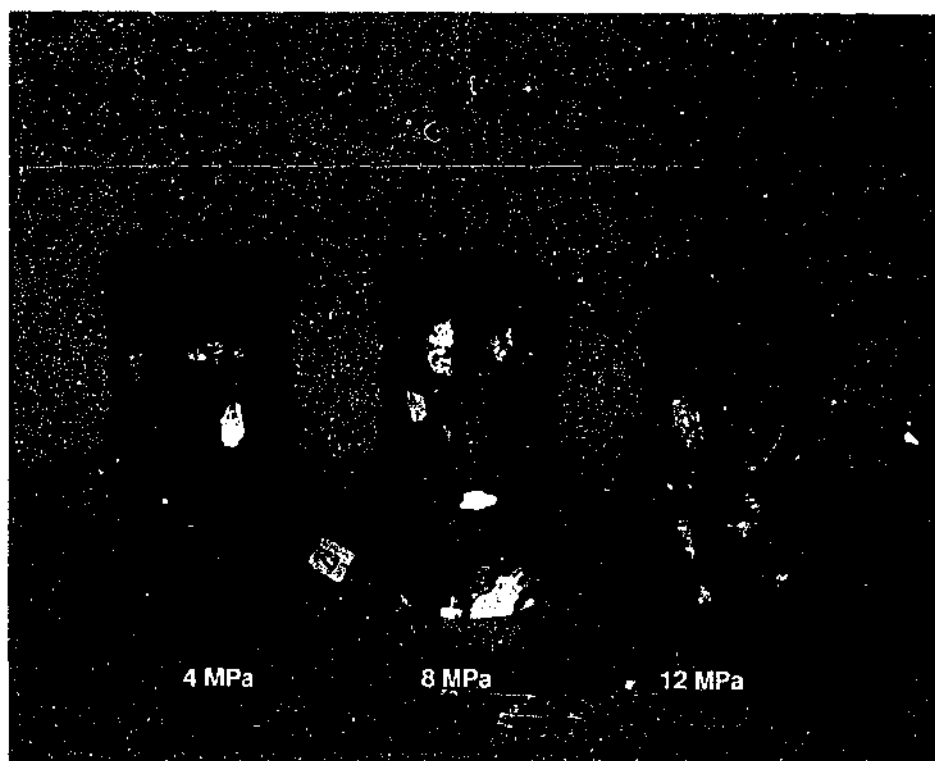
Ductility of the specimen with 12 MPa confining pressure in Grade 60 concrete is higher than that of the specimen with 8 MPa confining pressure as expected.

The damage due to each cycle changes with the unloading stress as shown by the Loading Regime 2 test series.

The thickness of the hysteresis loop increases with the increasing unloading strain for Grade 60 concrete. When unloaded in the "initial elastic region", a different curve is traced in the axial stress-axial strain plane while this is not the case in the axial stress-lateral strain plane.



(a). Loading Regime 1



(b). Loading Regime 2

Figure 8.9: Tested specimens for Grade 60 concrete.

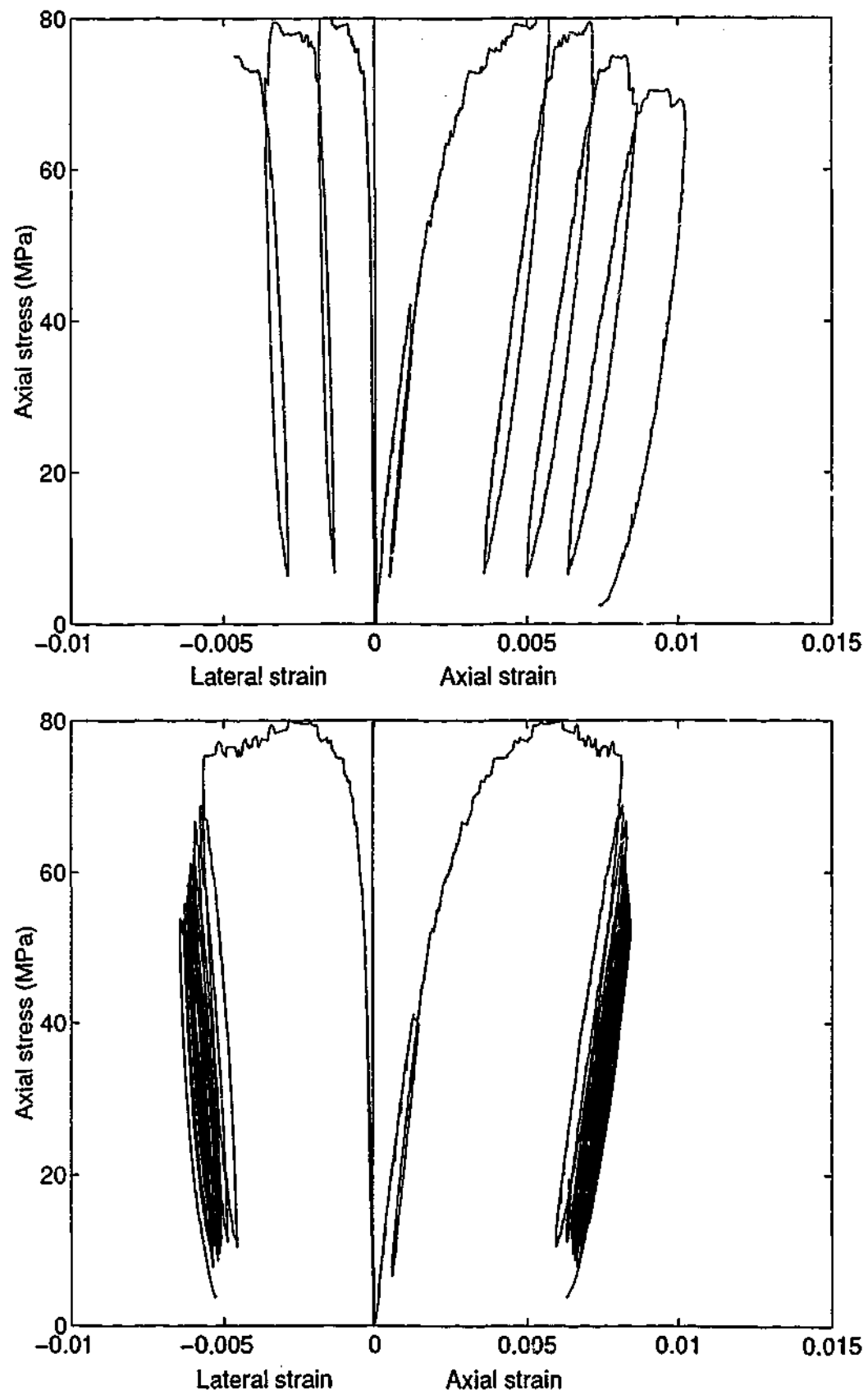


Figure 8.10: Grade 60 concrete with 4 MPa confining pressure.

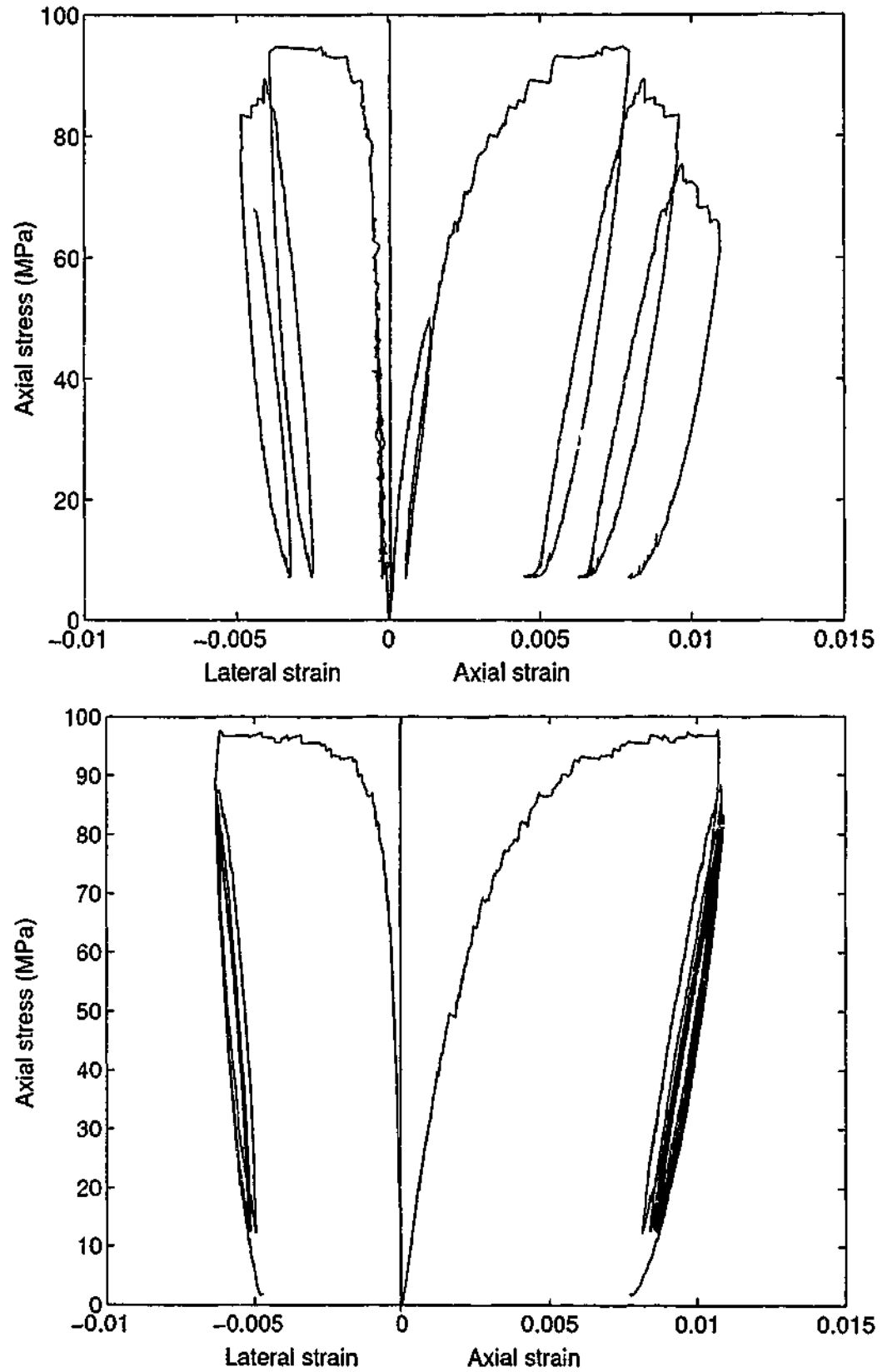


Figure 8.11: Grade 60 concrete with 8 MPa confining pressure.

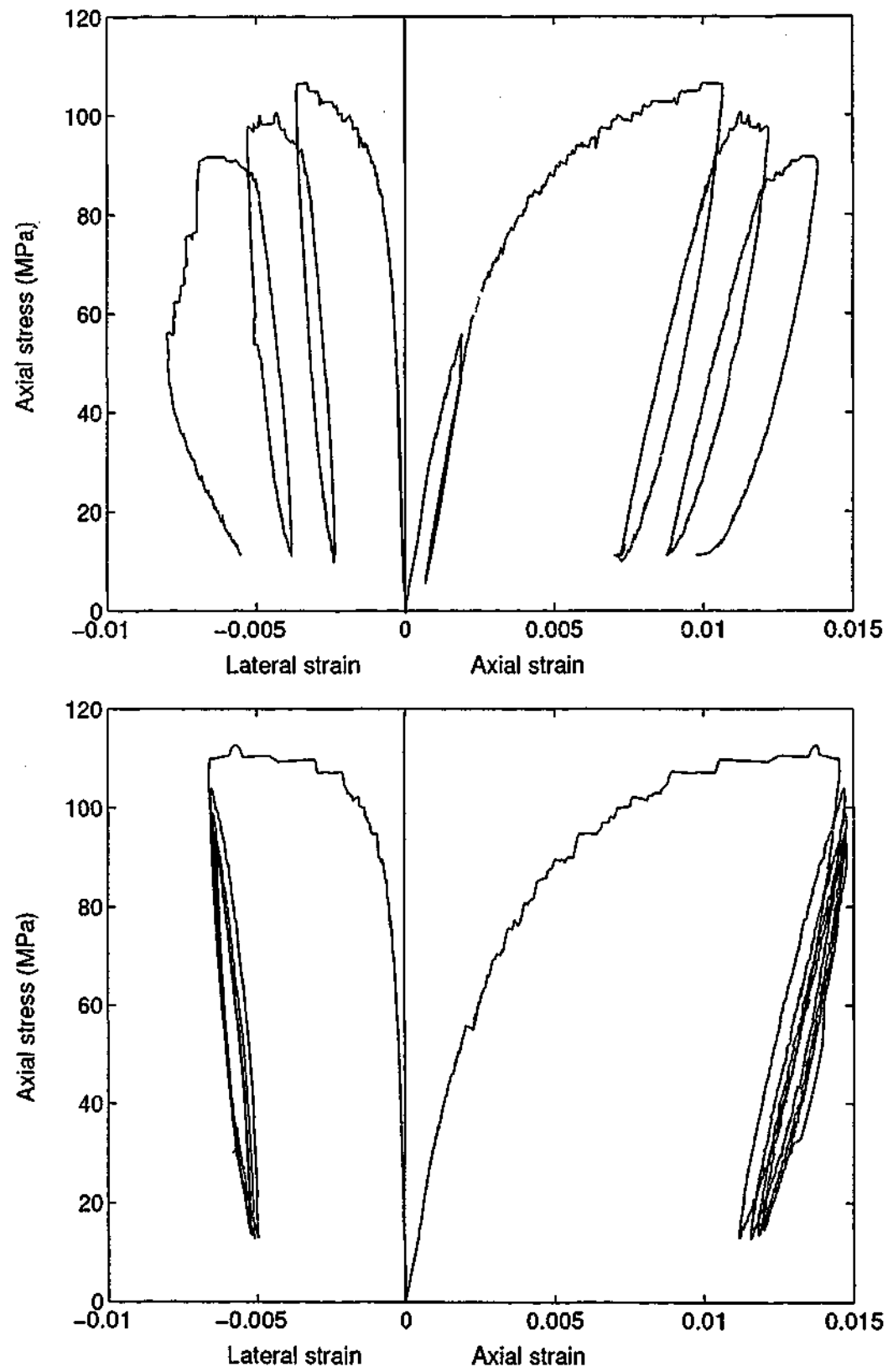


Figure 8.12: Grade 60 concrete with 12 MPa confining pressure.

8.3.3 Grade 80 test series

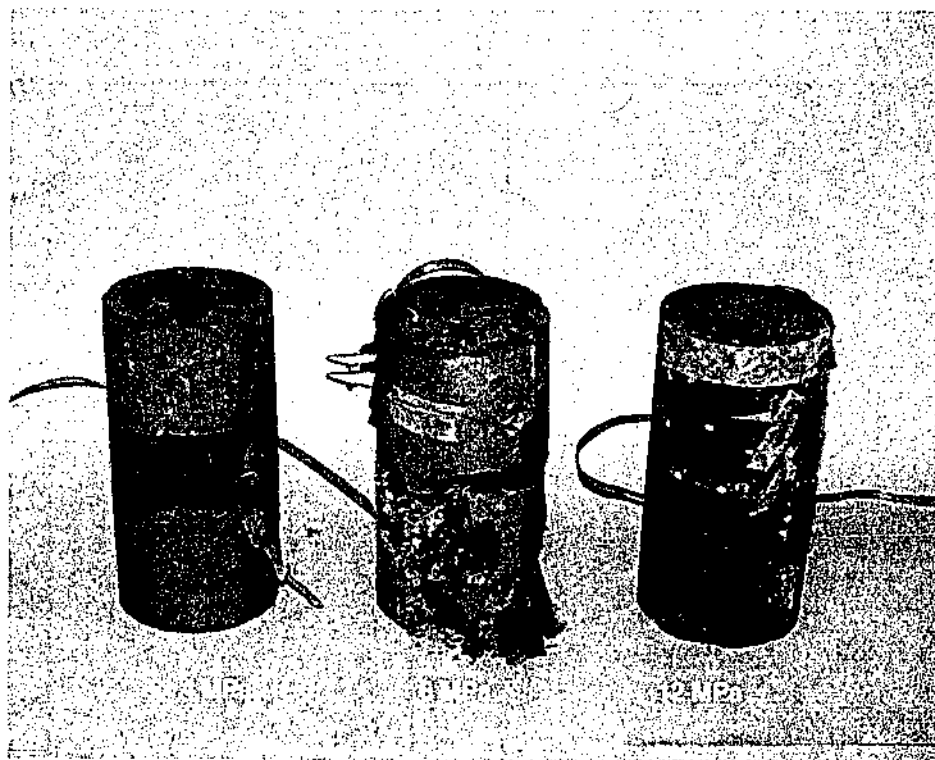
The tested Grade 80 concrete specimens are shown in Figure 8.13. Cracks were visible in most of Grade 80 test specimens. When the specimens were tested with 4 MPa confining pressure, it was impossible to get a cycle around the peak stress. When the specimen in Loading Regime 1 was unloaded just beyond the peak point, a significant strain increment was observed before unloading thus allowing to get only one cycle. Therefore in an attempt to obtain few cycles in the specimen used for Loading Regime 1 with 8 MPa confining pressure, the specimen fractured before ending the test. The failure plane for this specimen passed through the coarse aggregate. It was observed in this specimen that the cracking has passed through the strain gauges as well which proves the unreliability in the strain gauges after the peak point.

Figures 8.14-8.16 show the axial stress-axial strain and axial stress-lateral strain curves for Grade 80 concrete. The increase in peak strength is proportional to the level of confinement. 4 MPa increase in the lateral confinement has increased the peak strength by around 20 MPa.

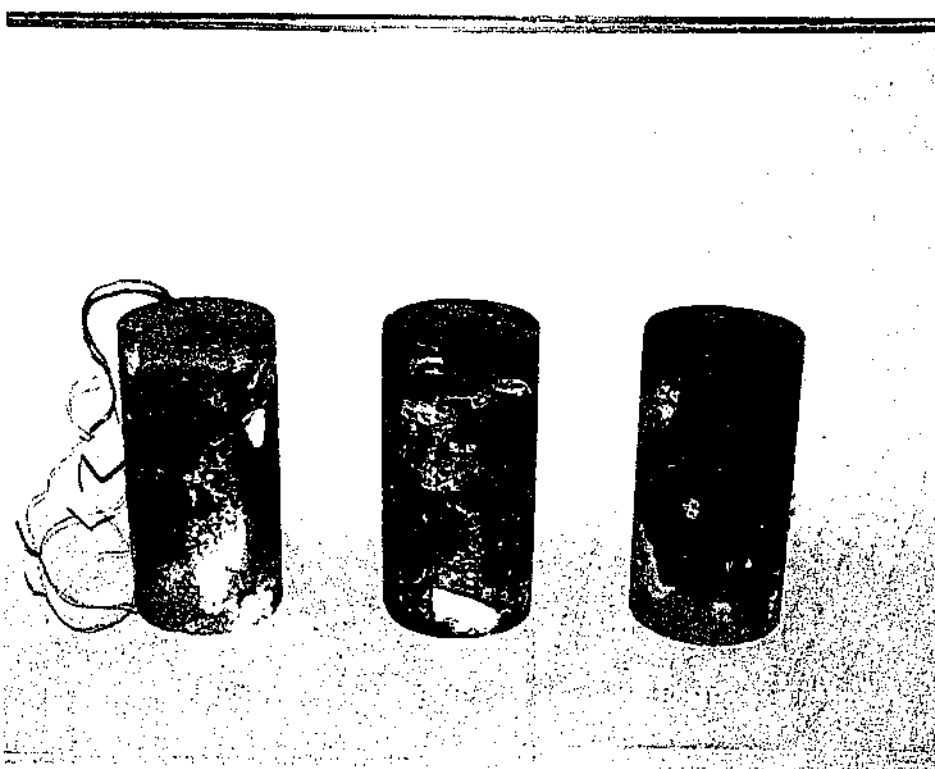
From Figure 8.15, it is evident that the lateral strains do not sound correct. This must be due to a malfunction in the clip gauge. Therefore the clip gauge was tested again before proceeding to the next tests.

Ductility of the specimen with 8 MPa confining pressure in Grade 80 concrete is higher than that of the specimen with 4 MPa confining pressure as expected.

The damage due to each cycle changes with the unloading stress as shown by the test series. The observation about the thickness of the hysteresis loops is similar to that made for Grade 40 and 60 concrete.



(a). Loading Regime 1



(b). Loading Regime 2

Figure 8.13: Tested specimens for Grade 80 concrete.

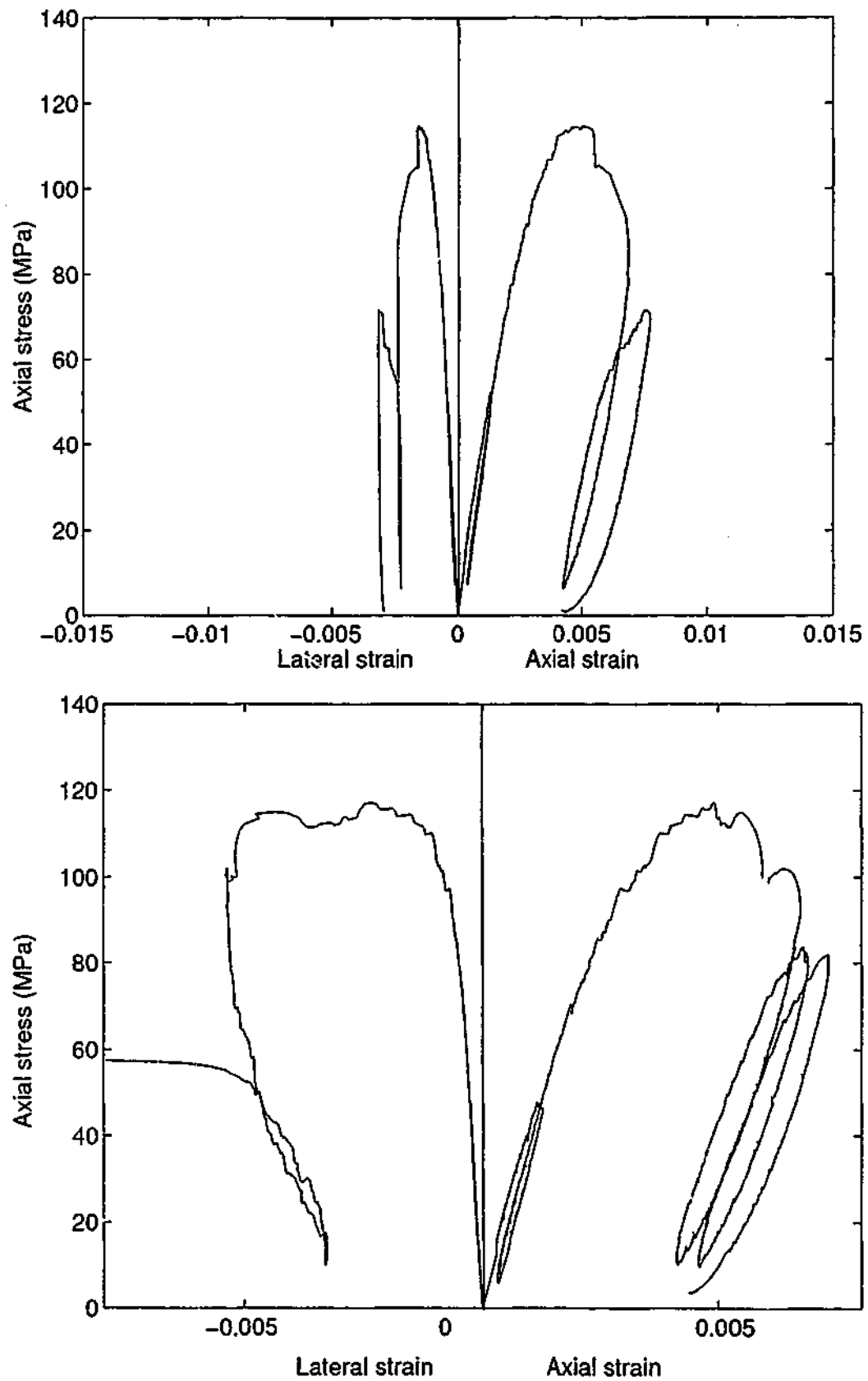


Figure 8.14: Grade 80 concrete with 4 MPa confining pressure.

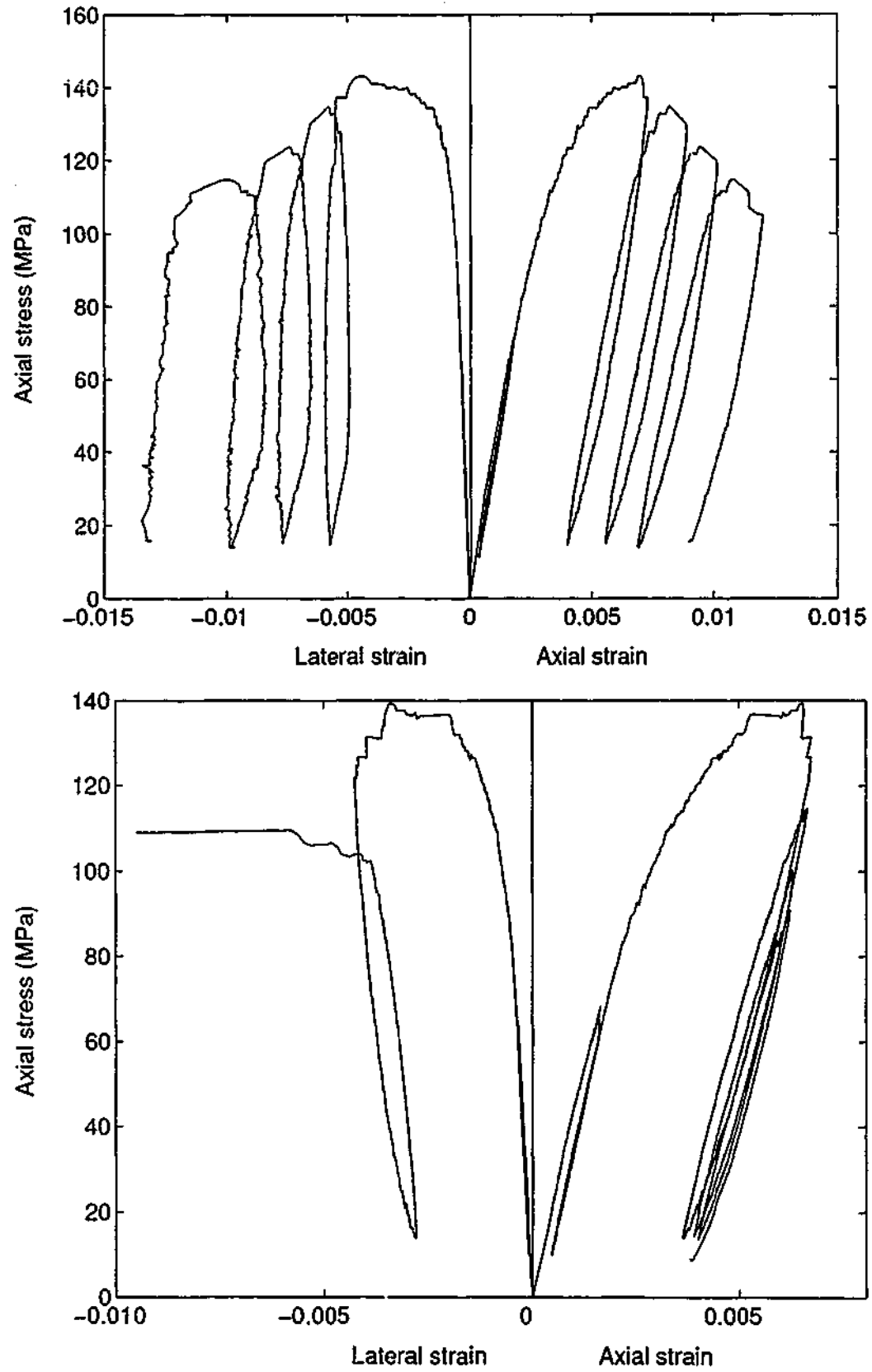


Figure 8.15: Grade 80 concrete with 8 MPa confining pressure.

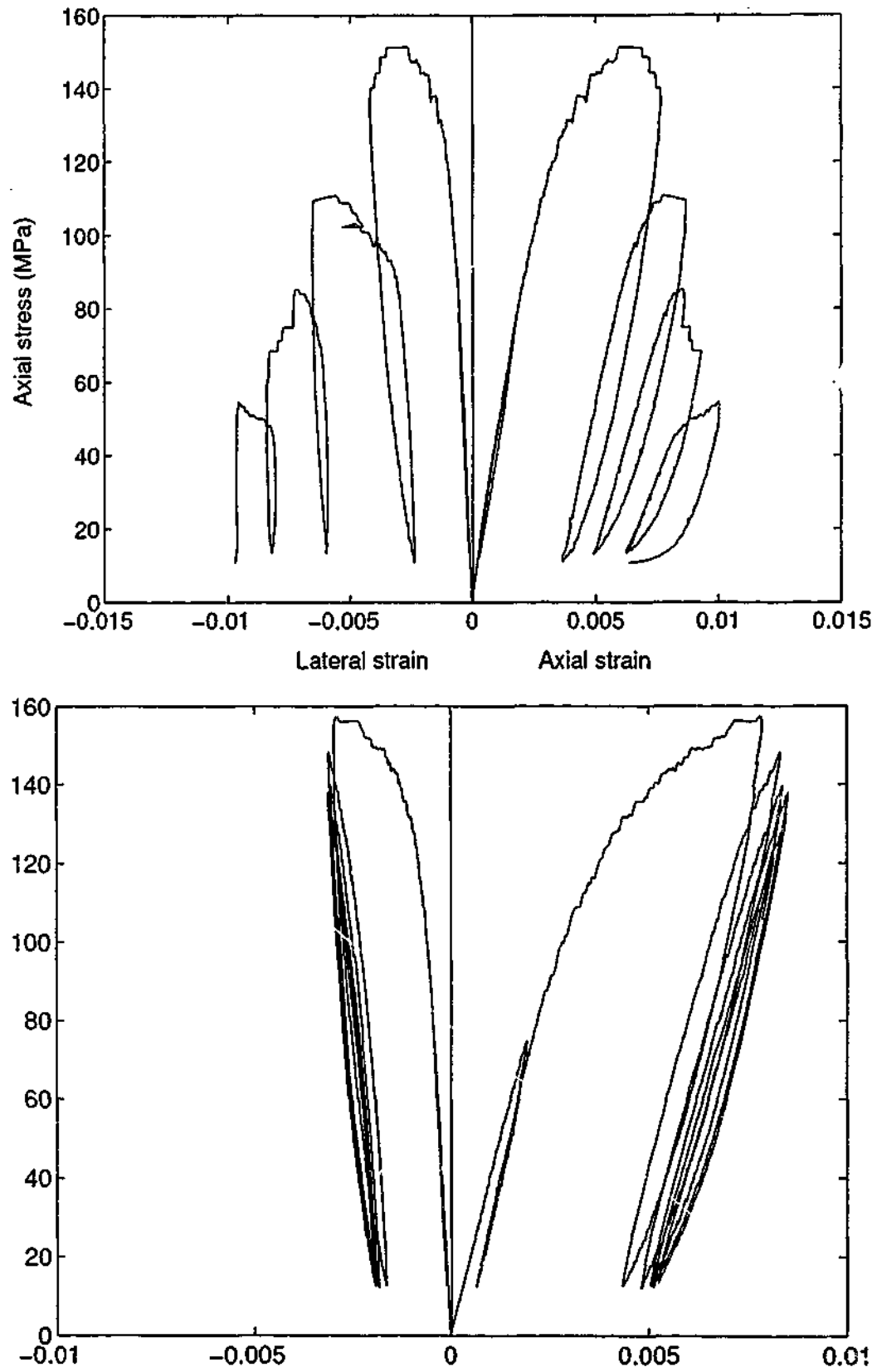


Figure 8.16: Grade 80 concrete with 12 MPa confining pressure.

8.3.4 Grade 100 test series

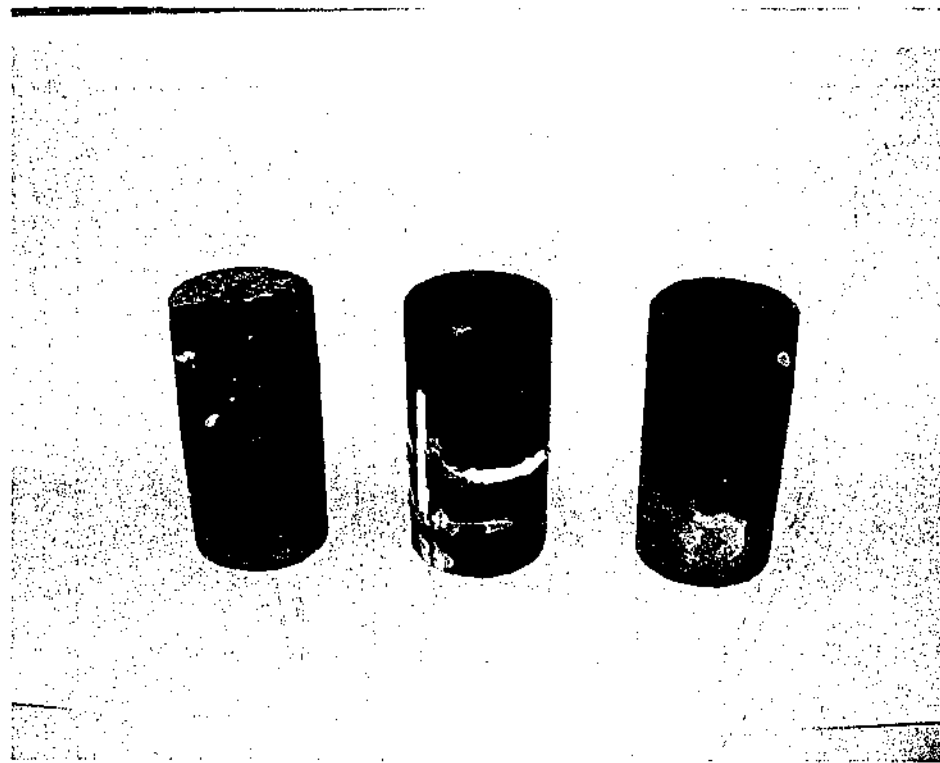
Figure 8.17 shows the tested Grade 100 concrete specimens at the end of testing. Special care was taken in testing these specimens to make sure they do not explode inside the tri-axial cell damaging the membrane. However, cracks propagated in some of the specimens thus damaging the strain gauges.

The axial stress-axial strain and axial stress-lateral strain curves for Grade 100 concrete are shown in Figures 8.18-8.20. The increase in peak strength is proportional to the level of confinement.

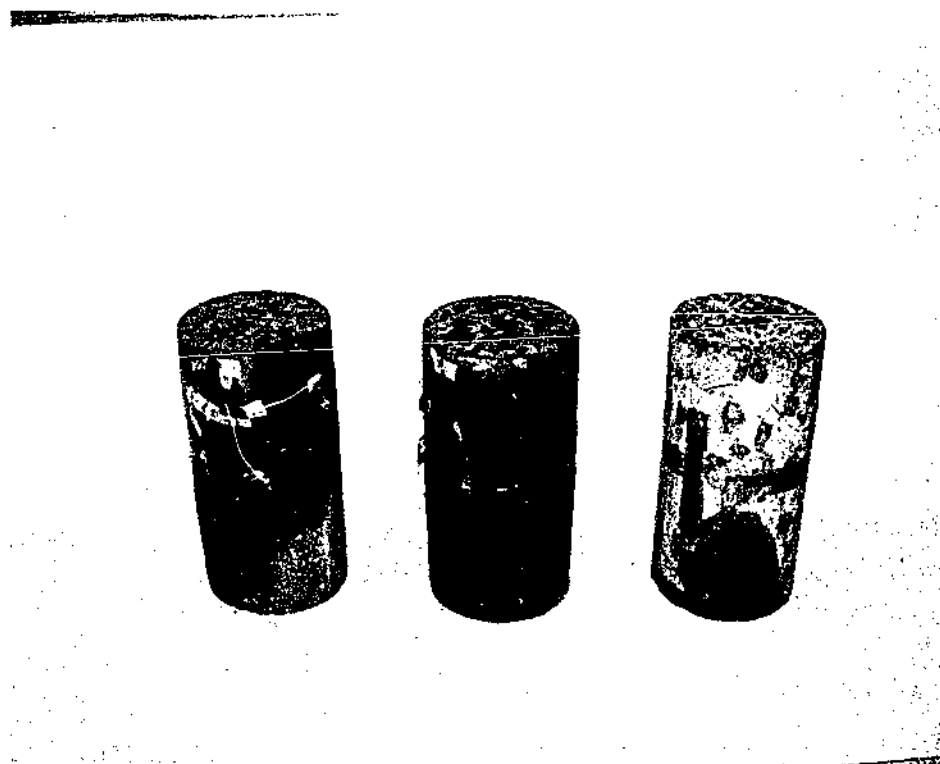
In Loading Regime 1 with 4 MPa confining pressure, attempting to unload around the peak point resulted in a dramatic increase in the axial strain thus only one cycle could be obtained. Therefore, the experimental program was modified for Grade 100 concrete such that a number of cycles are attempted before the peak point is reached. This was successful in several of the specimens.

When the stress-strain curves for Grade 100 concrete are considered, a significant ductility improvements are not found when the confining pressures are increased.

It was observed that the observations made about the damage in concrete, thickness of the hysteresis loop and the behaviour of unloading and reloading in the "initial elastic region" are still valid for Grade 100 concrete.



(a). Loading Regime 1



(b). Loading Regime 2

Figure 8.17: Tested specimens for Grade 100 concrete.

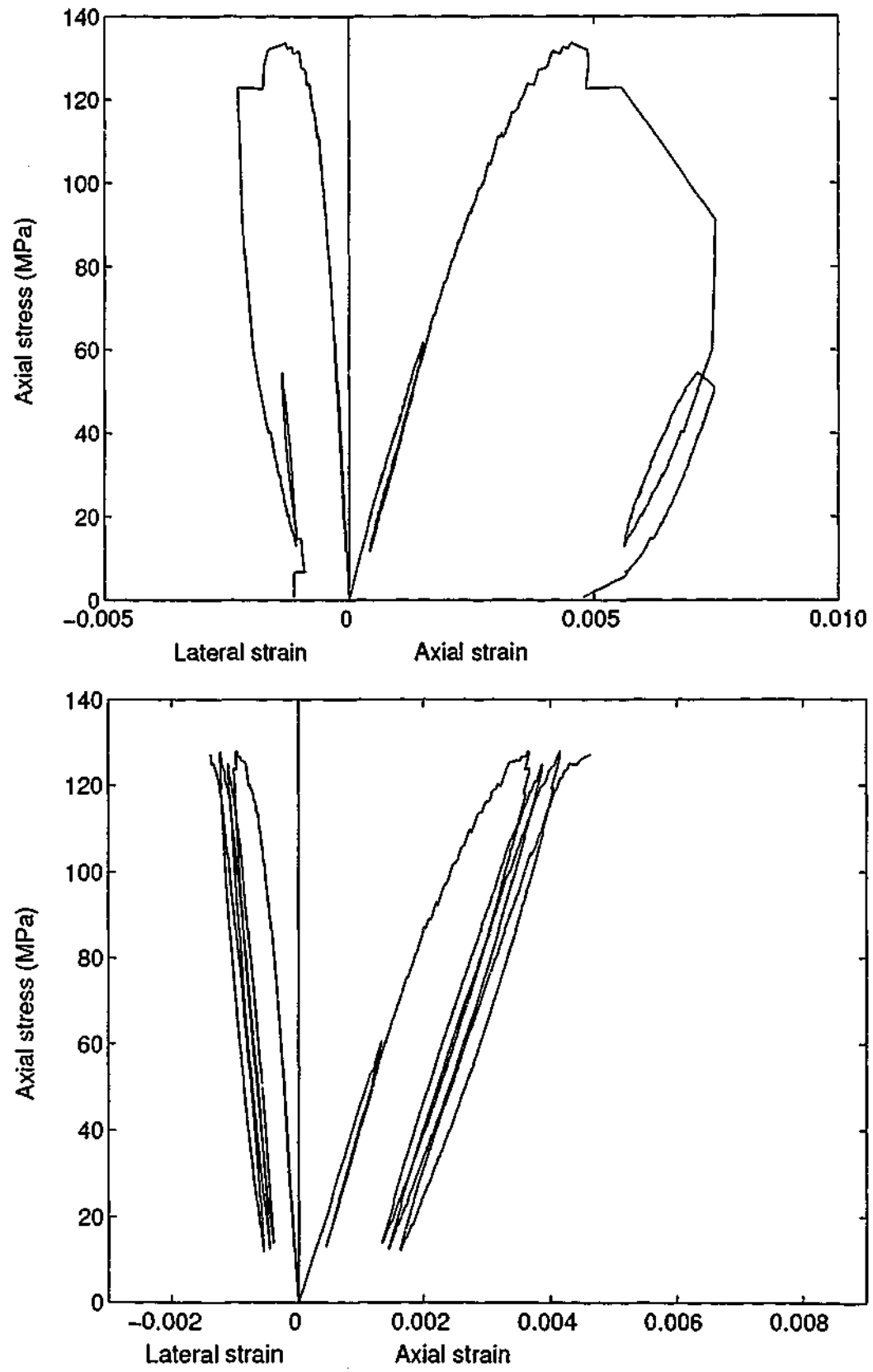


Figure 8.18: Grade 100 concrete with 4 MPa confining pressure.

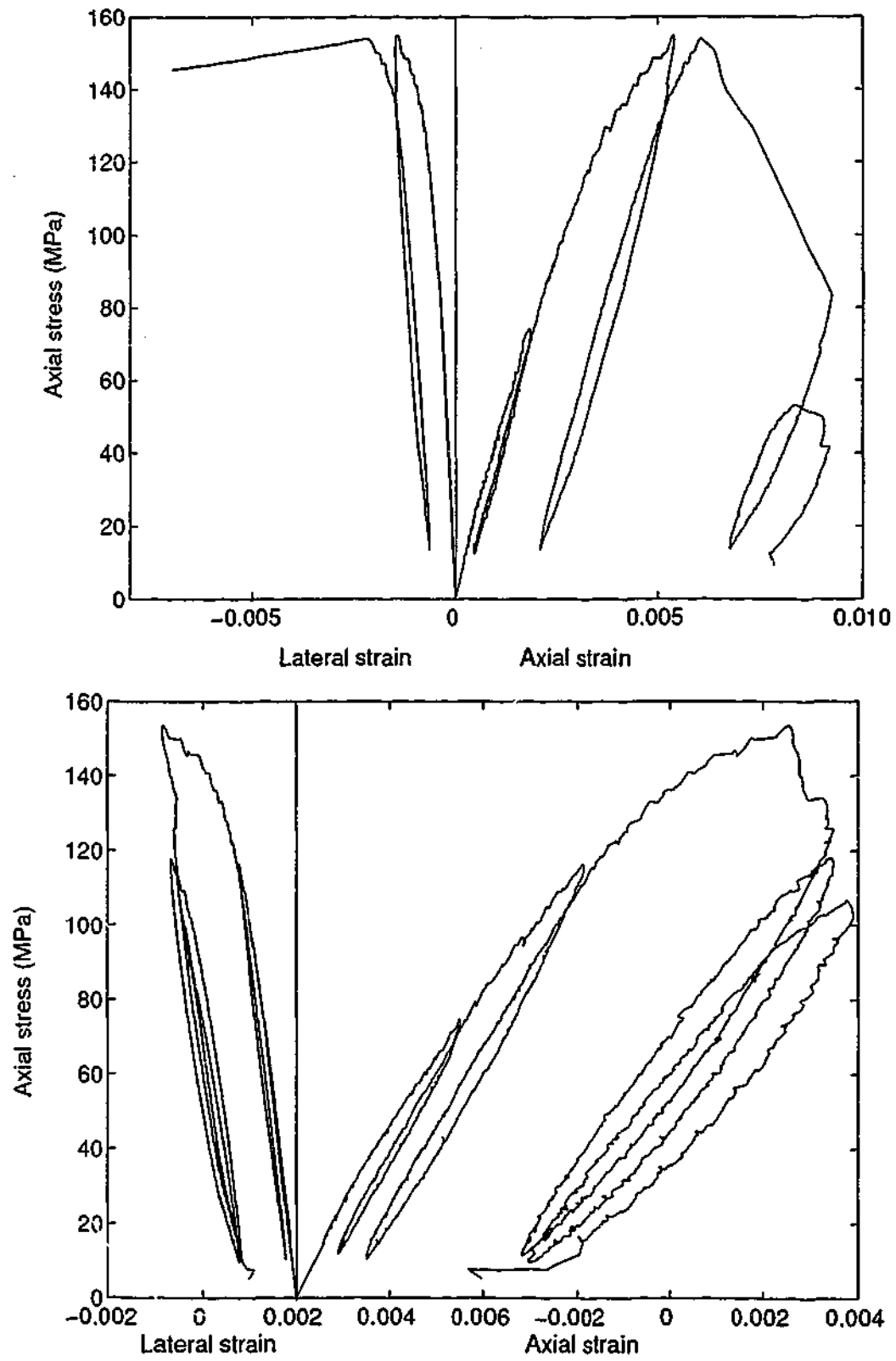


Figure 8.19: Grade 100 concrete with 8 MPa confining pressure.

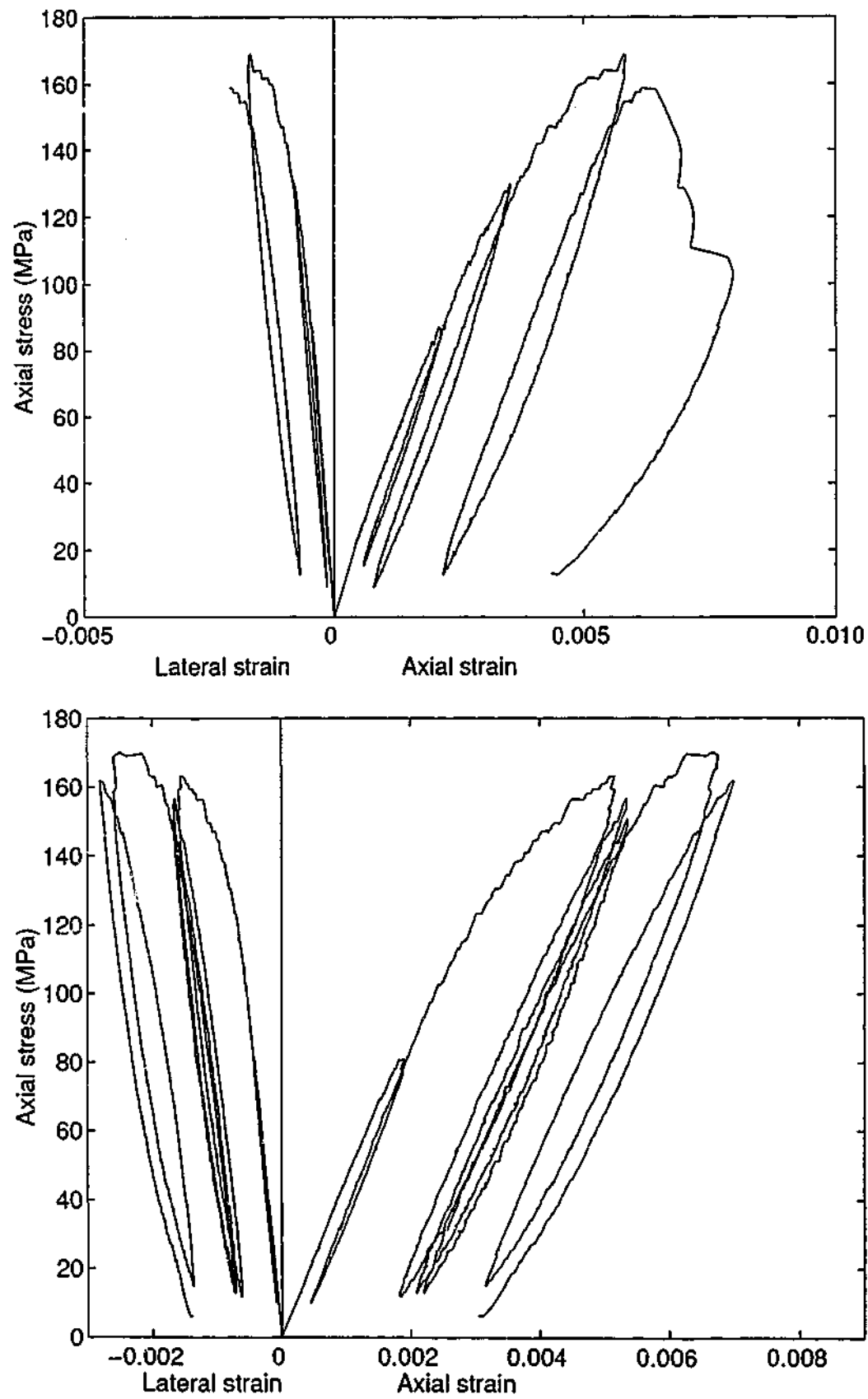


Figure 8.20: Grade 100 concrete with 12 MPa confining pressure.

8.4 Discussion

Several observations about ductility, shape of hysteresis loops, envelope curve, stress reduction due to unloading and reloading cycle and Poisson's ratio, were made from the experimental results reported in this section.

8.4.1 Envelope curve

"It is commonly believed that the monotonic loading curve forms the envelope for cyclic loading curves." This form of modelling has been developed by previous researchers for unconfined concrete (Sinha et al. 1964 and Karsan and Jirsa 1969). Later Karsan and Jirsa (1969) and Mander et al. (1988b) showed that it is a reasonable assumption for confined concrete as well. However, the experimental program carried out by the author for NSC and HSC and presented in this chapter, shows that this is valid for the ascending branch but is invalid for the descending branch (Figures 8.21-8.24).

8.4.2 Hysteresis loops

There is a small difference in the thickness of the loops depending on the unloading stress and the number of cycles. This is similar to the experimental results reported for NSC (Desayi et al. 1979; Sakai and Kawashima 2000). However, some of the experimental results for NSC show that the thickness of the loops increases with increasing unloading strain (Sinha et al. 1964; Karsan and Jirsa 1969).

8.4.3 Stress loss during hysteresis loops (damage)

The damage can be seen to vary depending on the strain and stress value of the unloading point. This is compatible with the experimental results reported in the literature for NSC (Sinha et al. 1964; Karsan and Jirsa 1969; Desayi et al. 1979; Sakai and Kawashima 2000). This stress reduction increases with the number of cycles. Similarly in Loading Regime 2 of the experiments, when there are a number of cycles from the same unloading strain, the stress reduction increases with the increasing number of cycles. This has also been proven to be true by previous researchers for NSC (Sakai and Kawashima 2000).

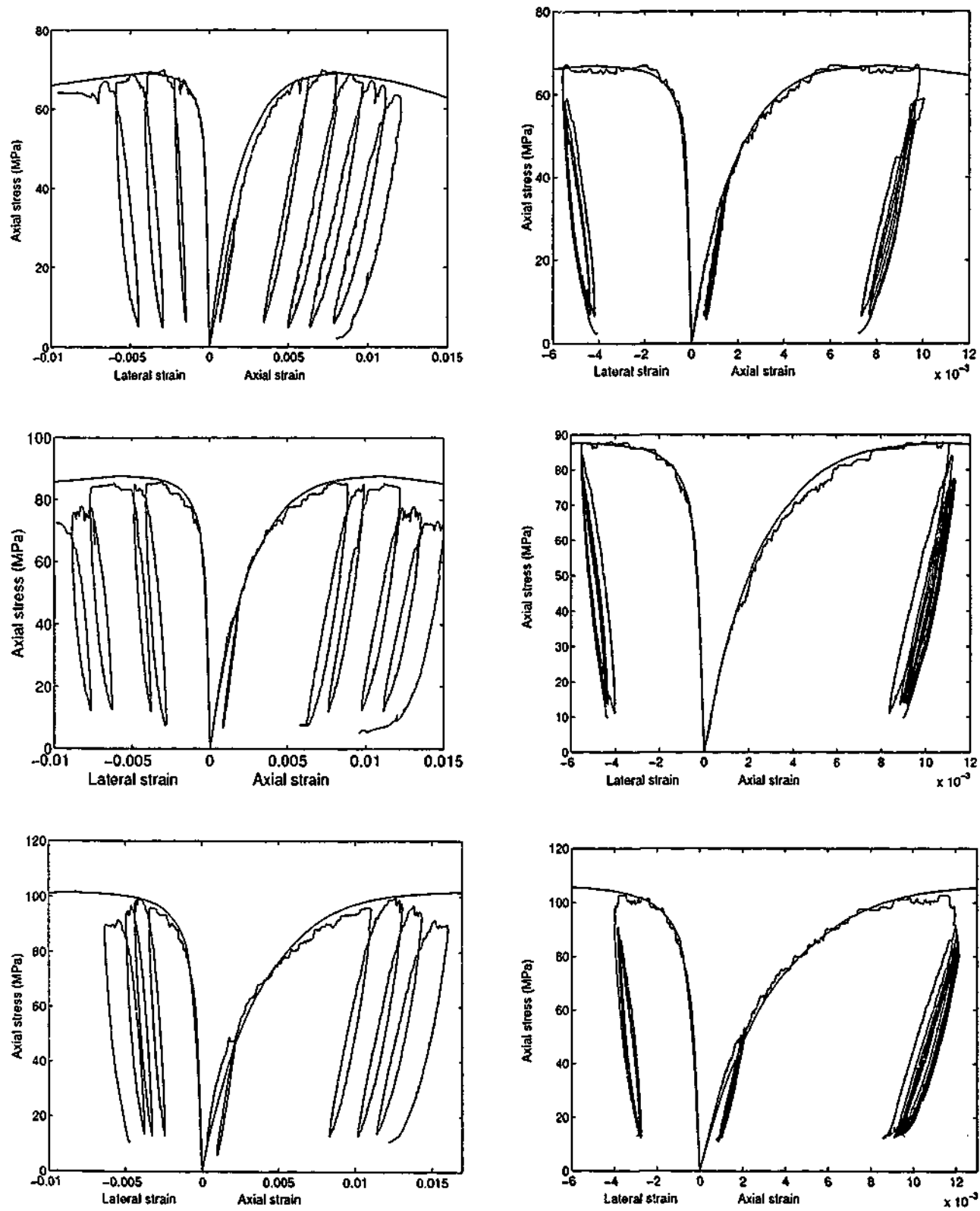


Figure 8.21: Comparison of monotonic and cyclic loading curves for 44 MPa concrete.

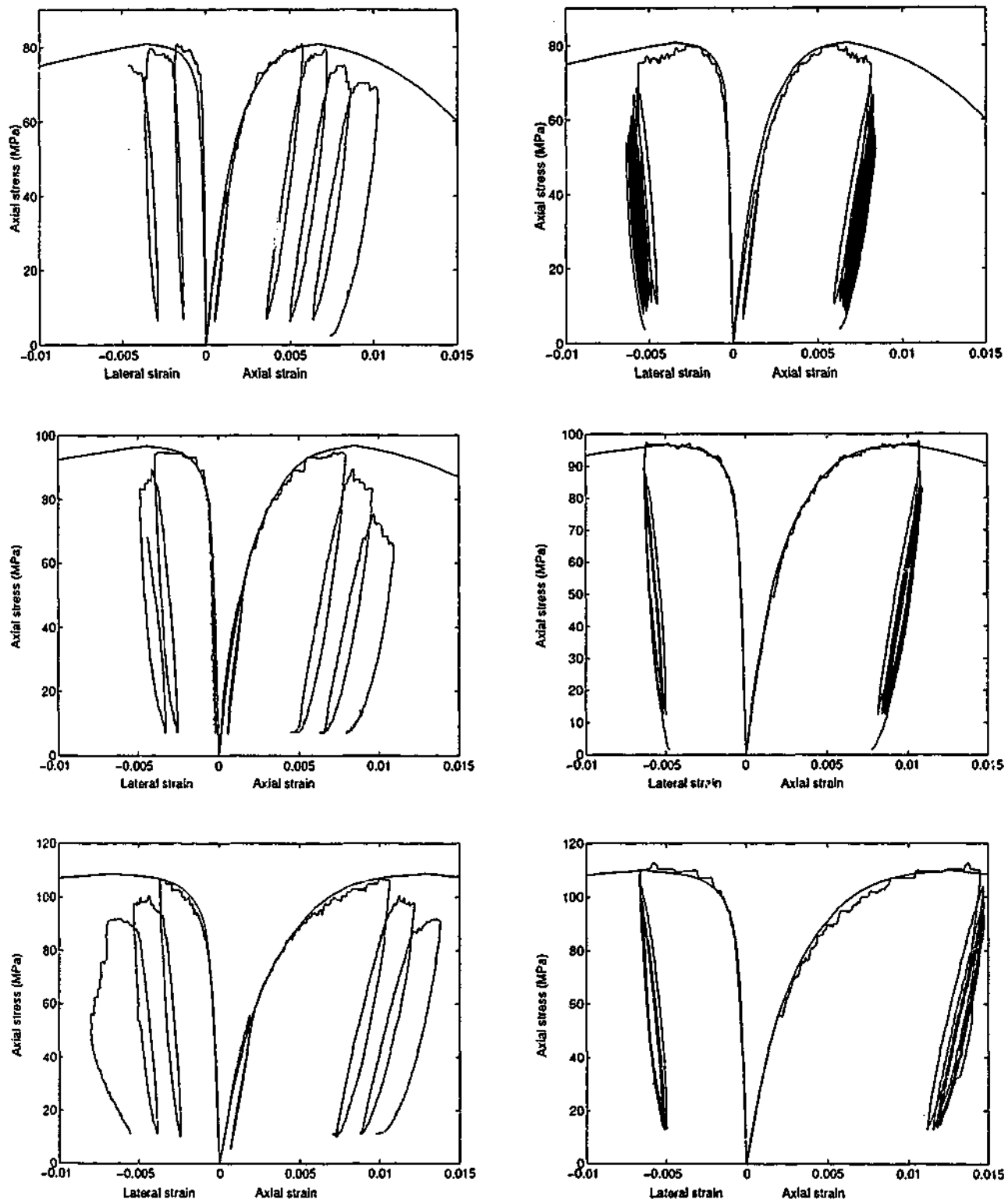


Figure 8.22: Comparison of monotonic and cyclic loading curves for 58 MPa concrete.

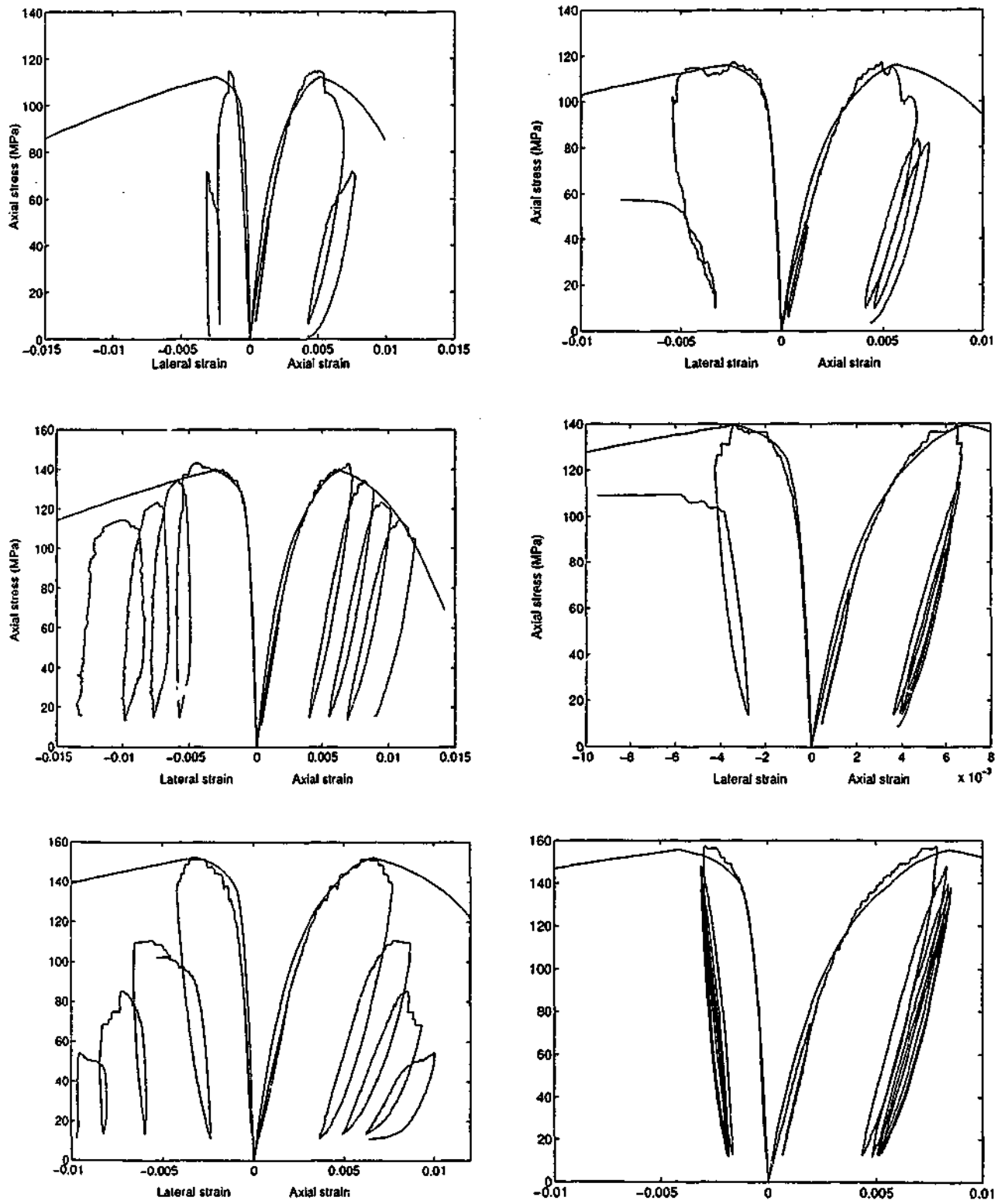


Figure 8.23: Comparison of monotonic and cyclic loading curves for 83 MPa concrete.

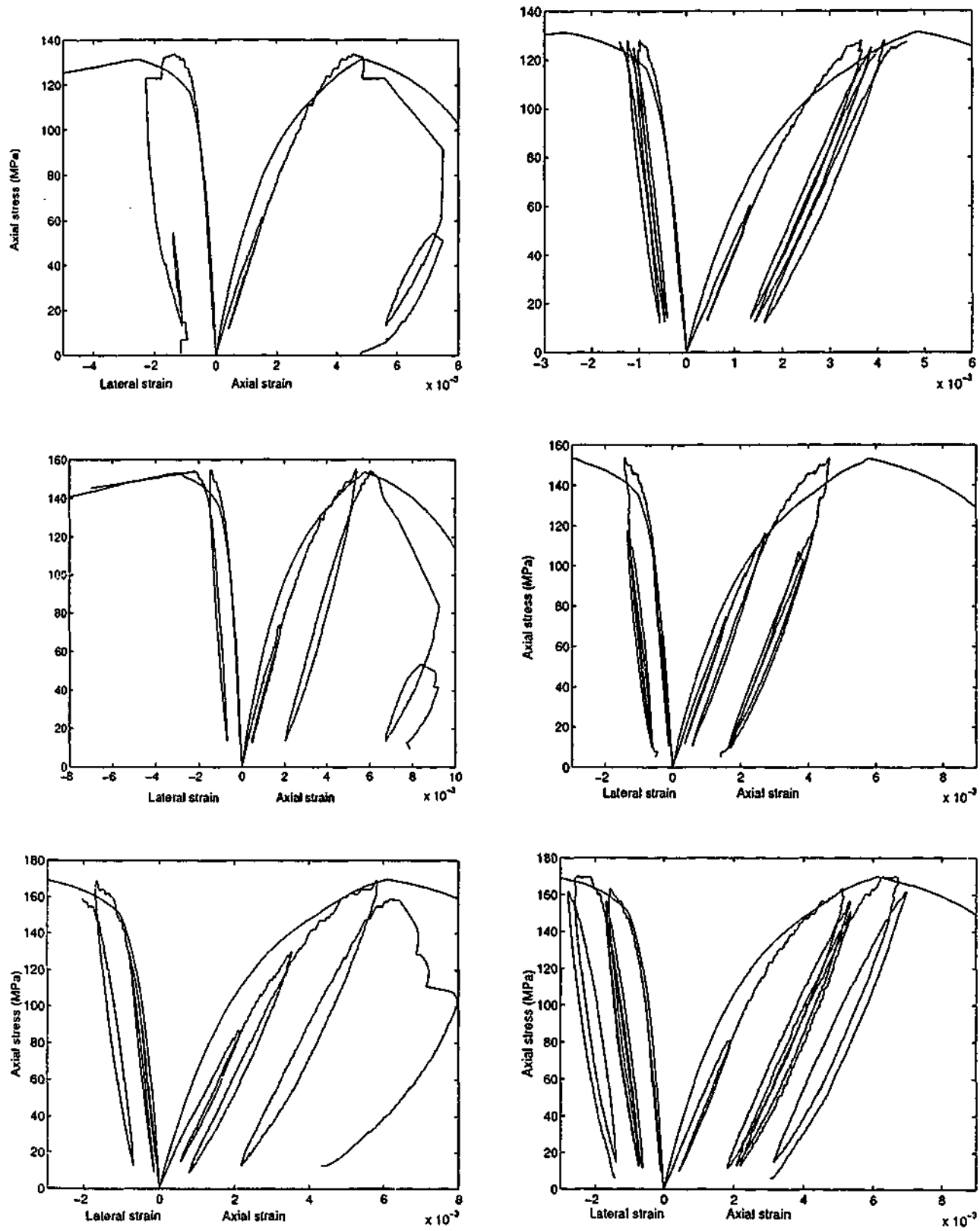


Figure 8.24: Comparison of monotonic and cyclic loading curves for 106 MPa concrete.

8.4.4 Poisson's ratio

Poisson's ratio is an important parameter specially when lateral confinement is involved. When the monotonically increasing loading is considered, initial Poisson's ratio was a constant for a particular concrete strength (Candappa et al. 2001) at the "initial elastic region". This "initial elastic region" was defined using β_i (axial stress to peak stress ratio), which is 0.7 for compressive strengths less than 40 MPa and 0.8 for compressive strengths greater than 60 MPa (Candappa et al. 2001). When loaded beyond the initial elastic region, Poisson's ratio rapidly increases to high values (Candappa et al. 2001).

From the experimental results in this study, it is found that the Poisson's ratio decreases when the unloading occurs in the initial elastic region. This can be observed in Figures 8.25-8.28 where the unloading of axial strain curves and lateral strain curves outside the initial elastic region show significantly different behaviour to the ones unloaded in the initial elastic region.

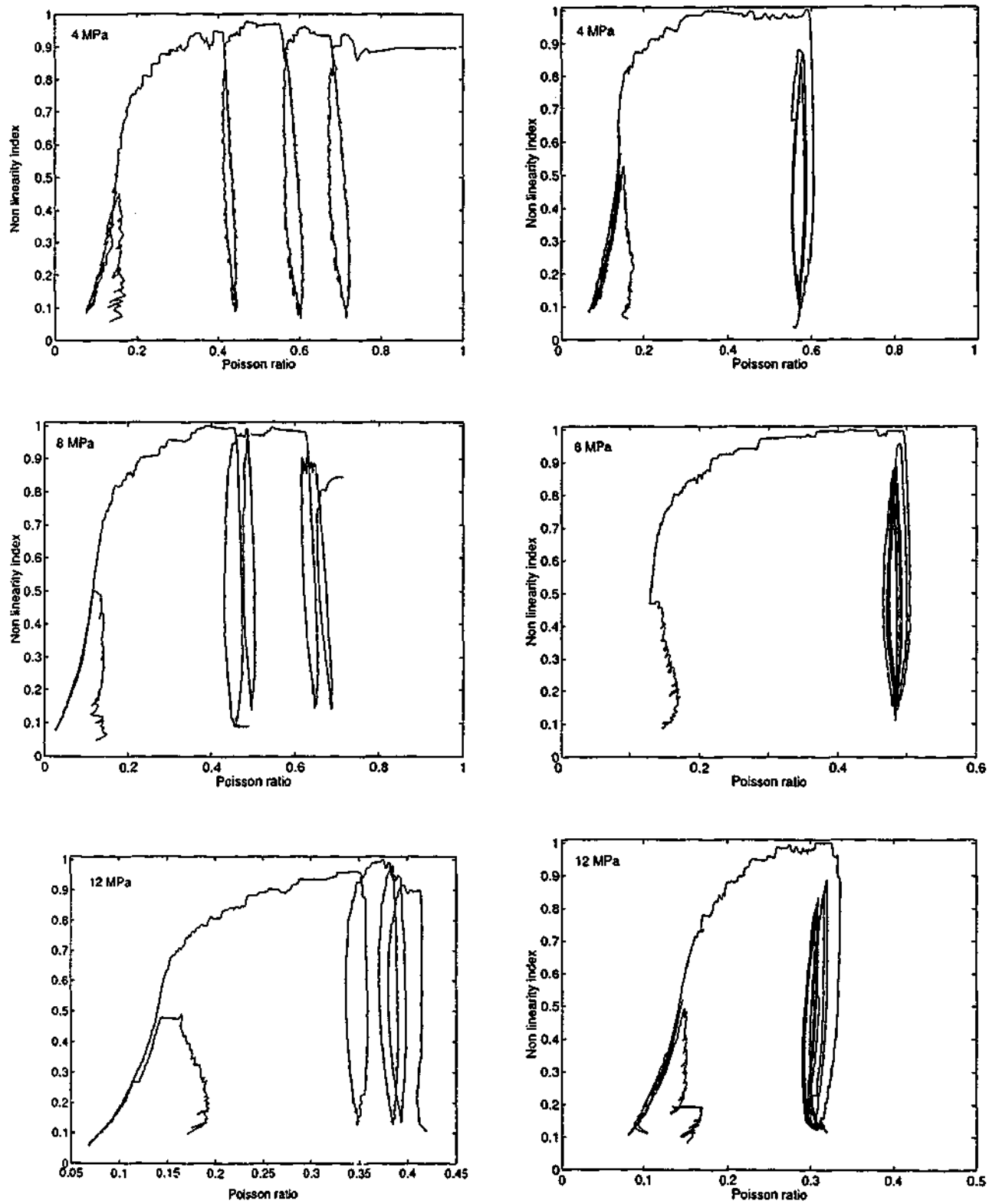


Figure 8.25: Behaviour of Poisson's ratio for 44 MPa concrete.

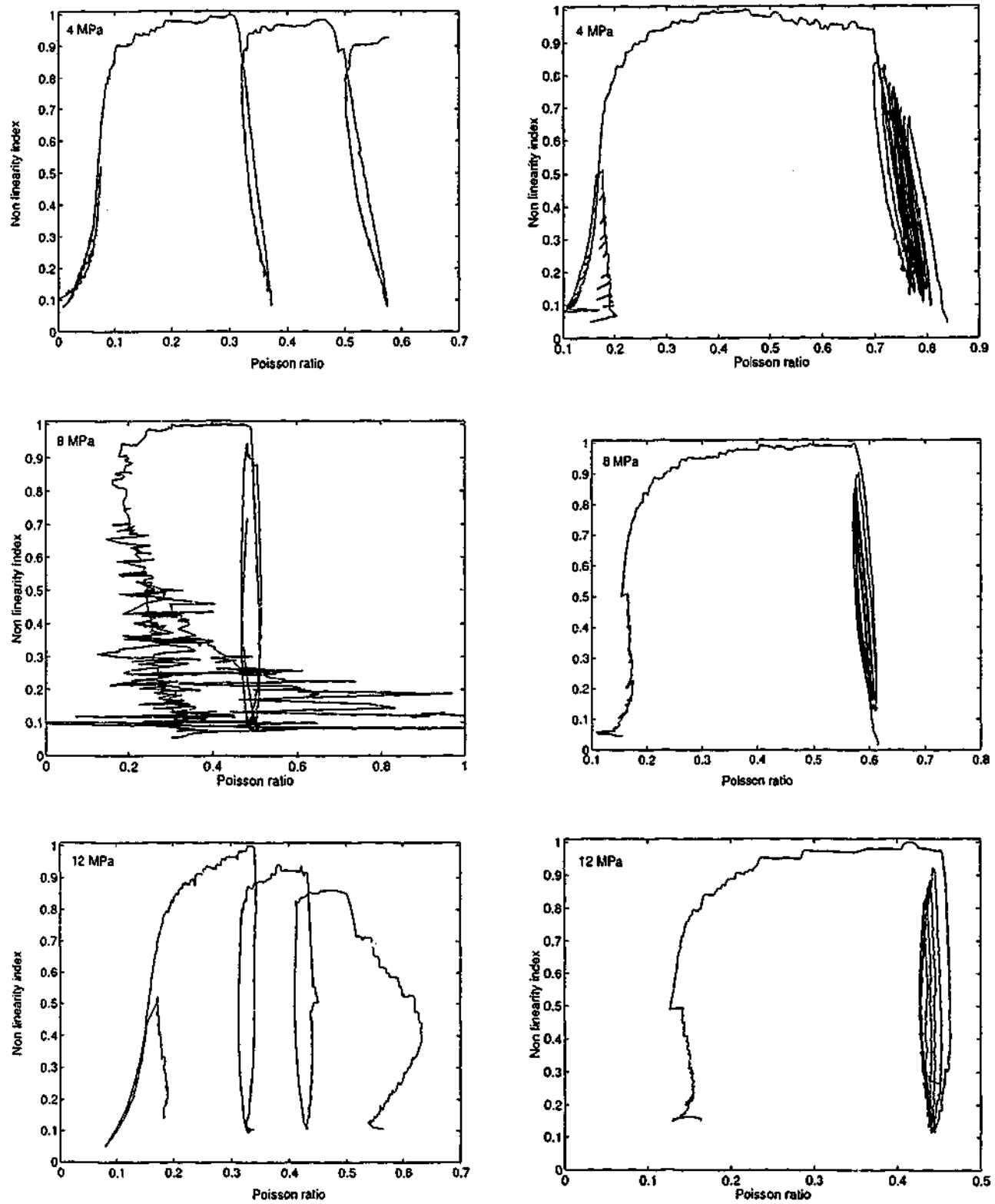


Figure 8.26: Behaviour of Poisson's ratio for 58 MPa concrete.

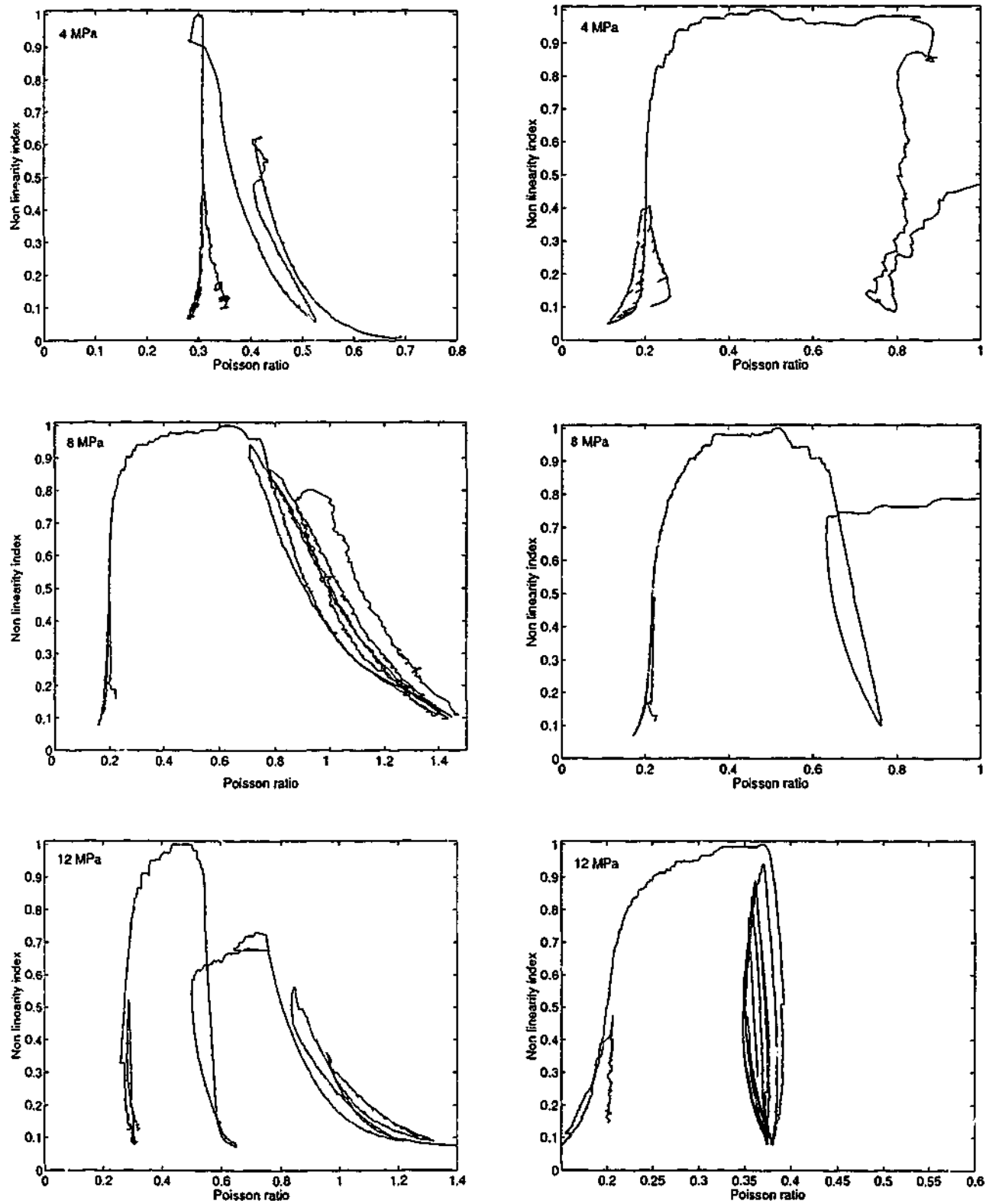


Figure 8.27: Behaviour of Poisson's ratio for 83 MPa concrete.

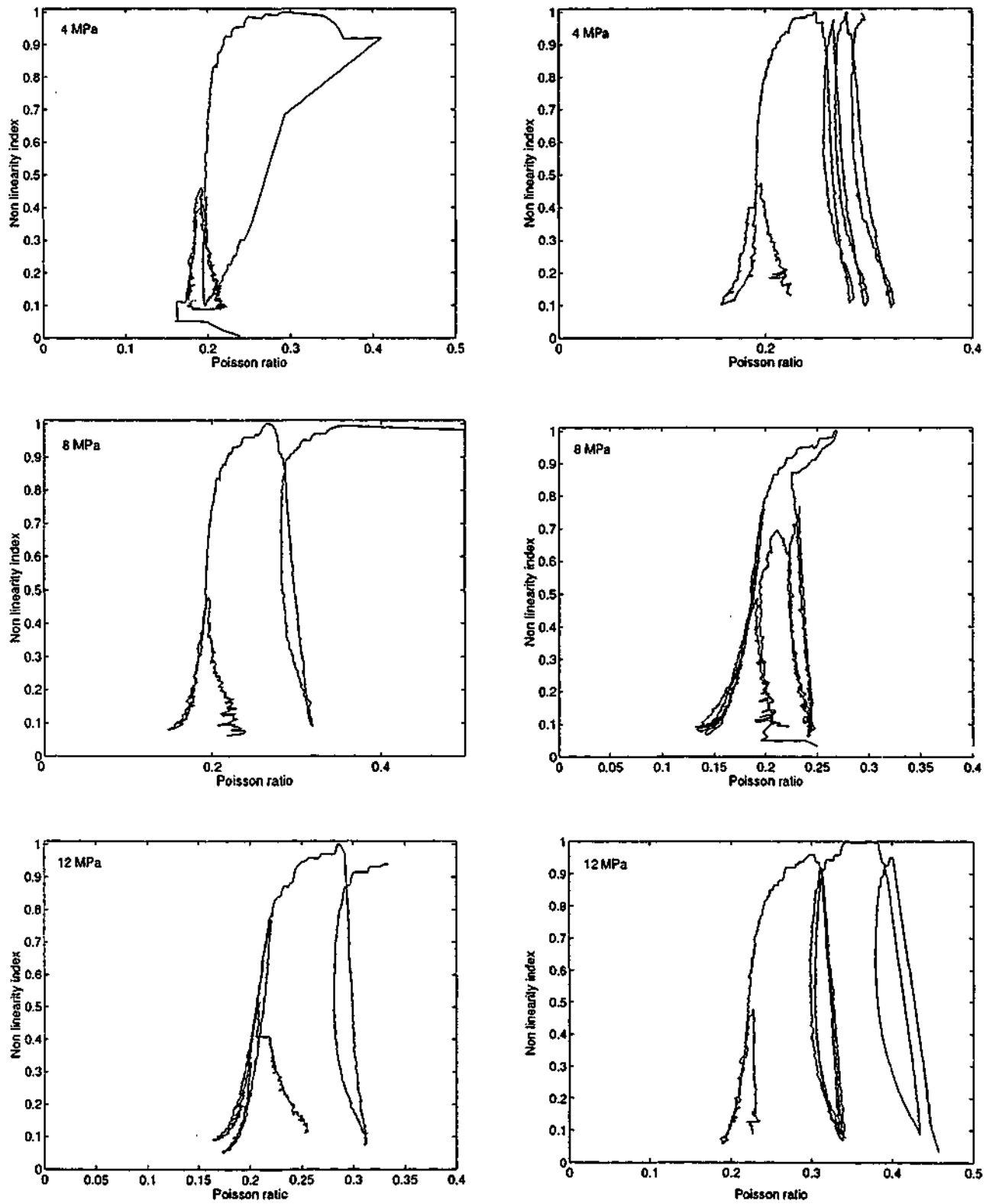


Figure 8.28: Behaviour of Poisson's ratio for 106 MPa concrete.

8.5 Conclusions

The following conclusions can be made from the experimental results reported in this chapter.

- It is generally agreed among the researchers that the monotonic loading stress-strain curve can be assumed to form the envelope curve for the cyclic loading stress-strain response. According to the experimental results, this needs modifications.
- When the monotonically increasing loading is considered, initial Poisson's ratio is a constant for a particular concrete strength (Candappa et al. 2001) in the "initial elastic region". If unloading occurs in this "initial elastic region", axial strains decrease more rapidly than the lateral strains, hence resulting in a reduction in Poisson's ratio. When reloading occurs after this unloading, the axial and lateral strains and Poisson's ratio values will return to the same values as those prior to the unloading occurred, in the "initial elastic region".
- An interesting observation in the initial elastic region is that the axial strain curves unload parallel to the initial tangent modulus whereas the lateral strain unloads along the same loading curve.
- The shape of the hysteresis loops in Loading Regime 1 of the experimental program is in agreement with those reported for normal strength concrete in the literature (Desayi et al. 1979; Sakai and Kawashima 2000).
- In Loading Regime 1 of experiments, the thickness of the loop, stress reduction (damage) in each unloading reloading cycle and the slope of the unloading curves (plastic strain) vary depending on the unloading point (strain and stress), uniaxial strength of concrete and applied confining pressure.
- In Loading Regime 2 of experiments about 20% decrease in stress occurs with about 2-3 cycles in specimens subjected to 4 MPa confining pressures whereas the same occurs in about 10 cycles in specimens subjected to 12 MPa confining pressures.

The experimental data presented in this chapter forms the basis for the development of a constitutive model for confined HSC subjected to cyclic loading.

Chapter 9

CYCLIC LOADS: Development of a constitutive model for confined concrete

9.1 Introduction

This chapter presents a constitutive model developed for high strength concrete with uniform lateral confinement subjected to cyclic axial compression. It is based on the results of an experimental program carried out for normal and high strength concrete as described in the previous two chapters. Unconfined compressive strengths of concrete were 44, 58, 83 and 106 MPa. Uniform confining pressures applied were 4, 8 and 12 MPa. The stress-strain model presented in this chapter is developed using triaxial test results, which are conducted under well-controlled conditions, where direct measurement of axial and lateral strains has been possible. Ability to estimate the axial as well as lateral strains in confined concrete is a superior attribute of the proposed model. When concrete is analysed for passive confinement (such as the one provided by reinforcement), estimating the lateral strain is important because the lateral confinement directly depends on it. The proposed model can be used for modelling HSC in seismic analysis of structures, where confining of concrete by reinforcement is essential for ductility.

During an earthquake, the structures are subjected to cyclic lateral forces. In performing a structural analysis in such a region, the effect of earthquake loadings on the structure needs to be analysed. Therefore understanding of behaviour of concrete and confining material (steel) with cyclic loading is necessary in such analysis. There are

experimental studies reported in the literature for the behaviour of unconfined NSC subjected to cyclic axial compression (Sinha et al. 1964, Karsan and Jirsa 1969, Desayi et al. 1979). Similar studies were reported for confined NSC (20-49 MPa) subjected to cyclic axial compression (Desayi et al. 1979, Shah et al. 1983, Mander et al. 1988b, Watanabe and Muguruma 1988, Sakai and Kawashima 2000). No experimental observations as such were reported for HSC in the literature. The available stress-strain curves for unconfined and confined NSC represent the variation of axial stress with axial strain only.

In the seismic design of reinforced concrete structures, ensuring sufficient level of ductility is important for energy absorption. With the increased use of HSC in structures, the issue of ductility improvements has become a critical issue. It is a common practice to use confining reinforcement in both earthquake resisting structures and other structures, to increase the ductility of the structural members. Since the confinement provided by lateral steel reinforcement changes with cyclic loading, developing a methodology for the behaviour of columns under cyclic loading is difficult based on column tests only. Therefore it is necessary to establish a complete deformational behaviour including both axial and lateral deformation of laterally confined HSC with cyclic axial compression. The author aimed at developing a constitutive model for the behavior of HSC with lateral confinement subjected to cyclic axial compression.

The outcomes of this chapter are to be published in a research paper, Lokuge et al. (accepted for publication in 2003 in Journal of Materials in Civil Engineering, ASCE).

9.2 Comparison of the experimental results with the existing models

The model proposed by Mander et al. (1988b) is the most widely used model among the research community for cyclic loading of concrete and the model proposed by Sakai and Kawashima (2000) is the most recent model reported in the literature for the same analysis. The results from these two models are compared with the experimental observations by the author for NSC and HSC. Appendix A reports these comparisons. Although these models are applied for HSC, they are originally developed based on NSC. It is observed from the study of cyclic axial load on NSC (confined or unconfined) that the experimental curves are in reasonable agreement with the estimated curves from the models. But, if

unloading starts from the latter part of the descending curve there is a difference in the experimental and estimated hysteresis loops. The comparison of experimental results from this study with the estimated curves from the two models explained earlier (Appendix A) are summarised for each strength grade in the following sections.

9.2.1 Grade 40 concrete

In Loading Regime 1 of Grade 40 concrete with 4 MPa confining pressure, it is observed that the thickness of the hysteresis loops were almost the same as those corresponding to experimental results. However, it is interesting to note that the plastic strains are overestimated in both the compared models. In Mander et al. (1988b) model, the estimation of plastic strains become closer to the experimental plastic strain with increasing axial strain. In Loading Regime 1 of Grade 40 concrete with 8 MPa confining pressure, the estimated loop thickness using Mander et al. (1988b) model is higher than that for experimental results. But the plastic strains were almost the same. When the results obtained from Sakai and Kawashima (2000) model are considered, the loop thickness was compatible but plastic strains were overestimated. In Loading Regime 1 of Grade 40 concrete with 12 MPa confining pressure, the loop thicknesses obtained from Mander et al. (1988b) model were higher than those for experimental results. However, the loop thicknesses corresponding to Sakai and Kawashima (2000) model were compatible. In both models plastic strains were overestimated.

9.2.2 Grade 60 concrete

In Loading Regime 1 of Grade 60 concrete with 4 MPa confining pressure, Mander et al. (1988b) model compares well with the experimental results. For the same Sakai and Kawashima (2000) model overestimated the plastic strains. This was the same for Loading Regime 1 of Grade 60 concrete with 8 MPa confining pressure. When the confining pressure was increased to 12 MPa, the loop thickness proposed by Mander et al. (1988b) was higher than that for experimental results. In this case Sakai and Kawashima (2000) model overestimated the plastic strains.

9.2.3 Grade 80 concrete

In Loading Regime 1 of Grade 80 concrete with 4 MPa confining pressure, Mander et al. (1988b) model estimated the plastic strains to be similar to experimental results while Sakai and Kawashima (2000) overestimated the same. This was the same for Loading Regime 1 of Grade 80 concrete with 8 MPa confining pressure. The experimental results for Loading Regime 1 of Grade 80 concrete with 12 MPa confining pressure do not seem correct and therefore not compared.

9.2.4 Grade 100 concrete

In Grade 100 concrete Mander et al. (1988b) model estimated the plastic strains to be close to those in the experimental results. However, the loop thickness was predicted to be higher from that model than the experimental results. Sakai and Kawashima (2000) overestimated the plastic strains in all cases.

In all the compared results, the ascending branch of the envelope curve compares well with those corresponding to experimental results. However for all the experiments carried out, it is noted that the descending branch of the envelope curve does not match with those in the experimental results.

9.3 Preliminary modelling process

The stress-strain models available in the literature for the static loading of HSC, can model only the axial stress and axial strain relationships. All of them were based on column tests. Therefore several attempts have been made in developing axial stress, axial strain and lateral strain relationships for confined HSC subjected to cyclic loading. They are described in detail in the following section.

9.3.1 Different attempted approaches

With the processed data for the 4 compressive strengths, 3 confining pressures and 2 loading regimes, the author searched for possibilities in establishing axial stress, axial strain and lateral strain relationships for unloading and reloading cycles. At this point it was aimed to use the stress-strain model developed by the author in Chapter 3 for monotonically increasing loading to predict the envelope curve for cyclic loading. The

first obvious concern was to extend the available stress-strain models for NSC to model the axial stress and lateral strain relationship of HSC subjected to cyclic axial compression. The second approach was to attempt extending Candappa (2000)'s model as it can predict both axial and lateral strains. Then an attempt was made to search for a common pattern in all the unloading and reloading curves separately. As a result, total energy was analysed with axial strain as the third attempt. It was possible to model the required behaviour using this method. However, an issue came up about the meaning of total energy versus axial strain relationships and concluded that it would be more meaningful if a relationship of total energy versus volumetric strain is considered.

Finally it was possible to find a common pattern in shear stress versus shear strain curves for unloading and reloading respectively. The theory that concrete failure is a Mohr-Coulomb type shear failure has been put forward by Nielsen (1999). Therefore the final approach was compatible with the theory proposed by Nielsen (1999). The same concept was used earlier to develop the constitutive model for confined HSC subjected to monotonically increasing loadings. However, all the four attempts made are described below.

Extending the available NSC stress-strain models

There are several models reported in the literature (Desayi et al. 1979; Watanabe and Murguruma 1988; Mander et al. 1988b; Sakai and Kawashima 2000) to establish the axial stress axial strain relationship for confined NSC subjected to cyclic loading. They are based on column tests and are described in detail in Chapter 6. The axial stress-axial strain relationships obtained for confined HSC from the experimental program described in the previous chapter can therefore be compared with these models. These comparisons are shown in Appendix A. If the same models are to be extended to model the lateral strains, there must be a relationship for the behaviour of Poisson's ratio. Therefore Poisson's ratio values were plotted against axial strain values for all 4 compressive strengths of concrete and 3 confining pressures used by Candappa (2000) and presented in Figure 9.1.

The curves were different in each grade of concrete for each confining pressure applied. Therefore a common pattern could not be observed. Due to these reasons the idea of extending the available stress-strain models for confined NSC to model the constitutive behaviour of confined HSC with cyclic loading was abandoned.

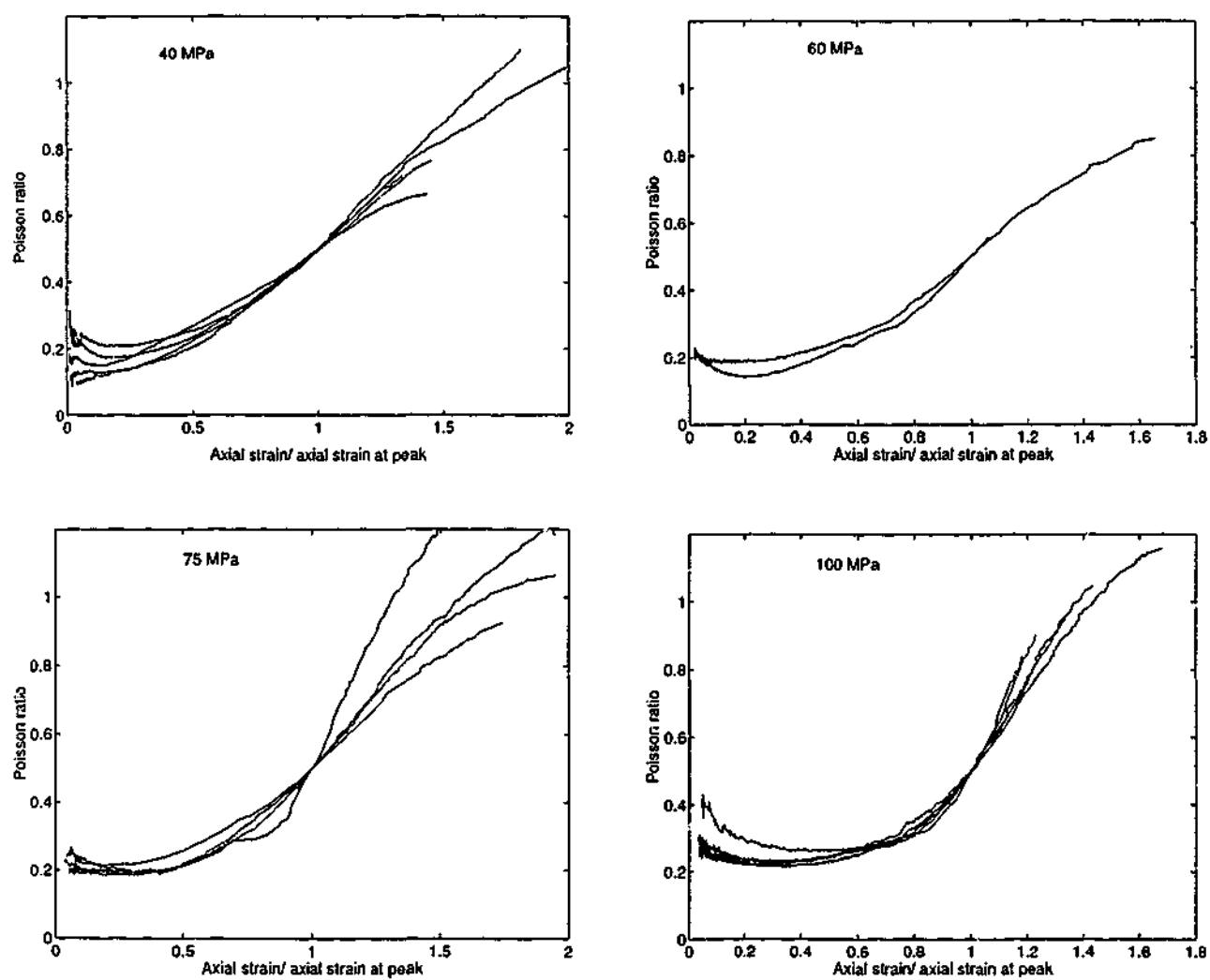


Figure 9.1: Poisson's ratio versus axial strain for monotonically increasing loads.

Extending Candappa (2000) model

Candappa (2000) developed axial stress, axial strain and lateral strain relationships for HSC subjected to lateral confinement. This model is the first and the only model among the many models available, which can model axial stress lateral strain relationships. Furthermore this model was based on the triaxial tests on HSC. The author investigated all the stress-strain models for static loading available in the literature and found that Candappa (2000)'s model is a possible model which can be considered to extend in establishing the constitutive behaviour of HSC with lateral confinement subjected to cyclic axial compression. The major reason for this selection was its ability to model the lateral strains. However, it is a stress-based model and therefore iterations are needed in the calculation of stress-strain behaviour and it is unnecessarily complicated. Further, Candappa (2000) used basic nonlinear elastic relationships as the main equations in establishing stress-strain behaviour under static loading. The validity of these relationships in unloading and reloading cycles is uncertain. Candappa (2000) used Poisson's ratio and secant value of Young's modulus to model statically loaded confined concrete. Using the experimental results reported in previous chapter it is possible to model the Poisson's ratio behaviour for the unloading reloading cycles but finding secant value of Young's modulus for this is a problem. Therefore the idea of extending Candappa (2000)'s model to estimate the behaviour of confined concrete subjected to cyclic loading was abandoned.

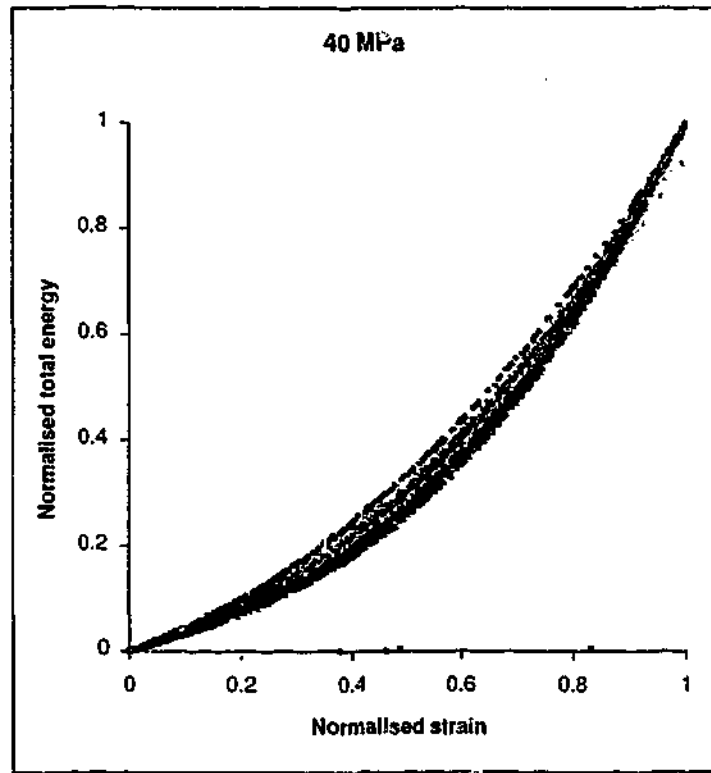
Energy approach

Energy dissipation in concrete has been addressed by many researchers in the literature (Mander et al. 1988b). It is interesting to note that the normalised total energy versus normalised strain curves for unloading branches had a similarity for a particular grade of concrete irrespective of the confining pressure applied (Figures 9.2-9.3).

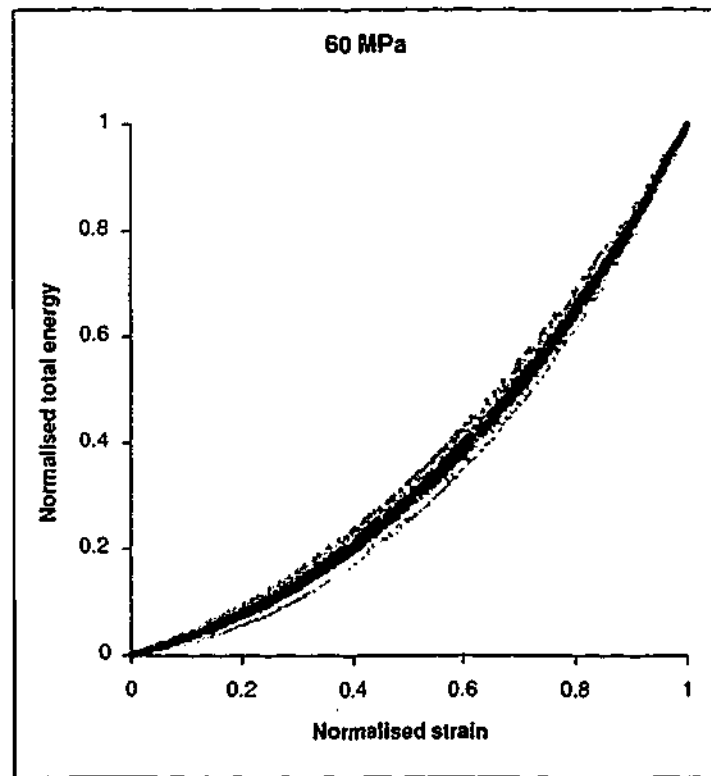
Normalised total energy, \bar{E} and normalised strain, $\bar{\epsilon}$ are defined as,

$$\bar{E} = \frac{E - E_{pl}}{E_{unt} - E_{pl}} \quad \text{and} \quad \bar{\epsilon} = \frac{\epsilon_1 - \epsilon_{pl}}{\epsilon_{un} - \epsilon_{pl}} \quad (9.1)$$

where E is the energy at any stress and strain state in the unloading branch, ϵ_1 is the corresponding axial strain, E_{pl} is the total energy at the plastic strain point (area under the loading curve ABC - area under the unloading curve CD), ϵ_{pl} is the plastic strain, and E_{unt} and ϵ_{un} are the total energy and strain at the unloading point. These parameters

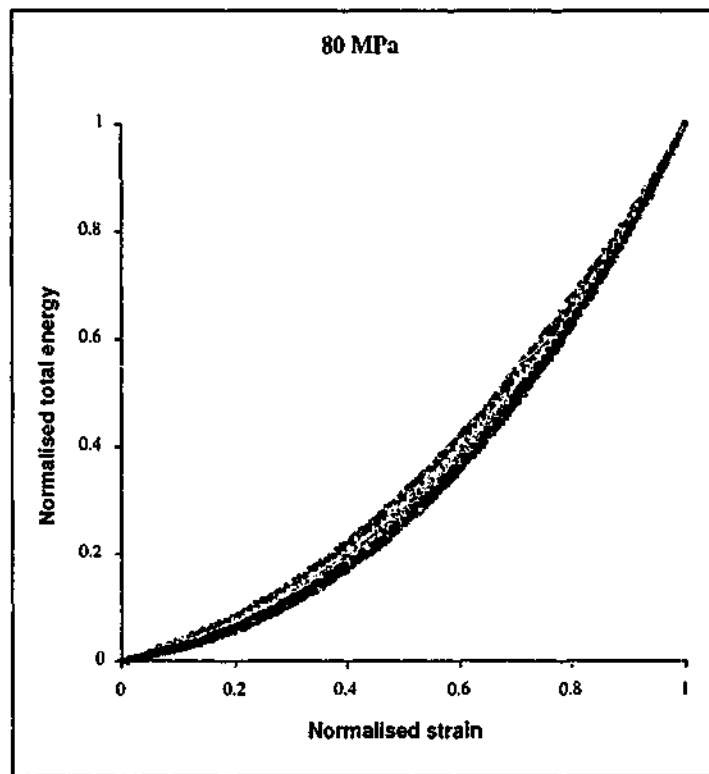


Grade 40 concrete

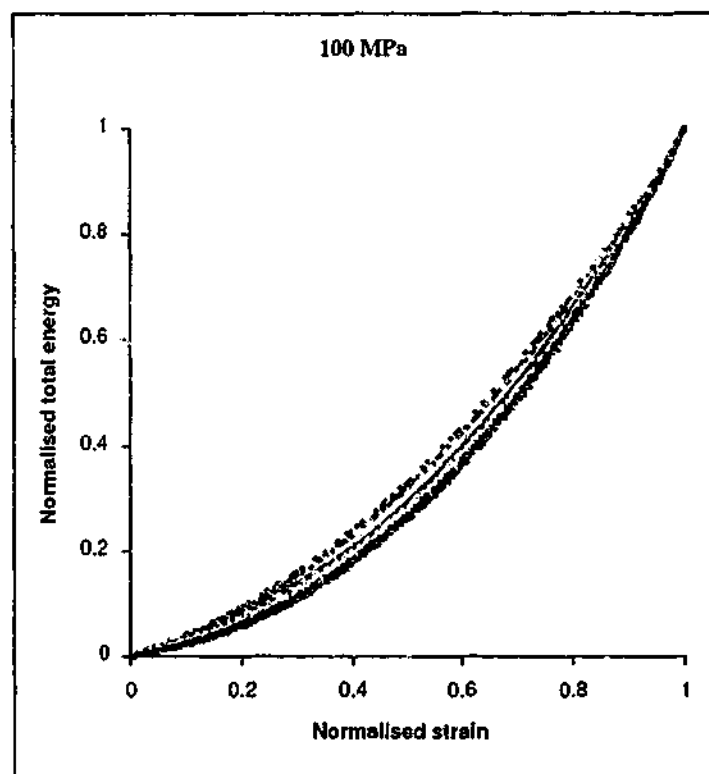


Grade 60 concrete

Figure 9.2: Normalised total energy versus strain for unloading branches.



Grade 80 concrete



Grade 100 concrete

Figure 9.3: Normalised total energy versus strain for unloading branches.

are defined in Figure 9.4.

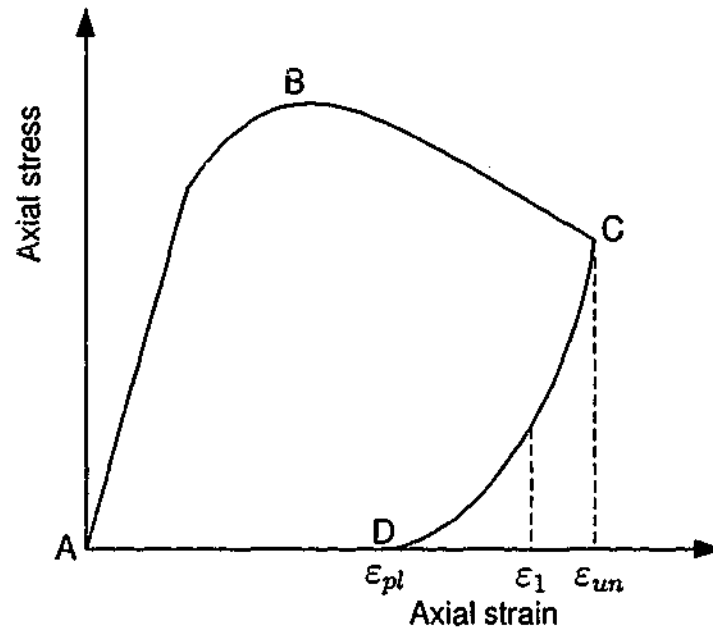


Figure 9.4: Definitions used in energy approach.

Figure 9.5 shows a stress-strain curve including an unloading branch. "A" is the unloading point, "C" is the plastic strain point and "B" is any stress and strain point in the unloading branch.

Normalised total energy versus normalised strain curves for unloading branches are shown in Figures 9.2-9.3. This relationship can be found in a form shown in Equation (9.2) for a particular concrete grade regardless of the confining pressure applied.

$$\bar{E} = f(\bar{\epsilon}). \quad (9.2)$$

Substituting for normalised total energy, \bar{E} and normalised strain, $\bar{\epsilon}$ from Equation (9.1),

$$\frac{E - E_{pl}}{E_{unt} - E_{pl}} = f\left(\frac{\epsilon_1 - \epsilon_{pl}}{\epsilon_{un} - \epsilon_{pl}}\right). \quad (9.3)$$

Rearranging Equation (9.3), a relationship between E and ϵ_1 can be found which may be of the form,

$$E = F(\epsilon_1). \quad (9.4)$$

Energy released in concrete during unloading will be the area under the unloading stress-strain curve as shown in Figure 9.5.

$$E = \int g(\bar{\epsilon}_1) d\bar{\epsilon}_1 \times \text{volume}. \quad (9.5)$$

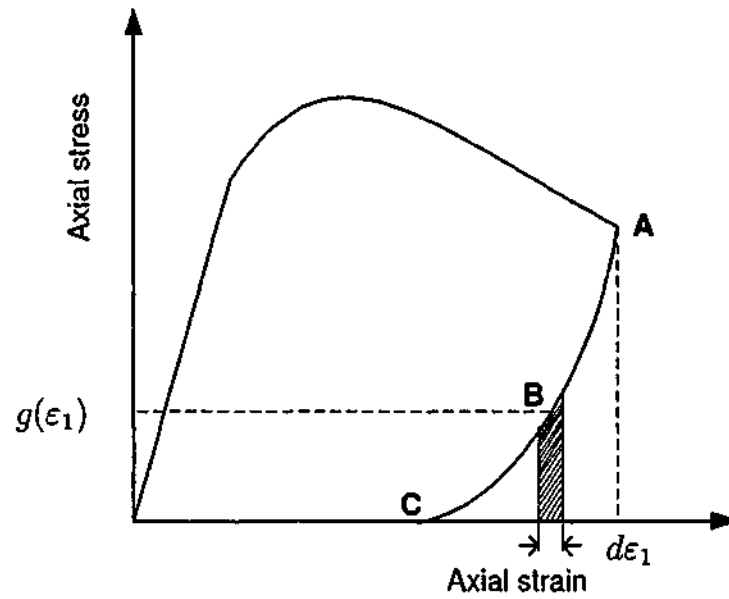


Figure 9.5: Energy during unloading.

$g(\epsilon_1)$ is the axial stress-strain function for unloading curve. Energy at a point in the unloading branch, E is obtained by subtracting the energy released during unloading from the energy absorbed during loading until unloading starts. It can be defined as,

$$\begin{aligned} E &= E_{unt} - \int_{\epsilon_1}^{\epsilon_{un}} g(\epsilon_1) d\epsilon_1 \times V \\ &= E_{unt} - [G(\epsilon_{un}) - G(\epsilon_1)] \times V \end{aligned} \quad (9.6)$$

where,

$$\begin{aligned} \int g(\epsilon_1) d\epsilon_1 &= G(\epsilon_1) + C \quad \text{or} \\ \frac{d}{d\epsilon_1} [G(\epsilon_1) + C] &= g(\epsilon_1). \end{aligned} \quad (9.7)$$

In Equation (9.6), E_{unt} is the energy at the point of unloading which is a constant for a particular unloading curve and $G(\epsilon_{un})$ is the area under the unloading stress-strain curve which again is a constant for a particular concrete grade and a confining pressure (Figure 9.6). Differentiating Equation (9.6) with respect to ϵ_1 ,

$$\begin{aligned} \frac{dE}{d\epsilon_1} &= V \frac{d}{d\epsilon_1} G(\epsilon_1) \\ &= V g(\epsilon_1) \end{aligned} \quad (9.8)$$

where V is the volume of concrete and $g(\epsilon_1)$ is any stress level in the unloading branch.

Differentiation of Equation (9.3) will result in,

$$\frac{1}{E_{unt} - E_{pl}} \times \frac{dE}{d\varepsilon_1} = \left(\frac{d}{d\bar{\varepsilon}} f(\bar{\varepsilon}) \right) \times \left(\frac{d}{d\varepsilon_1} \bar{\varepsilon} \right). \quad (9.9)$$

Substituting Equation (9.8) in Equation (9.9)

$$g(\varepsilon_1) = \frac{E_{unt} - E_{pl}}{V} \times \left(\frac{d}{d\bar{\varepsilon}} f(\bar{\varepsilon}) \right) \times \left(\frac{1}{\varepsilon_{un} - \varepsilon_{pl}} \right). \quad (9.10)$$

In Equation (9.10), E_{unt} is the energy at point of unloading which can be calculated from the envelope curve, ε_{un} is the unloading strain and ε_{pl} is the plastic strain. E_{pl} is the energy at plastic strain point that can be obtained by subtracting the energy released during unloading from the energy at the point of unloading. Therefore stress-strain curve for the unloading is completely defined by Equation (9.10).

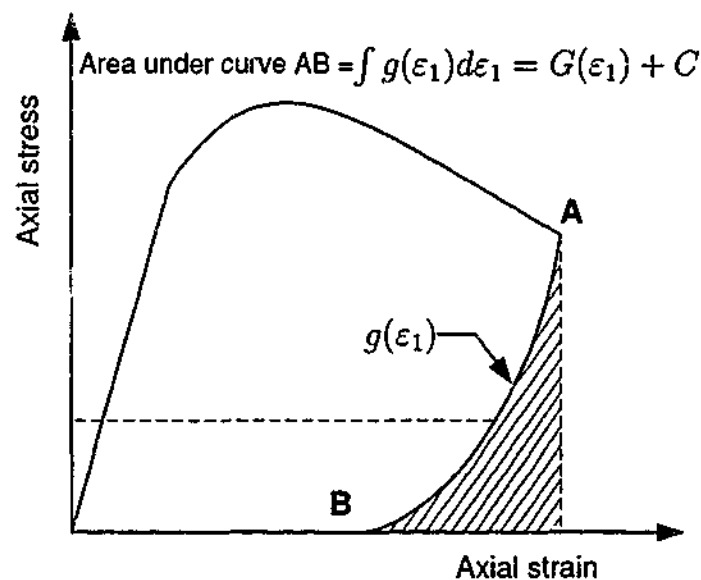


Figure 9.6: Dissipated energy during unloading.

Several problems were identified in this approach. Energy was calculated using axial stress and axial strain only disregarding the lateral stress and lateral strain. However, the work done by the lateral forces cannot be neglected for high confining pressures (Figure 9.7). Mander et al. (1988b) showed that total strain energy per unit volume required to "fail" concrete would be the area under the stress-strain curve of confined concrete. Nevertheless total energy will be the total work done due to axial stress, strain and lateral stress and strain. The interpretation of the energy calculated using only axial stress and strain is not complete. Finally it was decided that the total energy versus volumetric

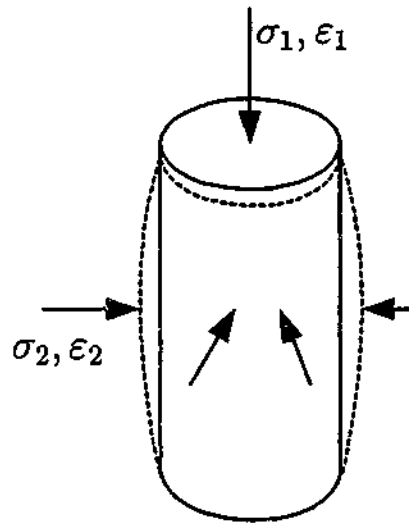


Figure 9.7: Stress-strain state of a laterally confined concrete cylinder.

strain curves are more meaningful than the curves for total energy versus axial strain. This approach was attempted first for the monotonically increasing axial load on confined HSC.

9.3.2 Shear failure approach

The theory that concrete failure is a Mohr-Coulomb shear failure is widely held by many researchers in this field. Nielsen (1999) provides the background to this theory and applications of this theory for structural analysis.

When the Mohr circle for concrete stresses as shown in Figure 9.8 touches the boundary line corresponding to sliding failure, the failure takes place. When the shear stress $|\tau|$ in a section exceeds the *sliding resistance*, shear failure is assumed to occur. Cohesion, denoted by c and the internal friction denoted by ϕ form the sliding resistance. Due to symmetry, the Mohr circle touches the boundary lines corresponding to sliding failure at two points. Therefore sliding failure will occur in two sections that form the angle $(90^\circ - \phi)$ with each other (Figure 9.9).

In the shear approach in modelling the unloading branches of cyclically loaded confined concrete, maximum shear stress and maximum shear strain at any stress-strain state were considered. Direction of these maximum shear stress and strain will change during the test progress. The planes they act are different from one stress-strain state to another. For all the unloading branches in four grades of concrete and three confining pressures, the maximum shear stress factor versus maximum shear strain factor graphs were plotted.

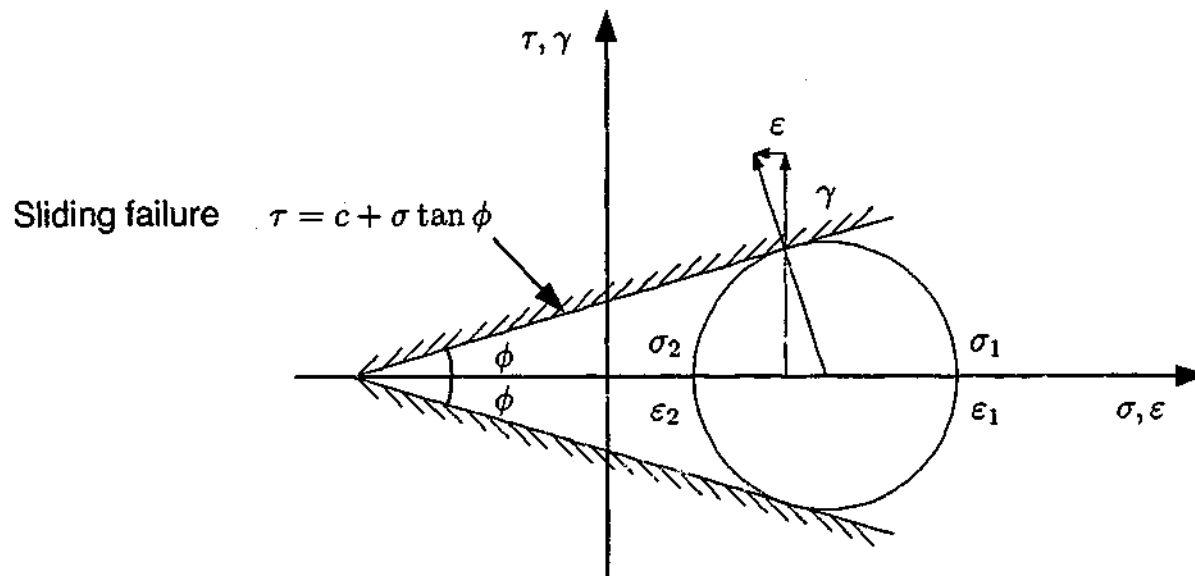


Figure 9.8: Mohr's circle for a stress/ strain field.

These factors are defined as in Equation (9.11) with respect to maximum shear stress and strain at unloading point and plastic strain point.

$$\bar{\tau}_{un} = \frac{\tau - \tau_{pl}}{\tau_{un} - \tau_{pl}} \quad \text{and} \quad \bar{\varepsilon}_{un} = \frac{\varepsilon_1 - \varepsilon_{pl}}{\varepsilon_{un} - \varepsilon_{pl}} \quad (9.11)$$

Irrespective of the confining pressure applied, the curves converged to one line for each grade of concrete as can be seen in Figures 9.10-9.13. Therefore it was decided that shear failure approach would be a reasonable method to model the unloading branches in cyclic loading of confined concrete.

9.4 Description of the proposed model

Model formulation is based on the experimental program carried out by the author which is described in the previous chapter. It is usually assumed that the monotonic loading stress-strain curve forms the envelope curve for the cyclic loading stress-strain response. This was proposed by Sinha et al. (1964) and Karsan and Jirsa (1969) for unconfined concrete. Later Karsan and Jirsa (1969) and Mander et al. (1988b) showed that it is a reasonable assumption for reinforced concrete as well. However, the experimental program carried out by the author for NSC and HSC and presented in Chapter 7, shows that this is valid for the ascending branch but needs to be modified for the descending branch. Key components outlining the model are shown in Figure 9.14. The aim of the study is to find

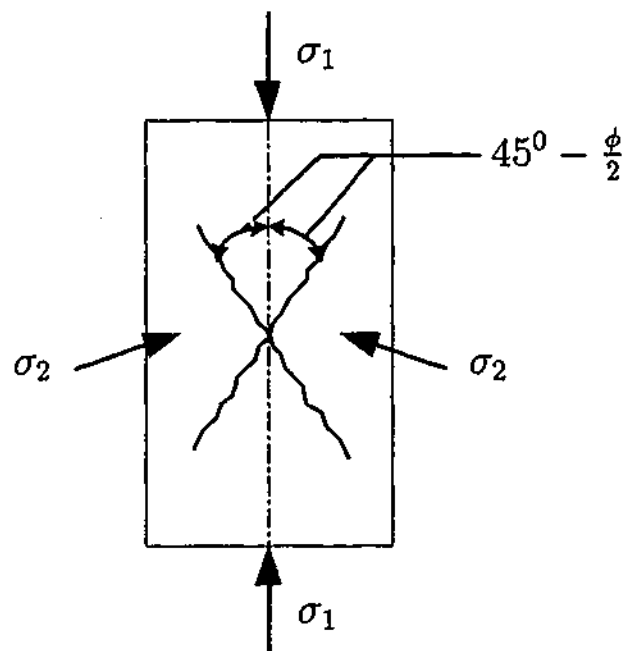


Figure 9.9: Failure sections in concrete under compression.

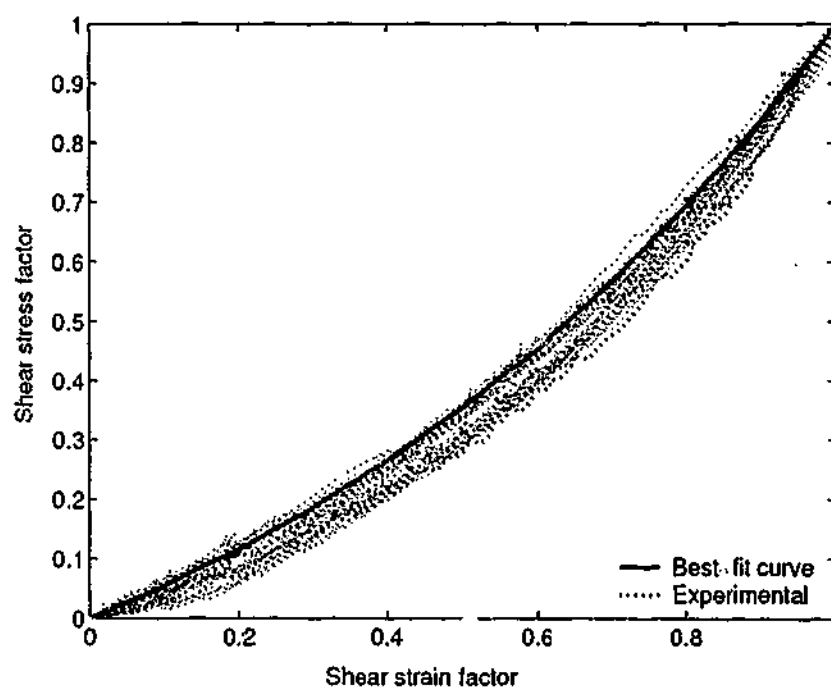


Figure 9.10: Shear stress factor versus shear strain factor for unloading branches of Grade 40 concrete.

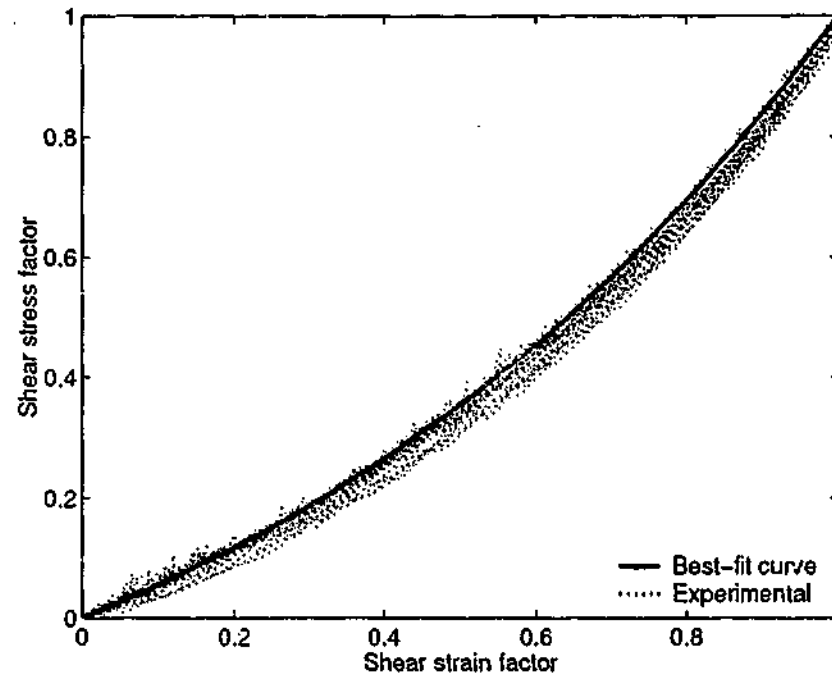


Figure 9.11: Shear stress factor versus shear strain factor for unloading branches of Grade 60 concrete.

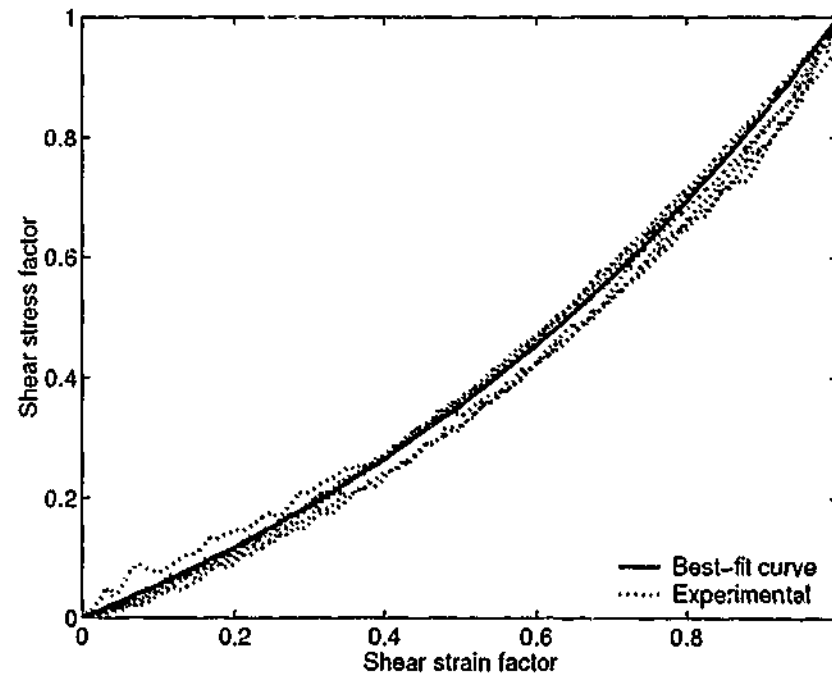


Figure 9.12: Shear stress factor versus shear strain factor for unloading branches of Grade 80 concrete.

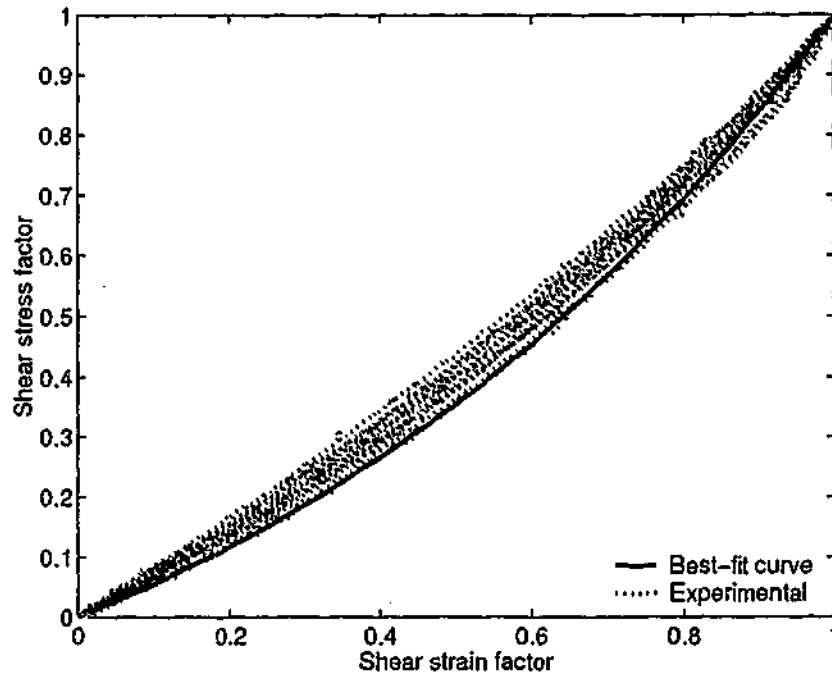


Figure 9.13: Shear stress factor versus shear strain factor for unloading branches of Grade 100 concrete.

axial stress (σ_1), axial strain (ϵ_1), confining pressure (f_l) and lateral strain (ϵ_2) for each of the curves described below:

1. Ascending branch of monotonic loading curve (AB)
2. Unloading curve (BC, GH)
 - Determination of plastic strain (ϵ_{pl})
3. Reloading curve (DE, HJ)
4. Parabolic transition curve (EF, JK)
5. Modified envelope curve for the descending branch (FG, KL)

9.4.1 Ascending branch of monotonic loading curve (AB)

Figure 9.14 shows the main parameters of the stress-strain curves used for modelling. The modelling of the ascending branch (AB) is based on experimental work carried out by Candappa et al. (2001) to model the constitutive behavior of HSC subjected to lateral confinement under monotonically increasing axial load. Candappa et al. (2001) carried out 24 tests consisting of 4 different uniaxial compressive strengths and 3 different

following equation was obtained for the ascending branch.

$$\sigma_1 = 2\tau_{mp} \left[1 - e^{-m_2 \left(\frac{\epsilon_1 + \epsilon_2}{2\gamma_{mp}} \right)} \right] + f_l. \quad (9.13)$$

ϵ_1 and ϵ_2 are axial and lateral strains respectively, σ_1 is the axial stress, f_l is the confining pressure. τ_{mp} and γ_{mp} are the maximum shear stress and strain at peak stress defined as,

$$\tau_{mp} = \frac{f_{cc} - f_l}{2} \quad \text{and} \quad \gamma_{mp} = \frac{\epsilon_{cc} + \epsilon'_{cc}}{2} \quad (9.14)$$

where f_{cc} is the peak axial stress of confined concrete, ϵ_{cc} (compression positive) and ϵ'_{cc} (expansion positive) are the corresponding axial and lateral strains respectively. m_2 is a material parameter which depends on the uniaxial strength of concrete.

$$m_2 = -0.0427f_c + 7.7381. \quad (9.15)$$

Peak axial stress of confined concrete (f_{cc}) is defined as (Attard and Setunge, 1996),

$$\frac{f_{cc}}{f_c} = \left(\frac{f_l}{f_t} + 1 \right)^k \quad (9.16)$$

where k is a constant given by,

$$k = 1.25 \left(1 + 0.062 \frac{f_l}{f_c} \right) (f_c)^{-0.21} \quad (9.17)$$

and f_t is the tensile strength. The tensile strength is given by,

$$f_t = 0.288(f_c)^{0.67}. \quad (9.18)$$

Attard and Setunge (1996) suggested equations for axial strain corresponding to peak axial stress ϵ_{cc} ,

$$\frac{\epsilon_{cc}}{\epsilon_{co}} = 1 + (17 - 0.06f_c) \left(\frac{f_l}{f_c} \right) \quad (9.19)$$

where f_l is the confining pressure and ϵ_{co} is the axial strain corresponding to peak uniaxial compressive strength (generally assumed to be 0.002). It is derived in Section 3.6.4 of Chapter 3 that,

$$\epsilon'_{cc} = 0.5\epsilon_{cc}. \quad (9.20)$$

ϵ_{cc} and ϵ'_{cc} are the axial and lateral strains corresponding to peak axial stress (f_{cc}).

In order to find a relationship between axial strain and lateral strain, curves were plotted for normalised lateral strain (with respect to lateral strain at peak stress), versus normalised axial strain (with respect to axial strain at peak stress). The curves were found to have a similar shape for a particular compressive strength irrespective of the confining pressure applied. Gradient of these curves is related to the Poisson's ratio. Initially it has a constant gradient which is compatible with Hooke's law. Candappa et al. (2001) proposed that initial Poisson's ratio (ν_i^a) is a constant.

$$\nu_i^a = 0.15 \quad (9.21)$$

The constant Poisson's ratio, ie. lateral strain is proportional to axial strain, is only valid for low axial strains. For high axial strains, the lateral strains increased at a higher rate than for low axial strains, thus increasing the Poisson's ratio. It can be approximated by a pair wise equation.

$$\frac{\varepsilon_2}{\varepsilon'_{cc}} = \begin{cases} \nu_i^a \left(\frac{\varepsilon_1}{\varepsilon_{cc}} \right) & \text{if } \varepsilon_1 \leq \varepsilon', \\ \left(\frac{\varepsilon_1}{\varepsilon_{cc}} \right)^{m_1} & \text{if } \varepsilon_1 > \varepsilon'. \end{cases} \quad (9.22)$$

ε' can be obtained by equating the right hand side of this equation at $\varepsilon_1 = \varepsilon'$. m_1 is a material parameter which depends on the uniaxial concrete strength.

$$m_1 = 0.0177f_c + 1.2818. \quad (9.23)$$

For an assigned axial strain (ε_1), lateral strain (ε_2) can be found using Equation (9.22). Therefore these equations together with the material parameters (m_1, m_2), completely define the ascending branch of the stress-strain curve for confined concrete.

9.4.2 Determination of plastic strain (ε_{pl})

In order to establish the unloading curve from the compressive loading curve, a plastic strain (ε_{pl}) based on the coordinates at the unloading point ($\varepsilon_{un}, \sigma_{un}$) needs to be determined. The procedure used here is a modified version of the one proposed by Mander et al. (1988b) for both confined and unconfined concrete. Axial plastic strain ($\varepsilon_{1,pl}$) and lateral plastic strain ($\varepsilon_{2,pl}$) are defined in a similar way. The plastic strain ε_{pl} depends

on the strain ε_a at the intersection of the initial tangent and the plastic unloading secant slopes (Figure 9.14).

$$\varepsilon_a = a\sqrt{\varepsilon_{1,un}\varepsilon_{cc}} \quad (9.24)$$

The value of a will be the greater of either

$$a = \frac{4\varepsilon_{cc}}{\varepsilon_{cc} + \varepsilon_{1,un}} \quad \text{OR} \quad \frac{0.09\varepsilon_{1,un}}{\varepsilon_{cc}} \quad (9.25)$$

for axial plastic strain ($\varepsilon_{1,pl}$). But for lateral plastic strain ($\varepsilon_{2,pl}$) value of a will be the smaller of the two alternatives in Equation (9.25) with corresponding lateral strains instead of the axial strains ie. ε_{cc} replaced by ε'_{cc} and $\varepsilon_{1,un}$ replaced by $\varepsilon_{2,un}$. Plastic strain on the secant line between ε_a and ε_{un} is given by,

$$\varepsilon_{pl} = \frac{(\varepsilon_{un} + \varepsilon_a)\sigma_{un}}{(\sigma_{un} + E_c\varepsilon_a)} \quad (9.26)$$

where $(\varepsilon_{un}, \sigma_{un})$ is the unloading point and E_c is modulus of elasticity of concrete. E_c is defined in Australian Standards, AS3600 (2001),

$$E_c = 0.043\rho^{1.5}\sqrt{f_{cm}} \quad \text{MPa} \quad (9.27)$$

where, ρ is the density of concrete in kg/m^3 , f_{cm} is the mean value of the compressive strength of concrete, in MPa. ACI 363 (1984) has recommended the following equation for HSC:

$$E_c = (3320\sqrt{f_c} + 6900) \left(\frac{\rho}{2320}\right)^{1.5} \quad \text{MPa} \quad (9.28)$$

where f_c is the uniaxial strength of concrete in MPa. Equation (9.28) has been taken from the work of Carrasquillo et al. (1981). However Attard and Setunge (1994) compared the elastic modulus of concrete using experimental results and predictions from Equations (9.27) and (9.28). They concluded that Equation (9.27) gives reasonable values for E_c for mixes with the aggregates used in Australia. Therefore throughout this study, Equation (9.27) has been used in calculating elastic modulus of concrete.

9.4.3 Unloading curve (BC, GH)

Figure 9.14 shows the parameters used to define the unloading curves. Formulation of the unloading curves is based on the experimental program carried out by the author for 24 tests with 4 different compressive strengths, 3 different confining pressures and 2 loading

regimes. One loading regime has 3-4 unloading curves while the other loading regime has a number of unloading curves. There are all together 72 unloading curves in all these 24 tests. The author looked for a common pattern in all the curves. It is found that shear stress factor and shear strain factor relationship has a similar behaviour regardless of the concrete strength and confining pressure applied (Figure 9.15). Results from all strength grades and confining pressures are included in the figure.

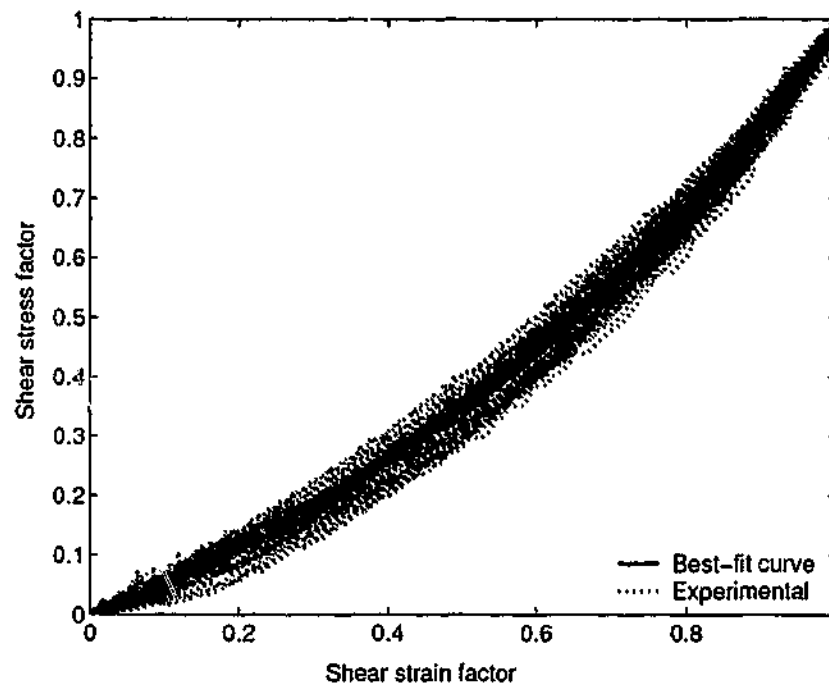


Figure 9.15: Shear stress factor versus shear strain factor for 72 unloading branches.

Various other methods such as total energy with volumetric strain etc. were attempted, but none of these provided such a close pattern as the shear stress versus shear strain factor. It is the innovative feature of the model formulation of unloading curves. Shear stress factor versus shear strain factor relationship is found to be as in Equation (9.29).

$$\bar{\tau}_{un} = 0.43(e^{1.2\bar{\gamma}_{un}} - 1). \quad (9.29)$$

The correlation factor is used to estimate the closeness of the best fit curve (Equation 9.29) to the test data. It is defined as the covariance of two data sets divided by the product of their standard deviations. The correlation factor for the 72 curves is 0.9943. $\bar{\tau}_{un}$ is the shear stress factor and $\bar{\gamma}_{un}$ is the shear strain factor for unloading curves. These factors are defined as,

$$\bar{\tau}_{un} = \frac{\tau - \tau_{pl}}{\tau_{un} - \tau_{pl}} \quad \text{and} \quad \bar{\gamma}_{un} = \frac{\gamma - \gamma_{pl}}{\gamma_{un} - \gamma_{pl}} \quad (9.30)$$

where τ and γ are the maximum shear stress and strain at any axial and lateral stress state.

$$\tau = \frac{\sigma_1 - f_l}{2} \quad \text{and} \quad \gamma = \frac{\epsilon_1 + \epsilon_2}{2}. \quad (9.31)$$

τ_{pl} and γ_{pl} are the maximum shear stress and shear strain at plastic strain point, τ_{un} and γ_{un} are the maximum shear stress and strain at the point of unloading. These are defined similar to Equation (9.31).

$$\tau_{pl} = \frac{\sigma_{pl} - f_l}{2} \quad \text{and} \quad \gamma_{pl} = \frac{\epsilon_{1,pl} + \epsilon_{2,pl}}{2}. \quad (9.32)$$

τ_{un} and γ_{un} are the maximum shear stress and shear strain at the point of unloading.

$$\tau_{un} = \frac{\sigma_{un} - f_l}{2} \quad \text{and} \quad \gamma_{un} = \frac{\epsilon_{1,un} + \epsilon_{2,un}}{2}. \quad (9.33)$$

Since the envelope curve is known, coordinates at unloading point are known. Axial stress (σ_1), axial strain (ϵ_1) and lateral strain (ϵ_2) are the unknowns in the above equations (Equations 9.29-9.31).

Axial strain lateral strain relationship

The graphs of normalised axial strain ($\bar{\epsilon}_{1,un}$) and normalised lateral strain ($\bar{\epsilon}_{2,un}$) for a particular concrete strength (f_c) have close similarity irrespective of the confining pressure applied. There were 21 unloading curves for 44 MPa concrete for all 3 confining pressures applied. Similarly there were 22, 9 and 20 unloading curves for 58, 83 and 106 MPa concrete respectively. Curves are shown in Figures 9.16-9.19.

Different relationships of normalised axial strain ($\bar{\epsilon}_{1,un}$) and normalised lateral strain ($\bar{\epsilon}_{2,un}$) for the unloading curves were established for the four grades of concrete. The relationship between these two parameters is found to be as in Equation (9.34). The correlation factors for the 21, 22, 9 and 20 curves in 44, 58, 83 and 106 MPa concrete were 0.9909, 0.9968, 0.9973 and 0.9970 respectively.

$$\bar{\epsilon}_{2,un} = \bar{\epsilon}_{1,un}^{1/q}. \quad (9.34)$$

q is a concrete material parameter and found to be,

$$q = -0.0035f_c + 1.445. \quad (9.35)$$

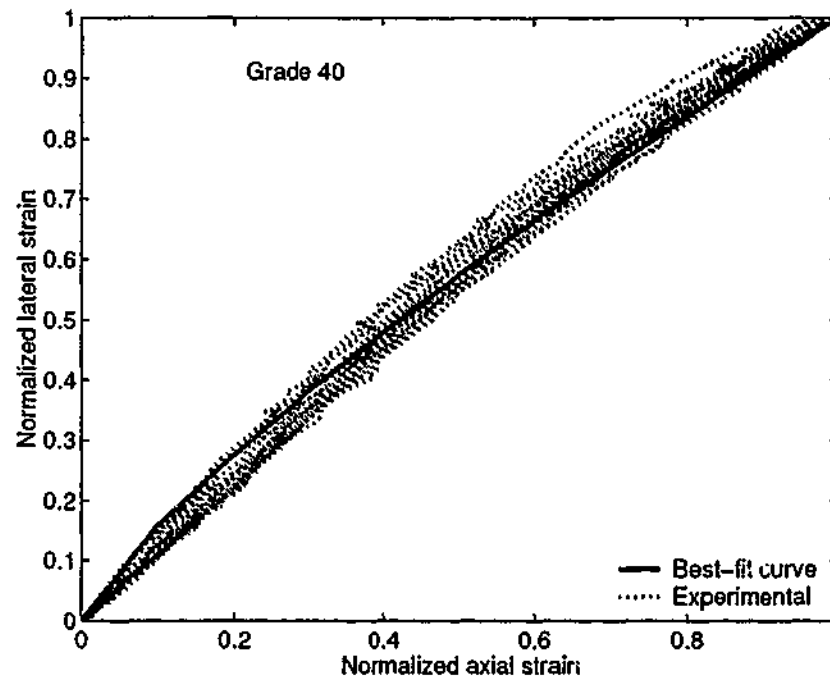


Figure 9.16: Normalised lateral strain versus normalised axial strain for 21 unloading curves in Grade 40 concrete.

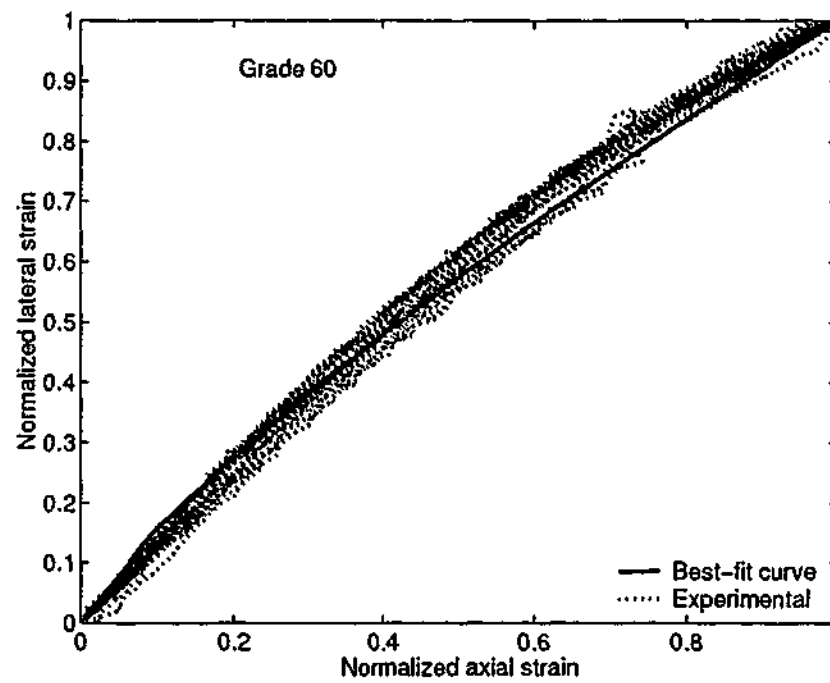


Figure 9.17: Normalised lateral strain versus normalised axial strain for 22 unloading curves in Grade 60 concrete.

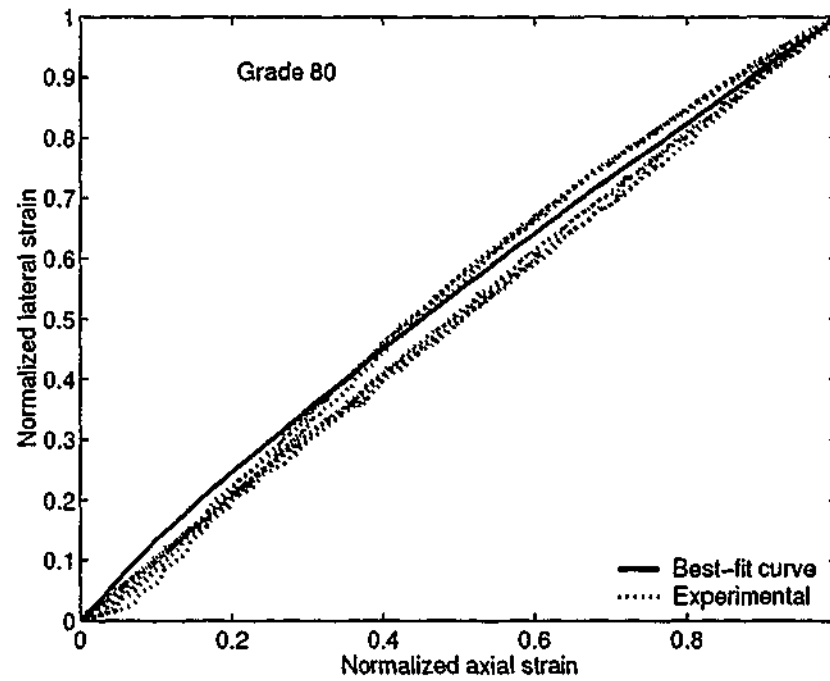


Figure 9.18: Normalised lateral strain versus normalised axial strain for 9 unloading curves in Grade 80 concrete.

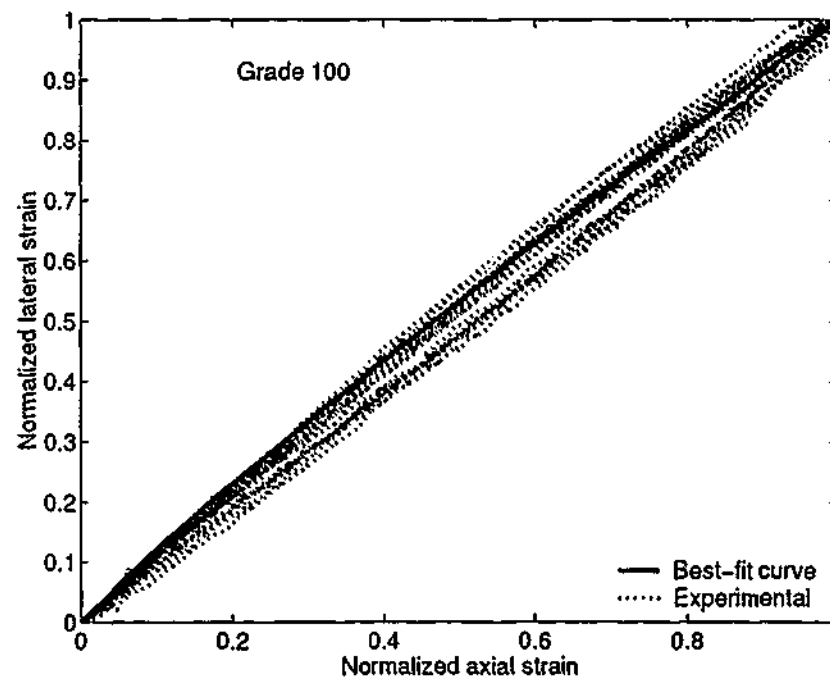


Figure 9.19: Normalised lateral strain versus normalised axial strain for 20 unloading curves in Grade 100 concrete.

$\bar{\varepsilon}_{1,un}$ is normalised axial strain and $\bar{\varepsilon}_{2,un}$ is normalised lateral strain. They are defined as,

$$\bar{\varepsilon}_{1,un} = \frac{\varepsilon_1 - \varepsilon_{1,pl}}{\varepsilon_{1,un} - \varepsilon_{1,pl}} \quad \text{and} \quad \bar{\varepsilon}_{2,un} = \frac{\varepsilon_2 - \varepsilon_{2,pl}}{\varepsilon_{2,un} - \varepsilon_{2,pl}} \quad (9.36)$$

where $\varepsilon_1, \varepsilon_2$ are the axial and lateral strains in the unloading branch, $\varepsilon_{1,un}$ and $\varepsilon_{2,un}$ are the axial and lateral strains at the unloading point and $\varepsilon_{1,pl}$ and $\varepsilon_{2,pl}$ are the plastic axial and lateral strains. For a given unloading axial strain (ε_1), Equation (9.34) is used to find the corresponding lateral strain (ε_2). Substituting values for (ε_1) and (ε_2) in Equation (9.29) will give the remaining parameter, axial stress (σ_1).

9.4.4 Reloading curve (DE, HJ)

Figure 9.14 shows the parameters used to define the reloading curves. The point of reloading ($\varepsilon_{ro}, \sigma_{ro}$) can be either from the unloading curve (loop GHJK) or from the cracked state (loop BCDEF). If it is from the cracked state, $\varepsilon_{ro} = (\varepsilon_{pl} - \varepsilon_{ts})$ and $\sigma_{ro} = 0$ as shown in Figure 9.14. ε_{ts} is the tensile strain and is given by,

$$\varepsilon_{ts} = \frac{f_t}{E_c} \quad (9.37)$$

where f_t is the tensile strength of concrete (given by Equation 9.18) and E_c is the modulus of elasticity of concrete. After the coordinates of the reloading point are determined, establishing reloading curves are the same for both situations. A stress-strain relationship which accounts for the degradation due to cyclic behavior is derived between reloading strain (ε_{ro}) and unloading strain (ε_{un}), to a reduced axial stress (σ_{new}) which is defined by Mander et al. (1988b),

$$\sigma_{new} = 0.92\sigma_{un} + 0.08\sigma_{ro}. \quad (9.38)$$

Formulation of reloading curves is based on the 24 test results of the experimental program carried out by author. There are 65 reloading curves considered in the analysis. Number of reloading curves is less than that of unloading curves because experiments were usually terminated with the unloading. Figure 9.20 shows shear stress factor versus shear strain factor for 65 reloading branches. Similar to the ascending branch of monotonic loading curve (AB) and unloading curve (BC and GH), author found that relationship between shear stress factor, $\bar{\tau}_{re}$ and shear strain factor $\bar{\gamma}_{re}$ for reloading curves was independent of the compressive strength of concrete and confining pressure applied similar to unloading

curves. It is found to be as in Equation (9.39). The correlation factor for the 65 curves is 0.9954.

$$\bar{\tau}_{re} = \sqrt{2} \log_e(\bar{\gamma}_{re} + 1). \quad (9.39)$$

This equation is a form of mirror image of the equation for unloading, Equation (9.29). $\bar{\tau}_{re}$ is shear stress factor and $\bar{\gamma}_{re}$ is shear strain factor for reloading curves.

$$\bar{\tau}_{re} = \frac{\tau - \tau_{pl}}{\tau_{new} - \tau_{pl}} \quad \text{and} \quad \bar{\gamma}_{re} = \frac{\gamma - \gamma_{pl}}{\gamma_{new} - \gamma_{pl}}. \quad (9.40)$$

τ and γ are the maximum shear stress and strain at any axial and lateral stress state (defined in Equation 9.31), τ_{pl} and γ_{pl} are the maximum shear stress and strain at plastic strain point (point C in Figure 9.14) and τ_{new} and γ_{new} are the maximum shear stress and strain at the returning point of the reloading branch (points E or J in Figure 9.14). Equation (9.39) defines the reloading branch. However, the relationship between axial strain (ε_1) and lateral strain (ε_2) is necessary for Equation (9.39) to be complete.

Axial strain lateral strain relationship

The graphs of normalised axial strain ($\bar{\varepsilon}_{1,re}$) and normalised lateral strain ($\bar{\varepsilon}_{2,re}$) for reloading curves for a particular concrete strength (f_c) are similar irrespective of the confining pressure applied. There were 21 reloading curves for 44 MPa concrete for all three confining pressures applied. Similarly there were 18, 8 and 18 unloading curves for 58, 83 and 106 MPa concrete respectively. These curves are shown in Figures 9.21-9.24 and are similar to the curves shown in Figures 9.16-9.19. Different relationships of normalised axial strain ($\bar{\varepsilon}_{1,re}$) and normalised lateral strain ($\bar{\varepsilon}_{2,re}$) for the reloading curves were established for the four grades of concrete. The relationship between these two parameters is a mirror image of the similar relationship defined for unloading curves as in Equation (9.34).

It is found to be as in Equation (9.41). The correlation factors for the 21, 18, 8 and 18 curves in 44, 58, 83 and 106 MPa concrete were 0.9934, 0.9969, 0.9913 and 0.9961 respectively.

$$\bar{\varepsilon}_{2,re} = \bar{\varepsilon}_{1,re}^q. \quad (9.41)$$

Material parameter q is the same defined in Equation (9.35) and $\bar{\varepsilon}_{1,re}$ is normalised axial strain and $\bar{\varepsilon}_{2,re}$ is normalised lateral strain defined as,

$$\bar{\varepsilon}_{1,re} = \frac{\varepsilon_1 - \varepsilon_{1,pl}}{\varepsilon_{1,new} - \varepsilon_{1,pl}} \quad \text{and} \quad \bar{\varepsilon}_{2,re} = \frac{\varepsilon_2 - \varepsilon_{2,pl}}{\varepsilon_{2,new} - \varepsilon_{2,pl}} \quad (9.42)$$

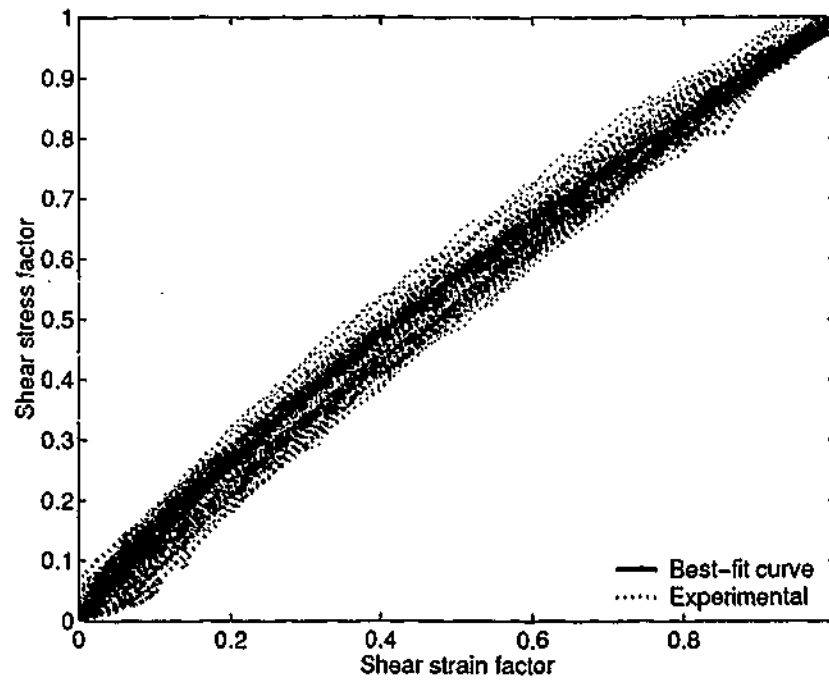


Figure 9.20: Shear stress factor versus shear strain factor for 65 reloading branches.

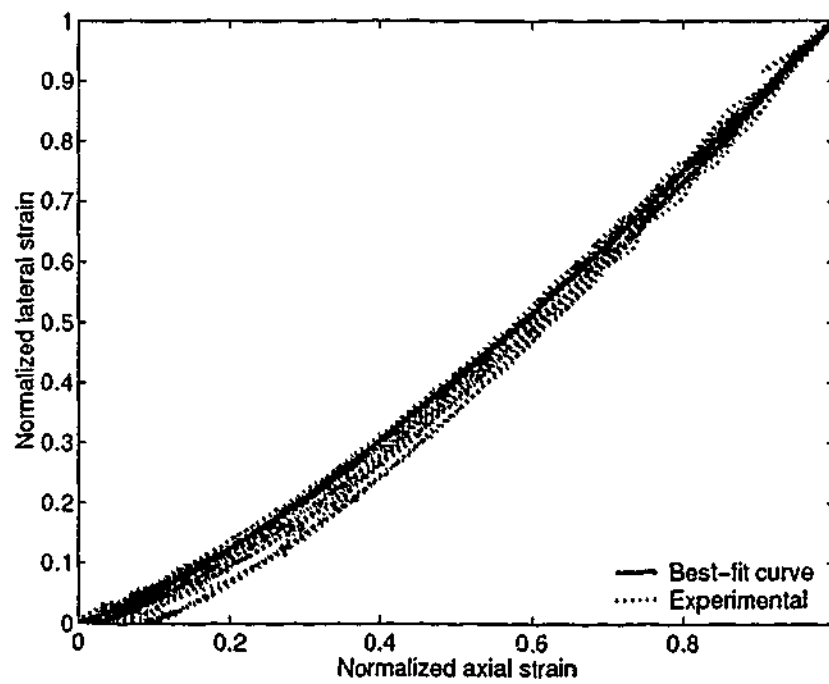


Figure 9.21: Normalised lateral strain versus normalised axial strain for 21 reloading curves in Grade 40 concrete.

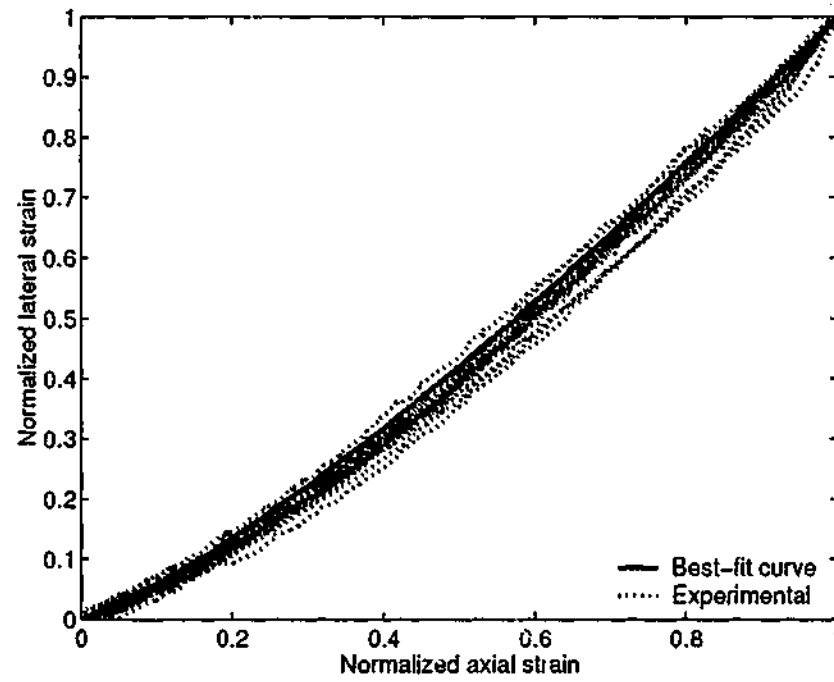


Figure 9.22: Normalised lateral strain versus normalised axial strain for 8 reloading curves in Grade 60 concrete.

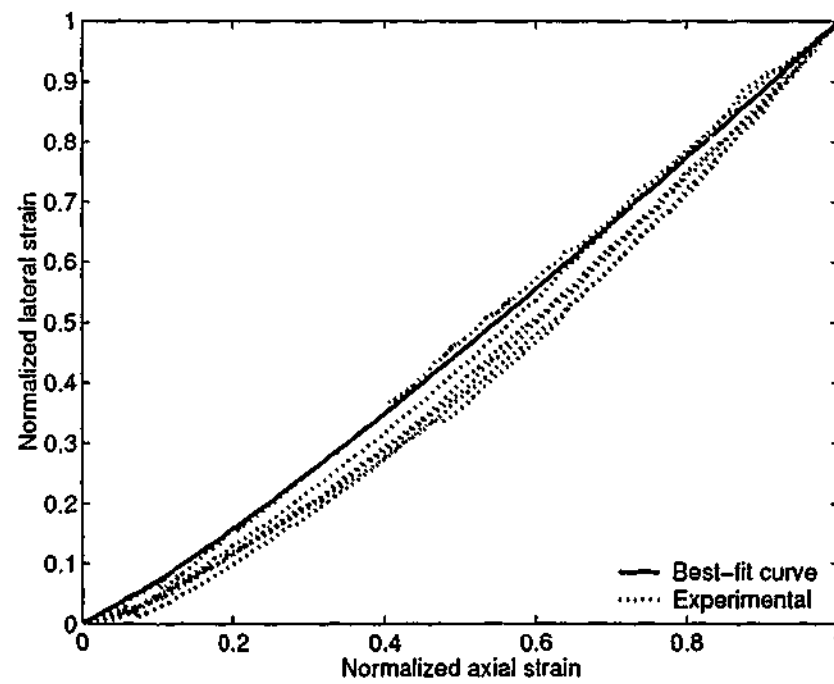


Figure 9.23: Normalised lateral strain versus normalised axial strain for 8 reloading curves in Grade 80 concrete.

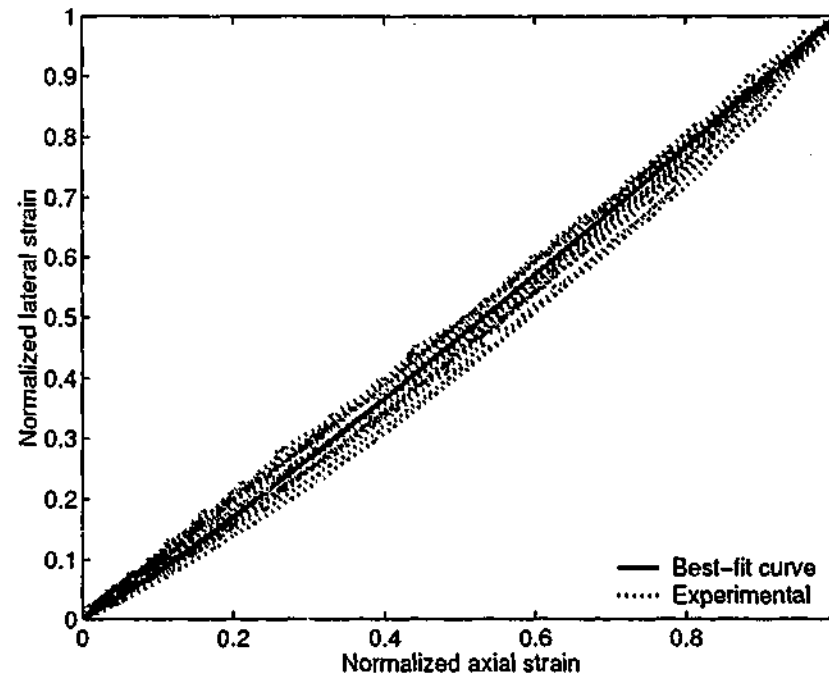


Figure 9.24: Normalised lateral strain versus normalised axial strain for 18 reloading curves in Grade 100 concrete.

where ε_1 , ε_2 are the axial and lateral strains in the reloading curve, $\varepsilon_{1,new}$ and $\varepsilon_{2,new}$ are the returning axial and lateral strains (corresponding to point E or J in Figure 9.14) which are the same as unloading strains ($\varepsilon_{1,un}$ and $\varepsilon_{2,un}$). $\varepsilon_{1,pl}$ and $\varepsilon_{2,pl}$ are the plastic axial and lateral strains. For a given axial strain in reloading curve, Equation (9.41) is used to find the corresponding lateral strain. Substituting values for ε_1 , ε_2 and f_l in Equation (9.39) will calculate the remaining parameter axial stress (σ_1).

If the unloading happened during the reloading before reaching the reduced axial stress (σ_{new}), it is called partial unloading (Otter and Naaman 1989). In this case, there are two extremes for the plastic strain. The lower limit is the plastic strain corresponding to previous unloading point. The upper limit is the plastic strain corresponding to the full reloading. Therefore plastic strain during partial reloading can be calculated by interpolation. Once the plastic strain is known, establishing reloading branch is the same for full and partial unloading. This has been addressed in the literature by Otter and Naaman (1989) for concrete composites.

9.4.5 Parabolic transition curve (EF, JK)

The point where the reloading curve joins the envelope curve (F or K in Figure 9.14) is defined by $(\epsilon_{re}, \sigma_{re})$. The common return strain (ϵ_{re}) is defined by Mander et al. (1988b),

$$\epsilon_{re} = \epsilon_{un} + \frac{(\sigma_{un} - \sigma_{new}) \times \left(2 + \frac{f_{cc}}{f_c}\right)}{E_{ro}} \quad (9.43)$$

where E_{ro} is the reloading point tangent modulus and is given by,

$$E_{ro} = \frac{\sigma_{ro} - \sigma_{new}}{\epsilon_{ro} - \epsilon_{un}} \quad (9.44)$$

Corresponding axial stress, σ_{re} is the return point axial stress calculated from the envelope curve. If the return point is in the ascending branch of the envelope curve, axial stress (σ_1) can be calculated directly from Equation (9.13). If it is in the descending branch, axial stress (σ_{re}) at the return point has to be calculated from the modified envelope curve. The author analysed the test results of the 24 specimens for cyclic loading and found that σ_{re} is a function of the number of hysteresis loop, n and given by,

$$\sigma_{re} = (1 - 0.01n)\sigma_{1,p} \quad (9.45)$$

where, $\sigma_{1,p}$ is the axial stress of envelope curve. The model formulation for the descending branch of the envelope curve is based on the 24 tests carried out by Candappa (2000). The author found that the shear stress factor versus shear strain factor was the same for a particular strength irrespective of the confining pressure applied. That relationship is found to be as in Equation (9.46).

$$\sigma_{1,p} = 2\tau_{mp} \left(e^{m_3 \left(\frac{\epsilon_1 + \epsilon_2}{2\gamma_{mp}} \right)^2} - m_3 \right) + f_l \quad (9.46)$$

τ_{mp} and γ_{mp} are the maximum shear stress and strain at peak stress defined in Equation (9.14), m_3 is a material parameter,

$$m_3 = -0.0003f_c - 0.0057. \quad (9.47)$$

A parabolic transition curve (Mander et al. 1988b) is then introduced between the reloading curve and the return coordinates $(\epsilon_{re}, \sigma_{re})$ of the modified envelope curve.

$$\sigma_1 = \sigma_{re} + E_{re}g + Ag^2 \quad (9.48)$$

where,

$$g = \varepsilon_1 - \varepsilon_{re}, \quad (9.49)$$

$$A = \frac{(\sigma_{new} - \sigma_{re}) - E_{re}(\varepsilon_{un} - \varepsilon_{re})}{(\varepsilon_{un} - \varepsilon_{re})^2}, \quad (9.50)$$

and E_{re} is the common return point tangent modulus.

9.4.6 Modified monotonic loading curve for the descending branch (FG or KL)

For a given axial strain (ε_1) in the envelope curve, axial stress (σ_1) can be found as,

$$\sigma_1 = (1 - 0.01n)\sigma_{1,p}. \quad (9.51)$$

This is used in estimating the axial stress (σ_1) values from the return point to the next unloading point if the return point is in the descending branch, where Equation (9.46) defines $\sigma_{1,p}$. If the return point is in the ascending branch, axial stress (σ_1) can be calculated directly from Equation (9.13).

9.5 Poisson's ratio

Poisson's ratio is an important parameter specially when lateral confinement is involved, since the confining pressure provided by steel depends on it. In studying monotonically increasing loads, Candappa et al. (2001) found that Poisson's ratio remained constant in the "initial elastic region" then starts to increase rapidly. The initial elastic region is defined by Candappa et al. (2001) as the region where the ratio of axial stress/peak axial stress is less than about 0.7 to 0.8. The value of 0.8 was found to be applicable to concretes with compressive strengths greater than 60 MPa while the value of 0.7 was found to be appropriate to concretes with less than 40 MPa compressive strengths.

Figures 8.25-8.28 of Chapter 8 are typical examples of non linearity index versus Poisson's ratio curves for a specimen with cyclic axial compression. As can be seen from the figures, when unloading occurs in the *initial elastic region*, the Poisson's ratio decreases. This phenomenon has not been reported before in the literature and will have significant implications to confining pressures during cyclic loadings. Figure 9.25 also shows the curves predicted by the model, which is capable of predicting the decreasing Poisson's ratio phenomenon.

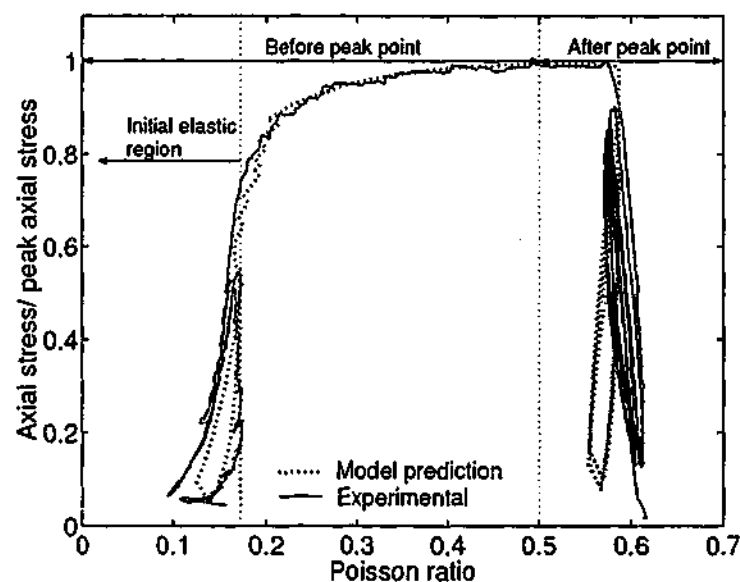


Figure 9.25: Variation of Poisson's ratio during hysteresis loops.

The decreasing Poisson's ratio phenomenon was investigated in all the test results from this study. It was found that the decreasing Poisson's ratio occurred only in cases where the unloading occurred in the *initial elastic region*. This can be confirmed by casual observations of Figures 8.25-8.28 of Chapter 8, where the unloading of axial strain curves and lateral strain curves show significantly different behaviour in the *initial elastic region*. The axial strain curves unload parallel to the initial tangent modulus whereas the lateral strain unloads along the same path as the loading curve.

9.6 Results

The procedure used in drawing stress-strain curves for confined concrete subjected to cyclic loading is summarised in Figure 9.26.

9.6.1 Comparison of the proposed model with the experimental results

Proposed model is developed from the experimental results obtained by the author for 24 specimens as described earlier. The stress-strain curves proposed by the model for all the concrete specimens tested are shown in Figures 9.27-9.38. These comparisons are not meant for validation of the model. However, they indicate how close the developed model follows the data it is based upon. Validation from independent data could not be performed because there are no HSC data available on cyclic loading.

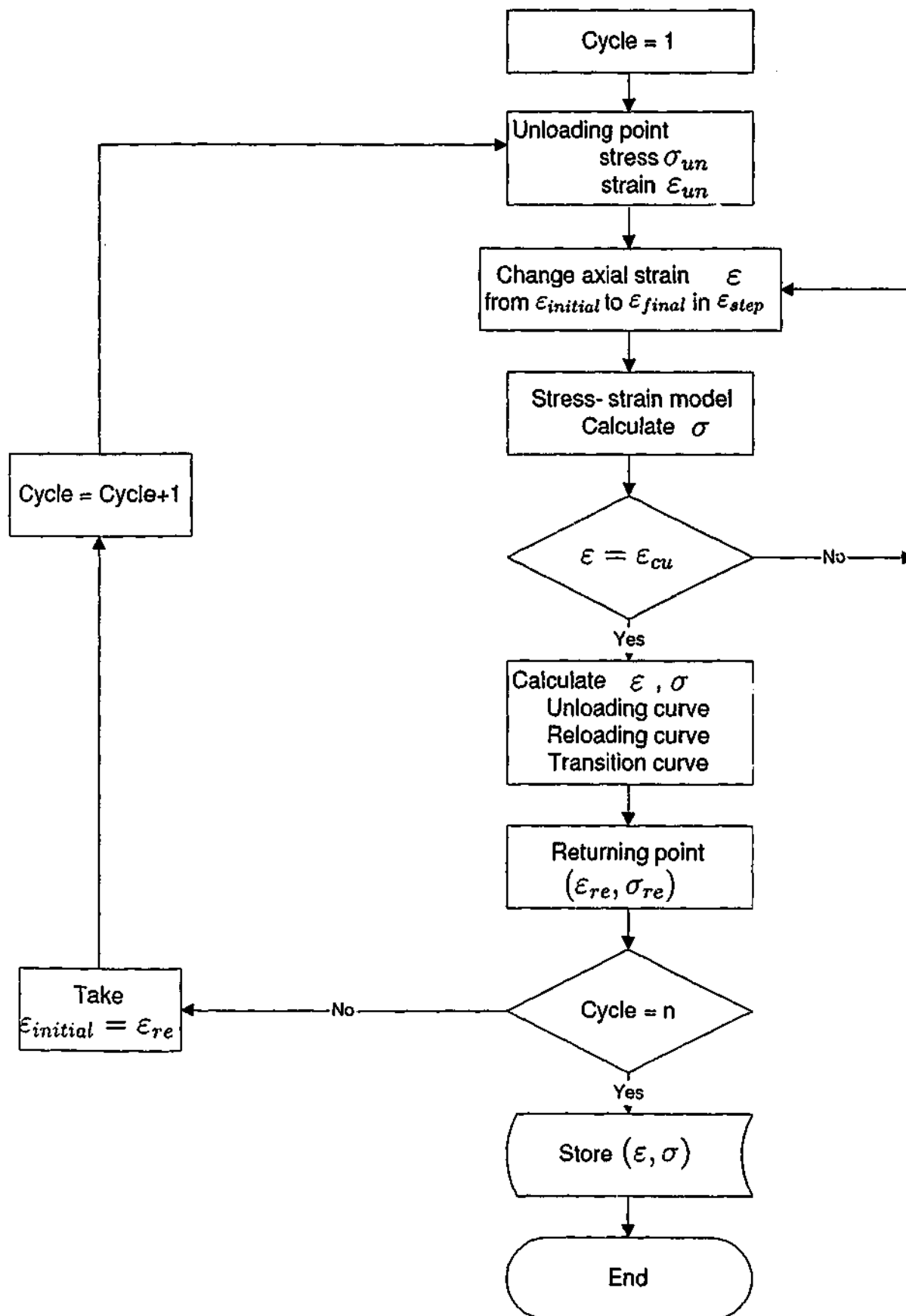


Figure 9.26: Procedure in drawing stress-strain curves for cyclically loaded concrete.

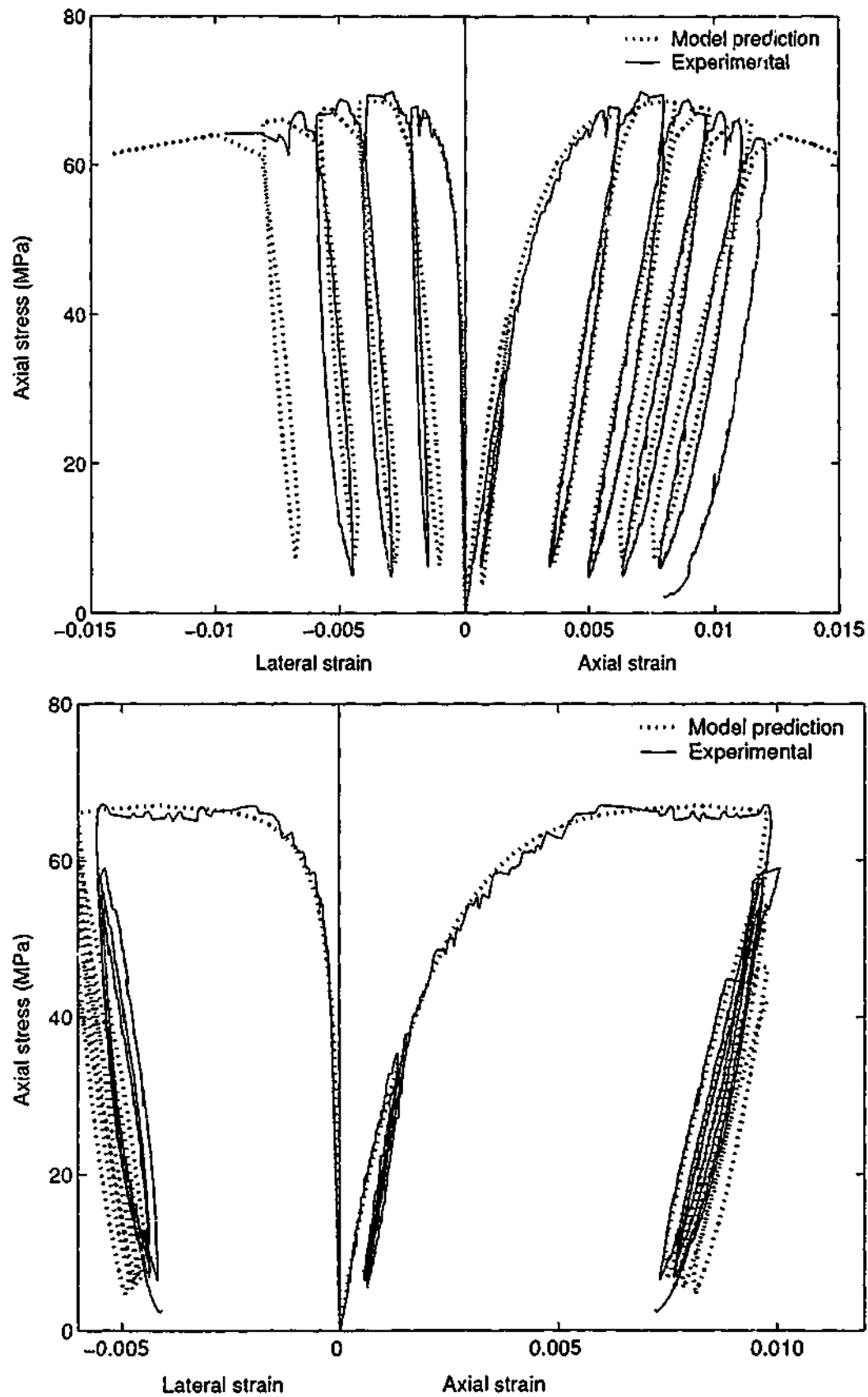


Figure 9.27: 44 MPa with 4 MPa confining pressure.

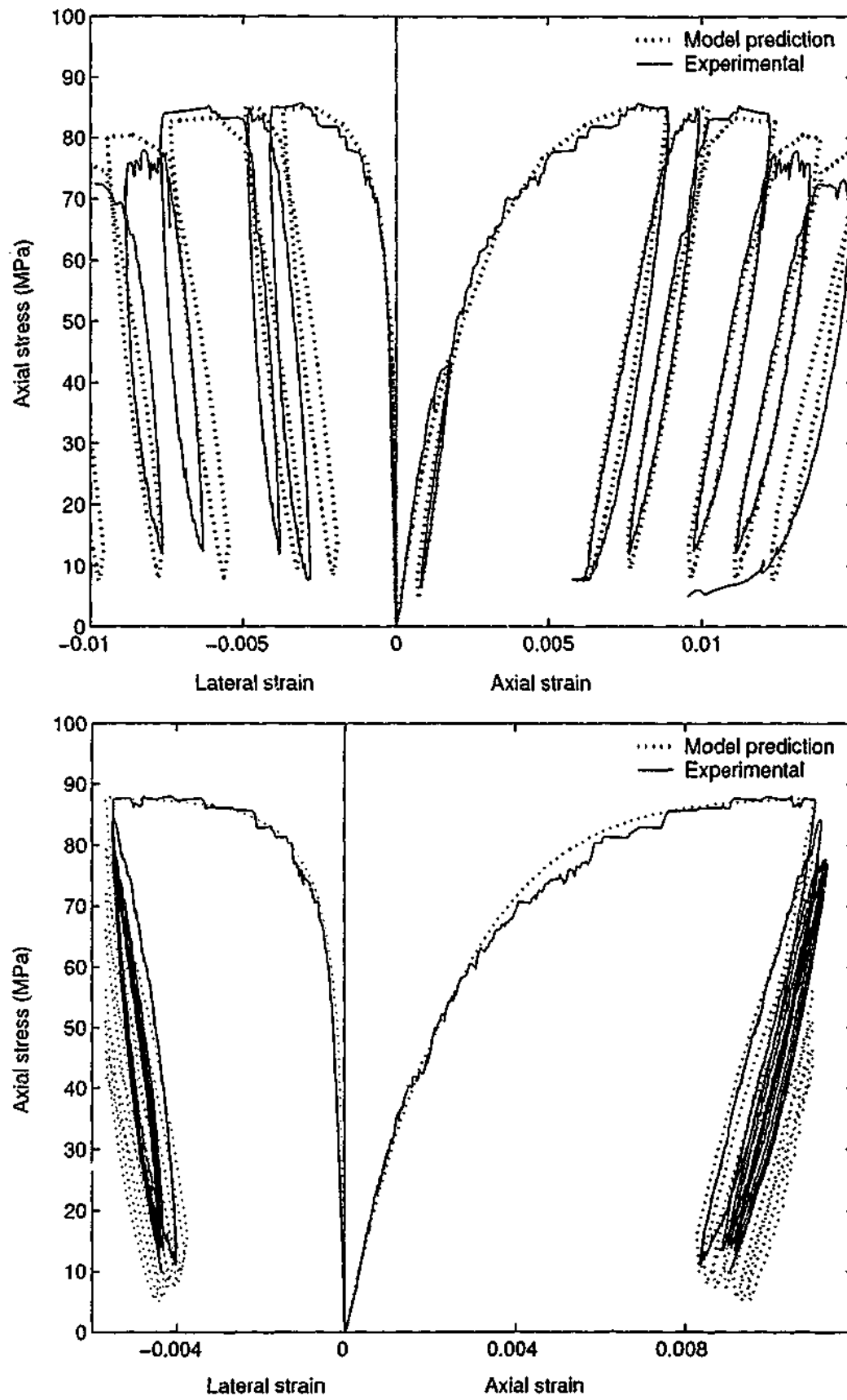


Figure 9.28: 44 MPa with 8 MPa confining pressure.

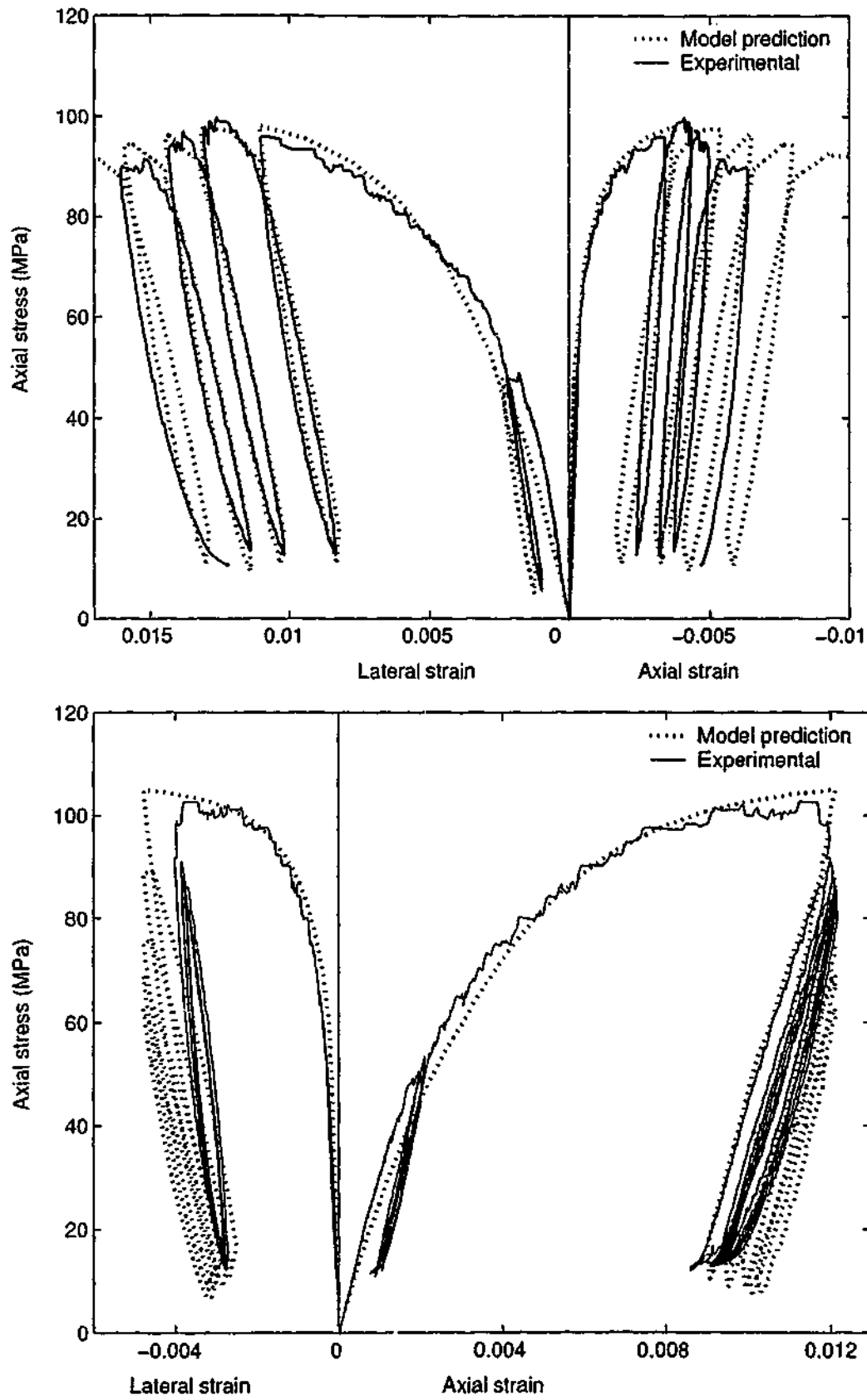


Figure 9.29: 44 MPa with 12 MPa confining pressure.

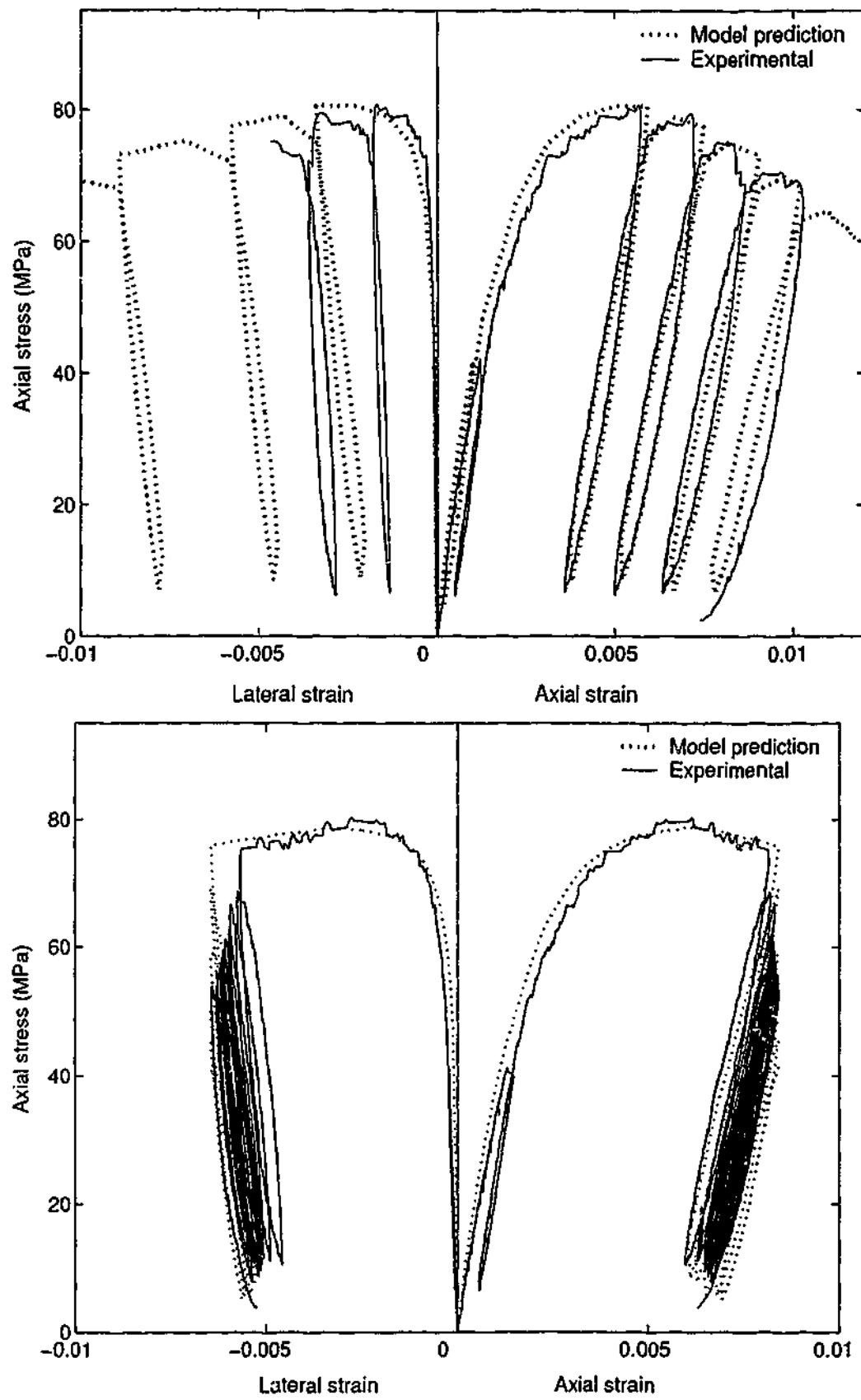


Figure 9.30: 58 MPa with 4 MPa confining pressure.

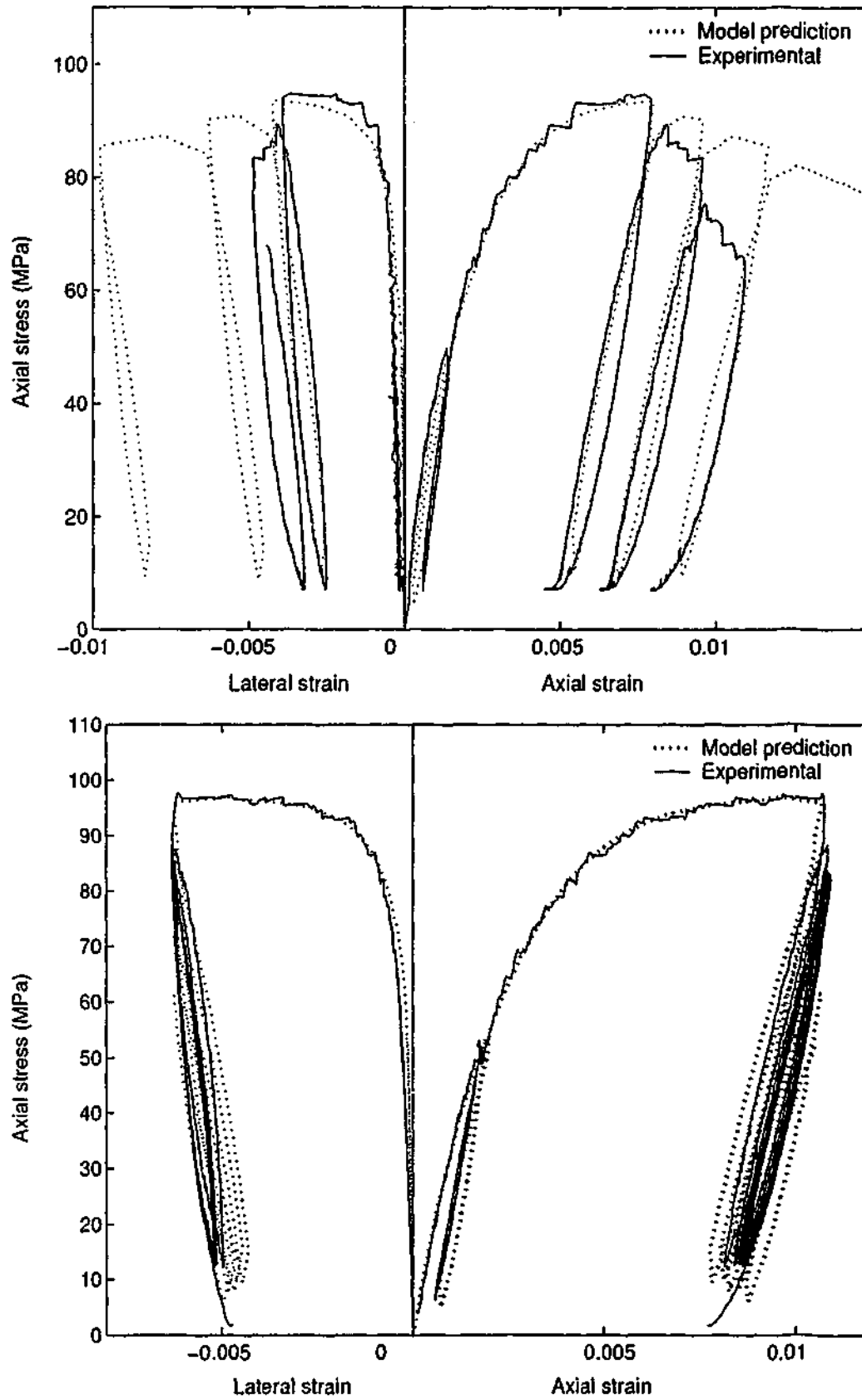


Figure 9.31: 58 MPa with 8 MPa confining pressure.

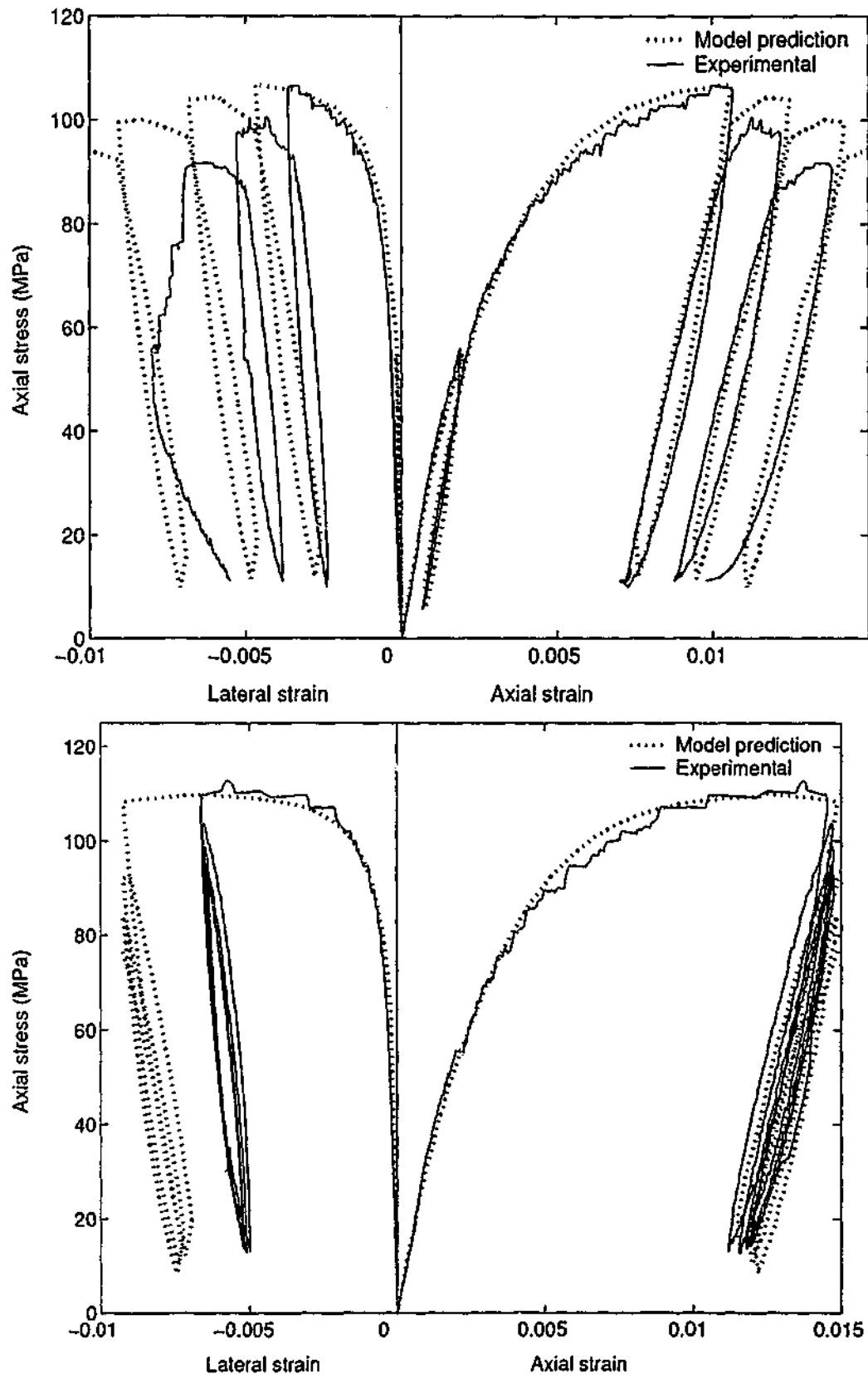


Figure 9.32: 58 MPa with 12 MPa confining pressure.

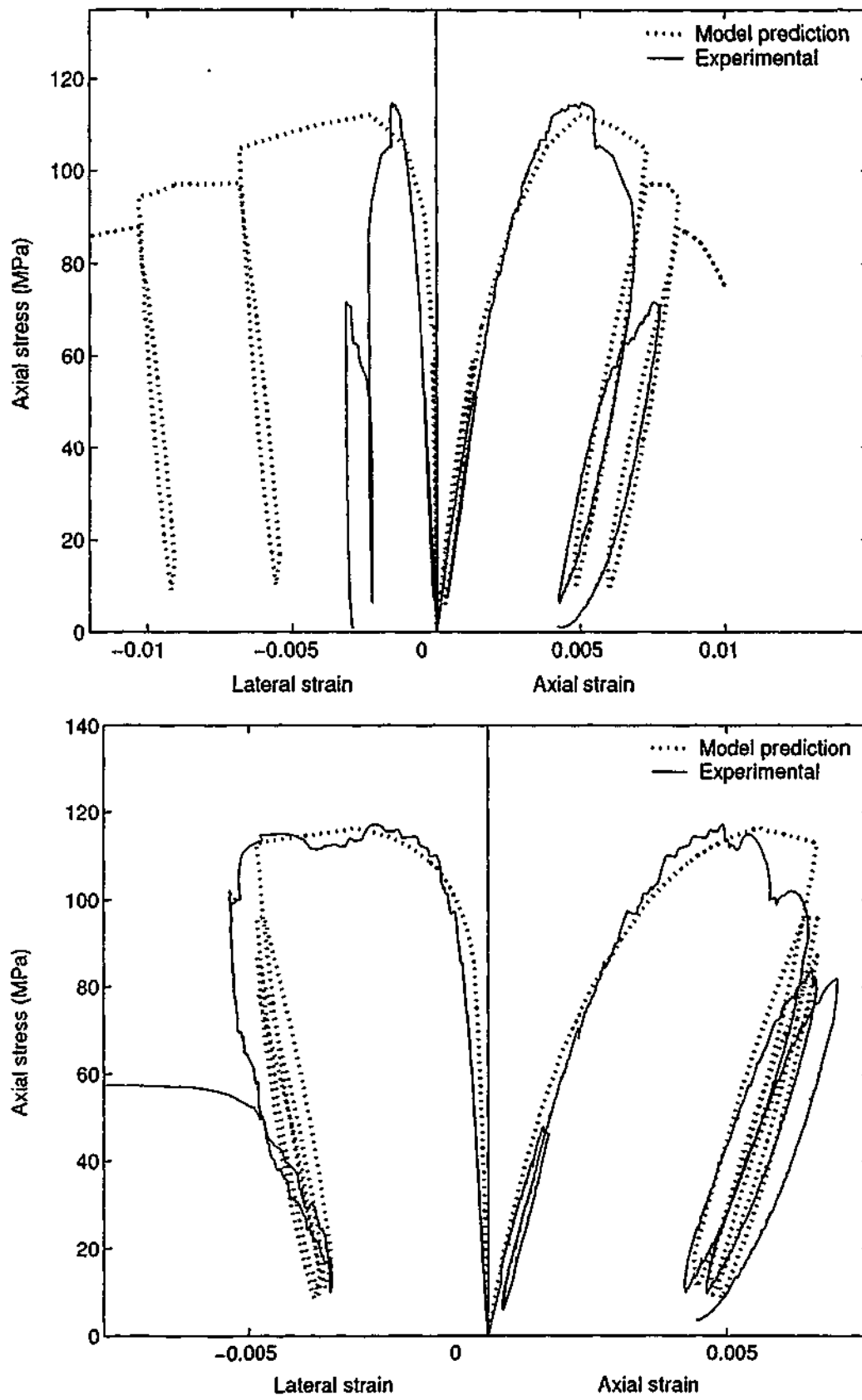


Figure 9.33: 83 MPa with 4 MPa confining pressure.

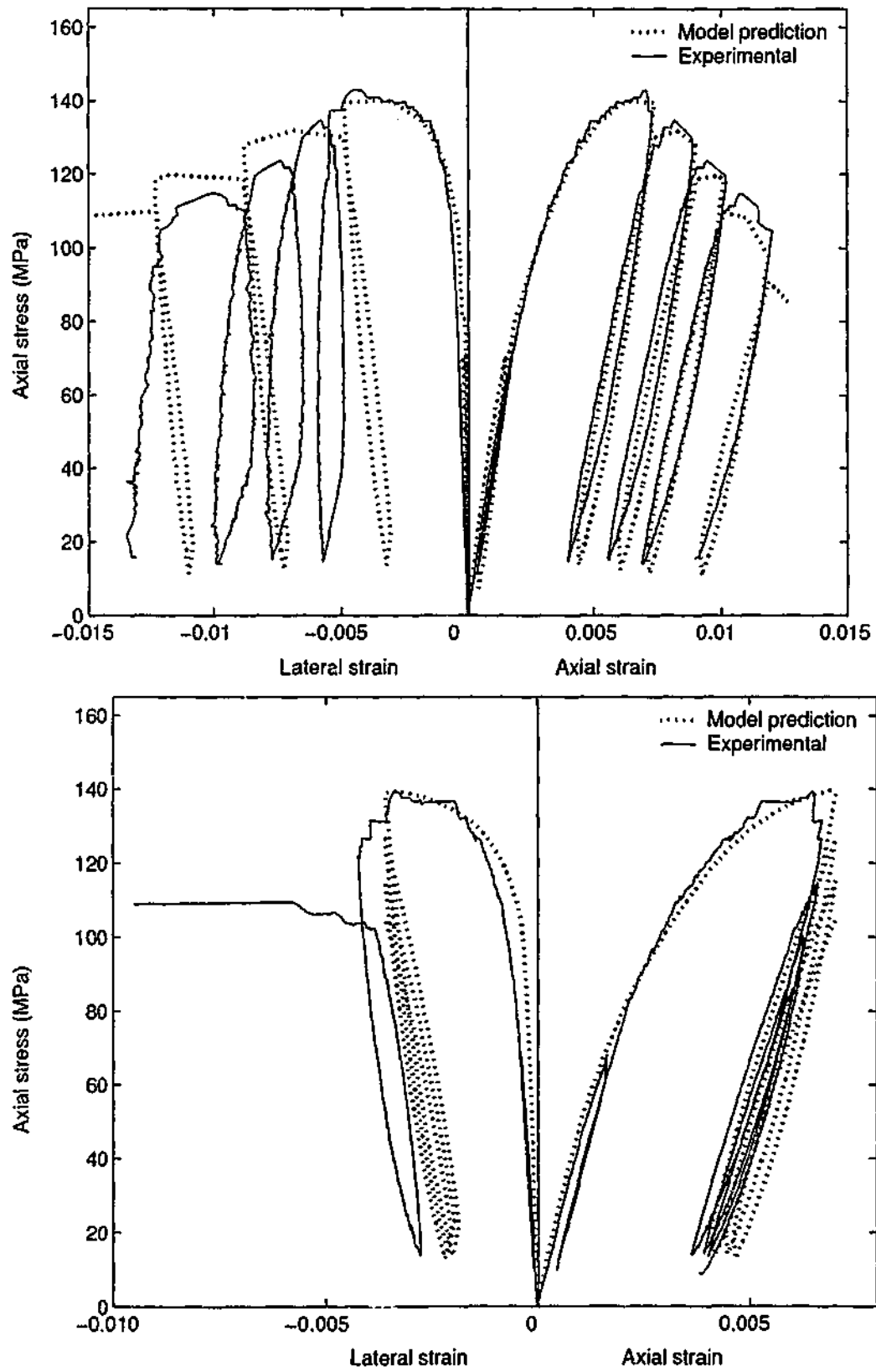


Figure 9.34: 83 MPa with 8 MPa confining pressure.

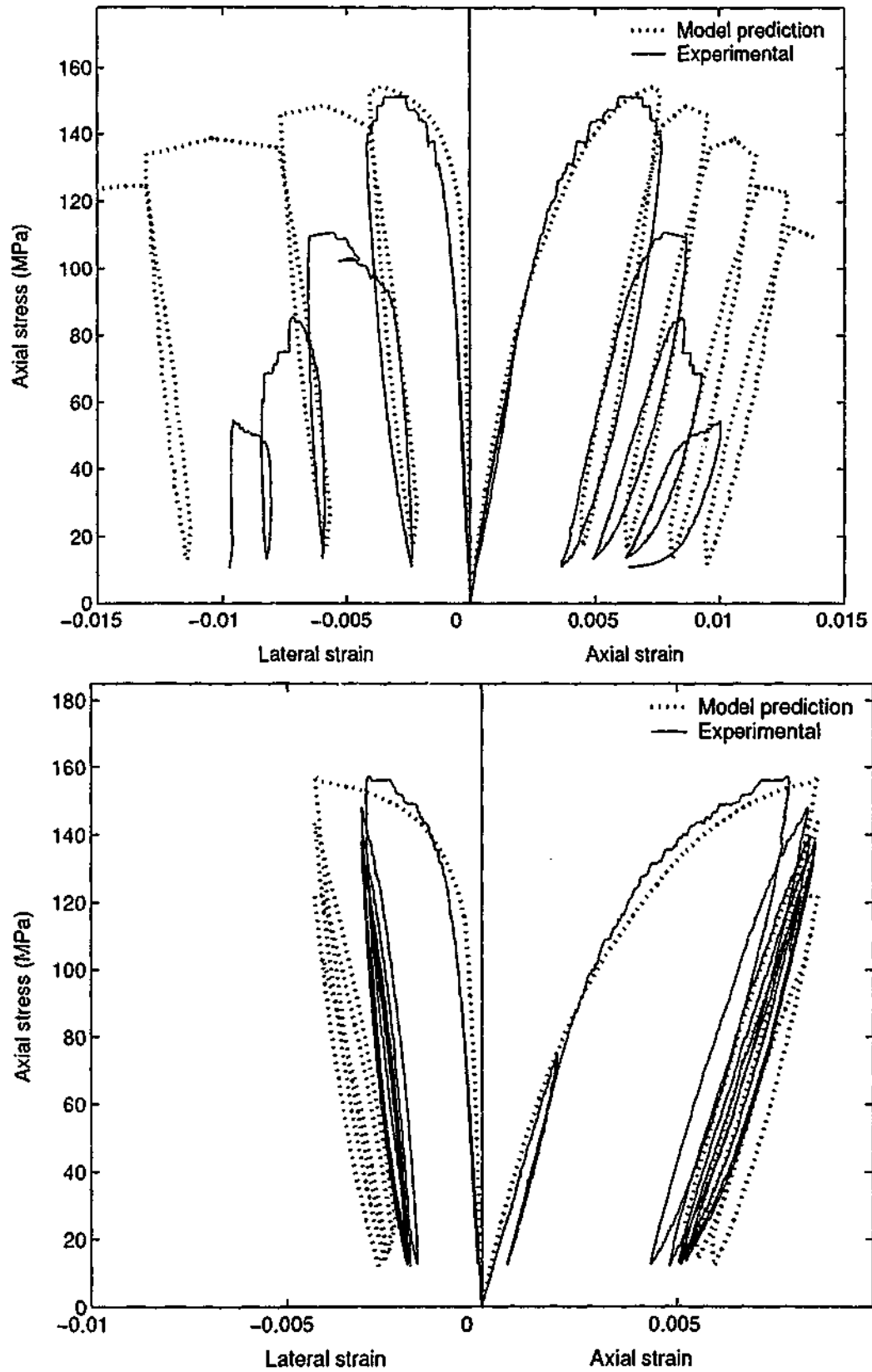


Figure 9.35: 83 MPa with 12 MPa confining pressure.

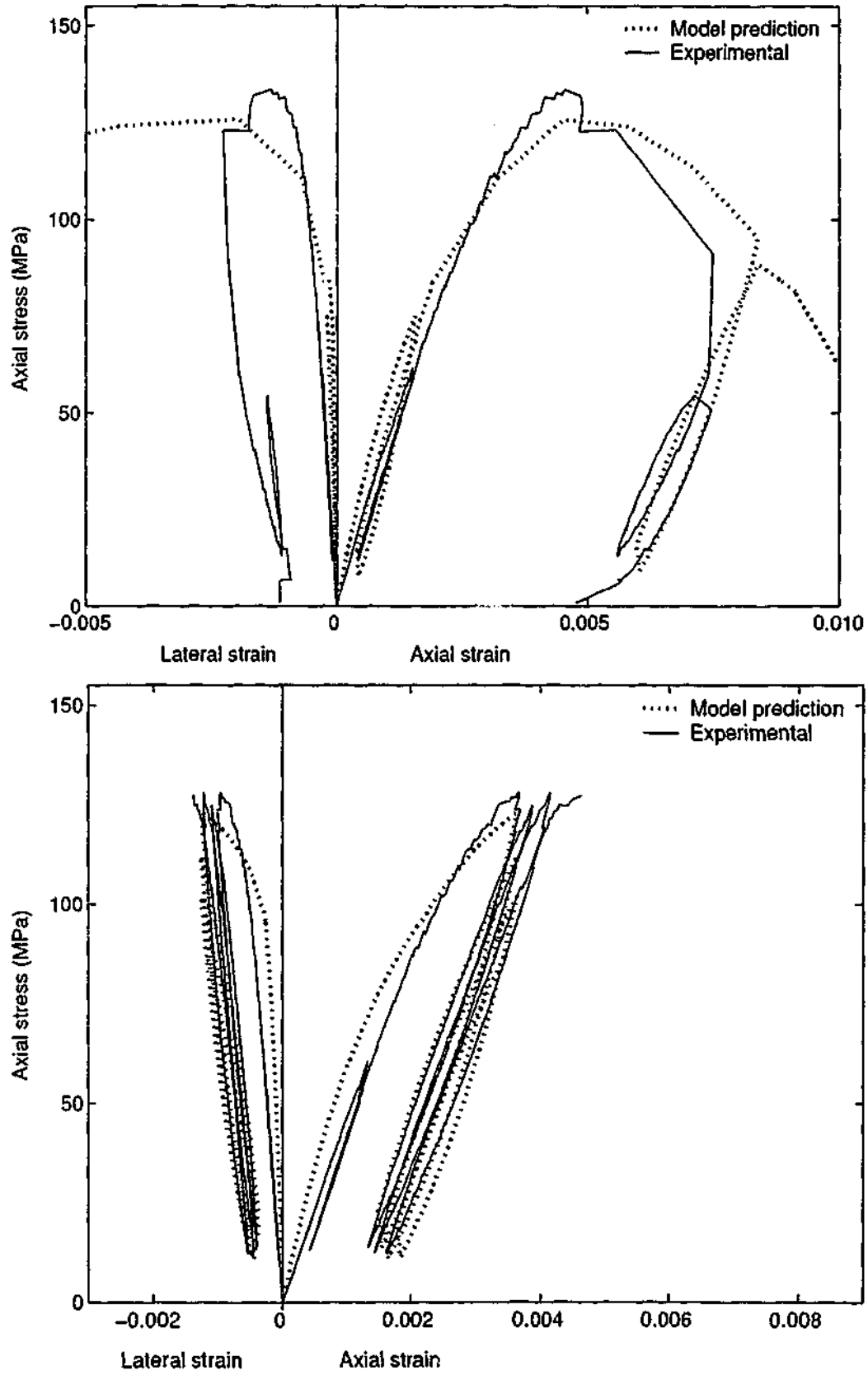


Figure 9.36: 106 MPa with 4 MPa confining pressure.

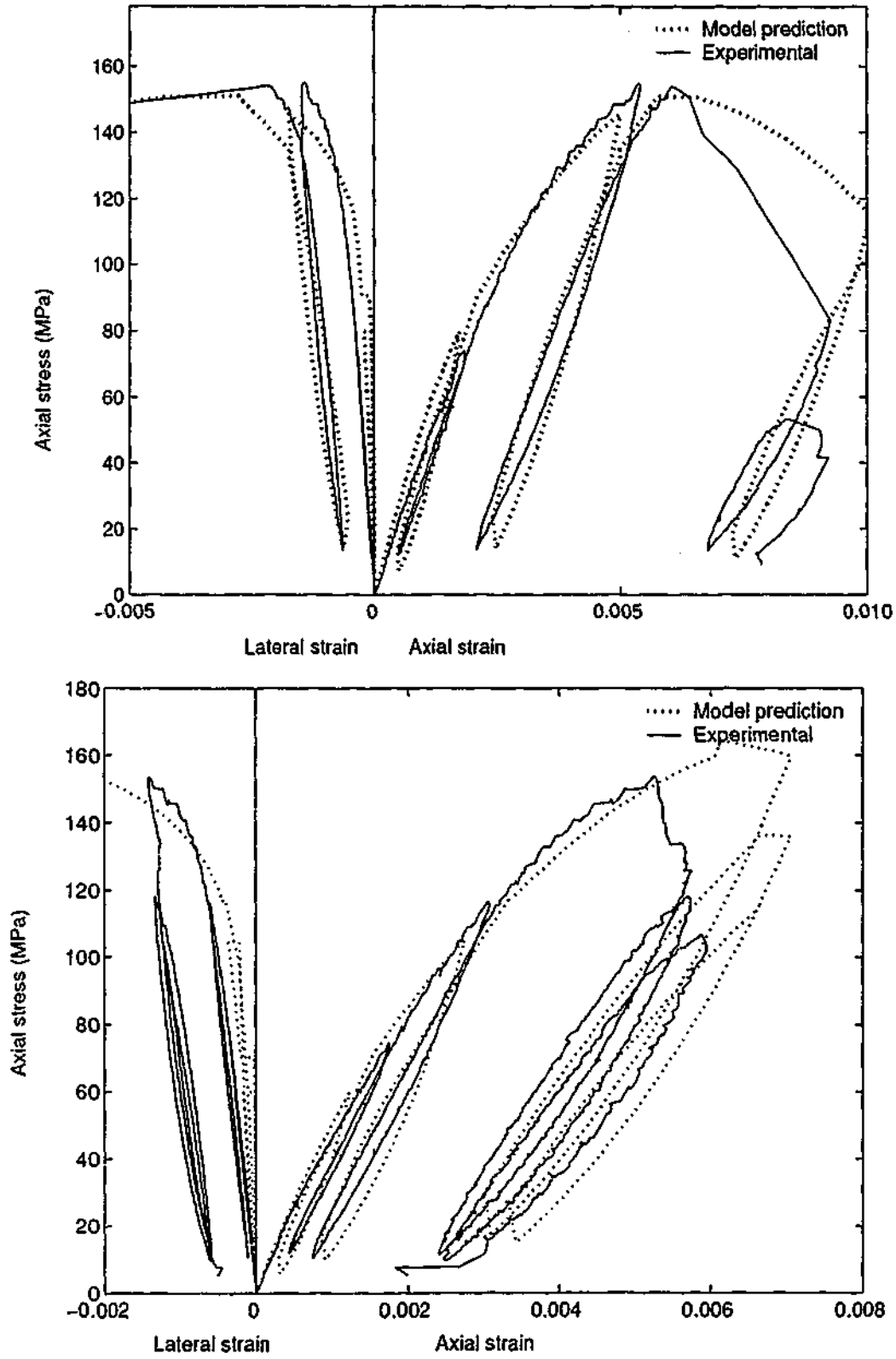


Figure 9.37: 106 MPa with 8 MPa confining pressure.

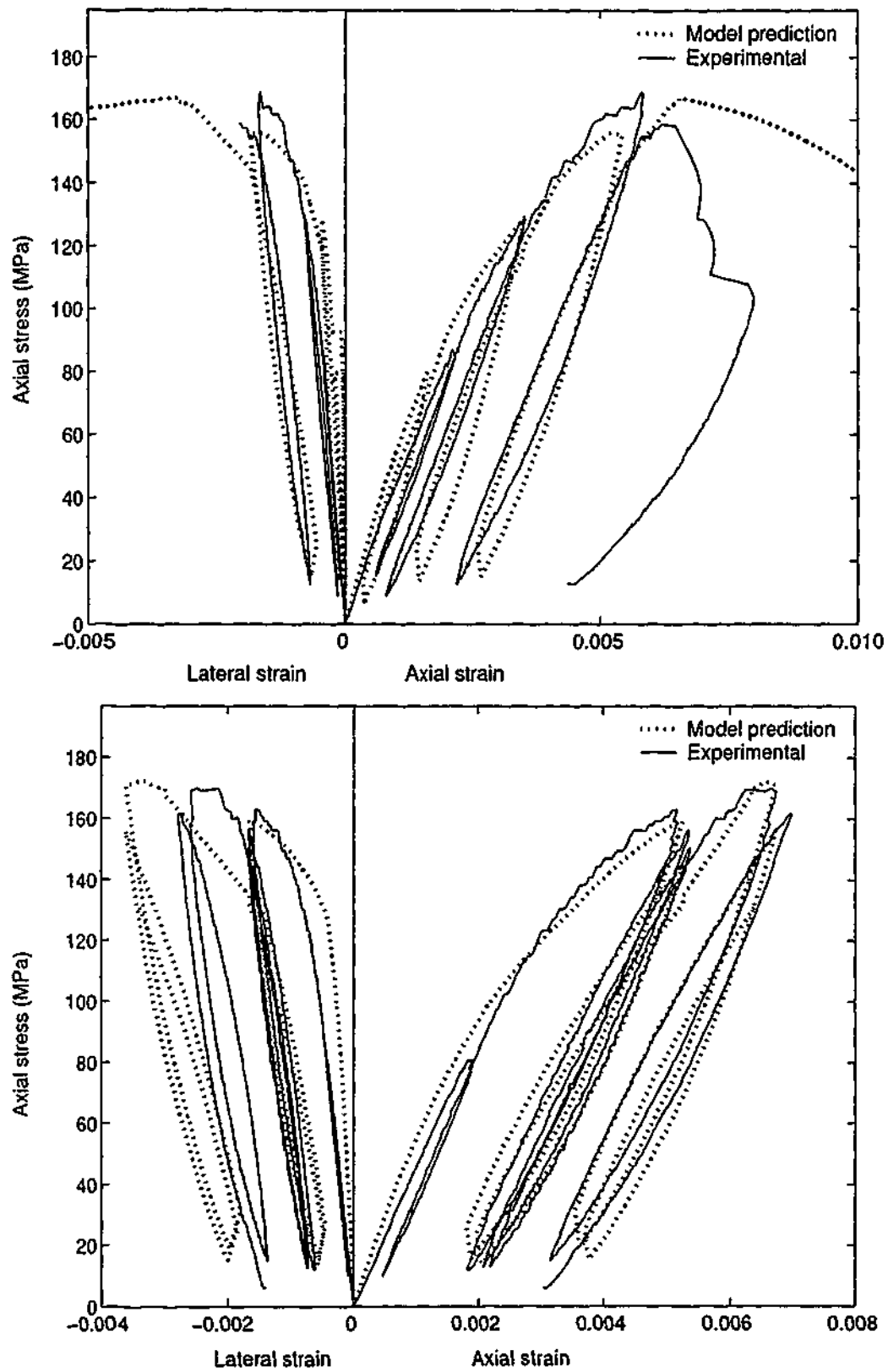


Figure 9.38: 106 MPa with 12 MPa confining pressure.

9.6.2 Comparison of the proposed model with experimental results reported in the literature

From available experiments reported in the literature for cyclic axial load on either confined or unconfined NSC, circular specimens were tested with the analytical model proposed. The model is developed based on the experimental results for concrete compressive strengths in 40-100 MPa range. But when it was compared for a concrete strength out of this range (17-23 MPa), still it shows a good agreement. Experimental curves are from the work reported by Desayi et al. (1979) (Figures 9.39-9.42).

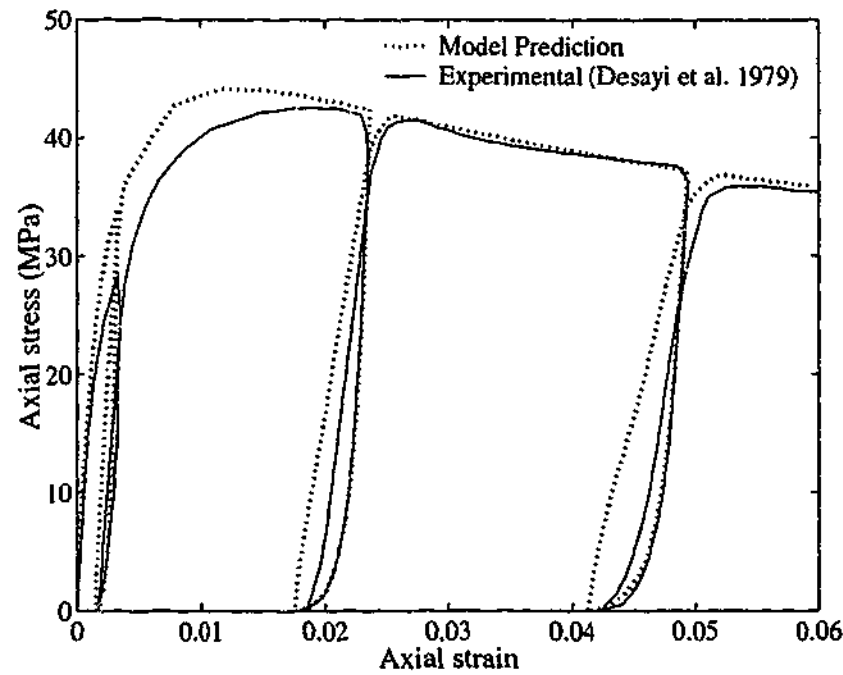


Figure 9.39: Model comparison with previous work (Desayi et al. 1979) for concrete with $f_c=22.3$ MPa.

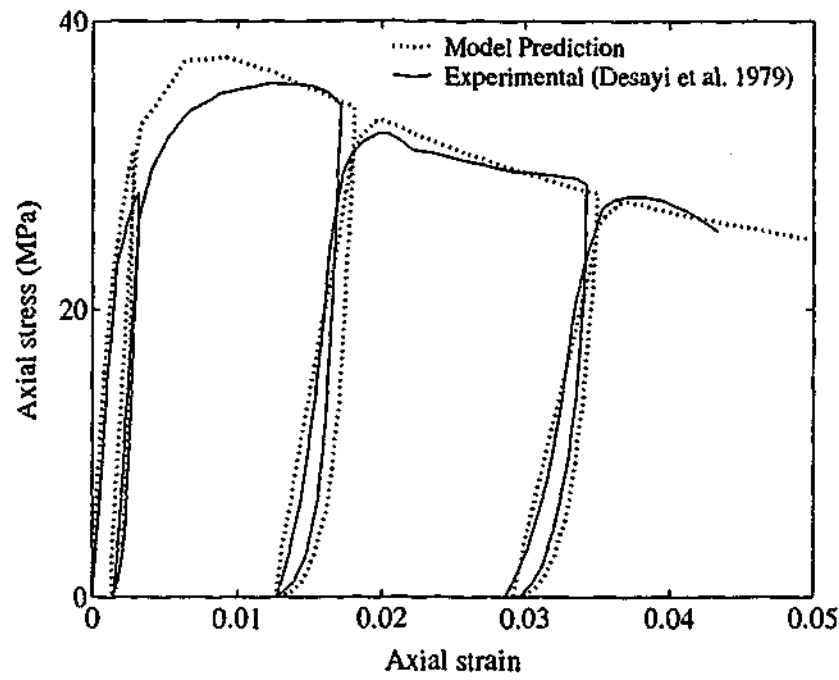


Figure 9.40: Model comparison with previous work (Desayi et al. 1979) for concrete with $f_c=23$ MPa.

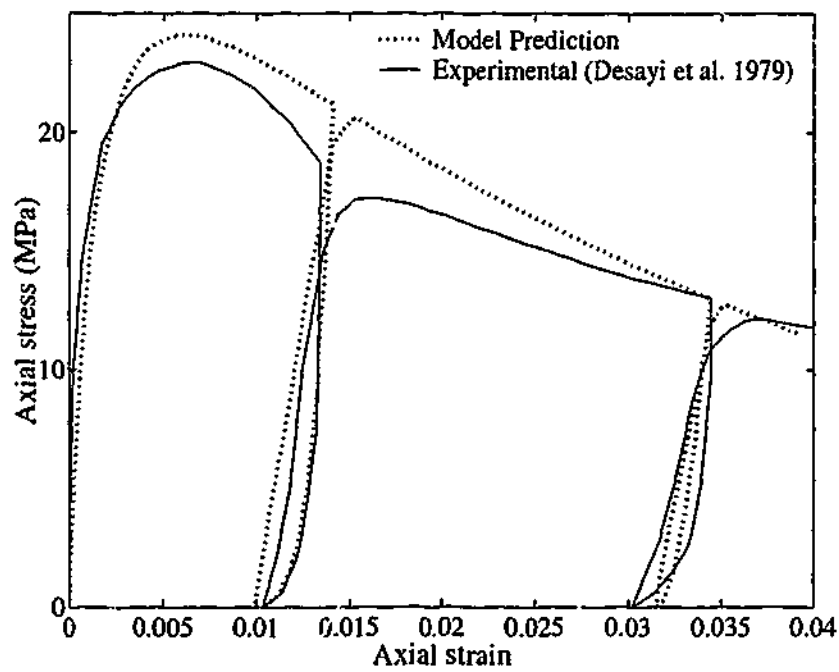


Figure 9.41: Model comparison with previous work (Desayi et al. 1979) for concrete with $f_c=17.8$ MPa.

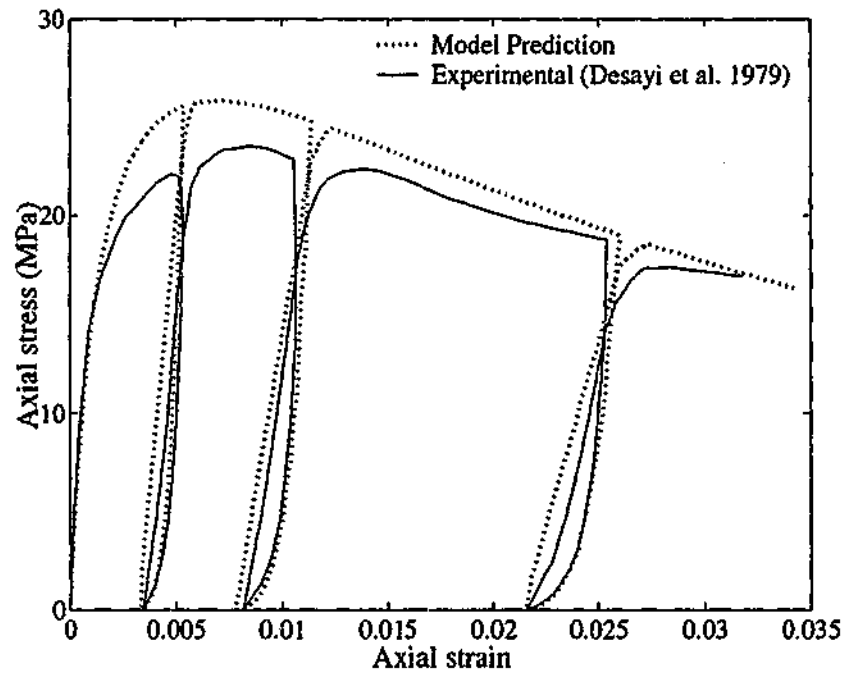


Figure 9.42: Model comparison with previous work (Desayi et al. 1979) for concrete with $f_c=18.7$ MPa.

9.7 Conclusions

- The model for concrete subjected to cyclic loading, proposed in this paper comprises four components; namely, (1). envelope curve (for both ascending and modified descending curves), (2). unloading curve, (3). reloading curve and (4). parabolic transition curve.

The envelope curve of the proposed model is based on the 24 experimental results reported by Candappa et al. (2001) as well as previous work presented by Attard and Setunge (1996) Attard and Setunge 1996. Unloading and reloading branches were developed based on the 24 tests carried out by the authors. Parabolic transition curve is the one proposed by Mander et al. (1988b) Mander et al. 1988a and plastic strain is a modified version of that proposed by Mander et al. (1988b).

- Envelope curve, unloading and reloading curves are derived using shear stress versus shear strain relationships.
 - Proved by previous researchers for unconfined and confined NSC
 - For HSC, it is valid only for the ascending branch

- For HSC, descending branch is modified by scaling down the corresponding stresses.
- Model is proposed using 24 test results for NSC and HSC with active lateral confinement subjected to cyclic axial compression. Using an iterative procedure, it can easily be applied to model the same with passive confinement.
- The Poisson's ratio is constant in the initial elastic region, and rapidly increases when loaded beyond this region.
- When unloading occurs in the initial elastic region, the Poisson's ratio decreases; and increases back to the same value when reloading occurs. The model proposed in this study is capable of modelling the phenomenon of decreasing Poisson's ratio.

A constitutive model is proposed in this chapter for the behaviour of HSC subjected to active lateral confinement and cyclic loading. It can easily be extended for HSC with passive confinement. The proposed model is to be applied for column analysis in the next chapter.

Chapter 10

CYCLIC LOADS:

Prediction of load-deformation characteristics of columns

10.1 Introduction

The use of high strength concrete (HSC) in columns in high seismic regions requires additional care in the design due to its lower level of ductility than the ductility available in NSC. Proper confinement or using the high yield strength lateral reinforcement is capable of increasing the ductility of HSC.

Most of the structural failures during recent earthquakes were attributed to poor column behaviour. In concrete structures, the ability to withstand strong earthquakes depends mainly on the formation of plastic hinges and their capability of energy absorption and dissipation without a major loss of strength capacity. Within the plastic hinge, all the inelastic deformations are assumed to occur. The region outside the hinge is assumed to remain elastic at all times.

It is preferable to design structures with strong columns and weak beams with plastic hinges forming in the beams and not in columns. However, it may not always be possible to design structures like this, and hinges may develop in columns. Therefore the possibility of plastic hinge formation at HSC column ends demands a sufficient level of ductility to safeguard the structures in seismic areas. This is an added ductility requirement to the already existing ductility need in HSC than that in NSC.

This chapter identifies the necessity to investigate the column behaviour for earthquake loadings. It then presents several experimental programs carried out around the world

to observe the behaviour of concrete columns under axial load and cyclic lateral loads simulating the ground motion in an earthquake. Having identified the gaps in knowledge in this area, an analytical procedure is described in detail to estimate the behaviour of HSC columns subjected to combined axial load and cyclic flexure. It uses the novel concrete constitutive model developed in Chapter 9 for the cyclic behaviour of HSC. A computer program coded in Visual Basic is developed in implementing this. The predicted behaviour of HSC columns under axial load and cyclic flexure, is compared with the reported experimental results.

10.2 Examples for poor design of columns

Columns are the most essential elements in the moment-resistant frame of buildings. Structural behaviour during recent earthquakes has indicated that majority of the structural failures are due to poor column behaviour. Hachinohe City Library damaged during the 1968 Tokachi-Oki earthquake in Japan has good examples of structural failures due to poor column behaviour (Saatcioglu and Ozcebe 1989). During the 1971 San Fernando earthquake, Olive View Hospital damaged due to the plastic hinging concentrated in the columns of the bottom storey (Park and Sampson 1972). Most of the column failures were caused by high shear stresses, lack of concrete confinement and bidirectional load effects. Saatcioglu and Ozcebe (1989) reported some examples for each effect. The short columns at the Macuto-Sheraton Hotel damaged during the 1967 Caracas, Venezuela earthquake is a good example of column failure due to high shear stress reversals. During the 1985 Mexico City earthquake, many column failures were caused due to poor concrete confinement. The failure of columns of the Imperial County Services Building during the 1979 Imperial Valley earthquake is a good example for structural failures due to bidirectional loading effects. Figure 10.1 shows three photos of column failures during Kobe 1995 earthquake. These failures are due to few confining reinforcement and bad detailing resulted in improper confinement.

Therefore in performing a structural analysis for earthquake loadings, it is of great importance to design columns with sufficient level of ductility in order to minimise the chances of a possible failure.

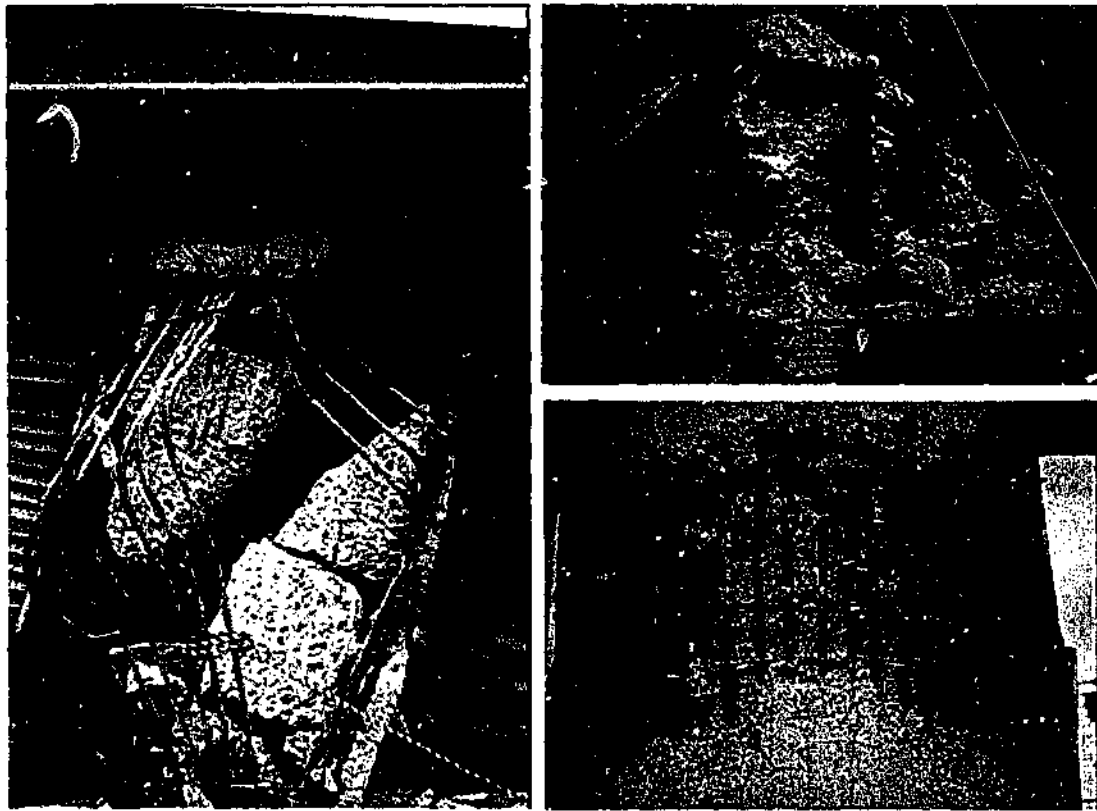


Figure 10.1: Column failures in Kobe 1995 earthquake (EQE 1995).

10.3 Previous work on the behaviour of columns under cyclic flexure and constant axial load

Studies on the behaviour of NSC (Watson and Park 1994; Priestley and Park 1987) and HSC columns (Ozcebe and Saatcioglu 1987; Saatcioglu and Ozcebe 1989; Muguruma and Watanabe 1990; Bing et al. 1991; Thomsen and Wallace 1994; Azizinamini et al. 1994; Sheikh et al. 1994; Bayrak and Sheikh 1998; Saatcioglu and Baingo 1999; Ahn et al. 2000; Legeron and Paultre 2000; Martirosyan and Xiao 2001) subjected to axial load and cyclic lateral forces have been progressing from well over 15 years. A large number of experimental programs have been reported in the literature to study this behaviour. Each experimental program differs from one another in compressive strength of concrete, size and shape of columns, configuration of reinforcement and the axial load level. Very few researchers compared the experimental results with the analytical findings (Thomsen and Wallace 1994; Assa and Nishiyama 1998; Kwan and Billington 2001).

10.3.1 Experimental programs

The aims of all the experimental programs carried out were to observe the effects of the following parameters in the behaviour of concrete columns subjected to axial load and cyclic flexure.

- Concrete compressive strength
- Axial load level
- Amount, configuration, spacing and yield strength of transverse reinforcement

The following parameters have been used in discussing the behaviour of columns.

- Ductility
- Plastic hinge length
- Spalling of cover
- Comparison with code provisions

10.3.2 Effect of concrete compressive strength

Majority of the researchers investigated the flexural capacity and ductility of square HSC columns subjected to constant axial load and cyclic lateral loads. Azizinamini et al. (1994) tested columns with a cross section of 305×305 mm, representing 2/3-scale model of an 457×457 mm prototype column. They tested 9 square columns of the same size and reported that increasing the compressive strength from 54 to 101 MPa resulted in approximately 25% reduction in the ductility. Many researchers (Muguruma and Watanabe 1990; Ahn et al. 2000) supported this idea. Muguruma and Watanabe (1990) tested 8 square columns (200×200 mm) using concrete compressive strengths of 85.7 and 115.8 MPa. Ahn et al. (2000) tested 20 square columns (240×240 mm) with concrete compressive strengths of 25, 52 and 70 MPa. Recently, Xiao and Henry (2002) tested 6 full-scale square HSC columns (510×510 mm) with compressive strengths of 63 MPa.

Saatcioglu and Baingo (1999) have conducted experiments on circular columns under constant axial compression and incrementally increasing lateral deformation reversals.

They concluded that increasing compressive strength will result in decreasing ductility unless proper confinement is provided.

Ductility of HSC columns subjected to combined axial load and cyclic flexure, decreases with the increasing compressive strength. However, this can be overcome if the HSC columns are sufficiently confined.

10.3.3 Effect of transverse reinforcement

Azizinamini et al. (1994) reported that decreasing the spacing of transverse reinforcement from 66.7 to 41.3 mm resulted in approximately 40% increase in ductility. According to their experimental and analytical studies for square HSC columns, the ductility of HSC columns is proportional to the volume of transverse reinforcement. Same idea was supported by Martirosyan and Xiao (2001) using six 1/3-1/2 scale HSC short columns. Furthermore, Legeron and Paultre (2000) and Ahn et al. (200) concluded that the tie spacing has significant effect on the behaviour of the columns.

Usage of high yield strength transverse reinforcement is suggested as a promising solution for the brittle nature of HSC and the problems associated with closer spacing of low yield strength transverse steel (Saatcioglu and Ozcebe 1989; Muguruma and Watanabe 1990; Azizinamini et al. 1994; Thomsen and Wallace 1994; Saatcioglu and Baingo 1999). However with the use of high yield strength transverse steel, the increment in spacing may increase the likelihood of buckling. It is proposed that further research work is needed in this aspect because the use of high strength transverse reinforcement to increase spacing is limited due to the potential adverse effects of buckling. On the other hand, Azizinamini et al. (1994) reported that yield strength of transverse reinforcement had no influence on the ductility, if the column is subjected to an axial load lower than 20% of the column axial load capacity.

Ozcebe and Saatcioglu (1987) tested full scale square columns (350 × 350 mm) to investigate the effect of confinement in the columns when subjected to seismic loading. The compressive strengths used had a range of 32-40 MPa. They concluded that proper choice of transverse steel arrangement is more feasible than reducing the tie spacing to achieve the same level of confinement.

By considering spiral reinforcement and circular hoops, Saatcioglu and Baingo (1999) concluded that although both columns with spiral steel and circular hoops behaved in a

similar manner, the spiral reinforcement was more effective in controlling the stability of longitudinal reinforcement than the circular hoops at later stages of inelastic behaviour. However, the performance of concrete columns during recent earthquakes showed that a failure in spiral reinforcement would lead to a complete unwinding of the spiral. Therefore the long believed potential benefits of continuity provided by spiral steel is said to be questionable when used in high seismic regions.

Ductility of HSC columns under axial load and cyclic lateral forces can be improved by,

- decreasing the spacing of transverse reinforcement,
- using high yield strength transverse reinforcement,
- choosing proper configuration of transverse reinforcement or
- using circular hoops instead of the spirals.

10.3.4 Effect of axial load

Saatcioglu and Ozcebe (1989) tested full scale square columns to illustrate the effects of axial load and lateral reinforcement on column ductility. The compressive strengths used were in the range of 30-50 MPa. They considered 2 levels of axial load, zero and 20% of concentric design axial load capacity and demonstrated the response as the accelerated strength and stiffness degradation. Azizinamini et al. (1994) compared the effect of NSC and HSC columns separately with different axial load levels. Three levels were selected in their analysis representing 20, 30 and 40% of nominal column load capacity. For NSC columns increasing axial load level from 30 to 40% reduced the ductility by 30%.

In Azizinamini et al. (1994) study for HSC columns, increasing axial load level from 20 to 30%, reduced the ductility by 17%. They concluded that ductility of HSC columns is inversely proportional to the level of axial load. Bayrak and Sheikh (1998) used realistically sized HSC and ultra HSC columns with moderate to high axial load levels. They concluded that a high axial load level increases the rate of stiffness degradation with every cycle and adversely affect the cyclic performance of HSC columns. Similar observation was reported by Legeron and Paultre (2000), Legeron et al. (1997) and Paultre et al. (2001) for HSC using axial load levels of 15, 25, 40 and 52%, Murguruma and Watanabe

(1990) using comparatively high axial load levels of 25 and 63% and Ahn et al. (2000) using axial load levels of 30 and 50%.

It is documented in the previously published research work, that increase in axial load level will result in decrease in the ductility for NSC (Watson and Park 1994) and HSC (Legeron and Paultre 2000; Ahn et al. 2000).

10.3.5 Ductility

Several definitions for ductility and deformability are available in the literature. In seismic design, the inelastic behaviour is generally quantified by both the ductility parameter and energy dissipation capacity. The main drawback in using this ductility parameter is the lack of generally accepted definition among the research community, for the yielding of a reinforced concrete member. Legeron and Paultre (2000) defined this point as the intersection of the maximum load and the elastic branch of the idealised curve which is secant to the real curve at 75% of maximum load.

Bayrak and Sheikh (1998) and Sheikh et al. (1994) defined ductility and toughness using parameters shown in Figure 10.2. Curvature ductility factor (μ_ϕ) is defined as,

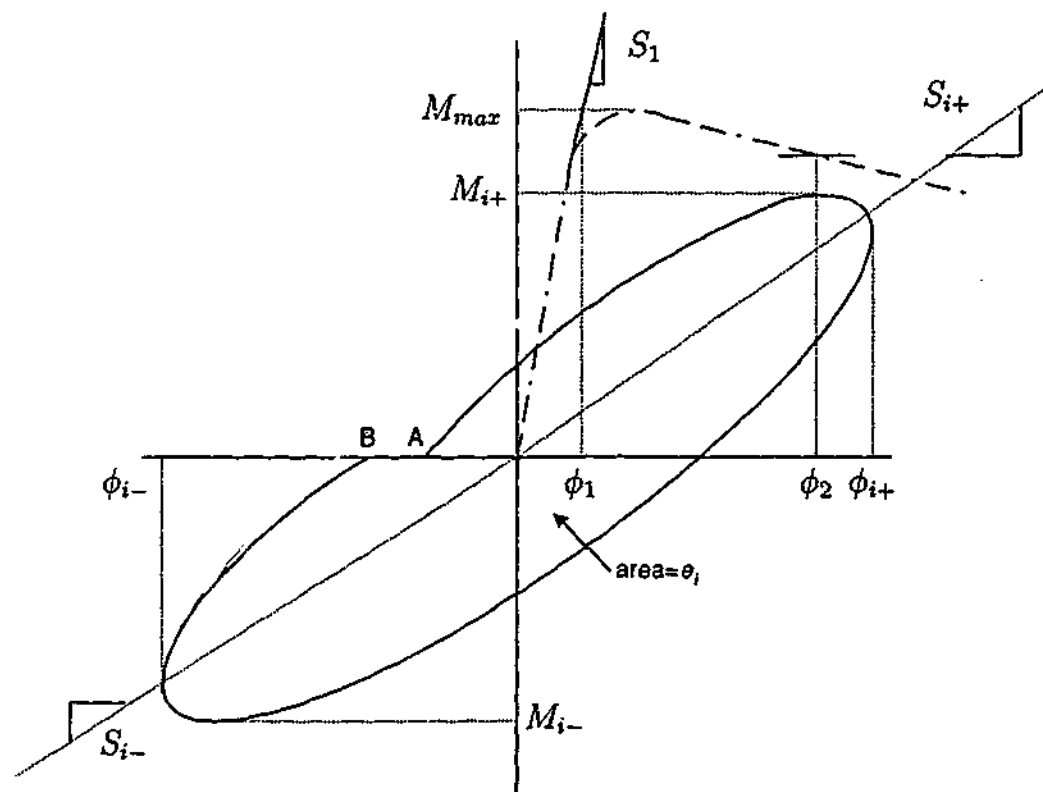


Figure 10.2: Section ductility parameters.

$$\mu_\phi = \frac{\phi_2}{\phi_1} \quad (10.1)$$

Cumulative ductility ratio (N_ϕ) is given as,

$$N_\phi = \sum_{i=1}^m \frac{\phi_i}{\phi_1} \quad (10.2)$$

where, ϕ_i is defined by,

$$\phi_i = \frac{1}{2}(\phi_{i+} + \phi_{i-}) \quad (10.3)$$

Energy-damage indicator (E) is given by,

$$E = \frac{1}{M_{max}\phi_1} \sum_{i=1}^m e_i \frac{l_p}{B} \left(\frac{S_i}{S_1} \right) \left(\frac{\phi_i}{\phi_1} \right)^2 \quad (10.4)$$

where, e_i is the area enclosed in cycle i of the $M - \phi$ curve, l_p is the most damaged region, B is the section depth of specimen and S_i is given by,

$$S_i = \frac{1}{2}(S_{i+} + S_{i-}) \quad (10.5)$$

It is observed that HSC specimens have low deformability, energy absorption and dissipation capacity (Bayrak and Sheikh 1998; Saatcioglu and Baingo 1999).

However in this study, these ductility parameters have not been utilised because of the unavailability of digital experimental data for comparison.

10.3.6 Length of plastic hinge

A guarantee in the stability of a concrete structure is the ultimate aim in any structural design. In a seismic design, it depends on the formation of plastic hinges and their capacity to absorb and dissipate energy without a major strength loss. When the structure is subjected to earthquake loadings, all the inelastic deformations are assumed to occur within the plastic hinge length while the outside region remains elastic. As most of the experimental programs reported the load-displacement relationships instead of the moment-curvature relationships, plastic hinge length is needed to calculate the deflections from the curvatures. This is described in detail later in Section 10.6.2.

Plastic hinge length has been approximated by several empirical equations in the previous studies (Sheikh et al. 1994; Assa and Nishiyama 1998). However, the researchers tend to use experimental observations to determine plastic hinge length. For the square

columns (305 × 305 mm) tested by Azizinamini et al. (1994), the length of plastic hinge for columns of HSC was approximately 254 mm from the beam stub, and that for NSC columns was approximately 305 mm. Assa and Nishiyama (1998) approximated the plastic hinge length with the column section depth, which is the normal approximation used by many researchers.

In general, Watson and Park (1994) observed that the length of plastic hinge zone increases with the axial load level for the NSC columns they tested. A similar observation was reported by Legeron and Paultre (2000) for the HSC columns.

10.3.7 Spalling of cover

Azizinamini et al. (1994) reported that the first crushing of cover concrete for all HSC columns (compressive strengths greater than 97 MPa), was observed during the first cycle at displacement ductility ratio of 1. For the other specimens, spalling of cover concrete was observed at a displacement ductility ratio of 2 or 3. In general with spalling of concrete, there was a drop in horizontal load carrying capacity of the test columns. However, Saatcioglu and Baingo (1999) have observed that the cover concrete does not contribute to sufficient adverse effects to make a prominent difference in ductility.

Legeron and Paultre (2000) reported that for the tested HSC columns, the strength loss due to cover spalling increases with the increasing axial load.

10.3.8 Code provisions

By investigating the horizontal load versus the horizontal displacement of the tested columns, Azizinamini et al. (1994) concluded that ACI provisions overestimated the horizontal load carrying capacity of the test columns with compressive strengths greater than 97 MPa. They suggested an equivalent rectangular compressive block for HSC. It has the intensity of $0.63f_c$ rather than $0.85f_c$ and the depth of 0.67 times the depth of neutral axis. They concluded that HSC columns under axial load levels below 20% of their axial load capacity and designed in accordance with the seismic provisions of ACI 318-89, have sufficient ductility. However, Watson and Park (1994) found that greater quantity of lateral reinforcement than that recommended by ACI 318-89 and NZS 3101 (1989), is necessary when the axial load is high. Bayrak and Sheikh (1998) reported that a column with 70% more reinforcement than the ACI 318-95 requirements, behaved in a

very ductile way.

Bing et al. (1991) tested five HSC columns (350×350 mm cross section) subjected to constant axial load and cyclic lateral loads to investigate the New Zealand code provisions when applied to HSC columns. Investigated compressive strengths ranged from 93-98 MPa. They have modified the constitutive model proposed by Mander et al. (1988b) to take into account the behaviour of HSC and concluded that the amount of confining reinforcement required in HSC columns in seismic areas is not reliably given by NZS 3101 (1989) equations. A cyclic moment-curvature analysis was performed by Watson et al. (1994) for a range of reinforced concrete columns to derive design charts to determine curvature ductility factors.

It is emphasised the need to include axial load level in the code provisions for transverse reinforcement requirement.

10.3.9 Behaviour of HSC columns under cyclic loading

Thomsen and Wallace (1994) conducted experiments on reinforced HSC columns and compared with analytical results. They concluded that lateral load-top displacement envelopes based on the analytical stress-strain model yielded very similar results for specimens without axial load, while noticeable differences are observed for specimens with high axial loads. However, the model slightly over-predicts column stiffness as the specimens approach their peak strengths.

Assa and Nishiyama (1998) and Kwan and Billington (2001) presented analytical methods based on finite element approach to establish the load-deformation behaviour of HSC column under seismic loading. Analytical work reported by Assa and Nishiyama (1998) was validated with the experimental results from the literature (Muguruma and Watanabe 1990; Bing et al. 1991; Azizinamini et al. 1994).

Most of the analytical procedures developed so far for the behaviour of confined concrete columns under axial load and cyclic lateral loads, were based on idealised cyclic behaviour of concrete. The empirical equations used for that behaviour, provide only the axial stress and axial strain relationships. The experimental programs for HSC columns, reveal that proper confinement is essential to obtain a sufficient level of ductility. However, the confining pressure depends on the lateral dilation or the lateral strain of concrete. Therefore if the model for cyclic behaviour of concrete has the capability of modelling the

lateral strains, it is possible to find the actual confinement provided by the lateral reinforcement. Such a constitutive model for concrete was developed for HSC in Chapter 9. The computational procedure based on that model, to analyse the behaviour of HSC columns subjected to axial load and cyclic flexure, is described in the next section.

10.4 Computational procedure

10.4.1 Basic assumptions

Load-deformation relations for columns subjected to combined axial load and flexure are obtained using the following assumptions.

- Plane sections remain plane after bending.
- Perfect bond between the longitudinal steel and the concrete is assumed thus it is possible to get the strain of the longitudinal steel as that of the surrounding concrete at the same distance from the neutral axis.
- In the tensile zone of the cross section, only tension steel resist the tensile forces and concrete does not resist any tensile force.

10.4.2 Methodology

Figure 10.3(a) shows the cross section details of the column considered in the analysis. The width and depth of the section are B and D respectively. It has m number of layers of longitudinal steel. The distance to the m^{th} layer from the top of the section is dr_m . For the purpose of the analysis, the section is divided into n number of horizontal strips (slices) as shown in Figure 10.3(b). The thickness of each strip, t will be,

$$t = \frac{D}{n} \quad (10.6)$$

Since the loading history is known, the curvatures are predefined. For a given curvature ϕ and an assumed top strain ε_t the strain distribution is known (Figure 10.3(c)). Consider the i^{th} strip at a distance d_i ,

$$d_i = (i - 0.5)t \quad (10.7)$$

from the top of the section. The average strain in this i^{th} strip will be,

$$\varepsilon_i = \varepsilon_t - \phi d_i \quad (10.8)$$

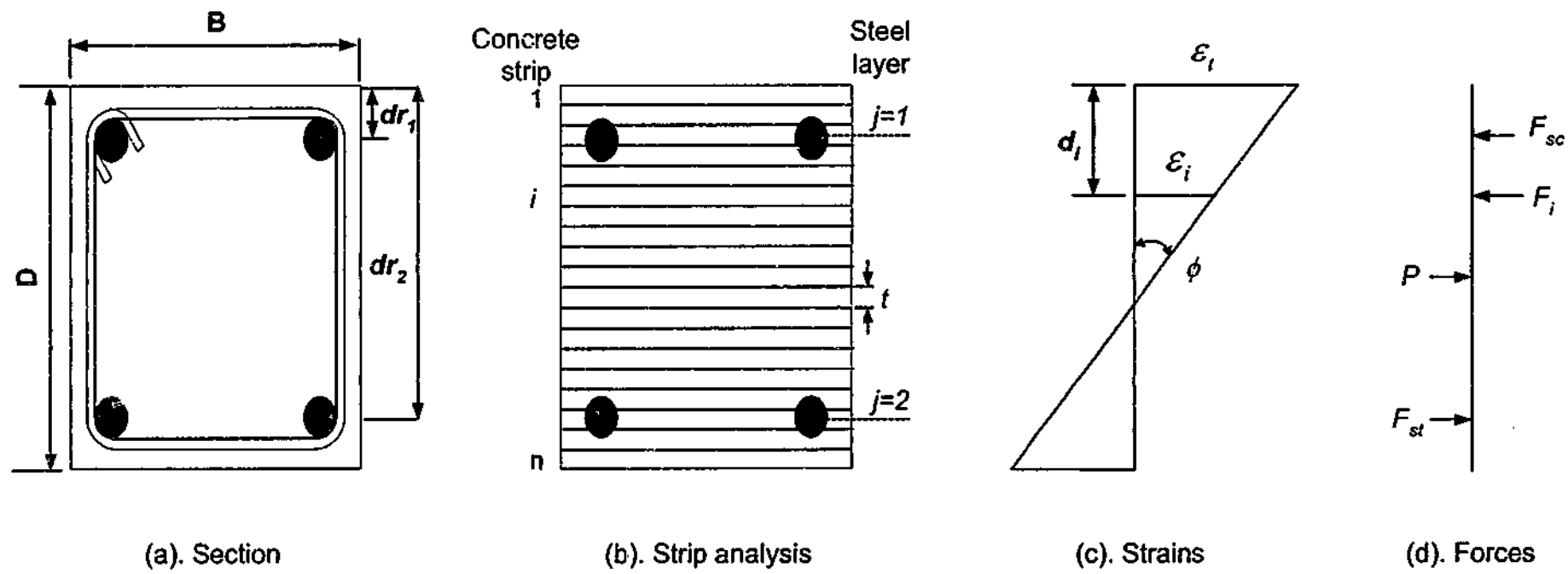


Figure 10.3 Basis for the column analysis

Each strip has confined concrete and unconfined concrete. Stresses in confined and unconfined concrete of these strips are calculated using the corresponding constitutive models that can depict the cyclic behaviour. Therefore force in each strip, F_i will be,

$$F_i = f_{i,con}A_{i,con} + f_{i,uncon}A_{i,uncon} \quad (10.9)$$

where $f_{i,con}$ and $f_{i,uncon}$ are the confined and unconfined concrete stresses and $A_{i,con}$ and $A_{i,uncon}$ are the areas of confined and unconfined concrete in the i^{th} strip. Summation of the forces in all the strips will result in the total force due to concrete, F_{cc} as,

$$F_{cc} = \sum_{i=1}^n F_i. \quad (10.10)$$

The strain corresponding to the j^{th} layer of longitudinal steel, ϵ_j can be calculated from the strain distribution,

$$\epsilon_j = \epsilon_t - \phi dr_j. \quad (10.11)$$

The stress corresponding to the strain in this layer of longitudinal steel, $f_{s,j}$ is then computed using the constitutive model for steel that has the ability to model the cyclic behaviour. If the total area of longitudinal steel in the j^{th} layer is $A_{s,j}$, the force can be calculated using,

$$F_{s,j} = f_{s,j}A_{s,j}. \quad (10.12)$$

Summation of all the forces in steel gives the total force due to steel,

$$F_{cs} = \sum_{j=1}^m F_{s,j}. \quad (10.13)$$

For force equilibrium shown in Figure 10.3(d),

$$P_{calc} = F_{cc} + F_{cs} \quad (10.14)$$

where P_{calc} is the calculated axial force. This calculated P_{calc} may not be the same as the actual axial load (P) because it is for a given ϕ and the assigned ϵ_t . Therefore a convergence algorithm is used to iterate ϵ_t until calculated axial load is sufficiently close enough to the actual axial load. Moment is then computed as follows:

$$M = \sum_{j=1}^m F_{s,j}dr_j + \sum_{i=1}^n F_i d_i. \quad (10.15)$$

The above procedure is performed for a series of deformation history of the section to obtain the moment-curvature relationships.

10.5 Computer program

10.5.1 General description

The computational procedure described in the previous section has been implemented in a computer program. The objective of the program is to establish the moment versus curvature relationships of confined concrete columns subjected to constant axial load and lateral load reversals. The constitutive models used for behaviour of concrete under monotonically increasing loading (modified to account for the envelope curve) and cyclic loading are explained in detail in Chapters 3 and 9 respectively. The model used for the cyclic behaviour of steel was the same as that used by Lim (1986). Chapter 6 gives a complete description of this steel model. The number of points to be plotted per cycle and the number of horizontal strips to be considered in the analysis can be specified as input parameters. The program is coded in Visual Basic. A general flowchart for the computer program is given in Figure 10.4 and the subroutines involved are described in the next section.

10.5.2 Program outline

The organisation of the subroutine library for analysis of columns subjected to constant axial load and cyclic lateral loads is shown in Figure 10.5. This section gives a detailed description of each subroutine.

Main initialises the input data, performs the necessary calculations and saves the final results to an output file. It includes the following subroutines.

- Initialise
- OptimumForce
- StoreResults

Initialise reads the input data for the column section details, properties of concrete, steel and initialises the parameters involved. The required information for the computer program is given using the user interface as shown in Figure 10.6. The input data are as follows:

- Section details

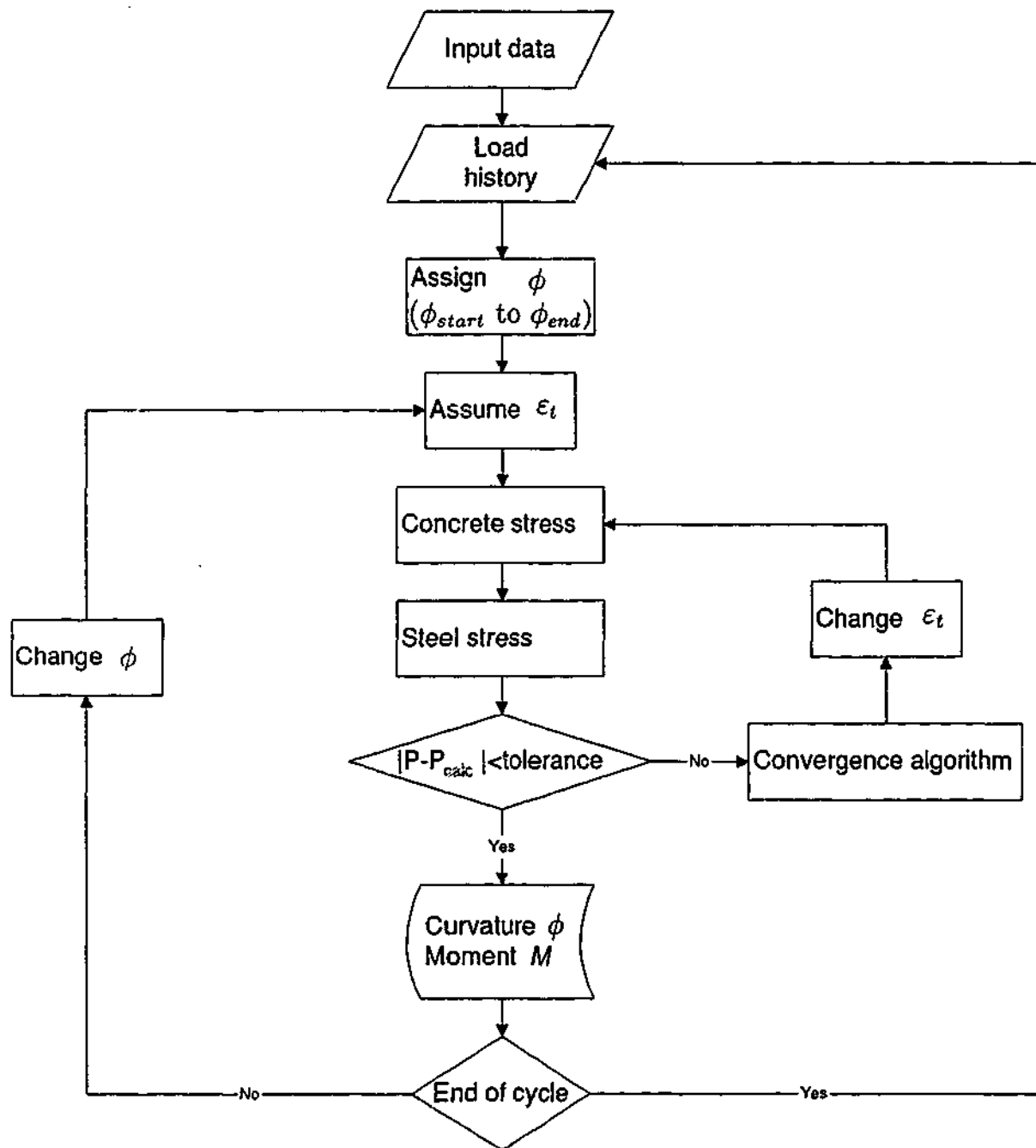


Figure 10.4: Flowchart for the column analysis.

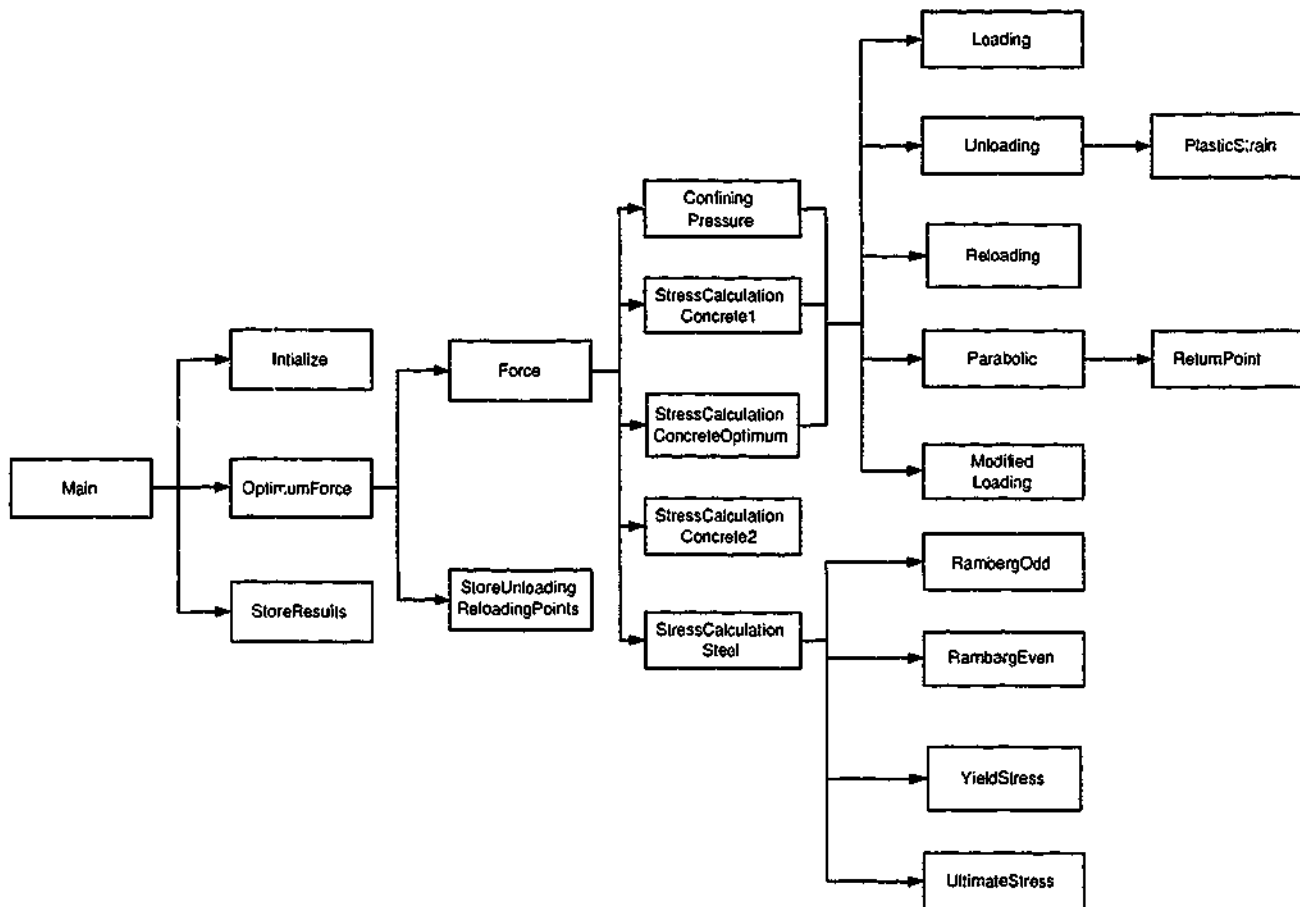


Figure 10.5: Structure of subroutines for the computer program.

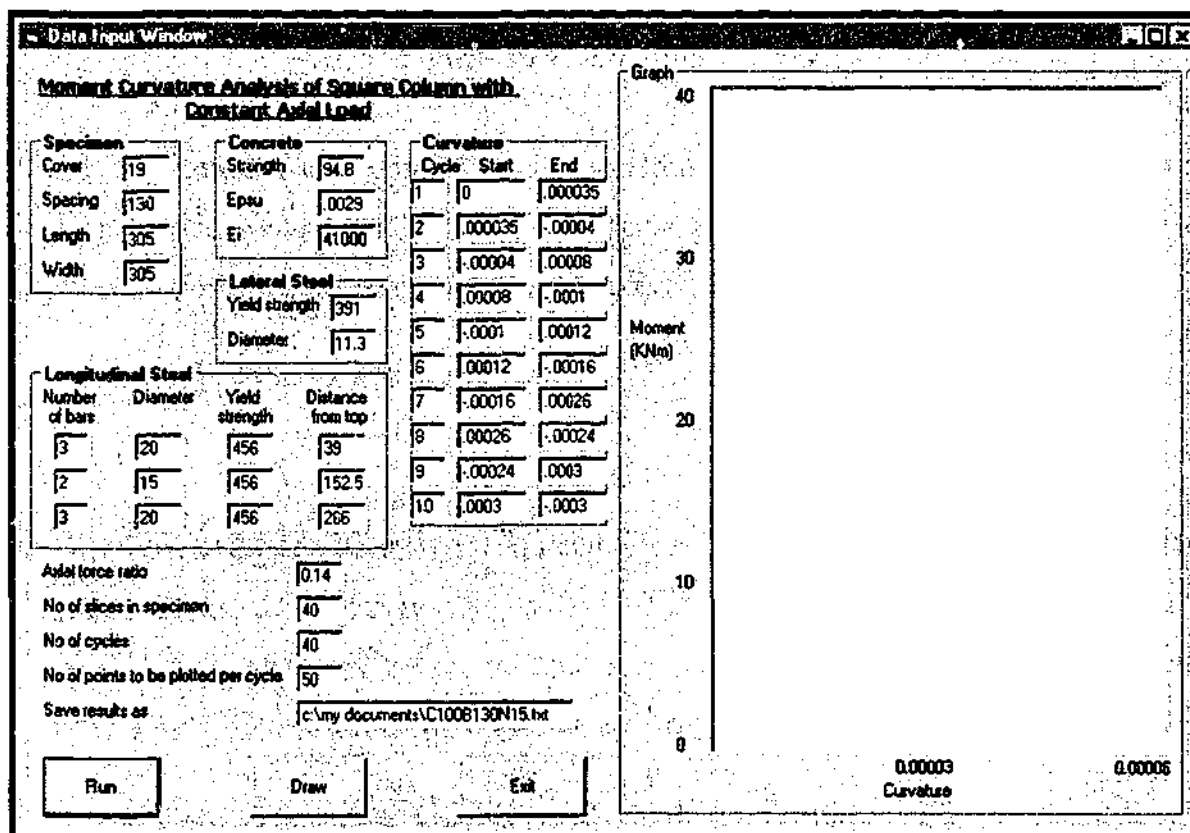


Figure 10.6: User interface.

- Properties of concrete
- Steel reinforcement (longitudinal and lateral) details
- Axial load
- Number of cycles and loading history (Figure 10.7)
- Number of slices in specimen cross section to be considered
- Number of points to be plotted per cycle
- File name for output results

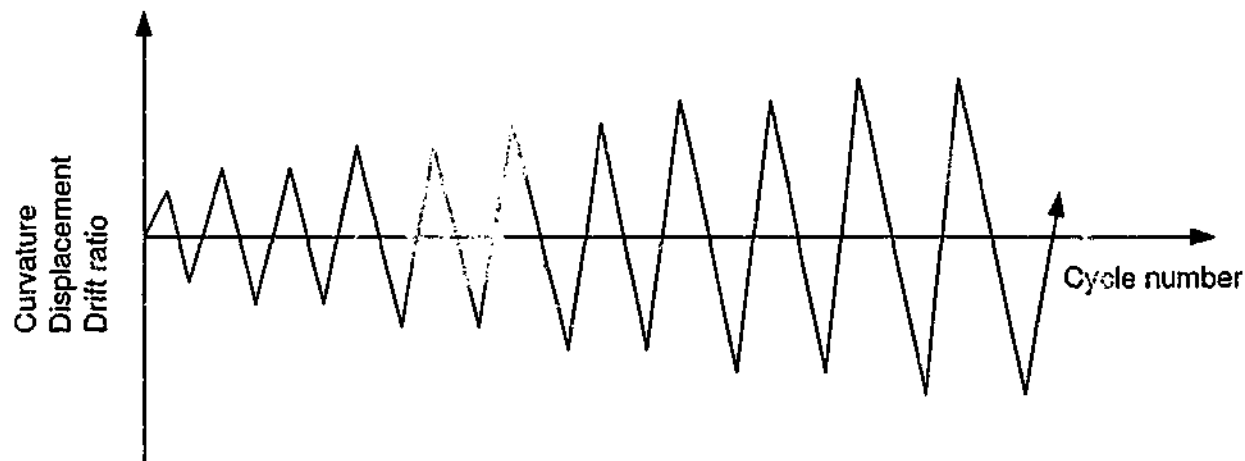


Figure 10.7: Loading history.

OptimumForce uses a convergence algorithm to calculate the axial load close enough to the given axial load. The optimisation procedure is explained in Figure 10.8. There are several other subroutines involved in this subroutine.

- StoreUnloadingReloadingPoints
- Force

StoreUnloadingReloadingPoints stores the stress and strain values after the optimisation, to utilise in the progress of loading, unloading or reloading of concrete. The storing procedure is done for each slice of concrete in the cross section considered. This subroutine consists of two phases:

- Storing coordinates of unloading point
- Storing coordinates of reloading point

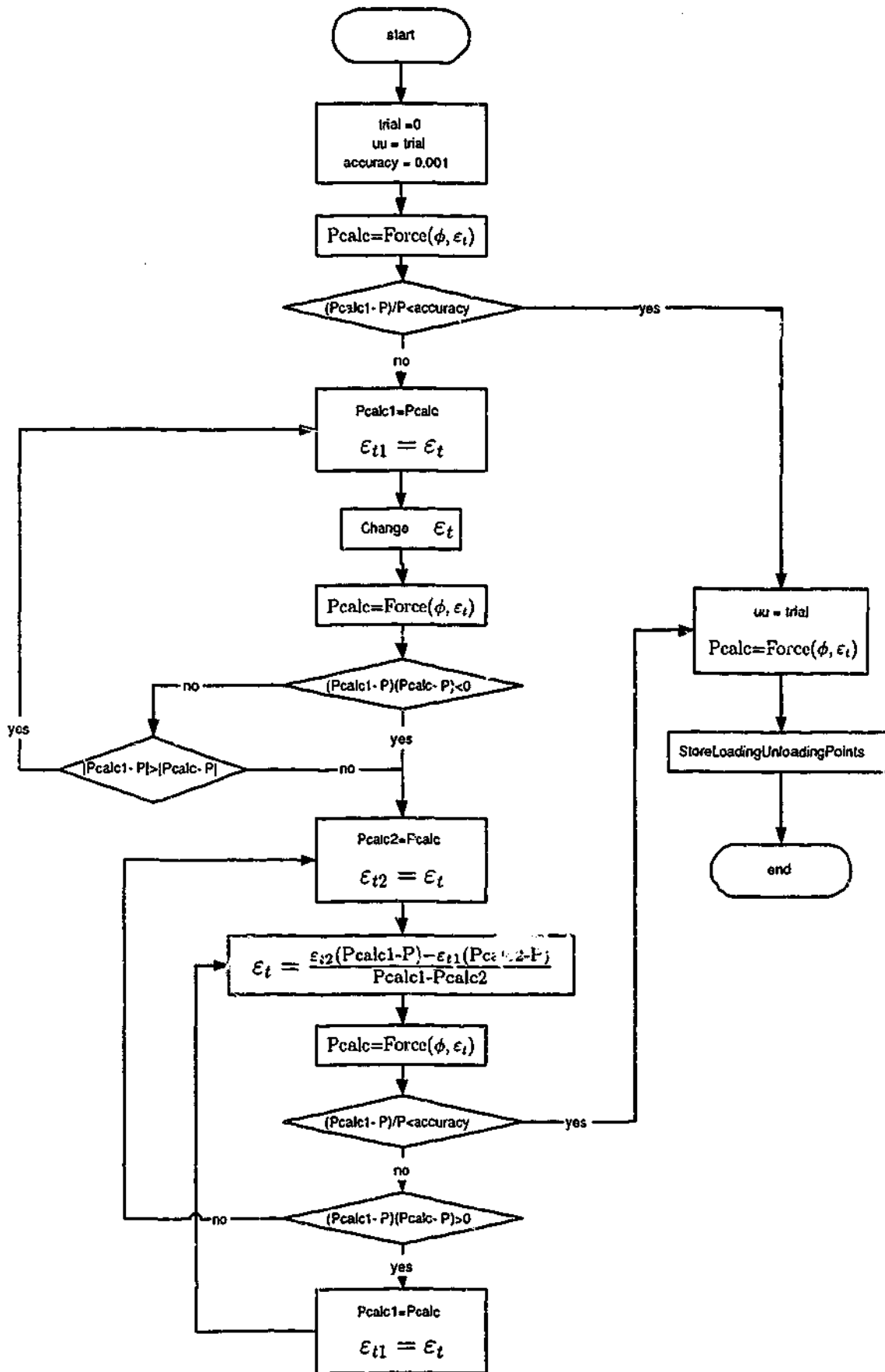


Figure 10.8: Convergence algorithm in finding axial load.

The procedure used to implement this is described in Figure 10.9. "cc" is a value used to differentiate the relevant loading path ("cc"=1 means the unloading path), $(\epsilon_{un}, \sigma_{un})$ is the unloading point, $(\epsilon_{ro}, \sigma_{ro})$ is the reloading point and p is the current loop considered. For example $\epsilon(i, p)$ is the strain in the i^{th} slice in loop p .

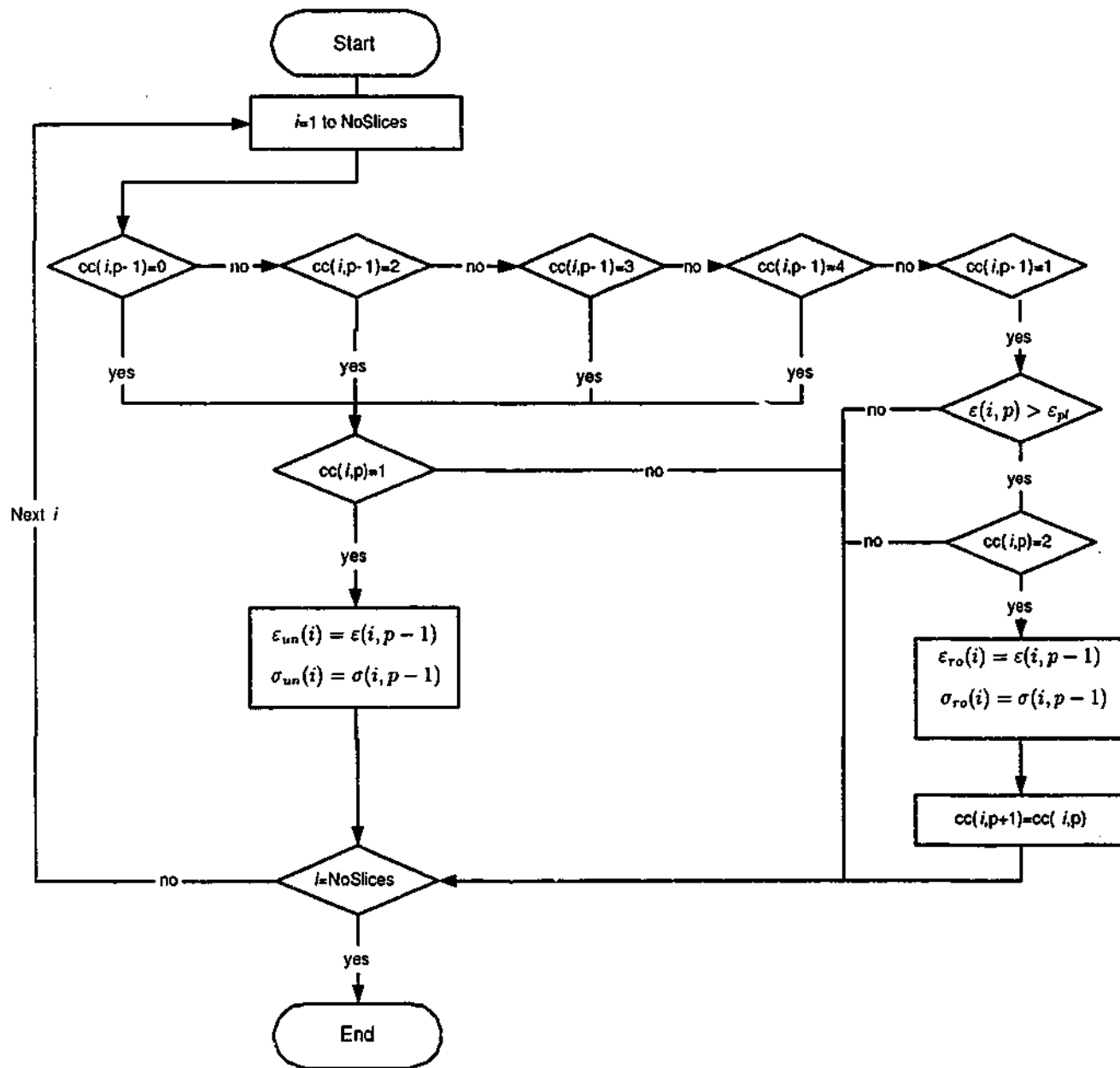


Figure 10.9: Storing unloading and reloading coordinates.

Force utilises the constitutive models for concrete and steel and calculates the concrete stress in each slice of the section and steel stress in each layer of steel. There are few other subroutines inside this subroutine to perform these.

- ConfiningPressure

- StressCalculationConcrete1
- StressCalculationConcreteOptimum
- StressCalculationConcrete2
- StressCalculationSteel

Figure 10.10 shows the process of the force calculations. i denotes the i^{th} slice of concrete, j denotes the j^{th} layer of steel, $f_{sy}(j)$ and $F_{su}(j)$ are the yield and ultimate stresses corresponding to the j^{th} layer of steel. $ENXConf$, $ENXUnconf$ are the force due to confined, unconfined concrete in each slice. $ENSteel$ and $EMSteel$ are the force and moment resulting from the j^{th} layer of steel. EN and EM are the resultant force and the moment.

ConfiningPressure computes the confining pressure exerted by the lateral reinforcement. Lateral strains in each slice of concrete is calculated from the constitutive model proposed earlier. Resulting strain in lateral steel is computed using these strains. The confining pressure corresponding to this strain can be computed using the constitutive model for lateral steel.

StressCalculationConcrete1 calculates the stresses in each slice of concrete using the constitutive models for monotonically increasing load and cyclic load. Loading, unloading, reloading, parabolic and modified loading are differentiated using the "cc" values. Figure 10.11 shows "cc" values corresponding to each loading path. The calculation is based on the "cc" value of the previous loop. It is assumed that the "cc" value for the current loop will follow the previous loading path. This is composed of the following subroutines.

- Loading
- Unloading
- Reloading
- Parabolic
- ModifiedLoading

The selection of the loading path according to the "cc" values is given in Figure 10.12.

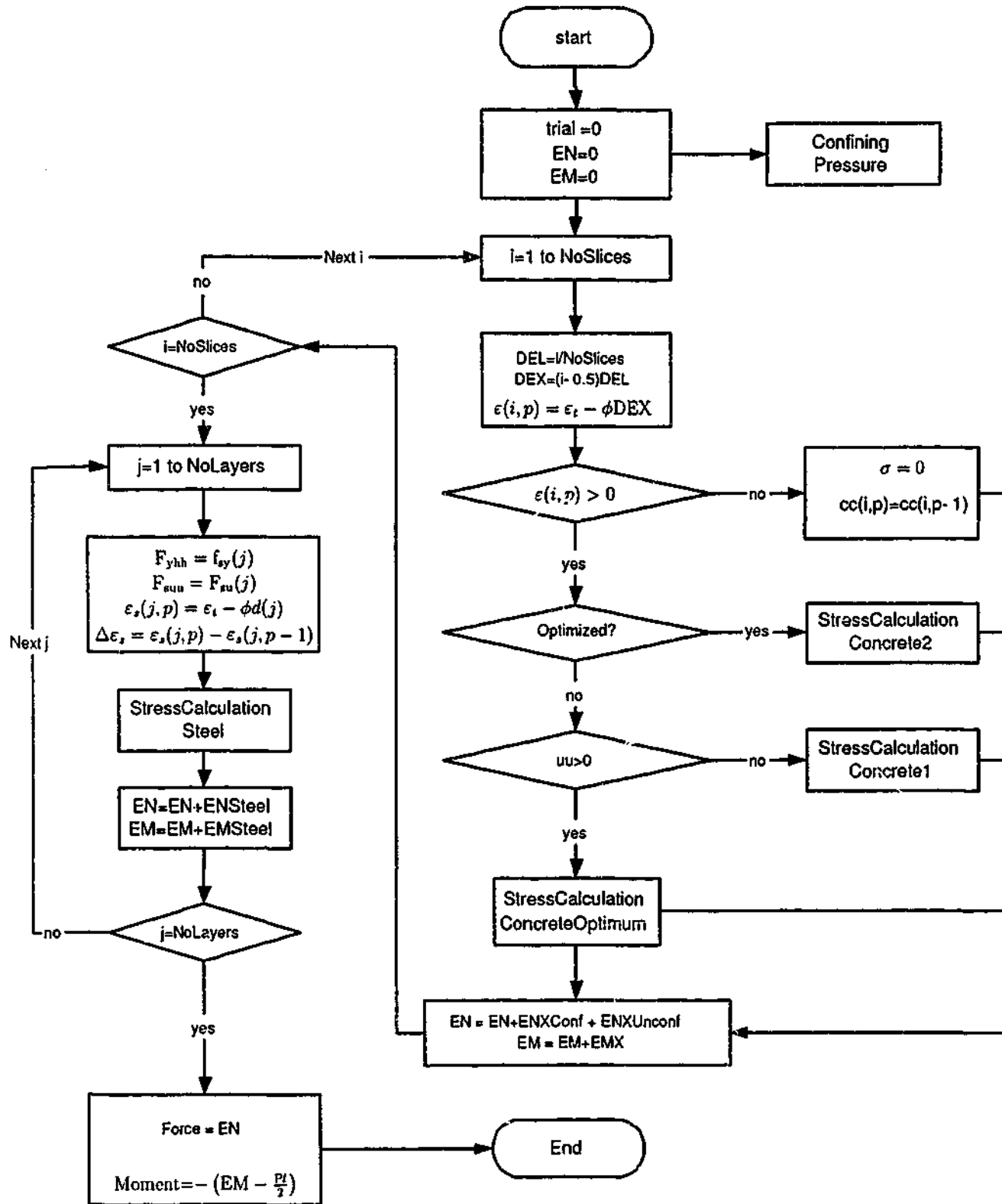


Figure 10.10: Axial load calculation.

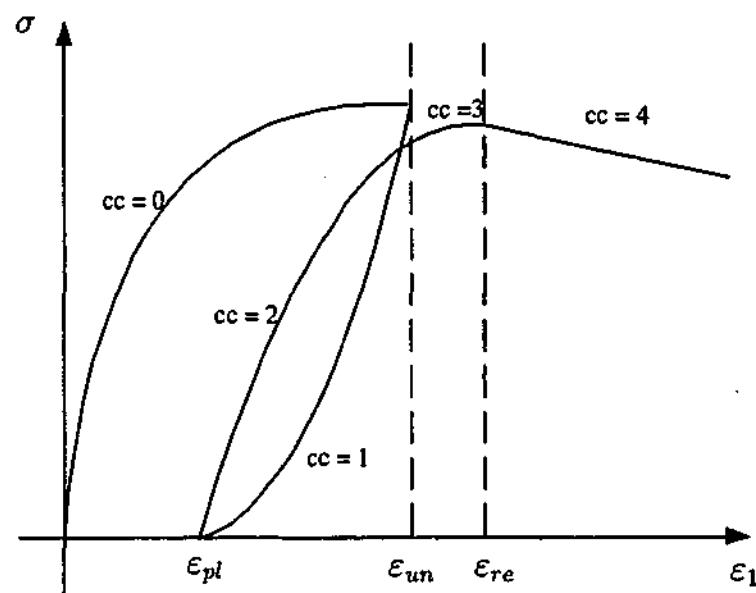


Figure 10.11: "cc" values for each loading path in concrete.

StressCalculationConcreteOptimum uses the same subroutines as in subroutine **StressCalculationConcrete1** and calculates the stresses in each slice of concrete. Calculations are based on the "cc" values of the previous loop but they are updated for the current loop with the optimised values in this subroutine. The procedure used in updating the "cc" values is shown in Figure 10.13.

StressCalculationConcrete2 uses the "cc" values of the current loop defined in subroutine **StressCalculationConcreteOptimum** for the optimised values. It calculates the final optimum stresses in each slice of concrete.

Loading computes the stress in concrete using the constitutive model for monotonically

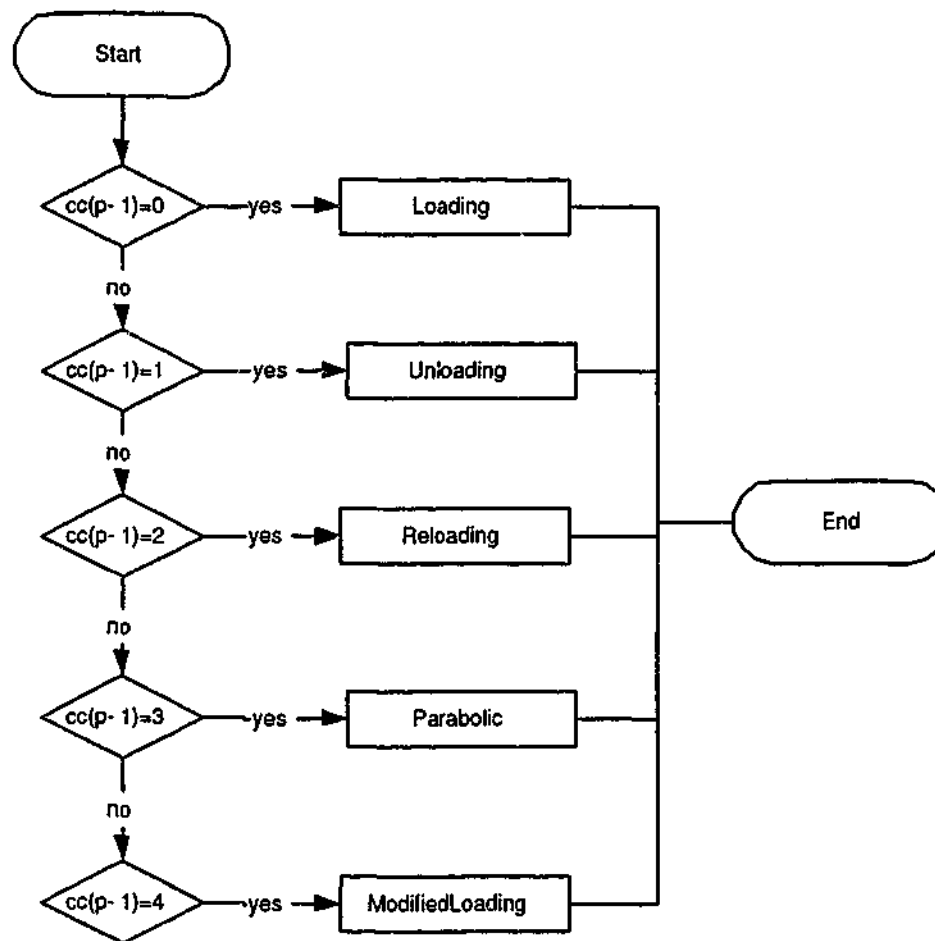


Figure 10.12: Determination of stress in concrete from different loading paths.

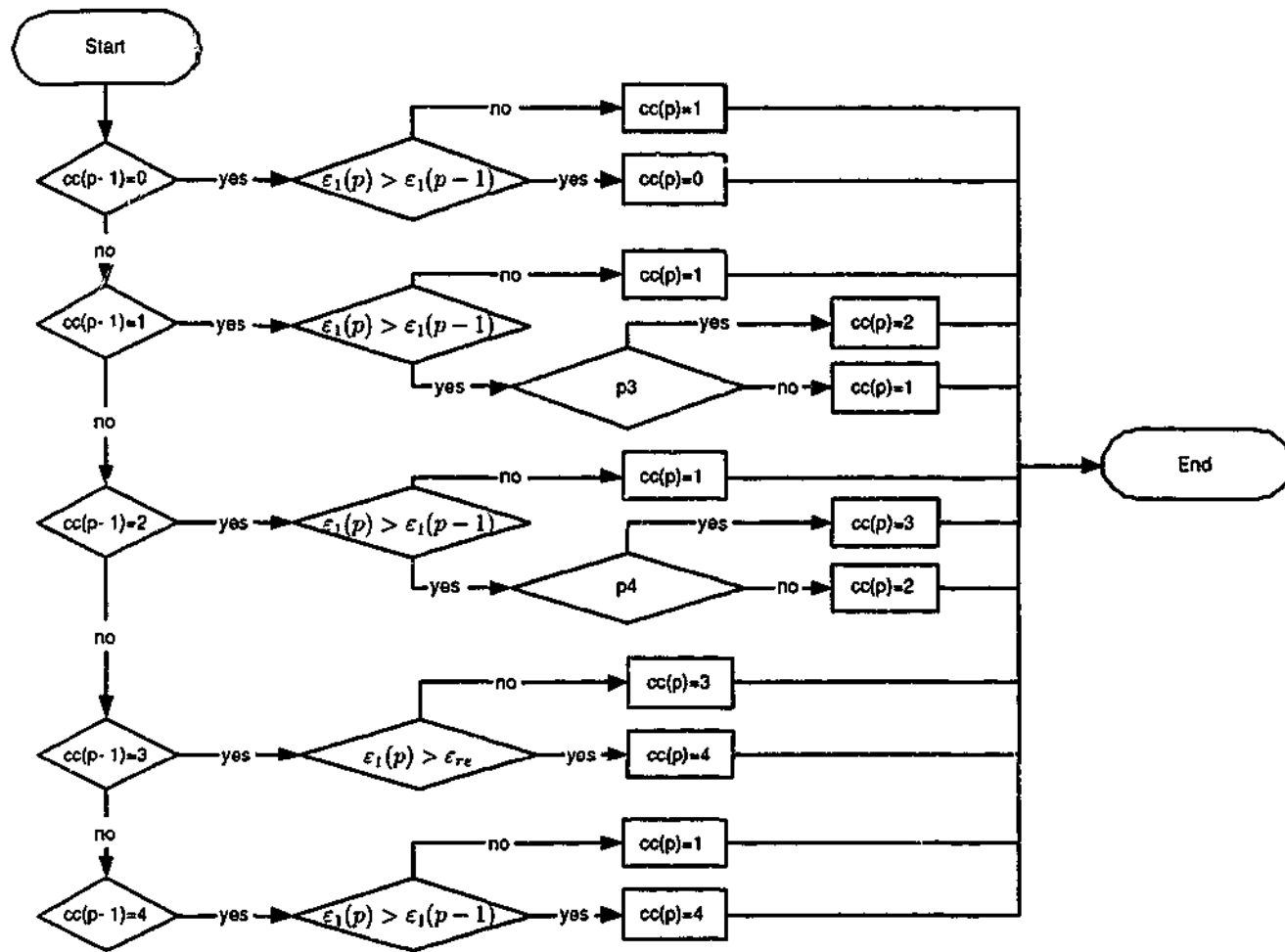


Figure 10.13: Assigning the loading path for each slice of concrete.

increasing load, described in Chapter 3. The ascending branch is defined as follows:

$$\sigma_1 = 2\tau_{mp} \left[1 - e^{-m_2 \left(\frac{\epsilon_1 + \epsilon_2}{2\gamma_{mp}} \right)} \right] + f_l$$

$$\tau_{mp} = \frac{f_{cc} - f_l}{2} \quad \text{and} \quad \gamma_{mp} = \frac{\epsilon_{cc} + \epsilon'_{cc}}{2}$$

$$m_2 = -0.0427f_c + 7.7381$$

$$\frac{f_{cc}}{f_c} = \left(\frac{f_l}{f_c} + 1 \right)^k$$

$$k = 1.25 \left(1 + 0.062 \frac{f_l}{f_c} \right) (f_c)^{-0.21}$$

$$f_l = 0.288(f_c)^{0.67}$$

$$\frac{\epsilon_{cc}}{\epsilon_{cc}'} = 1 + (17 - 0.06f_c) \left(\frac{f_l}{f_c} \right)$$

$$\epsilon_{cc}' = 0.5\epsilon_{cc}$$

$$\nu_i^a = 0.15$$

$$\frac{\epsilon_2}{\epsilon_{cc}'} = \begin{cases} \nu_i^a \left(\frac{\epsilon_1}{\epsilon_{cc}'} \right) & \text{if } \epsilon_1 \leq \epsilon_{cc}', \\ \left(\frac{\epsilon_1}{\epsilon_{cc}'} \right)^{m_1} & \text{if } \epsilon_1 > \epsilon_{cc}' \end{cases}$$

$$m_1 = 0.0177f_c + 1.2818$$

Unloading uses another subroutine to calculate the plastic strains for each slice. Concrete stresses are calculated for each slice using the coordinates of unloading point (stored in subroutine StoreUnloadingReloadingPoints) and plastic strain. The stress calculation is performed only for the strains greater than the plastic strain. If the

strain is less than the plastic strain, the stress is zero.

$$\begin{aligned}\bar{\tau}_{un} &= 0.43(e^{1.2\bar{\gamma}_{un}} - 1) \\ \bar{\tau}_{un} &= \frac{\tau - \tau_{pl}}{\tau_{un} - \tau_{pl}} \quad \text{and} \quad \bar{\gamma}_{un} = \frac{\gamma - \gamma_{pl}}{\gamma_{un} - \gamma_{pl}} \\ \tau &= \frac{\sigma_1 - f_l}{2} \quad \text{and} \quad \gamma = \frac{\epsilon_1 + \epsilon_2}{2} \\ \bar{\epsilon}_{1,un} &= \frac{\epsilon_1 - \epsilon_{1,pl}}{\epsilon_{1,un} - \epsilon_{1,pl}} \quad \text{and} \quad \bar{\epsilon}_{2,un} = \frac{\epsilon_2 - \epsilon_{2,pl}}{\epsilon_{2,un} - \epsilon_{2,pl}} \\ \bar{\epsilon}_{2,un} &= \bar{\epsilon}_{1,un}^{1/q} \\ q &= -0.0035f_c + 1.445\end{aligned}$$

PlasticStrain evaluates the residual strain during unloading using the method proposed by Mander et al. (1988b).

$$\epsilon_a = a\sqrt{\epsilon_{1,un}\epsilon_{cc}}$$

The value of a will be the greater of either

$$a = \frac{4\epsilon_{cc}}{\epsilon_{cc} + \epsilon_{1,un}} \quad \text{or} \quad \frac{0.09\epsilon_{1,un}}{\epsilon_{cc}}$$

and,

$$\begin{aligned}\epsilon_{pl} &= \frac{(\epsilon_{un} + \epsilon_a)\sigma_{un}}{(\sigma_{un} + E_c\epsilon_a)} \\ E_c &= 0.043\rho^{1.5}\sqrt{f_{cm}}\end{aligned}$$

Reloading determines the reloading stress for each slice of concrete using the corresponding plastic strain. Reloading path is confined to a strain range which should be greater than plastic strain and less than unloading strain. But the upper limit can be less than the unloading strain for the case of partial reloading.

$$\begin{aligned}\sigma_{new} &= 0.92\sigma_{un} + 0.08\sigma_{ro} \\ \bar{\tau}_{re} &= \sqrt{2}\log_e(\bar{\gamma}_{re} + 1) \\ \bar{\tau}_{re} &= \frac{\tau - \tau_{pl}}{\tau_{new} - \tau_{pl}} \quad \text{and} \quad \bar{\gamma}_{re} = \frac{\gamma - \gamma_{pl}}{\gamma_{new} - \gamma_{pl}} \\ \bar{\epsilon}_{1,re} &= \frac{\epsilon_1 - \epsilon_{1,pl}}{\epsilon_{1,new} - \epsilon_{1,pl}} \quad \text{and} \quad \bar{\epsilon}_{2,re} = \frac{\epsilon_2 - \epsilon_{2,pl}}{\epsilon_{2,new} - \epsilon_{2,pl}} \\ \bar{\epsilon}_{2,re} &= \bar{\epsilon}_{1,re}^q\end{aligned}$$

Parabolic uses another subroutine to calculate the return point in the envelope curve.

Parabolic curve is defined from the unloading strain upto the return strain in the envelope curve.

$$\begin{aligned}\sigma_1 &= \sigma_{re} + E_{re}g + Ag^2 \\ g &= \epsilon_1 - \epsilon_{re} \\ A &= \frac{(\sigma_{new} - \sigma_{re}) - E_{re}(\epsilon_{un} - \epsilon_{re})}{(\epsilon_{un} - \epsilon_{re})^2}\end{aligned}$$

ReturnPoint calculates the return point coordinates of the parabolic curve.

$$\begin{aligned}\epsilon_{re} &= \epsilon_{un} + \frac{(\sigma_{un} - \sigma_{new}) \times \left(2 + \frac{f_{cc}}{f_c}\right)}{E_{ro}} \\ E_{ro} &= \frac{\sigma_{ro} - \sigma_{new}}{\epsilon_{ro} - \epsilon_{un}} \\ \sigma_{re} &= (1 - 0.01n)\sigma_{1,p}\end{aligned}$$

ModifiedLoading computes the concrete stress in each slice for strain values greater than that at the return point until another unloading takes place.

$$\begin{aligned}\sigma_1 &= (1 - 0.01n)\sigma_{1,p} \\ \sigma_{1,p} &= 2\tau_{mp} \left(e^{m_3 \left(\frac{\epsilon_1 + \epsilon_2}{2\gamma_{mp}} \right)^2} - m_3 \right) + f_l \\ m_3 &= -0.0003f_c - 0.0057\end{aligned}$$

StressCalculationSteel computes the stress in each steel layer using the constitutive model described earlier. It uses the following subroutines.

- RambergOdd
- RambergEven
- YieldStress
- UltimateStress

The status of the steel layer (whether it is in linear or non linear section) is defined using the parameter "mm". Figure 10.14 shows the "mm" values corresponding to each loading path in steel.

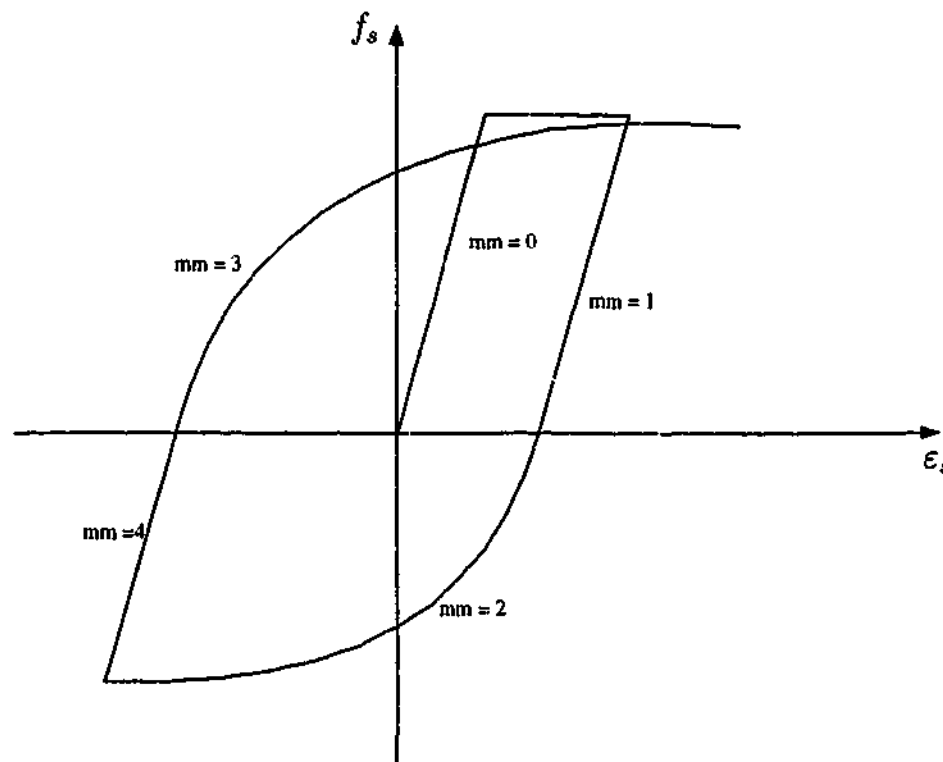


Figure 10.14: "mm" values for each loading path in steel.

The procedure used in updating the parameter, "mm" is shown in Figure 10.15. ϵ_s is the steel strain and $\Delta\epsilon(p)$ is the subtraction of the steel strain corresponding to the previous loop ($p - 1$) from that at the current loop (p). $(\epsilon_{un,s}, f_{un,s})$ is the steel unloading point and f_s is the steel stress. The general procedure used in evaluating the stresses in each steel layer is shown in Figure 10.16.

RambergOdd calculates the stress in the nonlinear loading path corresponding to the "odd" loading runs in steel.

$$\epsilon_s - \epsilon_{si} = \frac{f_s}{E_s} \left(1 + \left| \frac{f_s}{f_{ch}} \right|^{r-1} \right)$$

$$f_{ch} = f_y \left[\frac{0.744}{\ln(1 + 1000\epsilon_{ip})} - \frac{0.071}{1 - \exp(1000\epsilon_{ip})} + 0.241 \right]$$

$$r_{odd} = \frac{4.489}{\ln(n + 1)} - \frac{6.026}{\exp(n) - 1} + 0.297$$

RambergEven calculates the stress in the nonlinear loading path corresponding to the "even" loading runs in steel.

$$r_{even} = \frac{2.197}{\ln(n + 1)} - \frac{0.469}{\exp(n) - 1} + 3.043$$

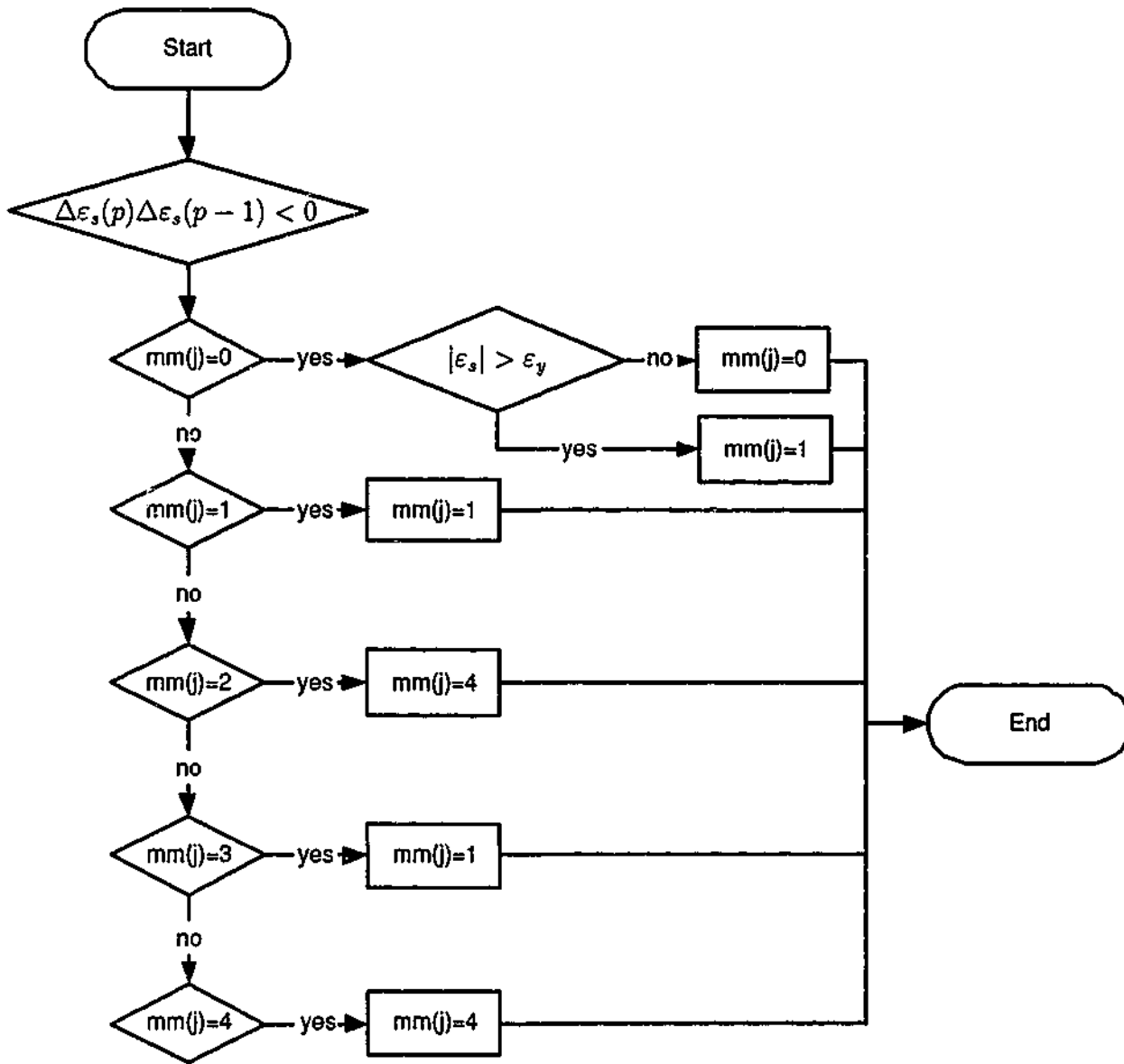


Figure 10.15: Assigning the loading path for each layer of steel.

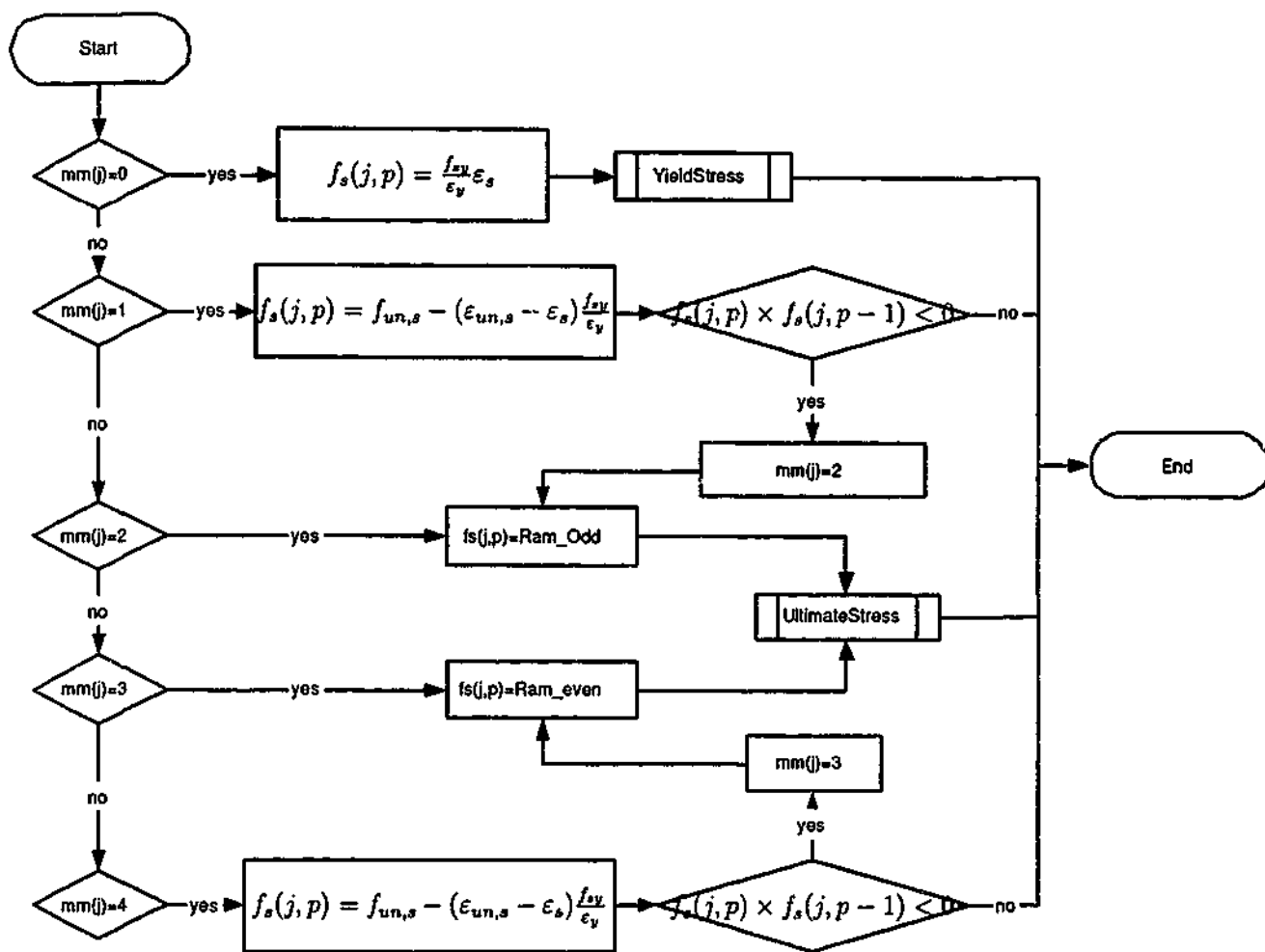


Figure 10.16: Procedure used in calculating steel stresses.

YieldStress defines the yielding of longitudinal steel.

UltimateStress defines the upper limit for the steel stress.

StoreResults stores the output results from the program in a user specified text file which can be opened in Excel spread sheet and the following relationships can be plotted using it.

- Moment-curvature (load-displacement)
- Stress-strain for any concrete layer
- Stress-strain for each of the steel layers

10.6 Comparison with experimental results

Four of the six columns reported by Legeron and Paultre (2000) have been selected in this study to validate the proposed methodology because of the high compressive strengths (100 MPa) and large column sizes (350 × 350 mm). However, the comparison is also extended for a comparatively small column (200 × 200 mm) reported by Matamoros and Sozen (2003) with 70 MPa compressive strength as it was the most recent study documented on similar investigation.

10.6.1 Experimental program

Legeron and Paultre (2000) reported experimental results for the behaviour of six confined concrete columns with constant axial load and cyclic flexure. The compressive strength of the tested large scale columns (305 × 305 mm) was in the range of 92-104 MPa.

Each specimen was given a name, which relates to the strength, reinforcement arrangement, the spacing of lateral reinforcement and the axial load level. For example, the specimen C100B60N15 represents a 100 MPa concrete column with the lateral reinforcement arrangement "B", having a centre-to-centre tie spacing of 60 mm and subjected to a axial load level of 15% of the column capacity. The dimensions and details of the reinforcement arrangements for the tested columns are given in Table 10.1(a) and Figure 10.17(a). Dimension "B" was 305 mm in Legeron and Paultre (2000) study. No. 20 (diameter 19.5 mm and yield strength 451 MPa) and No. 15 bars (diameter 16 mm and

yield strength 494 MPa) were used as longitudinal reinforcement. No. 10 bars (diameter 11.3 mm and yield strength 391 MPa) were used as lateral reinforcement.

A specifically designed frame was used by Legeron and Paultre (2000) to test the specimens. The axial load was applied using high strength bars tensioned by hydraulic jacks. The horizontal load was applied using an actuator at the tip of the specimen, 2 m from base of the column. The specimen represents a 4 m high column in a building. The horizontal tip displacement was measured using LVDT. Legeron and Paultre (2000) reported experimental results for horizontal load and tip displacement relationships.

Recently Matamoros and Sozen (2003) reported experimental investigations for the similar behaviour of confined concrete. Columns were made of NSC (35 MPa) and HSC (69 MPa) and had cross section of 200 × 200 mm (dimension "B" in Figure 10.17(b)). The experimental variables were the axial load, loading history and compressive strength of concrete. The specimens were named according to the compressive strength of concrete and the applied axial load level. For example C7010 specimen used 70 MPa concrete and the applied constant axial load was about 10% of the column capacity. The dimensions and the details of the reinforcement arrangements for the tested columns are given in Table 10.1(b) and Figure 10.17(b). No. 5 bars with yield strength of 585 MPa was used as longitudinal reinforcement while No. 3 bars with yield strength 400 MPa was used as lateral reinforcement. The lateral reinforcement ratio was 1%. The amount and distribution of lateral reinforcement was the same for all the specimens. The specimens were designed to simulate a beam column connection. They presented the experimental results in the form of moment-curvature relationships and load-displacement relationships.

The computer program described in Section 10.5 establishes moment-curvature curves. Since Legeron and Paultre (2000) presented the experimental results as force versus displacement relationships, it is necessary to translate the predicted moment versus curvature relationships into force versus displacement relationships. The section below describes how this is performed.

10.6.2 Load versus displacement relationship

Figure 10.18 shows a typical column used in the previous experimental investigations. The stub represents rigid member such as a beam-column joint or a slab foundation. The specimen represents a column with a height of $2L$ in a typical building where the point of

Table 10.1: Details of test specimens.
 (a) Legeron and Paultre (2000) experiments

Specimen	f_c (MPa)	Spacing (mm)	$\frac{F}{A_g f_c}$
C100B60N15	92.4	60	0.14
C100B130N15	94.8	130	0.14
C100B130N25	97.7	130	0.26
C100B130N40	104.3	130	0.39

(b) Matamoros and Sozen (2003) experiments

Specimen	f_c (MPa)	Spacing (mm)	$\frac{F}{A_g f_c}$
C7010	70	75	10

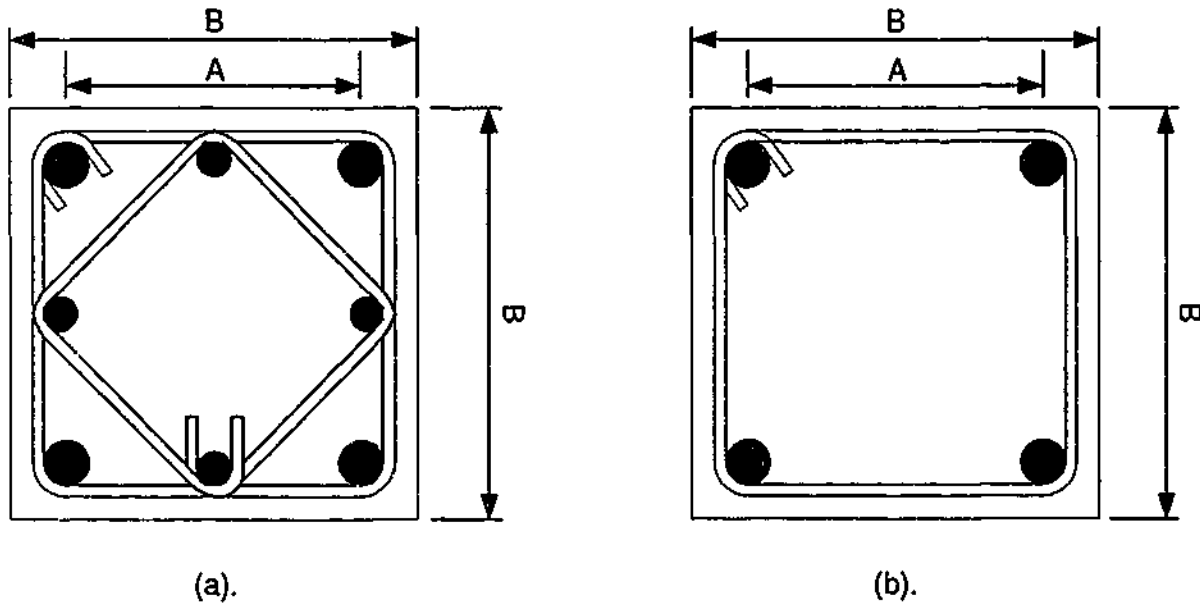


Figure 10.17: Details of column specimens.

contraflexure is assumed to be at the mid height level. Constant axial load, P is applied at the tip of the specimen. F is the horizontal load, L is the column height from the base and l_p is the plastic hinge length. A critical section at the mid height of the plastic hinge length has been selected for the analysis.

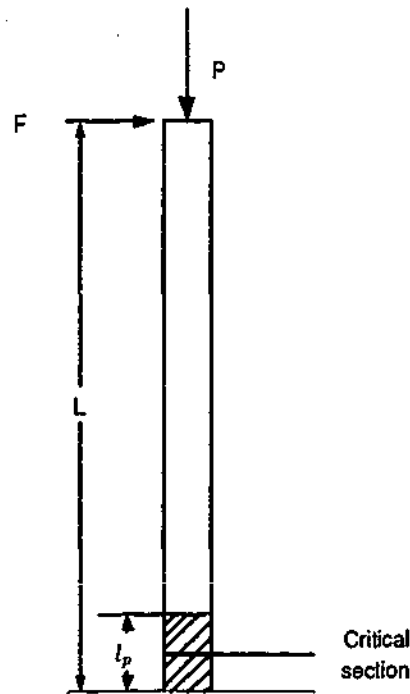


Figure 10.18: Typical column section used in the analysis.

When the column is subjected to axial load and lateral forces, it deflects horizontally. It is assumed that flexural deformation consists of two parts as shown in Figure 10.19. Δf_1 is the displacement due to the rotation of plastic hinge and Δf_2 is displacement due to elastic bending of the column along its length. Δf_1 can be calculated as follows:

$$\Delta f_1 = \theta \left(L - \frac{l_p}{2} \right). \quad (10.16)$$

θ can be defined in terms of curvature (ϕ) and plastic hinge length (l_p).

$$\theta = \phi \times l_p. \quad (10.17)$$

The elastic bending of column along its length is similar to the behaviour of a cantilever subjected to a vertical force at the free end. Δf_2 can be defined as,

$$\Delta f_2 = \frac{F(L - l_p)^3}{3(EI)_{eff}}. \quad (10.18)$$

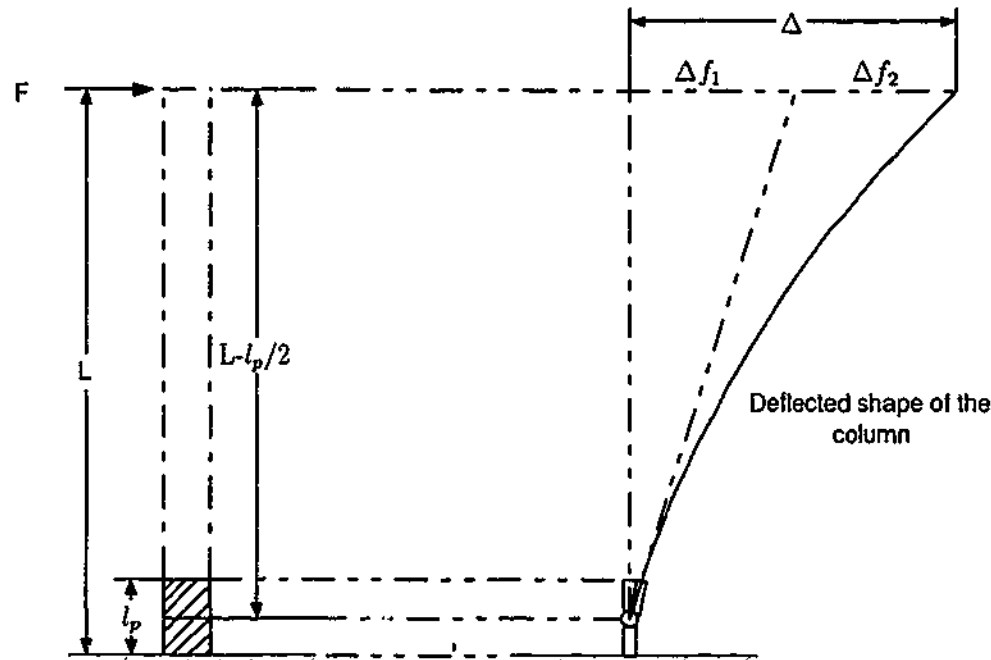


Figure 10.19: Curvature and displacement relationships.

Therefore the total displacement (Δ) is,

$$\begin{aligned} \Delta &= \Delta f_1 + \Delta f_2 \\ &= \phi \times l_p \left(L - \frac{l_p}{2} \right) + \frac{F(L - l_p)^3}{3(EI)_{eff}} \end{aligned} \quad (10.19)$$

The relationship between the horizontal load (F) and moment (M) is as follows:

$$M = F \left(L - \frac{l_p}{2} \right). \quad (10.20)$$

In the reported experimental programs for the flexural behaviour of columns subjected to constant axial load and cyclic flexure, load history is specified either by the displacement limits or the drift ratio limits. Using the procedure described here, the moment versus curvature relationships obtained from the computer program described in Section 10.5, can be converted to load (Equation 10.20) versus displacement (Equation 10.19) relationships.

Plastic hinge lengths assumed for the calculations are shown in Table 10.2 for each specimen.

10.6.3 Predicted and experimental behaviour

The predicted behaviour for the selected columns are shown in Figures 10.20-10.24. They were obtained using the computer program described in Section 10.5. The digital data for

Table 10.2: Plastic hinge length for selected specimens.

Specimen	Hinge length (mm)
C7010	100
C100B60N15	205
C100B130N15	185
C100B130N25	315
C100B130N40	600

the experimental results were not available for the author. Superimposing the experimental and predicted behaviour was not performed due to the confusion with too many lines. Instead the experimental result is shown separately as part "a" and predicted behaviour is shown as part "b" of each figure.

10.6.4 Discussion

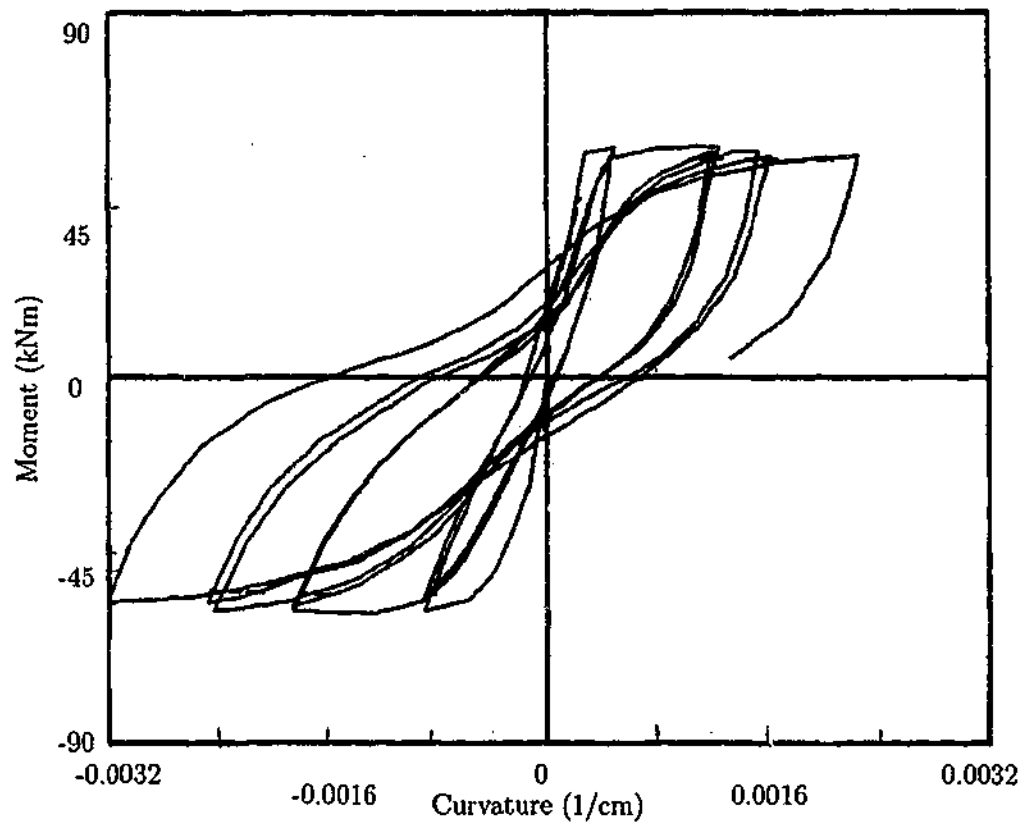
C7010 specimen

The predicted moment-curvature relationship shown in Figure 10.20(b) for C7010 column compares fairly well with the experimental results in terms of maximum moments, general shape of the curve and the strength deterioration in each cycle.

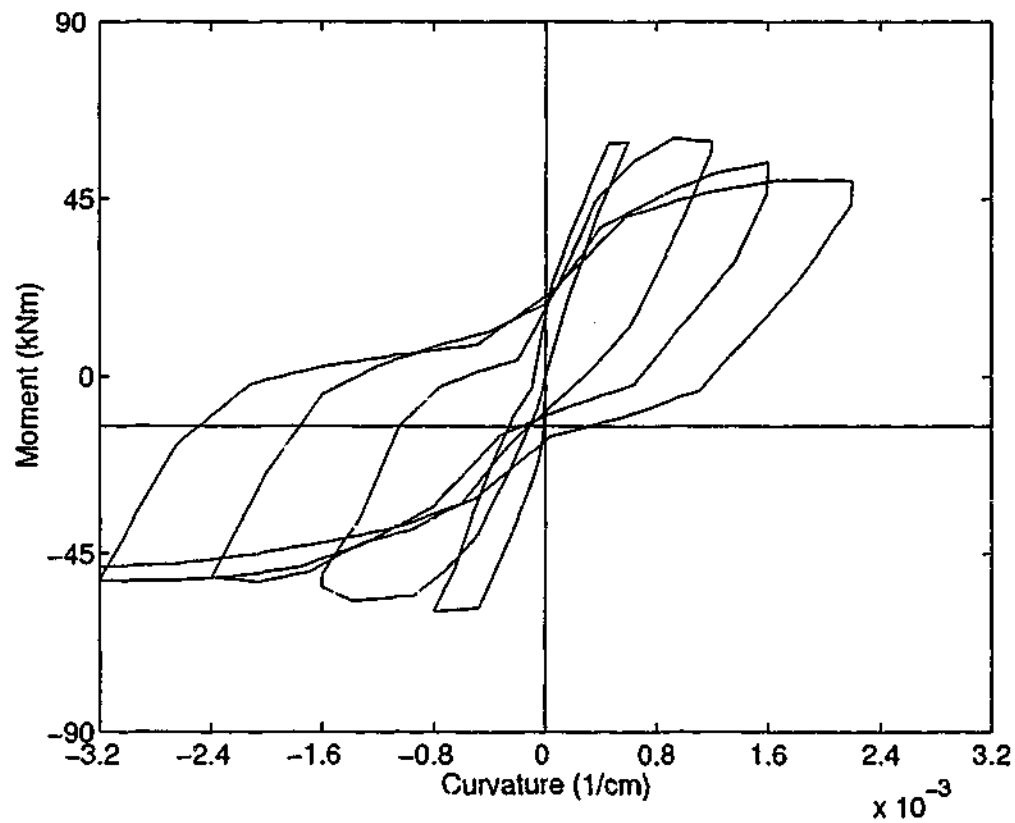
However, pinching is more pronounced in the predicted results than the experimental results. The predicted initial descending slopes were almost the same as experimental results. With the increasing number of cycles, the descending slope of the experimental curve becomes steeper than that of the predicted curve.

C100B60N15 specimen

Although in the predicted behaviour, the general shape, pinching and maximum horizontal loads agree with the experimental results for column C100B60N15 (Figure 10.21), the displacements are underestimated in the predicted curve. It may be due to the approximate method (Section 10.6.2) used to convert the moment-curvature relationships to load-displacement relationships. Furthermore, the displacement is sensitive to the assumed plastic hinge length and this may be another reason. The descending slopes of the experimental curve is higher for higher displacements than those for the predicted curve. With accurate information on plastic hinge length, the procedure would yield

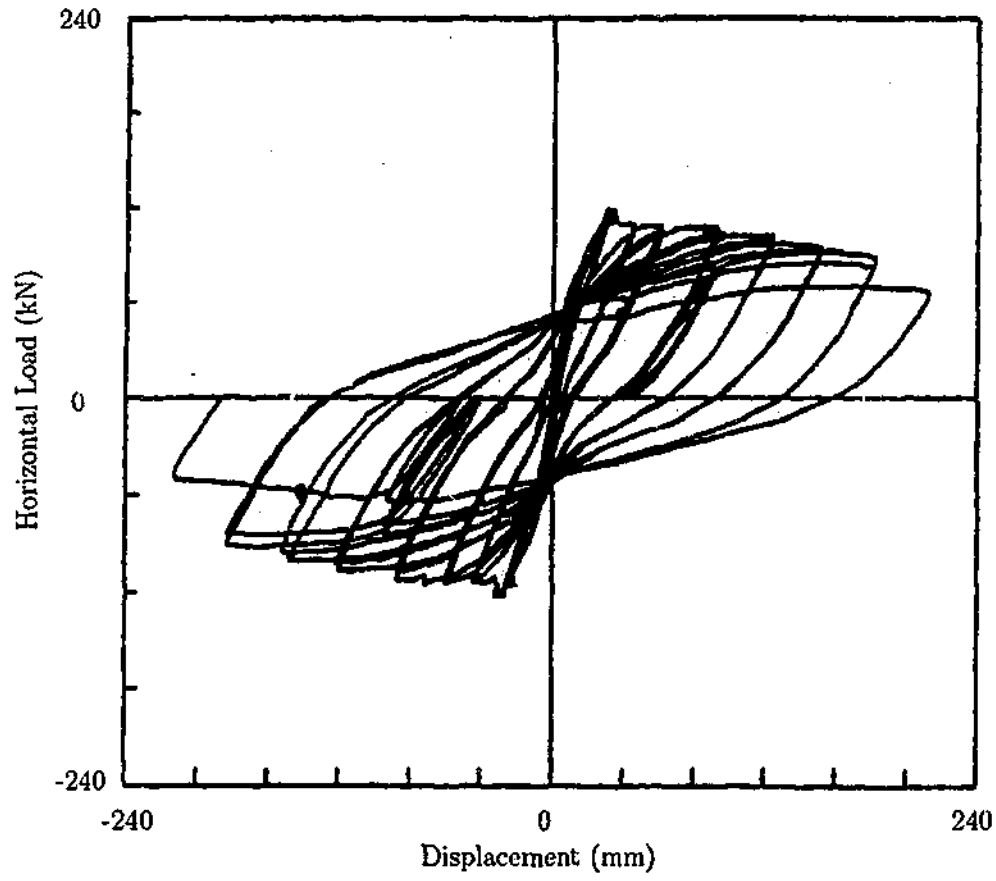


(a). Experimental results

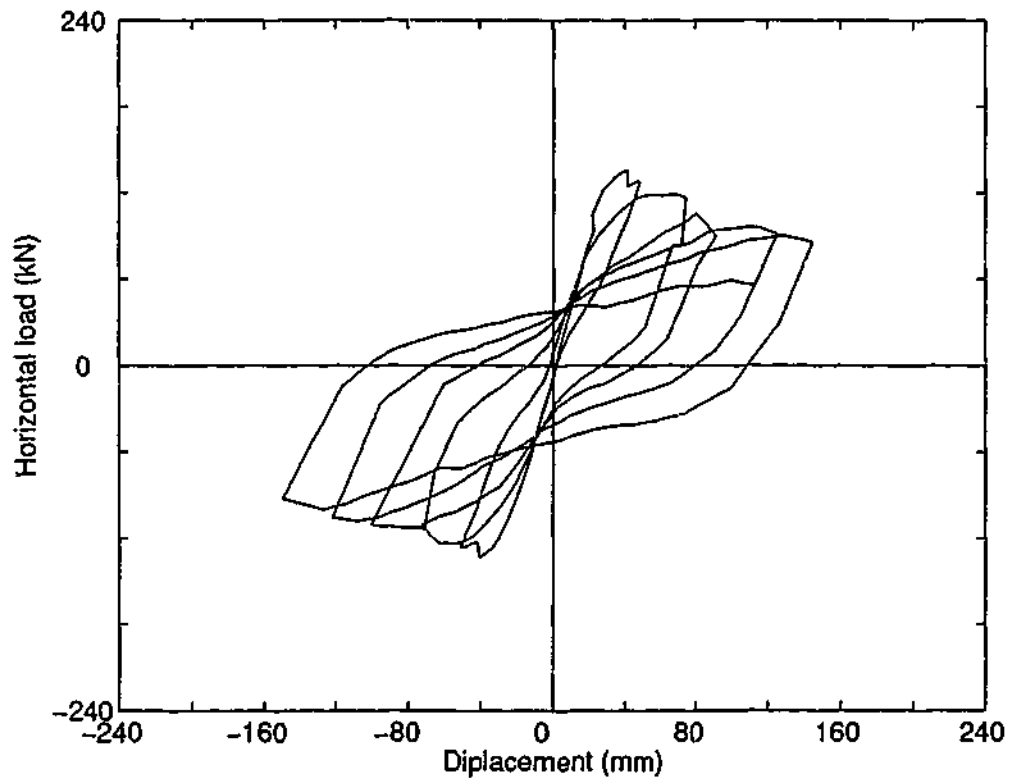


(b). Predicted results

Figure 10.20: Comparison for C7010 column reported by Matamoros and Sozen (2003).

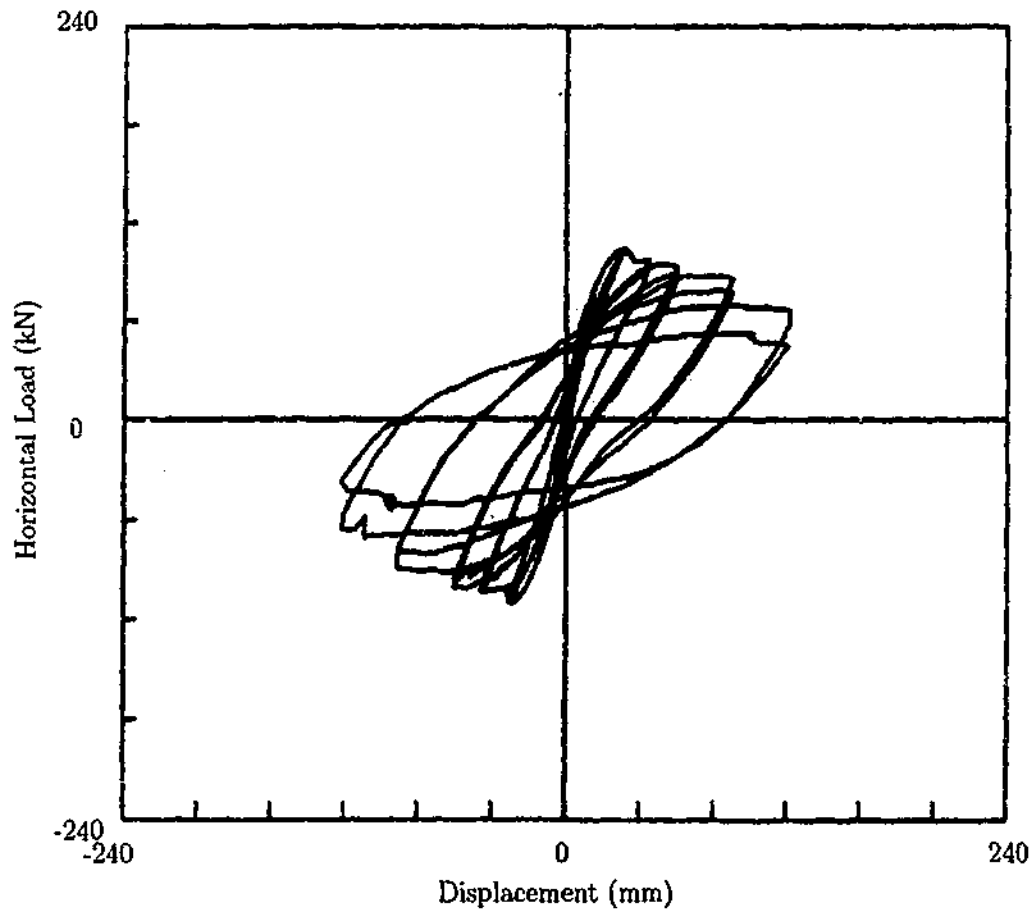


(a). Experimental results

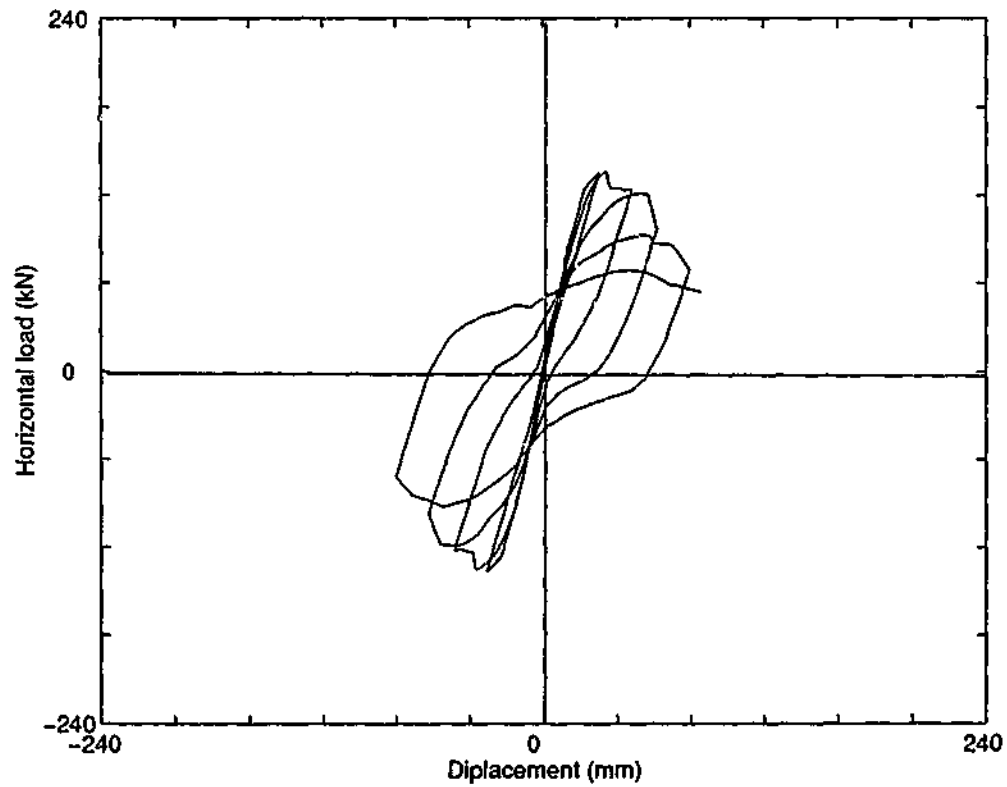


(b). Predicted results

Figure 10.21: Comparison for C100B60N15 column reported by Legeron and Paultre (2000).

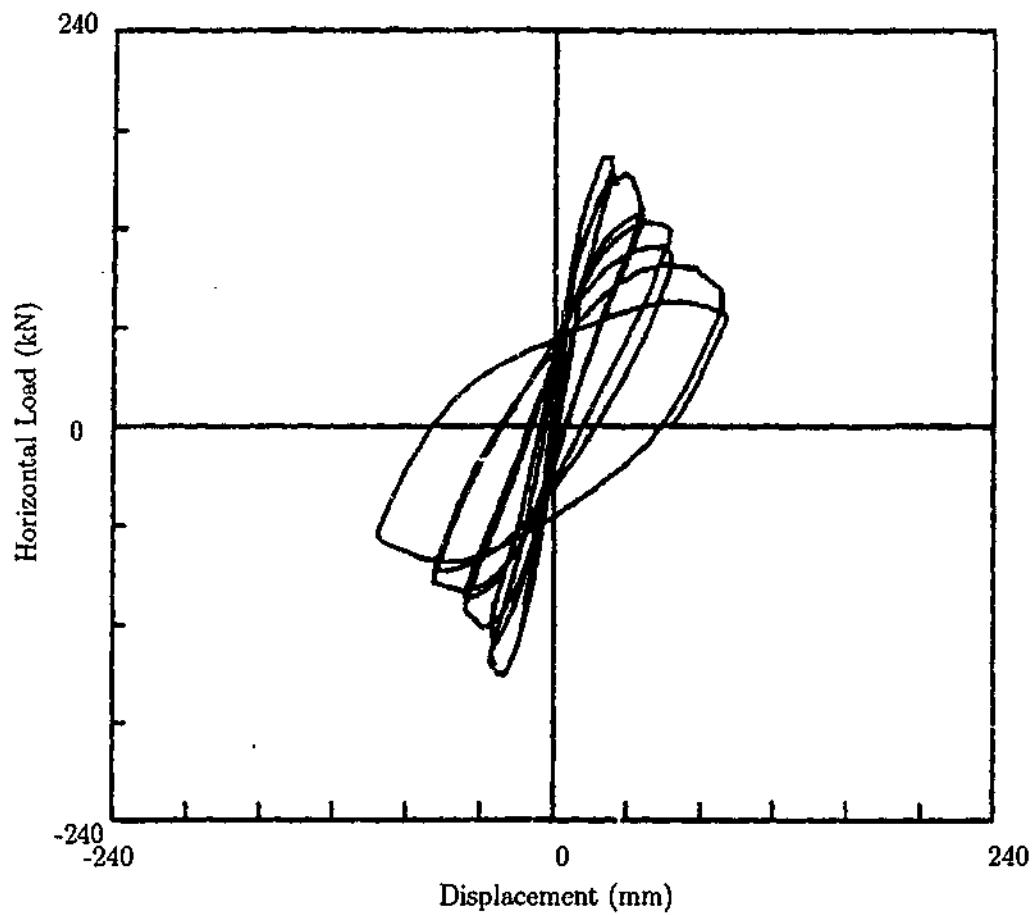


(a). Experimental results

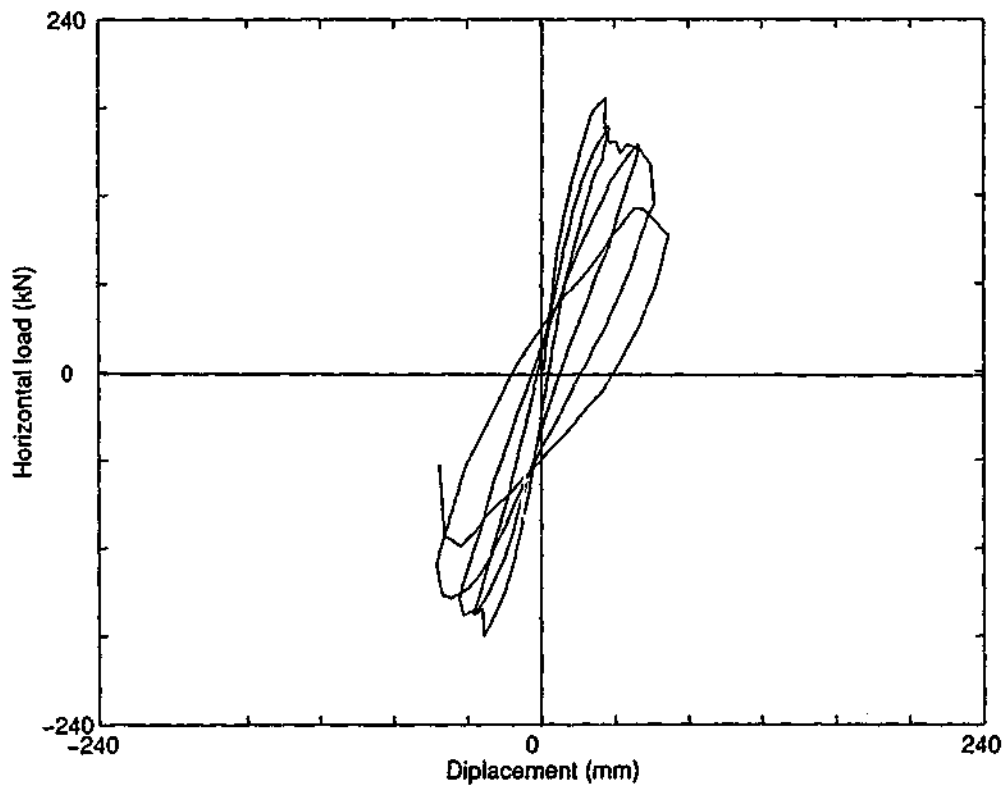


(b). Predicted results

Figure 10.22: Comparison for C100B130N15 column reported by Legeron and Paultre (2000).

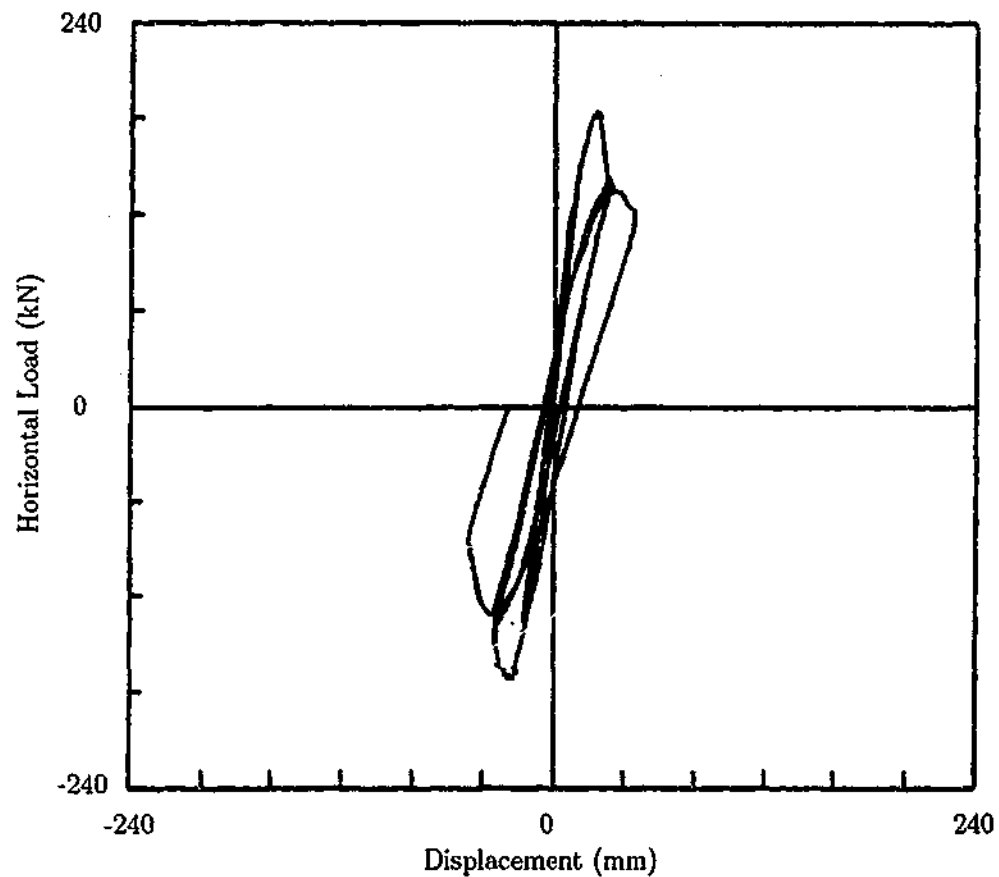


(a). Experimental results

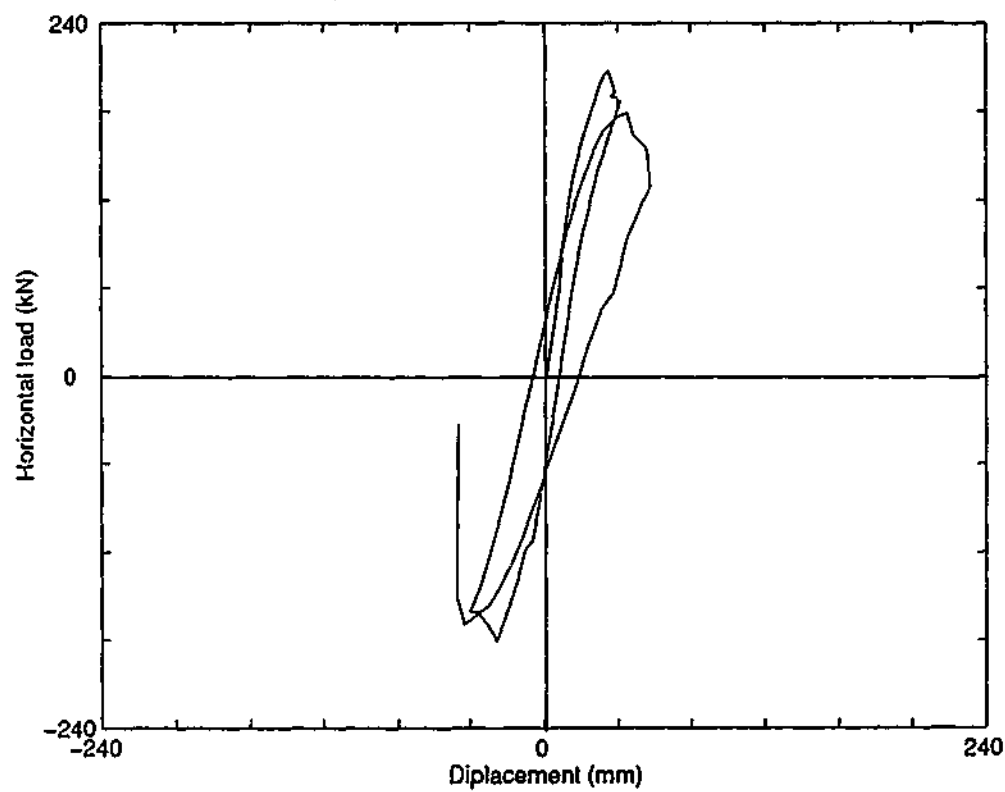


(b). Predicted results

Figure 10.23: Comparison for C100B130N25 column reported by Legeron and Paultre (2000).



(a). Experimental results



(b). Predicted results

Figure 10.24: Comparison for C100B130N40 column reported by Legeron and Paultre (2000).

results closer to those of experiments.

C100B130N15 specimen

The specimen, C100B130N15 differs from the specimen C100B60N15 in terms of only the spacing of the lateral spacing. The predicted curve shown in Figure 10.21(b) shows a more ductile behaviour than that shown in Figure 10.22(b). Predicted curve shows fairly brittle behaviour compared with the experimental curve for the specimen C100B130N15.

It was unable to get many cycles for larger displacements due to specimen failure. For low strains, the slopes of the descending curves compare well. Pinching is more pronounced in the predicted behaviour than the experimental results.

C100B130N25 specimen

Compared with specimen C100B130N15, the only difference in specimen C100B130N25 is the increase in the axial load. It is concluded by Legeron and Paultre (2000) that the increase in axial load will result in a decrease in ductility. A similar behaviour can be observed from the predicted curves as well. The slopes of the descending curves are almost the same for both the predicted and experimental results. Unlike in specimens C100B60N15 and C100B130N15, this specimen does not show the pinching effect. The horizontal loads are higher in the predicted curve than in the experimental curve. The strength loss due to cover spalling is higher than that corresponding to specimen C100B130N15 with lower axial load level than the specimen C100B130N25.

C100B130N40 specimen

The shape and the slopes of the predicted curve agree well with those of the experimental curve as shown in Figure 10.24. However, the maximum horizontal load is overestimated in the predicted curve. The ductility observed in this column with higher axial load levels, is lower than that for lower axial load levels (specimens C100B130N25 and C100B130N15). Crack closing or the pinching effect is not clearly visible in both experimental and predicted curves. It is observed that the strength loss due to cover spalling is higher than those corresponding to specimens C100B130N15 and C100B130N25.

In general, a difference in the slope of the descending curves can be observed for high strain levels. At this point, section might have cracked and only the steel couple must be

acting alone. Thus this difference may be due to the slope in the stress-strain curve for steel itself. In the methodology developed in this chapter, Ramberg-Osgood relationship is used for the cyclic behaviour of steel. This relationship needs to be modified according to the comparisons in this chapter.

10.7 Conclusions

Review of previous work reported in this chapter shows that a number of experimental programs have been reported for the behaviour of HSC columns subjected to cyclic loading. This chapter developed an analytical method using a novel constitutive model (described in Chapter 9) for HSC to predict the behaviour of HSC columns under earthquake loadings. The conclusions that resulted from this chapter are summarised below:

- The constitutive models developed in Chapter 3 for monotonically increasing loads and in Chapter 9 for cyclic loads, are capable of predicting the behaviour of HSC column subjected to earthquake loadings.
- Proposed methodology for the behaviour of HSC columns subjected to combined axial load and cyclic flexure shows good agreement between the predicted and experimental results. It is capable of predicting characteristics of inelastic cyclic response such as,
 - Strength degradation due to successive cycles of loading
 - Stiffness degradation due to concrete cracking and steel yielding
 - Stiffness increase due to crack closing (flexural pinching)
- The proposed analytical method is capable of establishing the following phenomenon, which have been also observed from the experiments.
 - Increase in axial load level, decreases the ductility.
 - Increase in axial load, increases strength and stiffness degradation, hence decreases energy dissipation capacity of the section.
 - Increase in axial load, increases the loss of column capacity due to the spalling of cover.

- Reducing the spacing of transverse reinforcement, increases ductility.
- Proposed methodology can be used to investigate the code provisions for seismic design.

Chapter 11

Conclusions and recommendations

11.1 Conclusions

The work reported in this thesis has significantly contributed to the knowledge base of behaviour of laterally confined HSC columns under static and cyclic loading. A fundamental model has been developed for the constitutive behaviour of HSC under triaxial loading regimes. Complex analytical procedures have been developed to apply the model to predict the behaviour of structural elements. Major conclusions and observations are summarised in this chapter.

11.1.1 Monotonically increasing loads

A strain-based constitutive model has been developed for confined HSC subjected to monotonically increasing loading. It is based on the 24 triaxial test results previously reported.

Observations

- It is observed from the experimental results for both monotonically increasing and cyclic loading of confined HSC that, when confined concrete is subjected to an axial stress, its volume initially decreases. Beyond a certain stress level, this trend reverses and the volume starts to increase. At this turning point, volumetric strain is the maximum. The axial strain at this point increases with the increasing concrete strength. For example, axial strain at the turning point is $0.5\epsilon_{cc}$ for 40 MPa concrete and $0.7\epsilon_{cc}$ for 100 MPa concrete; where ϵ_{cc} is the axial strain at peak axial stress.
- When the volume of concrete increases, there is a point where it returns to the

original unloaded volume. It is observed from the experimental results that this point corresponds to the peak axial stress. In other words, volumetric strain is zero at this point. Therefore, magnitude of lateral strain at peak axial stress is half of corresponding axial strain.

Conclusions

A constitutive model for monotonically increasing load has been developed based on test results with active confinement. It is shown to be giving satisfactory results for several applications.

The model is shown to be capable of predicting the behaviour of HSC columns with passive confinement by carbon fibre wraps.

The model is used to establish the behaviour of laterally confined short as well as slender HSC columns subjected to eccentric static loading. Proposed analytical procedure gives accurate results as it uses the confining pressure applied by lateral steel which changes with lateral dilation of concrete.

The model has the capability of predicting the behaviour of reinforced concrete column-slab joints with HSC in columns and a weaker layer of slab concrete in the joint.

In each application, model predictions found to be comparable with the relevant experimental results reported in the literature.

11.1.2 Cyclic loads

As an extension of the constitutive model developed for monotonically increasing load, a strain-based constitutive model is proposed for confined HSC subjected to cyclic loading. It consists of envelope curve (same as the one proposed in the first part of this thesis for monotonically increasing load), unloading and reloading curves (based on experimental investigations by the author) and a parabolic transition curve (modified version of a curve reported in the literature).

Observations

- Previous researchers were in general agreement that the envelope curve for cyclic loading for unconfined and confined NSC is similar to the stress-strain curve of

monotonically increasing load. From the experimental results for confined HSC, it is observed that this is acceptable in the ascending branch of the stress-strain curve of HSC but not for the descending branch. The descending branch of the envelope curve has to be modified by scaling down the corresponding stresses for HSC.

- In the initial elastic region, Poisson's ratio remains a constant and beyond this region, it increases with the increasing load.
- An unloading in the initial elastic region, results in a decreasing Poisson's ratio. Reloading increases it back to the same value. The proposed model is capable of modelling this decreasing/increasing phenomenon of Poisson's ratio.
- When unloading and reloading cycles occurs in the initial elastic region, the axial stress versus axial strain diagram exhibits a different behaviour to the axial stress versus lateral strain diagram. The axial stress versus lateral strain curves follow the same line during unloading and reloading cycles as expected. However, in the axial stress versus axial strain curves, the unloading does not follow the original loading curve and the reloading curve is different to the unloading curve. This aspect of different behaviour in axial strain and lateral strain is the reason for the decreasing/increasing phenomenon stated above.

Conclusions

The proposed constitutive model for cyclic loads can be applied for column analysis in seismic regions. It is proven to be giving satisfactory comparisons for the behaviour of confined HSC columns with axial load and cyclic flexure.

11.1.3 Important features of both models

- Strain-based. For a given axial strain, a strain-based constitutive model has the ability to calculate the corresponding axial stress directly. However, for a given axial strain a stress-based constitutive model uses an iterative procedure to calculate the corresponding axial stress. Therefore a strain-based constitutive model for concrete is desirable in a structural analysis.

- Ability to predict the axial stress, axial strain and lateral strain relationships for both HSC and NSC.
- The applications are not limited to certain size of columns or configurations, since the models are developed based on the triaxial tests.
- Unlike in the models based on column tests, no assumptions about the confinement effectiveness are included in developing these models.

11.2 Recommendations

There are still many applications of the two constitutive models for monotonically increasing loads and for cyclic loads which require further investigation. A few of them are suggested here.

- The constitutive model developed for HSC with monotonically increasing loading can be applied for analysing HSC columns with different methods of lateral confinement such as steel tubes and FRP composites. Therefore the applicability of the model for a wider range of confinement levels can be investigated.
- Application of the constitutive model for monotonically increasing loads in eccentrically loaded slender columns needs further investigations. A refined curvature-deflection model is likely to improve the analytical model.
- Using the constitutive model for cyclic loading of HSC, a parametric study can be conducted for the behaviour of confined HSC columns subjected to earthquake loadings. This is likely to reveal the influence of the various parameters on the earthquake response.

Effect of high strain rates on the behaviour of HSC subjected to monotonically increasing loading has been addressed by only few researchers in the literature (Fu et al. 1991a; Fu et al. 1991b; Bing et al. 2000). There have not been any studies reported on the effect of high strain rates on the behaviour of HSC subjected to cyclic loading. Therefore the experimental program described in this thesis for slow strain rates can be extended for high strain rates.

There are a number of researchers who did experimental analysis on HSC columns subjected to combined constant axial compression and reversed cyclic flexure and made design recommendations. Nevertheless it is reported that none of the current codes (ACI Code or New Zealand Standard) provide adequate amount of steel reinforcement to ensure a good level of ductility (Legeron and Paultre 2000). The ACI Code requirements are too conservative in the case of low axial load levels whereas they are insufficient for high axial load levels. Only New Zealand Standard considers axial load level in transverse steel requirements. The analytical procedures developed in this study may be used to review the current design code guidelines for earthquake resistant structures and to give design recommendations.

Appendix A

Comparison of experimental results with the existing models for monotonically increasing loads

Axial stress and axial strain relationships of the results obtained from the major experimental program for four grades of concrete, three confining pressures and two loading regimes, were compared with the models proposed by Mander et al. (1988b) and Sakai and Kawashima (2000).

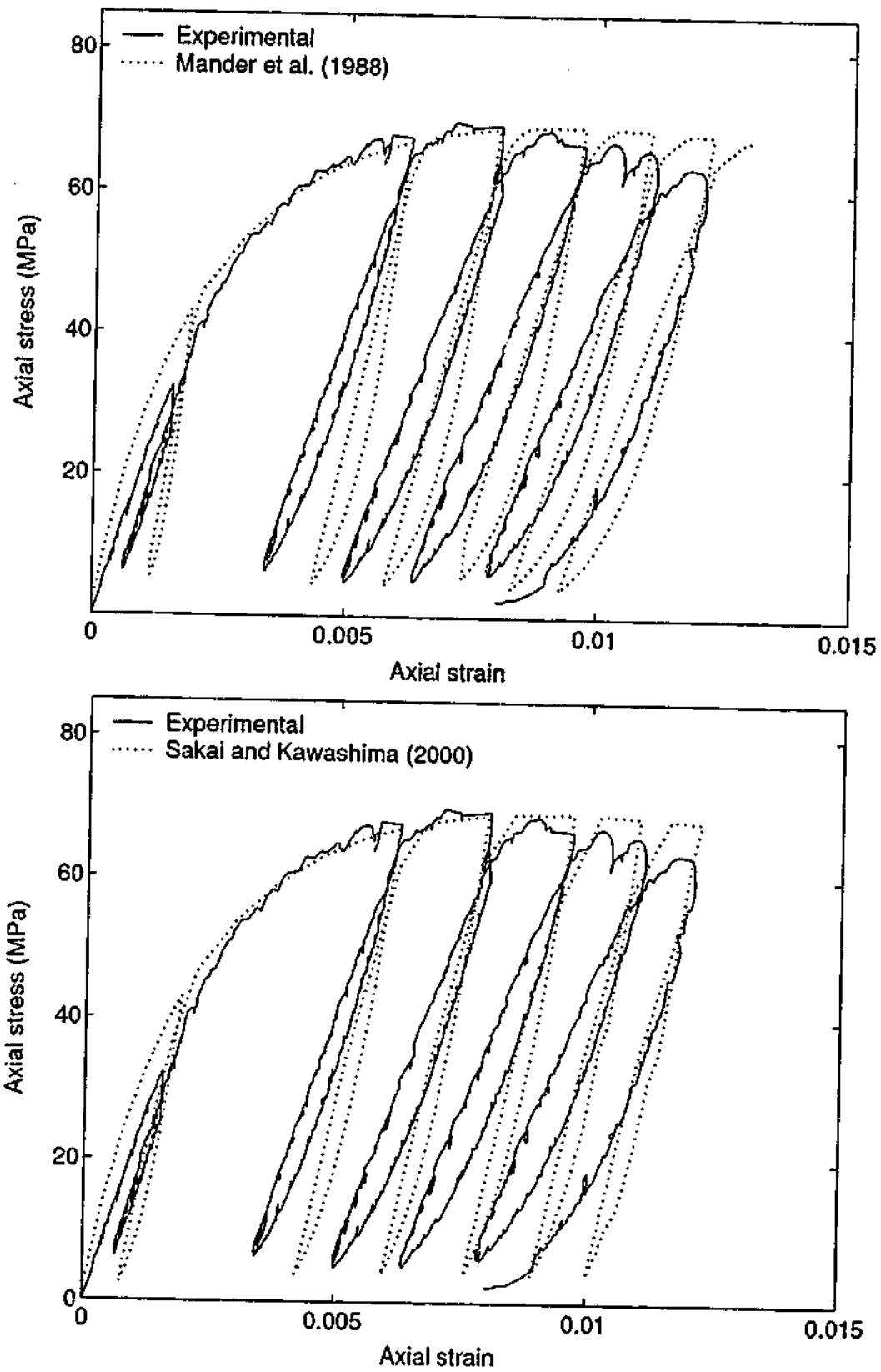


Figure A.1: Loading regime 1 of Grade 40 concrete with 4 MPa confining pressure.

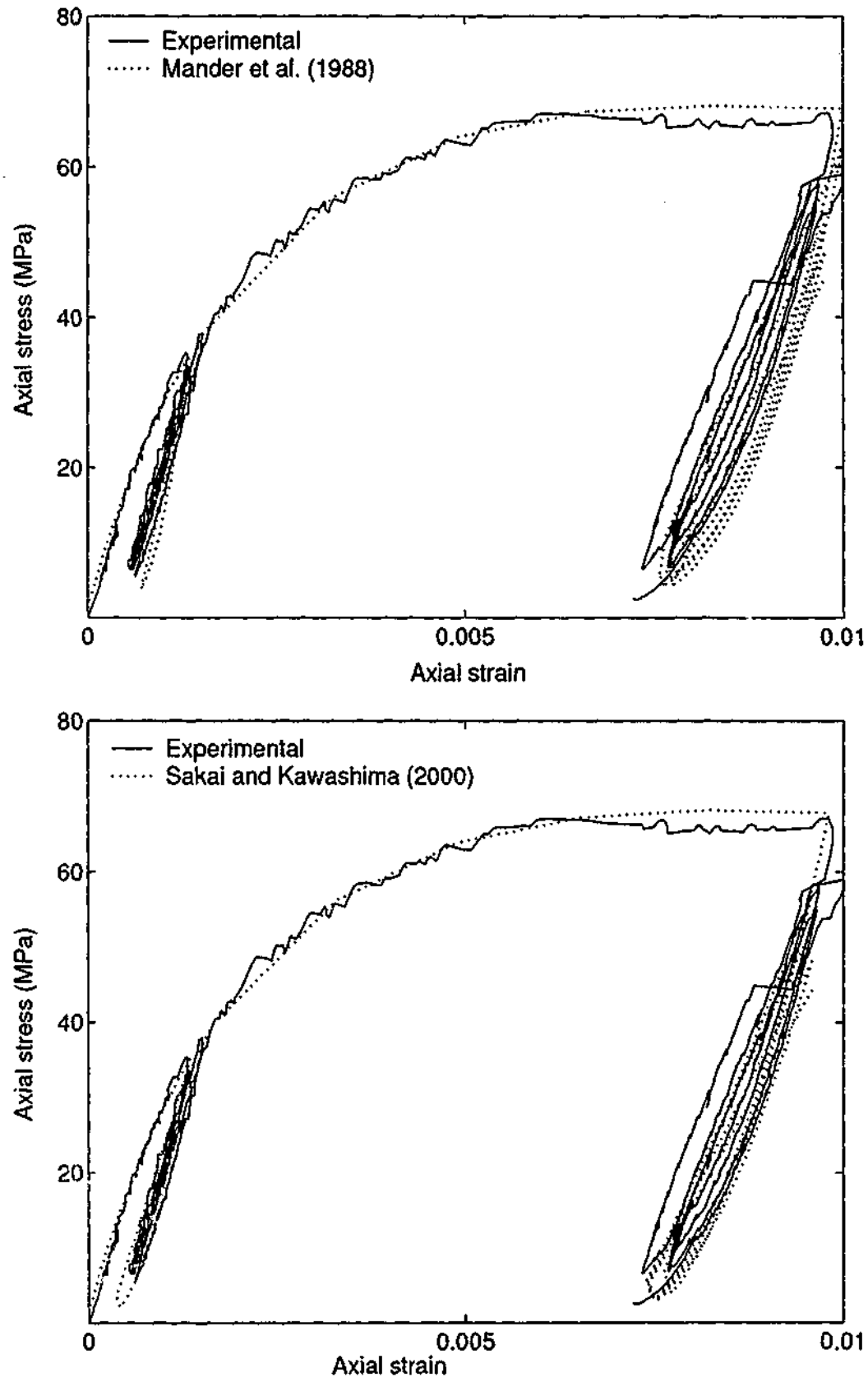


Figure A.2: Loading regime 2 of Grade 40 concrete with 4 MPa confining pressure.

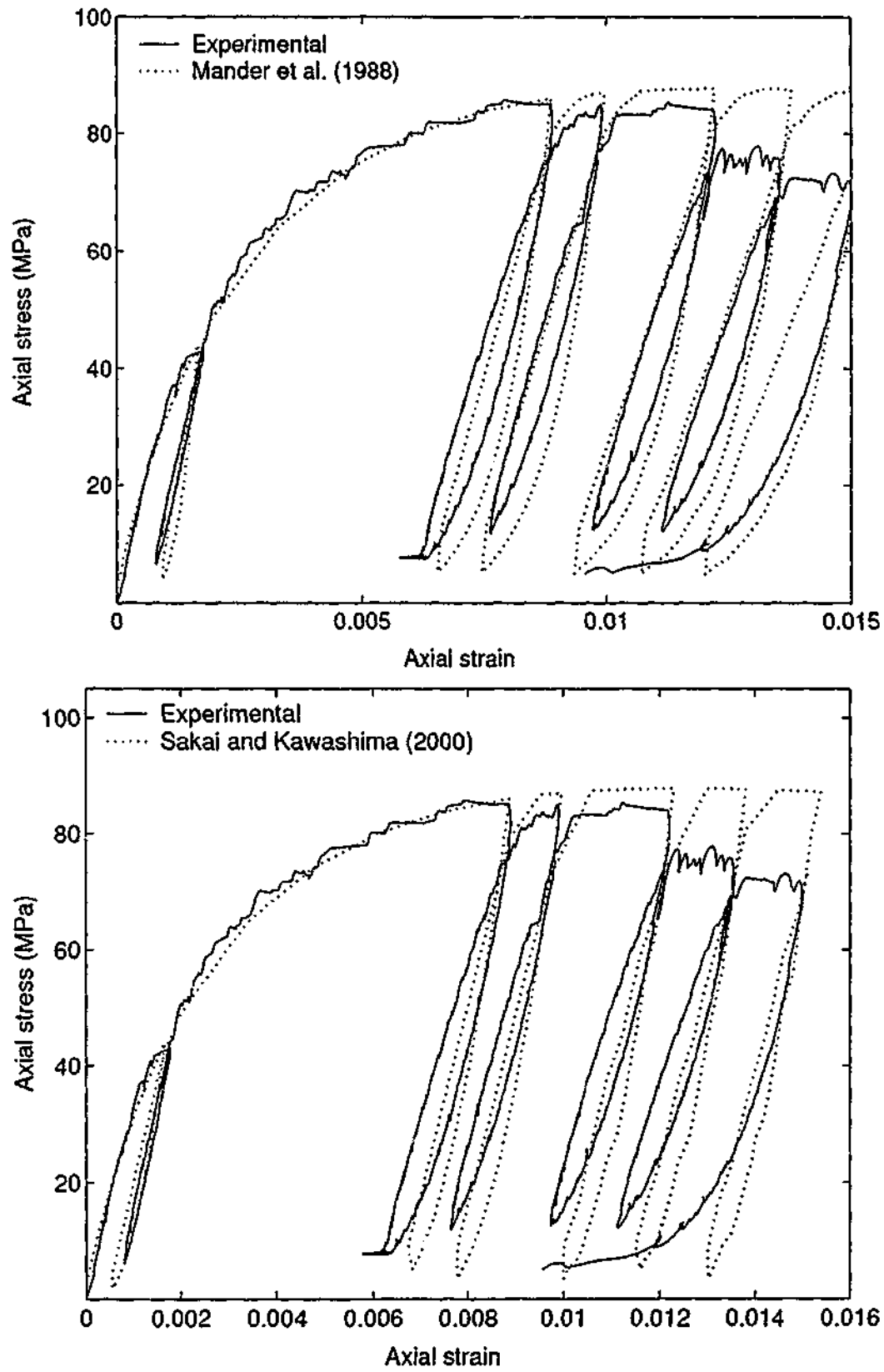


Figure A.3: Loading regime 1 of Grade 40 concrete with 8 MPa confining pressure.

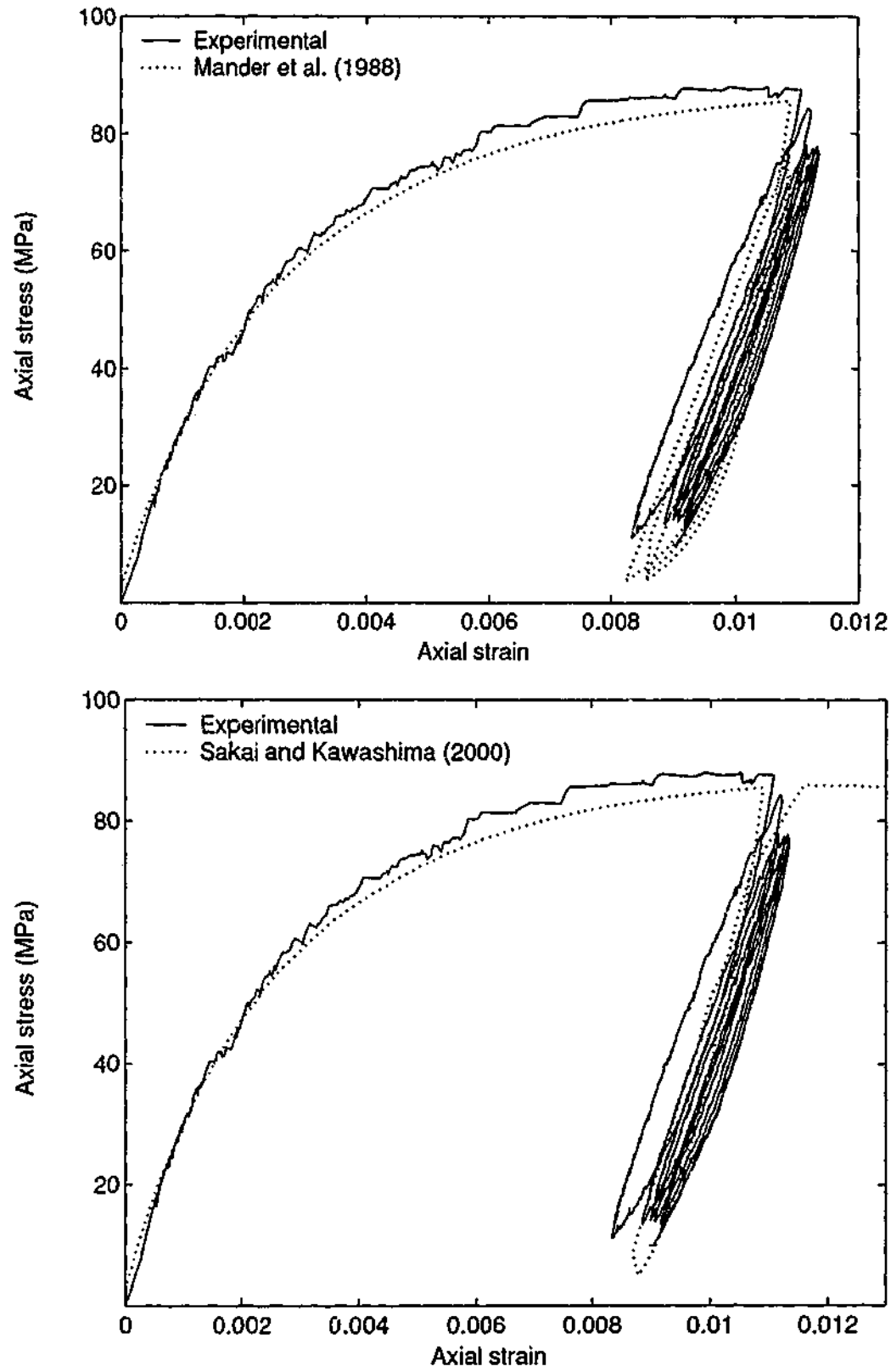


Figure A.4: Loading regime 2 of Grade 40 concrete with 8 MPa confining pressure.

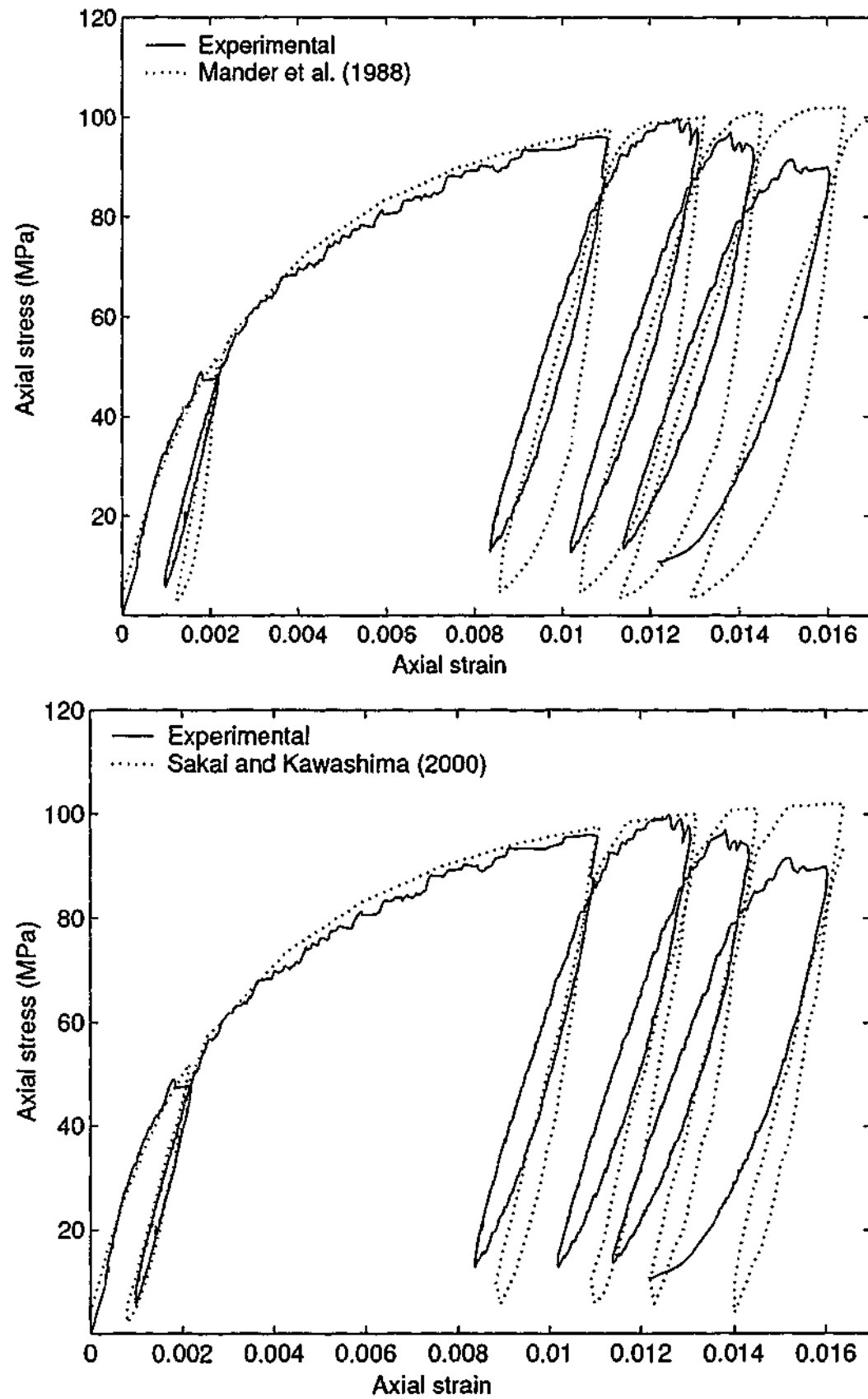


Figure A.5: Loading regime 1 of Grade 40 concrete with 12 MPa confining pressure.

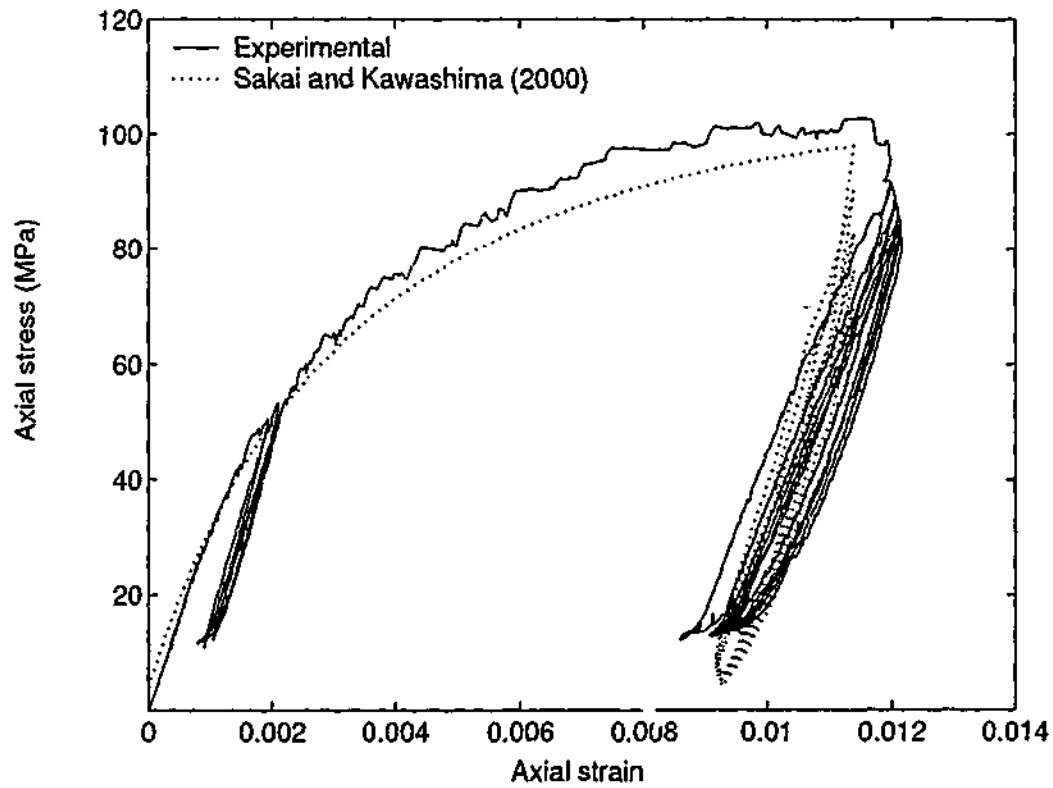
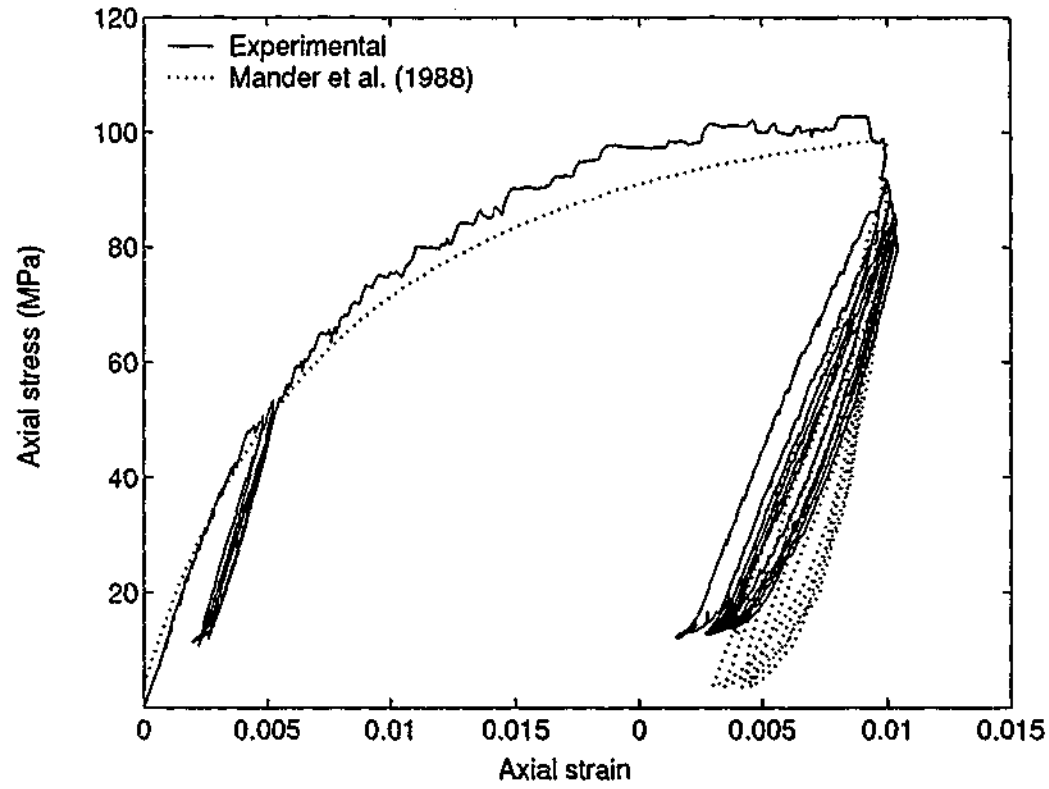


Figure A.6: Loading regime 2 of Grade 40 concrete with 12 MPa confining pressure.

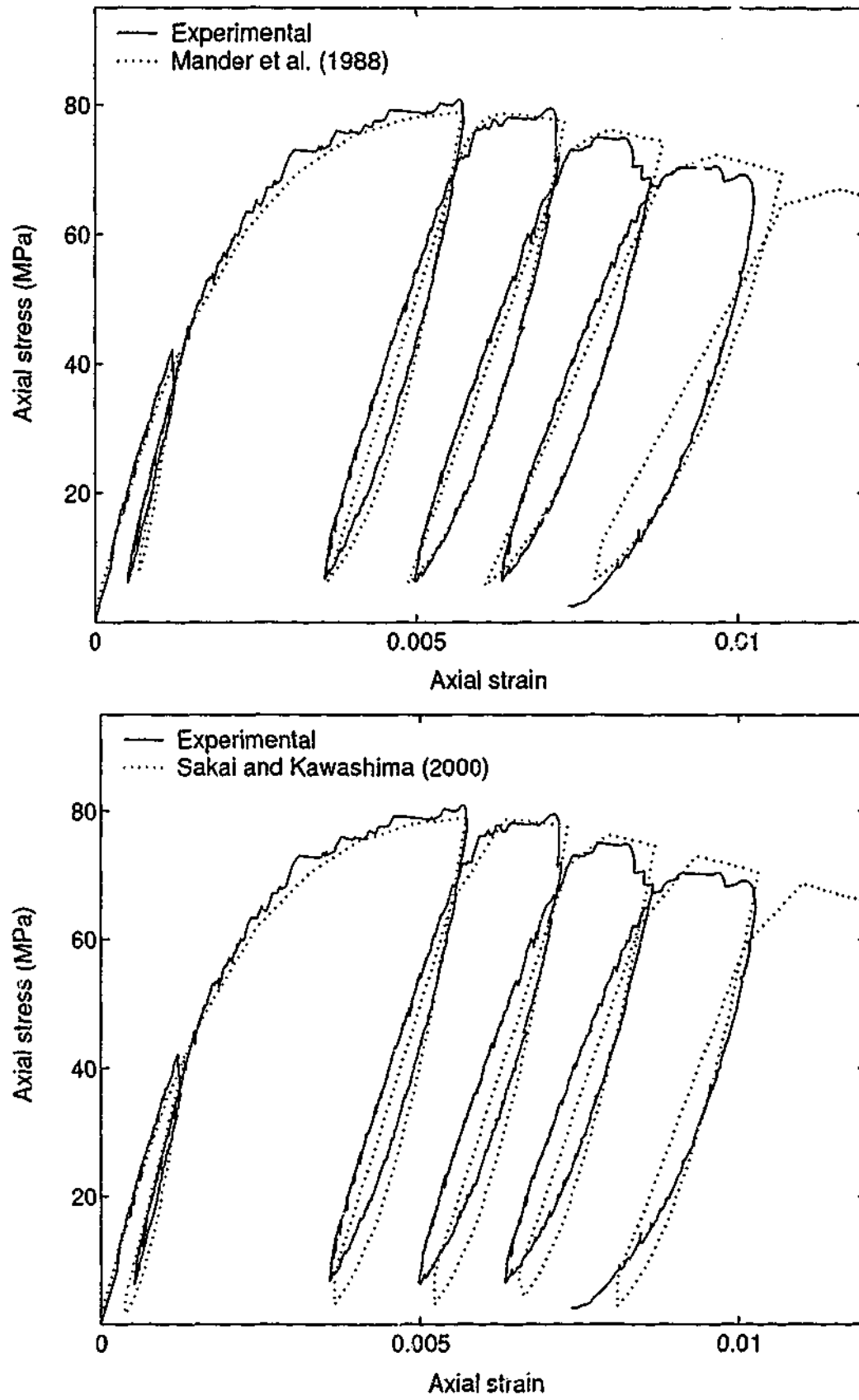


Figure A.7: Loading regime 1 of Grade 60 concrete with 4 MPa confining pressure.

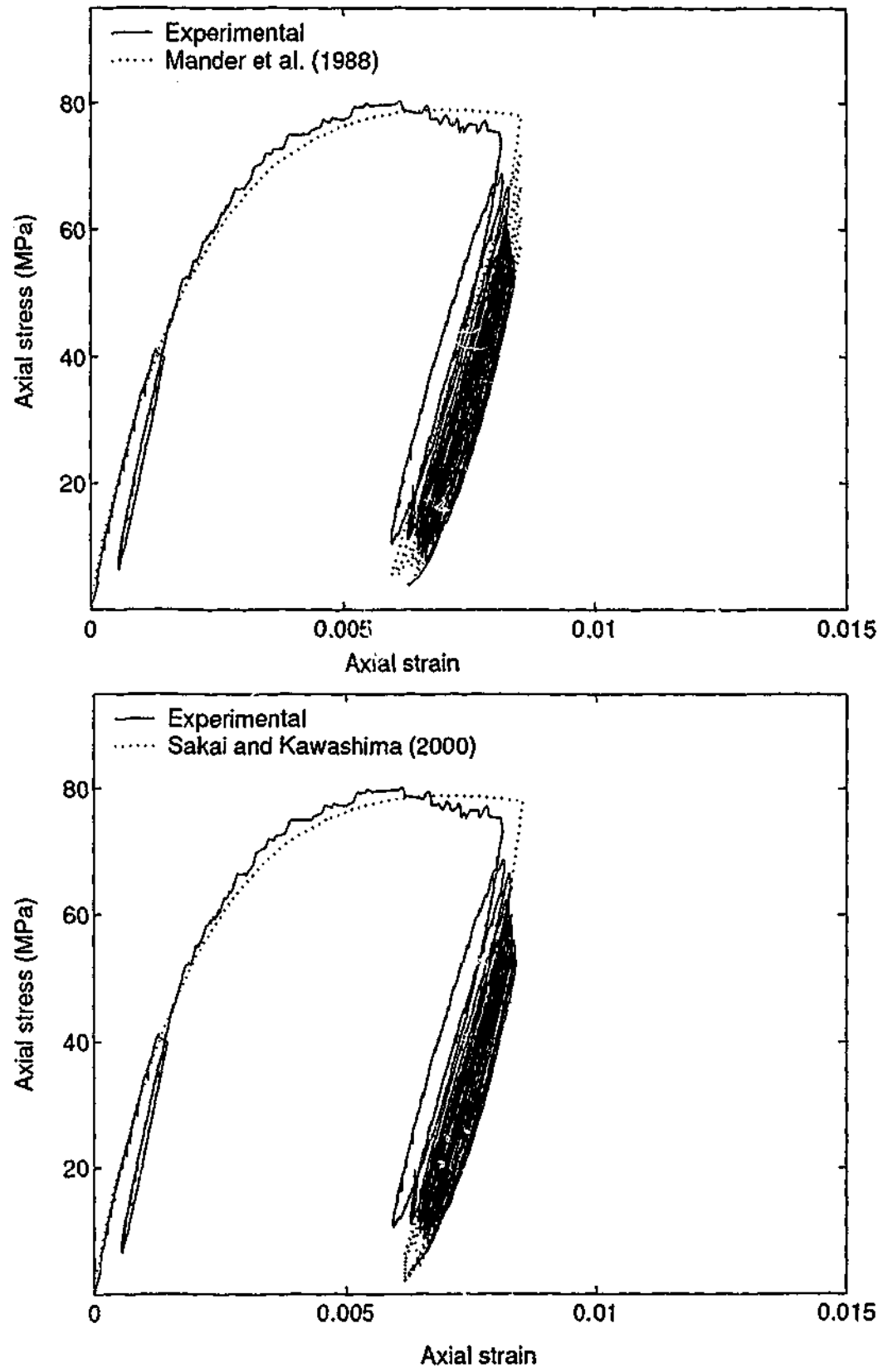


Figure A.8: Loading regime 2 of Grade 60 concrete with 4 MPa confining pressure.

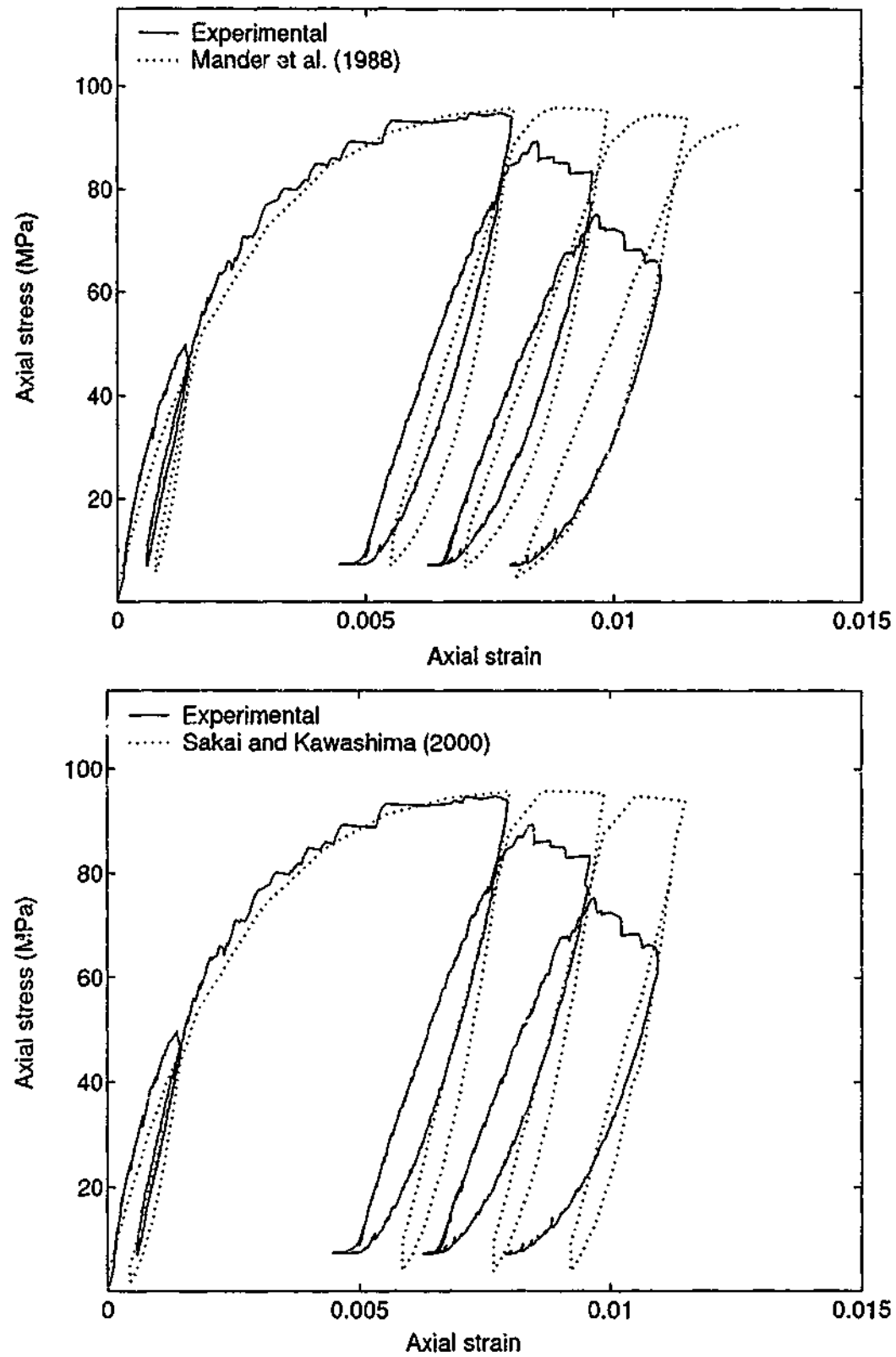


Figure A.9: Loading regime 1 of Grade 60 concrete with 8 MPa confining pressure.

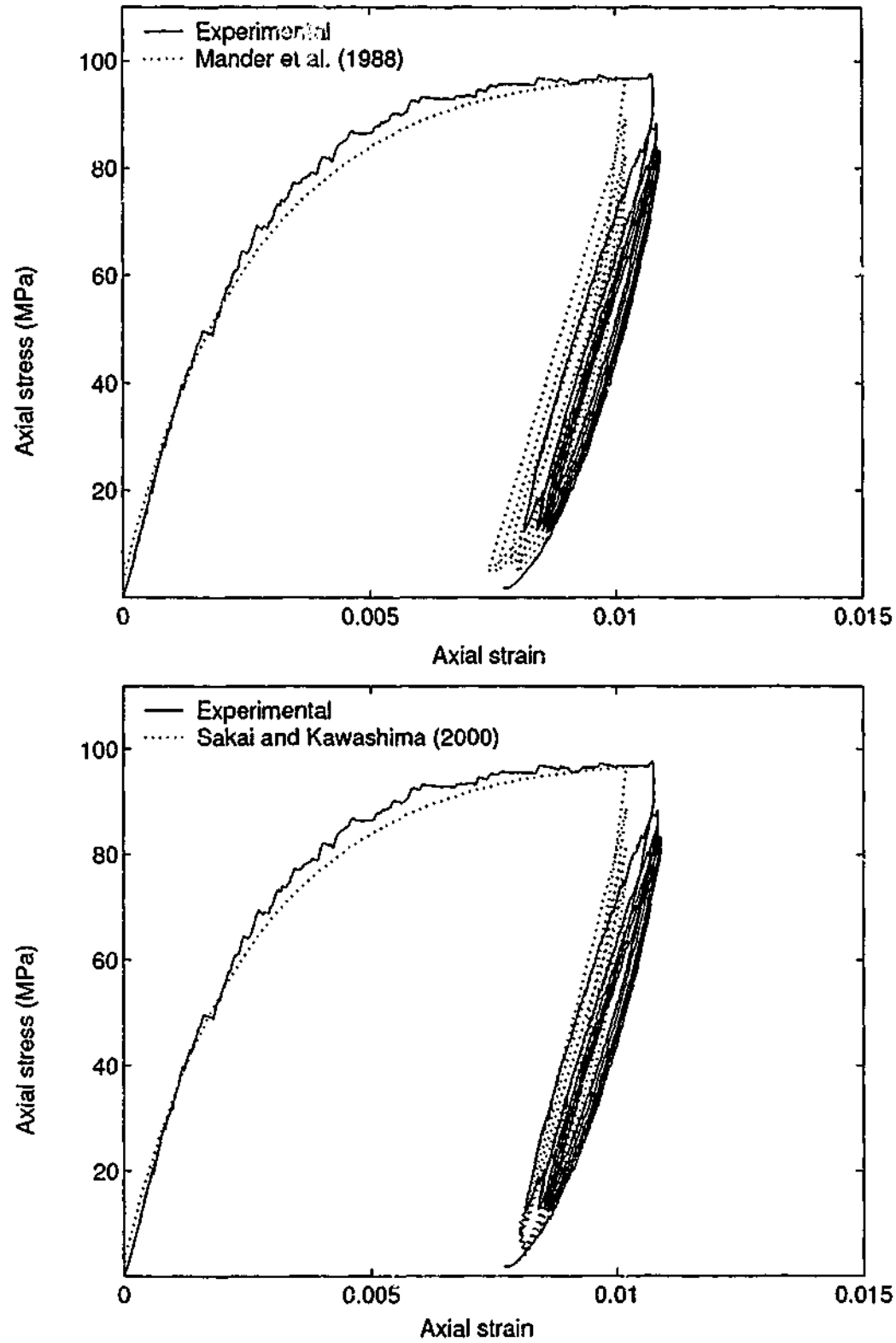


Figure A.10: Loading regime 2 of Grade 60 concrete with 8 MPa confining pressure.

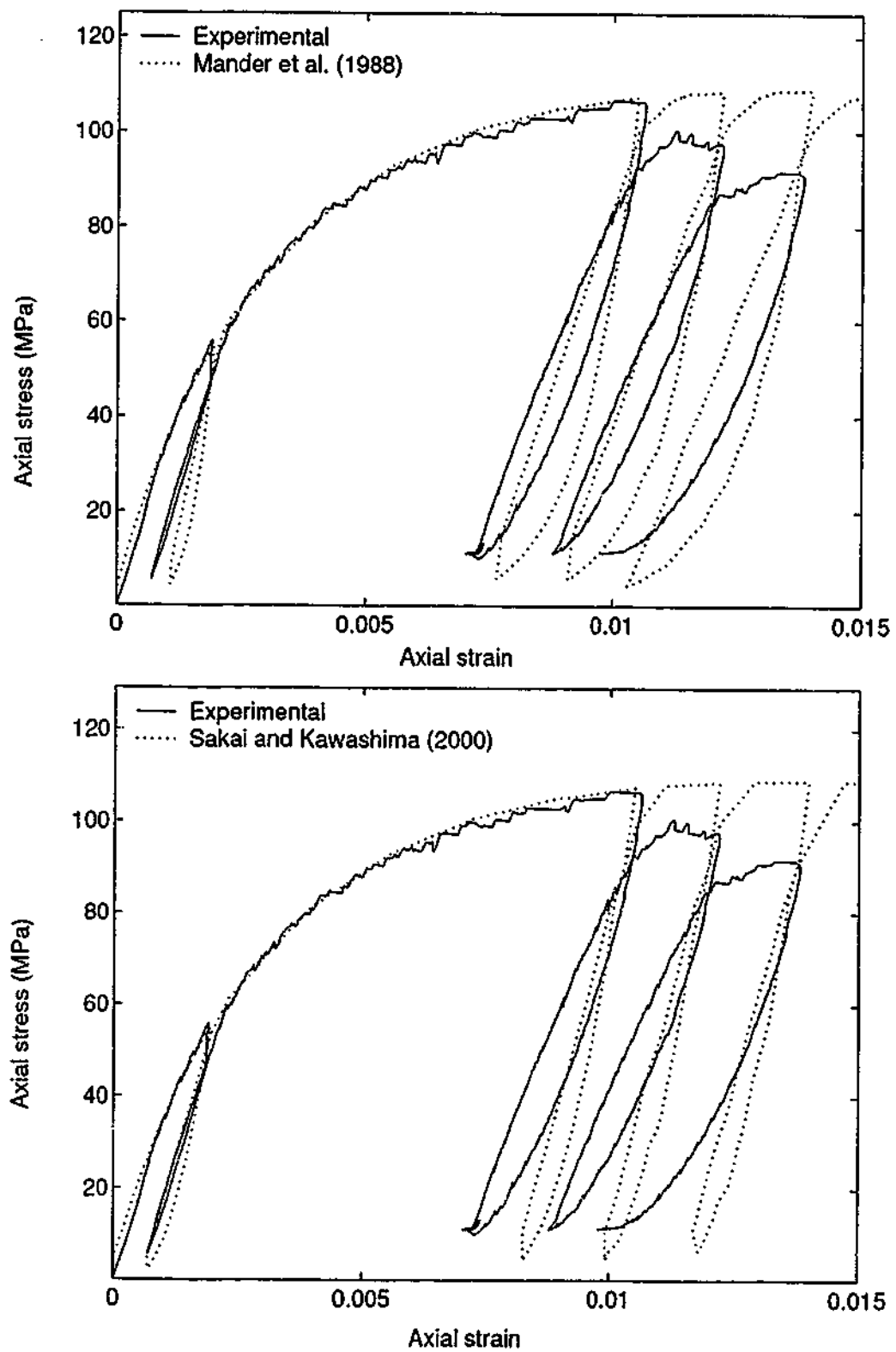


Figure A.11: Loading regime 1 of Grade 60 concrete with 12 MPa confining pressure.

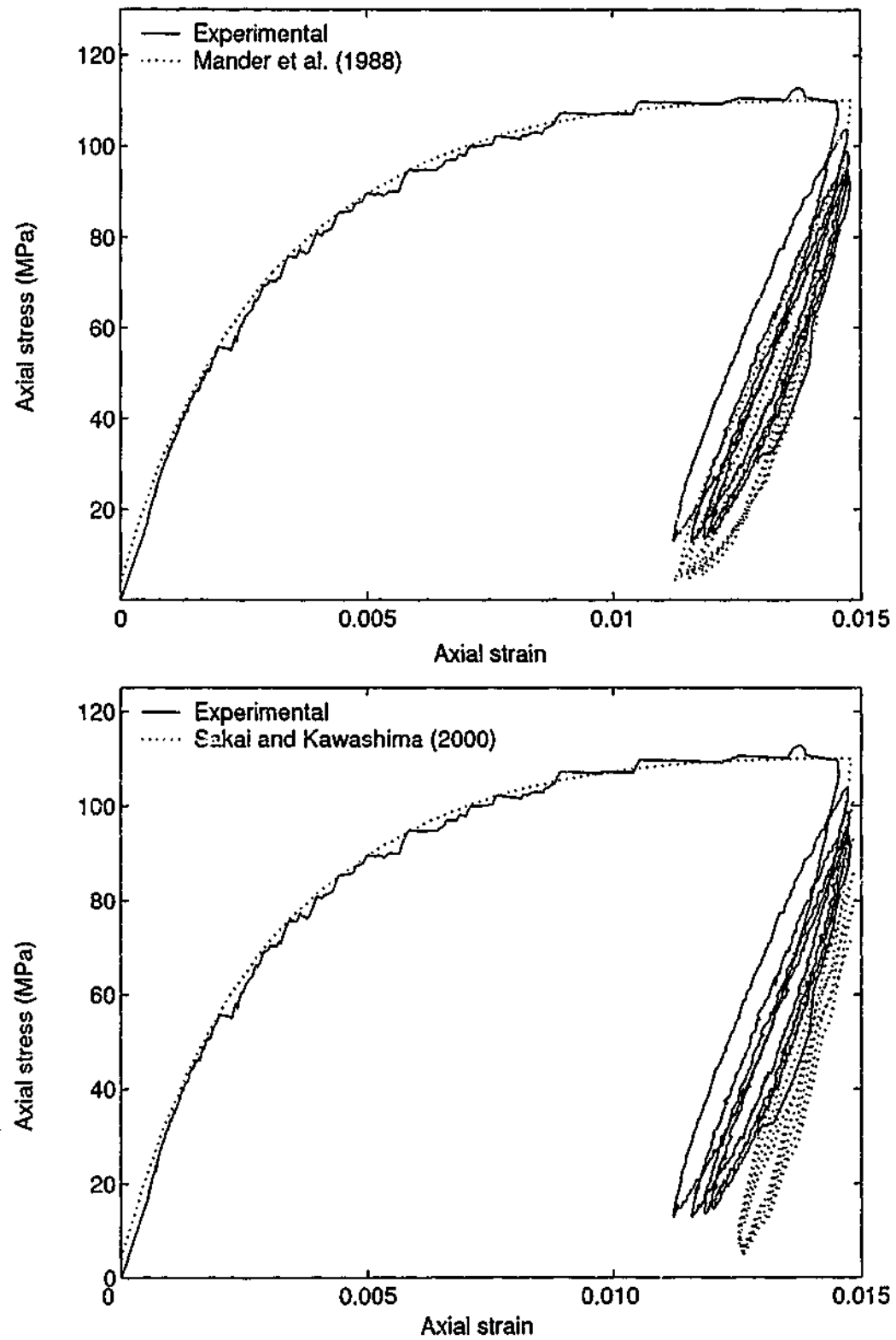


Figure A.12: Loading regime 2 of Grade 60 concrete with 12 MPa confining pressure.

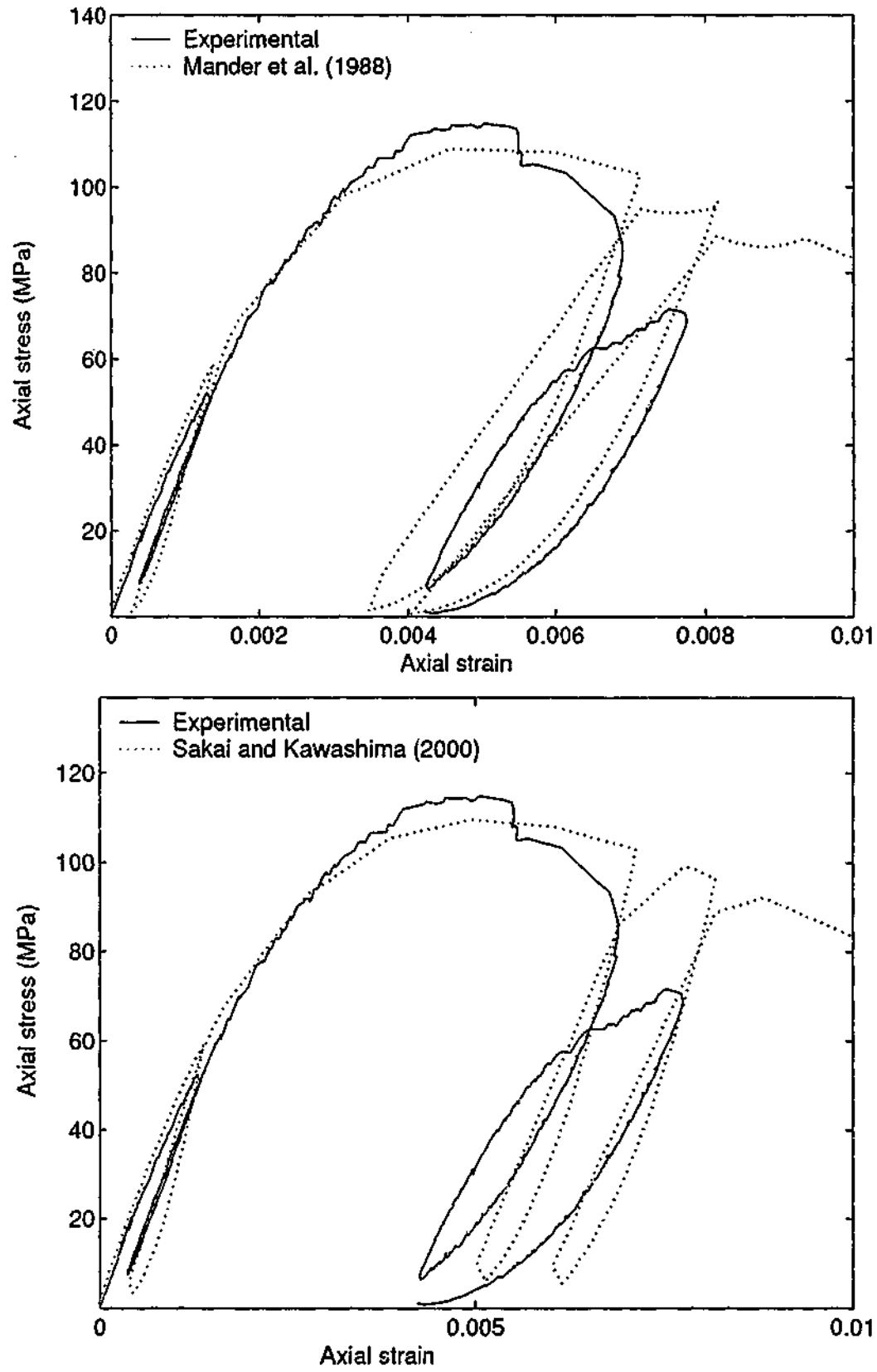


Figure A.13: Loading regime 1 of Grade 80 concrete with 4 MPa confining pressure.

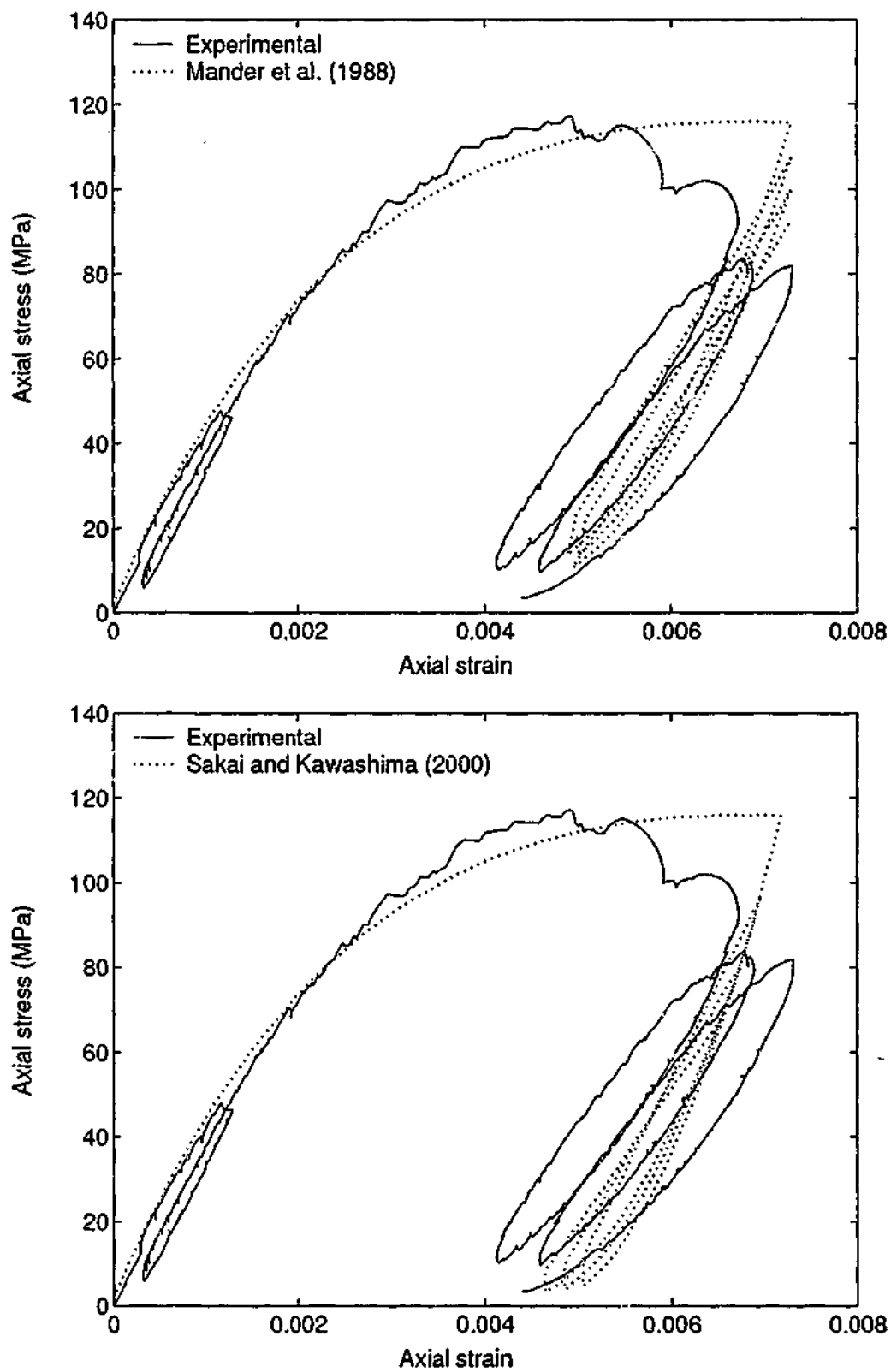


Figure A.14: Loading regime 2 of Grade 80 concrete with 4 MPa confining pressure.

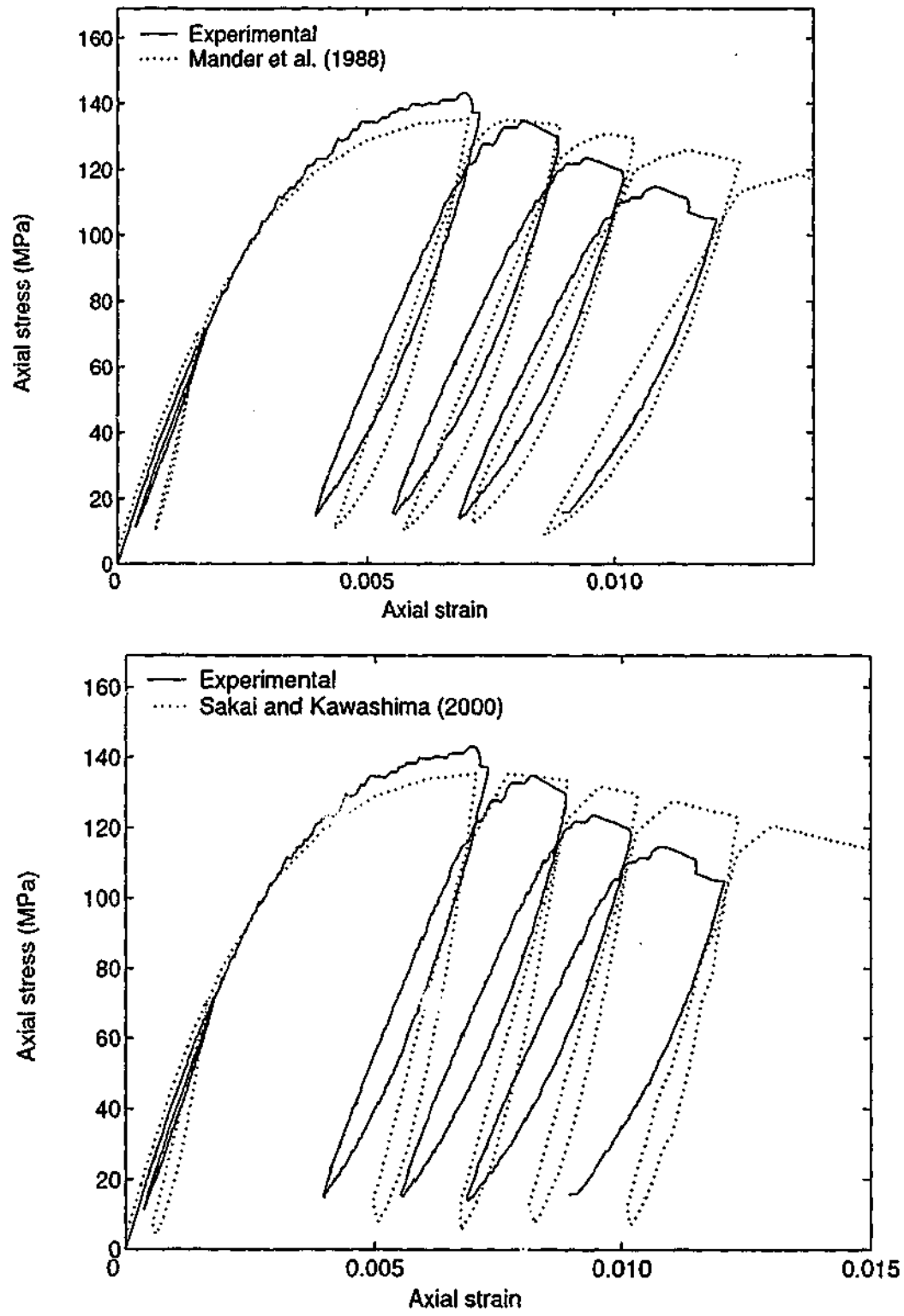


Figure A.15: Loading regime 1 of Grade 80 concrete with 8 MPa confining pressure.

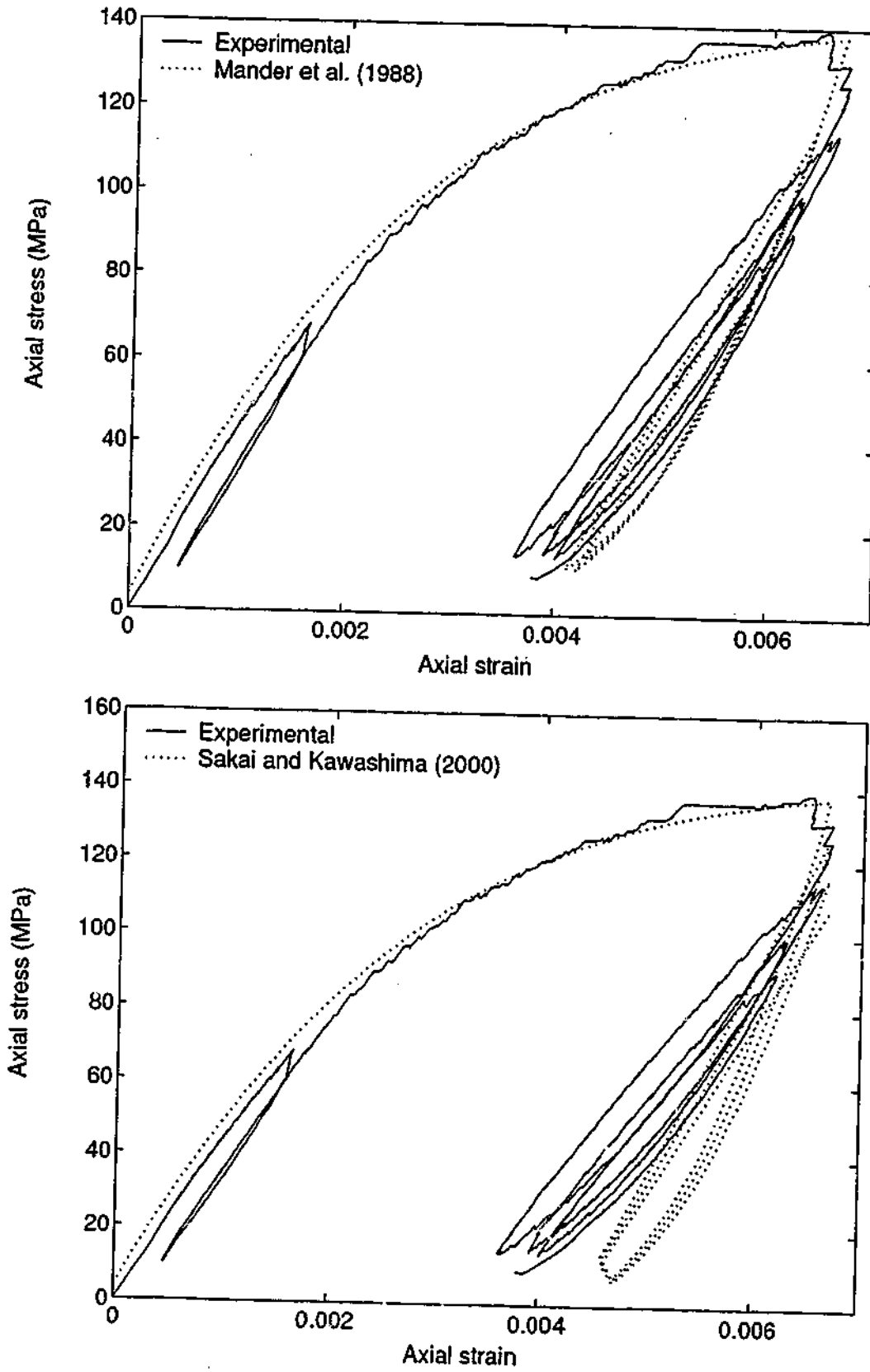


Figure A.16: Loading regime 2 of Grade 80 concrete with 8 MPa confining pressure.

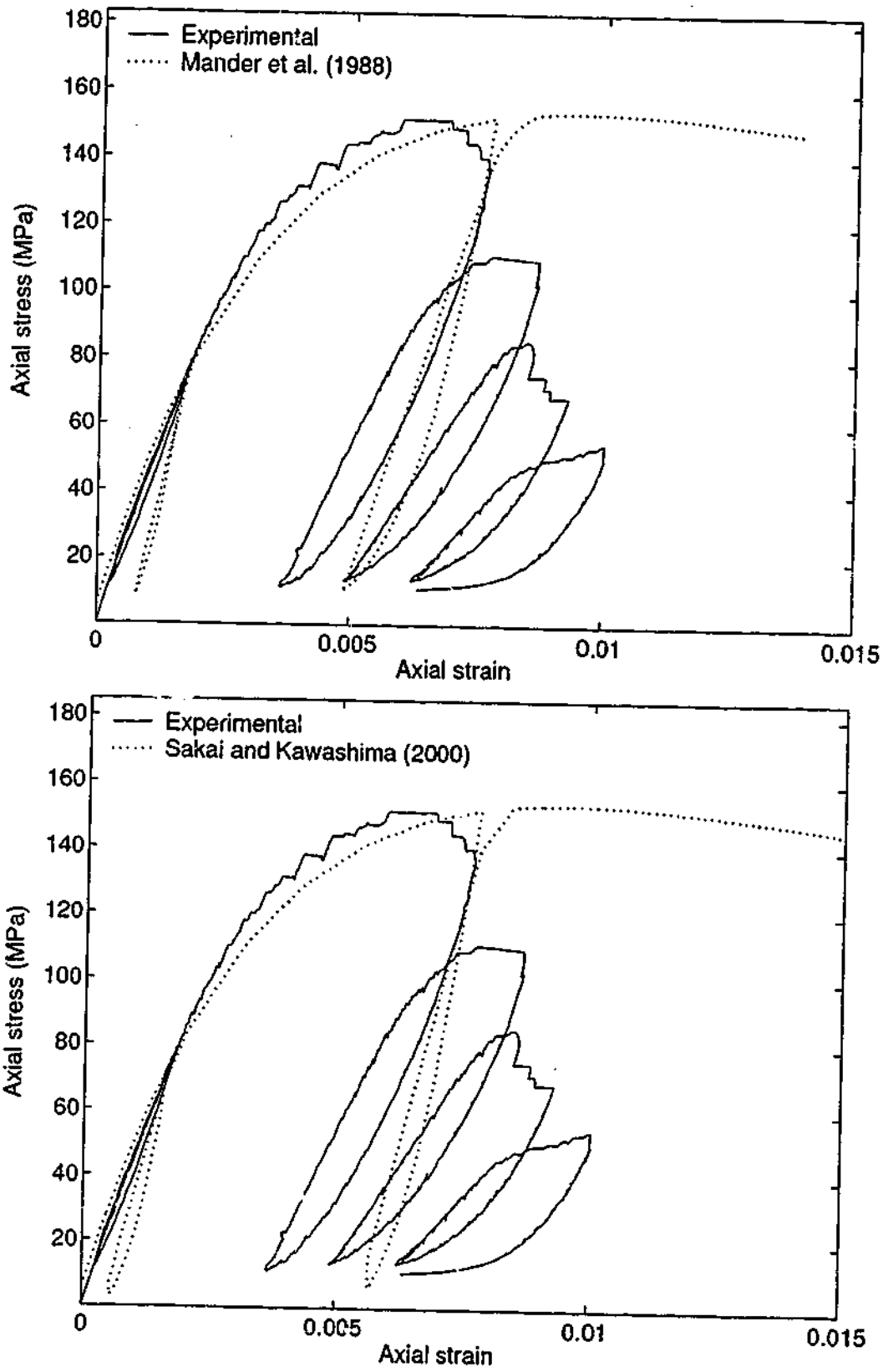


Figure A.17: Loading regime 1 of Grade 80 concrete with 12 MPa confining pressure.

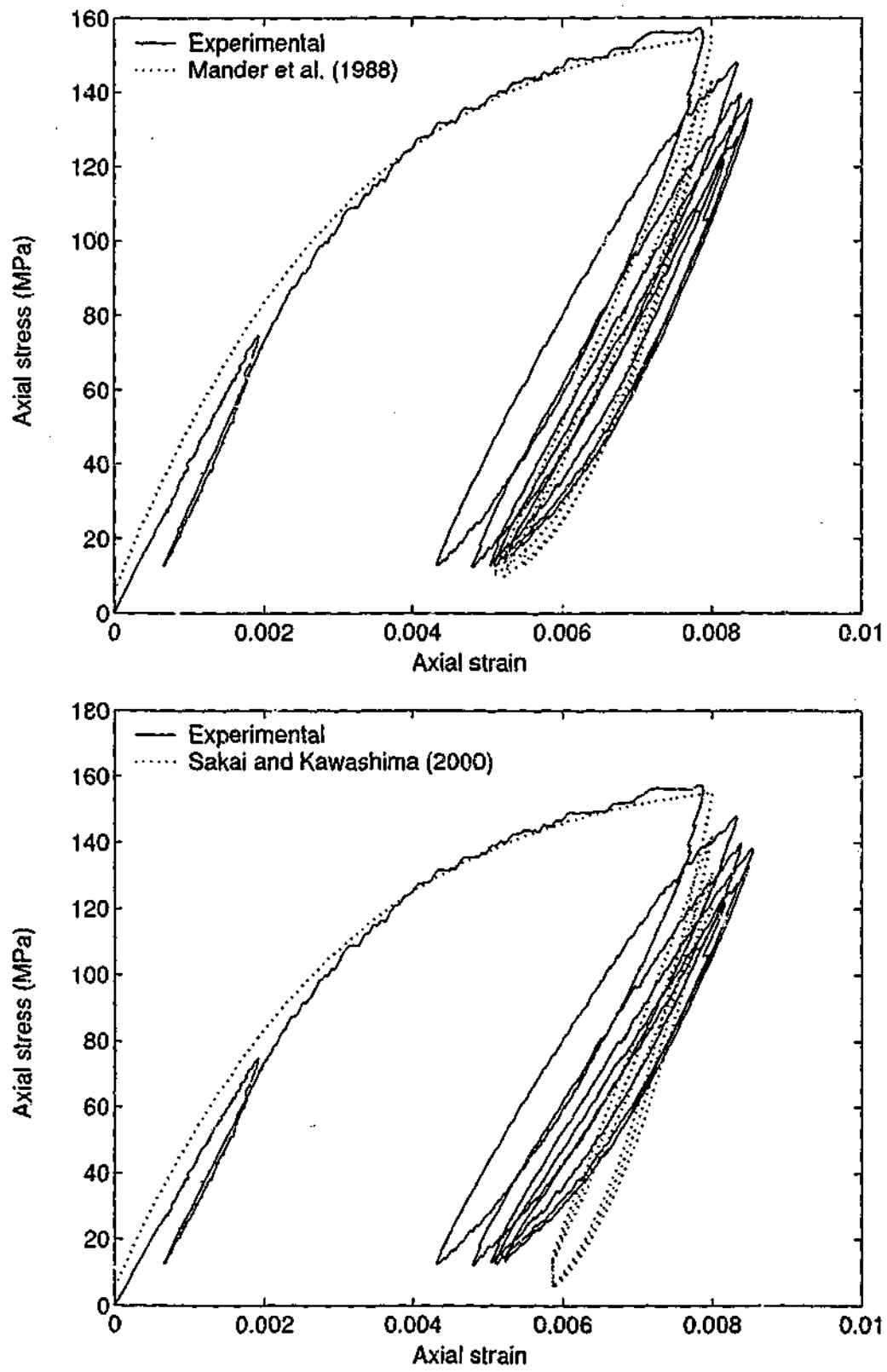


Figure A.18: Loading regime 2 of Grade 80 concrete with 12 MPa confining pressure.

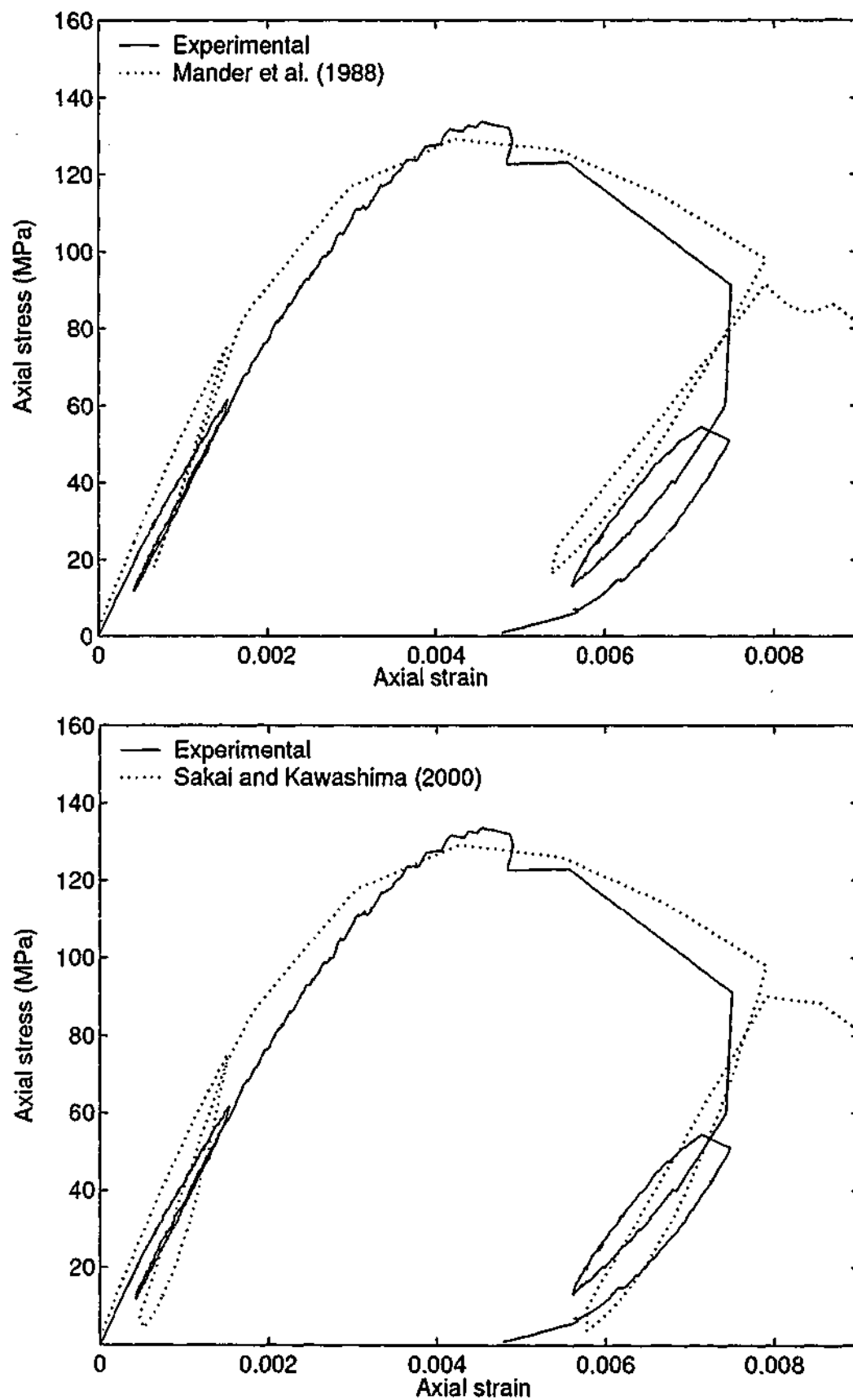


Figure A.19: Loading regime 1 of Grade 100 concrete with 4 MPa confining pressure.

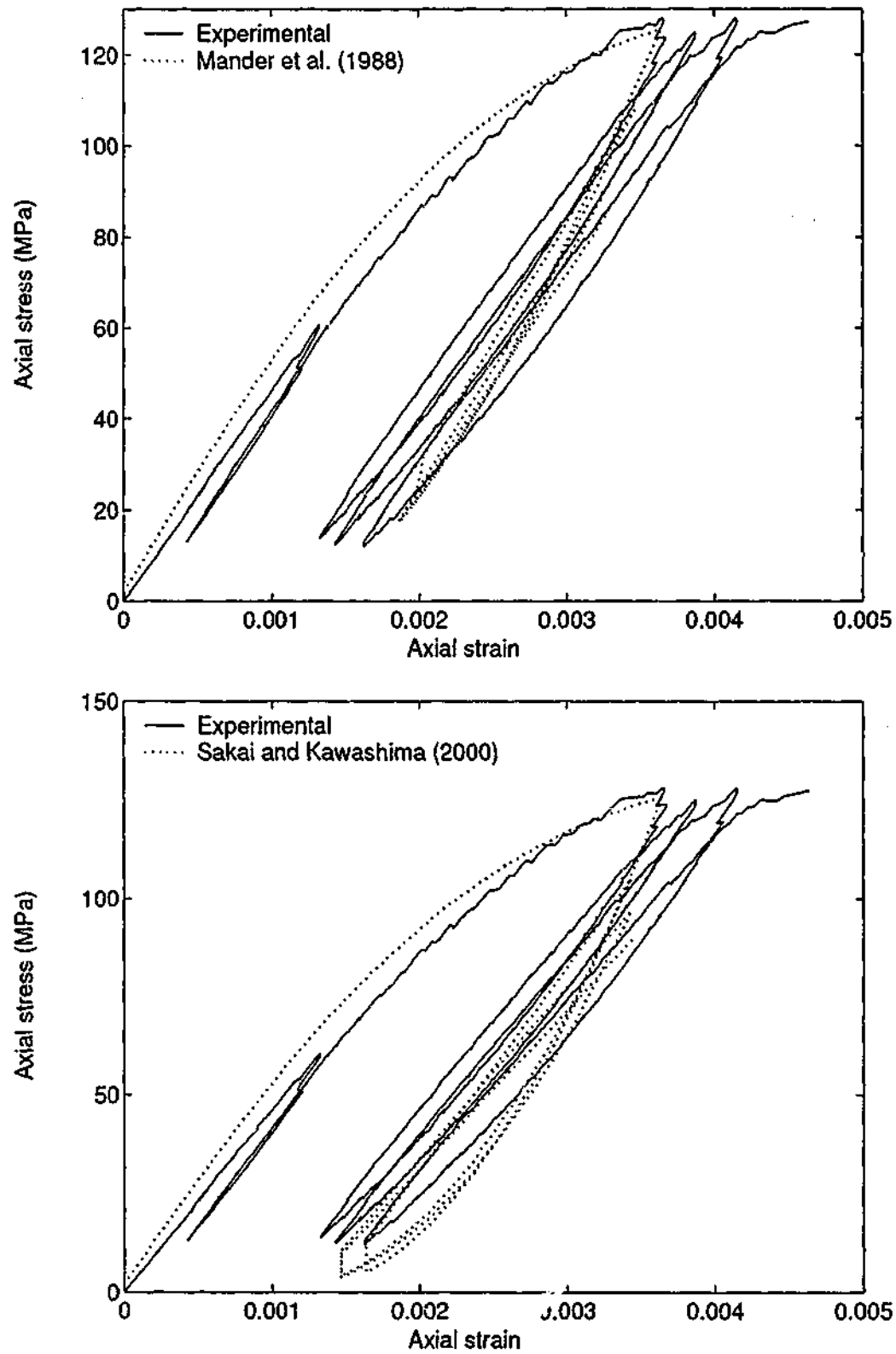


Figure A.20: Loading regime 2 of Grade 100 concrete with 4 MPa confining pressure.

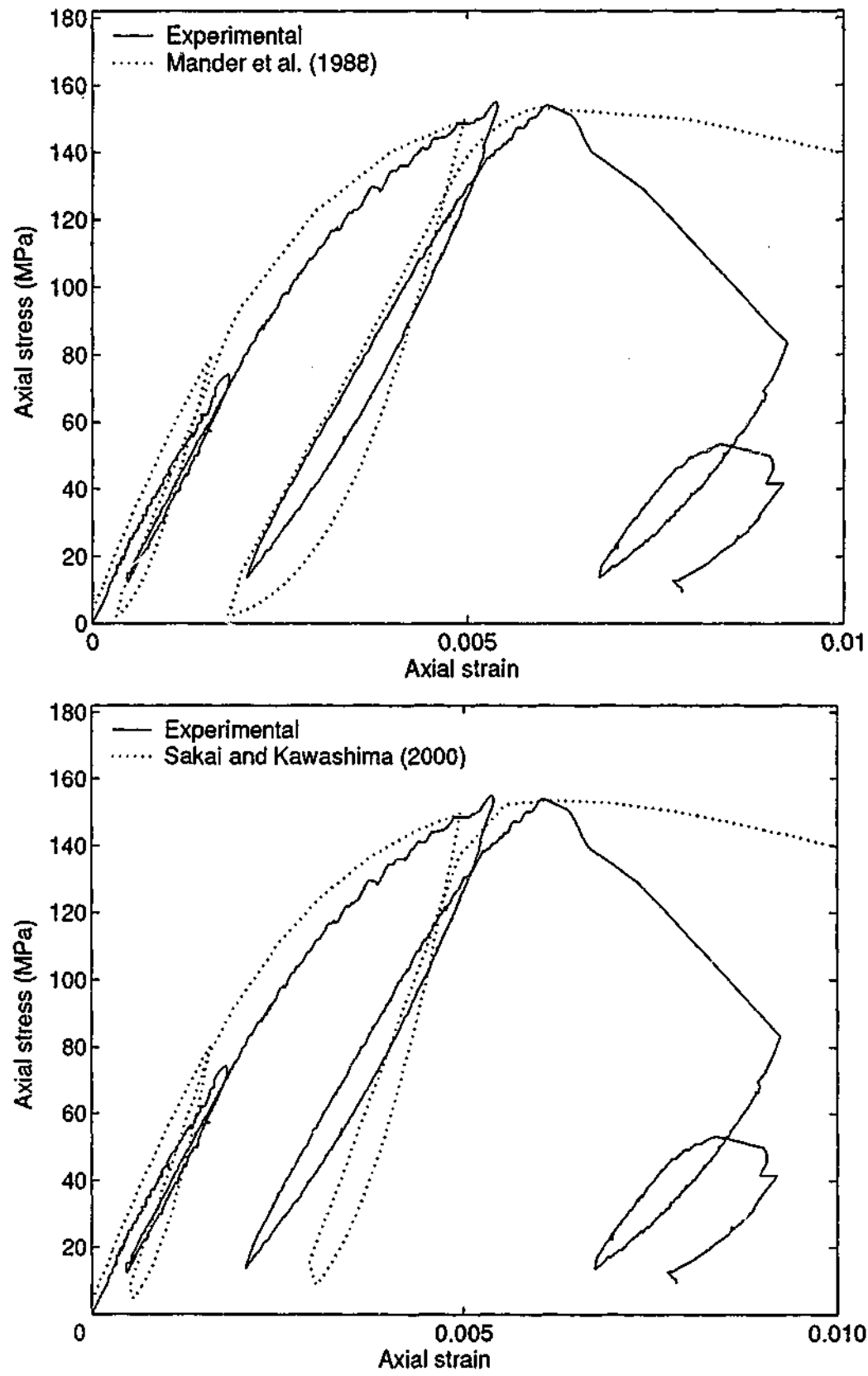


Figure A.21: Loading regime 1 of Grade 100 concrete with 8 MPa confining pressure.

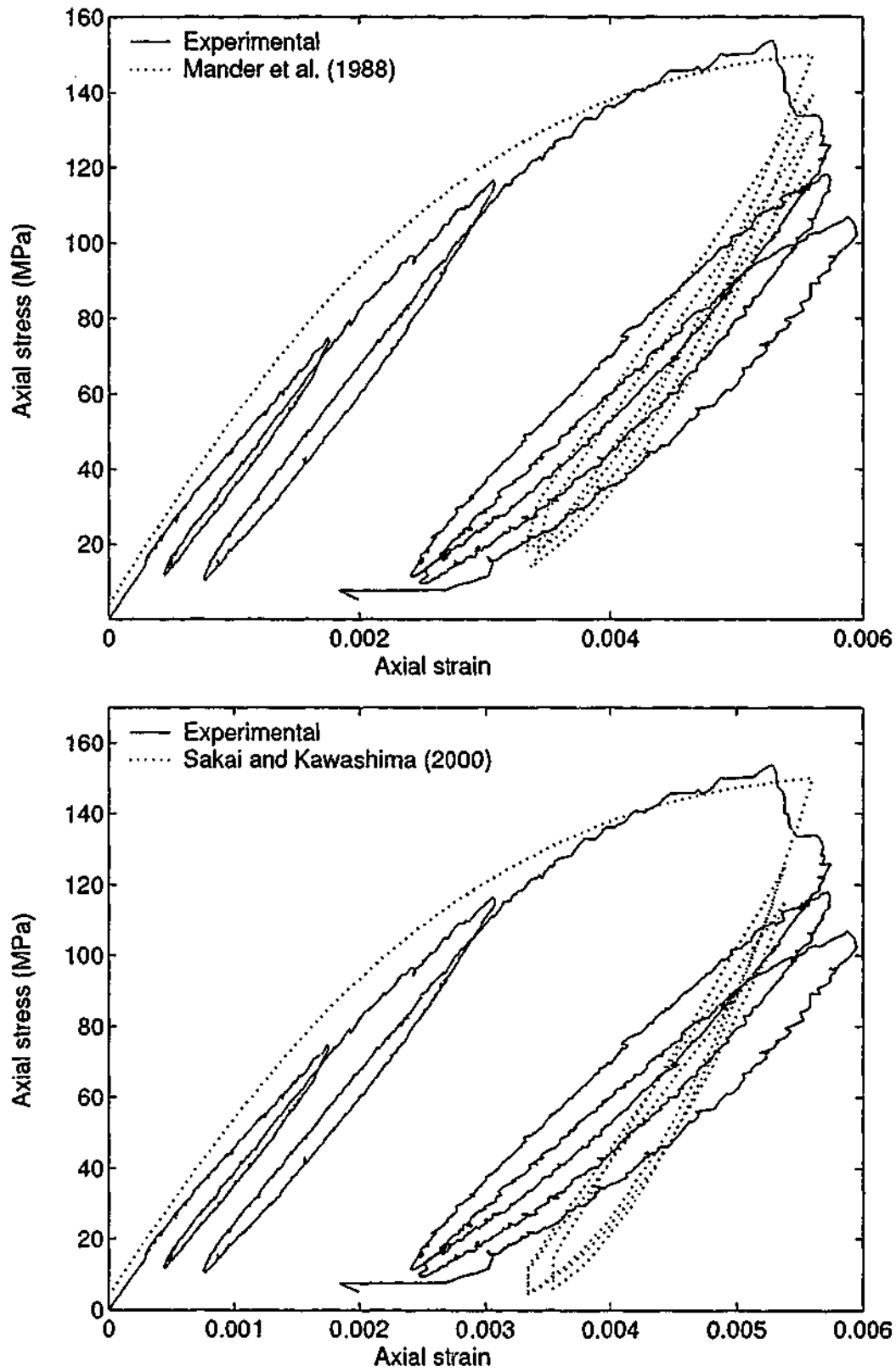


Figure A.22: Loading regime 2 of Grade 100 concrete with 8 MPa confining pressure.

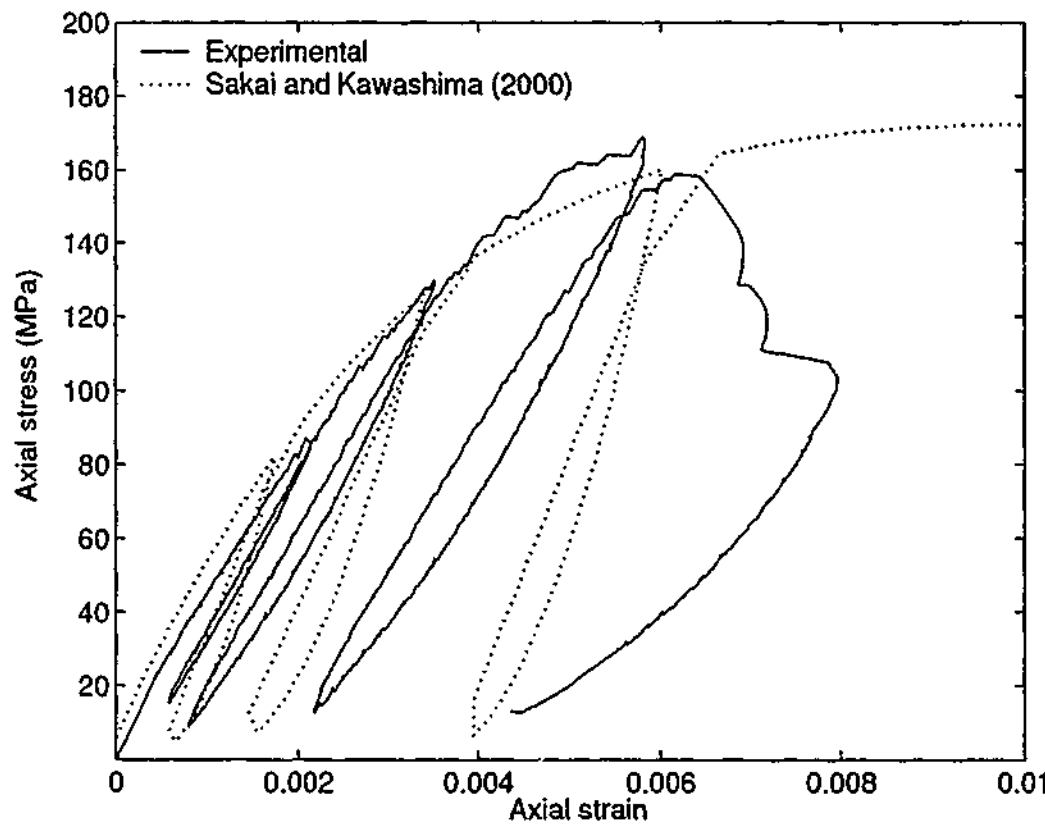
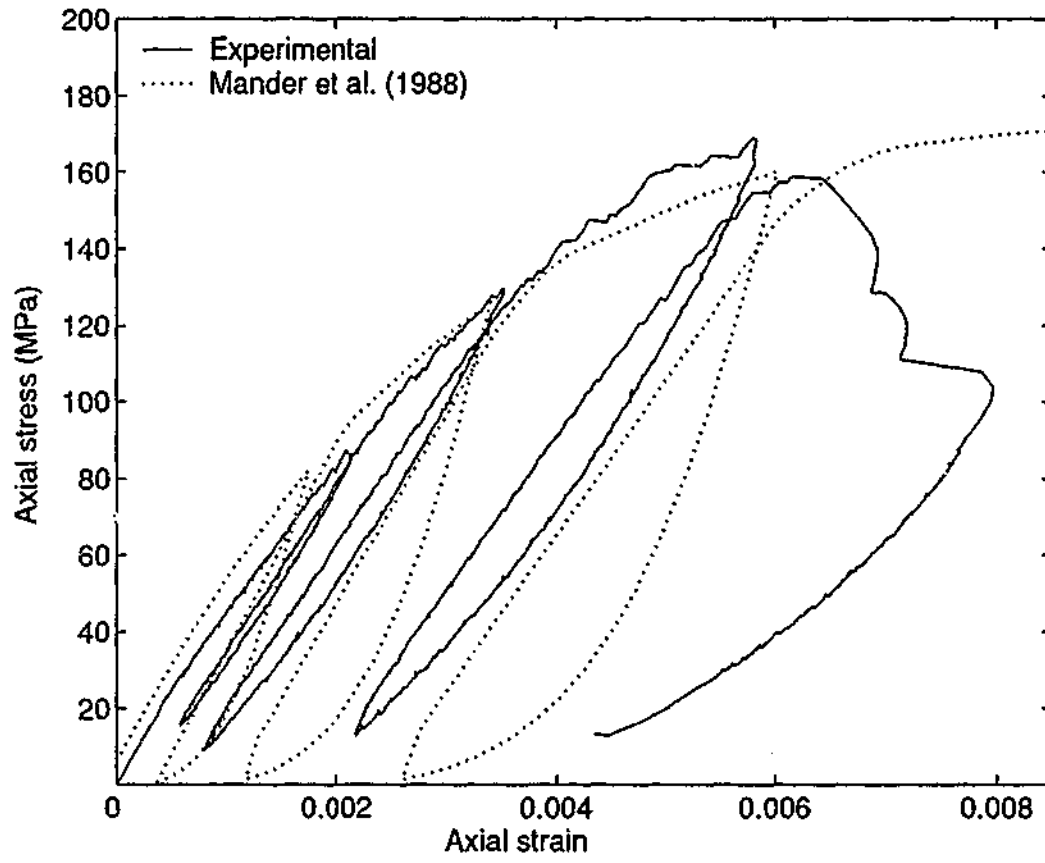


Figure A.23: Loading regime 1 of Grade 100 concrete with 12 MPa confining pressure.

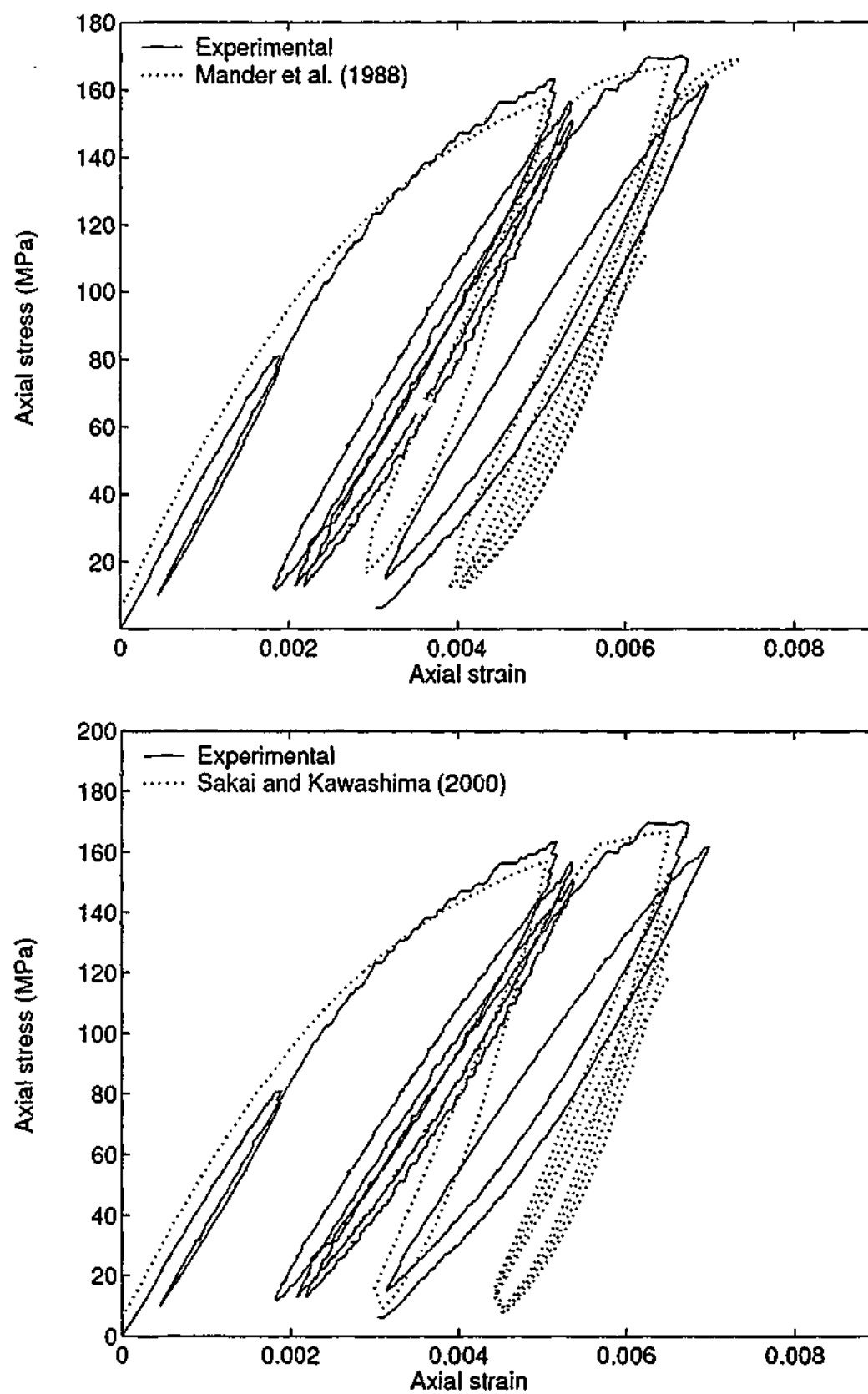


Figure A.24: Loading regime 2 of Grade 100 concrete with 12 MPa confining pressure.

Bibliography

- ACI318-89 (1989). *Building Code Requirements for Reinforced Concrete and Commentary (ACI 318-89/ACI 318R-89)* American Concrete Institute, Detroit.
- ACI318-99 (1999). *Building Code Requirements for Structural Concrete (ACI 318-99) and Commentary (ACI 318R99)* American Concrete Institute, Detroit.
- ACI363 (1984). "State-of-the-Art Report on High-Strength Concrete." *ACI Journal*, Proceedings 81(4), pp. 364-411.
- Ahmad, S. H. and Mallare, M. P. (1994). "A comparative study of models for confinement of concrete by circular spirals." *Magazine of Concrete Research*, 46(166), pp. 49-56.
- Ahmad, S. H. and Shah, S. P. (1982). "Stress-strain curves of concrete confined by spiral reinforcement." *ACI Journal*, 79(6), pp. 484-490.
- Ahn, J. M., Lee, J. Y., Bahn, B. Y., and Shin, S. W. (2000). "An experimental study of the behaviour of high strength reinforced concrete columns subjected to reversed cyclic shear under constant axial compression." *Magazine of Concrete Research*, 52(3), pp. 209-218.
- Aoyama, H. and Noguchi, H. (1979). "Mechanical properties of concrete under load cycles idealizing seismic actions." *Proc., State of the Art Report, AICAP-CEB Symposium on Structural Concrete under Seismic Actions*, Rome, Italy, pp. 31-62.
- AS1012 (2000). *Methods of testing concrete* Standards Association of Australia.
- AS3600 (2001). *Concrete Structures* Australian Standard, Standards Association of Australia.
- Assa, B. and Nishiyama, M. (1998). "Prediction of load displacement curve of high strength concrete columns under simulated seismic loading." *ACI Structural Journal*, 95(5), pp. 547-557.

- Assa, B., Nishiyama, M., and Watanabe, F. (2001a). "New approach for modeling confined concrete. I: Circular columns." *Journal of Structural Engineering*, 127(7), pp. 743-750.
- Assa, B., Nishiyama, M., and Watanabe, F. (2001b). "New approach for modelling confined concrete. II: Rectangular columns." *Journal of Structural Engineering*, 127(7), pp. 751-757.
- Attard, M. M. and Foster, S. J. (1995). "Ductility of high strength concrete columns." Technical Report UNICIV R-344, School of Civil Engineering, The University of New South Wales, Australia.
- Attard, M. M. and Setunge, S. (1994). "The stress-strain relationship of confined and unconfined normal and high strength concretes." Technical Report UNICIV R-341, School of Civil Engineering, The University of New South Wales, Australia.
- Attard, M. M. and Setunge, S. (1996). "Stress-strain relationship of confined and unconfined concrete." *ACI Materials Journal*, 93(5), pp. 432-442.
- Attard, M. M. and Stewart, M. G. (1998). "A two parameter stress block for high-strength concrete." *ACI Structural Journal*, 95(3), pp. 305-316.
- Azizinamini, A. (1995). "Can high-strength concrete be used in a ductile way?." *Concrete International*, 17(3), pp. 48-51.
- Azizinamini, A., Kuska, S. S. B., Brungardt, P., and Hatfield, E. (1994). "Seismic behaviour of square high-strength concrete columns." *ACI Structural Journal*, 91(3), pp. 336-347.
- Bayrak, O. and Sheikh, S. A. (1998). "Confinement reinforcement design considerations for ductile HSC columns." *Journal of Structural Engineering*, 124(9), pp. 999-1010.
- Bianchini, A. C., Woods, R. E., and Kesler, C. E. (1961). "Effect of floor concrete strength on column strength." *ACI Journal*, 31(11), pp. 1149-1169.
- Bing, L., Park, R., and Tanaka, H. (1991). "Effect of confinement on the behaviour of high strength concrete columns under seismic loading." *Proc., Pacific Conference on Earthquake Engineering*, New Zealand, pp. 183-194.
- Bing, L., Park, R., and Tanaka, H. (2000). "Constitutive behaviour of high-strength concrete under dynamic loads." *ACI Structural Journal*, 97(4), pp. 619-629.

- Biolzi, L., Guerrini, G. L., and Rosati, G. (1997). "Overall structural behaviour of high strength concrete specimens." *Construction and Building Materials*, 11(1), pp. 57-63.
- Candappa, D. (2000). *The constitutive behaviour of high strength concrete under lateral confinement* PhD Thesis, Monash University, Australia.
- Candappa, D. P., Sanjayan, J. G., and Setunge, S. (2001). "Complete triaxial stress-strain curves of high-strength concrete." *Journal of Materials in Civil Engineering*, 13(3), pp. 209-215.
- Candappa, D. P., Setunge, S., and Sanjayan, J. G. (1999). "Stress versus strain relationship of high strength concrete under high lateral confinement." *Cement and Concrete Research*, 29(12), pp. 1977-1982.
- Carrasquillo, R. L., Slate, F. O., and Nilson, A. H. (1981). "Properties of high-strength concrete subject to short-term loads." *ACI Journal*, 78(3), pp. 171-178.
- Carreira, D. J. and Chu, K. H. (1985). "Stress-strain relationship for plain concrete in compression." *ACI Journal*, 83(6), pp. 797-804.
- Chan, S. Y. N. and Anson, M. (1994). "High-strength concrete: The Hong Kong experience." *Magazine of Concrete Research*, 46(169), pp. 235-236.
- Cheong, H. K. and Perry, S. H. (1993). "Cyclic loading of laterally confined concrete columns." *Materials and Structures*, 26(163), pp. 557-562.
- Chung, H.-S., Yang, K.-H., Lee, Y.-H., and Eun, H.-C. (2002). "Stress-strain curve of laterally confined concrete." *JEST: Engineering Structures-Elsevier*, 24(9), pp. 1153-1163.
- Claeson, C. and Gylltoft, K. (1998). "Slender high-strength concrete columns subjected to eccentric loading." *Journal of Structural Engineering*, 124(3), pp. 233-240.
- CSA-A23.3 (1994). *Design of Concrete Structures for Buildings* Canadian Standards Association, Rexdale, Ontario.
- Cusson, D. and Paultre, P. (1994). "High strength concrete columns confined by rectangular ties." *Journal of Structural Engineering*, 120(3), pp. 783-804.
- Cusson, D. and Paultre, P. (1995). "Stress-strain model for confined high strength concrete." *Journal of Structural Engineering*, 121(3), pp. 468-477.

- Dahl, K. K. B. (1992). "A failure criterion for normal and high strength concrete." Technical Report 5.6, Technical University of Denmark, Denmark.
- Darwin, D. and Pecknold, D. A. (1976). "Analysis of RC shear panels under cyclic loading." *Journal of Structural Division, ASCE*, 102(2), pp. 355-369.
- Darwin, D. and Pecknold, D. A. (1977). "Analysis of cyclic loading of plane R/C structures." *Computers and Structures*, 7, pp. 137-147.
- Desayi, P., Iyengar, K. T. S. R., and Reddy, T. S. (1979). "Stress-strain characteristics of concrete confined in steel spirals under repeated loading." *Materials and Structures*, 12(71), pp. 375-383.
- Diniz, S. M. C. and Frangopol, D. M. (1997). "Strength and ductility simulation of high-strength concrete columns." *Journal of Structural Engineering*, 123(10), pp. 1365-1374.
- Dodd, J. I. and Restrepo-posada, J. I. (1995). "Model for predicting cyclic behaviour of reinforcing steel." *Journal of Structural Engineering*, 121(3), pp. 433-445.
- El-Dash, K. M. and Ahmad, S. H. (1995). "A model for stress-strain relationship of spirally confined normal and high-strength concrete columns." *Magazine of Concrete Research*, 47(171), pp. 177-184.
- Elmorsi, M. M., Kianoush, R. M., and Tso, W. K. (1998). "Nonlinear analysis of cyclically loaded reinforced concrete structures." *ACI Structural Journal*, 95(6), pp. 725-739.
- EQE (1995). "The January 17, 1995 Kobe Earthquake." EQE Summary Report, <http://www.eqe.com/publications/kobe/building.htm>.
- Fafitis, A. and Shah, S. P. (1985). "Lateral reinforcement for high-strength concrete columns." *ACI Special Publication*, SP 87-12, pp. 213-232.
- FIP/CEB (1990). "High strength concrete." State of the Art Report 90/1, FIP Publication.
- Foster, S. J. and Attard, M. M. (1997). "Experimental tests on eccentrically loaded high strength concrete columns." *ACI Structural Journal*, 94(3), pp. 295-303.
- Foster, S. J., Liu, J., and Sheikh, S. A. (1998). "Cover spalling in HSC columns loaded in concentric compression." *Journal of Structural Engineering*, 124(12), pp. 1431-1437.

- Fu, H. C., Erki, M. A., and Seckin, M. (1991a). "Review of effects of loading rate on concrete in compression." *Journal of Structural Engineering*, 117(12), pp. 3645-3659.
- Fu, H. C., Erki, M. A., and Seckin, M. (1991b). "Review of effects of loading rate on reinforced concrete." *Journal of Structural Engineering*, 117(12), pp. 3660-3679.
- Gamble, W. L. and Klinar, J. D. (1991). "Tests on high-strength concrete columns with intervening floor slabs." *Journal of Structural Engineering*, 117(5), pp. 1462-1476.
- Ghosh, S. K. (1997). "High strength concrete in regions of high seismicity." *Proc., The 1997 15th Structures Congress. Part 2 (of 2)*, pp. 1001-1005.
- Hadi, M. (2001). "Behavior of high strength concrete columns confined with helices." *Concrete in Australia*, pp. 10-13.
- Hadi, M. N. S. and Ai-samaraie, N. H. (2001). "Behavior of confined high strength concrete." *Proc., Third International Conference on Concrete under Severe Conditions*, The University of Columbia, Vancouver, Canada.
- Han, B. S., Shin, S. W., and Bahn, B. Y. (2003). "A model of confined concrete in high-strength reinforced concrete tied columns." *Magazine of Concrete Research*, 55(3), pp. 203-214.
- Hognestad, E., Hanson, N. W., and McHenry, D. (1955). "Concrete stress distribution in ultimate strength design." *ACI Journal*, 52(4), pp. 455-480.
- Hoshikuma, J., Kawashima, K., Nagaya, K., and Taylor, A. W. (1997). "Stress-strain model for confined reinforced concrete in bridge piers." *Journal of Structural Engineering*, 123(5), pp. 624-633.
- Hsu, L. S. and Hsu, C. T. T. (1994). "Complete stress-strain behaviour of high-strength concrete under compression." *Magazine of Concrete Research*, 46(169), pp. 301-312.
- Hu, Q. and Zhu, J. (1994). "Utilisation of high-strength concrete in tall buildings." *Structural Design of Tall Buildings*, 3(4), pp. 269-274.
- Ibrahim, H. H. H. and MacGregor, J. G. (1996). "Tests of eccentrically loaded high-strength concrete columns." *ACI Structural Journal*, 93(5), pp. 585-594.
- Issa, M. A. and Tobaa, H. (1994). "Strength and ductility enhancement in high-strength confined concrete." *Magazine of Concrete Research*, 46(168), pp. 177-189.

- Joen, P. H. and Park, R. (1990). "Flexural strength and ductility analysis of spirally reinforced prestressed concrete piles." *PCI Journal*, 35(4), pp. 64-83.
- Karsan, I. D. and Jirsa, J. O. (1969). "Behaviour of concrete under compressive loadings." *Journal of the Structural Division. Proceedings of the American Society of Civil Engineers*, 95(12), pp. 2543-2563.
- Karsan, I. D. and Jirsa, J. O. (1970). "Behaviour of concrete under varying strain gradient." *Journal of Structural Engineering*, 96(8), pp. 1675-1696.
- Kayani, M. K. (1992). *Load transfer from high-strength concrete columns through lower strength concrete slabs* PhD Thesis, Department of Civil Engineering, University of Illinois, Urbana-Champaign 111 pp.
- Kent, D. C. and Park, R. (1971). "Flexural members with confined concrete." *Journal of the Structural Division, Proceedings of the ASCE*, 97(7), pp. 1969-1990.
- Kwan, W. P. and Billington, S. L. (2001). "Simulation of structural concrete under cyclic load." *Journal of Structural Engineering*, 127(12), pp. 1391-1401.
- Laogan, B. T. and Elnashai, A. S. (1999). "Structural performance and economics of tall high strength buildings in seismic regions." *The Structural Design of Tall Buildings*, 8, pp. 171-204.
- Legeron, F., Mongeau, D., and Fautre, P. (1997). "Behaviour of high-strength concrete columns under combined flexure and axial loads." *Proceedings of the 1997 Annual Conference of the Canadian Society for Civil Engineering*, 7(7), pp. 163-172.
- Legeron, F. and Paultre, P. (2000). "Behaviour of high-strength concrete columns under cyclic flexure and constant axial load." *ACI Structural Journal*, 97(4), pp. 591-601.
- Lim, K. K. (1986). "Inelastic cyclic responses of reinforced concrete." Master Thesis, Dept. of Civil Engineering, Monash University, Australia.
- Liu, J., Foster, S. J., and Attard, M. M. (1998). "Behaviour of tied high strength concrete columns loaded in concentric compression." Technical Report UNICIV R-372, School of Civil and Environmental Engineering, The University of New South Wales, Australia.
- Liu, J., Foster, S. J., and Attard, M. M. (2000). "Strength of tied high-strength concrete columns loaded in concentric compression." *ACI Structural Journal*, 97(1), pp. 149-156.

- Lloyd, N. A. and Rangan, B. V. (1993). "High strength concrete: A review." Technical Report No. 1/93, Curtin University of Technology, Perth, Western Australia.
- Lloyd, N. A. and Rangan, B. V. (1995). "High strength concrete columns under eccentric compression." Technical Report No. 1/95, Curtin University of Technology, Perth, Western Australia.
- Lloyd, N. A. and Rangan, B. V. (1996). "Studies on high strength concrete columns under eccentric compression." *ACI Structural Journal*, 93(6), pp. 631-638.
- Lokuge, W. P., Sanjayan, J. G., and Setunge, S. (2000a). "Design of high strength concrete columns for ductility." *Concrete in Australia, Journal of the Concrete Institute of Australia*, 26(3), pp. 17-20.
- Lokuge, W. P., Sanjayan, J. G., and Setunge, S. (2002a). "Stress strain relationship of high strength concrete subjected to cyclic loading." *Proc., International Association for Bridge and Structural Engineering Symposium*, Volume 86, Melbourne, Australia, (CD-ROM), 9pp.
- Lokuge, W. P., Sanjayan, J. G., and Setunge, S. (2003a). "Constitutive model for confined high strength concrete subjected to cyclic loadings." *Approved for publication in the Journal of Materials in Civil Engineering, ASCE*.
- Lokuge, W. P., Sanjayan, J. G., and Setunge, S. (2003b). "Stress strain model for laterally confined concrete." *Approved for publication in the Journal of Materials in Civil Engineering, ASCE*.
- Lokuge, W. P., Sanjayan, J. G., and Setunge, S. (2003c). "Triaxial test results of high strength concrete subjected to cyclic loading." *Magazine of Concrete Research*, 55(4), pp. 321-329.
- Lokuge, W. P., Setunge, S., Mendis, P., and Sanjayan, J. G. (2002b). "Prediction of strength of interior high-strength concrete column-slab joints." *Proc., The 17th Australasian Conference on the Mechanics of Structures and Materials*, Volume 86, Queensland, Australia, pp. 185-190.
- Lokuge, W. P., Setunge, S., and Sanjayan, G. J. (2000b). "Lateral reinforcement requirement in high-strength concrete columns." *Proc., International Conference "Our World in Concrete and Structures"*, Singapore, pp. 411-417.

- Lokuge, W. P., Setunge, S., and Sanjayan, J. G. (2003d). "Modelling eccentrically loaded high-strength concrete columns." *Magazine of Concrete Research*, 55(4), pp. 331-341.
- Lorenzis, L. D. (2001). "A comparative study of models on confinement of concrete cylinders with FRP composites." Research report, Chalmers University of Technology, Göteborg, Sweden.
- Madas, P. and Elnashai, A. S. (1992). "A new passive confinement model for the analysis of concrete structures subjected to cyclic and transient dynamic loading." *Earthquake Engineering and Structural Dynamics*, 21(5), pp. 409-431.
- Maher, A. and Darwin, D. (1980). "Mortar constituent of concrete in compression." SM Report No. 5, Structural Engineering and Engineering Materials, University of Kansas Ctr. for Res., Lawrence, Kans.
- Mander, J. B., Priestley, J. N., and Park, R. (1988a). "Observed stress-strain behaviour on confined concrete." *Journal of Structural Engineering*, 114(8), pp. 1827-1849.
- Mander, J. B., Priestley, M. J. N., and Park, R. (1988b). "Theoretical stress-strain model for confined concrete." *Journal of Structural Engineering*, 114(8), pp. 1804-1826.
- Mansur, M. A., Chin, M. S., and Wee, T. H. (1997). "Stress-strain relationship of confined high-strength plain and fiber concrete." *Journal of Materials in Civil Engineering*, 9(4), pp. 171-179.
- Martinez, S., Nilson, A. H., and Slate, F. O. (1984). "Spirally reinforced high-strength concrete columns." *ACI Journal*, 81(5), pp. 431-442.
- Martirosyan, A. and Xiao, Y. (2001). "Flexural shear behaviour of high strength concrete short columns." *Earthquake Spectra*, 17(4), pp. 679-695.
- Matamoros, A. B. and Sozen, M. A. (2003). "Drift limits of high strength concrete columns subjected to load reversals." *Journal of Structural Engineering*, 129(3), pp. 297-313.
- McHarg, P. J., Cook, W. D., Mitchell, D., and Yoon, Y.-S. (2000). "Improved transmission of high-strength concrete column loads through normal strength concrete slabs." *ACI Structural Journal*, 97(1), pp. 157-165.
- Mendis, P., Pendyala, R., and Setunge, S. (2000). "Stress-strain model to predict the full-range moment curvature behaviour of high-strength concrete sections." *Magazine of Concrete Research*, 52(4), pp. 227-234.

- Muguruma, H. and Watanabe, F. (1990). "Ductility improvement of high strength concrete columns with lateral confinement." *ACI Special Publication, High strength concrete*, SP-121, pp. 47-60.
- Nielsen, M. P. (1999). *Limit analysis and concrete plasticity* Boca Raton, CRC Press.
- NZS3101 (1989). *Code of Practice for the Design of Concrete Structures; Commentary on the Design of Concrete Structures; Amendment No. 1 to NZS 3101 Standards* Association of New Zealand, Wellington, New Zealand.
- Ospina, C. E. and Alexander, S. D. B. (1997). "Transmission of high-strength concrete column loads through concrete slabs." *Structural Engineering Report 214*, Dept. of Civil Engineering, University of Alberta, Edmonton, Canada.
- Ospina, C. E. and Alexander, S. D. B. (1998). "Transmission of interior concrete column loads through floors." *Journal of Structural Engineering*, 124(6), pp. 602-610.
- Otter, D. E. and Naaman, A. E. (1988). "Properties of steel fiber reinforced concrete under cyclic loading." *ACI Materials Journal*, 85(4), pp. 254-261.
- Otter, D. E. and Naaman, A. E. (1989). "Model for response of concrete to random compressive loads." *Journal of Structural Engineering*, 115(11), pp. 2794-2809.
- Ottosen, N. S. (1979). "Constitutive model for short-time loading of concrete." *Journal of the Engineering Mechanics Division, Proceedings of the ASCE*, 105(1), pp. 127-141.
- Ozcebe, G. and Saatcioglu, M. (1987). "Confinement of concrete columns for seismic loading." *ACI Structural Journal*, 84(4), pp. 308-315.
- Park, R., Kent, D. C., and Sampson, R. A. (1972). "Reinforced concrete members with cyclic loading." *Journal of Structural Division, ASCE*, 98(7), pp. 1341-1360.
- Park, R., Priestley, M. J. N., and Gill, W. D. (1982). "Ductility of square-confined concrete columns." *Journal of the Structural Division, Proceedings of the ASCE*, 108(4), pp. 929-950.
- Park, R. and Sampson, R. (1972). "Ductility of reinforced concrete column sections in seismic design." *ACI Journal, Proceedings*, 69(9), pp. 543-551.
- Paultre, P., Legeron, F., and Daniel, M. (2001). "Influence of concrete strength and transverse reinforcement yield strength on behaviour of high strength concrete columns." *ACI Structural Journal*, 98(4), pp. 490-501.

- Peng, X., Meyer, C., and Fang, L. (1997). "Thermomechanically consistent continuum damage model for concrete materials." *Journal of Engineering Mechanics*, 123(1), pp. 60-69.
- Perry, S. H. and Cheong, H. K. (1991). "Stress-strain behaviour of laterally confined concrete columns." *Magazine of Concrete Research*, 43(156), pp. 187-196.
- Pessiki, S. and Pieroni, A. (1997). "Axial load behaviour of large-scale spirally-reinforced high-strength concrete columns." *ACI Structural Journal*, 94(3), pp. 304-314.
- Poh, K. W. (1997). "General stress-strain equation." *Journal of Materials in Civil Engineering*, 9(4), pp. 214-217.
- Popovics, S. (1973). "A numerical approach to the complete stress-strain curve of concrete." *Cement and Concrete Research*, 3(5), pp. 583-599.
- Portella, J., Mendis, P., and Baweja, D. (1999). "Transmission of high strength concrete column loads through slabs." *Proc., 16th Australasian Conference on the Mechanics of Structures and Materials*, Sydney, pp. 139-144.
- Priestley, M. J. N. and Park, R. (1987). "Strength and ductility of concrete bridge columns under seismic loading." *ACI Structural Journal*, 84(8), pp. 61-76.
- Rangan, B. V. (1990). "Strength of reinforced concrete slender columns." *ACI Structural Journal*, 87(1), pp. 32-38.
- Rangan, B. V. (1991). "Strength of high strength concrete columns." *Civil Engineering Transactions, The Institute of Engineers, Australia*, CE33(4), pp. 293-298.
- Rangan, V. (1998). "High-performance high-strength concrete: Design recommendations." *Concrete International*, 20(11), pp. 63-68.
- Rashid, M. A., Mansur, M. A., and Paramasivam, P. (2002). "Correlations between mechanical properties of high-strength concrete." *Journal of Materials in Civil Engineering*, 14(3), pp. 230-238.
- Razvi, S. and Saatcioglu, M. (1999). "Confinement model for high-strength concrete." *Journal of Structural Engineering*, 125(3), pp. 281-289.
- Razvi, S. R. and Saatcioglu, M. (1994). "Strength and deformability of confined high strength columns." *ACI Structural Journal*, 91(6), pp. 678-687.

- Saatcioglu, M. and Baingo, D. (1999). "Circular high-strength concrete columns under simulated seismic loading." *Journal of Structural Engineering*, 125(3), pp. 272-280.
- Saatcioglu, M. and Ozcebe, G. (1989). "Response of reinforced concrete columns to simulated seismic loading." *ACI Structural Journal*, 86(1), pp. 3-12.
- Saatcioglu, M. and Razvi, S. R. (1992). "Strength and ductility of confined concrete." *Journal of Structural Engineering*, 118(6), pp. 1590-1607.
- Saatcioglu, M., Salamat, A. H., and Razvi, S. R. (1995). "Confined columns under eccentric loading." *Journal of Structural Engineering*, 121(11), pp. 1547-1556.
- Sakai, J. and Kawashima, K. (2000). "An unloading and reloading stress-strain model for concrete confined by tie reinforcements." *Proc., The 12th World Conference on Earthquake Engineering (12WCEE 2000), Auckland, New Zealand*, pp. 1-8.
- Samra, Raed M Deeb, N. A. A. and Madi, U. R. (1996). "Transverse steel content in spiral concrete columns subject to eccentric loading." *ACI Structural Journal*, 93(4), pp. 412-419.
- Samra, R. M. (1990). "Ductility analysis of confined columns." *Journal of Structural Engineering*, 116(11), pp. 3148-3161.
- Sargin, M. (1971). "Stress strain relationship for concrete and the analysis of structural concrete sections." Technical Report Study No.4, Solid Mechanics Division, University of Waterloo, Ontario.
- Sargin, M., Ghosh, S. K., and Handa, V. K. (1971). "Effects of lateral reinforcement upon the strength and deformation properties of concrete." *Magazine of Concrete Research*, 23(75-76), pp. 99-110.
- Scott, B. D., Park, R., and Priestley, N. (1982). "Stress-strain behaviour of concrete confined by overlapping hoops at low and high strain rates." *ACI Journal*, 79(1), pp. 13-27.
- Setunge, S. (1993). *Structural properties of very high strength concrete* PhD Thesis, Monash University, Australia.
- Setunge, S., Mendis, P. A., and Darvall, P. L. (1994). "Full range moment curvature behaviour of reinforced concrete sections." *Proc., Australian Structural Engineering Conference*, pp. 507-514 Institute of Engineers, Australia.

- Shah, S. P., Fafitis, A., and Arnold, R. (1983). "Cyclic loading of spirally reinforced concrete." *Journal of Structural Engineering*, 109(7), pp. 1695-1710.
- Shams, M. and Saadeghvaziri, M. A. (1997). "State of the art of concrete-filled steel tubular columns." *ACI Structural Journal*, 94(5), pp. 558-571.
- Sheikh, S. A., Shah, D. V., and Khoury, S. S. (1994). "Confinement of high-strength concrete columns." *ACI Structural Journal*, 91(1), pp. 100-111.
- Sheikh, S. A. and Uzumeri, S. M. (1980). "Strength and ductility of tied concrete columns." *Journal of the Structural Division, Proceedings of the ASCE*, 106(5), pp. 1079-1102.
- Sheikh, S. A. and Uzumeri, S. M. (1982). "Analytical model for concrete confinement in tied columns." *Journal of Structural Engineering*, 108(12), pp. 2703-2722.
- Sheikh, S. A. and Yeh, C. C. (1992). "Analytical moment-curvature relations for tied concrete columns." *Journal of Structural Engineering*, 118(2), pp. 529-544.
- Siao, W. B. (1994). "Reinforced concrete column strength at beam/slab and column intersection." *ACI Structural Journal*, 91(1), pp. 3-9.
- Sinha, B. P., Gerstle, L. H., and Tulin, L. G. (1964). "Stress-strain relationships for concrete under cyclic loading." *Journal of the American Concrete Institute*, 61(2), pp. 195-211.
- Thomsen, J. H. and Wallace, J. W. (1994). "Lateral load behaviour of reinforced concrete columns constructed using high-strength materials." *ACI Materials Journal*, 91(5), pp. 605-615.
- Wang, P. T., Shah, S. P., and Naaman, A. E. (1978). "Stress-strain curves of normal and lightweight concrete in compression." *ACI Journal*, 75(11), pp. 603-611.
- Warner, R. F., Rangan, B. V., Hall, A. S., and Faulkes, K. A. (1998). *Concrete Structures* Addison Wesley Longman, Australia.
- Watanabe, F. and Muguruma, H. (1988). "Toward the ductility design of concrete members - Overview of researchers in Kyoto University." *Proc., Pacific Concrete Conference*, pp. 89-100, New-Zealand.

- Watson, S. and Park, R. (1994). "Simulated seismic load tests on reinforced concrete columns." *Journal of Structural Engineering*, 120(6), pp. 1825-1849.
- Watson, S., Zahn, F. A., and Park, R. (1994). "Confining reinforcement for concrete columns." *Journal of Structural Engineering*, 120(6), pp. 1798-1824.
- Wee, T. H., Chin, M. S., and Mansur, M. A. (1996). "Stress-strain relationship of high-strength concrete in compression." *Journal of Materials in Civil Engineering*, 8(2), pp. 70-76.
- Xiao, Y. and Henry, W. Y. (2002). "Experimental studies on full-scale high strength concrete columns." *ACI Structural Journal*, 99(2), pp. 199-207.
- Xiao, Y. and Wu, H. (2000). "Compressive behaviour of concrete confined by carbon fibre composite jackets." *Journal of Materials in Civil Engineering*, 12(2), pp. 139-146.
- Xie, J., Elwi, A. E., and MacGregor, J. G. (1997). "Performance of high-strength concrete tied columns- A parametric study." *ACI Structural Journal*, 94(2), pp. 91-102.
- Xie, J., MacGregor, J. G., and Elwi, A. E. (1996). "Numerical investigation of eccentrically loaded high-strength concrete tied columns." *ACI Structural Journal*, 93(4), pp. 449-461.
- Yankelevsky, D. Z. and Reinhardt, H. W. (1987). "Model for cyclic compressive behaviour of concrete." *Journal of Structural Engineering*, 113(2), pp. 228-240.
- Zhang, X., Guo, Z., and Wang, C. (1984). "Experimental investigation of complete stress-strain curves of concrete confined by stirrups under cyclic loading." *Proc., Eighth World Conference on Earthquake Engineering, San Francisco, California*, pp. 845-852.